

# NUMERICAL MODELLING OF MIXING AND SEPARATING OF FLUID FLOWS THROUGH POROUS MEDIA

Rahim Bux Khokhar

A thesis submitted in partial fulfilment of the requirements of the  
University of Hertfordshire for the degree of Doctor of Philosophy

The programme of research was carried out in the School of  
Engineering and Technology, University of Hertfordshire, Hatfield,  
UK

January 2017

---

## Abstract

In present finite element study, the dynamics of incompressible isothermal flows of Newtonian and two generalised non-Newtonian models through complex mixing-separating planar channel and circular pipe filled with and without porous media, including Darcy's term in momentum equation, is presented. Whilst, in literature this problem is solved only for planar channel flows of Newtonian and viscoelastic fluids. The primary aim of this study is to examine the laminar flow behaviour of Newtonian and inelastic non-Newtonian fluids, and investigate the robustness of the numerical algorithm. The rheological properties of non-Newtonian fluids are defined utilising a range of constitutive equations, for inelastic non-Newtonian fluids non-linear viscous models, such as Power Law and Bird-Carreau models are used to capture the shear thinning behaviour of fluids.

To simulate such complex flows, steady-state solutions are sought employing time-dependent finite element algorithm. Temporal derivatives are discretised using second order Taylor series expansion, while, spatial discretisation is achieved through Galerkin approximation in combination to deal with incompressibility a pressure-correction scheme adopted. In order to achieve the algorithm of semi-implicit form Darcy's-Brinkman equation is utilized for the conversion in Darcy's terms and diffusion, while Crank-Nicolson approach is adopted for stability and acceleration. Simple and complex flows for various complex flow bifurcations of the combined mixing-separating geometries, for both two-dimensional planar channel in Cartesian coordinates, as well as axisymmetric circular tube in cylindrical polar coordinates system are investigated. These geometries consist of a two-inverted channel and pipe flows connected through a gap in

---

common partitions, initially filled with non-porous materials and later with homogeneous porous materials. Computational domain is having variety it has been investigated with many configurations. These computational domains have been appeared in industrial applications of combined mixing and separating of fluid flows both for porous and non-porous materials. Fully developed velocity profile is applied on both inlets of the domain by imposing analytical solutions found during current study for porous materials.

Numerical study has been conducted by varying flow rates and flow direction due to a variety in the domain. The influence of varying flow rates and flow directions are analysed on flow structure. Also the impact of increasing inertia, permeability and power law index on flow behaviour and pressure difference are investigated. From predicted solution of present numerical study, for Newtonian fluids a close agreement is realised between numerical solutions and experimental data.

During simulations, it has been noticed that enhancing fluid inertia (flow rates), and permeability has visible effects on the flow domains. When the Reynolds number value increases the size and power of the vortex for recirculation increases. Under varying flow rates an early activity of vortex development was observed. During change in flow directions reversed flow showed more inertial effects as compared with unidirectional flows. Less significant influence of inertia has been observed in domains filled with porous media as compared with non-porous. The power law model has more effects on inertia and pressure as compared with Bird Carreau model. Change in the value of permeability gave significant impact on pressure difference.

Numerical simulations for the domain and fluids flow investigated in this study are encountered in the real life of mixing and separating applications in the industry.

---

Especially this purely quantitative numerical investigation of flows through porous medium will open more avenues for future researchers and scientists.

---

## Acknowledgements

First and above all, I praise God, the almighty for providing me this chance, granting me the competence, strong nerves, fitness and tolerance for conducting this research study in which I have progressed well. I would like to express my sincere appreciation to my supervisors Dr. Y. K. Chen and Dr. Y. Xu for their excellent guidance, motivation, continuous support and patience during write up period without whom I would have never been able to finish my write up. They always made themselves available to listen, discuss and provide helpful suggestions during all ups and downs.

It would be injustice if I do not express my deepest gratitude to worthy supervisors and honoured promoters during the first three years of research work; Dr. R. K. Calay and Dr. Pargat Singh. Without their warm cheer, sympathetic supervision and critical comments, I would not have been able to grow as an independent researcher.

I would like to thank the people from STRI, Mrs. Lorraine Nicholls, Miss Michaela Guarnieri, Avis and Emma for their continuous support and respect throughout my stay in the University. I would like to thank Dr. Saeed, Dr. Colin Robert and Dr. Adeel Loya for their advice and help in preparing this thesis.

I would like to give credit to Dr. Baloch and Dr. Solangi for their continuous support and encouragement. I would like to thank Dr. Uqaili, Dr. Tauha Ali, Registrar and Director Planning and Development, MUET, Jamshoro for their support in final stages to allow me to finish my degree smoothly. I am thankful to my friends in Pakistan especially Imdad Ali Qureshi, Abdullah Mahar, Dost Mohammad Sahito and many other sweet friends for their love and care.

I also want to thank my friends in the UK for their ingenuous support, care and unwavering love for me, my wife and for my kids. I would like to thank them especially during my final year of study where I was withdrawn by UH authorities due to financial crisis. They are shoulder to shoulder with me to date. I especially thank *Ada* Dr. Lahku Luhana *sahib* and his family for the way they supported us throughout the whole stay in UK. I want to say big thanks to *Ada* Dr. Ali Gul Metlo *sahib* for his support and helping us in the last stages of my PhD. I am also highly obliged to *Ada* Abdul Jabar Qureshi *sahib* for helping us during visa renewal times.

I cannot finish without thanking my family.

I would like to thank my entire family especially my mother, she remained as a spiritual support for me in all aspects of my life. I would like to say thanks to Mr Abdul Haque Bhatti *sahib* and my mother-in-law for getting in touch with my family all the time during our stay in UK.

I want to express my appreciation and deepest gratefulness to my lovely and sweet kids Faraz Ahmed Khokhar, Bilal Khokhar and Asad Khokhar for being nice human beings. They have been immensely patient and understanding. In particular, my elder son Faraz who gave me support in many ways; emotionally, financially and technically during write up period and all other difficult situations.

Last but not least, and most importantly, I would like to thank my wonderful wife Kousar Parveen Bhatti. Without her support, motivation and courage, I could not have finished this work.

---

## List of Contents

Abstract.....	i
Acknowledgements.....	iv
List of Contents.....	vi
List of Figures.....	xi
Nomenclature.....	xv
Greek Nomenclature.....	xviii
Chapter 1. Introduction.....	1
1.1 Historical Background.....	1
1.2 Motivations.....	3
1.3 Aims and objectives.....	3
1.3.1 Aims.....	4
1.3.2 Objectives.....	4
1.4 Layout of the dissertation.....	7
Chapter 2. Theory of Porous Media and Literature Review.....	10
2.1 Introduction.....	10
2.2 Representative Elementary Volume (REV).....	14
2.3 Basic equations of porous materials.....	16
2.3.1 Porosity.....	16
2.3.2 Darcy velocity.....	17
2.3.3 Momentum equation: Darcy's Law.....	18
2.3.4 Darcy's law: Permeability.....	18
2.3.5 Darcy's Brinkman's equation.....	19
2.4 Pseudo-plastic (shear-thinning) fluids.....	20
2.5 Literature review.....	21
2.5.1 Channel flows.....	21
2.5.2 Pipe flows.....	25
2.6 Research gaps.....	27
2.7 Summary.....	30
Chapter 3. Basic Governing System of Equations.....	32
3.1 Introduction.....	32

---

3.2 Basic equations .....	32
3.2.1 Equation of continuity (compressibility) .....	33
3.2.2 Principle of conservation of mass (incompressibility) .....	33
3.2.3 Momentum equation (principal of conservation of momentum) .....	34
3.3 Dimensionless system of equations .....	38
3.4 Initial and boundary conditions .....	39
3.5 Governing system of equations for porous medium .....	41
3.6 Material functions and rheometry .....	42
3.6.1 Steady simple shear flows .....	44
3.7 Governing system of equations (cylindrical polar co-ordinates) .....	45
3.8 Summary .....	46
Chapter 4. Implementation of Numerical Scheme .....	47
4.1 Introduction .....	47
4.2 Taylor–Galerkin/Pressure–Correction Scheme .....	48
4.3 Semi–implicit time–stepping scheme .....	49
4.3.1 Cartesian co-ordinates .....	49
4.3.2 Finite Element Discretisation .....	52
4.3.3 Cylindrical polar co-ordinates .....	56
4.4 Solution methods for resultant system of equations/Mass matrix construction	59
4.5 Stream function .....	61
4.6 Summary .....	66
Chapter 5. Reverse and Unidirectional Flows of Newtonian Fluids in a Channel .....	68
5.1 Introduction .....	68
5.2 Problem specification .....	69
5.3 Governing system of equations .....	72
5.4 Numerical results and discussion .....	74
5.4.1 Mixing and separating of Newtonian fluid flows in a channel filled with non-porous media (Geometry 1 $G_1$ ) .....	74
5.4.2 Mixing and separating of Newtonian fluid flows in a channel filled with non-porous media ( $G_2$ ) .....	90

---

5.4.3	Mixing of separating of Newtonian fluid flow in a channel filled with non-porous media ( $G_3$ ) .....	99
5.4.4	Unidirectional flow of Newtonian fluid in a channel filled with non-porous media ( $G_4$ ) .....	112
5.5	Summary .....	117
Chapter 6.	Mixing and Separating of Newtonian Fluid Flows in a Channel Filled with Porous Media .....	121
6.1	Introduction.....	121
6.2	Problem specification .....	121
6.3	Governing system of equations.....	123
6.4	Numerical scheme and weak formulation .....	123
6.5	Numerical prediction and discussion.....	124
6.5.1	Mixing and separating of Newtonian fluid flows in a channel filled with porous media ( $G_1$ ).....	125
6.5.2	Mixing and separating of Newtonian fluid flows in a channel through porous media ( $G_2$ ) .....	136
6.5.3	Mixing and separating of Newtonian fluid flows in a channel through porous media ( $G_3$ ) .....	143
6.5.4	Unidirectional flows of Newtonian fluid in a channel filled with porous media ( $G_4$ ) .....	155
6.6	Summary .....	158
Chapter 7.	Newtonian Fluid Flows in a Pipe Filled with and without a Porous Media	161
7.1	Introduction.....	161
7.2	Problem specification .....	161
7.3	Governing system of equations.....	162
7.3.1	Non-dimensional system of equations.....	164
7.3.2	Initial and boundary conditions.....	165
7.4	Numerical scheme.....	166
7.5	Results and discussions.....	167
7.5.1	Mixing and separating of Newtonian fluid flows in a pipe.....	168
7.5.2	Newtonian flows in a pipe filled with non-porous media .....	168

---

7.5.3 Mixing and separating of Newtonian fluid flows in a pipe filled with porous media .....	174
7.6 Summary .....	181
Chapter 8. Flows of Non–Newtonian Fluids through Tubes Occupied with and without a Porous Material.....	183
8.1 Introduction.....	183
8.2 Problem specification .....	183
8.3 The Power law model .....	185
8.4 The Bird-Carreau model .....	187
8.5 Governing system of equations.....	188
8.5.1 Initial and boundary conditions.....	190
8.6 Numerical scheme and fully discrete system of weak formulation .....	191
8.7 Numerical results and discussions .....	192
8.7.1 Mixing and separating of non-Newtonian fluid flows in a pipe filled with porous media (Power law model).....	192
8.7.2 The influence of inertia on flow structure .....	193
8.7.3 Effects of changing flow rates and permeability on pressure .....	200
8.7.4 Mixing and separating of non-Newtonian fluid flows in a pipe filled with porous media (Bird-Carreau model) .....	203
8.7.5 Influence of inertia on flow structure.....	203
8.7.6 Effects of Power Law and Bird Carreau model on pressure when pipes are filled without porous media.....	209
8.8 Summary.....	210
Chapter 9. Discussion .....	212
9.1 Introduction .....	212
9.2 Channel flows through non-porous media .....	212
9.3 Channel flows through porous media .....	219
9.4 Pipe flows through non-porous media .....	222
9.5 Pipe flows through porous media.....	223
Chapter 10. Conclusions and Future Suggestions .....	226
10.1 Introduction .....	226
10.2 Conclusion on channel flows .....	226

---

10.3 Conclusions on pipe flows .....	227
10.4 Novelties of the research project .....	228
10.5 Recommendations for future work .....	229
Appendix-A .....	232
Publications.....	232
Appendix-B.....	233
Analytical solution.....	233
Steady–state analytical solution of one–dimensional Darcy’s–Brinkman equation to impose boundary condition on the inlets of combined mixing–separating domain	233
Appendix-C.....	238
Flow Chart of the of finite element scheme.....	238
Appendix-D .....	241
Two dimensional code .....	241
Appendix–E .....	251
Numerically simulated results with velocity profiles, colour bars and velocity vectors .....	251
Bibliography .....	451

---

## List of Figures

Figure 2.1 (a)Examples of natural porous material: (A) beach sand, (B) sandstone, (C) limestone, (D) rye bread, (E) wood, and (F) human lung. (Nield, 1999). ..	12
Figure 2.2 (b) Diagram showing several types of Rock interstices (A) well sorted sedimentary deposit having high porosity; (B) poorly sorted sedimentary deposit having low porosity; (C) well sorted sedimentary deposit consisting of pebbles that are themselves porous, so that the deposit as whole have high porosity; (D) well sorted sedimentary deposit whose porosity has been diminished by the deposition of mineral material in the interstices; (E) Rock rendered porous by solution; (F) Rock rendered porous by fracturing Bear (1988).....	13
Figure 2.3[(a)-(d)] Images of Porous Media (Taken from google images).....	14
Figure 2.4 The representative elementary volume (REV) Nield (1999). .....	15
Figure 5.1 Geometries of the computational domain and mesh; (a) Diagram of combined mixing and separating flows with two inlets and two outlets (Reverse flow) , $G_1$ , (b) Unidirectional flow with two inlets and one outlet, $G_2$ , (c) Reverse flow with two inlets and one outlet, $G_3$ , (d) Unidirectional flow with one inlet and one outlet, $G_4$ and (e) Finite element mesh used in the simulation. ....	71
Figure 5.2 Streamline function for combined mixing and separating of Newtonian fluid flows for equal (1, 1) flow rate in a both channel arms, increasing Re from top to bottom. ....	78
Figure 5.3 Streamline functions for combined mixing and separating of Newtonian fluid flows of unequal (1, 1.5) flow rate in both channel arms, increasing Re from top to bottom. ....	82
Figure 5.4 Streamline functions for combined mixing and separating of fluid flow for unequal (1, 2) flow rate in both arms of channel, increasing Re from top to bottom. ....	86
Figure 5.5 Comparison of maximum scaled pressure with increasing inertia at different flow rates in a channel filled with non-Porous Media. ....	89
Figure 5.6 Streamline functions for unidirectional flows of Newtonian fluids for equal (1, 1) flow rate in both arms of a channel, increasing Re from top to bottom. .	92
Figure 5.7 Streamline functions for combined mixing and separating of fluid flow for unequal (1, 1.5) flow rate in both arms of channel, increasing Re from top to bottom. ....	94

---

Figure 5.8 Streamline functions of unidirectional flows Newtonian fluid for unequal (1, 2) flow rate in both arms of channel filled with non-porous media, increasing Re from top to bottom.....	96
Figure 5.9 Comparison of maximum scaled pressure with increasing inertia at different flow rates in a channel filled with non-Porous Media .....	99
Figure 5.10 Streamline functions for combined mixing and separating of Newtonian fluid flows for equal (1, 1) flow rate in both arms of channel filled with non-porous media, increasing Re from top to bottom.....	10302
Figure 5.11 Streamline functions for combined mixing and separating of Newtonian fluid flow for unequal (1, 1.5) flow rate in both arms of a channel, increasing Re from top to bottom. ....	10706
Figure 5.12 Streamline functions for combined mixing and separating of Newtonian fluid flows for equal (1, 1) flow rate in both arms of channel filled with non-porous media, increasing Re from top to bottom.....	10908
Figure 5.13 Comparison of maximum scaled pressure with increasing inertia at different flow rates in a channel filled with non-Porous media.....	1121
Figure 5.14 Streamline function for unidirectional Newtonian fluid flows in a channel filled with non-porous media, increasing Re from top to bottom.....	1165
Figure 5.15 Maximum scaled pressure with increasing inertia in a channel filled with non-porous media. ....	11716
Figure 6.1 Streamline functions for combined mixing and separating flows of Newtonian fluids of equal (1, 1) flow rate in a channel filled with the porous medium, increasing Re from top to bottom. ....	126
Figure 6.2 Streamline functions for combined mixing and separating flows of Newtonian fluids of unequal (1, 1.5) flow rate in a channel filled with the porous medium, increasing Re from top to bottom. ....	129
Figure 6.3 Streamline functions for combined mixing and separating flows of Newtonian fluids of unequal (1, 2) flow rate in a channel filled with the porous medium, increasing Re from top to bottom. ....	13532
Figure 6.4 Streamline functions for unidirectional flows of Newtonian fluid of equal (1, 1) flow rate in a channel through porous medium, increasing Re from top to bottom. ....	13835
Figure 6.5 Streamline functions for unidirectional flows of Newtonian fluid of unequal (1, 1.5) flow rate in a channel through porous medium, increasing Re from top to bottom. ....	1408
Figure 6.6 Streamline functions for unidirectional flows of Newtonian fluid of unequal (1, 2) flow rate in a channel through porous medium, increasing Re from top to bottom. ....	14240
Figure 6.7 Streamline functions for mixing and separating of Newtonian fluid flows for equal (1, 1) flow rate in a channel through porous medium, increasing Re from top to bottom. ....	14745

---

Figure 6.8 Streamline functions of mixing and separating of Newtonian fluid flows for unequal (1, 1.5) flow rate in a channel filled with porous medium, increasing Re from top to bottom.....	15048
Figure 6.9 Streamline functions of mixing and separating of Newtonian fluid flows for unequal (1, 2) flow rate in a channel filled with porous medium, increasing Re from top to bottom.....	15351
Figure 6.10 Comparison of maximum scaled pressure with increasing inertia at different flow rates in a channel filled with Porous Media .....	1553
Figure 6.11 Streamline function for unidirectional flows of Newtonian fluid in a channel filled with Porous Media, increasing Re from top to bottom. ....	15755
Figure 6.12 Maximum scaled pressure with increasing inertia in unidirectional flows of Newtonian Fluids in a channel filled with Porous Media.....	15856
Figure 7.1 Geometries of the computational domain and mesh; (a) Geometry of mixing and separating fluid flows in a cylindrical pipe, (b) Finite element mesh. ....	16260
Figure 7.2 Streamlines for Newtonian mixing-separating flow of equal (1, 1) flow rate in a pipe filled with the non-porous medium, increasing Re from top to bottom. ....	17068
Figure 7.3 Streamlines for Newtonian mixing-separating flow of unequal (1, 2) flow rate in a pipe filled with the non-porous medium, increasing Re from top to bottom. ....	17271
Figure 7.4 Comparison of maximum scaled pressure with inertia at different flow rates in Pipes filled with non-Porous Media.....	17473
Figure 7.5 Streamline functions for Newtonian combined mixing and separating flow of equal flow rate (1, 1) in a pipe filled with a porous medium, increasing Re from top to bottom. ....	175
Figure 7.6 Streamline functions for Newtonian combined mixing and separating flow of unequal flow rate (1, 2) in a pipe filled with a porous medium, increasing Re from top to bottom. ....	176
Figure 7.7 Comparison of maximum scaled pressure with inertia at different flow rates in Pipes filled with Porous Media .....	18078
Figure 8.1 Graph of shear–rate dependent viscosity of Power law model. ....	184
Figure 8.2 Variation of viscosity with shear rate according to Carreau model. ....	186
Figure 8.3 Streamline function of non-Newtonian fluid flows for Power law model under changing values of power law index from 0.9 to 0.7 with increasing Reynolds number from Re=1 to 6000, from top to bottom. (a) Under an equal (1, 1) and unequal (1, 2) flow rates, (b) Under an equal (1, 1) and unequal (1, 2) flow rates, (c) under an equal (1, 1) and unequal (1, 2) flow rates.....	198
Figure 8.4 [(a)-(b)] Pressure difference for an equal (1, 1) and unequal (1, 2) flow rates with changing power law index from 0.9 to 0.7 and with increasing Reynolds number from 1 to 6000. Re increasing from top to bottom. ....	201

---

Figure 8.5 Streamline function of non-Newtonian fluid flows for Bird Carreau model under changing values of power law index from 0.9 to 0.7 with increasing Reynolds number from $Re=1$ to 6000, from top to bottom. (a) Under an equal (1, 1) and unequal (1, 2) flow rates, (b) Under an equal (1, 1) and unequal (1, 2) flow rates, (c) under an equal (1, 1) and unequal (1, 2) flow rates.....	2036
Figure 8.6 Comparison of Power Law and Bird Carreau model on pressure.....	20808
Figure 9.1 Numerical Results Compared with the experimental Results of (Cochrane et al., 1981)..	20816
Figure 9.2 Numerical Results Compared with the experimental results of [(Cochrane et al., 1981) and (Walters and Webster, 1982)]..	20817

---

**Nomenclature**

$a$	Flow rates (1, 1.5 and 2)
$b$	Right hand side vector in matrix equation
$D_a$	Darcy's number
$D_1, D_2$	Velocity gradient matrices
$\frac{D}{Dt}$	Substantial derivative
$\underline{\underline{d}}$	Strain rate of deformation tensor
$F$	Body forces
$H^1(\Omega)^2$	Sobolev space
$L^2(\Omega)$	Hilbert space
$J$	Pressure gradient matrix
$k$	Incremental viscosity
$K$	Stiffness matrix
$L$	Length of a domain
$L_c$	Characteristic length of a channel
$M$	Mass matrix
$M_d$	Diagonal version of the matrix
$n, N$	Power law index
$N(V)$	Non-linear advection matrix
$P$	Pressure
$Q$	Pressure difference vector

---

$Q_1, Q_2$	Flow rates in domain
$r$	Axisymmetric cylindrical coordinate in radial direction
Re	Reynolds number
$R_i$	Radius of the inner pipe
$R_o$	Radius of the outer pipe
$S$	Diffusion matrix
$s$	Iteration number in matrix equation
$t$	Time
$\underline{\underline{T}}$	Rate of deformation tensor
$T_p$	Temperature under constant pressure
$u$	Horizontal component
$u_p$	Flow rate in porous media
$U_m, V_m$	Maximum velocities at the inlets of a channel
$\mathbf{v}$	Velocity field
$v$	Vertical component
$V$	Nodal velocity vector
$V_c$	Characteristic velocity
$V_p$	Average fluid velocity in porous media
$v_{fp}$	Volume element consisting of the fluid in a porous media
$v_{mp}$	Volume element the medium in a porous media
$v_r$	Radial velocity component

---

$v_z$	Axial velocity component
$v_t$	Partial derivative of velocity w.r.t. time
$V_1, V_2$	Maximum velocities at the inlets of a pipe
$w$	Weight function
$X$	Velocity solution vector in matrix
$z$	Axisymmetric cylindrical coordinate in axial direction

---

## Greek Nomenclature

$\alpha$	Relaxation time
$\beta$	Separation gap between inserted plates in the domain
$\Gamma$	Boundary of the domain
$\gamma$	Shear rate
$\Delta$	Differential operator
$\delta$	Components of unit vector
$\theta$	Theta (used for theta method)
$\kappa$	Permeability
$\lambda$	Relaxation time
$\mu$	Fluid viscosity
$\xi$	Positive acceleration operator
$\rho$	Fluid density
$\sigma$	Cauchy's stress tensor
$\tau$	Shear stress
$\nu$	Kinematic viscosity
$\varphi$	Quadratic basis function
$\psi, \Phi$	Shape functions
$\omega$	Porosity
$\Omega$	Domain of the interest
$\tilde{\mu}$	effective viscosity
$\tau_y$	Yield stress
$\nabla^2$	Laplacian operator

---

$\mu_p$	Plastic viscosity
$\mu_0$	Zero shear stress viscosity
$\dot{\varepsilon}$	Extensional or elongational rate
$\frac{\partial p}{\partial x}$	Pressure gradient
$\mu_\infty$	Viscosity at infinite time
$\mathfrak{T}$	Component of temporal domain
$\tilde{\mu}$	Effective viscosity
$\Delta t$	Time step
$\dagger$	Transpose of matrix
$II_d$ and $III_d$	Second and third invariants of rate of strain tensor
$\mathfrak{R}^2$	Real domain in two dimensions
$\langle \rangle$	Inner product

---

## Chapter 1. Introduction

### 1.1 Historical Background

Over last 50 years, in computational fluid dynamics it is witnessed that the laminar flow of various fluids passing through complex channels and pipes filled with porous material and without porous material have persisted a very important and an interesting topic of industrial significance, particularly in many fields of processing industries. Normally, due to complex flow phenomena of non-Newtonian fluids that displays very complex rheological behaviour and complexity of domain makes industrial problems much vigorous to handle. Therefore, presence of these complications give impetus and many challenges to mathematicians and scientists. Numerous industrial examples can be described, however, only few applications are highlighted, such as crude oil extraction and enhanced oil recovery in petroleum industries, ceramic, chemical, cosmetic, drying, filtration, food and pharmaceutical processes industries, various reactors and many other applications [(Walters and Webster et al, 1982), (Baloch, et al. 1995a) , (Tanner, 2000), (Xia and Sun, 2002), (Al-Nimr and Aldoss, 2004), (Hossain, et al., 2009),(Afonso, et al., 2011) , (Echendu, et al., 2011), (Zhou, et al., 2012), and (Hossain, et al., 2013)].

Incompressible laminar flows of fluids have been investigated in complex domains filled with or without porous media [(Baloch, et al., 1995a), (Alazmi and Vafai, 2001), (Al-Nimr and Aldoss, 2004) and (Echendu, et al., 2011)]. In the last few decades, development in modern high-speed computers has advanced to develop numerical algorithms that are sophisticated in design. The complex flow physics using computer simulations in a domain filled with porous material has been implemented practically and

---

recognized and further developed by the institutes of the world (Al-Nimr and Aldoss, 2004). An anticipated characteristic of the Computational Fluid Dynamics (CFD) approach due to the performance capability in parameter based simulations. Since last three decades, a significant progress has augmented the evolutionary knowledge related to numerical instabilities and nature of flow, like turbulence and unsteadiness. Mathematical modelling of the flow phenomena through combined mixing and separating along with other modifications, see the initial work of [(Cochrane, et al., 1981 and 1982) and (Walters and Hafez, 1982)], solved experimentally and numerically adopting finite difference method, followed a few two dimensional analysis by (Baloch et al., 1995a) employing finite element algorithm and (Afonso et al., 2008) used finite volume technique.

Flow in mixing and separating along with other modifications in a rectangular channels and pipes filled with or without porous media, presents many an interesting flow phenomena, such as, presence singularities at sharp corners, development of trailing edge, lip and longitudinal vortices, flow transition, meandering effects and turbulence all arise in the same domain [Cochrane et al., 1981), (Baloch et al., 1995a) and (Afonso et al., 2008) and (Echendu et al., 2011)].

(Baloch et al., 1995a), also simulated mixing and separating flow utilising time dependent finite element technique for the solution of highly elastic flows. For elastic flows a so called Taylor-Petrov-Galerkin algorithm is used. The method known as pressure-correction is applied for achieving the incompressibility with accuracy in second order. For Newtonian fluid flows, these authors, an equal flow rates in both arms of a channel

had adopted. For viscoelastic simulations, a class of shear thinning Phan–Thien and Tanner (PTT) (Phan–(Thien and Tanner, 1977 and 1978), constitutive model has been used to display shear–thinning effects numerically and the impact of variations in gap width between inserted parallel plates. Also different material parameters and flow conditions investigated.

(Afonso et al., 2011) calculated the lower values of inertia effect on the flow rate using the same geometry, even the creeping flow or limited vanishing inertia. In the latest study by (Echendu et al., 2011), for both Newtonian and viscoelastic fluids, a numerical study has also been performed for same flow domain.

## **1.2 Motivations**

The fundamental motivation of the current study is designing, predicting, and analysing the numerical algorithm to address the phenomena of complex flow within Newtonian and non–Newtonian fluids; this is considered to be one of the challenging problems in the past for computational rheologists (Walters and Webster, 2003). This is due to industrial importance of many complex problems, rheological behaviour of non–Newtonian fluids and flow through porous materials in many processing industries.

## **1.3 Aims and objectives**

The aims and objectives for the current research are given in this section for the Newtonian and non-Newtonian fluid flows of combined mixing and separating in a channel and circular pipes filled with porous and without porous media.

### 1.3.1 Aims

The aim of this research work is the further development of the sophisticated numerical model for both Newtonian and non–Newtonian fluids in combined flow mixing and separating within the circular pipes and rectangular channels in non – existence and existence of homogeneous of porous material.

### 1.3.2 Objectives

1. To analyse the past literature on numerical solutions and experiments relevant to the current aim and objectives
2. To validate the model and predictions made in the current study against past researches, numerical solutions, and experiments.
3. General discussions on flow behaviour of predicted steady–state solution of isothermal complex laminar flow of Newtonian and non–Newtonian fluids will be presented.

For Newtonian and non–Newtonian fluids, research into the laminar flow through channels and pipes filled with porous material the flow structure, development of eddies and pressure drop is a field of importance for scientists and engineers. In this light, current study has been stimulated to explore insight mathematical influence of the inertia (Reynolds number) and pressure drop on the flow phenomena in both rectangular channels and circular pipes filled with homogeneous porous materials. In many research papers in the past, mixing and separation of fluids in channels and pipes has been considered as the primary aim of the studies. Due to relevance to many industrial applications, this classical problem has fascinated significant consideration, because of its complex flow arrangement. Recently, this problem is considered as benchmark

problem for comparison and validation purpose, due presence of singularities at sharp corners and development of complex flow structure, present challenges to both experimental and numerical analysts which facilitates experimental calibrations or numerical implementations. Within these channels, nonetheless, the flow phenomena is very complex.

This study, identify a critical inertial value (Reynolds number), at which inertia influence on the development of embryo vortices and with increasing inertia, become more visible, demonstrate the presence of inertial effects on vortex enhancement and pressure difference. Secondly, this study intends to illustrate the effects of Reynolds numbers generates the onset of instability. On the two-dimensional flows in a rectangular channel, the numerical simulations have been lead to study the flow structure, vortex enhancement and appreciates the impact at various Reynolds number values. Research investigations in the literature shows only few results for different configurations for mixing and separating flow problem obtained with experimental and different numerical schemes. There is still need to consider variety of combinations along with changing fluid materials, flow directions and flow rates.

In this study a numerical investigation of mixing and separating flows in channels and pipes filled with homogeneous porous media will be addressed for its importance in the physical applications like [(Neale and Nader 1974), (Adler, 1992), (Abu-Hijleh and Al-Nimr, 2001), (Alazmi and Vafai, 2001), (Alkam et al., 2001) and (Al-Nimr and Aldoss, 2004)]. Adopting a finite element technique, a steady two-dimensional flow structure, development of vortices and flow bifurcation in rectangular channels at different flow-

rates will be investigated. Effects of the inertia on the size of recirculation, location and number of vortices will be determined along with flow patterns. Numerical predicted flow structure will be compared with the other numerical as well as experimental flow structure as reported by former investigators. Furthermore, this research work also investigates new features of the vortices enhancement and structure by changing in flow rates. The distinctive feature of flow structure will be displayed. The study investigates the varying flow rates for the inertia force and its effect. The influence of the Reynolds number value changes on the flow of the entire domain and flow patterns were studied.

In the current study, isothermal laminar flow of Newtonian and non-Newtonian fluids passing through complex geometry has been considered. Many other complex flow domains also very important to address, however, due to occurrence of singularities at sharp corners where fluid enters in the vicinity of these sharp corners, such as, entry flow geometries are practically very important. The geometry of mixing and separation has same phenomena of flow in context of the development of complex vortices. The comprehensive deliberation is intentionally restricted to those investigations which are directly relate to the mixing and separating geometry experiments and numerical results. The research study selected specify a promising agreement between experiment and simulation. However, at the end of this research study as a matter of fact with the pleasure it is acknowledge that still there are too many problematic questions persist to be focused in future work.

### **1.4 Layout of the dissertation**

This report consists of ten chapters. Chapter–01, comprises an introduction with historical background of the research. Motivations got from the history for selecting this research project. In the end aims and objectives are set.

Chapter–02, depicts theory of porous media with its basic equations. In the end literature review with critical approach is given. Table has been given for identified research gaps along with summary.

Chapter–03, details the governing system of equations along with their dimensionless forms. This chapter also provides initial and boundary conditions used for the domain with and without porous media. The chapter also gives description of the rheometry and material functions for steady shear flows.

Chapter–04, details and analyses the theoretical and practical application of cylindrical co-ordinate and Cartesian through numerical scheme. Explicit and implicit schemes used in current work are given in detail. Finite element discretization, solutions methods for resultant system of equations/Mass matrix construction, theory for stream function are also given.

Chapter–05, details and analyses the Newtonian fluid's simulated results of varying flow directions and rates within the channel filled with non-porous media. In all numerical simulations the effects of inertia on vortex development, influence of relative flow rates on flow structure with changing in flow directions, effects on pressure and mixing

separating effects all are discussed in detail. Possible comparisons are made against available experimental and numerical data available in an open literature.

Chapter-06, presents numerically simulated solutions of flow passing through mixing-separating planar channel filled with porous material of Newtonian fluids. Impact of change in material parameters and its influence on inertia has been analysed to see the effects of Darcy's number in Darcy's-Brinkman's transport momentum equation. Effects of inertia with changing flow rates and flow directions are examined on the flow domain and maximum pressure. The study analyses the Newtonian fluid flows for the effects of mixing and separating using the varied permeability values in the domain.

Chapter-07, reports Newtonian flows in circular pipes filled with a porous and non-porous media using cylindrical coordinates system. The chapter discusses the inertia effects on the structure and pattern of flow due to flow rate changes.

Chapter-08, analyses the application of non-linear viscous models within the flow of non-Newtonian fluid employed for the models; Bird Carreau and Power law in the cylindrical pipes, which is demonstrated through change of the flow rates and power law index with and without porous media.

Chapter-09, covers general discussions on the accuracy and stability of numerical scheme used and results produced from chapter five to eight for both channel and pipe flows. Here comparisons are made when Newtonian and non-Newtonian fluid flows are passing

through a channel and pipe filled with and without porous media. Numerical results are also compared with experimental results.

Finally Chapter–10, summarises the main findings from the overall study including novilities of this research project. In the end some recommendations have been made for the future research in this area.

## Chapter 2. Theory of Porous Media and Literature Review

### 2.1 Introduction

In the field of computational fluid dynamics, the prediction of the non-linear system of Partial Differential Equations (PDEs) govern the simple as well as complex flows of both compressible or incompressible fluids, whereas fluids are Newtonian or non-Newtonian have been given considerable attention in the open literature [(Chorin, 1968), (Whitaker, 1986), (Bear, 1988), (Kakac, 1991), (Anderson, 1995), (Temam, 1995), (Ingham, 1998), (Nield, 1999), (Löhner, 2001), (Walters and Webster, 2003), (Versteeg and Malalasekera, 2007) and (Vafai, 2010)].

During recent years, research in flow of fluids through porous material has received significantly high interest and attracted the attention devoted by engineers and scientists, due to its many industrial and real life applications. These are exemplified in diversified subjects, such as, applied mathematics, chemical processing industries (chemical reactors), civil (ground water hydrology, snow and soil mechanics), petroleum (reservoir engineering), environmental, mechanical, biological and biomedical (haemodynamic), and nuclear engineering, geothermal physics, food science and many other applications. There are several studies based on the porous media and flow rates of fluids. It is therefore, appropriate and timely to undertake a new critical estimation of modern evidences (Ingham, 1998).

Porous materials are defined as solids containing pores or as bulk material containing of solid particles in between presence spaces. Mainly, it is characterised by its porosity and

ratio between spaces to the bulk material. Permeability, the measure of the flow conductivity, also characterised porous materials. In real life application, such as, purifying drinking water, filtration process, also use porous media, for example, activated carbon or porous ceramics, eliminating slit and sand particles (Kōzō Ishizaki, et al. 1998).

In chemical, cosmetic and food processing industries, many processes, include fluid passing through complex tubes, conduits, and other processing type of equipment. In processes, flow become laminar which characterises the fluid move with small velocity, where inertial force is relatively small compared to viscous force. In many cases it arises, such as, sinking films, in thin capillaries, flow through porous material, flow around immersed bodies, and highly viscous diffusion dominant fluids. To describe the diffusion of fluid in porous media is through tortuosity, which is a property of curve being tortuous (twisted: with numerous turns), and several attempts have been made to compute the property (Heldman, 2003).

There are many examples of porous medium, such as, porous soil, porous or fissured rocks, fibrous aggregates, loaf of bread, ceramics, sand filters, and filter paper are just few. Somewhat less obvious but still part of this group is also a good example of porous material which is large geologic formations of caustic limestone, where open passages such as solution channels or caverns may be of substantial size and far apart. All of these materials have some characteristic in common that permit them to be grouped and classified as porous medium (Bear, 1988).

In figure 2.1(a) and 2.2 (b), different rick spaces and natural porous materials are specified as examples. Various other images of porous media taken from Google images are also given in Figure[2.3(a-d)]. Advancements in flow through porous material lead to extended sophisticated models for the Darcy's law, Darcy's–Brinkman equation is applicable for large flow velocities and Darcy's–Brinkman–Forchheimer's equation takes into account the microscopic behaviour at low inertial values and boundary effects.

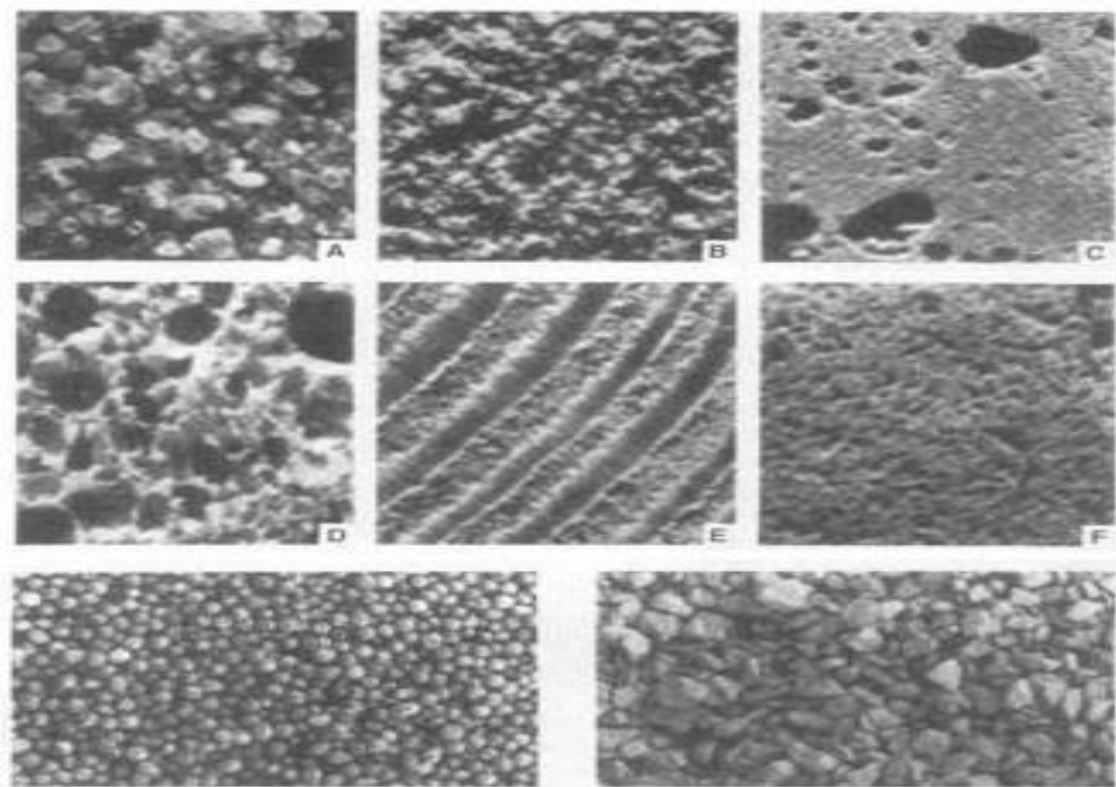


Figure 2.1 (a): Normal porous material: (A) Shore Sand, (B) Stone, (C) Mineral, (D) Dough, (E) Timber, and (F) Lungs (Nield, 1999).

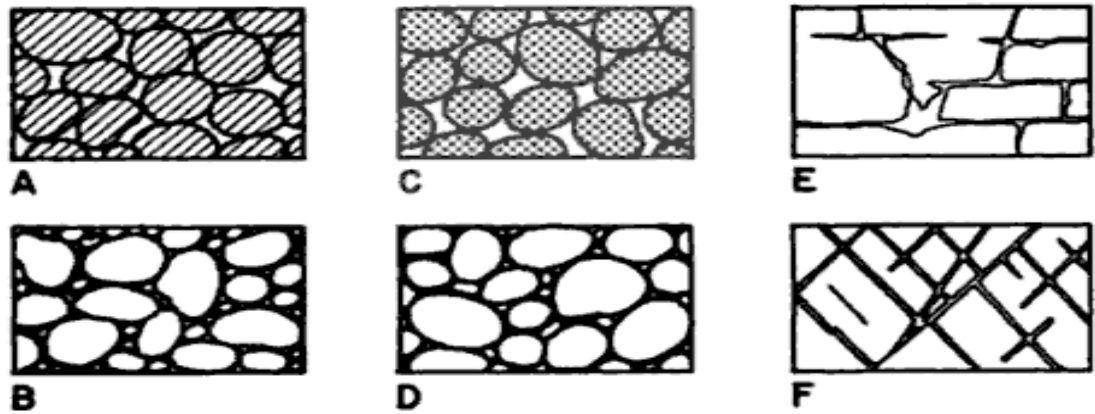
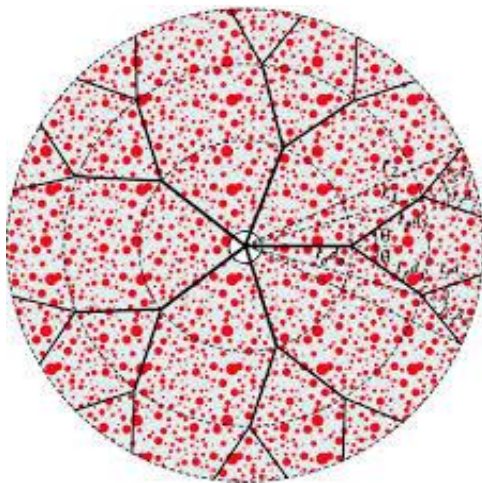
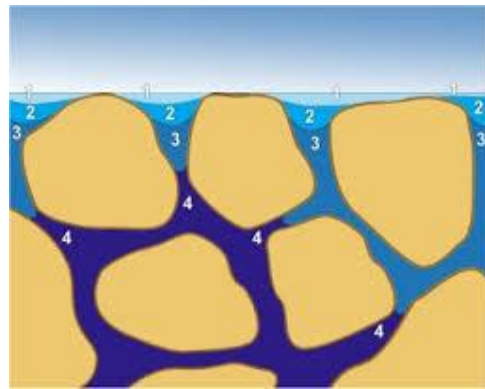


Figure 2. 2 (b): Diagram showing several types of Rock interstices (A) well sorted sedimentary deposit having high porosity; (B) poorly sorted sedimentary deposit having low porosity; (C) well sorted sedimentary deposit consisting of pebbles that are themselves porous, so that the deposit as whole have high porosity; (D) well sorted sedimentary deposit whose porosity has been diminished by the deposition of mineral material in the interstices; (E) Rock rendered porous by solution; (F) Rock rendered porous by fracturing Bear (1988).



(a)



(b)

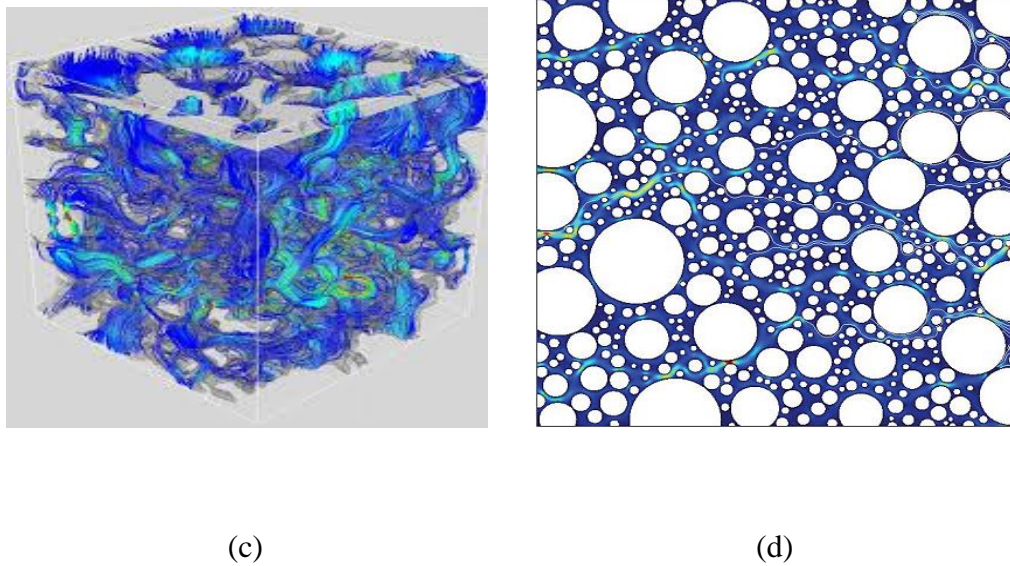


Figure 2.3(a–d): Images of Porous Media (Taken from google images).

## 2.2 Representative Elementary Volume (REV)

The regular mathematical equations were employed to develop macroscopic variables and governing laws via normal approach. It is achieved through means of macroscopic equations with three dimensional volume above the mean value as well as for the two-dimensional areas with several pores. For obtaining mean, there are couple means, one is spatial way, while, other is through statistical approach. For special method, a macroscopic variable is described as a proper average over an adequately substantial illustrative elementary volume (Aboubacar, et al., 2004). This approach is used to produce value at the REV centroid for the variable, considering the results are independent of the REV size. The Figure 2.3 evidences the measure of REV length with the ample higher values of the macroscopic flow field in the pore gauge. The figure illustrates the comparison of the flow magnitude areas and gaps with transitional size. Employing statistical technique, an average is over a collection of probable nature of pore, which is

macroscopically similar. Usually, the collection of the statistical data is applied for the complete sample or all data collected. This is likely when statistical uniformity is presumed (Nield, 1999). If anyone who is interested only in evolving the relationship between the space-averaged measures is not apprehensive regarding their variation, then the solutions acquired by adopting both approach is necessarily similar. In this case, simpler approach based on the (REV) may be adopted. In recent years, various problems have been simulated adopting a statistical approach (Nield, 1999).

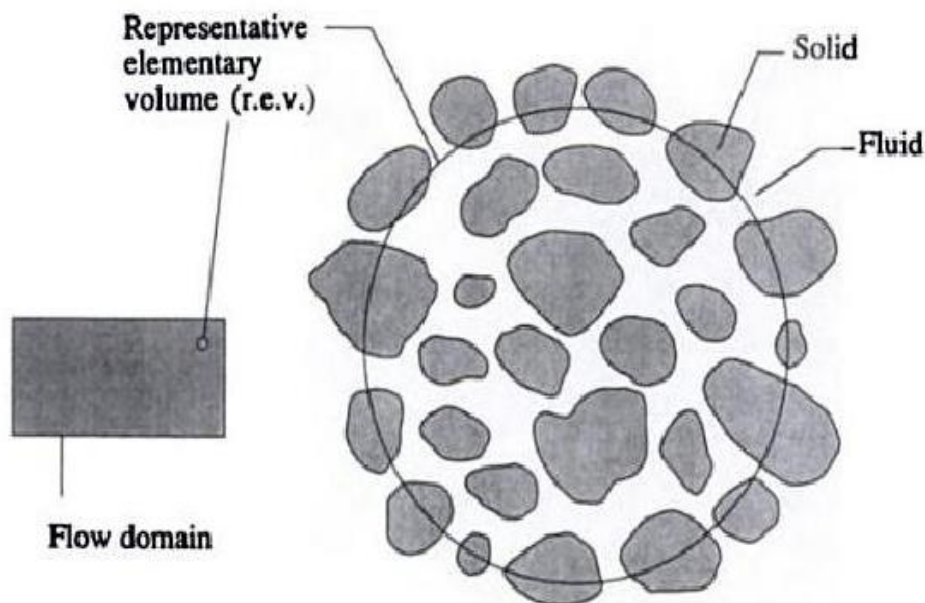


Figure 2.4: The representative elementary volume (REV) (Nield, 1999).

In various fields of engineering and applied sciences, alike, bio- and chemo-fluid and solid mechanics, one has frequently tackle continuum mechanics problems that cannot be categorised exclusively. In fact, the problems can be characterised, that necessitate a cohesive behaviour of volumetrically coupled solid collections. Fundamentally, plunge into the kinds of both blends of porous material. Considering the subsequent arguments the engineering problem can be analysed from various perspectives for example the

deformation of the coupled solid analysis. Also, analysing the literature on porous media is reflected mostly towards the bio–mechanical research problems; thus, comparative studies on intervertebral disk, cartilage, study of bones, etc. (Ehlers and Bluhm, 2002).

### **2.3 Basic equations of porous materials**

The field of porous media is explored due to global interests in the problems, such as, surface environment, sub–surface groundwater pollution and energy problems. Fields of an application, includes numerous examples, such as, the insulation of buildings, chemical reactors, recovery methods, petroleum reservoirs, and etc. (Nield and Bejan, 2006). Porous material is comprising of solids with gaps. It is presumed the solids are either inflexible (in normal conditions) or goes under slight deformation. The gaps (the pores) allows to pass the single or many fluids through the media. In the single phase, two phase and three–phase flows, the void may be saturated by a single (simple), two (liquid and gas share the void space), and three (void spaces share oil, water and gas) fluids. In nature, porous material is non–homogeneous.

#### **2.3.1 Porosity**

The Porosity ( $\omega$ ) represents the bulk volume as a part of a porous matrix in the empty spaces, whereas  $(1-\omega)$  remains the solids part of the material. Isotropic medium remain unidirectional in the “surface porosity”, normally, homogeneous ( $\omega$ ) or the porosity is fraction of pore volume to the total volume (Nield and Bejan, 2006). Total porosity is defined as the ration of the entire pore space in a rock to its bulk volume. I-e, Porosity = pore volume/bulk volume and can be expressed in terms of symbol as below:

---

In this procedure, describing ' $\omega$ ', by assumption that all the void spaces are connected. One has to face the situation where few pores are disconnected from the rest. An “effective porosity” is introduced, which is the ratio between linked spaces to bulk volume. Effective porosity is defined as total porosity less the fraction of the pore space occupied by shale or clay. In a very clean sands, total porosity is equal to effective porosity. For normal materials, ' $\omega$ ' does not more than 0.6. The value of ' $\omega$ ' is varied between 0.2595 (rhombohedral packing) to 0.4764 (cubic packing) values within the solid sphere beds having uniform diameter, or values are between rhombohedral and cubic packing. In artificial materials, such as, metallic foams ' $\omega$ ' may reach to one (Nield and Bejan, 2006).

### 2.3.2 Darcy velocity

The construction of continuum model is considered for the REV approach centred on the porous media (Nield, 1999). For consistent volume means to be obtained, they introduced a Cartesian frame of reference and considered suitably large volume of elements against the pore volumes. Alternatively, one can say that, means are insensitive on element choice. This approach is unique because it compares the elements' volume  $V_{mp}$  for the matrix and  $V_{fp}$  for the fluid only by its' means. Here,  $\mathbf{v} = (u, v, w)$  denotes the fluid's mean flow velocity as illustrated. This quantity of fluid velocity has been given a variety of names by different authors like seepage velocity, superficial velocity, volumetric flux density, filtration velocity, and Darcy velocity. But the Darcy velocity is preferred, as it is unique and brief. The  $\mathbf{v}$  represents the relationship of the fluid velocity  $v_{fp}$  with

intrinsic velocity  $V_p$  means with the help of the procedure derived by Dupuit-Forchheimer, as illustrated below (Nield and Bejan, 2006):

$$\mathbf{v} = \omega V_p \quad (2.1)$$

### 2.3.3 Momentum equation: Darcy's Law

Firstly, in absence of the porous media the equation for time dependent momentum is employed. For steady-state unidirectional flow, a Navier-Stokes equation is used. Whilst, for flow through homogeneous porous matrix a Darcy's–Brinkman transport equation is adopted and are given in this section below. At this stage, body forces such as gravity; has been neglected and these appropriate terms added easily at the later stages.

### 2.3.4 Darcy's law: Permeability

To investigation has been made in hydrology of water supply of Dijon (Darcy's, 1856) and his experiments on steady-state and homogeneous medium of unidirectional flows on the computational domain. A proportionality has been obtained between rate of fluid flow and pressure applied. This relationship in Cartesian coordinates is given by (Nield and Bejan, 2006):

$$u = -\frac{\kappa}{\mu} \frac{\partial p}{\partial x} \quad (2.2)$$

Here the coefficient  $\kappa$  is independent of fluid properties, however, it is related to allow ability of the medium, it has dimensions of (length)<sup>2</sup> and is called the specific permeability or intrinsic permeability of the medium, in case of single phase flow, it is

known as simple permeability. While,  $\mu$  is the dynamic viscosity of the fluid and  $\frac{\partial p}{\partial x}$  is

the pressure gradient in the flow direction.

In three dimensions, above equation can be generalised (Nield and Bejan, 2006) as:

$$\mathbf{v} = \mu^{-1} \kappa \nabla P \quad (2.3)$$

Generally, the permeability  $K$  is a second-order tensor, while, in case of isotropic media it is a scalar quantity and Equation- (2.3) is simplified as below:

$$\nabla P = -\frac{\mu}{\kappa} \mathbf{v} \quad (2.4)$$

In geophysics unit of permeability is Darcy, which equivalent to  $0.987 \times 10^{-2} m^2$ , while, in other fields it varies. By the outcomes of many experiments Darcy's law has been proved. By various ways its theoretical backing has been obtained with the help of either statistical models or deterministic.

### 2.3.5 Darcy's Brinkman's equation

This model is generally expressed as the Brinkman's equation. In the absence of inertial terms it takes the form (Nield and Bejan, 2006) as:

$$\nabla P = -\frac{\mu}{\kappa} \mathbf{v} + \tilde{\mu} \nabla^2 \mathbf{v} \quad (2.5)$$

Equation-(2.5) has two viscous terms. The first term is Darcy and the other is equivalent to the Laplacian term as seems in Navier-Stokes equation. The coefficient of second term  $\tilde{\mu}$  represents effective viscosity. Brinkman's sets  $\mu$  and  $\tilde{\mu}$  equal to each other. Equation (2.5) with parameter  $K$  (the permeability) reduces to the form of the Navier-Stokes equation as  $\kappa \rightarrow \infty$  and to Darcy equation as  $\kappa \rightarrow 0$ . Equation- (2.5) is also said to be Brinkman's extension to Darcy's law and it has been used in current research study for the fluid flows in channel and pipes filled with porous media.

#### 2.4 Pseudo-plastic (shear-thinning) fluids

Pseudo-plastic fluids show no yield value and the typical flow curve for these materials indicates that the ratio of shear stress to the rate of shear, which is known as viscosity, falls progressively with the shear rate and the flow curve becomes linear at only very high rate of shear. The logarithm plot of shear stress and shear rate for these materials is often found to be linear over many decades of shear rate, with a slope between zero and unity. As a result, an empirical function known as the power law is widely used to represent fluids of this type. This relation is written as (Tanner, 2000):

$$\mu(\dot{\gamma}) = \tau = k (\dot{\gamma})^{(n-1)} \quad (2.6)$$

Where,  $k$  and  $n$  are constants ( $n < 1$ ) for particular fluids.  $k$  is a measure of the consistency of the fluid, higher is the value of  $k$  the more viscous is the fluid;  $n$  is the measure of degree of non-Newtonian behaviour, the greater is the value of the  $n$  more pronounced are the non-Newtonian properties of the fluid. Over decades this index  $n$

may often be regarded as constant of shear rate.

## **2.5 Literature review**

Combined mixing-separating of Newtonian and non-Newtonian flows occurs as an important unit operation in many engineering and industrial application. This study has reported these applications in different sections of this thesis in detail. As the focus of this research is to model and simulate numerical results of Newtonian and non-Newtonian fluid flows in the channel as well as in circular pipes passing through non-porous and porous media. To further analyse the position literature review on various studies has been provided in the next section.

### **2.5.1 Channel flows**

In this section, initially the literature focused on the experimental and numerical computations and experiments on the method of finite difference (Cochrane, et al., 1981). The authors have analysed the flow of different fluids and illustrated variation and bifurcation in in flow structure in order to examine the effects of inertia under several situations. They employed only two inlets, i.e., both left bottom inflow and top right reversed flow (Cochrane, et al., 1982) happen at the same time. For both fluids, i.e., constant viscosity Newtonian and shear–rate dependent inelastic fluids, this standard problem established to investigate flow various features. They also employed viscoelastic fluid adopting an **upper convected Maxwell model**, however, in the numerical predictions show the limitation of inertial and elastic parameters.

For all the numerical simulations conducted in the research, there is no evidence of the presence of porous media. Study employs low Reynolds number fluid flows and only liquids like Boger fluids. Furthermore, the same study was extended by (Cochrane et al., 1982) using a steady-state advanced numerical scheme by utilising a finite difference discretisation. Geometry as shown in Figure 5.) in chapter five. Flow occurrence is presented in chapter five for further details.

In the study of (Walters and Webster, 1982), thinner plates with sharp re-entrant corners were used, they considered three different plate separation gap widths and two different flow rate configurations. One of biased unequal flow rates in the various inlet and outlet channel arms and the other with balanced flow rates. These researchers found the flow conditions, material parameters, and gap width for variation effects through experiment and numerical computation. They also considered low Reynolds numbers only for channel flows with finite difference technique. In this research study they used Maxwell model. They also used rectangular Cartesian coordinates and square elements for mesh.

Later, (Baloch, et al., 1995a) numerically simulated adopting finite element technique through so called, time-dependent Taylor-Galerkin/Pressure-Correction (TGPC) algorithm. The algorithm adopted in their research work was a semi-implicit form for constant viscosity fluid. For viscoelastic fluid; a Taylor-Petrov-Galerkin approximation along with linear constitutive Phan-Thien-Tanner (PTT) model was employed. In these flows, thin insert plates with sharp edges has been used. This study addressed the equal

flow rates and gap width variation for the centre and middle inserted plates. In their research study triangular elements were used.

After that, for low Reynolds number, (Afonso, et al., 2011) investigated this flow problem, and simulated only creeping flow using finite volume method. For viscoelastic simulations, an upper-convected Maxwell (UCM) model had been used numerically. The simulated results acknowledged a new study bi-stable bifurcation pattern at low inertia and high stability. In that numerical study, they focused on the effects of dimensionless Deborah number, gap size between plates and inertia. They simulated only channel flows without porous media.

The latest study conducted by (Echendu, et al., 2011), the numerical simulations were done for viscoelastic and constant viscosity fluid, when passed through combined mixing and separation flows within the configured channel. The investigation presented to realise the validities of a fractional staged finite element algorithm. For the complex inelastic flows, same scheme employed in the semi-implicit form of (TGPC) scheme. This study adopts the approach in arrangement with an executed viscous regularisation on the Herschel-Bulkley fluid model and its changes. The researchers found the outcomes based on pressure outlines, streamline forms, and velocity profiles. In that study power law and bingham models were used with fixed geometric gap width and only equal flow rates in both situations.

Contemporary literature tells interesting description of the rheological complex fluid behaviour in flow through a variety of porous media. From these analyses, numerous

correlations of flow phenomena of constant viscosity fluid and the rheology of functional viscosity of inelastic fluids have been attempted. The phenomenological aspects of these effects mainly have been focused (Savins, 1969).

Under different flow conditions in porous structures different complexities occurs and seem to be coupled with the unusual rheological behaviour of complex inelastic fluids. In the further study of [(Oden, 1970) and (Neale and Nader, 1974)], it has been observed that when various flows of fluid passed the shallow of porous domain, where the fluid has been flowing parallel to the shallow, the special effects of viscous shear in the free fluid will enter below the permeable surface to form which effects the boundary layer area in the porous media. The experimental data relating to steady, incompressible laminar flow through a two dimensional parallel channel have been reported by them (Neale and Nader, 1974) .

The inertia effect of microscopic coefficient and Darcy number value is more significant than the completely developed region as passing within the channel porous domain is decreased in the pore velocity magnitude. It has been found that forced convections can be significantly enhanced by putting of porous inserts on impermeable heated walls, provided that high active thermal conductivity and thick porous matter are used.

In the article of (Abu-Hijleh and Al-Nimr, 2001) the transient hydrodynamics behaviour of the fluid flows in a parallel plate channels partly filled with porous media was examined numerically again. Through the momentum equation, the study found local inertia effect with changes in the Newtonian flows of the channel imposed with pressure

gradient. The non-dimensional system of coupled partial differential equations is solved using the finite difference method on a uniform grid. It is found that the local inertial term is insignificant when Darcy number is less than  $10^{-06}$ , over the entire range of dynamic viscosity ratio between 0.1 to 10; Forchheimer coefficient between 0 to 10000 and all porous substrates thicknesses. The study also found that there is a deviation in the quasi-steady and transient models for the porous domain and decreased time.

In another numerical study of the transient hydrodynamics behaviour of inelastic non-Newtonian unidirectional flows of fluid in a parallel plate and horizontal channels through porous material has been conducted by (Al-Nimr and Aldoss, 2004). The effect of the macroscopic local inertia term in the porous region, momentum equation has been examined. They have solved the one-dimensional unsteady governing equations by finite volume method. The study found that there is no significant effect of the local inertial terms on the behaviour of the channel hydrodynamics with the value 0.5 power law index and for the complete ranges of Forchheimer and Darcy numbers. Furthermore, it is found that local inertia of microscopic level has significant effect if the Darcy and Forchheimer numbers used for the greater values of the power law index, predominantly for the lower Forchheimer numbers and high values of the Darcy numbers.

### **2.5.2 Pipe flows**

In the experimental study of (Escudier et al., 2005), he detailed mean velocity profile data for fully developed pipe flow of a wide range of shear thinning liquids together with two Newtonian control liquids. By using laser Doppler anemometry (LDA) as measurement technique all the experimental data were collected in unrelated research programs in UK,

Australia and France. The experimental velocity profile data, which have been presented, reveal to varying degrees' leavings from axisymmetry in fully developed circular tube flow of a wide range of inelastic non-Newtonian liquids with rheological characteristics including shear thinning viscosity, yield stress and viscoelasticity. In the majority of the cases, axisymmetric flow is observed for the laminar and turbulent flow conditions. The researchers found the way for symmetrical velocity profiles acquired considering the streams (laminar and turbulent) of all non-Newtonian fluids through the information gathered from each of the three labs prompt to state irregular results are concerns for the fluid dynamic device, it is as yet having not been perceived, as opposed to constraints in the stream.

In another experimental study by (Peixinho et al., 2005), detailed measurement were given in all laminar, transitional and turbulent circular tube flow of yield stress fluids. All three flows are conducted in cylindrical pipe, the length of the tube is considered 5.5m, while, inner diameter of tube is 30mm. The study examined the flow by using the Doppler approach with pressure quantities and axial velocity. The inertia value which is critical is solved through experiment through application of the laminar solutions; that are linked with phenomenological procedure as well as delimited. The first normal stress differences are similar for two non-Newtonian fluids. In laminar flow, the experimental velocity profiles and friction factors are well described by the theoretical solution.

Solution presented that the yield stress fluids adds to stabilise the flow and the transition. It has been noticed a growth of root mean square of the axial velocity outside a domain nearby the axis, while, it remains laminar level inside this area. When inertia increases,

the fluctuation increases within the whole segment because of the turbulent spots' apparition. For constant viscosity and shear-rate dependent inelastic fluids, depiction of the turbulent flow displays that the root mean square of axial velocity profile is alike excluding near the wall where the turbulent power is higher against constant viscosity fluids.

(Nield and Kuznetsov, 2007)'s simulations carried out for observing the influence of flow pulsation over the transport process in the laminar regime of developing parallel-plate channel or a circular pipe. For forced convection, a perturbation analytical solution is obtained of primitive variables velocity, pressure and temperature. For non-isothermal transient analysis approach is adopted using Nusslet number. That was created through applied pressure gradient that varies with small amplitude harmonically in time about a non-zero mean. It has been observed that oscillating quantity of the Nusslet number altered in degree and phase as the non-dimensional frequency increased. Nusslet number is based on the twice the initial length of the tube radius, following the pulsation cycle. The pulsation has no positive influence in augmentation of heat transfer within the examined range of pulsation frequency and amplitude.

## 2.6 Research gaps

In the following table research gaps are evident in the support and motivation of current study for the modelling of combined mixing and separating flow domains.

<b>Research study</b>	<b>Method</b>	<b>Material</b>	<b>domain</b>	<b>Gaps</b>	<b>Gaps Covered by</b>

					<b>current study</b>
Cochrane (1981)	Finite difference and upper convected Maxwell model	Newtonian and non-Newtonian	Channel	<ul style="list-style-type: none"> <li>➤ Channel filled without porous media</li> <li>➤ Circular pipe flows with and without porous</li> <li>➤ limited variety of flow bifurcations</li> <li>➤ Changing flow rates</li> <li>➤ Low Reynolds number</li> </ul>	<p>✓ Yes</p> <p>✓ Yes</p> <p>✓ Yes</p>
Walter (1982)	Finite difference and upper	Newtonian and non-	channel	<ul style="list-style-type: none"> <li>➤ channel without porous</li> <li>➤ no pipe flows</li> <li>➤ only equal low rates</li> </ul>	<p>✓ Yes</p> <p>✓ Yes</p> <p>✓ Yes</p>

	convected maxwell model	newtonian		➤ Low Reynolds number	✓ Yes  ✓ yes
Baloch (1995a)	Finite element with (TGPC) method	both	channel	<ul style="list-style-type: none"> <li>➤ channel without porous</li> <li>➤ no pipe flows</li> <li>➤ only equal low rates</li> <li>➤ no change in flow directions</li> </ul>	<ul style="list-style-type: none"> <li>✓ yes</li> <li>✓ yes</li> <li>✓ yes</li> <li>✓ yes</li> </ul>
Afonso (2011)	Finite volume method and UCMM	Newtonian and viscoelastic	channel	<ul style="list-style-type: none"> <li>➤ Channel without porous media</li> <li>➤ Creeping flow</li> <li>➤ Only equal flow rates</li> <li>➤ No change in flow direction</li> <li>➤ No pipe flows</li> </ul>	<ul style="list-style-type: none"> <li>✓ Yes</li> <li>✓ Yes</li> <li>✓ Yes</li> <li>✓ yes</li> <li>✓ yes</li> </ul>
Eschendu (2011)	Finite element,	Newtonian,	channel	➤ Channel without	✓ Yes

	SITGPC scheme  with Power law and Bingha m model	Herschel- Bulkley for non- Newtonia n		poro us medi a ➤ Only equal flow rates  ➤ equal rates only and one chan ge in flow direct ion  ➤	✓ Yes  ✓ yes
--	---	---	--	---	--------------------

## 2.7 Summary

After reviewing the literature, evident research gaps have given good insightment and motivations for current research study. In most of the cases only channel flows were studied without changing flow directions and flow rates in the arms of a computational domain. In the wide gap domain as shown in figure 5.1 in chapter five of this thesis, there are variety of ways to change flow directions and even flow rates as insertion of thin inserts in the middle of the channel from either side gives us numerous combinations. Newtonian and non-Newtonian flows in such complex domains is very hard to handle. For the set aims and objectives, firstly we found analytical solution to apply velocity profiles on the inlets of domain to pass fully developed flows. Secondly, using the developed code by Dr. Baloch and others authors have been extended to the requirements

of current study. Later, Newtonian and non-Newtonian have been analysed in circular pipes to monitor mixing and separating within the middle gap of inner and outer pipe. Complete description of pipe flows is available in chapter seven and eight.

Most of the authors in literature review have used limited options to explore the very important flows in channel and circular pipes. But in the current study, four different combinations of the channel along with the flow rates have been examined thoroughly to see the inertia effects, pressure drops and effects of porosity and changing fluids within the domains. Research on channel filled with porous media and circular pipes with and without porous media for Newtonian and non-Newtonian fluid flows in current study is new of its kind and will be very useful for future studies.

## **Chapter 3. Basic Governing System of Equations**

### **3.1 Introduction**

This chapter is based on analysing the equations of the basic field and its formulation which is universally applied in all types of fluids. The classification of materials is done in terms of the Newtonian or non-Newtonian fluid flow. In this study both type of the fluid materials are investigated. To capture the shear-thinning behaviour of non-Newtonian fluids the Power law and Bird–Carreau models are used. The details of these models could be found in chapter eight. As domain of interest is a channel and a pipe filled with or without porous media. For both cases transport equations are given. In first case, two-dimensional Navier-Stokes equations and their non-dimensional forms are given in Cartesian coordinates. For later in pipes flows continuity, and momentum equation are presented. The solution approach adopted is to solve the continuity, momentum transport equations subject to initial and boundary conditions for stresses, velocity and pressure in the whole domain. Dimensionless forms are produced for variables by incorporating their characteristic values.

### **3.2 Basic equations**

This section presents equations of the governing system that accomplishes the flow of fluids in the domain computations. The law of conservation of mass, momentum transport equations by the well know, Newton’s second law of motion are discussed.

### 3.2.1 Equation of continuity (compressibility)

At any point of time the continuity equation is connected with the mass conservation principle in 3 dimensional compressible domain and given by:

$$\frac{\partial \rho}{\partial t} + \nabla(\rho \mathbf{v}) = 0 \quad (3.1)$$

In Equation–(3.1),  $\nabla(\rho \mathbf{v}) = \text{div}(\rho \mathbf{v})$ , here  $\mathbf{v}$  represents the field of the vector for the flow field at any time as illustrated in the components of the local velocity  $u, v$  and  $w$ . Where,  $\rho$  represents the density of fluid. In Cartesian coordinates  $\mathbf{v}$ , is a function of the location  $(x, y, z)$ . The first term on the left hand side of the equation (3.1) is the rate of change in time of the density (mass per unit volume). In the second representation, the term is describes as the convective term which involves the elements across the boundaries via its net flow, while  $\nabla$  represents the gradient operator.

### 3.2.2 Principle of conservation of mass (incompressibility)

A material is said to be incompressible if, for all possible motions, the mass density satisfies the constraint that rate of change of mass vanishes  $(\dot{\rho} = 0)$ , it means inflow mass is equal to outflow mass. Therefore for incompressible isothermal fluids the density  $\rho$  is constant, the material derivative of mass density in Equation-(3.1) is zero and equation of continuity in vectorial notation reduces to:

$$\nabla \cdot \mathbf{v} = 0 \quad (3.2)$$

A velocity that satisfies the conservation of mass is said to be solenoidal. Almost all liquids are incompressible and satisfy the equation of continuity. However, there are liquids like foam and bubbles that are slightly compressible. In this study consideration is given to those liquids which are essentially incompressible and satisfy the equation of continuity (3.2). It can be considered from the equation (3.2) that the incompressible material for every motion is volume preserving.

### 3.2.3 Momentum equation (principal of conservation of momentum)

The second law of motion describes the momentum equation for the moving continuum, presenting the fluid particles' changing momentum rate equals to the combined forces on the particles. Two types of forces on the fluid particle are (a) Surface forces (pressure, viscous) (b) Body forces (gravitational force, centrifugal, centripetal, Coriolis and electromagnetic force).

Using the second law of motion for the transport equation to consider the x-component:

$$\sum F_x = \rho a_x \quad (3.3)$$

Where  $F_x$  is the force in x-direction will be equals to:

$$F_x = \nabla \cdot \boldsymbol{\sigma} + \rho g \nabla h \quad (3.4)$$

The equation (3.4), where  $\sigma$  presents Cauchy's stress tensor or simply stress tensor comes from Cauchy's formula, Stress tensor describes traction on any surface, whereas gravity and height are given by  $g, h$  respectively. First term of the equation (3.4) represents surface forces and second body forces.

The equation 3.3 defines the acceleration as  $a_x$ :

$$a_x = \frac{D\mathbf{v}}{Dt} = \left( \frac{\partial \mathbf{v}}{\partial t} + (\mathbf{v} \cdot \nabla) \mathbf{v} \right) \quad (3.5)$$

The equation (3.5) illustrates the material time derivative by  $\frac{D\mathbf{v}}{Dt}$  where  $t$  is the time.

Momentum equation in general vectorial notation form can be written as (Baloch, 1994):

$$\rho \left( \frac{\partial \mathbf{v}}{\partial t} + (\mathbf{v} \cdot \nabla) \mathbf{v} \right) = \nabla \cdot \boldsymbol{\sigma} + \rho \mathbf{F} \quad (3.6)$$

In case of incompressible fluids above equations Cauchy's stress tensor can be decomposed into the sum of Noll (1958):

$$\boldsymbol{\sigma} = -p\delta + \underline{\underline{\mathbf{T}}} \quad (3.7)$$

Where,  $p$  is the isotropic fluid pressure,  $\underline{\underline{\mathbf{T}}}$  is the extra stress tensors and  $\delta$  (Kronecker delta) denotes the components of a unit tensor. For an incompressible Newtonian viscous

fluid, the extra-stress is proportional to the rate of strain or deformation tensor and defined as:

$$\underline{\underline{\mathbf{T}}} = 2\mu\underline{\underline{\mathbf{d}}} \quad (3.8)$$

In equation (3.8)  $\mu$  is fluid dynamic viscosity and  $\underline{\underline{\mathbf{d}}}$  is the rate of deformation tensor defined as Baloch (1994):

$$\underline{\underline{\mathbf{d}}} = \frac{1}{2} \left( \frac{\partial v_i}{\partial x_j} + \frac{\partial v_j}{\partial x_i} \right) \quad (3.9)$$

In general notation:

$$\underline{\underline{\mathbf{d}}} = \frac{1}{2} [\nabla \mathbf{v} + (\nabla \mathbf{v})^\dagger] \quad (3.10)$$

Where,  $\dagger$  is transpose of tensor;

In expanded matrix notation form  $\underline{\underline{\mathbf{d}}}$  is written as follows:

$$\underline{\underline{\mathbf{d}}} = \frac{1}{2} \begin{pmatrix} 2 \frac{\partial u}{\partial x} & \left( \frac{\partial u}{\partial y} + \frac{\partial v}{\partial x} \right) & \left( \frac{\partial u}{\partial z} + \frac{\partial w}{\partial x} \right) \\ \left( \frac{\partial u}{\partial y} + \frac{\partial v}{\partial x} \right) & 2 \frac{\partial v}{\partial y} & \left( \frac{\partial v}{\partial z} + \frac{\partial w}{\partial y} \right) \\ \left( \frac{\partial u}{\partial z} + \frac{\partial w}{\partial x} \right) & \left( \frac{\partial v}{\partial z} + \frac{\partial w}{\partial y} \right) & 2 \frac{\partial w}{\partial z} \end{pmatrix} \quad (3.11)$$

In the absence of body forces and under linear functional dependency of the extra stress tensor  $\underline{\underline{\mathbf{T}}}$  on the rate of deformation tensor  $\underline{\underline{\mathbf{d}}}$  and utilising the equations [(3.2), (3.6) and (3.7)] into equation (3.8) gives Navier-Stokes equation as follows:

$$\rho \frac{\partial \mathbf{v}}{\partial t} = \nabla \cdot (2\mu \underline{\underline{\mathbf{d}}}) - \rho(\mathbf{v} \cdot \nabla) \mathbf{v} - \nabla p \quad (3.12)$$

For Newtonian fluid  $\mu$  is taken as constant. Hence equation (3.12) becomes (Baloch, 1994):

$$\frac{\partial \mathbf{v}}{\partial t} = \mu \nabla^2 \mathbf{v} - (\mathbf{v} \cdot \nabla) \mathbf{v} - \nabla p \quad (3.13)$$

Where,  $\nabla = \left( \frac{\partial}{\partial x} \mathbf{i} + \frac{\partial}{\partial y} \mathbf{j} + \frac{\partial}{\partial z} \mathbf{k} \right)$  which vector differential operator and known as

gradient and  $\nabla^2 = \frac{\partial^2}{\partial x^2} \mathbf{i} + \frac{\partial^2}{\partial y^2} \mathbf{j} + \frac{\partial^2}{\partial z^2} \mathbf{k}$  is a Laplacian operators.

### 3.3 Dimensionless system of equations

In dimensionless analysis, a dimensionless number or simply a number with dimension (1) is a pure number without any physical units. The characteristic velocity  $\mathbf{v}_c$ , length  $L_c$  and the time scale of  $\frac{L_c}{\mathbf{v}_c}$  are selected to invoke the non-dimensionalisation. For convenience the governing system of equations is cast into non-dimensional form. Dimensionless variables  $x^*$ ,  $\mathbf{v}^*$ ,  $p^*$  and  $t^*$  are defined by introducing suitable scales given as:

$$x = L_c x^*, \quad \mathbf{v} = \mathbf{v}_c \mathbf{v}^*, \quad p = \rho \mathbf{v}_c^2 p^*, \quad \text{and} \quad t = \frac{L_c}{\mathbf{v}_c} t^*$$

In the interest of clarity in presentation and without ambiguity all asterisk notation may be discarded and the Equation- (3.14) may be expressed non-dimensionally as Baloch (1994):

$$\frac{\partial \mathbf{v}}{\partial t} = \frac{1}{\text{Re}} \nabla^2 \mathbf{v} - (\mathbf{v} \cdot \nabla) \mathbf{v} - \nabla p \quad (3.14)$$

Where,  $\text{Re}$  is a Reynolds number and expressed as given below:

$$\text{Re} = \frac{\text{Inertia force}}{\text{friction force}} = \frac{\rho \mathbf{v}_c L_c}{\mu} \quad (3.15)$$

### 3.4 Initial and boundary conditions

To complete the problem specification, it is necessary to prescribe initial and boundary conditions. The above Equation- (3.14) is supplemented by boundary condition given in the form:

$$\mathbf{v}(x, 0) = \mathbf{v}_0(x) \quad (3.16)$$

Subject to

$$\nabla \cdot \mathbf{v}_0 = 0 \quad (3.17)$$

Boundary conditions on solid walls of the geometry and centrally inserted plates are taken as no slip conditions (all components of velocity field vanish). The steady Poiseuille flow profiles are imposed at both the entry and exit flow sections in both arms of a channel as shown in Equations- [(3.18a) and (3.18b)]. In the case of unequal flow rates and flow direction different boundary conditions have been found. For convenience pure approximation is considered and it is demonstrated for developing very frequent entrance in the regions of flow, as well as it does not reduce the solution accuracy. Transient simulations commence from quiescent initial conditions, or from two parallel but opposing flows, to obtain a steady state solution for fixed level of inertia. Subsequently, to accelerate the computation times for higher parameters values, prior steady state solutions are adopted as starting conditions. For material at both inlets:

$$u(y) = U_m (y-a)(b-y) \text{ at } x = 0 \quad (\text{Bottom left arm})$$

(3.18a)

$$u(y) = -V_m \{y-(b+\alpha)\}(2b+\alpha - y) \text{ at } x = 23L \quad (\text{Top right arm}) \quad (3.18b)$$

In equations[(3.18a) and (3.18b)]  $a, b$  are lower and upper coordinate of the wall of domain having  $b-a$  as height of the computational domains and  $\alpha = 0.0254L$  is thickness of the plate. Channel is having reasonable long length of  $23L$ , which reflects the fully developed flow at the inlets and outlets of it. Here  $L$  is characteristic length of a channel. For inlet flow imposed on bottom left arm the values of  $a, b$  are 0 and 1 respectively. The maximum velocity obtained for the equal rate of flow in the channel arm centre is given by  $U_m = V_m$ , whereas if there are an unequal rates of flow  $U_m$  and  $V_m$  presents the 1:15 and 1:2 ratios.

In the exit sections for both geometries, consistency with the fixed pressure ( $p = 0$ ) is achieved for the normal traction free conditions. With the application of numerical calculations for the flow fields approximation is made by checking the flow carefully for the regions and it does not affect the solutions' global accuracy. Whereas no cross flow is assumed at both inlets and outlets ( $v = 0$ ). Graphical representation of equation (3.18) is shown in figure 1 in appendix-B on page-234. These equations show velocity profile imposed on top and bottom channel arms.

### 3.5 Governing system of equations for porous medium

Consider spatial bounded domain  $\Omega \in \mathbb{R}^2$  with piecewise smooth boundary  $\Gamma$  and a temporal domain  $[0, \mathfrak{T}]$  with  $\mathbf{x}$  and  $t$  representing the associated spatial and time coordinates. In the absence of body forces, the corresponding equations for conservation of mass and Darcy-Brinkman momentum transport for an incompressible, isothermal, and isotropic flow through homogeneous porous media may be used to describe flow behaviour in both channel and pipes and is given by the following equation:

$$\rho \frac{\partial \mathbf{v}}{\partial t} = \nabla \cdot (2\mu \underline{\underline{d}}) - \rho(\mathbf{v} \cdot \nabla) \mathbf{v} - \nabla p - \frac{\omega \mu}{\kappa} \mathbf{v} \quad (3.19)$$

Where,  $\mathbf{v}(\mathbf{x}, t)$  is the velocity vector field,  $p(\mathbf{x}, t)$  is isotropic pressure (per unit density),  $\rho$  and  $\mu$  are fluid density and viscosity respectively. In the given equation  $\kappa$  represents the porous media's permeability, whereas  $\omega$  describes the porous media's porosity. The flow is considered to be hydro-dynamically fully developed hence velocity does not depend on transversal and radial direction of the channel and pipe respectively. Through the use of continuity equation, flow is given by the transversal direction function and in expression of the axial velocity. Equation (3.14) and (3.19) can be used to give the below equation (3.20) to express the same dimensionless form with its variables and scaling factors:

$$\frac{\partial \mathbf{v}}{\partial t} = \frac{1}{\text{Re}} \nabla^2 \mathbf{v} - (\mathbf{v} \cdot \nabla) \mathbf{v} - \nabla p - \frac{1}{\text{Re} D_a} \mathbf{v} \quad (3.20)$$

Here,  $D_a = \frac{\kappa \rho v_c}{\omega \mu L_c}$  represents the Darcy's non-dimensional number.

The fully developed flow in the hydro-dynamic velocity, it is not dependent on the pipe and channel's axial direction. The flow in the continuity equation is unidirectional and axial velocity expression presents it in the transversal direction of alone function.

For porous media an exact velocity profile is imposed by steady-state solutions obtained during this study as follows:

$$u(y) = U_{\max} \left[ 1 - \frac{\cosh \frac{y-a}{\sqrt{Da}} + \sinh \frac{b-y}{\sqrt{Da}}}{\sinh \frac{b-a}{\sqrt{Da}}} \right], \quad (3.21)$$

In equation (3.21) at bottom inlet at  $x=0$ ,  $U_{\max} = U_m$  where  $a=0$  and  $b=1$ . Whilst, at other inlet (top right)  $x=23L$ ,  $U_{\max} = V_m$  and here  $a=1.0254$  and  $b=2.0254$ . However, for all other boundaries same conditions are imposed as explained above. In Appendix-B, equation (3.21) has been derived for imposing velocity profiles on both inlets of a channel. Graphical representation is produced in the same appendix in its end as shown in figure 1.

### 3.6 Material functions and rheometry

Besides polymers, industry and nature provide with vast range of materials composed of complex polymeric elements in suspensions in fluid. At sufficiently high concentrations,

the suspended elements develop specific mutual interactions and therefore will be dealt with pasty materials. The flow is not possible when the force exerted on it is below the critical value. This type of materials are found in our daily lives and commonly used, for example the hair gel, marmalade, peanut butter, mayonnaise, solar cream, cosmetic cream, shaving cream, paint, modelling paste as well as in natural phenomenon lahars, snow, mudflows, debris, and mining slurries. Civil engineering, cosmetic and food industries also use pasty or granular materials for sorting or storing solid matter or forming product, with agent such as drilling fluids, concrete, cement paste, mortar glues, ceramic slip, foodstuff, paste, sludges, grains, sand, and powders (Coussot, 2005). The complexity arises in the non-Newtonian fluid mechanics is to find the relationship of various characteristics of the fluids with the macroscopic flow features for example in shear flow the viscous behaviour.

In order to find characteristics of the non-Newtonian fluids the material functions are employed, whereas through the use of rheometry simple flow functions, flow characteristics of material, and deformation is investigated. Other flows such as oscillatory shear flow and extensional flow are also important in the study of non-Newtonian fluid mechanics. For generalised non-Newtonian liquids, the viscosity is non-constant, and the relation between extra-stress tensor and rate of deformation is not a simple linear form, but some function of shear rate and elongational rate. The results from experimentally generated data for non-Newtonian flows are used to construct constitutive models from simple shear, oscillatory shear, uni and bi-axial extension and squeezing flows, with which predictions from mathematical models can be compared.

### 3.6.1 Steady simple shear flows

In the present work, concern will be uniaxial steady simple shear flow of complex inelastic non-Newtonian fluids. The isothermal generalised extra-stress tensor for an inelastic non-Newtonian fluid as determined by (Baloch, 1994):

$$\underline{\underline{T}} = 2\mu(\dot{\gamma})\underline{\underline{d}} \quad (3.22)$$

Considering the shear flow which is steady and simple,  $\dot{\gamma}$  defines rate of shear rate as:

$$\dot{\gamma} = 2\sqrt{II_d} \quad (3.23)$$

Here,  $II_d$  represents the strain tensor rate for the second invariants  $\underline{\underline{d}}$  that is present as equation 3.24 in axisymmetric frame:

$$II_d = \frac{1}{2}tr(\underline{\underline{d}}^2) = \frac{1}{2} \left[ \left( \frac{\partial v_r}{\partial r} \right)^2 + \left( \frac{\partial v_z}{\partial z} \right)^2 + \left( \frac{v_r}{r} \right)^2 + \frac{1}{4} \left( \frac{\partial v_r}{\partial z} + \frac{\partial v_z}{\partial r} \right)^2 \right] \quad (3.24)$$

It should be noted that the equation (3.22) is constitutive and beneficial for the identification of shear effect. The indices of power law are used in combination with the Bird-Carreau and Power law as the models of Shear thinning (Barnes et al., 1989).

### 3.7 Governing system of equations (cylindrical polar co–ordinates)

The equations of momentum transport and continuity can be utilised for modelling the porous material filled pipes with the Newtonian and non–Newtonian incompressible fluids having laminar flow. Fully established flow at both inlets is considered to be axi–symmetric and two dimensional. These governing equations for two dimensional cylindrical polar coordinates, in domain filled without porous media are reported by (Solangi, 2011). The equation for momentum transport and mass conservation can be utilised with or without porous material filled in the circular pipes. Equations for Newtonian fluids subject to the boundary conditions are given, in the absence of body force used for such domains are written in the cylindrical coordinates as:

$$\frac{\partial v_z}{\partial z} + \frac{1}{r} \frac{\partial (rv_r)}{\partial r} = 0 \quad (3.25)$$

r-component

$$\begin{aligned} \frac{\partial v_r}{\partial t} + v_r \frac{\partial v_r}{\partial z} + v_z \frac{\partial v_r}{\partial r} = \\ -\frac{1}{\rho} \frac{\partial p}{\partial r} + \frac{\mu}{\rho} \left( \frac{1}{r} \frac{\partial}{\partial r} \left( r \frac{\partial v_r}{\partial r} \right) + \frac{\partial^2 v_r}{\partial z^2} - \frac{v_r}{r^2} \right) - \frac{\omega \mu}{\rho K} v_r - \frac{1}{\rho} \frac{\partial p}{\partial r} \end{aligned} \quad (3.26)$$

z-component

$$\frac{\partial v_z}{\partial t} + v_z \frac{\partial v_z}{\partial z} + v_r \frac{\partial v_z}{\partial r} = -\frac{1}{\rho} \frac{\partial p}{\partial z} + \frac{\mu}{\rho} \left( \frac{1}{r} \frac{\partial}{\partial r} \left( r \frac{\partial v_z}{\partial r} \right) + \frac{\partial^2 v_z}{\partial z^2} \right) - \frac{\omega \mu}{\rho K} v_z - \frac{1}{\rho} \frac{\partial p}{\partial r} \quad (3.27)$$

Where,  $v_z$  and  $v_r$  are the axial and the radial velocity components,  $p$  is the isotropic pressure,  $\rho$  is the density of fluid and  $\mu$  represents the viscosity of fluid materials and  $K$  is the permeability of porous media.

---

Equations [(3.25)-(3.27)] are solved by imposing initial and boundary conditions. Their all necessary conditions along with non-dimensional form are discussed in chapter 7-8 for Newtonian and non-Newtonian flows in a domain presented in figure (7.1).

### 3.8 Summary

This chapter presented the fundamental governing equations which are used to control the fluid flows in the domain filled with or without porous media. The non-dimensionalisation along with appropriate initial and boundary conditions are defined. The Darcy's term in momentum equations has been added and implemented in code used along with other parameters. In latter chapters equations are presented for material functions and rheometry along with the equations monitor simple shear rate flows.

As focus of this research is to study fluid flows in channel and pipes therefore equations are given in Cartesian and cylindrical and polar coordinates along with Darcy's tem in momentum. Primary research has been extended to monitor flows through porous media in channel and pipes to observe the effects of porosity on flow domains by utilizing the appropriate numerical schemes presented in chapter 4 in detail for both coordinate systems.

To empose exact velocity profiels on both inlets of a channel filled with porous media, an analytical solution has been found by using the knowelge of solving differential equations. The complete derivation of analytical solution shown in an equation (3.21) is available in Appendix-B with its graphical representation as presented in Figure 1 of the same Appendix.

## Chapter 4. Implementation of Numerical Scheme

### 4.1 Introduction

This chapter covers the development of finite element scheme for the models introduced in chapter-03. For numerical simulation, the problem addressed in this investigation is combined mixing and separating flows. Computation of Newtonian and non-Newtonian fluids, flow through mixing-separating geometry filled with porous media and in absence is presented in chapter five to eight. The governing systems of equations employed in this study are in both Cartesian as well as cylindrical polar coordinates systems. To simulate steady-state and time-dependent problems, many sophisticated numerical algorithms can be found in the literature. To acquire the steady-state solutions there are numerous procedures, however, most popular method is Newton-Raphson's. Whilst, computation of time-dependent problems, in the open literature numerous algorithms are present, for example, the Taylor-Galerkin (Donea, 1984b), Least-Square (Carey and Jiang, 1988) and Lagrange-Galerkin methods. Further details about the Taylor-Galerkin scheme are discussed in chapter two.

The scheme of choice here is a multi-stage finite element technique. Initially, an explicit form of time-dependent Taylor-Galerkin scheme was improved (Townsend and Webster, 1987) by incorporating pressure-correction method to resolve pressure driven incompressible flows of Newtonian fluids. The algorithm was designed following the ideas of (Donea, 1984a and 1984b)) and to obtain a second order accurate solutions and adjust the incompressibility the work of (Van Kan, 1986) was followed.

Structuring of this scheme is suitable to solving large-scale problems and ease to implement in three-dimension. By a number of researchers, a computer program in FORTRAN has been developed based on Taylor–Galerkin/pressure–correction algorithm was made available at the start of the research described in this thesis in literature review. However, the present author has significantly enhanced the code and has contributed by incorporating Darcy’s term for flow through porous material in the momentum equation.

#### **4.2 Taylor–Galerkin/Pressure–Correction Scheme**

Central theme of Taylor–Galerkin scheme is to develop a procedure to capture transient as well as steady–state solution of fluid flow problems through efficient and highly accurate time–stepping scheme. Originally, algorithm has been presented (Donea, 1984b) to resolve the time–dependent flows of viscous fluids and the incompressibility condition is treated implicitly. In the algorithm, temporal discretisation is achieved through expansions of Taylor series. For second order temporal accuracy of results, a Lax–Wendroff approximation in two–step predictor–corrector scheme is employed. Algorithm also capture the higher order accuracy for time derivatives and consistent spatial derivatives. A significant augmentation in accuracy and stability is shown by the algorithm against Euler–Galerkin and Finite Difference methods [(Donea, 1984b) and (Hawken, et al., 1990)].

Pressure–correction/projection method has been suggested originally (Chorin, 1968) and in explicit form offered by (Fortin, et al., 1971). A further development of this operator separating method, after a linearized momentum analysis, leads to overall second order

---

accuracy and stability [(Peyret and Taylor, 1983) and (Kan, 1986)]. A so called TGPC algorithm [(Zienkiewicz and Codina, 1995) and (Zienkiewicz, et al., 2005)] presents the foundation for current numerical algorithm employed in this research. There are many other alike techniques related to finite difference literature may be found [(Lax and Wendroff, 1953), (Sod, 1978) and (Baloch, et al., 1994)]. For more details on steady-state and transient flows of Newtonian fluids can be found [(Hawken, et al., 1990) and (Tamaddon-Jahromi, et al., 1992)]. Whilst, for non-Newtonian fluids, has guided to experiment numerically extend the algorithm in semi-implicit and fully-implicit form of algorithm. For significant diffusion dominant flows, semi-implicit algorithm is realised numerically accurate, computationally efficient and stable, therefore, algorithm is advocated for such problems. As in this research study semi-implicit form of TGCP algorithm is employed. Therefore, only this method is described here.

### **4.3 Semi-implicit time-stepping scheme**

#### **4.3.1 Cartesian co-ordinates**

In literature it is indicated that, due to slow rate-of-convergence and inherent difficulties to deal with large time step ( $\Delta t$ ) of explicit schemes are computationally very expensive. Therefore, for the numerical simulation in this research work a semi-implicit form of TGCP algorithm is employed [(Hawken, et al., 1990), (Carew, et al., 1993), (Baloch, 1994), (Baloch, et al., 1995a) and (Solangi, et al., 2012b)]. The choice is purely recognised on its robustness of the algorithm and matter of fact, it enhance the accuracy, stability, efficiency and increase convergence rate at sufficiently larger time step. Fully implicit numerical algorithms commonly enhance the numerical stability properties, whereas, also computationally observed less cost effective. In the present research study,

---

only on the viscous or diffusive and Darcy's components of Darcy's–Brinkman equation, a Crank–Nicolson treatment is employed to deduce the TGCP scheme in semi–implicit form.

Adopting a semi–implicit approach on TGCP algorithm, for the governing system of equations (3.12 and 3.19), a semi–discrete system is obtained by expanding temporal domain  $(t_n, t_{n+1})$  in two steps through Taylor series expansion. In first step, a forward difference approach is applied up to half time step, keeping the philosophies of (Van Kan, 1986) in the finite element perspective to compute velocity vector field  $\mathbf{v}$  at half time step  $(n + \frac{1}{2})$  from initially given primitive variables  $(\mathbf{v}^n, p^n)$  at  $t = t_n$ . In second step, a central difference approach is employed to compute primitive variables  $(\mathbf{v}^{n+1}, p^{n+1})$  at full time step  $(t = t_{n+1})$ . For pressure term accommodating the incompressibility constraint, a Crank–Nicolson technique is applied to split this step in further two steps. In second step, a non–divergence–free velocity vector field is calculated utilising the information gathered from first step and initial given data. Whilst, in third step a pressure difference is obtained at full time step  $(t = t_{n+1})$ . At final fourth step, divergence–free velocity vector field  $(\mathbf{v}^{n+1})$  is computed from the information for pressure difference resulted at third step. The semi–discrete system of Darcy's–Brinkman equation in strong form and the algorithm in time difference is given as follows:

**Stage-1a:** Compute divergence free velocity field  $\mathbf{v}^{n+\frac{1}{2}}$  at half time step  $n+\frac{1}{2}$  from the given initial data for velocity vector field  $\mathbf{v}^n$  and pressure  $p^n$  at initial level  $n$ :

$$\begin{aligned} & \left( \frac{2}{\Delta t} - \frac{1}{2\text{Re}} \nabla^2 + \frac{1}{2\text{Re} D_a} \right) \left( \mathbf{v}^{n+\frac{1}{2}} - \mathbf{v}^n \right) \\ &= \left[ \frac{1}{\text{Re}} \nabla^2 \mathbf{v} - (\mathbf{v} \cdot \nabla) \mathbf{v} - \nabla p - \frac{1}{\text{Re} D_a} \mathbf{v} \right]^n \end{aligned} \quad (4.1a)$$

**Stage-1b:** Compute an intermediate non-solenoidal velocity field  $\mathbf{v}^*$  from velocity vector fields  $\mathbf{v}^{n+\frac{1}{2}}$  computed at  $n+\frac{1}{2}$  time step and pressure  $p^n$  at initial time step  $n$  after applying Crank-Nicolson treatment on pressure. (Crank-Nicolson uses average of an implicit and explicit methods):

$$\begin{aligned} & \left( \frac{1}{\Delta t} - \frac{1}{2\text{Re}} \nabla^2 + \frac{1}{\text{Re} D_a} \right) (\mathbf{v}^* - \mathbf{v}^n) \\ &= \left[ \frac{1}{\text{Re}} \nabla^2 \mathbf{v} - \nabla p - \frac{1}{\text{Re} D_a} \mathbf{v} \right]^n - (\mathbf{v} \cdot \nabla) \mathbf{v}^{n+\frac{1}{2}} \end{aligned} \quad (4.1b)$$

**Stage-2:** Having solved for non-divergence free velocity vector  $\mathbf{v}^*$ , now need to compute the pressure difference  $(p^{n+1} - p^n)$  with the help of Poisson equation at full time step interval  $(t_n, t_{n+1})$ , as given below:

$$\theta \nabla^2 (p^{n+1} - p^n) = \frac{1}{\Delta t} \nabla \cdot \mathbf{v}^* \quad (4.1c)$$

**Stage–3:** Finally, at this step three, compute the solutions for a solenoidal velocity field  $\mathbf{v}^{n+1}$  at the concluding of full time step  $(n+1)$  cycle utilising information gathered in stage–1b and stage–2, i.e.,  $\mathbf{v}^*$  and pressure difference  $(p^{n+1} - p^n)$  as follows:

$$\frac{2}{\Delta t}(\mathbf{v}^{n+1} - \mathbf{v}^*) = -\nabla(p^{n+1} - p^n) \quad (4.1d)$$

Here, initial time step index is represented by  $n$ . The choice of Crank–Nicolson  $\theta$  ( $=0.5$ ) is used [(Crank and Nicolson, 1996), (Baloch, et al., 1995a) and (Solangi, et al., 2012b)]. For Taylor–Galerkin/pressure–correction scheme, in first temporal fractional stage, the addition of mid–point temporal step, characterises the expansion from first to second order projection method.

### 4.3.2 Finite Element Discretisation

For spatial discretisation of above set of equations (4.1), are reorganise into a variational form using weighted technique and a finite element approximation. For shape and weight functions, following suitable definitions of Hilbert spaces  $(H^1(\Omega)^2)$  and vector valued Sobolev space functions are defined on  $\Omega \subset \mathbb{R}^2$ . Which are themselves and their first order derivatives are first order square–integrable  $L^2(\Omega)$  of scalar Hilbert space and second order square–integrable  $L^2(\Omega)$  of vector Hilbert space functions. For detail definitions reader is referred to [(Baloch, 1994) and (Solangi, 2011)]: represents the particular standard of:

$$V = \left\{ u^n \in H^1(\Omega)^2 \mid u \Gamma_1^n = b \right\} \quad (4.2a)$$

$$V_0 = \left\{ v \in H^1(\Omega)^2 \mid u \Gamma_1 = 0 \right\} \quad (4.2b)$$

For square-integrable functions, the conventional inner-product representation is defined as:

$$\langle f, g \rangle = \int_{\Omega} f(x)g(x)d\Omega \quad (4.3)$$

Let  $L^2(\Omega)$  be the scalar Hilbert space for square-integrable functions:

$$P = \left\{ q \in L^2(\Omega)^d \right\} \quad (4.4)$$

For set of equations (4.1), utilising above definition of spaces of test functions for both velocity and pressure  $V_0$  and  $P$  respectively, a weak formulation of problem is acquired.

Subsequently, integrating using inner product equation (4.4) over the spatial domain  $\Omega$ , the anticipated semi-discrete variational form of the above equations at different stages are:

$$\begin{aligned} \text{Stage-1a:} \quad & \left( \frac{2}{\Delta t} - \frac{1}{2\text{Re}} \nabla^2 + \frac{1}{2\text{Re} D_a} \right) \left( \mathbf{v}^{n+\frac{1}{2}} - \mathbf{v}^n, \mathbf{v} \right) \\ & = \left( \frac{1}{\text{Re}} \nabla^2 \mathbf{v} - (\mathbf{v} \cdot \nabla) \mathbf{v} - \frac{1}{\text{Re} D_a} \mathbf{v}, \mathbf{v} \right) - (\nabla p, q) \end{aligned} \quad (4.5a)$$

---


$$\begin{aligned}
 \text{Stage-1b:} \quad & \left( \frac{1}{\Delta t} - \frac{1}{2\text{Re}} \nabla^2 + \frac{1}{\text{Re } D_a} \right) (\mathbf{v}^* - \mathbf{v}^n, \mathbf{v}) \\
 & = \left( \frac{1}{\text{Re}} \nabla^2 \mathbf{v} - \frac{1}{\text{Re } D_a} \mathbf{v}, \mathbf{v} \right)^n - (\nabla p, q)^n - (\mathbf{v} \cdot \nabla \mathbf{v}^{n+\frac{1}{2}}, \mathbf{v})
 \end{aligned} \tag{4.5b}$$

$$\text{Stage-2:} \quad \theta \nabla^2 (p^{n+1} - p^n, q) = \frac{1}{\Delta t} (\nabla \cdot \mathbf{v}^*, \mathbf{v}) \tag{4.5c}$$

$$\text{Stage-3:} \quad \frac{2}{\Delta t} (\mathbf{v}^{n+1} - \mathbf{v}^*, \mathbf{v}) = -\nabla (p^{n+1} - p^n, q) \tag{4.5d}$$

To derived fully discrete system of the problem, describing proper finite dimensional subspaces  $V^h, V_0^h$  and  $P^h$  of  $V, V_0$  and  $P$  respectively. Adopting weighted residual technique, the above system of equations (4.5) are spatially discretised using finite element method by Galerkin approximation, where, weight function is taken equivalent to shape function. For velocity components  $(u, v)$  and pressure  $p$ , a piecewise quadratic shape functions and piecewise linear shape functions are adopted respectively over triangular mesh tessellations. Employing variable separating (temporal and spatial variables) technique, the approximate solutions of primitive variables,  $u(x, y, t)$ ,  $v(x, y, t)$  and  $p(x, y, t)$ , are introduced over finite spaces of following functions as:

$$u(x, y, t) \cong \sum_{j=1}^6 U_j^n(t) \Phi_j(x, y) \tag{4.6a}$$

$$v(x, y, t) \cong \sum_{j=1}^6 V_j^n(t) \Phi_j(x, y) \quad (4.6b)$$

$$p(x, y, t) \cong \sum_{k=1}^3 P_k(t) \psi_k(x, y) \quad (4.6c)$$

Where,  $\Phi_j$  and  $\psi_k$  are quadratic and linear shape functions respectively. In these equations (4.6) symbolisations are followed (Cuvelier, et al., 1986). Adopting divergence theorem, integrating by parts, the fully discrete system in the compact matrix form is:

**Stage-1a:**

$$\left\{ \frac{2M}{\Delta t} - \frac{1}{\text{Re}} \left( \frac{S}{2} + \frac{M}{D_a} \right) \right\} (\mathbf{V}^{n+\frac{1}{2}} - \mathbf{V}^n) = \left[ -\frac{1}{\text{Re}} (S\mathbf{V}_j) + J_1^\dagger p_k - N(\mathbf{V})\mathbf{V}_j - \frac{1}{\text{Re} D_a} M\mathbf{V}_j \right]^n \quad (4.7a)$$

**Stage-1b:**

$$\left[ \frac{M}{\Delta t} - \frac{1}{\text{Re}} \left( \frac{S}{2} + \frac{M}{D_a} \right) \right] (\mathbf{V}^* - \mathbf{V}^n) = \left[ -\frac{1}{\text{Re}} S\mathbf{V}_j - J_2^\dagger p_k - \frac{1}{\text{Re} D_a} M\mathbf{V}_j \right]^n - N(\mathbf{V})\mathbf{V}_j^{n+\frac{1}{2}} \quad (4.7b)$$

**Stage-2:**

$$K(p^{n+1} - p^n) = -\frac{2}{\Delta t} J\mathbf{V}_j^* \quad (4.7c)$$

**Stage-3:**

$$\frac{2M}{\Delta t} (\mathbf{V}_j^{n+1} - \mathbf{V}_j^*) = J^\dagger (p^{n+1} - p^n) \quad (4.7d)$$

Where  $M = \int \phi_i \phi_j d\Omega$  is a consistent mass matrix,

$$N(V) = \int \left\{ \varphi_i (\phi_l U_l) \frac{\partial \phi_j}{\partial x} + \varphi_i (\phi_l V_l) \frac{\partial \phi_j}{\partial y} \right\} d\Omega \text{ is a convection matrix,}$$

$$S = \int \left\{ \frac{\partial \phi_i}{\partial x} \frac{\partial \phi_j}{\partial x} + \frac{\partial \phi_i}{\partial y} \frac{\partial \phi_j}{\partial y} \right\} d\Omega \text{ is a momentum diffusion matrix,}$$

$$J_1 = \int \frac{\partial \psi_i}{\partial x} \phi_j d\Omega \text{ and } J_2 = \int \frac{\partial \psi_i}{\partial y} \phi_j d\Omega \text{ are divergence/pressure gradient matrix and}$$

$$J = (J_1, J_2) \text{ and } K = \int \left\{ \frac{\partial \psi_{ki}}{\partial x} \frac{\partial \psi_{kj}}{\partial x} + \frac{\partial \psi_{ki}}{\partial y} \frac{\partial \psi_{kj}}{\partial y} \right\} d\Omega \text{ is a pressure stiffness matrix. Here, } \dagger$$

is transpose of a matrix.  $V^n, V^*$  and  $V^{n+1}$  are nodal vectors of velocity field,  $p^n, p^{n+1}$  is pressure, and  $\Delta t$  is the time interval  $(t_n, t_{n+1})$ .

### 4.3.3 Cylindrical polar co-ordinates

The choice of algorithm for numerical simulation depends on precision, convergence rate, effectiveness and stability. Literature review shows that semi-implicit techniques are preferred over the explicit schemes, which have slow rate of convergence [(Hawken et al., 1990), (Carew et al., 1994), (Baloch, 1994), Solangi, 2011), (Solangi et al., 2012a) and (Solangi et al., 2013)]. For the enhancement of numerical stability, generally implicit methods are used; however, these methods are computationally no more expensive. The fully discrete semi-implicit system of equations with Darcy's term in addition is as follows:

**Stage-1(a):**

$$\left[ \frac{2}{\Delta t} M + \frac{1}{\text{Re}} \left( \frac{S_{rr}}{2} + \frac{M}{D_a} \right) \right] (V_{r,j}^{n+\frac{1}{2}} - V_{r,j}^n) = \left[ -\frac{1}{\text{Re}} \{S_{rr} + S_{rz}\} V_{r,j} - J_1^\dagger P_k \right]^n - N(V) V_{r,j}^n - \frac{1}{\text{Re} D_a} M V_{r,j}^n \quad (4.8a)$$

$$\left[ \frac{2}{\Delta t} M + \frac{1}{\text{Re}} \left( \frac{S_{zz}}{2} + \frac{M}{D_a} \right) \right] (V_{z,j}^{n+\frac{1}{2}} - V_{z,j}^n) = \left[ -\frac{1}{\text{Re}} \{S_{rz}^\dagger + S_{zz}\} V_{z,j} - J_2^\dagger P_k \right]^n - N(V) V_{z,j}^n - \frac{1}{\text{Re} D_a} M V_{z,j}^n \quad (4.8b)$$

**Stage-1(b):**

$$\left[ \frac{1}{\Delta t} M + \frac{1}{\text{Re}} \left( \frac{S_{rr}}{2} + \frac{M}{D_a} \right) \right] (V_{r,j}^* - V_{r,j}^n) = \left[ -\frac{1}{\text{Re}} \{S_{rr} + S_{rz}\} V_{r,j} - J_1^\dagger P_k \right]^n - N(V) V_{r,j}^{n+\frac{1}{2}} - \frac{1}{\text{Re} D_a} M V_{r,j}^n \quad (4.8c)$$

$$\left[ \frac{1}{\Delta t} M + \frac{1}{\text{Re}} \left( \frac{S_{zz}}{2} + \frac{M}{D_a} \right) \right] (V_{z,j}^* - V_{z,j}^n) = \left[ -\frac{1}{\text{Re}} \{S_{rz}^\dagger + S_{zz}\} V_{z,j} - J_2^\dagger P_k \right]^n - N(V) V_{z,j}^{n+\frac{1}{2}} - \frac{1}{\text{Re} D_a} M V_{z,j}^n \quad (4.8d)$$

**Stage-2:**

$$K(Q^{n+1}) = -\frac{2}{\Delta t} (J_1 V_{r,j} + J_2 V_{z,j}) \quad (4.8e)$$

**Stage-3:**

$$M(V_{r,j}^{n+1} - V_{r,j}^*) = \frac{\Delta t}{2} J_1^\dagger (p^{n+1} - p^n) \quad \text{“P” should be capital with subscript “j”} \quad (4.8f)$$

$$M(V_{z,j}^{n+1} - V_{z,j}^*) = \frac{\Delta t}{2} J_2^\dagger (p^{n+1} - p^n) \quad (4.8g)$$

where,  $M = \int_{\Omega} \Phi_i \Phi_j r d\Omega$ , is a mass matrix, (4.9a)

$$J_1 = \int_{\Omega} \psi_k \frac{\partial \Phi_j}{\partial r} r d\Omega + \int_{\Omega} \psi_k \Phi_j r d\Omega \quad \text{and} \quad (4.9b)$$

$$J_2 = \int_{\Omega} \psi_k \frac{\partial \Phi_j}{\partial z} r d\Omega, \quad \text{are Pressure gradient matrices,} \quad (4.9c)$$

$$N(V) = \int_{\Omega} \Phi_i \left( \Phi_l V_l \frac{\partial \Phi_j}{\partial r} + \Phi_l V_l \frac{\partial \Phi_j}{\partial z} \right) r d\Omega, \quad \text{is non-linear convection matrix,} \quad (4.9d)$$

While the momentum diffusion matrices are define as:

$$S = \begin{bmatrix} S_{rr} & S_{rz} \\ S_{rz}^t & S_{zz} \end{bmatrix} \quad (4.9e)$$

$$S_{rr} = \int_{\Omega} \left( 2 \frac{\partial \Phi_i}{\partial r} \frac{\partial \Phi_j}{\partial r} + \frac{\partial \Phi_i}{\partial z} \frac{\partial \Phi_j}{\partial z} + \frac{\Phi_i \Phi_j}{r^2} \right) r d\Omega \quad (4.9f)$$

$$S_{zz} = \int_{\Omega} \left( \frac{\partial \Phi_i}{\partial r} \frac{\partial \Phi_j}{\partial r} + 2 \frac{\partial \Phi_i}{\partial z} \frac{\partial \Phi_j}{\partial z} \right) r d\Omega \quad (4.9g)$$

$$S_{rz} = \int_{\Omega} \left( \frac{\partial \Phi_i}{\partial r} \frac{\partial \Phi_j}{\partial z} \right) r d\Omega \quad (4.9h)$$

$$K = \int \left\{ \frac{\partial \psi_{ki}}{\partial r} \frac{\partial \psi_{kj}}{\partial r} + \frac{\partial \psi_{ki}}{\partial z} \frac{\partial \psi_{kj}}{\partial z} \right\} d\Omega \text{ is a pressure stiffness matrix.} \quad (4.9I)$$

Here,  $\dagger$  is transpose of a matrix.  $V^n, V^*$  and  $V^{n+1}$  are nodal vectors of velocity field,  $p^n, p^{n+1}$  is pressure, and  $\Delta t$  is the time interval  $(t_n, t_{n+1})$ .  $V_j^n$  is a nodal velocity vector at time  $t_n$ ,  $V_j^*$  is an intermediate non-divergence-free velocity vector and  $V_j^{n+1}$  is a divergence-free velocity vector at time step  $t_{n+1}$ . In above equations  $p_k^n$  is a pressure vector and  $Q^{n+1} = p_k^{n+1} - p_k^n$  is a pressure difference vector. Where, subscripts  $i, j$ , and  $l$  are all six nodes (1, 2, ... 6) for quadratic triangular element for velocity components, while  $k, k1$  and  $k2$  are represents only vertex nodes (1, 2, 3) for pressure.

#### 4.4 Solution methods for resultant system of equations/Mass matrix construction

For numerical computation, initially at different stages, non-linear system of partial differential equations governing the flow, are reduced in the linear algebraic system of equations. The linearization is incorporated through finite element technique. Subsequently, finding the solutions of corresponding linear algebraic system of equations, the direct as well as iterative methods are employed. At stage-1(a, b) and stage-3, linear algebraic system of equations may be exhibited as:

$$M_{ij} X_j = b_i \quad (4.10)$$

---

Here, the augmented mass matrix of order ‘ $n$ ’ is represented by  $M = \begin{bmatrix} m_{11} & \cdots & m_{1n} \\ \vdots & \ddots & \vdots \\ m_{n1} & \cdots & m_{nn} \end{bmatrix}$ ,

whereas, solution vector  $X_j$  represents an unknown velocity difference over each time–step cycle  $[t_n, t_{n+1}]$  and  $b$  is related to a right–hand–side known column vector. On the left hand side of above linear algebraic system of equations (4.6), a symmetric coefficient mass matrix is present and it is solved through modified Jacobi’s iterative method and presented as:

$$M_d X^{(s+1)} = (M_d - M) X^{(s)} + b \quad (4.11)$$

Where  $M_d$  is denotes a diagonal version of mass matrix. To ensure the mass matrix diagonally dominant, a diagonal matrix is introduced. This diagonal matrix  $M_d$  is constructed through absolute row sum of mass matrix and derived from  $M$  (Donea, et al. 1982a).

For the solution of equation (4.7), the direct inversion of mass matrix ‘ $M$ ’ is circumvented, in order to save computation cost, an alternatively approach is adopted. At first and third stages, an explicit assembly of the consistent mass matrix is restricted. Therefore, element by element contributions of mass matrix is computed using Jacobi’s iterative technique. For planar flows, using exact integration, this choice is found to be suitable because it yields a fast convergence–rate with an adequate convergence is realised in only three or five iterations. The authors [(Hawken, et al., 1990) and (Ding, et

al., 1992)] have discussed the  $M_d$  for different choices. Whilst, unknown vector and iteration number are represented by  $X^{(s)}$  and  $s$  respectively. The diagonal mass matrix is taken as the absolute row sum and illustrated as below:

$$M_d = [m_{ij}^d] \quad (4.12a)$$

$$\text{Where, } m_{ij}^d = \begin{cases} 0 & \text{for } i \neq j \\ \sum_{k=1}^n |m_{ik}| & \text{for } i = j \end{cases} \quad (4.12b)$$

For axi-symmetric flow problem, a seven point Gauss quadrature method is applied to integrate the governing PDEs, therefore, a mass lumping ( $s = 1$ ) approach is adopted. As mass lumping always degrades convection results [(Gresho, et al. 19760 and (Baloch, 1994)]. However, in diffusion dominant flows mass lumping accelerates the convergence and stabilises the solution (Donea, et al., 1982a). A mixed type method is engaged by (Usmani, et al., 1993) the effects of mass lumping are well discussed in [(Fu, 1972), (Fujii, 1973), (Wood, 1990) and (Zienkiewicz and Taylor, 2000)]. Stream function calculator uses explicitly both lumped as well as higher number of mass iterations. Whilst, at stage two, for pressure difference, a Poisson equation is solved. At this stage a symmetric-positive-definite stiffness matrix is formed with a banded structure. Therefore, it is an appropriate to apply Cholesky's method.

#### 4.5 Stream function

In the analysis of fluid dynamic problems, the flow structure has great importance. Flow structure can be computed through stream function in two-space coordinate system which

---

have quantitatively of significant interest. However, in three–space coordinate system, for each dimensional face a multiple stream functions are desirable. For illustration flow structure, the computation of stream function has an important physical meaning and mathematically useful to visualise. The streamlines represent the flow field corresponding to the local velocity vectors. Solid boundaries of the flow can be interpreted through streamline, also quantitatively suitable, particularly in recirculation regions.

For planar flow, difference between two streamlines characterises the volume flow of fluid between the two positions. For the simulation of fluid flow problems using primitive variables, it is necessary to have a post processing facility of stream function generating in order to visualise clear picture of flow pattern. To draw streamlines from first node position to another location of node, it is necessary the information of stream function shall be present beforehand. A family of curves across the flow structure describes the stream function, while, can be computed from the velocity gradient. Whilst, in the steady–state solution situation the variation along a single streamline or path line of the fluid particles is constant in the flow field. For both coordinate systems, i.e., plane Cartesian and cylindrical polar coordinates, stream function satisfies Poisson's equation in. To compute stream function at the completion of finite element solver, it is appropriate to adopt FE approximation to simulate the equation. For an incompressible two–dimensional flow, a velocity vector potential ‘ $\Psi$ ’ can be presented, an applicable vector potential is:

$$V = \nabla \times \Psi \quad (4.13)$$

Where,  $\Psi = \{0, 0, \Psi\}$  represents the stream function.

Here we only address an axisymmetric frame of reference as the Cartesian coordinates in computation is a subclass. Let  $(v_r, v_z)$  be velocity components in axisymmetric cylindrical polar coordinate system  $(r, z)$  in radial and axial directions. Stream function  $\Psi(r, z)$  and fulfils the following relations between velocity components and stream-function (Baloch, 1994):

$$\frac{1}{r} \frac{\partial \Psi}{\partial r} = -v_z \text{ and } \frac{1}{r} \frac{\partial \Psi}{\partial z} = v_r \quad (4.14)$$

For computation purpose using pseudo time stepping procedure, above equation (4.14) gives the following scheme:

$$\frac{\partial \Psi}{\partial t} = \left( \frac{\partial^2 \Psi}{\partial r^2} + \frac{\partial^2 \Psi}{\partial z^2} \right) - r \frac{\partial v_z}{\partial r} - v_z + r \frac{\partial v_r}{\partial z} \quad (4.15)$$

After dividing by r gives:

$$\frac{1}{r} \frac{\partial \Psi}{\partial t} = \frac{1}{r} \left( \nabla^2 \Psi \right) - \frac{\partial v_z}{\partial r} - \frac{v_z}{r} + \frac{\partial v_r}{\partial z} \quad (4.16)$$

For time derivative in left hand side of the equation (4.16), employing forward time stepping scheme with step  $(\Delta t)$ , variation form of equation-(4.16) becomes:

$$\frac{1}{r} \left( \frac{\Psi^{n+1} - \Psi^n}{\Delta t} \right) = \frac{1}{r} (\nabla^2 \Psi^n) - \frac{\partial v_z}{\partial r} - \frac{v_z}{r} + \frac{\partial v_r}{\partial z} \quad (4.17)$$

Employing weighted residual technique, weak form of equation–(4.17) becomes:

$$\begin{aligned} \frac{1}{\Delta t} \int_{\Omega} \frac{w}{r} (\Psi^{n+1} - \Psi^n) r d\Omega &= \int_{\Omega} \frac{w}{r} (\nabla^2 \Psi^n) r d\Omega - \int_{\Omega} w \frac{\partial v_z}{\partial r} r d\Omega \\ &\quad - \int_{\Omega} w \frac{v_z}{r} r d\Omega + \int_{\Omega} w \frac{\partial v_r}{\partial z} r d\Omega \end{aligned} \quad (4.18)$$

A finite element approximation will be as follows:

$$(\Psi, v_r, v_z) = \sum_{i=1}^N (\Psi_j, V_r^j, V_z^j) \Phi_i(r, z) \quad (4.19)$$

Where, on  $j$  nodal point  $\Phi_j$  is the quadratic basis function, whereas, stream function'

$\Psi_j$ ', radial velocity and axial velocity components are represented by  $(V_r^j, V_z^j)$  in  $r$

and  $z$  directions respectively.

Adopting finite element Galerkin approximation in which weight function ( $w_i$ ) is taken

equivalent to shape function ( $\Phi_i$ ) and represented below (Baloch, 1994):

$$\sum_{i=1}^N w_i(x) = \sum_{i=1}^N \Phi_i(x) \quad (4.20)$$

Gives:

$$\begin{aligned} \frac{1}{\Delta t} \int_{\Omega} \Phi_i \Phi_j d\Omega \Delta \Psi_j^{n+1} = & \int_{\Omega} \Phi_i (\nabla^2 \Phi_j) d\Omega \Psi_j^n - \int_{\Omega} \Phi_i \frac{\partial \Phi_j}{\partial r} r d\Omega v_z^j \\ & - \int_{\Omega} \Phi_i \Phi_j d\Omega v_z^j + \int_{\Omega} \Phi_i \frac{\partial \Phi_j}{\partial z} r d\Omega v_r^j \end{aligned} \quad (4.21)$$

In order to reduce the second order derivatives of above equation (4.21), Green's theorem is used to integrate by parts and neglecting the boundary integrals by imposing Dirichlet boundary conditions, can be written as:

$$\begin{aligned} \frac{1}{\Delta t} \int_{\Omega} \Phi_i \Phi_j d\Omega \Delta \Psi_j^{n+1} = & - \int_{\Omega} \left\{ \frac{\partial \Phi_i}{\partial r} \frac{\partial \Phi_j}{\partial r} + \frac{\partial \Phi_i}{\partial z} \frac{\partial \Phi_j}{\partial z} \right\} d\Omega \Psi_j^n - \int_{\Omega} \Phi_i \frac{\partial \Phi_j}{\partial r} r d\Omega v_z^j \\ & - \int_{\Omega} \Phi_i \Phi_j d\Omega v_z^j + \int_{\Omega} \Phi_i \frac{\partial \Phi_j}{\partial z} r d\Omega v_r^j \end{aligned} \quad (4.22)$$

The above equation (4.22) is presented in its explicit and semi-implicit forms adopting matrix-vector notation as:

$$\frac{1}{\Delta t} M \Delta \Psi_j^{n+1} = -K \Psi_j^n - D_1 v_z^j - M v_z^j + D_2 v_r^j \quad (4.23)$$

$$\left( \frac{1}{\Delta t} M + \frac{K}{2} \right) \Delta \Psi_j^{n+1} = -K \Psi_j^n - D_1 v_z^j - M v_z^j + D_2 v_r^j \quad (4.24)$$

Where,  $M$  is called the mass like matrix with entries  $\int_{\Omega} \Phi_i \Phi_j d\Omega$  and  $K$  is known as

diffusion like stiffness matrix with the following entries:

$$\int_{\Omega} \left\{ \frac{\partial \Phi_i}{\partial r} \frac{\partial \Phi_j}{\partial r} + \frac{\partial \Phi_i}{\partial z} \frac{\partial \Phi_j}{\partial z} \right\} d\Omega$$

In equations (4.23 and 4.24),  $D_1$  and  $D_2$  are denoted as velocity gradient matrices with entries:

$$\int \Phi_i \frac{\partial \Phi_j}{\partial r} r d\Omega \text{ and } \int \Phi_i \frac{\partial \Phi_j}{\partial z} r d\Omega.$$

#### 4.6 Summary

For the simulation of mixing–separating flows through channels and pipes filled with porous material or without porous media, numerical algorithm employed is a semi–implicit finite element based Taylor–Galerkin/Pressure–Correction (TGPC) algorithm. Technique adopts a time marching process based on a fractional–steps formulation. Scheme has been implemented successfully in numerous flow circumstances [(Van Kan, 1986), (Carew, et al., 1993), (Carew, et al., 1994), (Baloch, et al., 1995a), (Qureshi, et al., 2004), (Solangi, et al., 2012a), (Solangi, et al., 2012b) and (Solangi, et al., 2013)]. None of them has tried to check its stability and convergence in a domain filled with porous media. In current study numerical scheme has been implemented on the benchmark problem of geometries used by (Cochrane, 1981) through porous media.

The semi–implicit scheme presented has been applied to simulate complex flows of Newtonian and non–Newtonian fluids under varying flow–rates and flow directions of

---

the domains introduced in chapters 5 to 8. Algorithm comprises, temporal discretisation through expansion of Taylor series in time (Donea, 1984a). At initial half time step a forward difference approach is adopted, while, for full time-step a central difference approach is employed. For computation of pressure-differential, a numerical algorithm is built to achieve a second order accuracy in time, an operator-split projection method is used (Van Kan, 1986). For spatial discretisation a finite element basis functions are used, i.e., linear and quadratic approximation for pressure velocities is achieved. These basis functions are defined over two-dimensional triangular elements. An iterative, modified Jacobi's, solver is used to compute velocity fields at stage-(1a and 1b) and stage-3. While, at stage-2, to Poisson equation for pressure-difference an explicit Choleski's technique is adopted [(Townsend and Webster, 1987) and (Hawken, et al., 1990)].

Convergence and stability of this scheme analysed in both coordinate system has been compared in channel and pipe flows on the basis of model used and discussed in chapter 4 and eight.

## Chapter 5. Reverse and Unidirectional Flows of Newtonian Fluids in a Channel

### 5.1 Introduction

This chapter covers numerically simulated results in a channel filled with and without porous channel. Four different settings from  $G_1$  to  $G_2$  are presented in figure (5.1). The domain is very much rich in changing flow directions along with varying flow rates in both channel arms. The hundreds of configurations are possible to get very interesting seniors but this study considers only four combinations. The continuity and momentum equations discussed in chapter three along with their appropriate initial and boundary conditions are solved for flows through non-porous and porous media. Two dimensional flows of Newtonian fluids are carried out in combined mixing separating geometry by using Cartesian co-ordinates system. An unsteady finite element scheme in combination with semi-implicit Taylor-Galerkin/Pressure correction scheme has been employed to get steady solutions. Details of this scheme are found in chapter four.

The domain is twofold one with reversed and unidirectional channel flows interacting through a gap in the common separating walls filled with Newtonian materials in both arms of a channel and later with reversed and unidirectional flows through porous media as shown in figure [5.1(a)-(b)]. The impact of increasing inertia, variation in flow directions, varying flow rate patterns in both channel arms and pressure difference are all studied in detail. Numerical simulations of Newtonian fluid flows in a channel are presented for the reversed and unidirectional domain shown in Figure (5.1). A computational domain is configured into four different settings from  $G_1$  to  $G_4$  shown in

---

figures [5.1(a) to 5.1(b)] by changing flow directions. In same figure finite element mesh used in the domain is also presented as shown in figure [5.1(e)].

In all four settings equal (1, 1) and unequal [(1, 1.5), (1, 2)] flow rates have been analysed initially channel filled with non-porous materials and later with porous. The numerical solutions are analysed by presenting streamline patterns, which are plotted at an equal interval in two flow regions, those of combined mixing and separating as well as for the other three configurations. In the mixing region contours are plotted from the separation line to centrally located plate, and in the unidirectional flow region from the channel wall to the separation line. In each case of reversed and unidirectional flows particularly for high values of Reynolds number streamline patterns are plotted at equal intervals to monitor clear activity of vortex development in all flow regions.

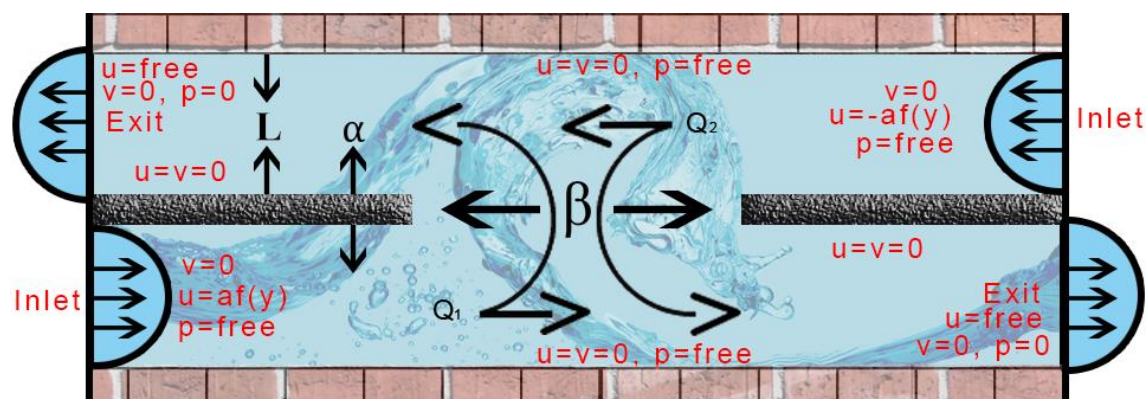
## 5.2 Problem specification

The particular details of combined mixing and separating geometry of reversed along with a unidirectional flow problem is given in Figures [5.1(a) to 5.1(d)] along with the finite element mesh used in this study shown in figure [5.1(e)]. As shown in Figure (5.1), configurations consist of two inlet and two outlet flows in a planar channel that is divided into two different sections by the intersection of two thin insert plates, placed horizontally in the central plane of a domain. The second has with two inlets from same direction one outlet in opposite. The third modified geometry is with again two inlets in opposite direction and one outlet. The last unidirectional geometry has one inlet from left bottom arm and an outlet from top right arm of a channel. In this study wide gap geometry with a separation gap width of  $\beta = 3L$  where  $L$  is taken as height of one arm of a channel has

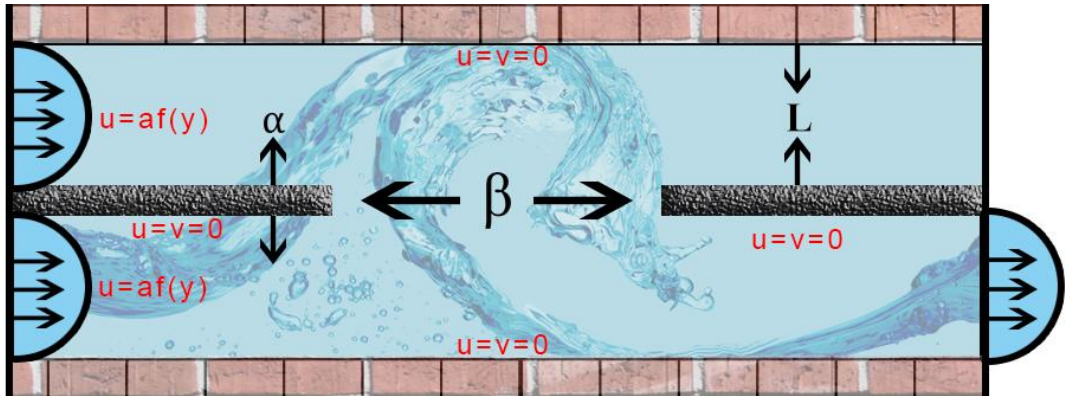
been studied. This facilitates an investigation of the impact of gap width on resultant flow structure.

Here same thickness of the plate which is  $\alpha = 0.0254L$  as in (Baloch et al., 1995a) has been taken. The length of a channel is reasonably good for reproducing developed flow at inlet and outlet of the flow domain. This research has preferred the wide gap geometry because in medium and narrow gap geometries it was observed that flow characteristics do not have some dramatic change. As mentioned by (Cochrane et al., 1981) it is very interesting geometry because flow rates and flow directions can be varied in several ways and the strength of the streams in the both the channel arms could be viewed by indicating arrows on the various figures. The flow domain is obtained by a uniform conformal mapping procedure and discretized into triangular elements. The total number of elements, nodes, boundary nodes, degrees of freedom and vertex nodes in a finite element mesh of the domain are 1328, 2853, 392, 6469 and 763 respectively.

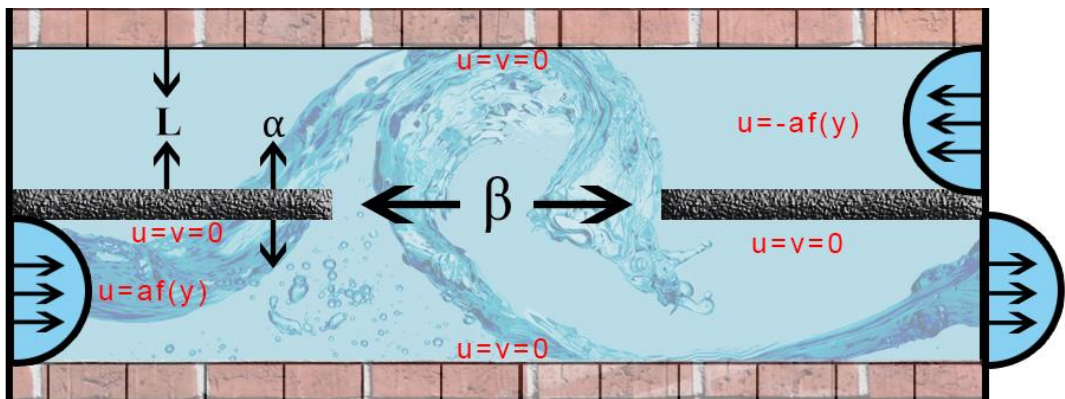
(a)



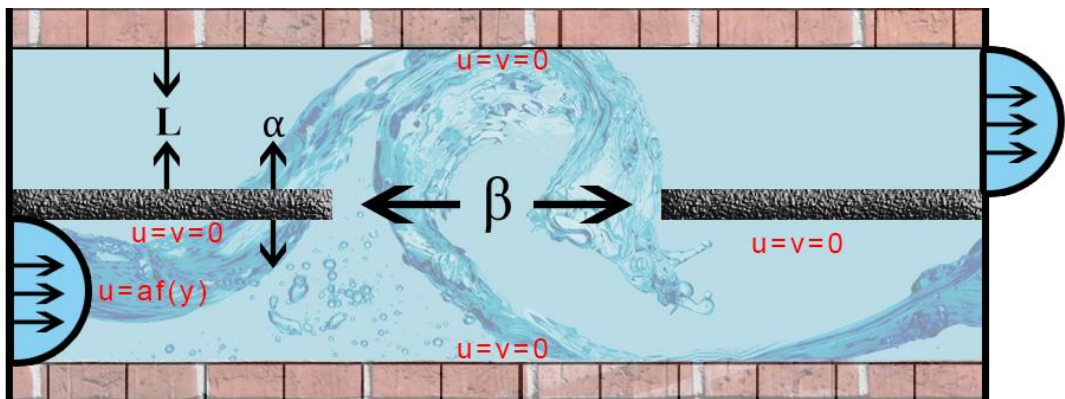
(b)



(c)



(d)



(e)

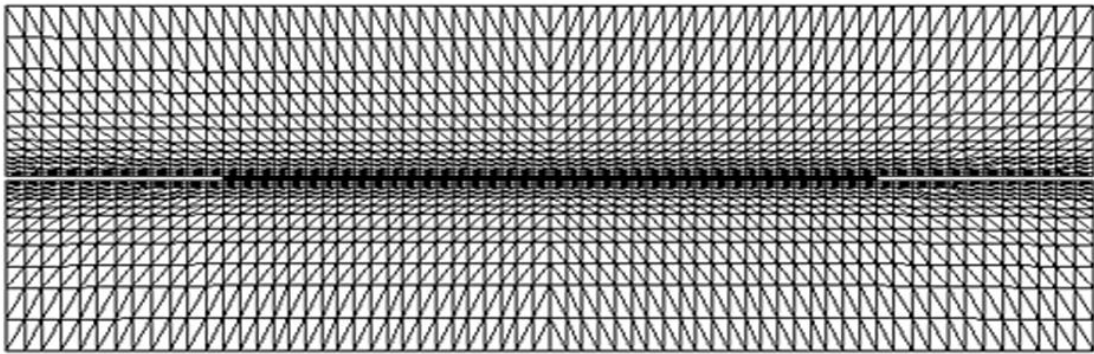


Figure 5.1 Geometries of the computational domain and mesh; (a) Diagram of combined mixing and separating flows with two inlets and two outlets (Reverse flow) ,  $G_1$ , (b) Unidirectional flow with two inlets and one outlet,  $G_2$ , (c) Reverse flow with two inlets and one outlet,  $G_3$ , (d) Unidirectional flow with one inlet and one outlet,  $G_4$  and (e) Finite element mesh used in the simulation.

Following the pioneer study (Baloch et al., 1995a) a proper choice of the time step has been made. A semi-implicit scheme has been employed by using Jacobi method to capture an accurate solution and typical time steps involved are  $\Delta t \leq 0.01$  for Newtonian problems. By employing five iterations per Jacobi step at a tolerance of  $10^{-6}$  a steady state solutions have been achieved.

### 5.3 Governing system of equations

For an analysis of an incompressible flow, the governing system of equations involves the conservation of mass and momentum transport equations. In the absence of body forces under isothermal condition within bounded region in space  $\Omega \rightarrow \mathfrak{R}^2$  with a smooth

piecewise boundary and time domain  $[0, \mathfrak{J}]$  with  $t$  and  $x$  are time and space respectively

the constitutive equations are defined as follows:

Continuity equation

$$\nabla \cdot \mathbf{v} = 0 \quad (5.1)$$

Where  $\mathbf{v}(x, t)$  the velocity is vector and  $\nabla$  is the gradient operator.

Momentum equation

$$\rho \frac{\partial \mathbf{v}}{\partial t} = \nabla \cdot (2\mu \underline{\underline{d}}) - \rho(\mathbf{v} \cdot \nabla) \mathbf{v} - \nabla p \quad (5.2)$$

Where,  $\mathbf{v}$  is a velocity of fluids,  $p(x, t)$  is the isotropic pressure (per unit density),  $\rho$  is the fluid density,  $\nabla$  is the gradient operator  $\mu$  is a Newtonian fluid viscosity and  $\underline{\underline{d}}$  is the rate of deformation tensor and it is defined as below:

$$\underline{\underline{d}} = \frac{1}{2} [\nabla \mathbf{V} + (\nabla \mathbf{V})^\dagger]. \text{ Where } \dagger \text{ denotes matrix transposition. For Newtonian fluid } \mu \text{ is}$$

assumed as constant.

The flow is considered to be hydro-dynamically fully developed hence velocity does not depend on axial direction of the channel. The flow is a unidirectional one and it is expressed in terms of axial velocity alone as a function of transversal direction. The non-dimensional system of equations along with appropriate initial and boundary conditions

could be found in chapter three. Governing system of equations are solved by employing a Taylor-Galerkin method which its numerical scheme and weak formulation is discussed in chapter four.

#### **5.4 Numerical results and discussion**

In this section, current study presents numerical solutions for Newtonian combining and separating flows in a channel filled with non-porous media. Investigations are given into flow stream patterns, vortex growth, pressure difference, due to changing flow rates and flow directions. Different combinations are given in Figures [5.1(a) to 5.1(d)] by changing flow directions and flow rates.

##### **5.4.1 Mixing and separating of Newtonian fluid flows in a channel filled with non-porous media (Geometry 1 $G_1$ )**

Figure 5.1(a) shows Newtonian fluid flows for combining and separating in a channel filled with a non-porous media. Insertion of the plates into computational domain creates two inlet and two outlet channel arms of equal dimension on opposing sides of the partition and placed separation gap of width  $\beta$ . The separation gap considered is  $\beta = 3L$  where  $L$  is a characteristic length taken as the height of an inlet arm of a channel. The thickness of the plate is taken as  $\alpha = 0.0254L$  and sufficiently long length of a channel is selected to reflect fully developed flow at entry and exit of the domain. Here effects of inertia, vortex size and its power are being discussed when channel is filled with a non-porous material. Comparisons will be made with inertial effects, pressure difference with the available results in open literature when a channel is filled with non-porous materials.

### 5.4.1.1 Equal (1, 1) flow rate

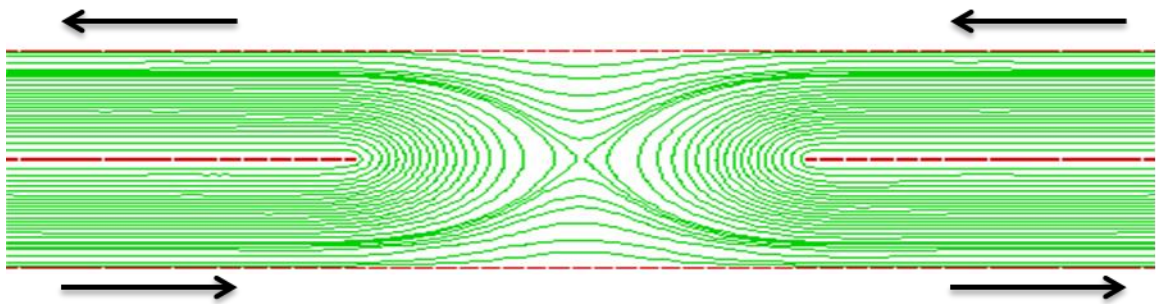
Equal (1, 1) rate is the volume of fluid passes per unit time into either channel arm is the same. As it has been discussed in chapter two  $U_m = V_m$ . In order to understand the effects of the inertia it is useful to first examine the flow of a Newtonian fluid and relative flow rates. The numerical results are presented in Figure 5.2 for increasing Reynolds number from ( $1 \leq Re \leq 200$ ). Starting from two parallel Poiseuille flows that are moving in opposite directions in upper and lower channel section of the geometry, solutions for unit Reynolds number have been got first. It is observed that the fluid responds to the presence of the gap and immediately breaks up, with flow mixing in both upper and lower exit sections of the geometry.

At  $Re = 15$  vortices development has been started near the walls in both arms of a channel. At  $Re = 15$  both vortices formed near the wall of upper and lower channel arms collide and merge in one and cover the middle gap of the domain. That single vortex grows in size and clearly forms an eddy. By adopting the same approach in increasing the value of  $Re$  the development of intensity of these vortices become more visible near the nip of the inserted plates in lower and upper channel arms as shown in figure (5.2) (at  $Re = 30$  to  $Re = 150$ ) by presenting symmetry with respect to each other.

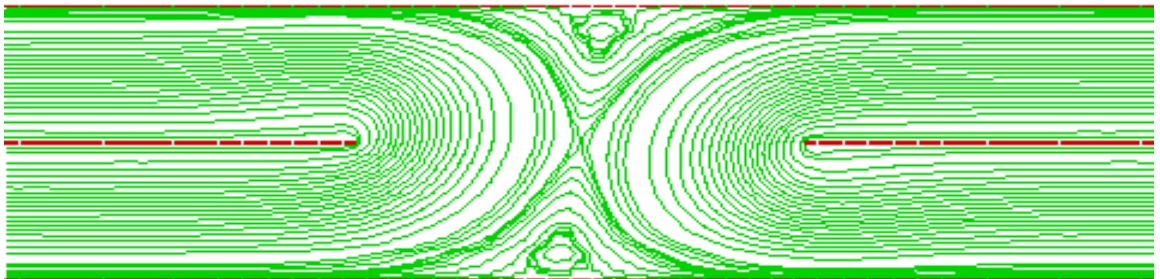
These independent vortices near the walls grow in size with increasing value of  $Re$  at exactly  $Re = 100$  these vortices become stable stretch in size and adjust their position on the wall. Eddy formed by the collision of two vortices in the middle gap increases in size grows horizontally and moves its position. Those eddies similarly start recirculation grow in size and forms two other eddies inside the bigger eddy and being symmetrically placed with respect to each other (at  $Re = 200$ ).

The core twin vortices near the boundary tend to become more twisted and stretched in the horizontal and vertical directions. Increasing the Reynolds number has an effect of increasing the size and strength of the central vortex and vortex behind the insert plates but with very high Reynolds number, vortices seem to divide into more vortices.

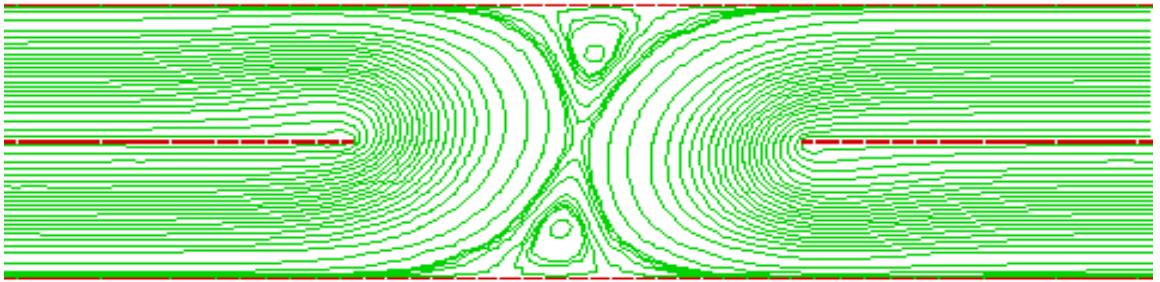
In equal (1, 1) flow rate flow was blocked by dominant recirculating vortices in the middle gap of the domain and that results in the flow of reversed (at  $Re=15$ ). Proper mixing of the fluids in middle gap has been observed.



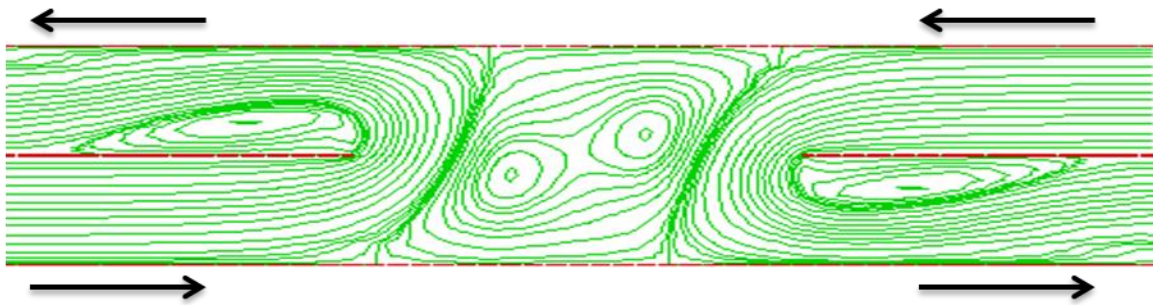
$Re=1$



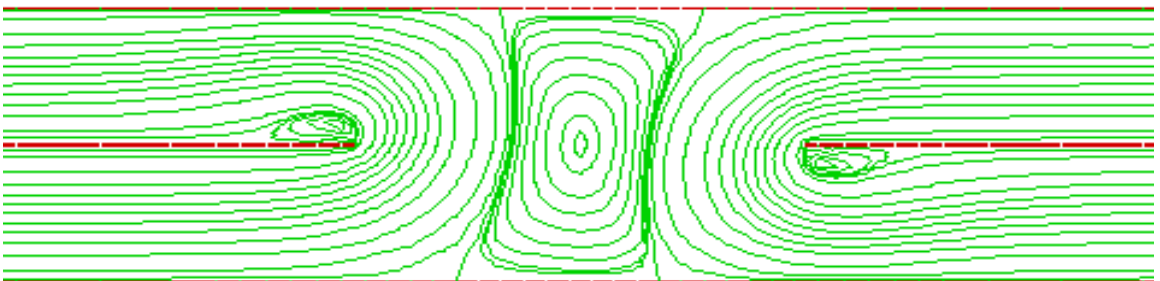
$Re=15$



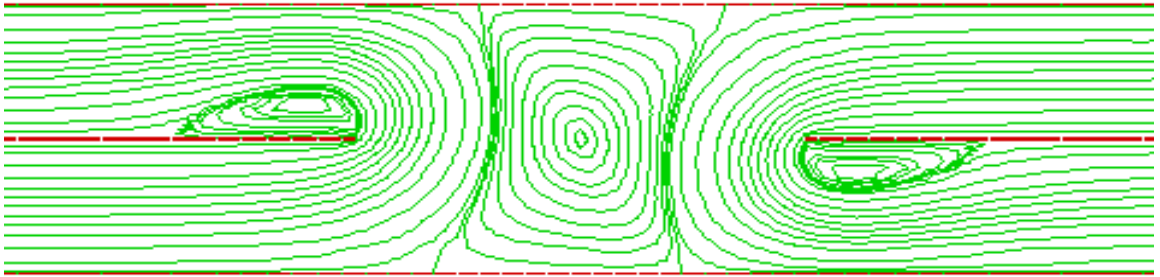
Re=16



Re=25



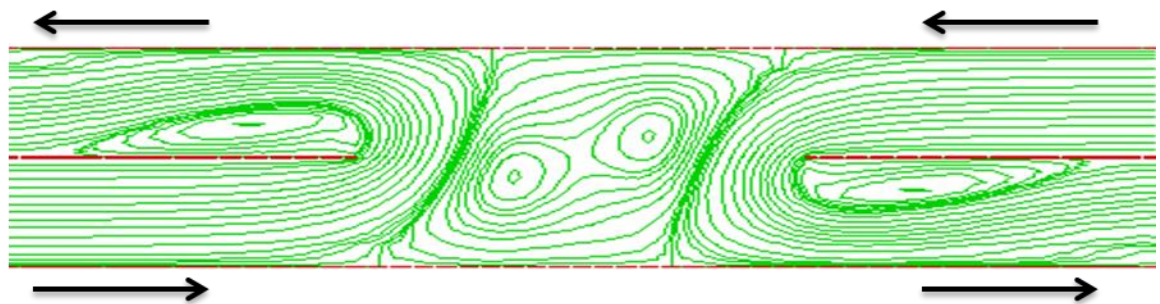
Re=30



Re=50



Re=150



Re=200

Re=200 (with small time step)

Figure 5.2 Streamline function for combined mixing and separating of Newtonian fluid flows for equal (1, 1) flow rate in a both channel arms, increasing Re from top to bottom.

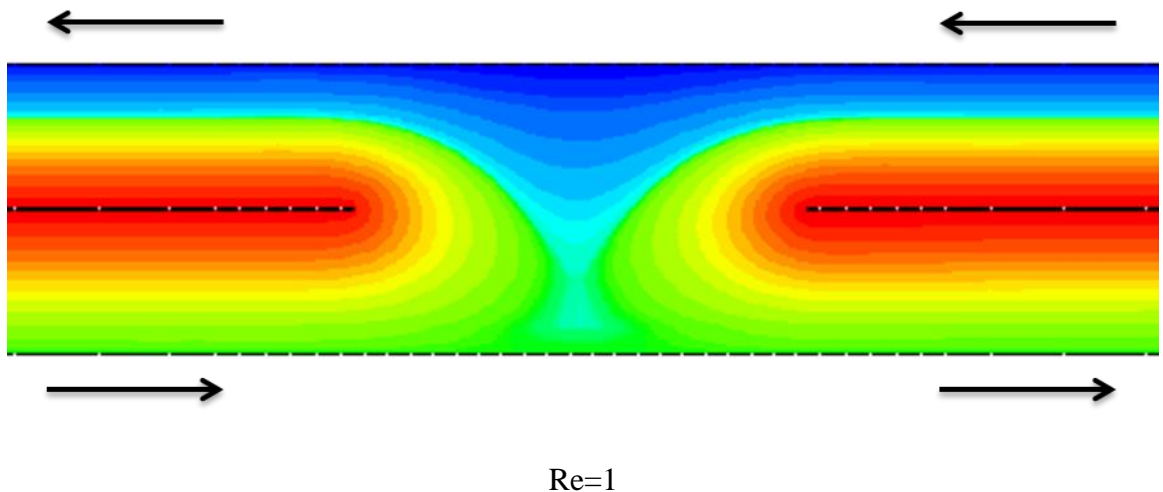
#### 5.4.1.2 Unequal (1, 1.5) flow rate

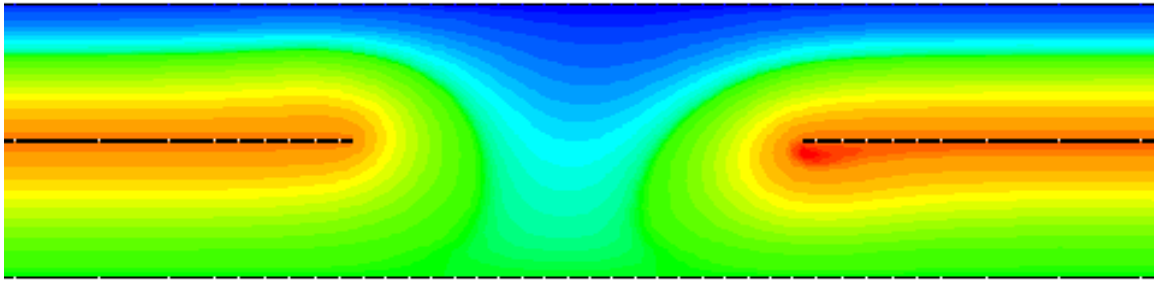
Numerical results for unequal (1, 1.5) flow rate of Newtonian flows in a channel are displayed in Figure- 5.3. In this case  $U_m = V_m$  and fluids passes from each channel arm takes the ratio 1:1.5. Again results are presented form the same domain but here flows rate has been changed in upper channel arm with increasing Reynolds numbers ( $1 \leq Re \leq 200$ ). Solutions are similarly started with Re=1, due change in upper channel arm flow has been pushed down in lower bottom arm of a channel and it has given rise to reversed flow. At Re=1 very weak vortex activity near the lip of sharp edge has been observed in in the right of lower channel arm towards the exit flow.

By adopting the same approach of increase in the value of Reynolds number as shown in section 5.4.1.1. It has been observed one more vortex growth near the wall in top channel arm in the centre of the domain wall (at Re=25) has been appeared.by increasing the value of Re vortex developed near the insert plate lie flat and adjust its position. It grows in size, become more stable, deeper and inclined with the wall. For further increase in the value of Re the intensity of vortex recirculation increases and vortex near the boundary wall pushes more towards the middle separation gap, grows in size and form an eddy as shown in figure (5.3) (at Re=100 to Re=200).

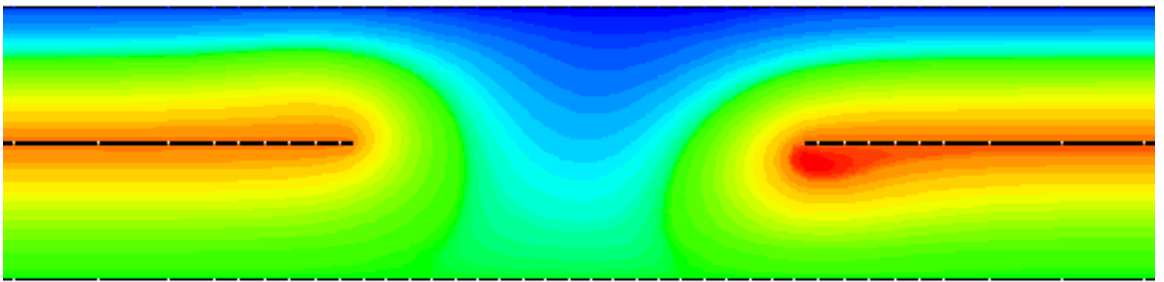
At  $Re=200$  another vortex appears in the top channel arm on the left downstream. All vortices development in all three different locations and have adopted the same pattern of growth in size, intensity, stability and with symmetry in streamlines. Similarly, here increasing the value of Reynolds number has the outcome of increasing the size strength, stability of the vortices as it was observed in the case of equal flow rate in section (5.4.1.1). Here flows are both unidirectional and reversed.

Vortex developed only on one wall of the upper channel whilst, in equal flow rate it appeared from either side of the domain in the middle of the wall. In lower a channel arm at  $Re=10$ , vortex appears only from one side near the central plate from its right. Another vortex on the other side of the central plate appears very late at  $Re=50$ .

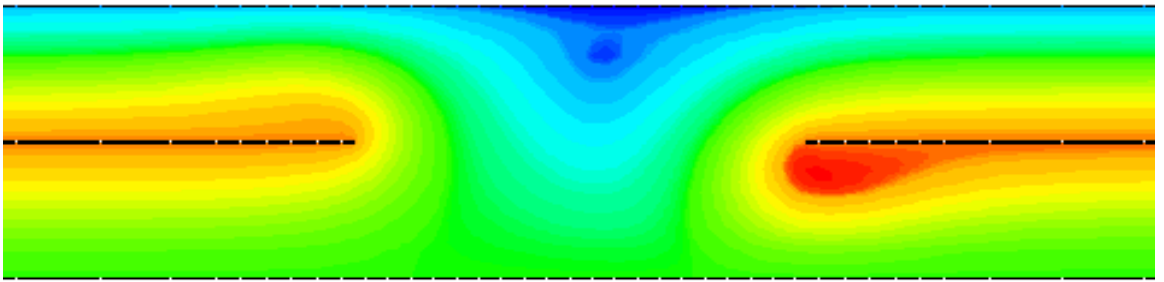




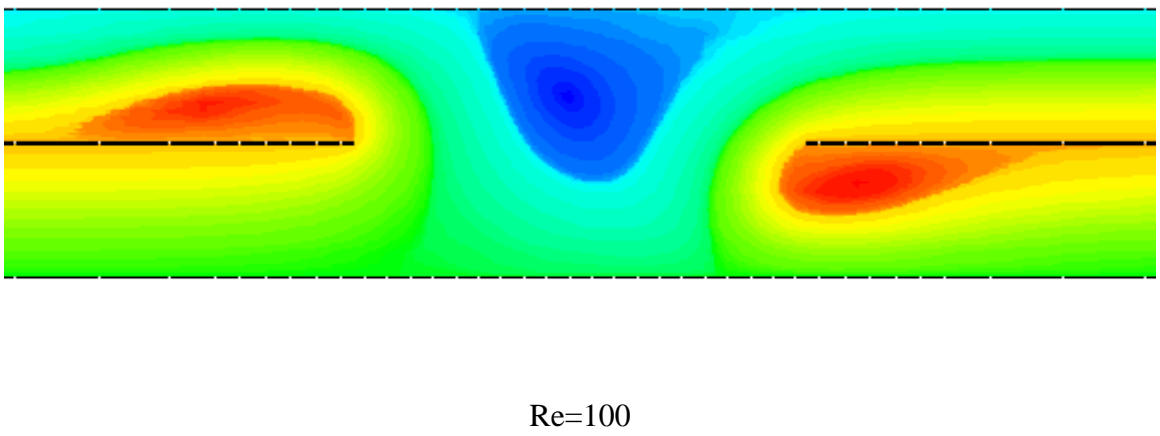
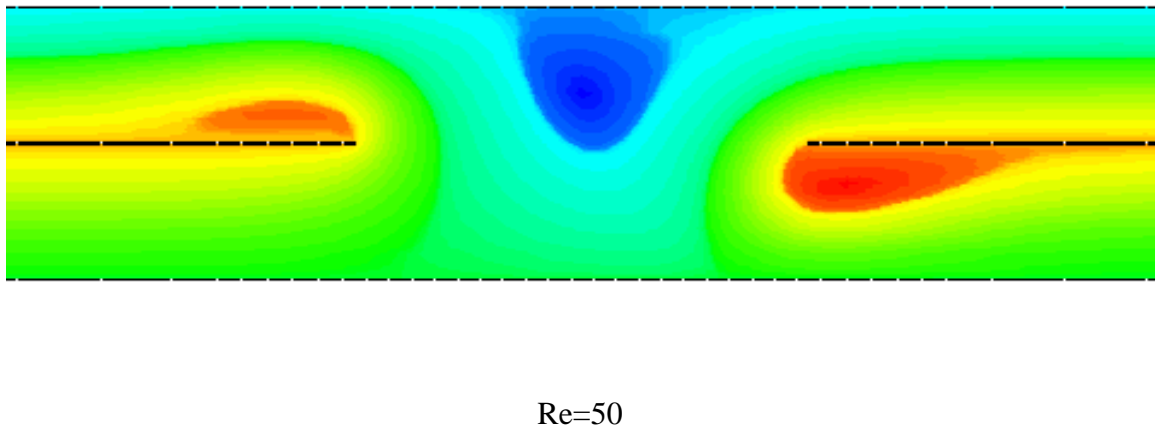
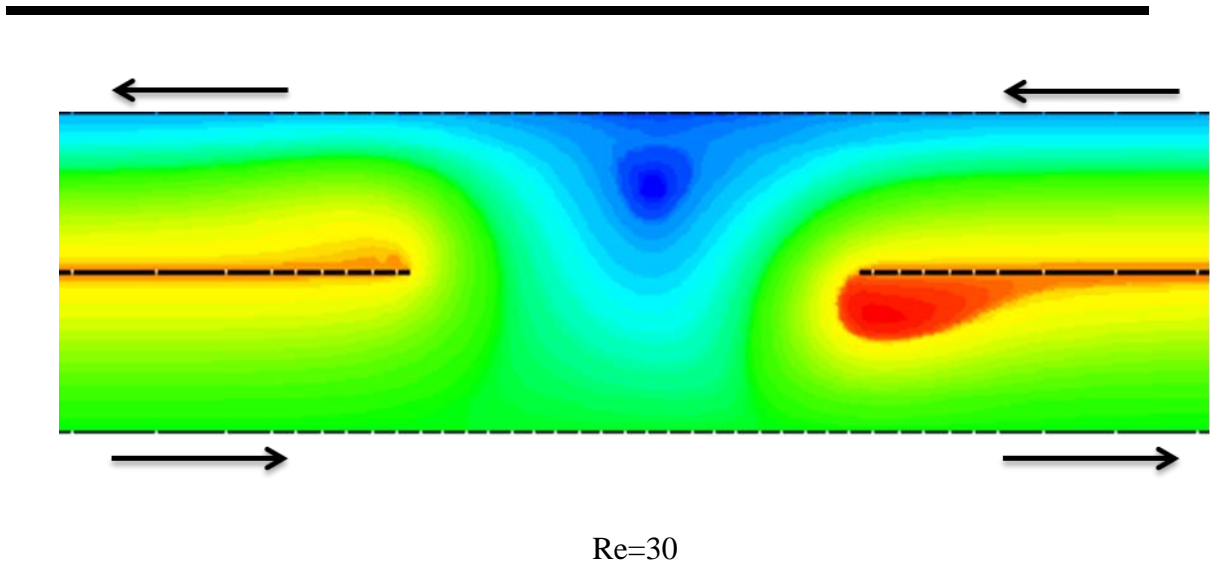
Re=10

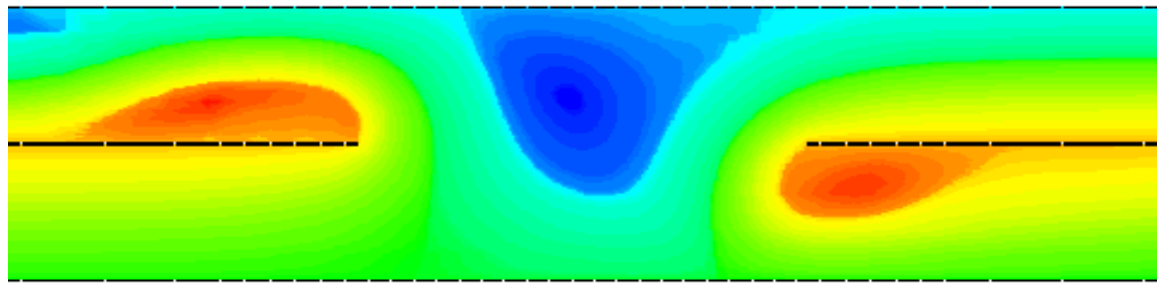


Re=15

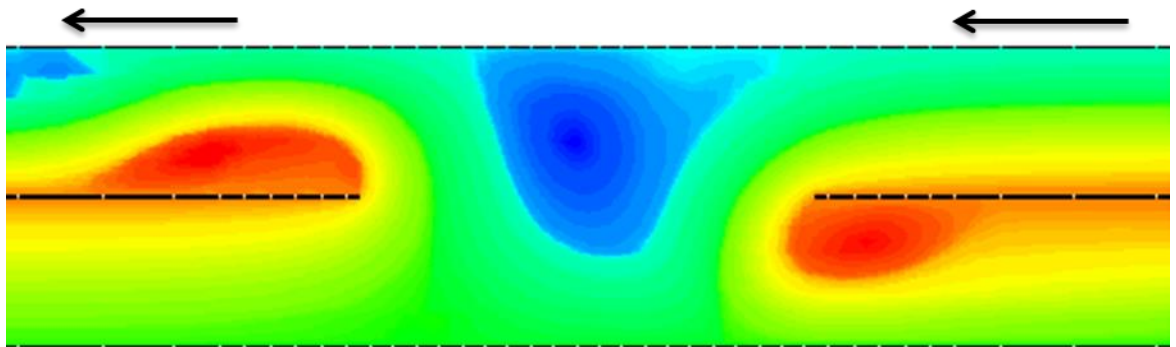


Re=25





Re=150



Re=200

Figure 5.3 Streamline functions for combined mixing and separating of Newtonian fluid flows of unequal (1, 1.5) flow rate in both channel arms, increasing Re from top to bottom.

#### 5.4.1.3 Unequal (1, 2) flow rate

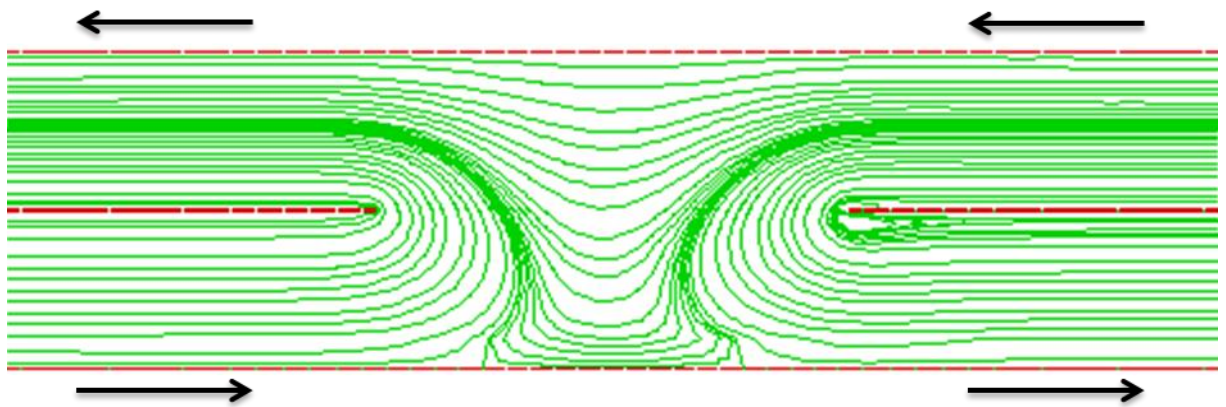
In this case fluid passes in lower and upper arm of a channel in the ratio of 1:2. It means volume of the fluid flows in upper channel arm is double as compared with lower channel arm. Unequal (1, 2) flows of Newtonian fluid filled in a channel for non-porous media are shown in figure (5.4). Calculations are presented for the same configuration with

increasing Reynolds numbers ( $1 \leq Re \leq 200$ ) for different flow rates in both a channel arms. Numerical simulations are giving streamline patterns, which are plotted at equal intervals in two flow regions, those of unidirectional and reversed flow. In the mixing region contours are plotted from the separation line to centrally located plate and in the unidirectional flow region from the channel wall to the separation line.

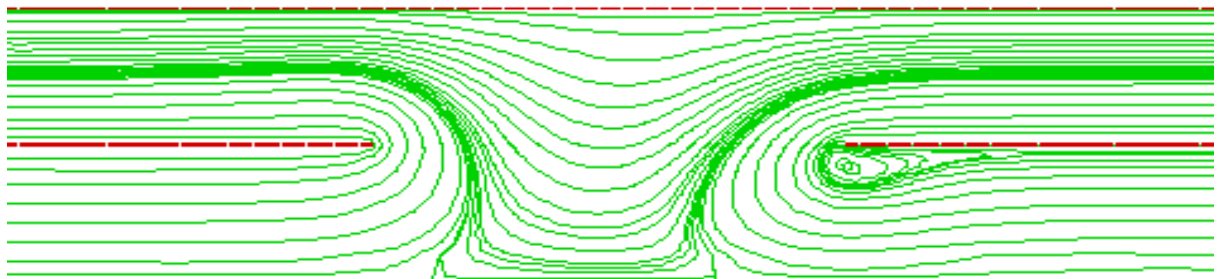
Results for double flow rate in upper arm of a channel are started with unit Reynolds number and very early activity of vortex development near the nip of edge of the central plate in bottom channel arm. Due to double flow rate in upper arm of the channel fluid has been pushed down in the lower channel. At  $Re=10$  vortex grow in size and becomes inclined towards the flow direction towards right. Very late development of other vortex appeared on the top channel at  $Re=50$  and higher Reynolds number. Moreover, the vortex was developed very late for higher values of  $Re$  at the top channel arm near the wall which again pushed down the flow in lower arm in the middle gap of the domain (at  $Re=50$ ). By increasing the value of  $Re$  inertial effects become more visible in the entire computational domain. These all three vortices recirculate and grow in size. These vortices developed at the plate adjust their position by lying horizontally on the plate. These vortices grow in size and shape with same lines of symmetry in both vertical and horizontal directions.

Once again like above unequal (1, 1.5) discussed in section (5.4.1.2). The unequal (1, 2) flow has more dramatic change in the flow structure. Vortices development has been in all three different locations of the computational domain like above discussed flow rate (1, 1.5). The vortexes are present in upper exit, lower exit near the insert plates and in the middle separation gap of the domain. Increasing the Reynolds number has the effect of

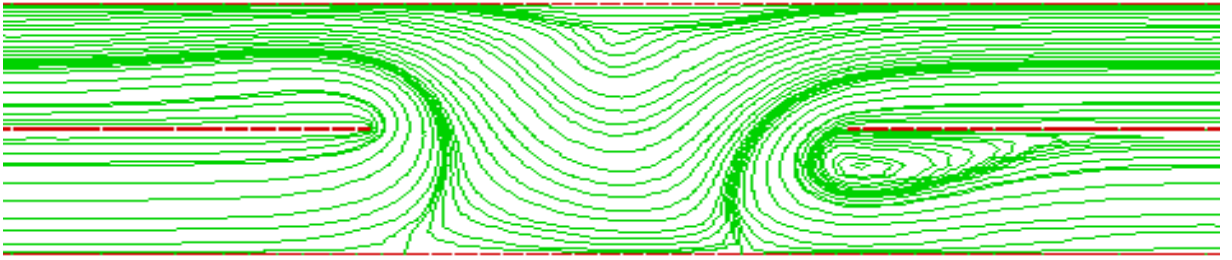
increasing the size, strength and intensity of the vortices as it was observed in unequal flow rate above and form eddies. Mixing and separating fluids have been noticed in the central gap. In all three configurations results are in very good agreement with experimental results.



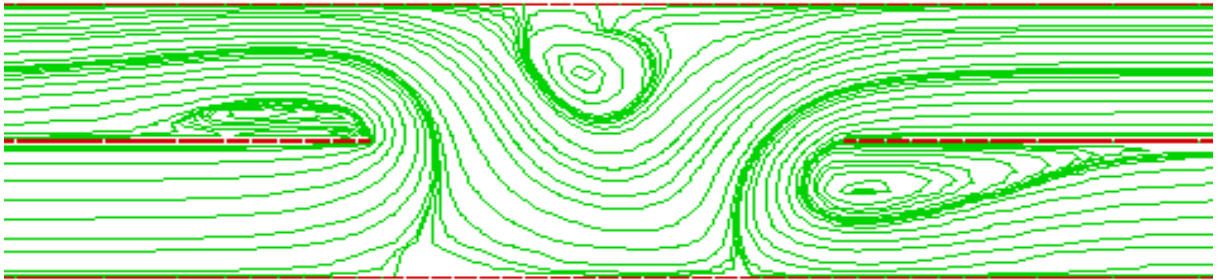
Re=1



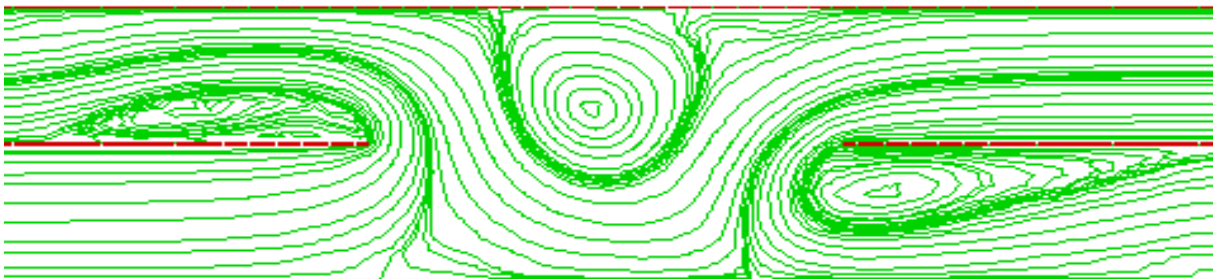
Re=10



Re=25



Re=50



Re=100

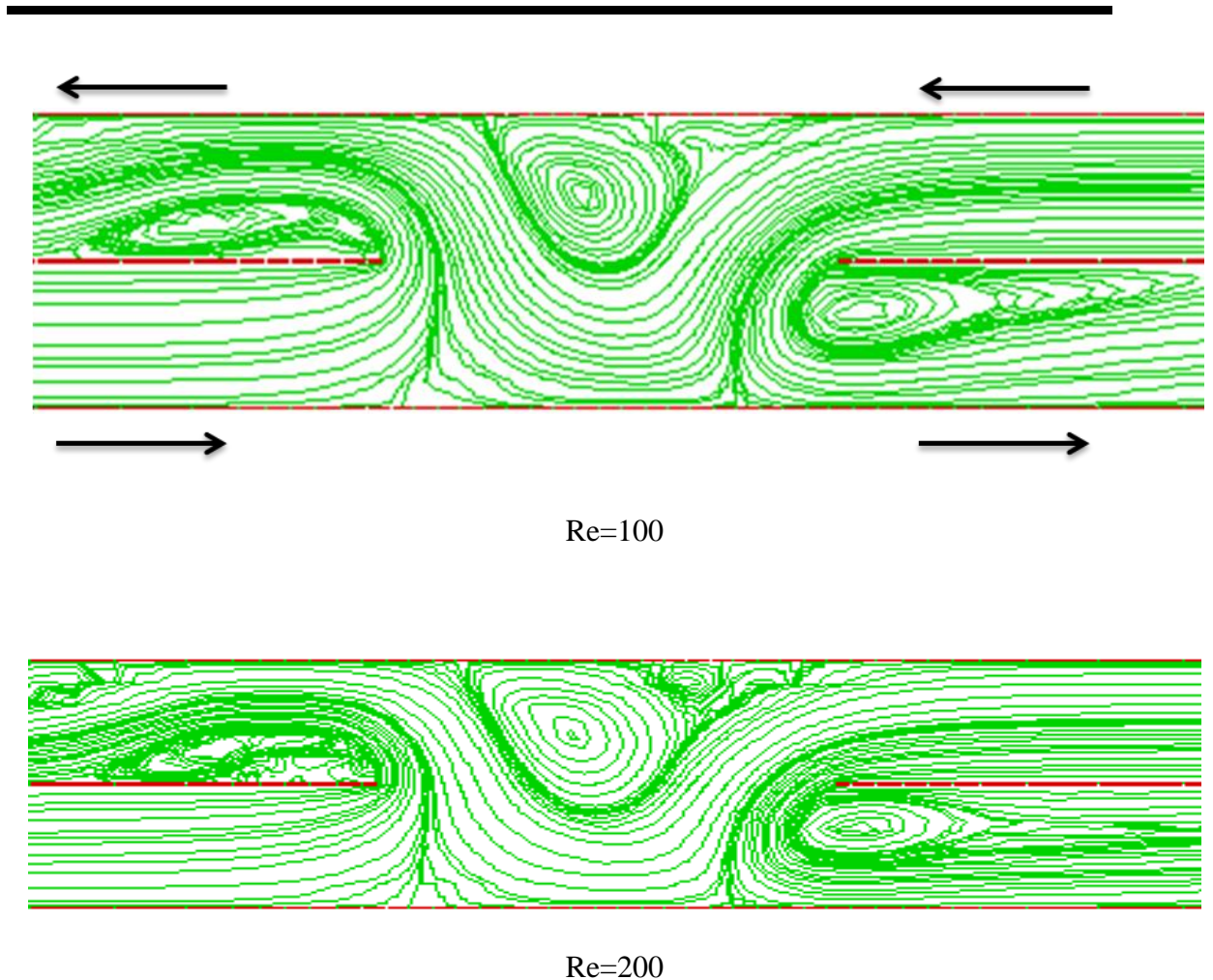


Figure 5.4 Streamline functions for combined mixing and separating of fluid flow for unequal (1, 2) flow rate in both arms of channel, increasing Re from top to bottom.

#### 5.4.1.4 Influence of unequal flow rate on flow structure

In unequal flow rates there is dramatic change in inertial effects of Newtonian fluid flows in a channel filled with non-porous materials. For both unequal flow rates numerical results are presented for in figures [(5.3) to (5.4)] above. Solutions are found for increasing Reynolds number and there is no any evidence of completely reversed flows as compared with equal flow rate. It can be seen that unidirectional flow has been increased as the flow rate changes but reversed flow still exists up to the end. Increase in flow rates in the top arm of a channel has increased the intensity of unidirectional flow

and vortex growth near the one end of a channel arm. That vortex is near the central plate is the bottom arm of a channel has been suppressed/decreased in strength which exits near the other end of centrally positioned plate. Here twin vortex which was appearing in the middle gap of separation gap of plate has changed its position in the top channel arm somewhere in the possible gap available near the upper wall of the channel. It is slowly coming down by pushing the flow in lower bottom channel arm.

By increasing value of Reynolds number vortex pattern diminishes in size and strength and they split into other smaller vortices. That affect is due to the relative flow rates. Furthermore, in contrast with equal flow rates in unequal flow rates have given more rises to vortex generation only in the top channel arm. There is no any evidence of vortex development in bottom channel arm in the middle of the boundary wall. Due to the changing flow rates in upper channel arm vortex in the upper channel near the edge on its left have vanished for initial values of  $Re$ . Very late activity of third vertex have been noticed when  $Re$  reaches up to 50. Flows are mixing and separating in the separation gap but mixing is not like as it was in equal flow rate.

#### **5.4.1.5 Effect of flow rates on pressure difference**

As shown in figure (5.5), non-dimensional scaled pressure verses Reynolds number (Inertia) is presented for Newtonian fluids in combined mixing and separating geometry. For all relative flow rates the value of Reynolds numbers are considered from  $1 \leq R \leq 200$ . For equal flow rate non-dimensional scaled maximum and minimum pressure obtained by current numerical scheme are, for equal flow rate,  $1 \leq p_s \leq 2.8013$ , for unequal (1,1.5) flow rate  $1 \leq p_s \leq 5.6551$ , and for unequal (1,2) flow rate,  $1 \leq p_s \leq 8.4396$

. Results are presented for increasing value of Re against non-dimensional scaled pressure

difference for all three relative flow rates and are scaled by  $p_s = \frac{Re \times \Delta p_{\max}}{(\Delta p_{\max})_{at Re=1}}$ . Where,  $p_s$

is scaled pressure difference,  $Re = \frac{\rho v L}{\mu}$  Reynolds number and  $\nabla p_{\max}$  is a non-

dimensional pressure difference.

It has been observed that increasing relative flow rates have shown effect of increase in pressure difference as presented in the following graph shown in Figure 5-5. In all three flow conditions an increase in pressure has been detected in all three relative increasing flow rates. When all three flow rates compared with each in an increasing order of Re, the change is obvious in figure (5.5). For initial values of Re from Re=1 to Re=50, pressure is minutely changed but for higher values of Re (from 100 to 200) obvious change is appearing. Increase in the value of Re along with relative flow rates in upper arm of a channel have increasing effects on pressure difference.

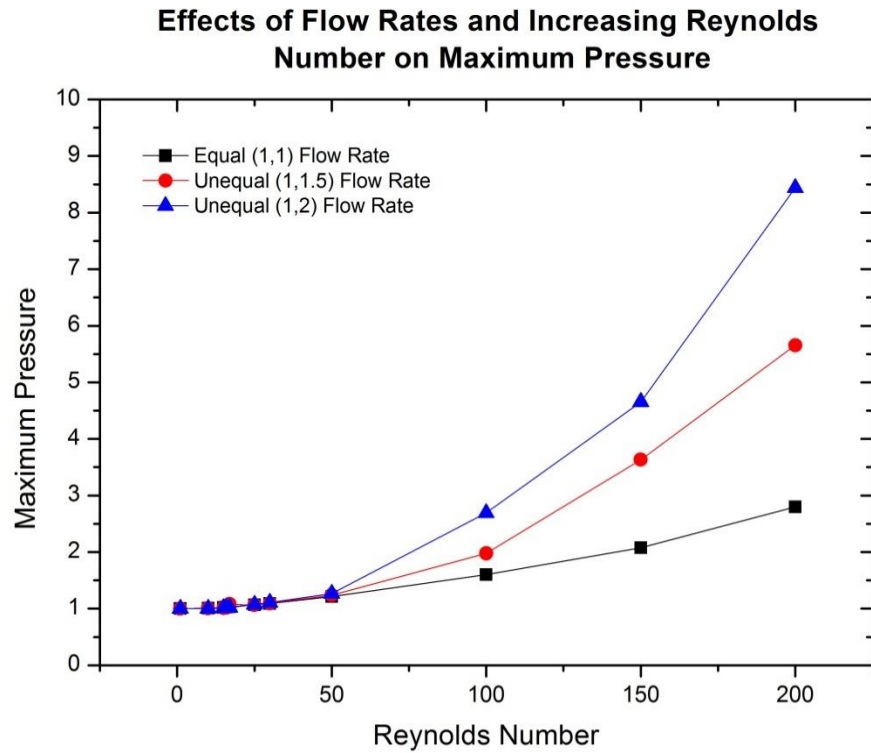


Figure 5.5 Comparison of maximum scaled pressure with increasing inertia at different flow rates in a channel filled with non-Porous Media.

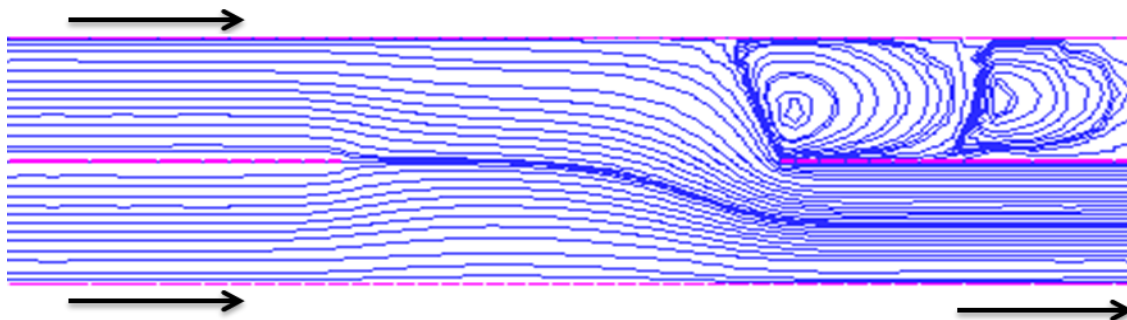
#### 5.4.2 Mixing and separating of Newtonian fluid flows in a channel filled with non-porous media ( $G_2$ )

In section 5.4.1 flow is reversed with two inlets, one in top channel arm from its right and another in bottom from its left. Flows are in opposite directions with other two outlets one from its right in bottom channel arm and other from its left in upper channel arm. Flow directions are shown in figure [5.1 (a)]. In  $G_2$  flow is unidirectional and domain is such that having two inlets from left side in each arm and only one outlet its right in lower arm as in figure [5.1 (b)]. Unidirectional Newtonian fluids have been passed in domain filled without porous media along with varying flow rates in both arms. The same

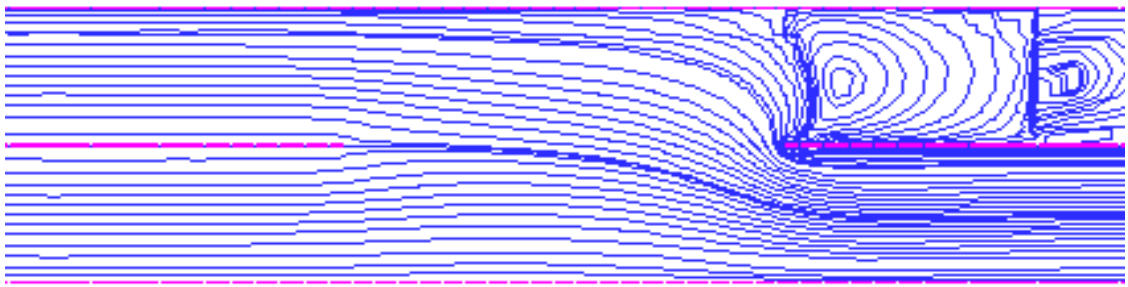
procedure as has been adopted for the presentation of streamline functions as discussed in above in section (5.4.1). In order to understand the effects of the inertia on flow structure and pressure difference flow of Newtonian fluids have been examined with relative flow rates.

#### 5.4.2.1 Equal (1, 1) flow rate

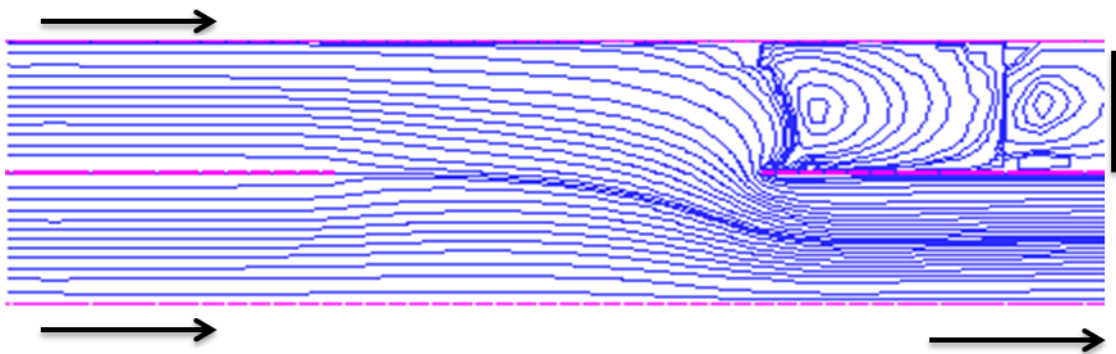
Numerical solutions of Newtonian fluid flows for equal flow rate in both channel arms of Reynolds numbers ( $1 \leq Re \leq 200$ ) are presented in figure (5.6). At  $Re=1$  two big vortices have been produced in downstream of upper arm of a channel to its right side of the computational domain. One vortex is on the nip of the sharp edge of the central plate located on the middle side of the channel on its right and the other is farther to its silent arm. By increasing the value of  $Re$ , vortex on the nip of sharp edge on its above arm of a channel increases in its size as shown in figure (5.6) (at  $Re=20, 30, 50, 100$  and  $150$ ). At  $Re = 150$  another inertial effect has been observed in the bottom channel arm near the central plate towards the exit. At  $Re=200$  both vortices are merged and one weak vortex move horizontally towards the blockage. As fluid flow is unidirectional therefore mixing has been observed in the separation gap and in lower arm of a channel towards the exit.



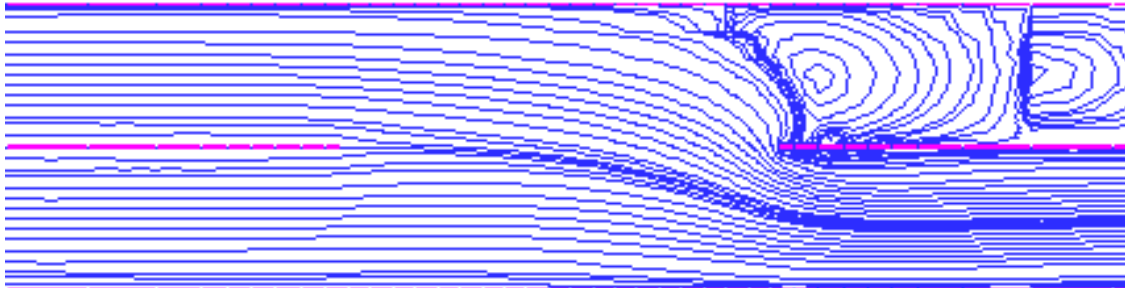
Re=1



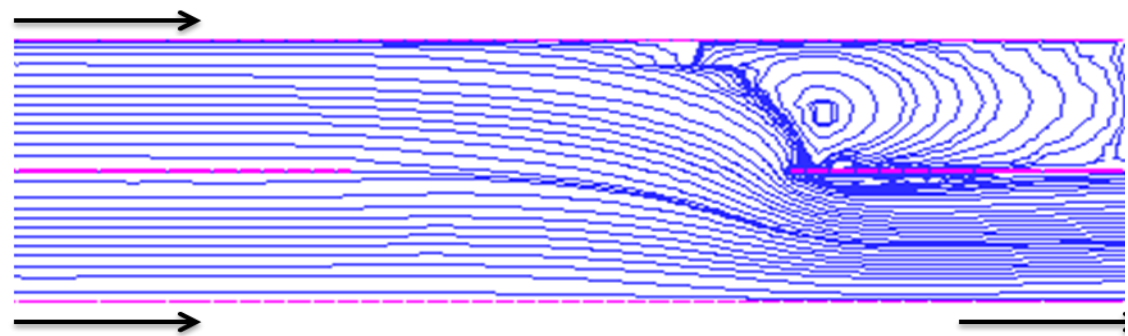
Re=20



Re=30



Re=100



Re=200

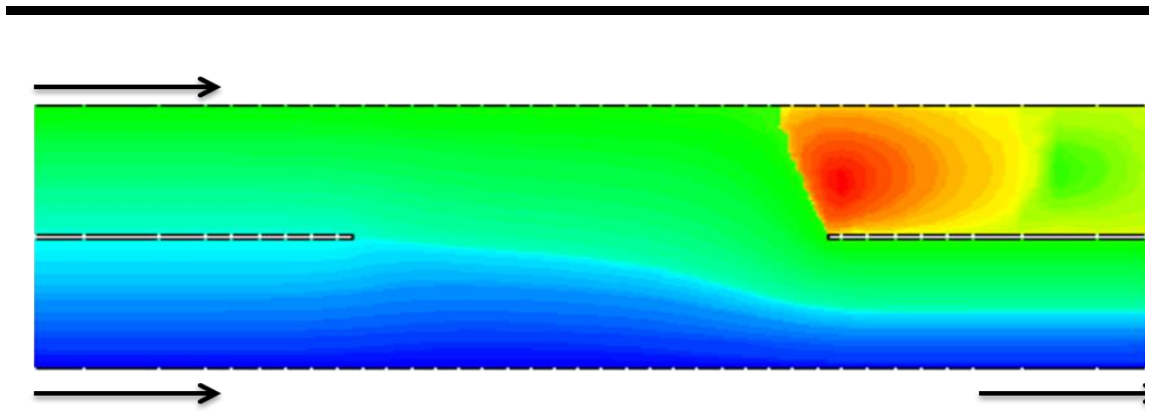
---

Figure 5.6 Streamline functions for unidirectional flows of Newtonian fluids for equal (1, 1) flow rate in both arms of a channel, increasing  $Re$  from top to bottom.

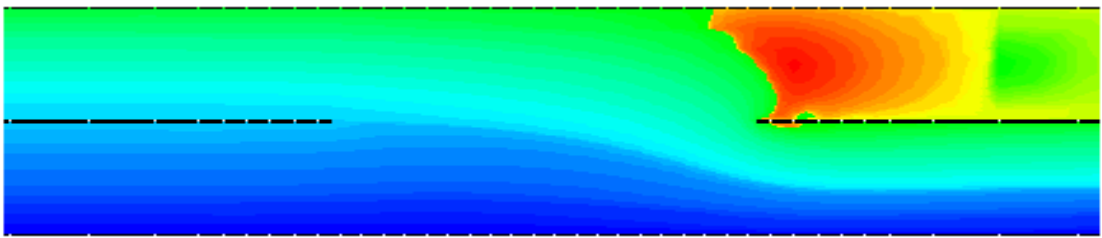
#### 5.4.2.2 Equal (1, 1) flow rate

Numerical Results are presented for same domain from  $Re=1$  to 200 in figure (5.7). The flow rate has been increased in upper channel to monitor change in inertia and mixing of fluids. Almost identical effect has been observed except one vortex development in lower arm near the inserted plate in the centre of the domain towards the exit. This vortex is stronger and bigger in size as compared with the one appeared in equal flow rate discussed in section (5.3.2.1). The same mixing effects have been monitored as was the case in equal flow rate. Early activity of vortex development has also been observed for lower Reynolds number. That vortex appeared near the centrally located plate on its right during increased value of Reynolds at  $Re=150$ . Vortex developed in silent arm has been a little bit pushed towards silent downstream of the top channel arm.

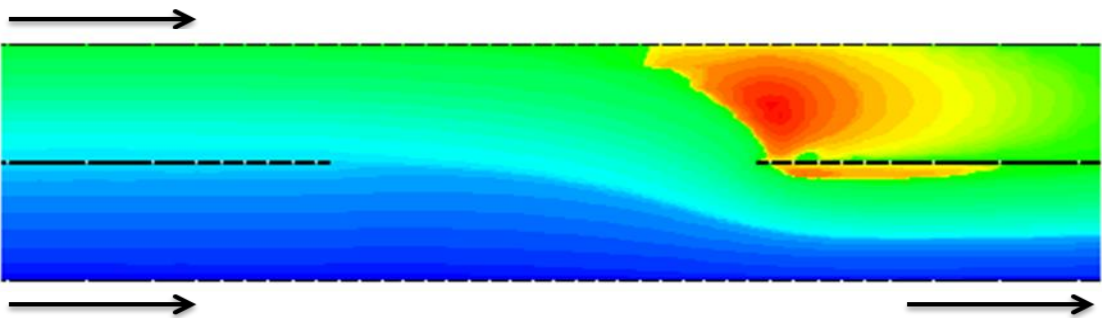
During varying flow rate merging of two vortices becomes too early with the increasing flow rate. The same mixing effects have been found as with of equal flow rate. Numerical results are compared with the experimental and numerical results produced by (Cochrane et al., 1981) and results presented are in very good agreement them. Comparisons of numerical results with experimental are given in chapter nine in figures [(9.1)-9.2] in chapter 9.



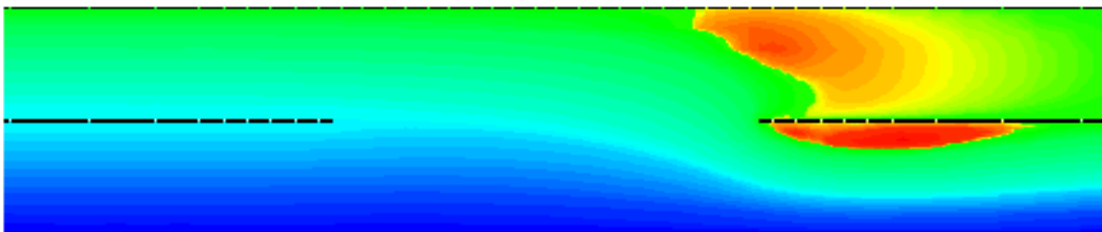
$Re=1$



$Re=50$



$Re=150$



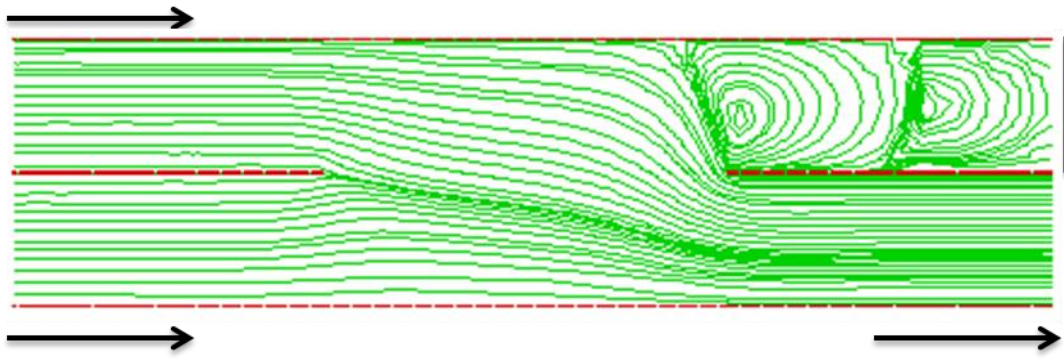
Re=200

Figure 5.7 Streamline functions for combined mixing and separating of fluid flow for unequal (1, 1.5) flow rate in both arms of channel, increasing Re from top to bottom.

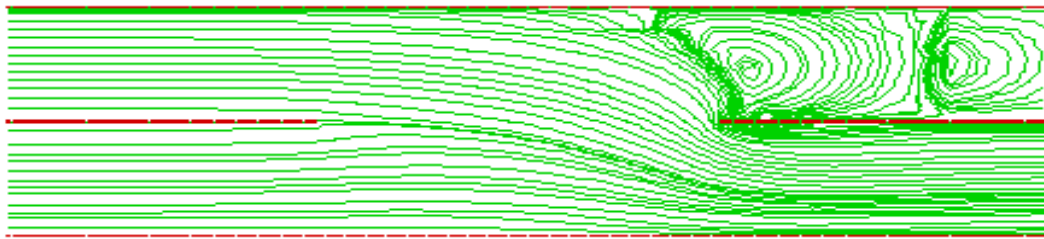
#### 5.4.2.3 Unequal (1, 2) flow rate

With fluid flowing rate is double in upper arm of a channel to see mixing and inertia effects. In Figure (5.8) numerically simulated results are presented form an identical unidirectional domain. From Re=1 to Re=150 same effect as have been observed except little bit more push to fluids in salient corner of the domain. At Re= 100 two vortices appeared in the silent corner merged more early i-e. At Re=100 as compared to above two flow rates in the same situation discussed in sections [(5.3.2.1) to (5.3.2.2)]. Moreover, another weak vortex influence has been seen in lower channel arm near the centrally positioned plate.

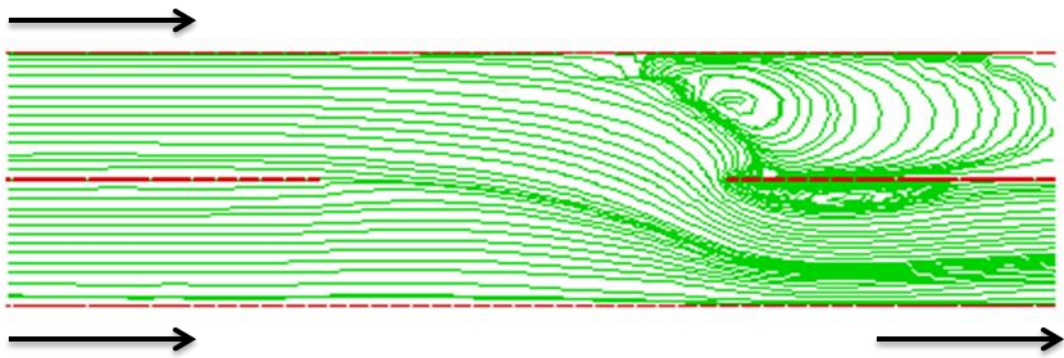
At Re=150 fluid has been pushed high on into a silent corner due to the double flow rate in upper arm of the channel. It is matter of common sense that fluid should be pushed there and it proves the strength of our numerical scheme and stability of the developed code. The vortex developed near the central plate grow in its size and adjust its position on the plate and moves towards the exit (at Re=150). The merged vortex breaks up into two vertices and these new vortices grow in its size and length. Mixing effects are literally same as observed in above two cases discussed in sections [(5.3.2.1) to (5.3.2.2)].



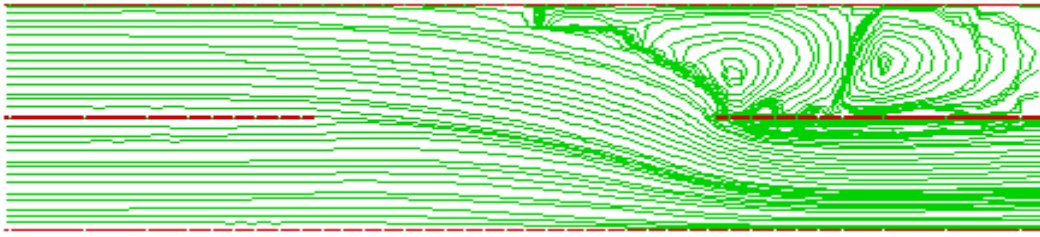
Re=1



Re=50



Re=100



Re=200

Figure 5.8 Streamline functions of unidirectional flows Newtonian fluid for unequal (1, 2) flow rate in both arms of channel filled with non-porous media, increasing Re from top to bottom.

#### 5.4.2.4 Effects of flow rate

For different flow rates numerical simulations of unequal [i.e. (1, 1.5) and (1, 2)] numerical results are shown in figures [(5.7) to (5.8)] for flows of Newtonian fluids in a channel filled with non-porous media. Changing flow rates has effects on early development of vortices and some push to fluid in silent corners of the domain in upper downstream towards blockage. Early merging of two vortices developed in the silent corners has been observed as compared to equal flow rates in both channel arms. In unidirectional flow one more stable vortex has been developed near the central position plate towards the exit of a bottom channel arm. More inertia has been noticed due to changing flow rates in upper channel arm. Merged vortices again break up into two by increasing the value of Re. Similar mixing effects were seen as those in equal flow rate.

#### 5.4.2.5 Effect of increasing inertia and flow rates on pressure

In figure (5.9), non-dimensional scaled pressure difference versus Reynolds number (Inertia forces) is presented for Newtonian fluids in combined mixing and separating geometry. For all relative flow rates the value of Reynolds numbers are considered from  $1 \leq Re \leq 200$ . For three different flow rates non-dimensional scaled maximum and minimum pressure difference were obtained, which are for equal flow rate  $1 \leq p_s \leq 2.4255$ , for unequal (1,1.5) flow rate  $1 \leq p_s \leq 2.5365$ , and for unequal (1,2) flow rate  $1 \leq p_s \leq 2.6374$ . Pressure difference for all three relative flow rates have been scaled the same way as above discussed in section (5.4.1.5).

Newtonian fluid flows in three relative flow conditions give an increase in pressure with increasing the values of Reynolds number. In this case pressure increases smoothly as compared to the relative flow rates of  $G_1$  discussed in section (5.4.1.5) and shown in Figure 5-5. In this situation as flow is unidirectional therefore increase in pressure difference is linear in nature as compared to reversed flow discussed in section (5.4.2.5) above. Compare figures [(5.5) to (5.9)].

On lower values of inertia there is no dramatic change but with further an increase the higher values of inertia show a significant change as depicted in below graph from lower to higher values of Reynolds number. In unidirectional flows curve of the flow rate is smooth. But in case of reversed flow pressure show more inertia effects for specially for higher values as show in figure (5.9) (from  $Re=100$  to  $Re=200$ ). In figure (5.9) pressure ranges from 1 to 3 units and in this case it is within 1 to 3 units. From  $Re=1$  to 50 there is

less variation but in the range of higher values of  $Re$  (at  $Re=100$  to  $200$ ) pressure shows obvious change.

### Effects of Flow Rates and Increasing Reynolds Number on Maximum Pressure

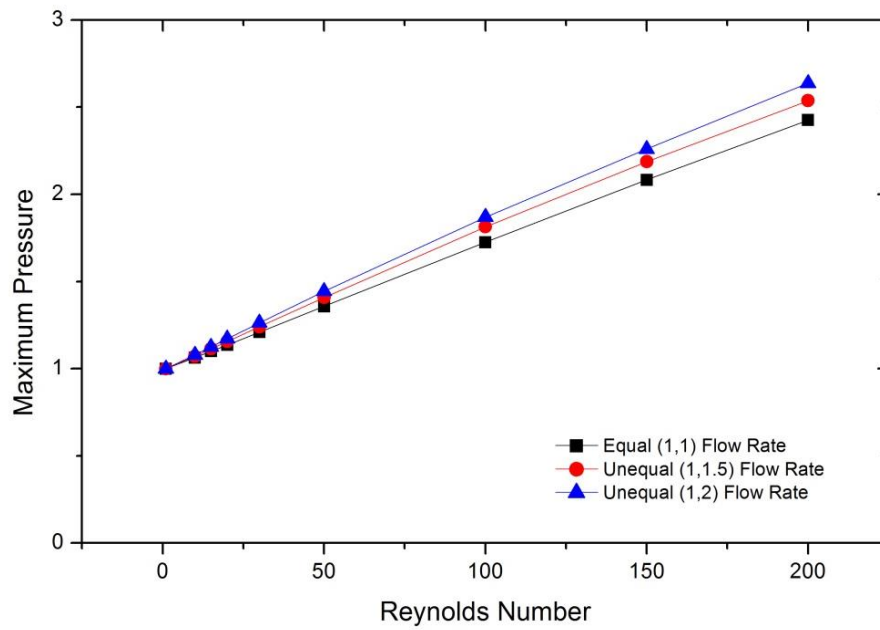


Figure 5.9 Comparison of maximum scaled pressure with increasing inertia at different flow rates in a channel filled with non-Porous Media

#### 5.4.3 Mixing of separating of Newtonian fluid flow in a channel filled with non-porous media ( $G_3$ )

In this configurations domain is having two inlets in opposite directions, first from its right in top channel arm and another from its left in bottom channel arm. In this setting outlet is only one and it is from right in bottom channel as shown in Figure [5.1(c)]. Numerical solutions of that reversed flow for Newtonian fluid in a channel filled with no porous media in it are presented in figures [(5.10) to (5.12)] for relative flow rates. The numerical results are analysed by presenting streamline patterns, which are plotted at an

equal interval in two flow regions for reversed flows. In this section in similar way as discussed in sections (5.4.1) and (5.4.2) flow rates have been changed in both arms to observe its special effects on flow structure. Effects of inertia, intensity, size and length of vortex development in flow structure and pressure difference have been discussed in the section.

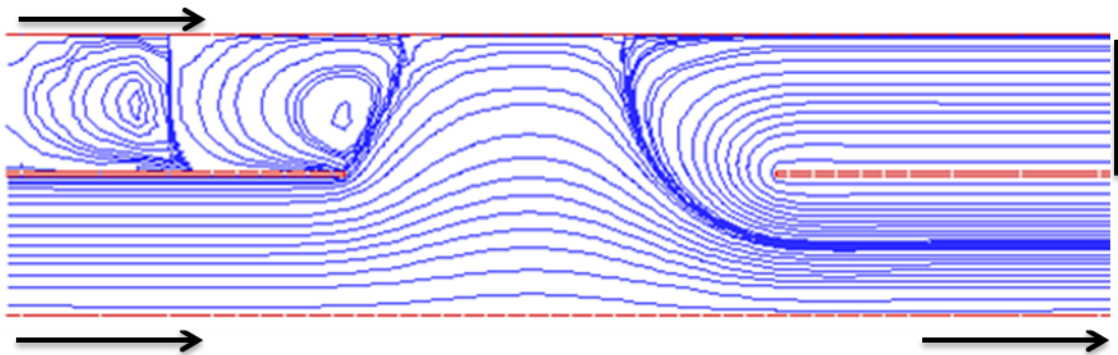
#### **5.4.3.1 Equal (1, 1) flow rate**

The numerical calculations are shown for equal (1, 1) in figure (5.10) with the increasing Reynolds numbers ( $1 \leq Re \leq 200$ ) for different flow bifurcations. It is observed that the fluid responds to the presence of the gap and immediately breaks up, with flow mixing in both upper and lower exit sections of the geometry as it has been seen in other settings discussed in sections (5.4.1) to (5.4.2). From  $Re=1$  to  $Re=15$  two strong vortices have been seen in the downstream of the above arm of the channel and the flow in above channel has been pushed towards the wall of upper arm of a channel in the middle gap of a domain. At  $Re=30$  one vortex has stretched horizontally in the whole middle gap of the top channel arm and the flow has been pushed to be reversed in the lower channel towards to the exit. Moreover, at  $Re=30$  a new activity of vortex development can be seen in the lower channel arm near the central plate at nip of it.

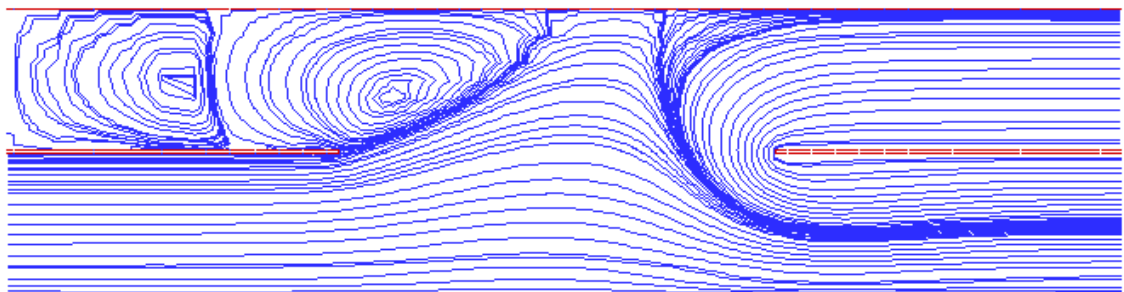
At  $Re=50$  another inertial effect has been noticed in the top channel arm near the wall. By increasing the value of inertia vortex grows in size and moves towards the lower channel arm and also pushes the flow in the lower arm of a channel (at  $Re=100$ ) in figure (5.10). At  $Re=150$  third vortex develops in the salient corner of the top arm. All other four vortices established in different locations of the domain, nurture in size and firm their

positions by moving horizontally and vertically. The third vortex developed in a upper channel arm on its left side in its downstream merged into one with second vortex near to it (at  $Re=200$ ) in figure (5.10).

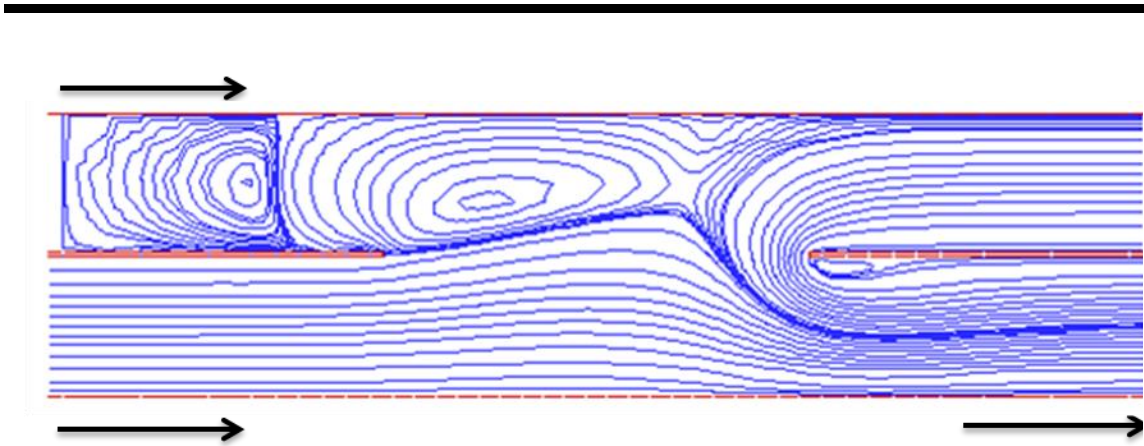
Changing flow directions of the fluid flows has shown their effects as increasing inertia in the computational domain especially in upper arm of a channel. Increasing the value Reynolds number has shown more inertial effects and has further strengthened the shape and size of vortices noticed in different locations. Flows are both reversed and unidirectional up to  $Re=200$ . Mixing and separating of fluids have been observed in the middle gap and in lower channel arm.



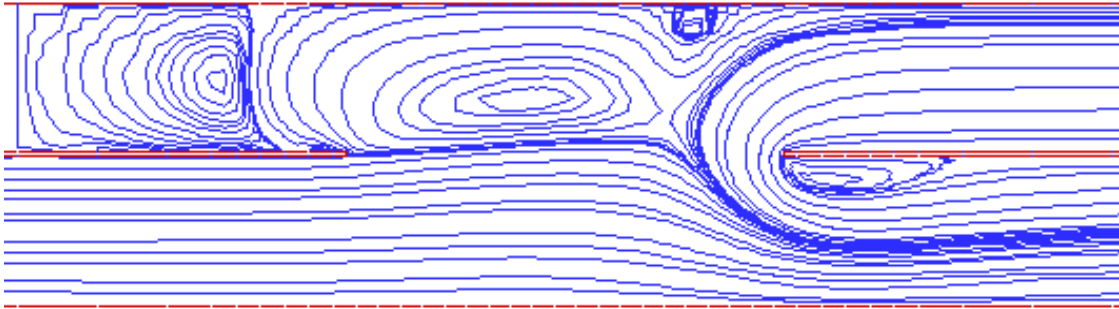
Re=1



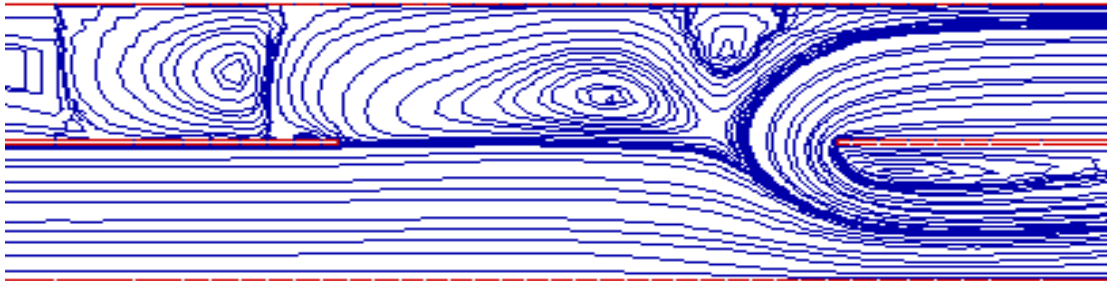
Re=15



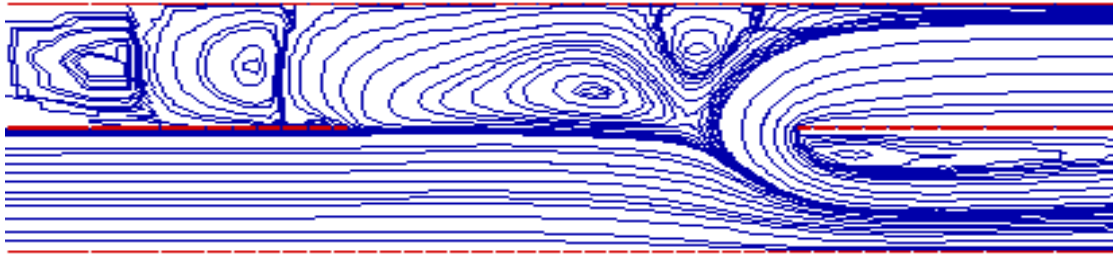
Re=30



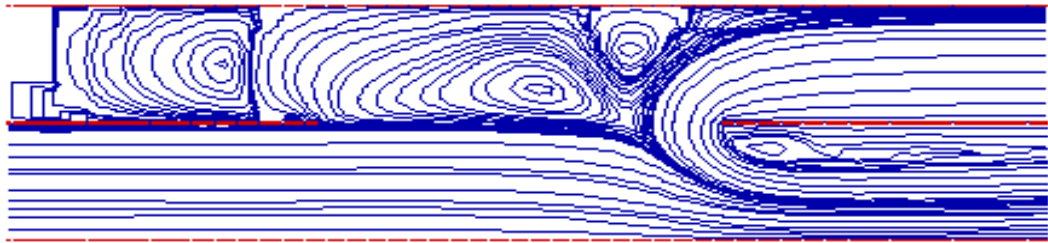
Re=50



Re=100



Re=150



Re=200

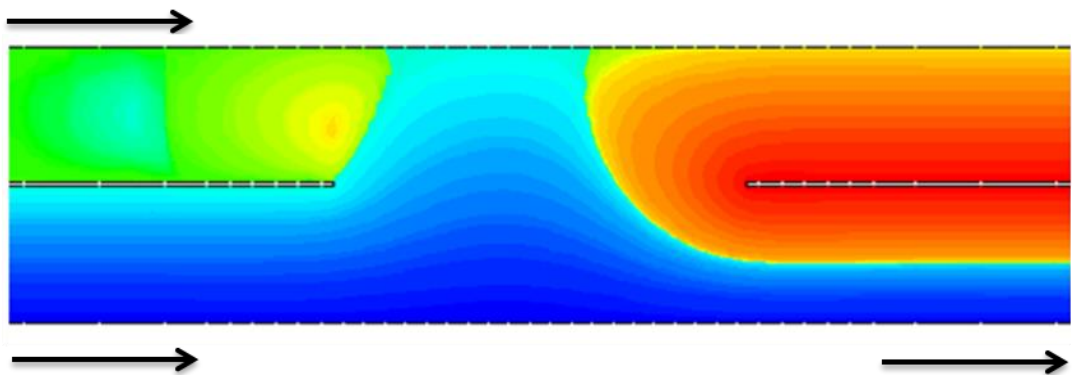
Figure 5.10 Streamline functions for combined mixing and separating of Newtonian fluid flows for equal (1, 1) flow rate in both arms of channel filled with non-porous media, increasing Re from top to bottom.

#### 5.4.3.2 Unequal (1, 1.5) flow rate

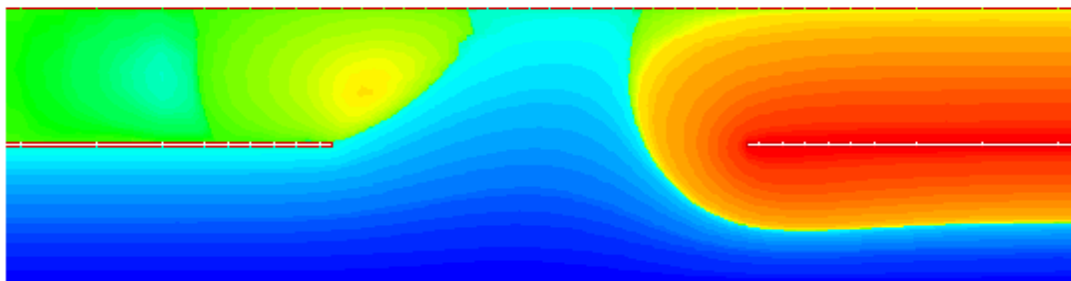
In unequal (1, 1.5) flow rate, numerical results for Newtonian flows in a channel filled with non-porous media are displayed in figure (5.11). In this section the flow has been increased in top arm of the channel to detect its special effects on flow design of the computational domain. Almost the same influence has been seen in vortex progress from  $Re=1$  to  $Re=20$  as shown in figure (5.9) of equal (1, 1) flow rate. Although an early

activity of vortex growth has been noted in lower channel towards exit near at the sharp edge of a central inserted plate (at  $Re=15$ ).

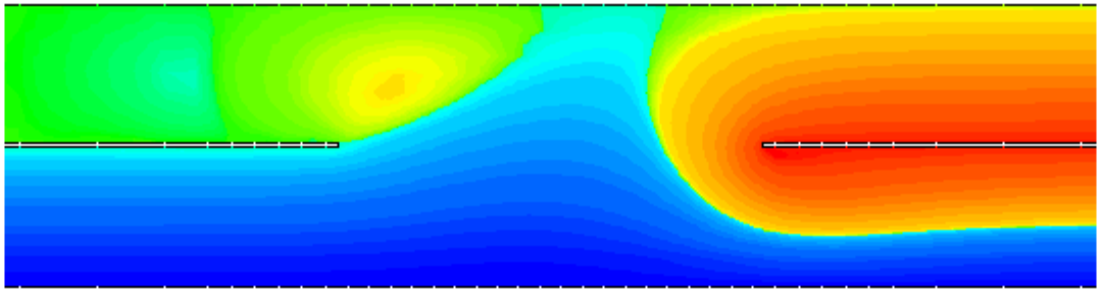
Further increasing the value of  $Re$  has given rise to more vortex development and intensity in its growth and size. Flows are both unidirectional and reversed but presence of unidirectional flows have pushed the flows back to lower channel by the growth in the size of vortices appeared in the top channel arm. The Same effects of splitting and merging again have been observed in the top channel arm in its salient corners as shown in figure (5.10). Mixing and separating appear either in upper arm or lower arm towards the outlet of the channel.



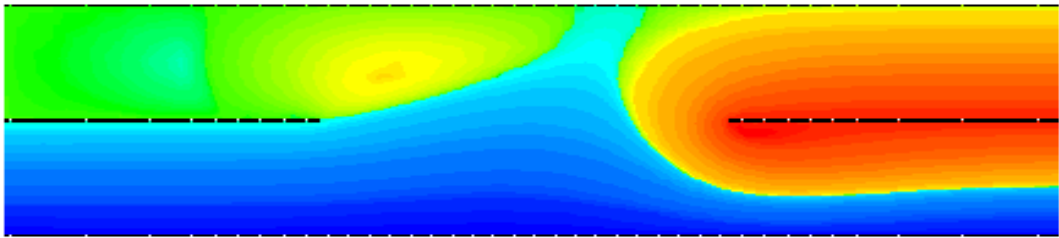
$Re=1$



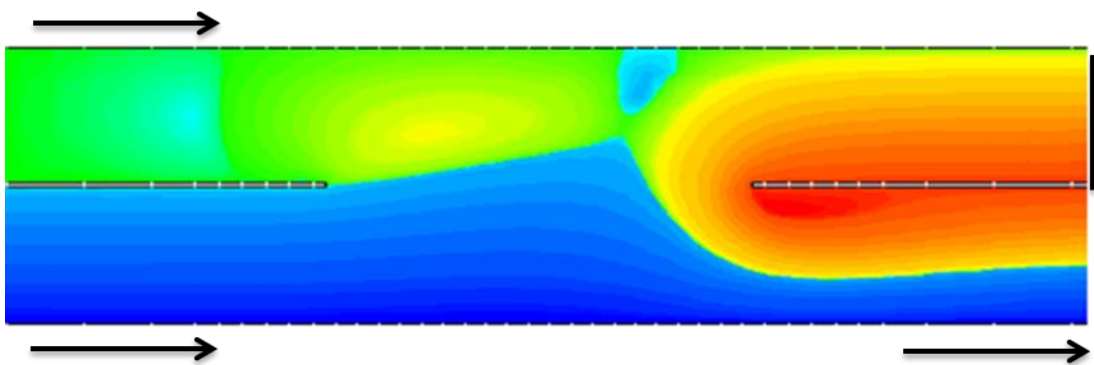
$Re=10$



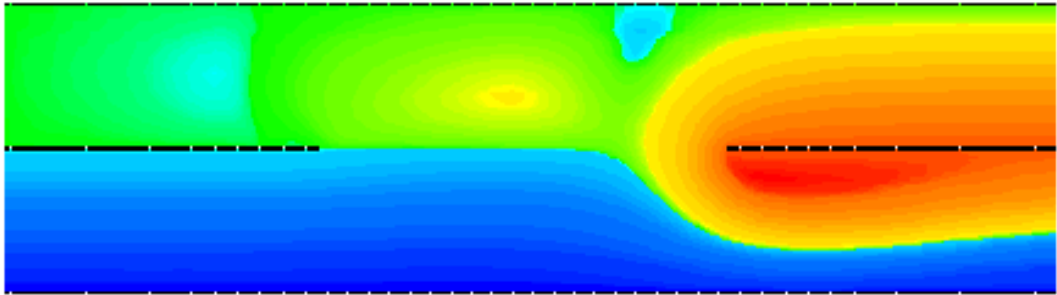
Re=15



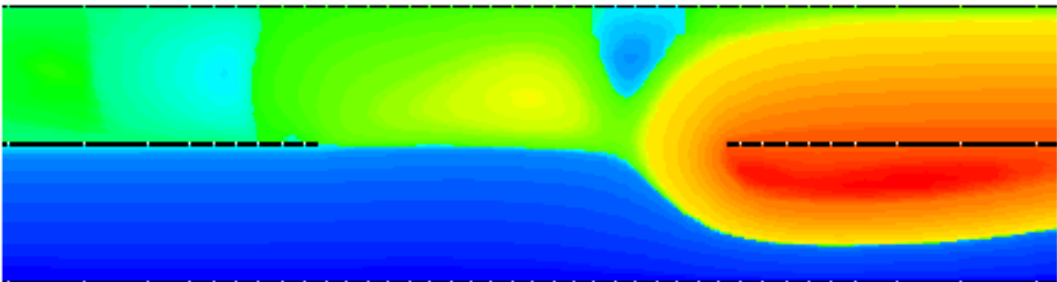
Re=20



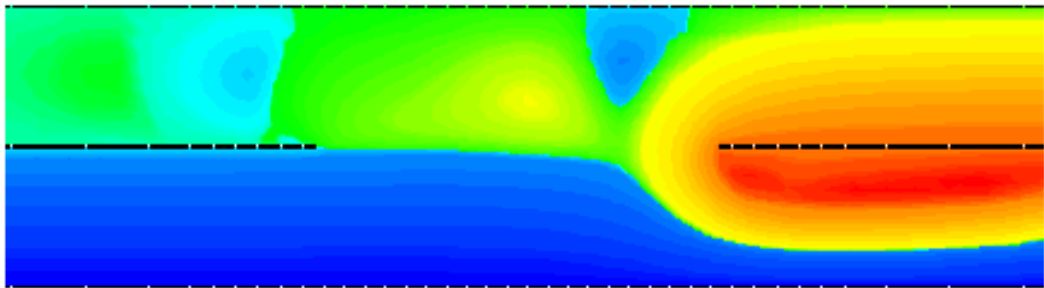
Re=30



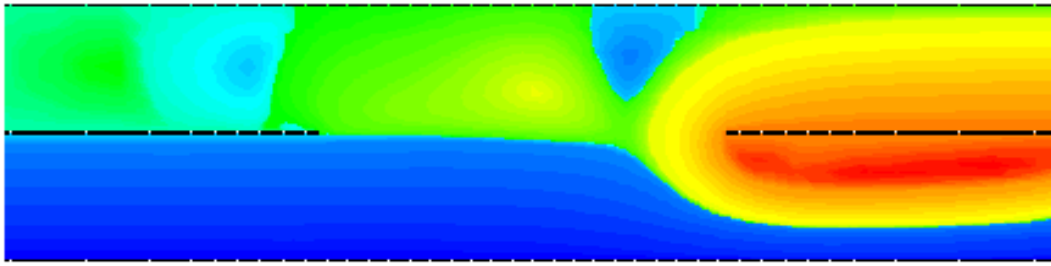
Re=50



Re=100



Re=150



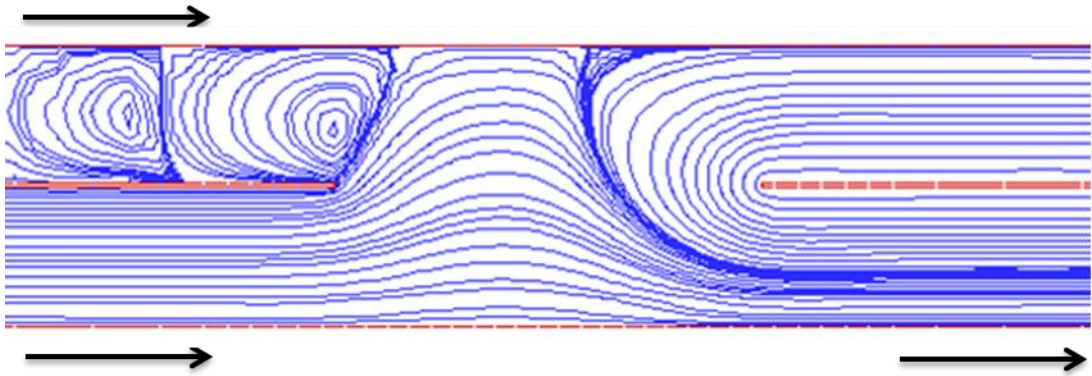
Re=200

Figure 5.11 Streamline functions for combined mixing and separating of Newtonian fluid flow for unequal (1, 1.5) flow rate in both arms of a channel, increasing Re from top to bottom.

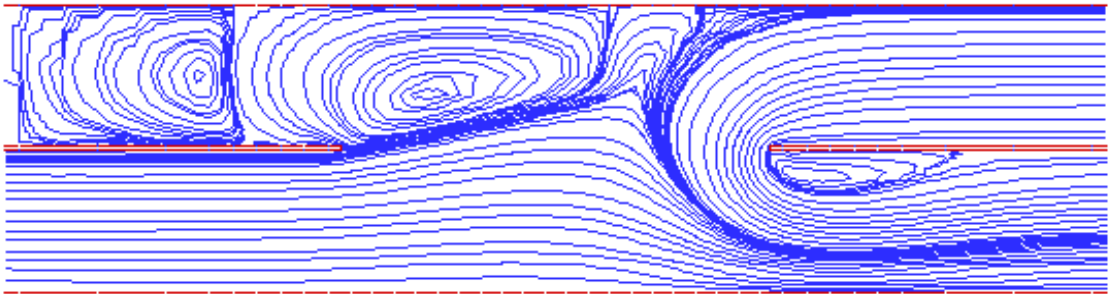
#### 5.4.3.3 Unequal (1, 2) flow rate

In this case flow rate in upper channel arm has been increased to its double when compared with the flow rate in its lower arm. A numerically simulated result for this purpose has been presented in figure (5.12) for same channel with the same settings except from the change in flow rate in the top arm. For value of  $Re=1$  to 20 the same effects of inertia have been noticed. For all other increasing number of  $Re$  same effect of vortices has been noticed except the raise more in size and in its adjusted shape as shown in figures [(5.10) to (5.11)]. Compare these similar effects as are shown in figures [(5.10) to (5.11)]. For higher values of  $Re$ , unidirectional flow in the bottom arm has been suppressed and has given strength to the reversed flow to the outlet of the channel fixed in the lower arm. Similar effects of inertia have been observed by changing flow rate in upper arm when compared to unequal (1, 1.5) flow rate discussed in section (5.3.3.2),

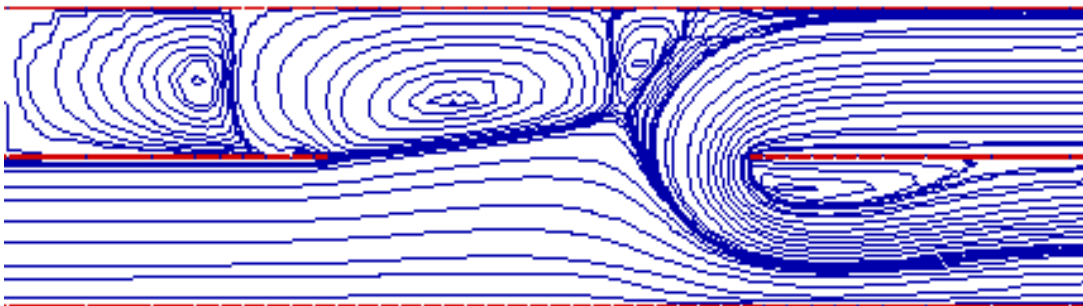
except unidirectional flow has been reduced in bottom arm towards its exit. Mixing only appears in either separation gap or in the lower channel in the downstream towards exit.



Re=1



Re=20



Re=30

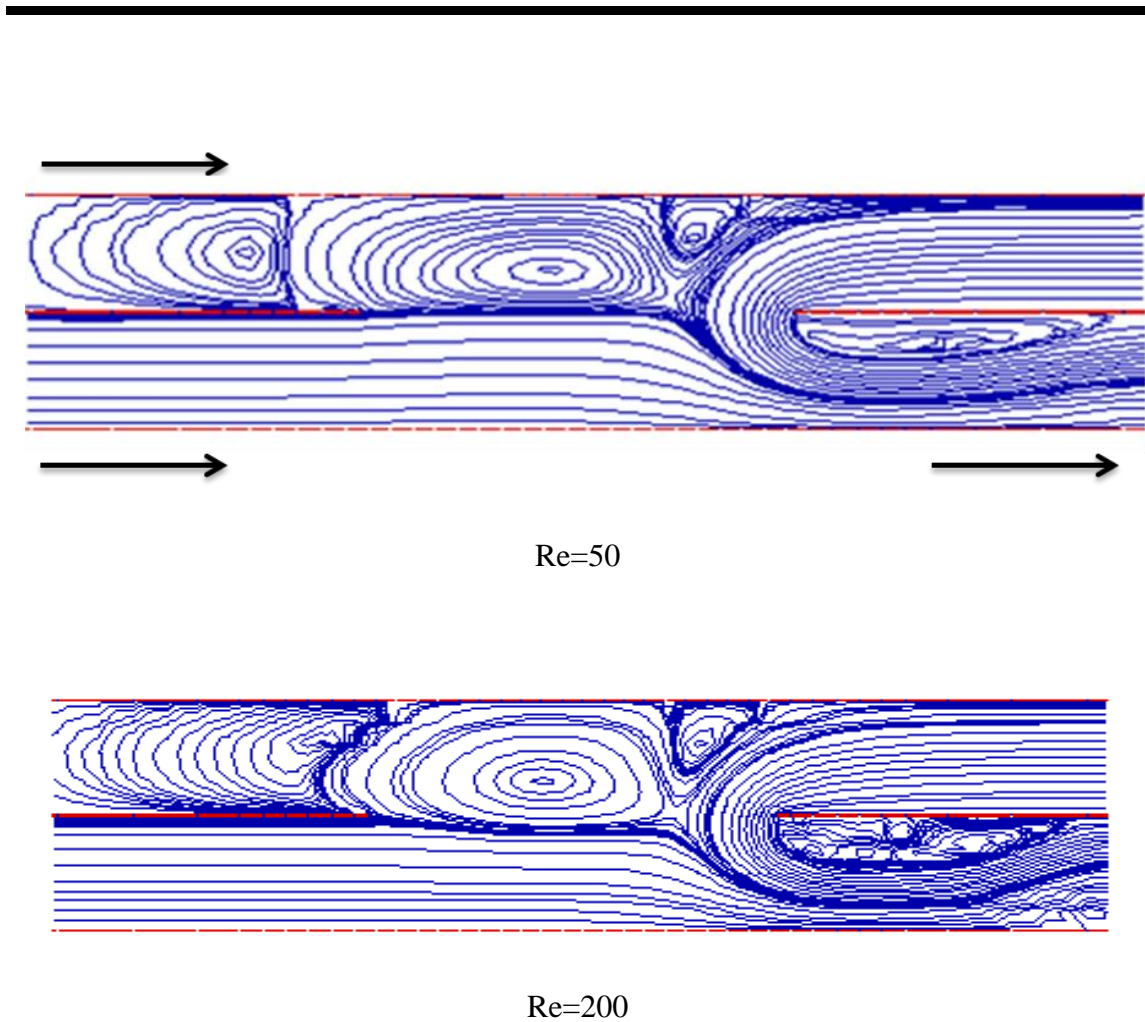


Figure 5.12 Streamline functions for combined mixing and separating of Newtonian fluid flows for equal (1, 1) flow rate in both arms of channel filled with non-porous media, increasing Re from top to bottom.

#### 5.4.3.4 Effects of flow rate

For different flow changing rates numerical simulation results for unequal flows of [i.e. (1, 1.5) and (1, 2)] in a channel filled with no porous media are given in figures [(5.11) to (5.12)]. Here reversed and unidirectional flows have been observed for both unequal flow

rates in the channel. Changing flow rate in upper arm has given rise to the early activity of vortex development as compared with the equal flow rate.

Increasing the value of  $Re$  has more effects of inertia as it can be seen from the growth in size, splitting and merging of vortices in the salient corner of the upper arm. Changing flow rate in the upper arm of the channel i-e from unequal (1, 1.5) to (1, 2) have suppressed the unidirectional flow in the lower arm in the downstream towards its outlet. Most of the mixing and separating have been seen either in lower arm or in the middle gap of the domain.

#### 5.4.3.5 Effects of increasing inertia on pressure difference

Results from Newtonian fluid flows are presented in figure (5.13) under the reversed flow condition with dual-inlet/single outlet for different flow rates in a channel [as shown in figure 5.1(c)]. In three different flow rates non-dimensional scaled maximum and minimum pressure obtained are, for equal (1, 1) flow rate  $1 \leq p_s \leq 5.8078$ , for unequal (1, 1.5) flow rate  $1 \leq p_s \leq 8.7263$ , and for unequal (1, 2) flow rate  $1 \leq p_s \leq 11.0048$ . In all three flow situations the values of Reynolds number are considered  $01 \leq Re \leq 200$  to monitor the influence of inertia and flow rates on pressure. Results of pressure difference verses Reynolds number shown in figure (5.13). Pressure difference are scaled and shown in vertical axis, whereas Reynolds number are in horizontal directions.

It is obvious in figure (5.13) the non-dimensional pressure difference increases with the increasing flow rates and varying values of Reynolds number. A pattern of the graph of pressure difference verses Reynolds number against flow rates show the same change as was observed in reversed flow direction discussed in section (5.4.1.5). The effects of

increasing inertia and flow rates are the same in the reversed flow conditions as shown in figure (5.5) and figure (5.13). Scaled pressure difference are directly proportional to Reynolds number because with increasing  $Re$  pressure difference increases. Pressure difference in relative flow rates are also depending on Reynolds number. Increase in the value of  $Re$  increases pressure difference in respective flow rates. As shown in figure (5.13), values of pressure difference in unequal (1, 1.5) are flow are higher than equal (1, 1) flow rate. Whereas values of pressure difference in unequal (1, 2) flow rate are greater than unequal (1, 1.5).

Pressure is directly affected by increasing inertia. Pressure is also affected by flow rates. The reversed flow rates have significant effects as compared with unidirectional flow compare figures [(5.5) and (5.13)] with figure (5.9). Reversed and unidirectional flows are depending on Reynolds number. Increase in the value of  $Re$  increased the scaled pressure but that increase is higher in case of reversed flow case. From  $Re=1$  to 50 there is no obvious dramatic change but from  $Re=100$  to  $Re=50$  it is very clear and depicted in graph.

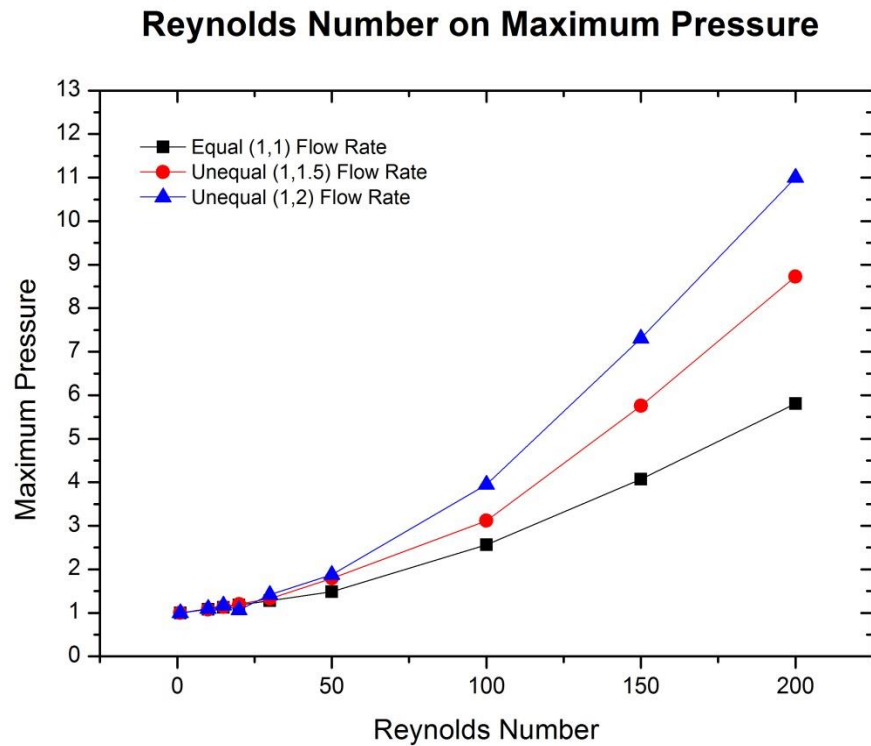


Figure 5.13 Comparison of maximum scaled pressure with increasing inertia at different flow rates in a channel with non-Porous media.

#### 5.4.4 Unidirectional flow of Newtonian fluid in a channel filled with non-porous media ( $G_4$ )

This configuration of unidirectional domain is having one inlet from the bottom arm from its left and one outlet from its right in the top channel arm as shown in [figure 5.1(d)]. It is obvious from the domain settings only equal flow rate could flow in each arm. The fluid flow enters from one arm and exits from the other. Numerical results for unidirectional flows of Newtonian fluids in a channel filled with non-porous medium are displayed in figure (5.14). The numerical solutions are analysed by presenting streamline patterns, which are plotted at an equal interval in two flow regions for unidirectional flows. Newtonian fluid Flows have been passed once again in the channel filled with non-

---

porous media with changing flow directions. The effects of inertia and their influence on pressure difference are discussed.

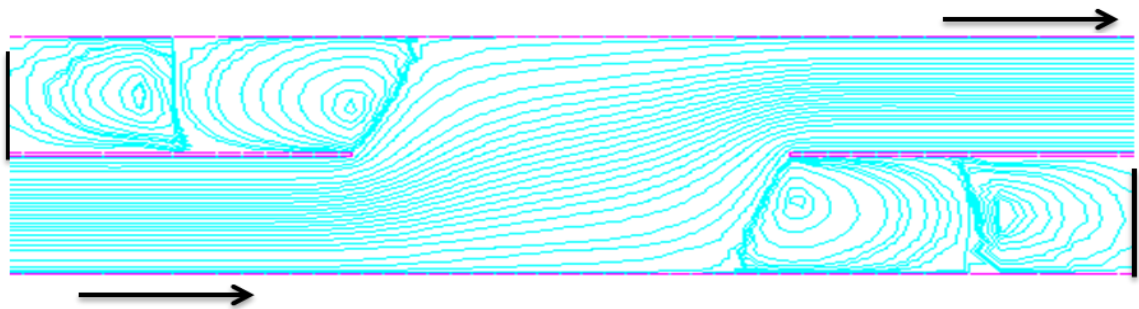
#### 5.4.4.1 Effects of inertia on flow structure

Figure 5-14 shows numerical results for the values of  $Re$ , from ( $1 \leq Re \leq 500$ ). Newtonian fluid flows in the channel filled with non-porous media are presented with streamline functions along with pressure difference. In order to understand the effects of inertia simulation are started with Reynolds number. At  $Re = 1$  a very strong and early growth of vortices in the salient arms of a channel near the sharp edge have been noticed. Vortex appeared on the top channel arm on the nip of a central plate grow in its size and started moving horizontally towards the middle gap in the top arm towards the exit as shown in figure (5.14) [at  $Re$  10, 25, 50, 100]. At  $Re=300$  a vortex developed near the central edge in lower channel also has started moving horizontally along with the wall of the channel.

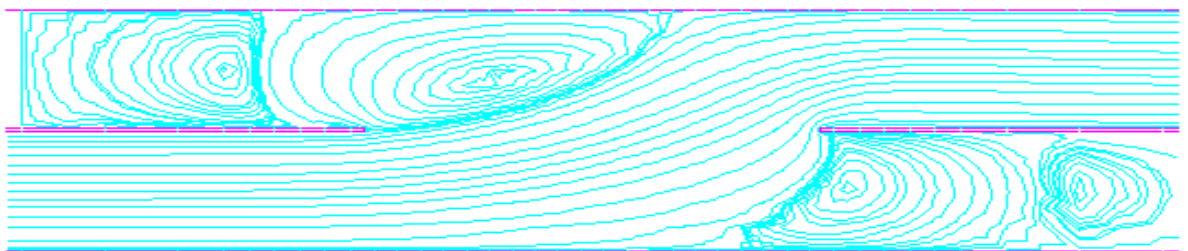
At  $Re=200$  third vortex has been noticed in the upper arm in its blockage side. That vortex grows in size vertically as well as horizontally and the intensity of recirculation of vortex has broken it into other smaller vortices. These vortices have given rise to formation of an eddy in the top arm of a channel. With an increase in the value of Reynolds number these small vortices formed a strong eddy which adjusted its position between solid boundary walls and thin insert plates placed in the middle of the geometry. That eddy further stretched in the direction of flow towards the exit. The growth of an eddy was observed in the horizontal direction of top channel arm. As the flow is coming from bottom arm of the channel and it is not giving it space to come down towards the gap. Above of it is a solid boundary wall which suppresses the developed eddy to down.

Enhancement of grown vortex/eddy is in horizontal direction in the direction of flow. That eddy has inclined towards exit due to flow direction that is the natural process.

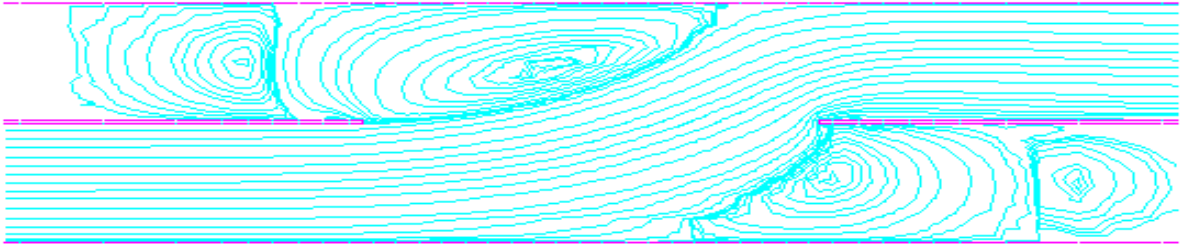
The vortex stretch is more in horizontal direction towards salient arm of the channel because the flow from its left suppresses its growth in that direction. Finally, that strong vortex adjusts its position on the boundary wall of bottom arm and form an eddy. It is observed that power of recirculation and its formation in size and shape of an eddy in the salient arm of top channel is strong. It could be compared with the other vortices near the insert plate in salient bottom arm of channel. Here study can find very strong behaviour of recirculating vortices with an increasing value of  $Re$  behind the centrally positioned insert plates as evident from figure (5.14). For the higher values  $Re$  the process of meandering has been noticed in the end.



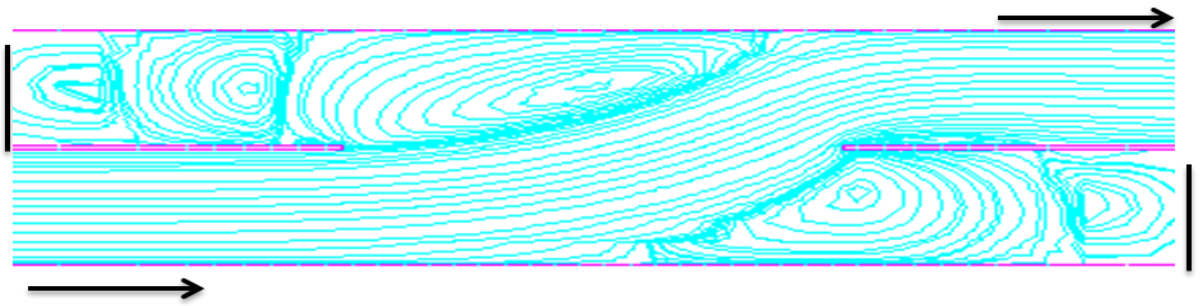
$Re=1$



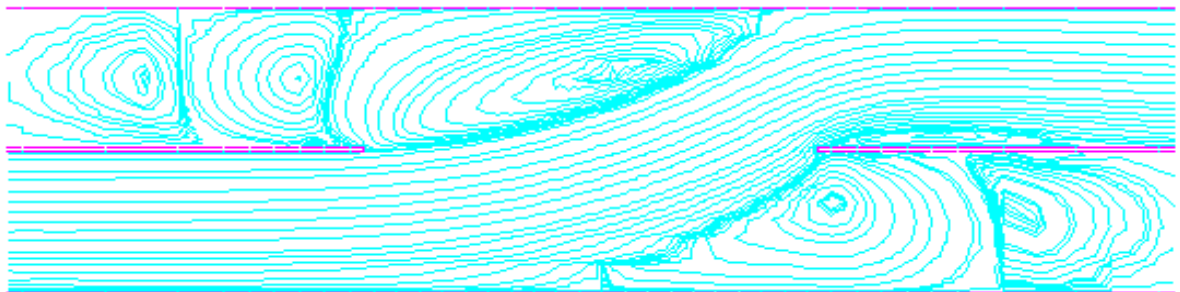
Re=50



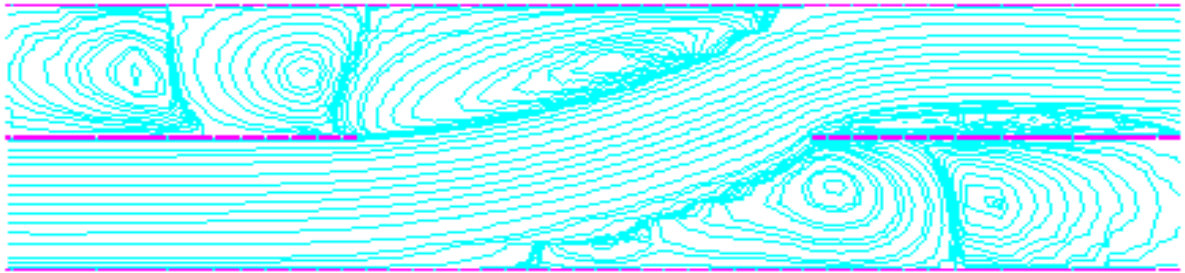
Re=100



Re=200



Re=300



Re=500

Figure 5.14 Streamline function for unidirectional Newtonian fluid flows in a channel filled with non-porous media, increasing Re from top to bottom.

#### 5.4.4.2 The influence of inertia on pressure difference

Figure (5.15) shows the effects of inertia on pressure with increasing the values of Reynolds number. Numerical simulations are carried out for unidirectional Newtonian fluid flows for the domain given in figure [5.1(d)]. Non-dimensional scaled pressure got for this purpose is  $1 \leq Re \leq 1.3571$  and shows an increase in its values as discussed in sections [(5.4.1.5), (5.4.2.5) and (5.4.3.5)] in all three flow conditions with an increasing values of Re. As flow settings are shown in figure [5.1. (d)], because of it flow is entered from bottom arm from its left and exits from top channel arm from its right of the domain. Therefore it is not possible run relative flow rates. That is why only equal (1, 1) flow rates are discussed.

In this case once again flow is unidirectional as was the case in section (5.3.2). Therefore, increase in values of pressure difference is linear in its nature and pressure rises linearly against inertial forces. Pressure difference and varying flow rates are influence with an

increasing inertia as shown in figures [(5.5), (5.9) and (5.13)]. As discussed in the beginning of this section (5.3.4) only equal (1, 1) are passed in this settings. This unidirectional flow setting agrees with the one discussed in section (5.3.2.5). Changes in pressure difference are similar to it.

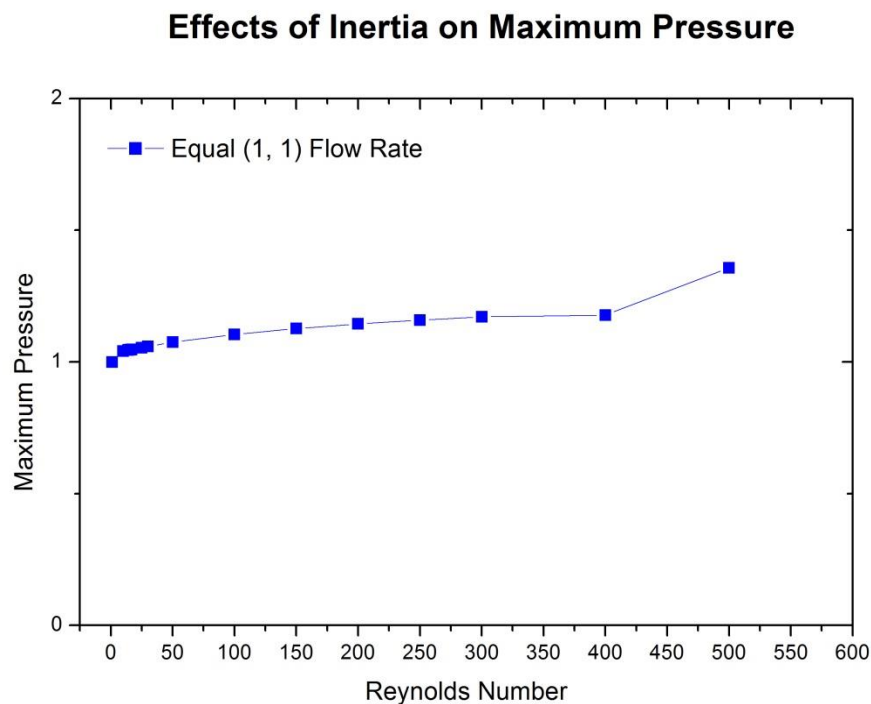


Figure 5.15 Maximum scaled pressure with increasing inertia in a channel filled with non-porous media.

## 5.5 Summary

The semi-implicit time-stepping Taylor-Galerkin/Pressure-Correction primitive variable finite element algorithm has been used. The scheme is found to be robust, stable and accurate in its predictions of steady and complex flows. For combined mixing and separating as well as unidirectional flows in a channel of Newtonian fluids different

bifurcations have been investigated by changing flow direction and flow rates. The results from two dimensional planar combined mixing and separating geometry as well as the other three modified settings of changing flow directions of unidirectional flows have shown that this algorithm gives an adequate mesh convergence for the full compressible Navier-stokes equation.

For monitoring the level of inertial effects on flow structure and pressure the value of Reynolds number was increased for equal and unequal flow rates for all changing flow directions of the flows in given computational domain. It has been observed that an increase in the value of Reynolds number has led to an increase the intensity of vortex development near both ends of centrally located plate and in the middle gap of the geometry for equal flow rates. Changes in flow rates have encouraged the unidirectional flow in top channel arm and decreased the power of vortex development near one end of centrally positioned plate towards more flow direction. With the unequal flow rate, an increase of the value of Reynolds number flow is both unidirectional as well as reversed up to the end in contrast with equal flow rate. Furthermore, an eddy formed in the middle gap of the channel which was the result from the collision of two small eddies appeared from the boundary walls from the mid of the geometry stable its position. That eddy stretched horizontally in case of equal flow rate. While, in the case of unequal flow rate, an eddy appeared only from the upper boundary wall slowly stretched down by pushing the flow of the top arm and stabilise its position just near the middle gap of the geometry in the end by showing process of meandering [shown in figure (5.14) at  $Re=400$  and  $500$ ].

In the case of unidirectional flows early activity of a vortex is observed in the salient arms of the channel when compared with other relative fluid flows in the same channel. The size of an eddy formed by the recirculating vortices in the bottom channel arm near the lower end of centrally placed plate diminishes in size with a further increase of the value of Reynolds number. This eddy developed into the side of top salient arm of the channel stretches vertically and more horizontally in the direction of the flow and adjusts its position in between the solid boundary walls and centrally located insert plates. Changing flow rates and flow directions has given rise to the intensity of recirculation in vortex growth and pressure difference. Increasing value of Reynolds number has the same outcome vortex intensity. Splitting of one vortex into more and further increase in the value of Reynolds number have resulted in again a merge of two or more vortices into one.

Under all three flow conditions, an increase in non-dimensional pressure difference has been observed by increasing the flow rate into the top arm of a channel along with the varying values of Reynolds number. In reversed flows a rise in the pressure is slightly different that in unidirectional flows. Patterns of growth in unidirectional flows show a linear change as compared with reversed flows as shown in figures [(5.9) and (5.13)]. Changing flow directions in Newtonian fluid flows either in reversed or unidirectional also has effects on pressure. It is clear when compared reversed flows with unidirectional domains as shown in figures [(5.5), (5.9), (5.13) and (5.15)]. Results achieved in this numerical study are in agreement with the published experimental results as shown in the discussion section of channel flows in chapter nine.

Stream functions are shown with velocity profiles and are alignment with vertical colour bars. Stream functions with contour number and its corresponding values are labelled. Contour types are presented in lines, flood and in some case lines and flood both. Velocity Vectors are also presented for selected Reynolds number. These results are presentrd in as extra appendix-E for all equal (1, 1) and unequal [(1,1.5) and (1,2)] flow rates for  $G_1 - G_4$  (domain of all four geometries) for non-porous media.

## **Chapter 6. Mixing and Separating of Newtonian Fluid Flows in a Channel Filled with Porous Media**

### **6.1 Introduction**

Modelling flow of fluids through a porous medium in complex geometries has been challenging and interesting topic for research in applied mathematics and engineering because it has applications in many important industries with examples in petroleum industry, food processing, pharmaceutical industry, ground water flow, nuclear reactors etc. Generally, industrial problems are much harder to tackle and present complex flow phenomena. Also fluids exhibit very complex rheological behaviour in several applications.

In this chapter flow behaviour of mixing and separating in channel is modelled by finite element method by using Taylor-Galerkin/Pressure-Correction scheme. The flow consists of two reversed settings and two unidirectional flows of Newtonian fluids having sudden gap in a channel filled with porous materials. The steady solutions are obtained through an unsteady finite element approach. The influence of increasing inertia, porosity and variation in flow rates are all studied. The algorithm is found to be stable up to Reynolds number 6000 and solutions are physically correct. The results were in agreement with published data in the porous channels for Newtonian fluids.

### **6.2 Problem specification**

Figures [5.1(a)-(d)] in chapter five have shown the schematic details of the two flow problems considered, i.e. (a) reverse flow and (b) unidirectional flow (c) Reversed flow and (d) unidirectional flow. The channel is divided into two sections by the two thin-plate

inserts. The inserts are placed horizontally in the same central plane of the geometry and separated by a gap of width of  $\beta$ . The separation gap  $\beta$  is  $3L$  where  $L$  a characteristic length is taken as the height of a single inlet channel arm. The thickness of the plate is taken as  $\alpha = 0.0254L$ . A sufficiently long length of channel of  $23L$  is selected to reproduce fully developed entry and exit flow. These specifications have allowed the numerical predictions for a direct comparison with experimental data and numerical results from the [(Al-Nimr and Aldoss 2004), (Cochrane et al.,1981), (Webster, 1982), (Baloch et al., 1995a), (Afonso et al., 2010) and (Echendu et al., 2011)].

The flow domain is discretised with triangular elements that are generated by a uniform conformal mapping technique. The mesh design is such that the minimum size of element is in the neighbourhood of the separation or gap region, this being  $0.003L$ . A finite element mesh on the domain has total number of elements, nodes, boundary nodes, vertex nodes and degrees of freedom are 1328, 2853, 392, 763, and 6469 respectively. The choice of appropriate time-step was made following the pioneer study by (Carew et al., 1993), governed principally by an explicit time-stepping scheme that depends on a measure of the mesh spacing (taken as the minimum radius of encircle over the triangular elements). A semi-implicit method is implemented with three Jacobi mass-matrix iterations to capture an accurate solution and typical time steps involved is  $\Delta t \leq 0.1$  for Newtonian problems. The steady-state solutions are achieved at a time-step relative increment tolerance of  $10^{-1}$  as used by [(Carew et al., 1993) and (Donea 1984b)]. As shown in figure (5.1), geometries of the computational domain and Finite element mesh are given to see the settings of inlets, outlets, initial and associated boundary conditions.

### **6.3 Governing system of equations**

Consider an unsteady, incompressible and laminar flow of Newtonian fluid in a channel filled with porous medium. The unsteadiness in the fluid flow is due to a suddenly imposed pressure gradient which drives the flow. The flow of Newtonian fluids through porous media assumed to be isotropic and homogeneous can be modelled through governing system equations which are conservation of mass and momentum transport (Darcy-Brinkman) has been given in chapter three. In same chapter initial and boundary conditions are given along with their non-dimensionalisation form in detail.

### **6.4 Numerical scheme and weak formulation**

In this study Taylor-Galerkin/Pressure-Correction scheme has been applied for obtaining steady solution. For viscoelastic flows this method was originally suggested by (Townsend and Webster, 1987) and it was further enhanced for Newtonian flows by (Hawken et al.,1990). After that (Carew et al.,1993), worked on this scheme for a range of other applications in other complex flows. Taylor Galerkin /Pressure-Correction technique was employed to simulate mixing and separating Newtonian flows in channels for non-porous and porous materials (Khokhar et al. 2013) and numerical results were presented under Reynolds number up 6000 for equal and unequal flow rates and for other settings up to 10000. The method contains temporal discretisation through Taylor series expansions in grouping with predictor-corrector scheme. In this multi-stage method, at stage-1 a non-divergence-free velocity is calculated first and then Poisson equation for pressure is solved at stage-2. At stage-3 a velocity field is corrected. At each time step of fractional stages of the scheme second order accuracy is achieved. Galerkin discretisation has been used for the momentum and continuity equations. Details of this scheme are

presented in chapter four. During these study analytical solutions found and other parameters used are included in code.

### **6.5 Numerical prediction and discussion**

Newtonian fluids are both shear-rate and strain-rate independent, manifesting a constant shear viscosity, zero first normal stress difference, and a constant extensional viscosity. Contemporary literature relates interesting descriptions of how rheologically complex fluids behave in flow in through a variety of porous media. Keeping in view the above facts the simulations are performed by extended code developed during current study. That code is already extended by incorporating parameters used for the study of channel flows through non-porous media. Newtonian fluid flows in a channel filled with a porous material are presented and the predictions are presented in the form of streamlines. Geometries are both reversed and unidirectional and all different bifurcations are given in figure (5.1). In this research value of porosity (Darcy's number) is one with varying values of permeability from 0.1 to 0.00001 and viscosity value is chosen 1 to monitor its effects on inertia and pressure on all three flow rates. With increasing Re increases the density of the fluid because of it numerical algorithm diverges. for adjustments values of permeability and size of time interval is decreased to make algorithm convergent up to the required level of accuracy. Therefore, we have adjusted time interval and value of permeability so that algorithm converges to the required accuracy. Inertial factor always changes due to change of Re (density) from 1 to 10000 in all four domains.

### **6.5.1 Mixing and separating of Newtonian fluid flows in a channel filled with porous media ( $G_1$ )**

The details of the particular combined mixing and separating flow problem are presented in figure [5.1 (a)] with same specification discussed in chapter five. In this section Newtonian flow in channel filled with porous media has been discussed. Mixing and separating effects on flow structure are focused in channel filled with Newtonian fluids.

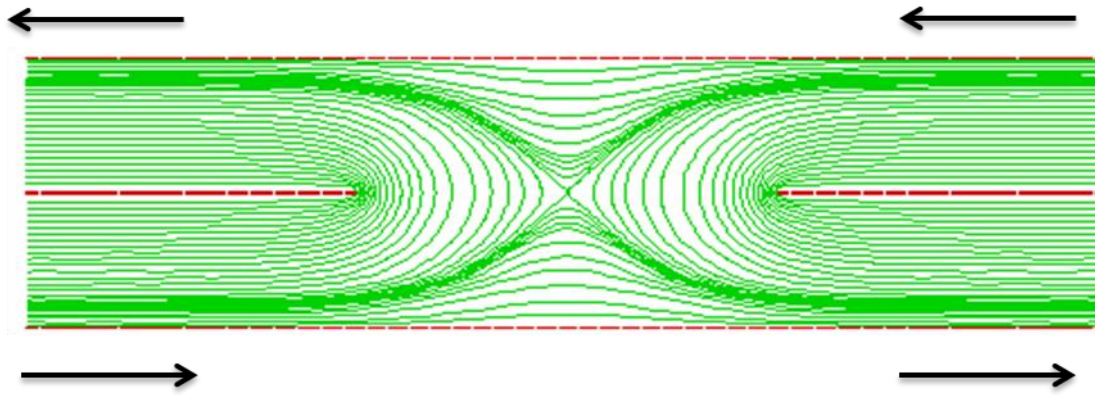
Numerical solutions are presented under different flow rates and flow directions by increasing the value of Reynolds number. The effects of inertia, vortex size and its intensity are discussed when channel is filled with a porous material. Inertial effects and changes in pressure difference will be compared with channel filled without porous media and other available open literature. The effects of porosity and permeability will be analysed on the flow structure will be discussed.

#### **6.5.1.1 Equal (1, 1) flow rate**

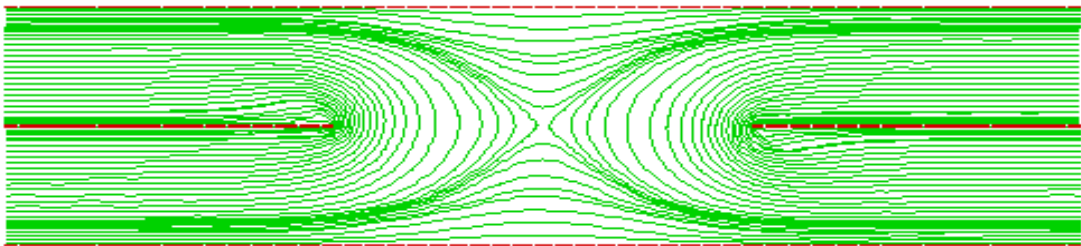
As shown in Figure 6-1, the effects of increasing Reynolds number of ( $1 \leq Re \leq 10000$ ) on relative flow rates are investigated. Attention is given to new features arising from a change of flow rates and flow conditions to test the performance of the algorithm and to reproduce the flow characteristics, especially any dramatic change in flow characteristics by opposing influences of flow inertia and flow rates in the channel. Numerical simulations are started with  $Re=1$  for both cases i.e. reverse and unidirectional flows to test the stability of the program and how it simulates in the presence of the gap in the middle and breaks up. This was necessary particularly in the reversing and mixing zones in both upper and lower exit sections of the geometry.

The solutions were obtained up to Reynolds number 10000 starting from  $Re=1$ . There is no development of vortex activity up to  $Re=4000$ . At the value of Reynolds number of  $Re=5000$  has been noticed the activity of very weak vortex near the centrally positioned insert plate on its lower and upper nip in the direction of exit flow. With a further increase in the value of  $Re$  a vortex developed at the nip of central plate disappears as shown in figure (6.1) (at  $Re=6000$  and 10000). There is no evidence of strong vortex development behaviour under low Reynolds number and it is the indication of very low opposing inertia effects on flow structure as was expected and reported in literature (Al-Nimr and Aldoss, 2004).

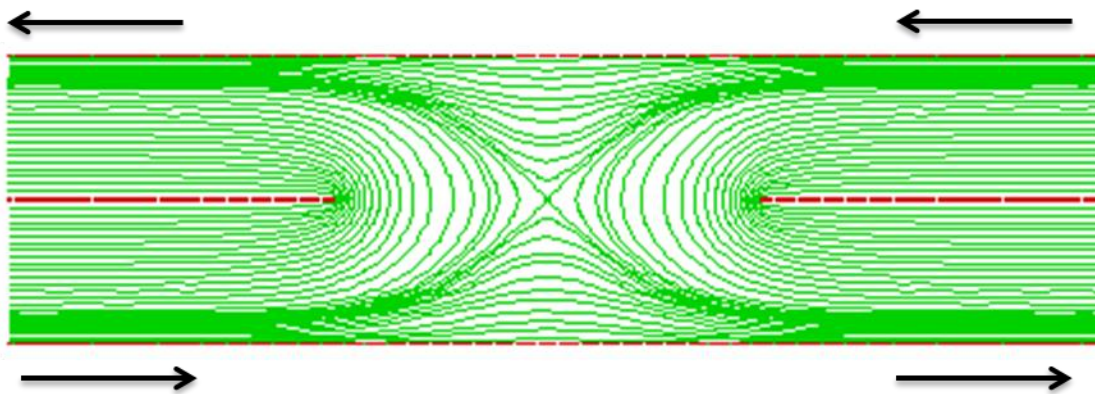
It has been observed that the macroscopic local inertial term has an insignificant effect on hydrodynamics behaviour of Newtonian fluids in porous medium domains. The simulation results are in very good agreement with similar results available in open literatures. Therefore, it is clear that porous medium domains of low Darcy numbers have very small transient time for all ranges of the microscopic inertial numbers. This implies that the effect of local inertia can be neglected because they have insignificant effects in porous domains.



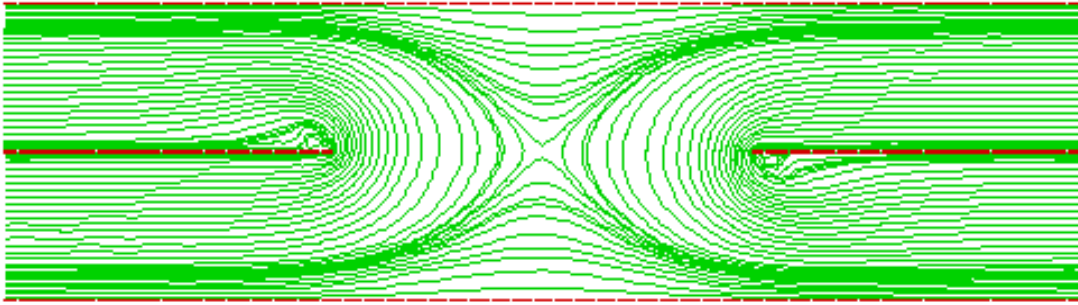
$Re=1$



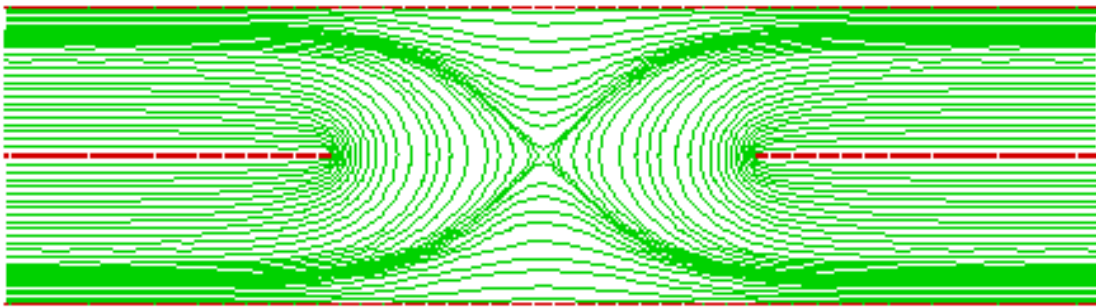
$Re=3000$



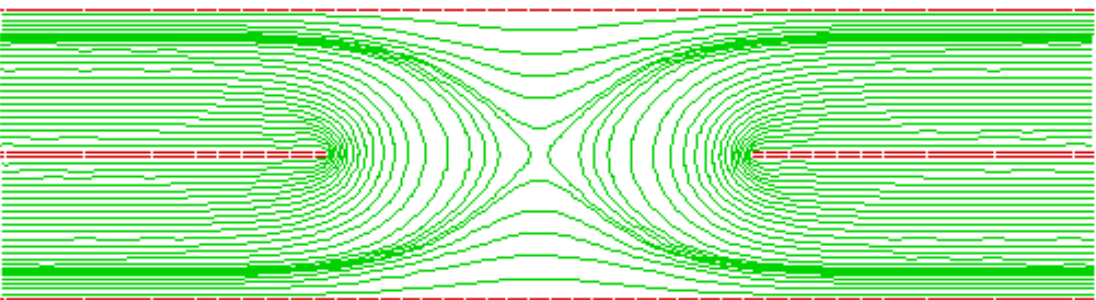
$Re=4000$



Re=5000



Re=6000



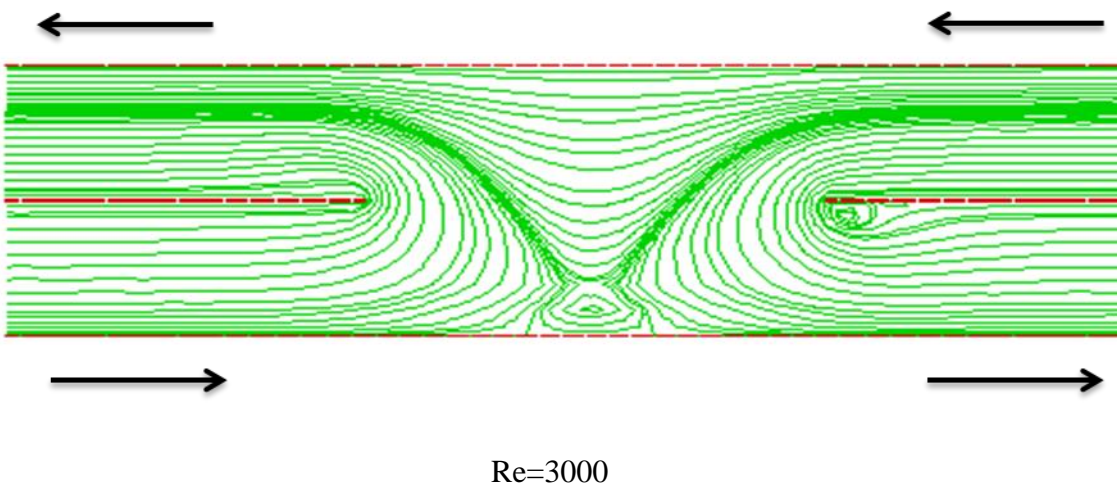
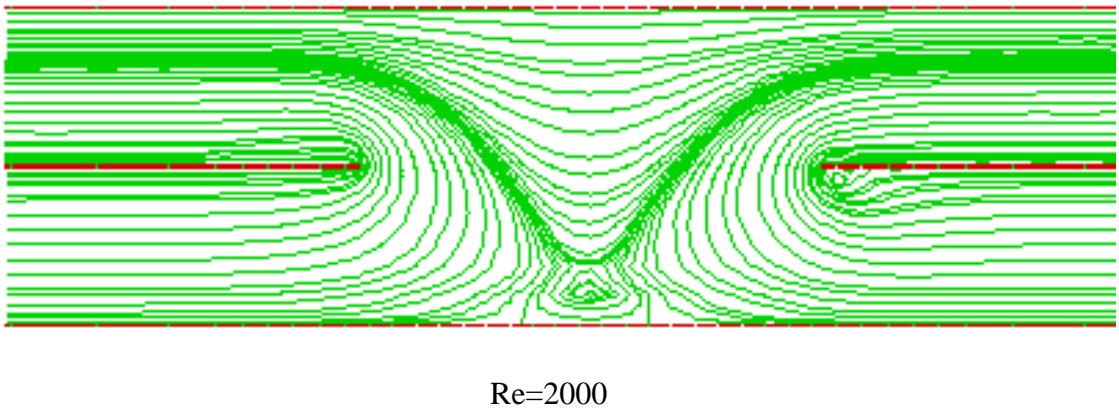
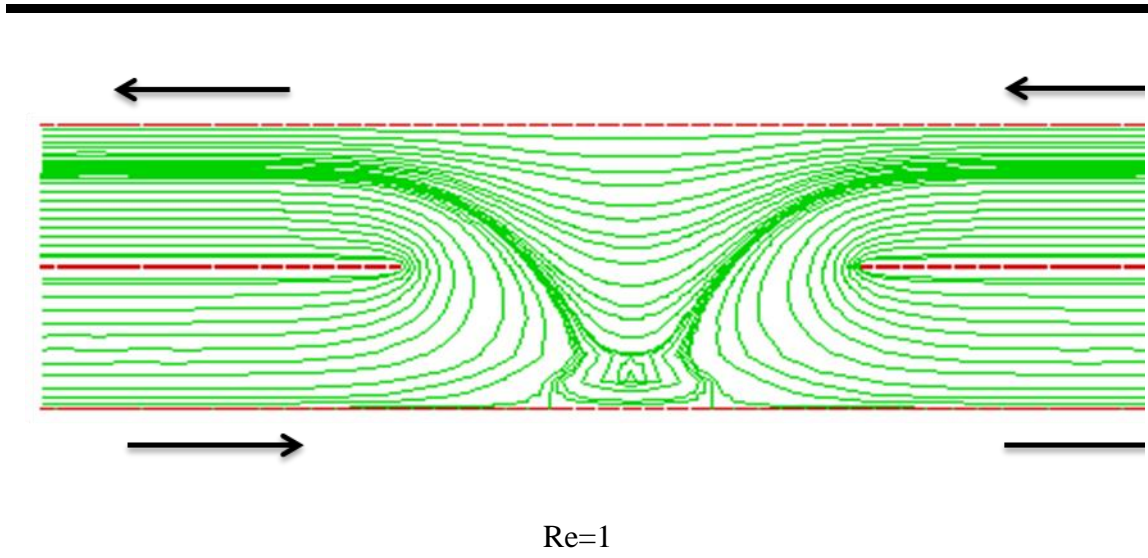
Re=10000

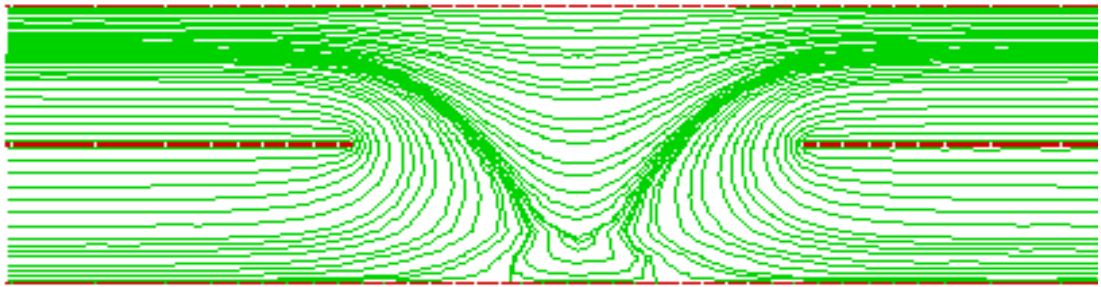
Figure 6.1 Streamline contours for combined mixing–separating flows of Newtonian fluids with equal (1, 1) flow rate in a channel filled with the porous medium, increasing Re from top to bottom at fixed Darcy’s number ( $Da=0.1$ ).

### 6.5.1.2 Unequal (1, 1.5) flow rate

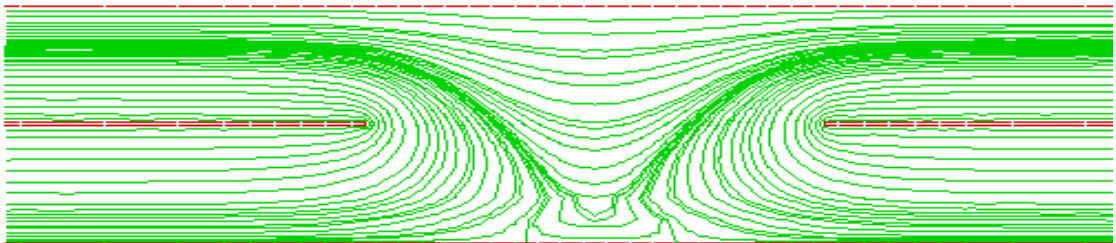
For unequal flow rates (1, 1.5) numerically simulated results are given in figure (6.2) in a channel filled with porous media. The simulations are performed with an increase of Reynolds numbers ( $1 \leq Re \leq 10000$ ) for different flow configurations. The two parallel flows of different flow rates in the top and bottom channel move in the opposite directions. At  $Re=1$  under unequal (1, 1.5) the flow rate in top channel arm, flow comes down in the lower channel and forms an eddy on the wall of lower channel in the middle gap of the domain. A very early response of weak vortex development near the edge of centrally positioned insert plate in the exit flow of bottom channel arm at  $Re = 2000$  was observed. This vortex grows in size and becomes stable at 3000. Early response of vortex development behaviour reveals that relative flows have some effects on opposing inertia of the flow structure. Continually increasing approach in the value of  $Re$  has led to effects of vanishing inertia but an eddy formed on the wall of lower channel wall still exists till the end.

It has been observed that presence of porous materials in the computational domain of Newtonian fluids flows has no significant effect on inertia as compared with channel filled without porous media. Due to the double flow rate top channel arm pushes fluid flow into lower channel arm; therefore, it encourages the reversed flow towards both exits of the computational domain. Due to a different flow rates in both channel arms, development of vortices was only observed on one side of the central positioned plate. That growth of vortices is on nip in the lower channel arm towards the exit.

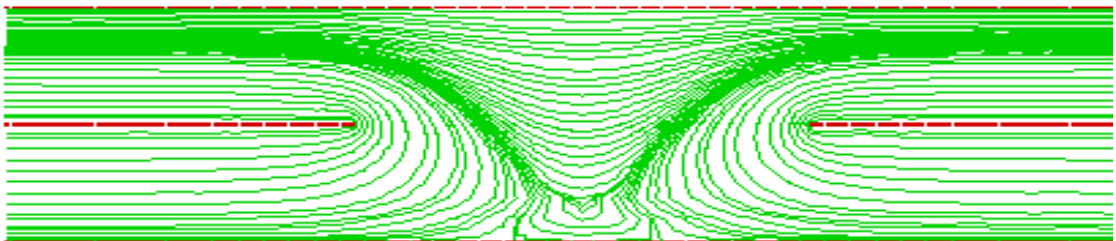




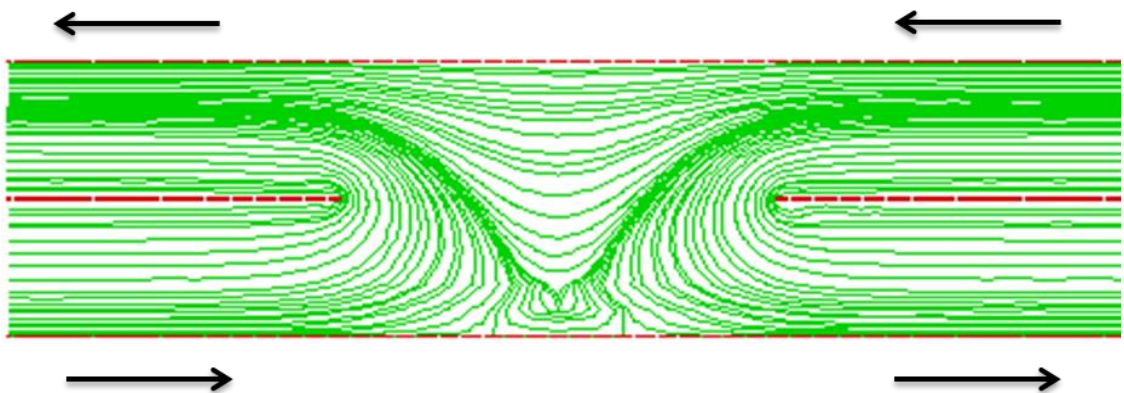
Re=4000



Re=5000



Re=6000



Re=10000

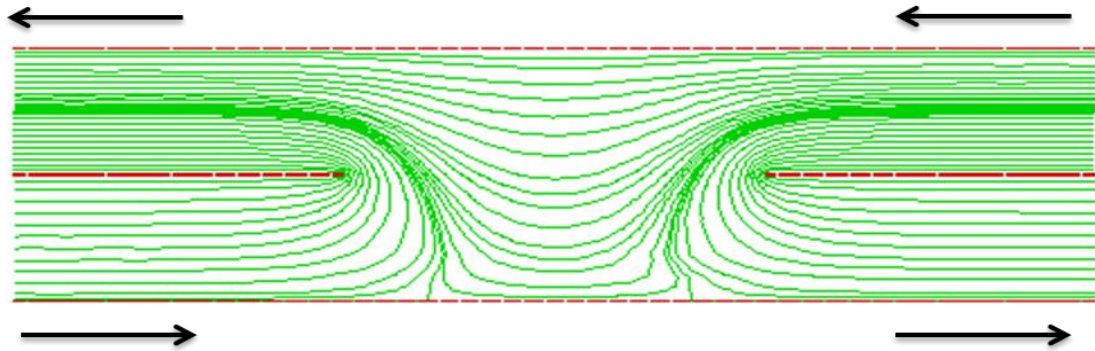
Figure 6.2 Streamline functions for combined mixing and separating flows of Newtonian fluids of unequal (1, 1.5) flow rate in a channel filled with the porous medium, increasing  $Re$  from top to bottom.

### 6.5.1.3 Unequal (1, 2) flow rate

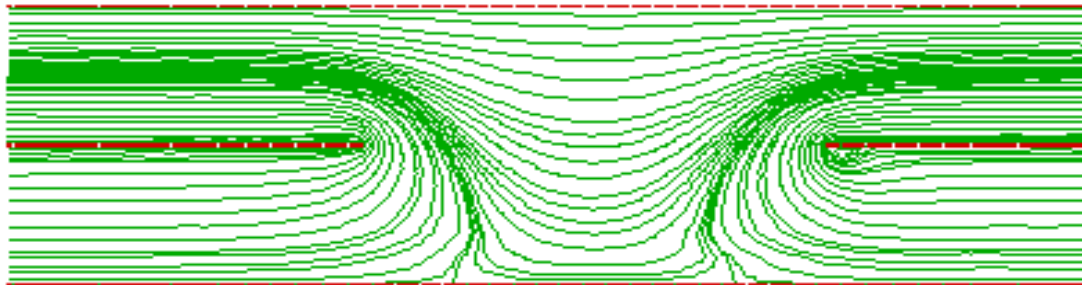
Figure (6.3) shows, numerically simulated results from Newtonian Fluid flows in a channel filled with porous medium for unequal (1, 2) flow rate in both arms of a channel. Similarly, to the above these results these numerical simulations are presented against  $Re=1$  to  $Re=10000$  in the form of streamlines. Once again simulation was started with  $Re=1$  it can be seen that pushing of flow in lower arm in the middle gap exits. That flow only touches the wall and moves back in the upper arm without forming and eddy as compared to flow rate (1, 1.5). An early existence of vortex development behind the one side of centrally positioned insert plate appeared. That vortex lies on nip of central plate in the direction of exit. As shown in figure (6.3) in the bottom channel at low Reynolds number  $Re = 2000$ . With a further increase of the value of Reynolds number, the vortices adjust their position inclined with the wall and become more stable as shown in Figure 6.3 (at  $Re= 3000, 4000$  and  $5000$ ).

Identical with unequal flow rate (1.1.5) vortices are observed only at insert plate of bottom arm of the exit flow channel on its nip. There is no other indication of vortex generation on the top channel arm near the insert plate in the mid of the geometry on its other side. Therefore, it is very clear that changing flow rates has some effects on opposing inertia of the flow structure with varying parameters of the fluids. It is evident that porous channel for flows of Newtonian fluids has less activity of vortices progress. It reflects fewer opposing inertia effects as the similar numerical results suggest. But results also

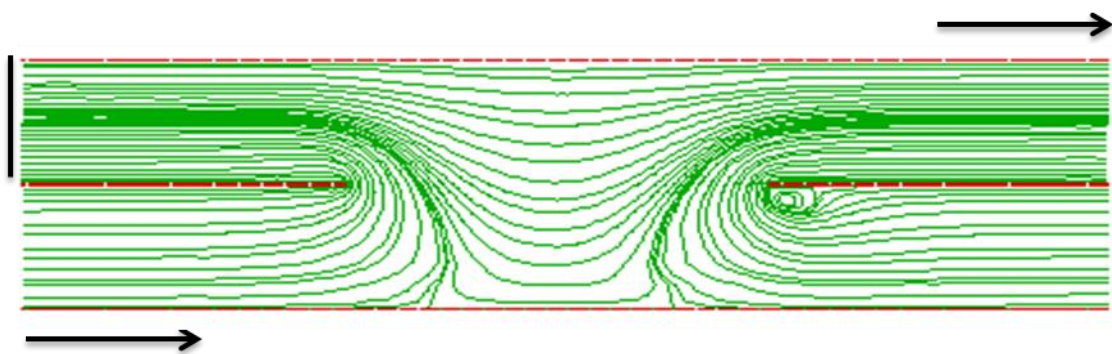
shows dissimilarity with flows in a channel filled with non-porous media discussed in chapter five of current study. Fluids are mixed in the middle gap of the domain and on the corners of the channel towards its exit.



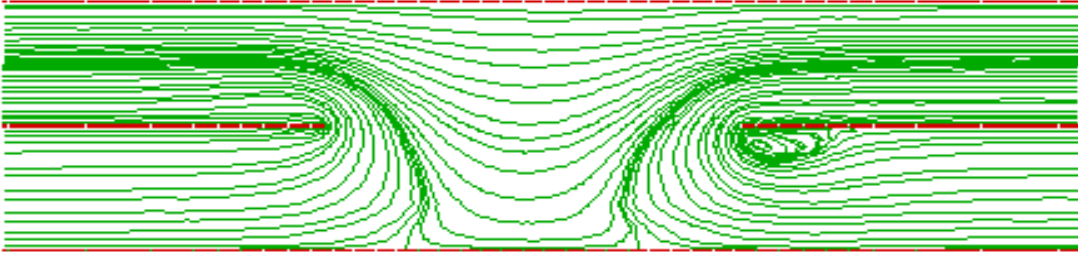
$Re=1$



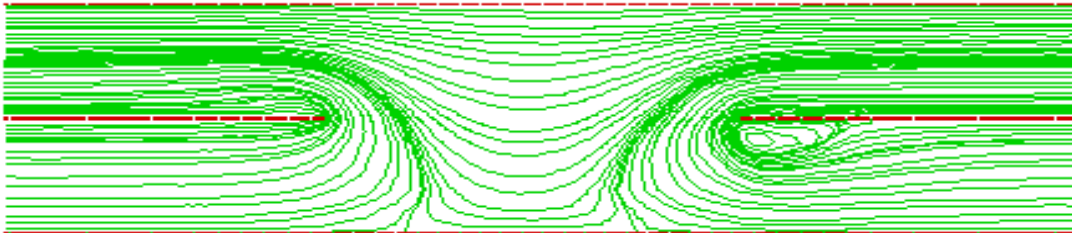
$Re=1000$



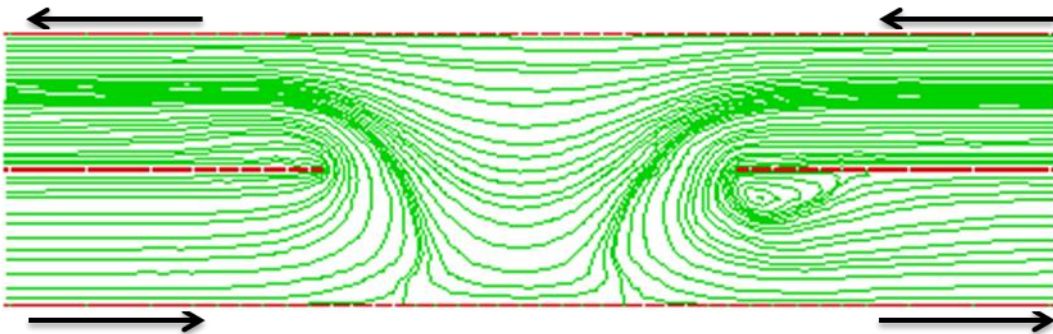
Re=2000



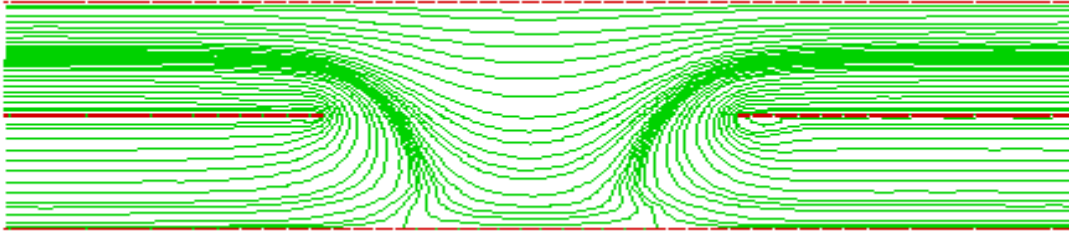
Re=3000



Re=4000



Re=5000



Re=10000

Figure 6.3 Streamline functions for combined mixing and separating flows of Newtonian fluids of unequal (1, 2) flow rate in a channel filled with the porous medium, increasing Re from top to bottom.

#### 6.5.1.4 Effects of flow rate

Streamline functions are presented in figures [(6.2) to (6.3)] for two unequal [(1, 1.5) and (1, 2)] flow rates in a channel filled with Newtonian fluids through porous media. The results are computed from Re=1 to 10000 to monitor the effects of opposing inertia on the structure of the flow domain. In numerically computed results of changing flow rates in two different channel arms with varying parameters of fluid, a very early activity of vortex development reveals the effects of changing flow rates. It can be seen that vortices are only found on one side of the channel. These developed vortices lie on the centrally located plate on its nip in the bottom channel arm.

Changing flow rates from equal (1, 1) to unequal (1, 1.5) has an influence on the vortex intensity which is the clear proof of more opposing inertia on the flow structures. Again changing flow rate from unequal (1, 1.5) to unequal (1, 2) in the top channel arm has its

effect on the flow structures. An early activity of vortex progress has been noticed as shown in figure (6.3) (at  $Re=2000$ ). Flow in lower channel has been pushed down in the middle gap of the domain towards the wall of a channel due to the presence of double flow rate in top channel arm.

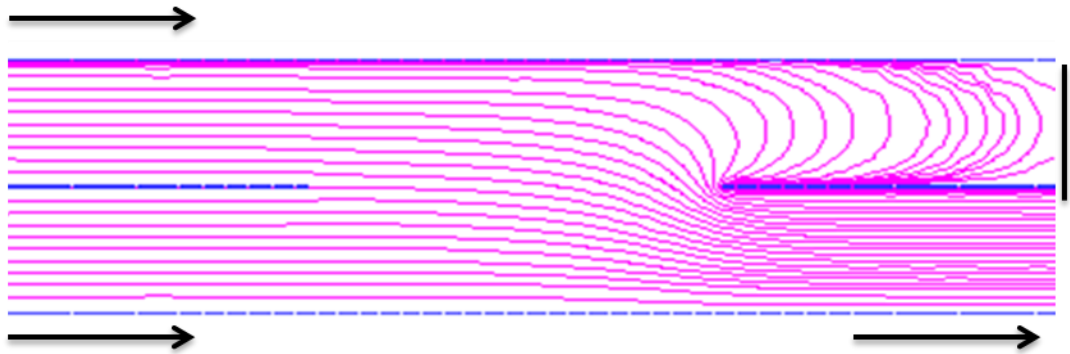
An eddy found in the middle gap near the wall under unequal (1, 1.5) flow rate vanishes due to double flow rate in the top arm. A push to flow down to the wall in lower channel arm can still be noticed till the end of increasing  $Re$  up to 10000 in double flow rate. Flows are both reversed and unidirectional. Mixing and separating have been observed but little a bit more change in reversed flow in lower channel arm towards the outlet. When both unequal rates are compared with equal flow rate with increasing inertia, in equal flow rate flows are balanced, mixing and separation is also smooth either in the separation gap or in the arms of both arms.

### **6.5.2 Mixing and separating of Newtonian fluid flows in a channel through porous media ( $G_2$ )**

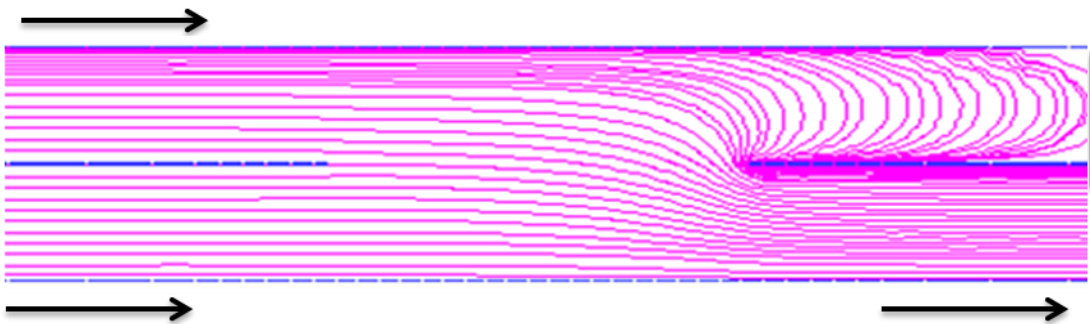
The details of the particular combined mixing and separating of unidirectional flows of Newtonian fluids in the same channel with changing flow directions is presented in Figure 5.1 (b) with the same specification as discussed in chapter five. In this chapter flows of Newtonian fluids are discussed in a channel through porous media. The channel has having two inlets from its left in both upper and lower arms and one outlet from right in its lower arm. Discussions will be made for changing flow directions and increasing the value of Reynolds number and effects on inertia, pressure difference and the presence of Darcy term in momentum equations.

### 6.5.2.1 Equal (1, 1) flow rate

The effects of increasing Reynolds number from ( $1 \leq Re \leq 1000$ ) for equal (1, 1) flow rates are presented in Figure (6.4). Attention is given to new features arising from changing of flow rates and flow directions to test the performance of the algorithm to reproduce the flow characteristics, especially any dramatic change in flow structure by opposing influences of flow inertia. No effects of opposing inertia has been noticed so far by increasing the value of  $Re$  up to 10000. Due to unidirectional flows and addition of Darcy's term there are no possessions of opposing inertia on the flow structure as compared with case of reversed flows discussed in section 6.5.1. Fluids mixes in the bottom arm towards to its exit.



R=1



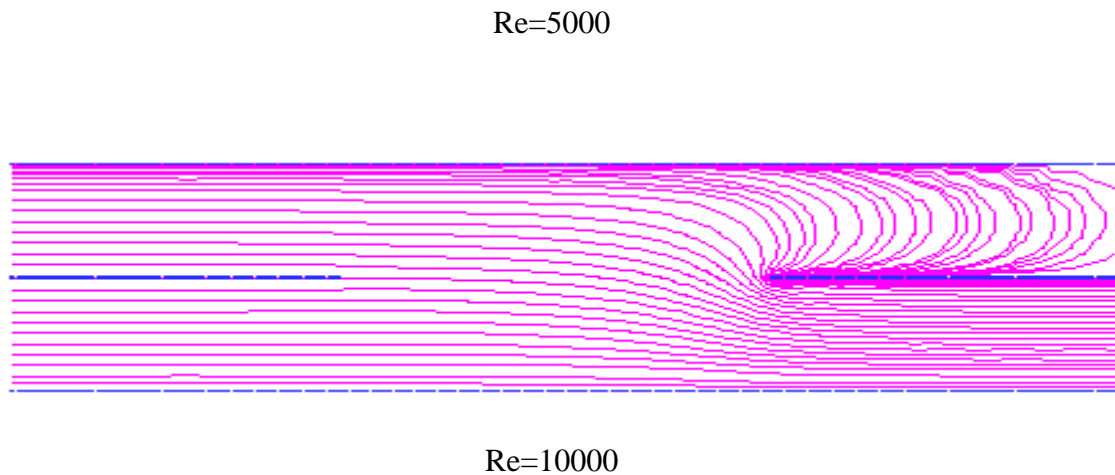


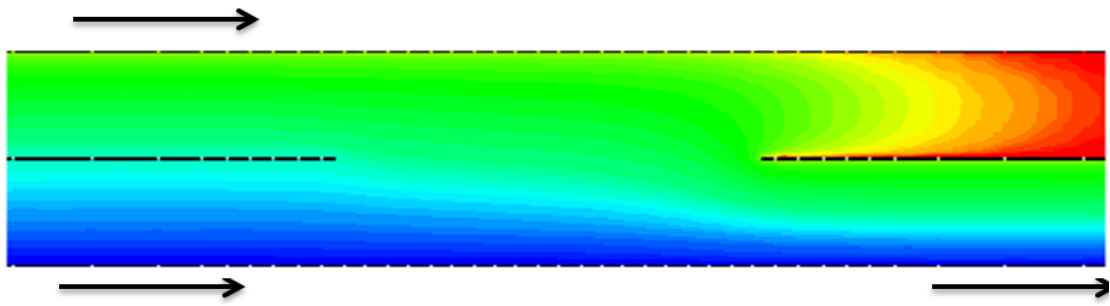
Figure 6.4 Streamline functions for unidirectional flows of Newtonian fluid of equal (1, 1) flow rate in a channel through porous medium, increasing Re from top to bottom.

### 6.5.2.2 Unequal (1, 1.5) flow rate

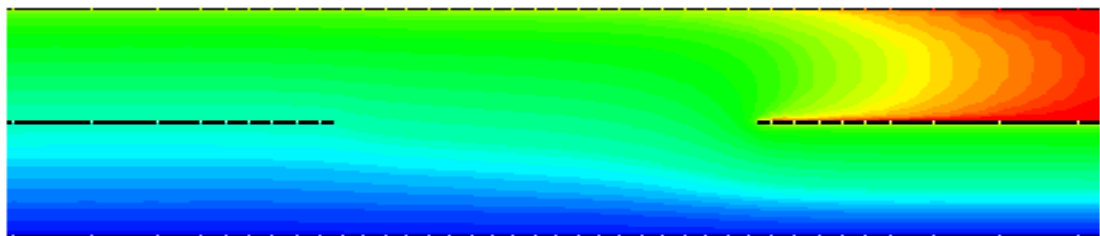
Numerically simulated results for unequal (1, 1.5) flow rate in a channel filled with Newtonians materials through porous media are presented in figure (6.5). The simulations were performed with increasing Reynolds numbers ( $1 \leq Re \leq 10000$ ) for different flow divisions. The two parallel flows of different flow rates in top and bottom channel arms move in the same directions towards the same exit in lower channel arm from its right. There is no existence of inertia on the flow structure except a little bit push to flow in lower arm towards the exit due to an increased flow rate in top channel arm.

It can be seen that increasing Re from lower to higher values up to 10000 gives little bit more push to the flow towards the wall of lower channel arm in its exit corner. No other effects of inertia are evident by changing flow rate as compared with channel filled with

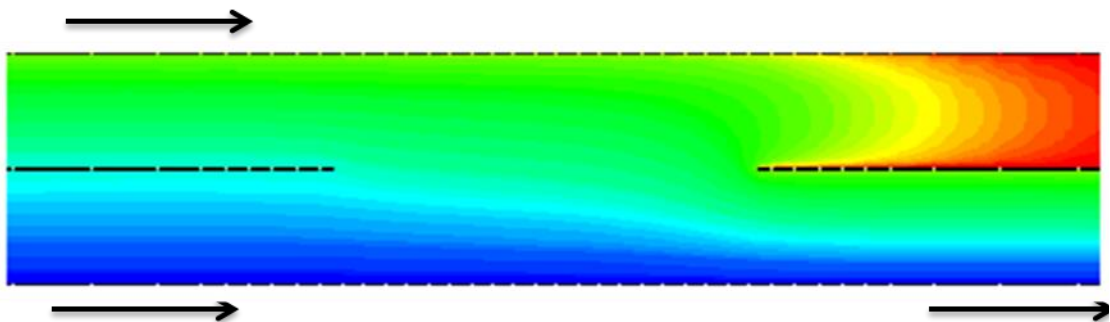
non-porous media in same settings. Due to unidirectional activities of fluid flows mixes in the lower channel arm towards its exit. With increasing  $Re$  up to 10000 no evidence of vortex generation has been found. Flows enter in the silent zone of above arm from its right but vortex generation is not noticed.



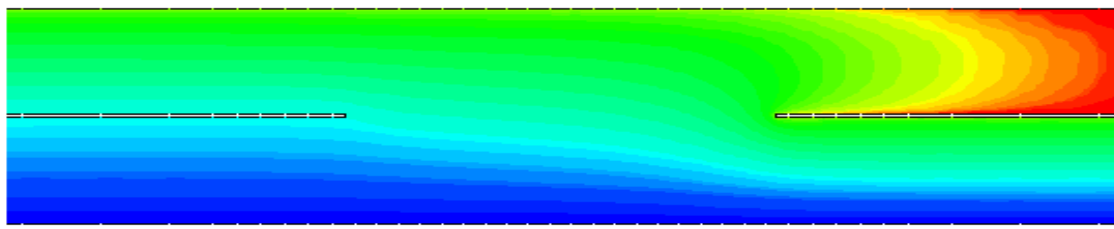
$Re=1$



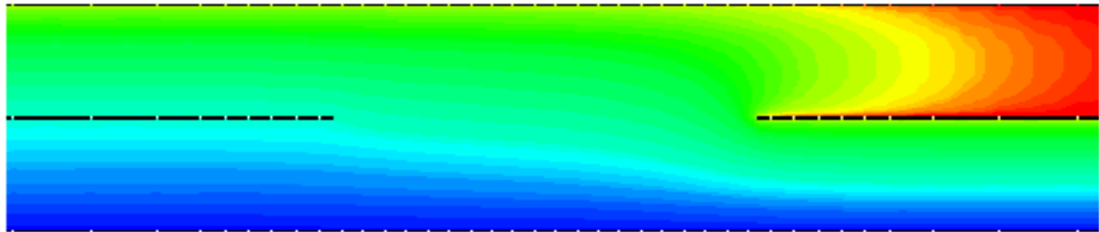
$Re=50$



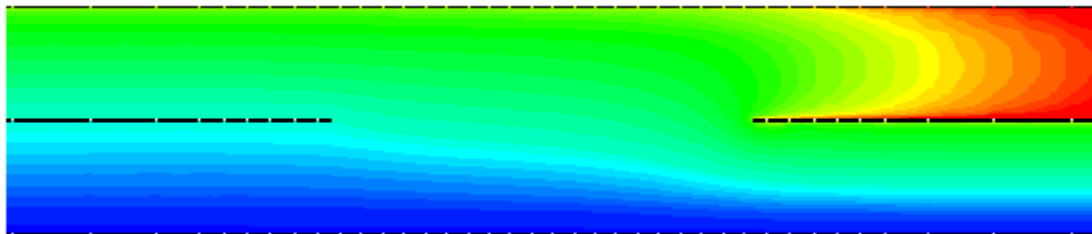
$Re=100$



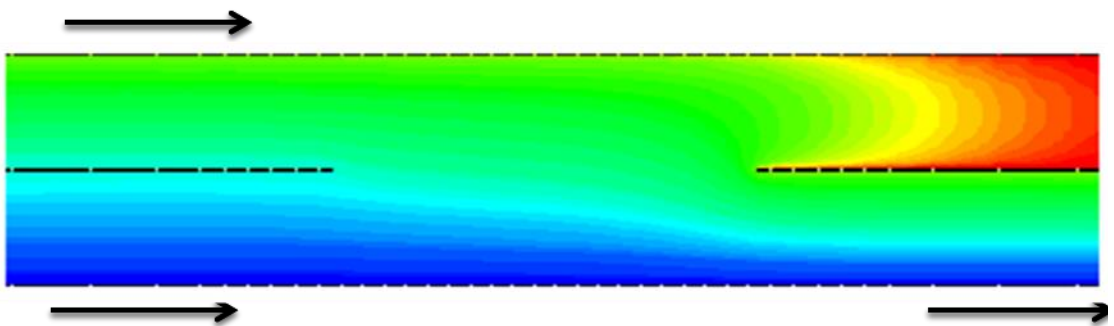
Re=500



Re=1000



Re=5000



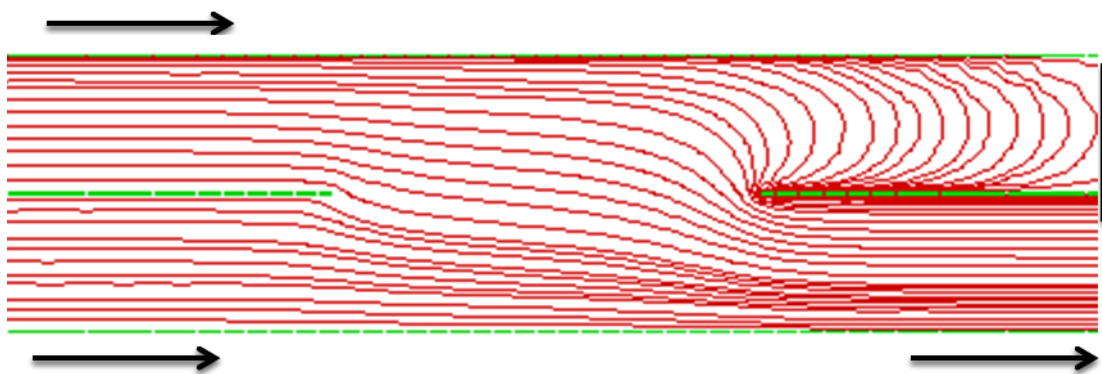
Re=10000

Figure 6.5 Streamline functions for unidirectional flows of Newtonian fluid of unequal (1, 1.5) flow rate in a channel through porous medium, increasing Re from top to bottom.

### 6.5.2.3 Unequal (1, 2) flow rate

In figure (6.6), numerical results from Newtonian Fluid flows in a channel filled with porous medium for unequal (1, 2) flow rate in both arms of a channel are presented. The simulations were performed with increasing Reynolds numbers ( $1 \leq Re \leq 10000$ ) for different flow partitions. There is no occurrence of opposing inertia on the flow structure except a little bit more push to flow in lower arm towards the exit. This is due to increased flow rate in top channel arm as compared with unequal (1, 1.5) or even with equal (1, 1) flow rate.

Increasing  $Re$  from smaller to larger values up to 10000 gives slightly more push to the flow towards the wall of lower channel arm in its exit corner. No other effects are evident by changing flow rate or fluid properties, compared with channel filled with non-porous media in same settings. Due to unidirectional actions of fluid flows mixes in the lower channel arm towards its departure. Because of no dramatic change on flow structure of the domain fewer results are given below in figure (6.7) as compared with the other two flow rates. These flow rates are presented in figures [(6.4) to (6.5)] above in channel filled with Newtonian materials through porous media.



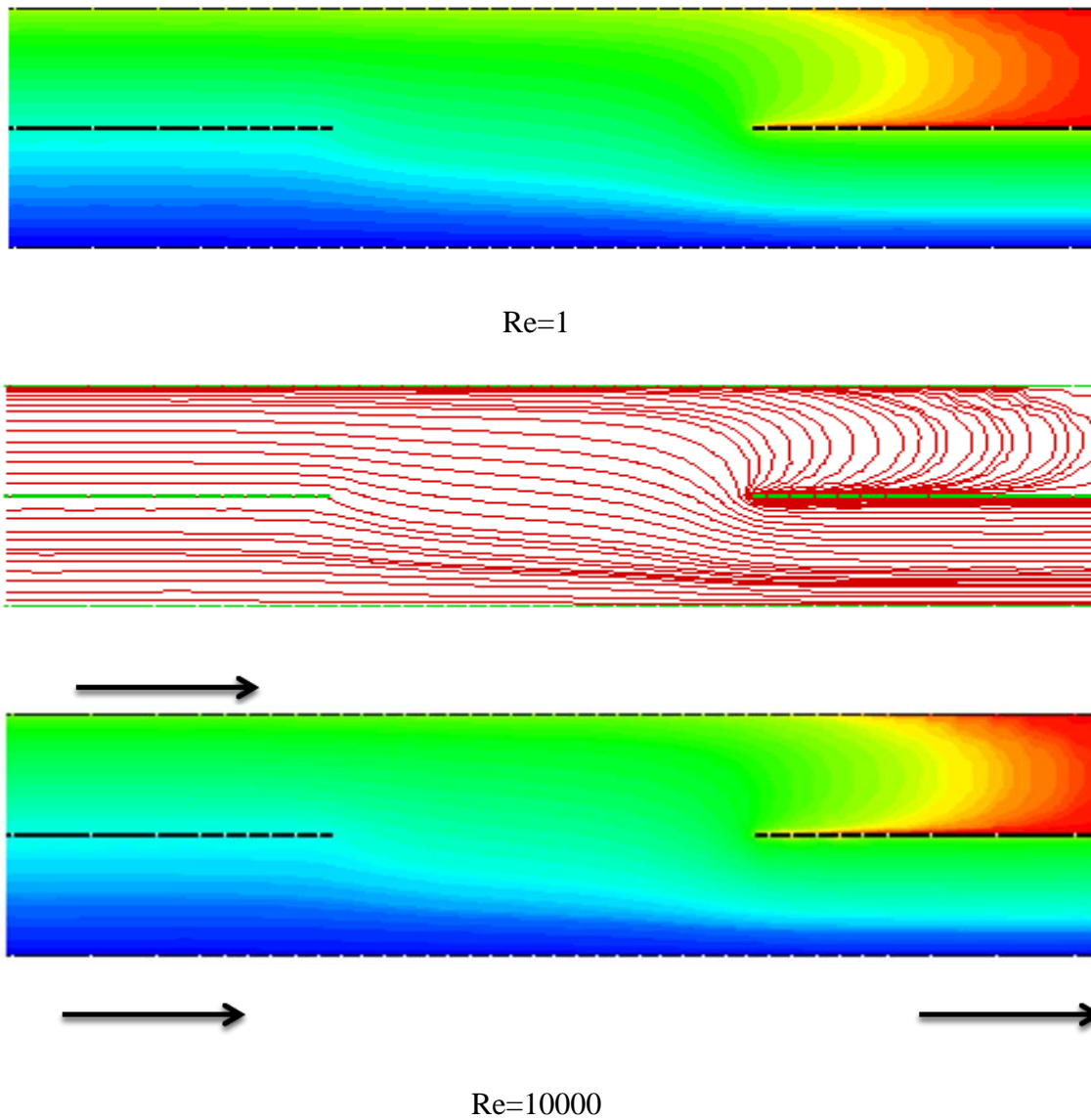


Figure 6.6 Streamline functions for unidirectional flows of Newtonian fluid of unequal (1, 2) flow rate in a channel through porous medium, increasing Re from top to bottom.

#### 6.5.2.4 Effects of change in flow rate

As shown in figures [(6.4) to (6.6)], there is no significance change on flow domain in it's all of the three different sections, lower channel arm, upper channel arm and in the

separation gap in the middle of the changing flow directions. Increasing flow rate in upper arm of the channel has given a soft push to the fluids flow in lower arm of the channel towards the exit of the fluids. As flow is unidirectional therefore mixing appears only in the lower arm of a channel towards its downstream. It is obvious that in all three flow rates not a single vortex generated by increasing the value of  $Re$ , in reversed flow case discussed in section (6.5.1), there was some evidence of inertia but in unidirectional case nothing has happened.

### **6.5.3 Mixing and separating of Newtonian fluid flows in a channel through porous media ( $G_3$ )**

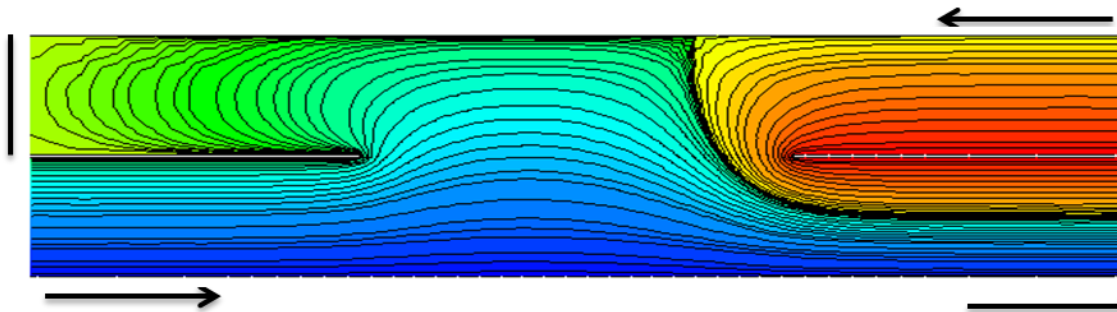
The details of the particular combined mixing and separating flows are presented in Figure 5.1 (c) with same specification discussed in chapter five. Flows of Newtonian fluids in the channel filled with porous will be discussed with increasing the value of Reynolds number. The flow is reversed two opposing inlets one from lower bottom arm from the left and the other from top arm from its right and one outlet is in lower arm from its right. Inertia effects, change in pressure difference and existence of the Darcy's number by changing flow rates in top arm of a channel will be focused.

#### **6.5.3.1 Equal (1, 1) flow rate**

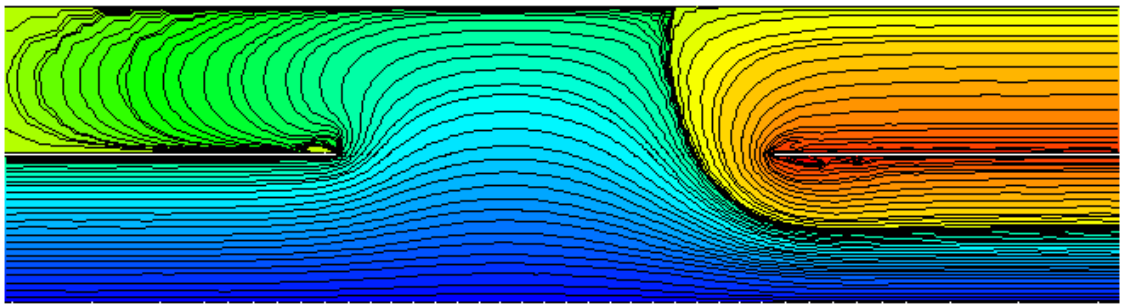
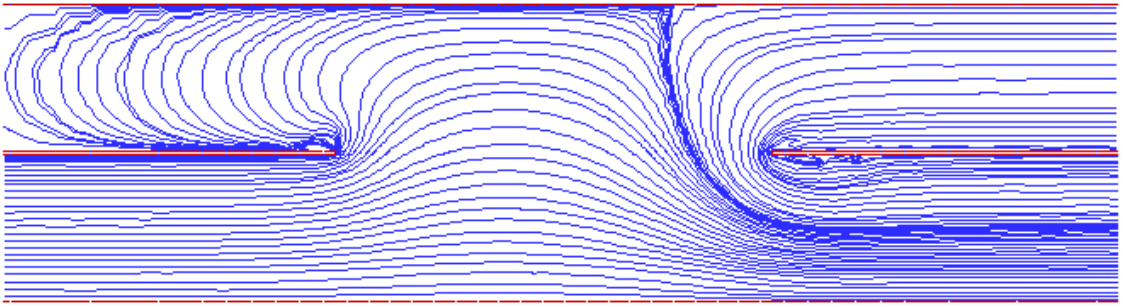
The effect of increasing Reynolds number from ( $1 \leq Re \leq 5000$ ) for relative flow rates of Newtonian fluids in a channel filled with porous media are displayed in figure (6.7). The results were obtained up to Reynolds number 5000. At  $Re=1$  movement of the flow from lower arms towards upper arm gives chance to reverse flow and blocks its mixing in the middle gap of the domain. Up to  $Re = 2000$  there is no significant activity of the vortex

development except a shift of the flow in upper arm. By Further increasing the value of  $Re$ , at  $Re=3000$  a very weak activity of vortex near the nip of a plate to the right in top arm has been noticed along with some recirculation in its right central plate on its lower side in the bottom channel arm. At  $Re=4000$ , the recirculation of vortex near the central plate on its right grows in its size and adjusts its position in the plate. The smaller eddies maintain their positions at an angle to the insert plates and seem to become more stable at  $Re=5000$  as shown in figure (6.7).

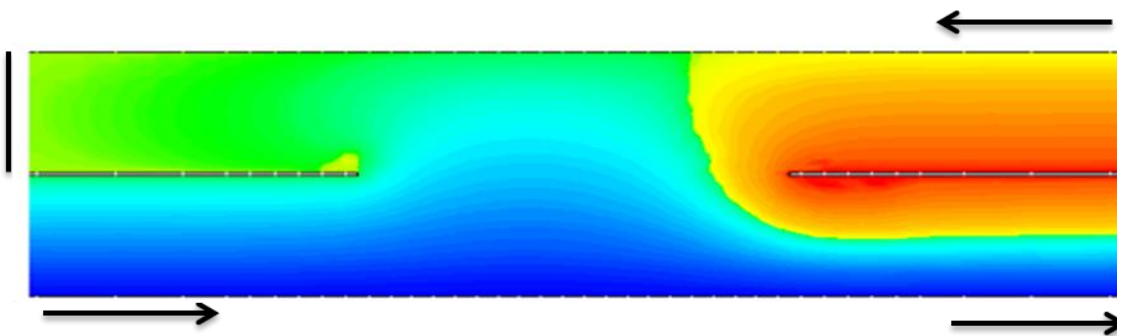
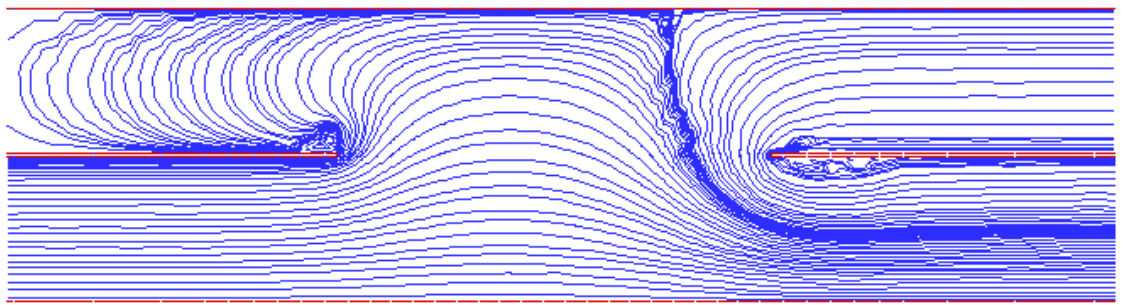
No evidence of strong vortex development behaviour for low Reynolds number and it is the indication of very low opposing inertia effects on flow structure as was expected and reported in paper (Al-Nimr and Aldoss, 2004). Both unidirectional and reversed flows have been observed with slightly more twist in reversed flow due to the movement of fluid flow in the upper arm towards its salient corner and in the middle gap up to the wall of top channel arm. The fluid mixes more in the lower channel arm in the section towards flow departures.

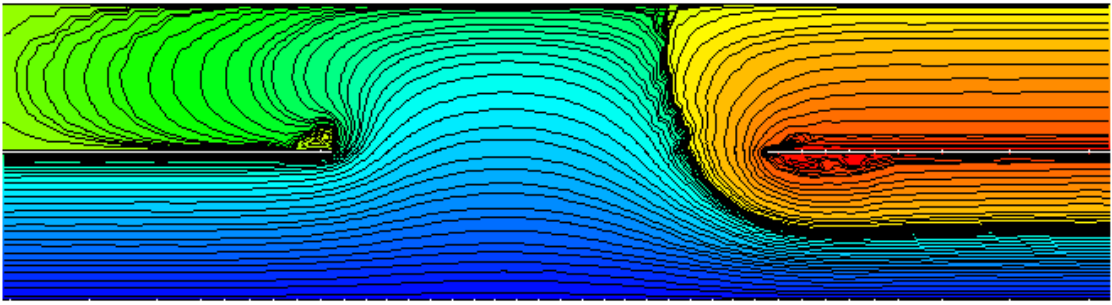


$Re=1$

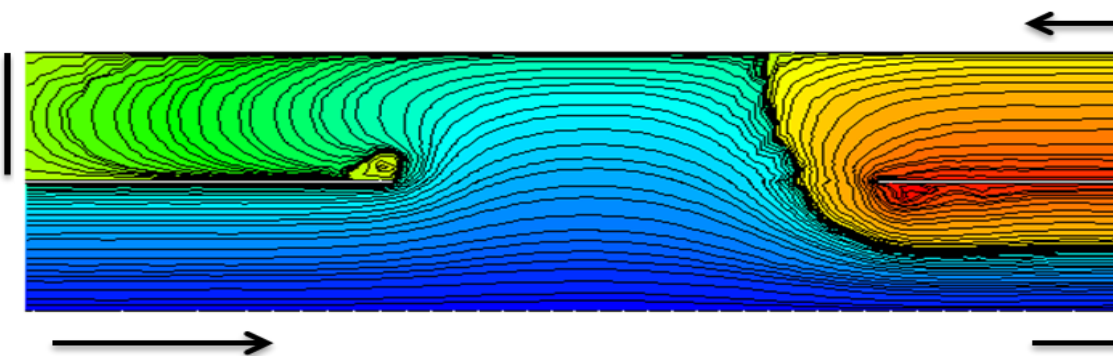
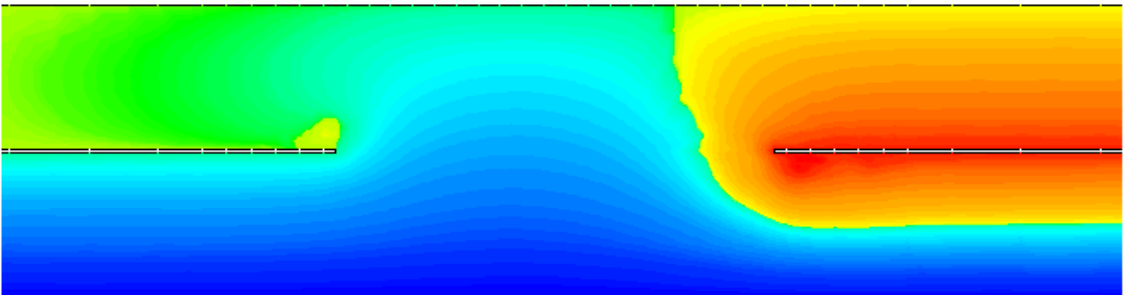
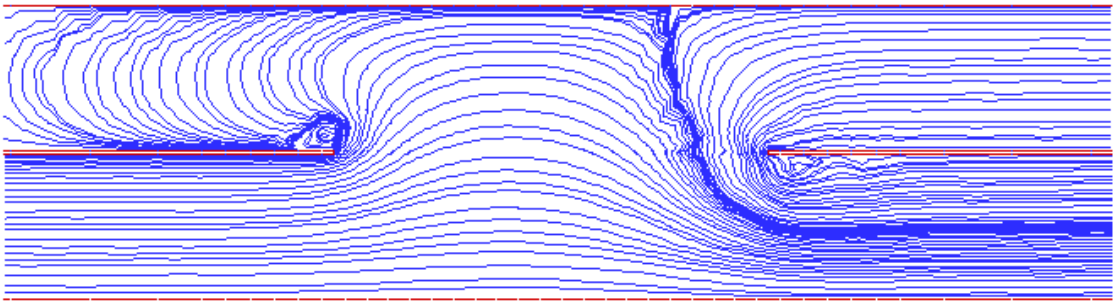


Re=2000





Re=4000



---

Re=5000

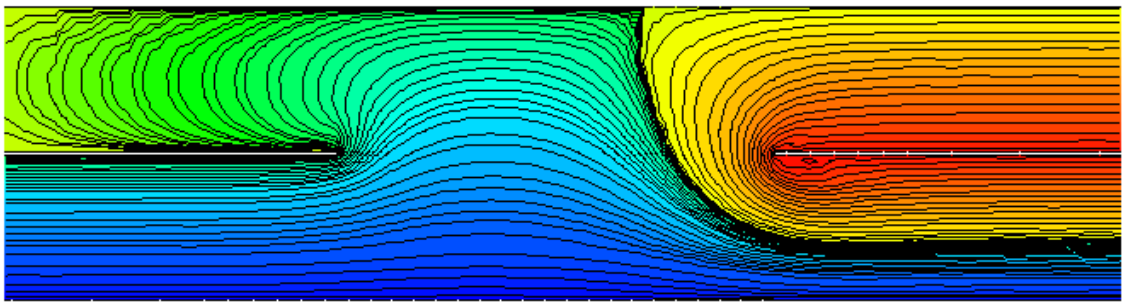
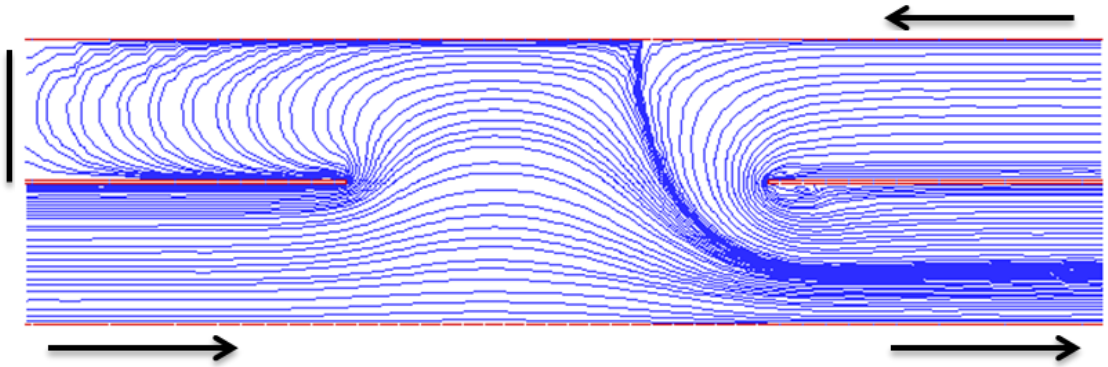
Figure 6.7 Streamline functions for mixing and separating of Newtonian fluid flows for equal (1, 1) flow rate in a channel through porous medium, increasing Re from top to bottom.

### 6.5.3.2 Unequal (1, 1.5) flow rate

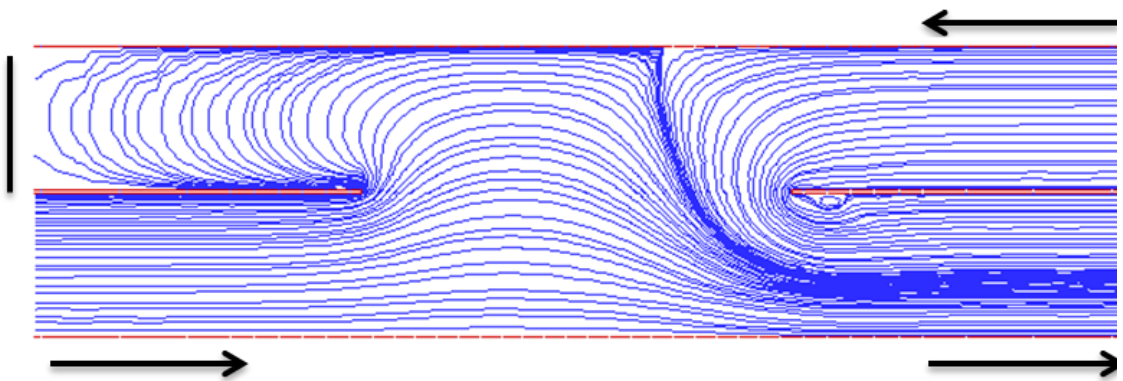
Numerical results from unequal (1, 1.5) flow rates of Newtonians in both arms of a channel filled porous media are presented in figure (6.8). The simulations were performed with increasing Reynolds numbers ( $1 \leq Re \leq 5000$ ). At  $Re = 2000$  a recirculation has been observed near the central plate fixed in the middle of the geometry in lower arm towards flow the exit. In the case of equal (1, 1) flow rate discussed in section 6.6.3.1 at  $Re = 2000$  weak vortex developed on the nip of central located plate vanishes in increasing flow rate. Comparison can be seen in figures [(6.7) and (6.8)] due to increased flow rate in top channel arm. At  $Re = 3000$ , a vortex near the one side of centrally positioned insert plates in the exit flow of bottom channel arm at grows in size and adjusts its position in the plate. At  $Re = 4000$  another weak vortex appeared near the centrally positioned insert plate lies flat in the plate in top channel arm. Both vortices developed in the plates near its edge adjust their position and become stable at 5000.

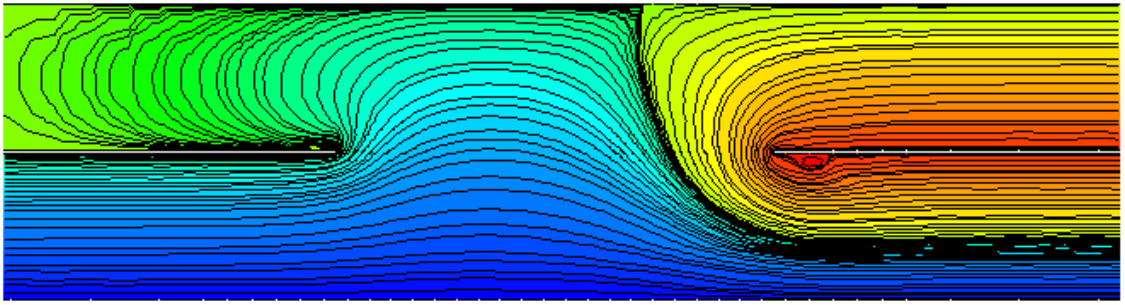
Changing flow rate in top channel arm has its effects on the late vortex development at the edge of central from its left in top channel arm. But increasing the value of Re again gives rise to its appearance again (at  $Re = 4000$ ) in figure (6.7). Other mixing and

separating effects are the same as mentioned in equal flow rate. Unidirectional and reversed flows behave the same way as discussed in sections [(6.5.1) to (6.5.2)] above.

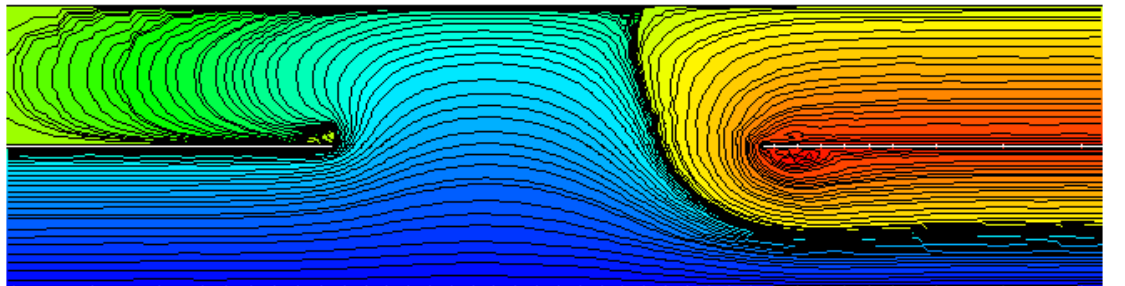
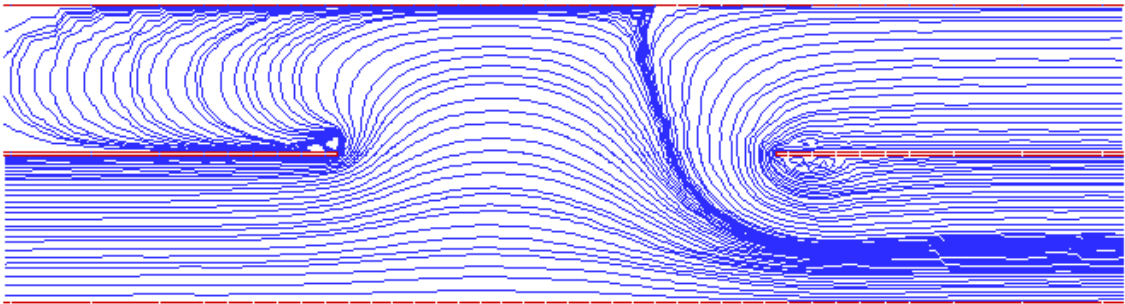


Re=2000

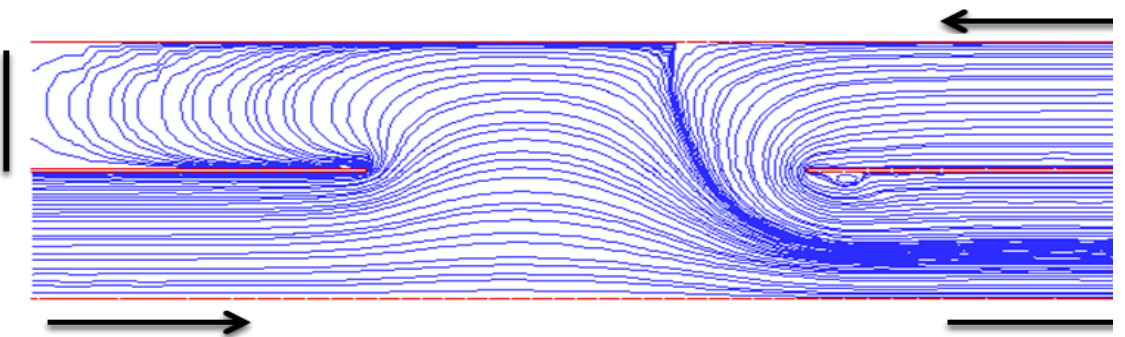


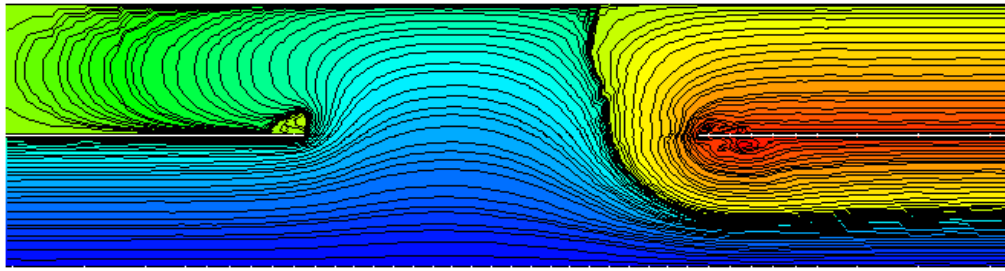


Re=3000



Re=4000





Re=5000

Figure 6.8 Streamline functions of mixing and separating of Newtonian fluid flows for unequal (1, 1.5) flow rate in a channel filled with porous medium, increasing Re from top to bottom.

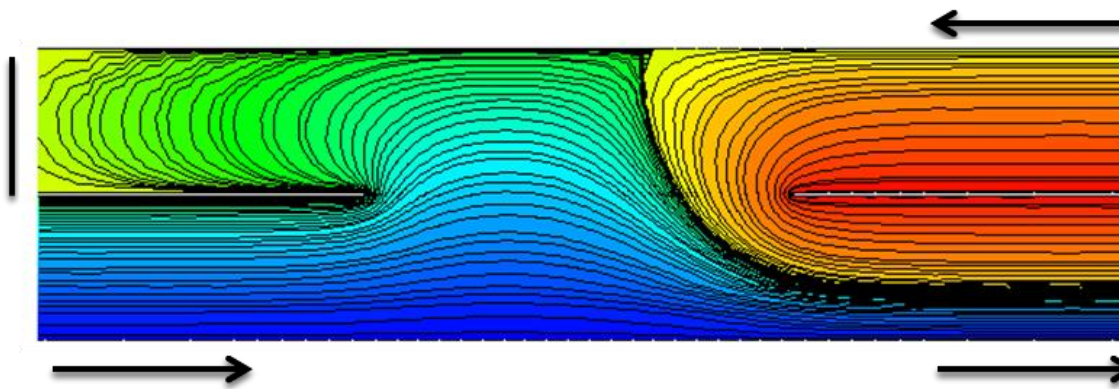
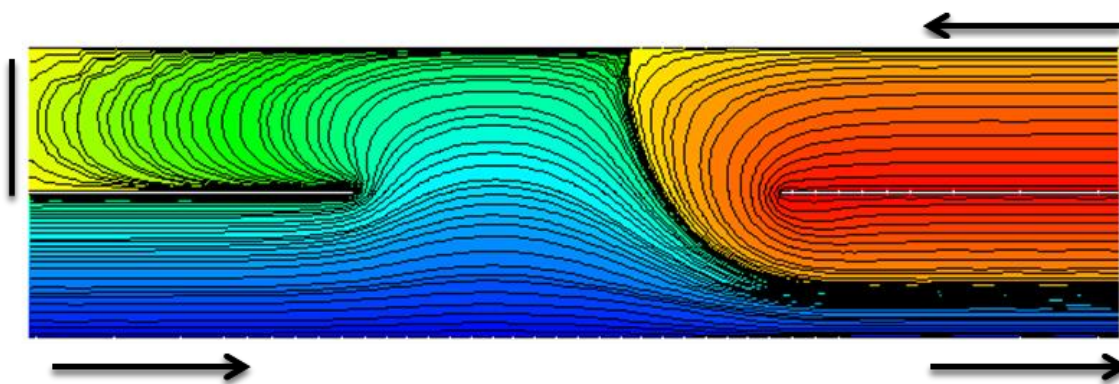
### 6.5.3.3 Unequal (1, 2) flow rate

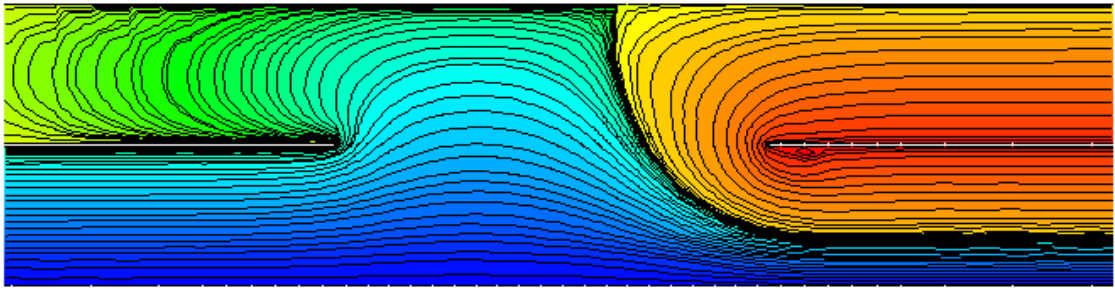
Figure (6.9), shows the results of numerical simulation from Newtonian Fluid flows in a channel filled with porous medium under unequal (1, 2) flow rate in both arms of the channel. Up to  $Re=1000$ , no evidence of vortex growth has been noticed in any section of the flow domain. At  $Re=2000$ , a smaller vortex appears at the near sharp edge of the central plate fixed from right in the bottom channel arm. The vortex grows in size at  $Re=3000$  and becomes more stable with the plate. At  $Re=4000$  another vortex develops at the edge of central fixed plate on its right of the top arm towards salient corner of the domain.

At  $Re=5000$  both vortices grow in size but a vortex on the right at the edge grows more, stick to both sides of the edge in lower and upper side, then splits into more smaller vortices and creates the situation of meandering. The intensity in the progress splitting into other smaller vortices shows visible opposing inertial effects with more increase in the value of Reynolds number. Changing flow rate in the top channel arm has its effects

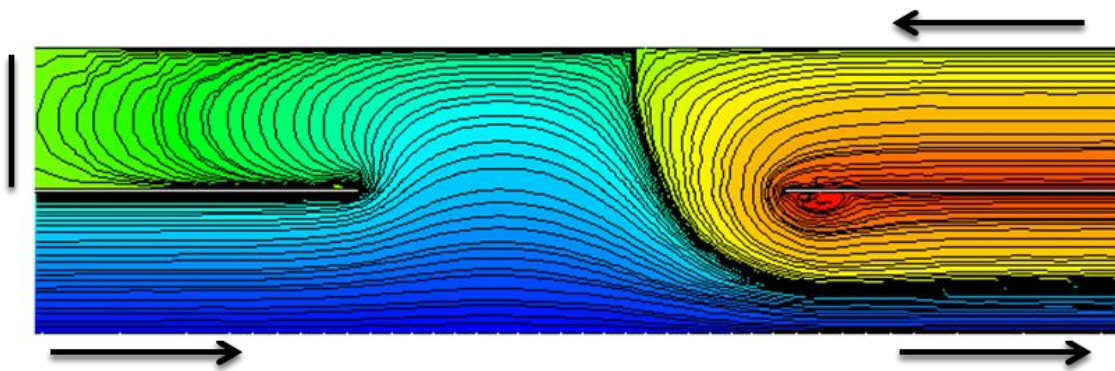
of late vortex development on the edge central from on its left in the top channel arm. Increasing the value of  $Re$  again gives rise to its appearance again as shown in figure (6.5) (at  $Re=4000$ ). Other mixing and separating effects are same as mentioned in equal flow rate. Unidirectional and reversed flow behaves the same way as discussed in sections (6.5.3.1) and (6.5.3.2) of equal flow rate.

Changing flow rate from unequal (1, 1.5) to (1, 2) in the top channel arm has more influence of inertia at the higher values of Reynolds number as shown in figure (6.9) (at  $Re=5000$ ) compared with other relevant flow rates discussed.

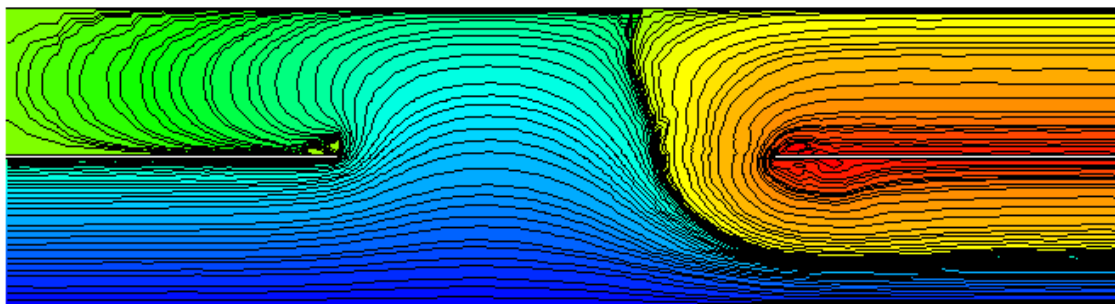
 $Re=1$  $Re=1000$



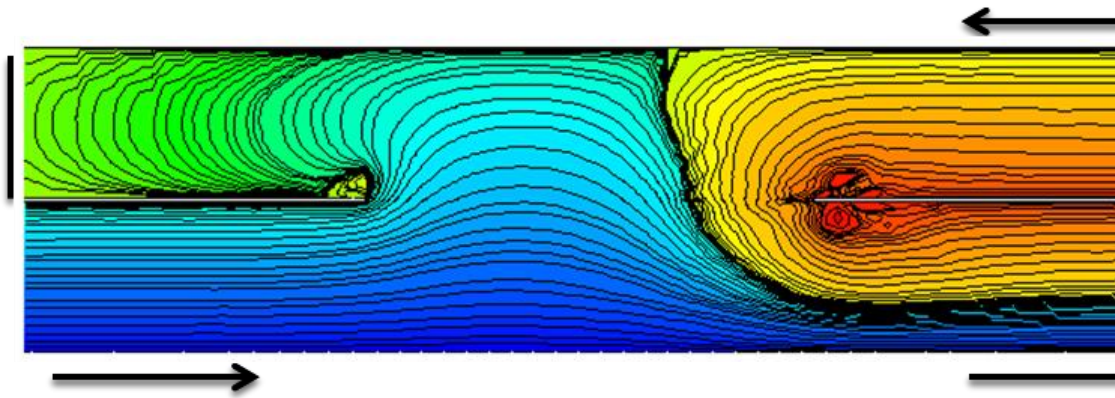
Re=2000



Re=3000



Re=4000



Re=5000

Figure 6.9 Streamline functions of mixing and separating of Newtonian fluid flows for unequal (1, 2) flow rate in a channel filled with porous medium, increasing Re from top to bottom.

#### 6.5.3.4 Effects of change in flow rate

Streamline functions are presented in figures [(6.8) to (6.9)] under unequal [(1, 1.5) and (1, 2)] flow rates in a channel filled with porous media for Newtonian materials. Changing flow rate in one of the upper arms has effects on vanishing vortex developed on the right side of the domain at the edge of central fixed plate. Increasing the value of Reynolds number along with double flow rate in top arm gives more strength and intensity to the formation of vortices. Spreading and splitting of one vortex into more or its generation have been observed and more recirculation indicates more inertial effects on the domain at its sharp edge towards the flow departure.

Solutions are found for the increasing value of Reynolds number along with changing flow rates in the top channel arm and no completely unidirectional flows are found. But reversed flow has been increased due to the movement of flow from lower to upper arm

in salient corner and middle separation gap up to the wall of the top channel arm. That reversed flow blocks the flow coming from upper channel arm towards the middle gap and forces to be reversed flow towards the outlet. Mixing only increases in the bottom channel arm in the section towards the exit.

#### **6.5.3.5 Effect of unidirectional flows and permeability on pressure**

Figure (6.10) shows the patterns of increasing inertia and three relative flow rates on pressure difference. Newtonian fluid flows in a channel filled with porous media have a variation of pressure difference in the channel with respect to increasing Reynolds number. For equal and unequal flow rates in the two arms of a channel the pressure difference increases nearly linear with the increasing Reynolds number and with varying flow rates. The value of permeability has been varied at different Reynolds number during varying flow rates, which gives shoot up to pressure. Change in the value of permeability has changed the value of pressure difference as shown in figure (6.10) (at  $Re=1000$  and  $2000$ ). Increase in the value of  $Re$  gives increase in pressure as shown in figure (6.10) during relative flow rates.

### Influence of Different Flow Rates on Maximum Pressure

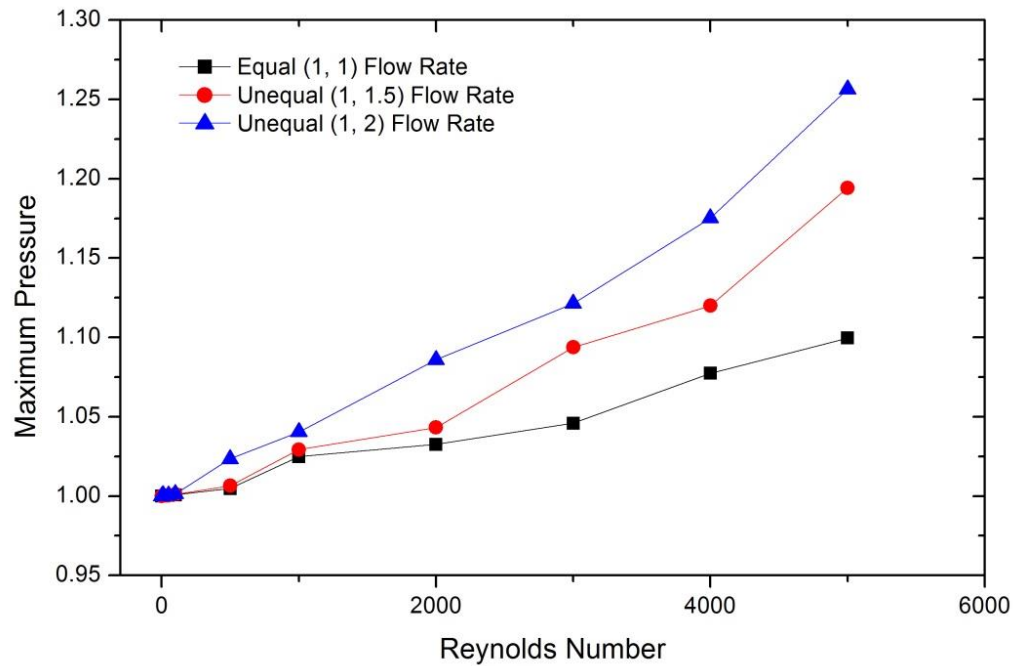


Figure 6.10 Comparison of maximum scaled pressure with increasing inertia at different flow rates in a channel filled with Porous Media

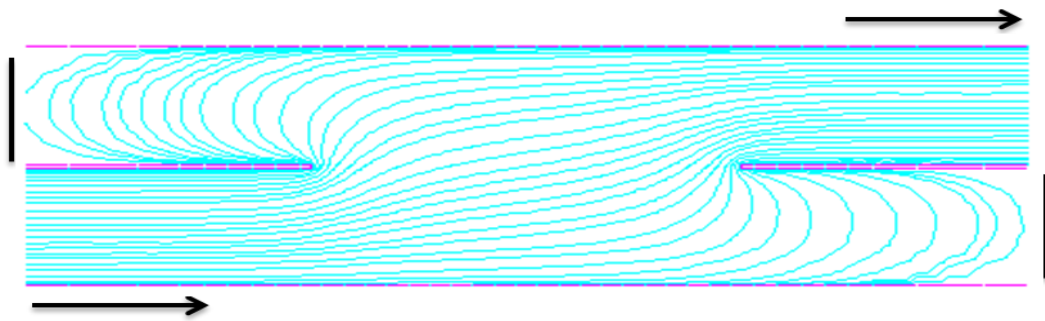
#### 6.5.4 Unidirectional flows of Newtonian fluid in a channel filled with porous media

( $G_4$ )

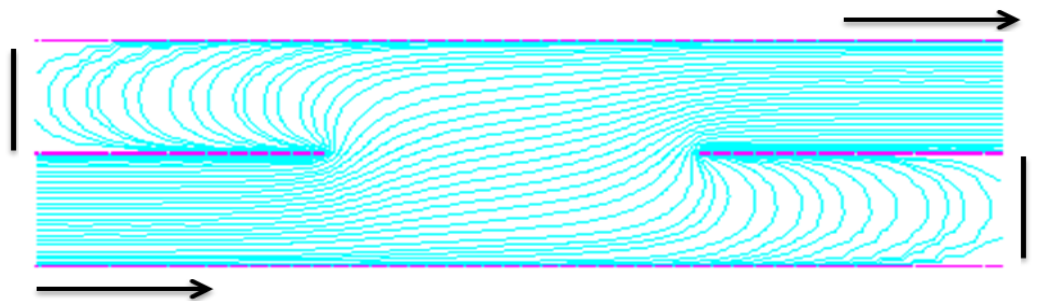
In this unidirectional flow condition given in figure [5.1(d)] development of a vortex and its intensity will be analysed along with pressure difference. In this case there is one inlet from the left in the lower arm and only one outlet from its right in the top arm of a channel. Effects of porosity and permeability will be compared with other flow rates and flow directions discussed in above three configurations ( $G_1, G_2$  and  $G_3$ ) and with the results discussed in a channel filled without porous media in chapter five.

#### 6.5.4.1 The influence of inertia on flow structure

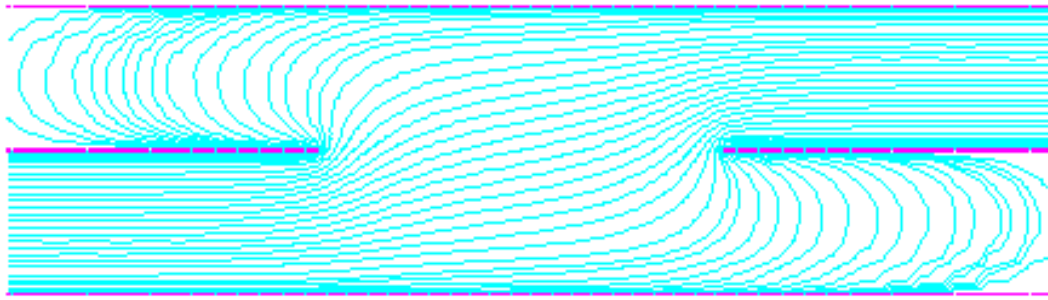
Unidirectional flows of Newtonian fluids, the simulations of are performed under Reynolds numbers ( $1 \leq Re \leq 10000$ ) in a channel filled with porous media and presented in figure (6.11). No vortex growth has been noticed even under higher Reynolds number up to  $Re=10000$ . Unidirectional flow inertial effects are negligible compared with the reversed flow cases. Further presence of porous materials has also high impact on the lesser chance for inertia compared with the channel filled with no porous media as shown in chapter five. It is evident that results are in very good agreement with the results available in open literature for fluid flows in channel (Al-Nimr and Aldoss, 2004).



$Re=1$



$Re=5000$



Re=10000

Figure 6.11 Streamline function for unidirectional flows of Newtonian fluid in a channel filled with Porous Media, increasing Re from top to bottom.

#### 6.5.4.2 Effects of flow rates and inertia on pressure

Figure (6.12) shows the variation of pressure difference in the channel through porous media with respect to increasing Reynolds number of Newtonian Fluid Flows. For unidirectional flow in the two arms of the channel the pressure difference increases non-linearly with the increasing Reynolds number, with the varying values. As it is obvious from graph in figure (6.12) at [Re=1 to 5000] growth is linear because the value of permeability ( $\kappa$ ) is fixed 0.001. After decreasing the value of  $\kappa=0.00001$  from Re=600 to 10000 the pressure increases and trend led to non-linear. Pressure difference is affected by varying the value of permeability and inertia. As under initial values of Re increase in pressure was very small and was not visible on graph. Therefore, vertical axis has been rescaled to show clear picture.

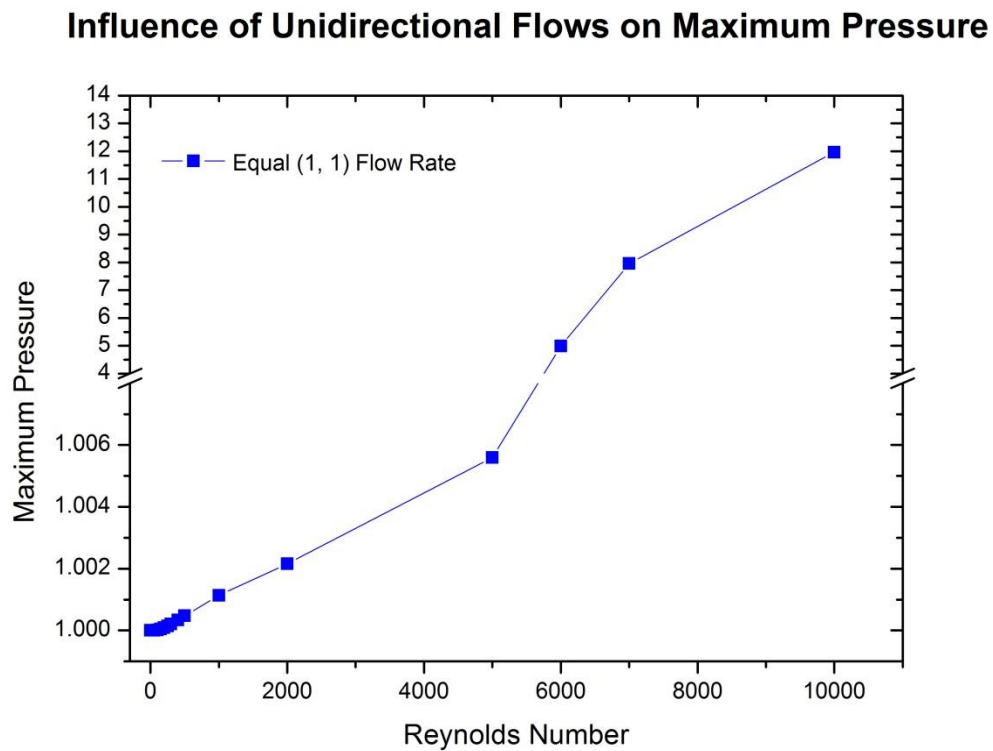


Figure 6.12 Maximum scaled pressure with increasing inertia in unidirectional flows of Newtonian Fluids in a channel filled with Porous Media.

## 6.6 Summary

In this chapter effects of inertia on flow domain, difference in pressure difference under inertia and permeability are investigated numerically. Newtonian flows are studied in a channel filled with porous media. Taylor-Galerkin/Pressure-Correction primitive variable finite element algorithm has been used. Reversed and unidirectional flows of Newtonian flows are investigated for varying flow rates and directions in a porous channel. The algorithm was found to be stable at Reynolds number from 1 to 10000 and accurate in its predictions of steady and complex flows. For mixing and separating as well as unidirectional flows, different bifurcations have been examined by changing flow direction and flows rates in the same domain filled with porous media. The algorithm

gives satisfactory mesh convergence for the full compressible Navier-stokes equation. The physics of the flow is also predicted realistically by the numerical scheme. The flow patterns are presented as streamlines. The level of inertial effects on the flow structure, non-dimensionlised scaled pressure difference along with porosity in the channel is presented.

Due to the presence of porous materials activity of vortex development was less than that in a channel filled without porous media. At a very high Reynolds number some vortices have been seen near the sharp edge of centrally fixed plate. Changing flow rates in the top channel arm has vanished the vortex developed from the left on the nip of the central plate at its near edge. In the case of unidirectional flow there was no activity of vortex progress as compared to reversed flow rate in the same computational domain. An increase of Reynolds number along with changing flow rates in the upper arm of a channel has led to an increase in the intensity of a vortex development near both ends of centrally located plates fixed of middle gap of the geometry for both equal and unequal flow rates. But the strength of vortex of the right of central plate is higher.

In all three flow rate conditions and increasing inertia, an increase in non-dimensional pressure difference has been observed by increasing the flow rate into the top arm of a channel. Patterns of pressure verses flow rate and inertia are changing with varying values permeability. Graph shown in figure (6.12) shows a linear increase in pressure for fixed values of permeability for initial values of  $Re$ . with higher values of inertia and smaller values of permeability, an increase in pressure is non-linear. An increasing flow rates has

an increasing effect in the value of pressure. Decreasing values of permeability has the same influence on pressure.

It has been observed that Newtonian fluid flows in a channel filled with porous media with an increasing inertial force have insignificant effects on vortex growth, intensity and size. This numerical scheme provides physically correct predictions and in very good agreement with the published results in open literatures. It is further determined that the inertial term has a negligible effect on the behaviour of the flow with power law index and the whole range of Darcy's and Forchheimer numbers. The mass of the liquid contained in the porous domain decreases with decreasing inertia premises. As a result, a very short time is required for the fluid to reach the steady state behaviour. It has been reported in literature as well (Alazmi and Vafai, 2001).

Most of the numerically simulated results are post processed to show many changes on the computational domain. Stream functions with velocity profiles and velocity vectors are presented for selected Reynolds numbers. stream functions with contour number and its corresponding values are labelled with vertically aligned colour bars. Contour types are presented in lines, flood and in some case lines and flood both. Velocity Vectors are also presented for selected Reynolds number. These results are shown in appendix-E and referenced in respective sections of the chapter-6 for  $G_1 - G_4$  (domain of all four Geometries) for all three flow rates for porous media.

---

## Chapter 7. Newtonian Fluid Flows in a Pipe Filled with and without a Porous Media

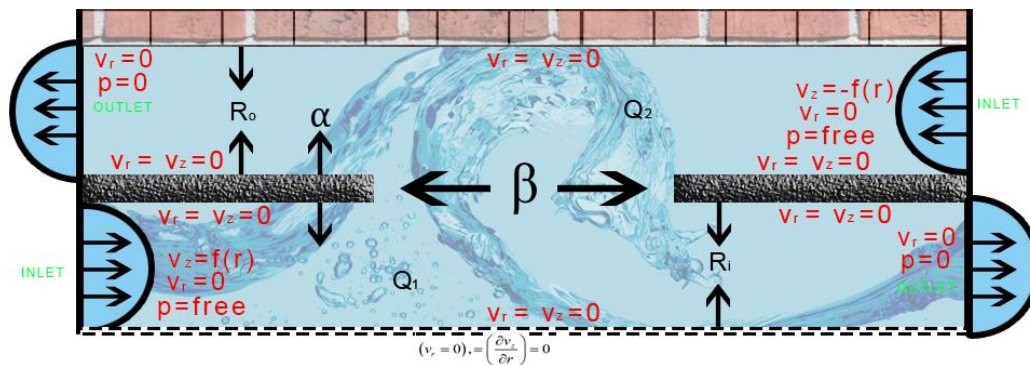
### 7.1 Introduction

Having investigated two dimensional planar channels with Cartesian coordinates in chapter five and six, two dimensional axi-symmetric combined mixing and separating flows in pipe/tube domain are focused in this chapter. These consist of one with reversed pipe and annular flows interacting through a gap in the common separating walls with Newtonian fluids in both cylinders. By using time dependent finite element approximation in the combination of semi-implicit Taylor-Galerkin/Pressure Correction scheme, steady results are obtained in cylindrical polar coordinates. The effects of increasing inertia on change in flow directions, varying flow rates and pressure difference configurations in both the central pipe and outer cylinder are considered. Due to unavailability of experimental data as well as numerical solutions in tubes or pipes the results were compared against channel flows [(Cochrane et al., 1981); (Webster, 1982); (Baloch et al., 1995a), (Afonso et al., 2011), (Khokhar et al., 2012) and (Khokhar et al., 2013)].

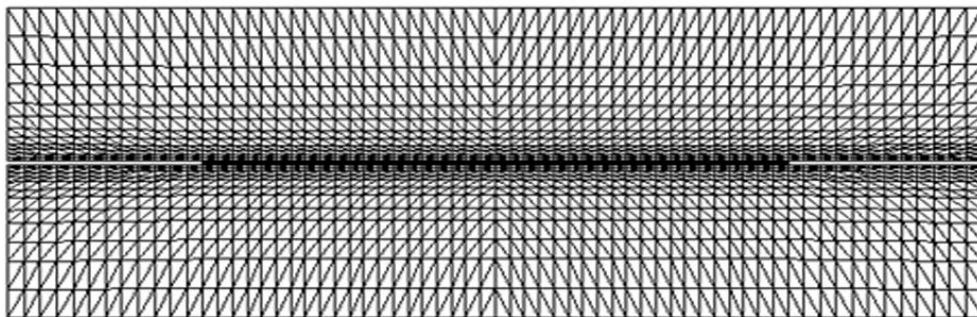
### 7.2 Problem specification

As shown in Figure [7.1(a)], the pipe is assumed as an inflexible circular tube, having two dimensional axial and radial directions. There are two pipes/cylinders one with small diameter, which is placed within another pipe of the large diameter. Fluid is flowing through both pipes, i.e., in the inner pipe from left side and in the outer cylinder from right side as an annular flow. In between inner pipe there is a gap in the centre of the cylinder, where fluid is mixing and separating at the same time (combine). Flow of fluid is being the same or different type by changing Reynolds number. Radius of the inner pipe is  $R_i$ , the outer pipe having  $R_o$  and

whereas  $\alpha = 0.0245$  is non-dimensional thickness of the inner pipe. In this research, flow of Newtonian fluids through combined pipe/cylinder with or without porous media is modelled. For the sake of simplicity similar mesh of planner domain discussed in chapter 5-6 has been used here after having had a study on mesh density. Typical mesh is shown in Figure [7.1(b)]. The total number of elements, nodes and degree-of-freedom are 5049, 19057 and 73953 respectively.



(a)



(b)

Figure 7.1 Geometries of the computational domain and mesh; (a) Geometry of mixing and separating fluid flows in a cylindrical pipe, (b) Finite element mesh.

### 7.3 Governing system of equations

Consider that the isothermal flow of incompressible Newtonian fluids in non-porous pipe and filled with porous media is to be axisymmetric in two dimensions, whilst the flow is fully

established at both inlets. The discussion of mass and momentum transport equations, which govern the flow of Newtonian fluids subject to the boundary conditions are written in the cylindrical polar coordinates as:

**Conservation of mass:**

$$\frac{\partial v_z}{\partial z} + \frac{1}{r} \frac{\partial (rv_r)}{\partial r} = 0 \quad (7.1)$$

**Darcy's–Brinkman transport component wise equations neglecting body force:**

r-component

$$\begin{aligned} \frac{\partial v_r}{\partial t} + v_z \frac{\partial v_r}{\partial z} + v_r \frac{\partial v_r}{\partial r} = \\ -\frac{1}{\rho} \frac{\partial p}{\partial r} + \frac{\mu}{\rho} \left( \frac{1}{r} \frac{\partial}{\partial r} \left( r \frac{\partial v_r}{\partial r} \right) + \frac{\partial^2 v_r}{\partial z^2} - \frac{v_r}{r^2} \right) - \frac{\omega \mu}{\rho \kappa} v_r - \frac{1}{\rho} \frac{\partial p}{\partial r} \end{aligned} \quad (7.2)$$

z-component

$$\frac{\partial v_z}{\partial t} + v_z \frac{\partial v_z}{\partial z} + v_r \frac{\partial v_z}{\partial r} = -\frac{1}{\rho} \frac{\partial p}{\partial z} + \frac{\mu}{\rho} \left( \frac{1}{r} \frac{\partial}{\partial r} \left( r \frac{\partial v_z}{\partial r} \right) + \frac{\partial^2 v_z}{\partial z^2} \right) - \frac{\omega \mu}{\rho \kappa} v_z - \frac{1}{\rho} \frac{\partial p}{\partial z} \quad (7.3)$$

Where,  $v_z$  and  $v_r$  are the axial and the radial velocity components,  $p$  is the isotropic pressure,  $\rho$  is the density of fluid and  $\mu$  represents the viscosity of fluid materials and  $K$  is the permeability of porous media. For non-porous simulations, the last Darcy's term will vanish in above both equations (7.2 and 7.3), and Darcy's–Brinkman equation will reduce in to Navier–Stokes equation.

### 7.3.1 Non-dimensional system of equations

In dimensionless analysis, a dimensionless number or a number with dimension (1) is a pure number without any physical units. For suitability, the governing system of equations is written in the following non-dimensional form by introducing the following dimensionless variables:

$$r^* = \frac{r}{R_c}, \quad z^* = \frac{z}{R_c}, \quad v_r^* = \frac{v_r}{V_c}, \quad \kappa = \kappa^* R_c^2 \frac{v_z}{V_c}, \quad t^* = \frac{t v}{R_c}, \quad p^* = \frac{p}{\rho V_c^2}$$

Where,  $V_c$  and  $R_c$  are characteristic velocity and length of pipe respectively,  $V_c$  is taken as velocity of the fluid and  $R_c$  is taken as radius of an inner pipe. Substituting these non-dimensional values in Equations [(7.2) to (7.3)] and discarding asterisks for brevity and simplicity, the system of Equations [(7.1) to (7.3)] may be rewritten as:

$$\frac{\partial v_z}{\partial z} + \frac{1}{r} \frac{\partial(rv_r)}{\partial r} = 0 \quad (7.4)$$

$$\frac{\partial v_r}{\partial t} + v_z \frac{\partial v_r}{\partial z} + v_r \frac{\partial v_r}{\partial r} = -\frac{\partial p}{\partial r} + \frac{1}{\text{Re}} \left( \frac{1}{r} \frac{\partial v_r}{\partial r} + \frac{\partial^2 v_r}{\partial z^2} - \frac{v_r}{r^2} \right) - \frac{1}{\text{Re} D_a} v_r \quad (7.5)$$

$$\frac{\partial v_z}{\partial t} + v_z \frac{\partial v_z}{\partial z} + v_r \frac{\partial v_z}{\partial r} = -\frac{\partial p}{\partial z} + \frac{1}{\text{Re}} \left( \frac{1}{r} \frac{\partial v_z}{\partial r} + \frac{\partial^2 v_z}{\partial z^2} \right) - \frac{1}{\text{Re} D_a} v_z \quad (7.6)$$

Where,  $D_a$  is Darcy's number and  $\text{Re}$  is a Reynolds number. They are defined as:

$$\text{Re} = \frac{\rho V_c R_c}{\mu}, \quad \text{and} \quad D_a = \frac{\kappa}{R_c^2} \quad (7.7)$$

### 7.3.2 Initial and boundary conditions

To present a well posed problem specification for the flow of fluid in pipe, it is essential to advise the proper initial and boundary conditions. To stipulate the value of  $\mathbf{v}_0$  at the initial time, the initial condition is taken as:

$$\mathbf{v}(z, 0) = \mathbf{v}_0(z); \text{ Subject to } \nabla \cdot \mathbf{v}_0 = 0.$$

For initial conditions, velocity vector field and pressure the simulations start with quiescent initial conditions as vanishing values of velocity vector and pressure and tractions-free velocity components are executed ( $v_r = v_z = p = 0$ ).

As shown in Figure7-1 (a), the boundary conditions are considered as fundamental conditions for simulation of the well posed problem. A normal traction free boundary condition is implied at the domain exit, at which a pressure datum of zero is fixed. The remaining surfaces are represented as solid walls where no-slip boundary conditions are taken  $v_r = v_z = 0$ . On axis of symmetry, Neumann conditions are imposed ( $v_r = 0, \frac{\partial v_z}{\partial r} = 0$ ). For the fluid flows through pipe/cylinder, flow proceeds from fully developed inlet velocity profile for both an inner tube and outer cylinder. On the inlet of a pipe, the non-dimensional analytic solution and axial based

velocity are defined without cross flow. The boundary conditions from both inlets either on inner or outer pipe are imposed as follows:

$$v_z = V_1(1-r^2) \quad (\text{On left inlet of inner pipe}) \quad (7.8)$$

And

$$v_z = V_2(r-a)(b-r) \quad (\text{On right inlet of outer cylinder}) \quad (7.9)$$

Where,  $V_1$  and  $V_2$  are maximum velocities based on flow rate,  $a = R_i + \alpha$  (where  $\alpha = 0.0254L$  is the thickness of the inserted plate in the middle of the geometry) and  $b = R_o$ . For axisymmetric flow velocity vector field axial and radial coordinates are  $v_r$  and  $v_z$  where  $v_r$  velocity is vector component in radial direction and  $v_z$  is velocity component in axial direction. In case of equal flow rate maximum velocities at the centre of a domain are  $V_1 = V_2$ , whilst, in an unequal flow rate  $V_1, V_2$  takes the ratio 1: 2 of fluid.

The mesh is designed in such a way that the minimum size of the element is chosen in the vicinity separation of  $0.003L$ . Finite element mesh on the domain is illustrated in Figure 7.1(b), where the total number of elements, number of nodes, number of boundary nodes and number of vertex nodes are 1328, 2853, 392, 763 respectively.

#### 7.4 Numerical scheme

Taylor-Galerkin/Pressure-Correction finite element method is well thought-out as a semi-implicit time stepping procedure has been employed to simulate the Navier-Stokes equations, along with the incompressibility constraints. To get highly accurate time-marching algorithm

is the basic tactic lying behind this method and is used to compute transient as well as steady flow problems proposed by (Donea,1984a)). In chapter 4, this method is discussed in detail and also applied in chapters (5-6).

Briefly, the Taylor-Galerkin based algorithm is a fractional step method, that semi discretises first in the temporal domain, using Taylor series expansion in time by adopting a two-step Lax-Wendroff approach and a pressure-correction procedure, to extract a time stepping scheme of second order accuracy. The discretisation is computed via a spatial Galerkin finite element method, where velocities are approximated quadratic basis functions and pressure is an approximated linear basis function to ensure Babuska-Brezzi condition in order to avoid superior oscillation in pressure [(Cuvelier et al., 1986) and (Johnson et al., 1990)]. Weak formulation of semi-implicit Taylor-Galerkin/Pressure-Correction algorithm for the domain filled with and without porous media has been presented in detail.

### **7.5 Results and discussions**

The flow domain was meshed by employing uniform conformal mappings, a technique which automatically aligned element sides with streamlines and preserved orthogonally of the elements. The flow was considered by examining inertia special effects on flow structure, impact of change in flow rates on flow structure, effects of flow on pressure difference and influence of porosity in the computational domain. Stream function calculated vortex length and intensity of recirculation of flows at different Reynolds number. Therefore, the computed results are presented by stream functions including pressure difference at inlet against Reynolds number for increasing Reynolds number. Velocity profiles were imposed at different axial locations and velocity profiles at axis of symmetry.

Critical Reynolds number values are identified for the formation of vortex development in different flow structures by changing flow rates. For vortex formation the range of Reynolds number values was taken from  $(1 \leq Re \leq 200)$  for non-porous and  $(1 \leq Re \leq 5000)$  for Newtonian fluid flows of pipe filled with non-porous and porous media. Values of  $Re$  (density) gives us inertia factor. for Newtonian fluid flows for both flow rates Darcy's number is 1, value of viscosity is 1 and permeability varies from 0.1 to 0.00001.

### **7.5.1 Mixing and separating of Newtonian fluid flows in a pipe**

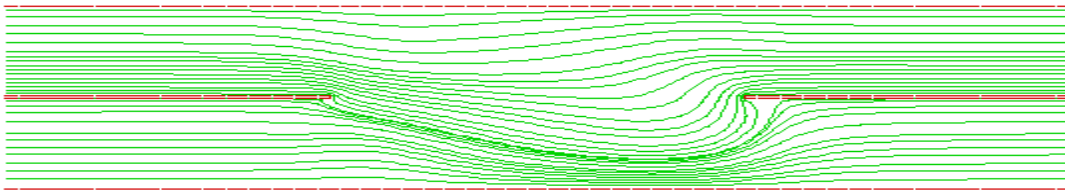
The domain of the problem shown in in Figure (7.1) is discretised into triangular elements, with mesh design of minimum element-size of  $0.025L$  with same specification discussed in chapters five and six. In this chapter instead of a channel, a circular pipe has been taken as test problem. Newtonian fluids are flowing in pipe filled with both non-porous and porous media. Numerical simulations are analysed by presenting streamline patterns and filled domain. The effects of changing flow rates, varying materials and impact of porous media will be examined on vortex development, its intensity and enhancement and pressure difference. Also results of pressure difference are computed at inlet against Reynolds number.

### **7.5.2 Newtonian flows in a pipe filled with non-porous media**

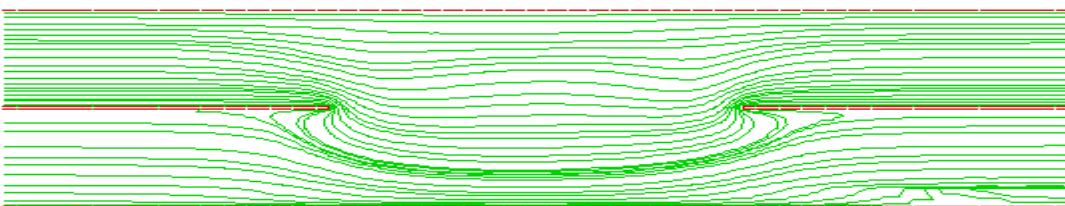
Flow outlines in a combing-separating formation are an important feature, found useful to start the presence of stagnant regions, and the productivity of overall progress. Flows of Newtonian fluid in a pipe filled with non-porous media have been displayed along with streamline projections in Figures [(7.2) to (7.3)]. In this section, numerical simulation of Newtonian fluids in combing-separating domain, investigation into influence of inertia through streamline patterns, vortex growth and impact of changing flow rate on flow structure are studied.

### 7.5.2.1 Equal (1, 1) flow rate

In case of equal flow rate maximum velocities at the centre of domain are  $V_1 = V_2$ . Whilst in case of unequal flow rate  $V_1$  and  $V_2$  takes the ration of fluids 1:2 as discussed in section 0. The impact of fluid inertia in terms of streamline projections has been displayed in Figure (7.2) with changing inertia in terms of the Reynolds numbers, from  $Re = 1$  to 200, respectively. It is found that the flow answers to the presence of the gap and breaks up, with some flow unidirectional, mixes in the gap and flow merging in both upper and lower exits of the domain ( $Re = 1$ ). It is observed that at equal (1, 1) flow rate, no significant activity of vortex generation has occurred in the centre of the domain, even at high Reynolds number. In all cases, the flow structure remains similar except pushing flow to internal pipe towards the line of symmetry. This flow phenomenon is not fully understood.



Re=1



Re=10

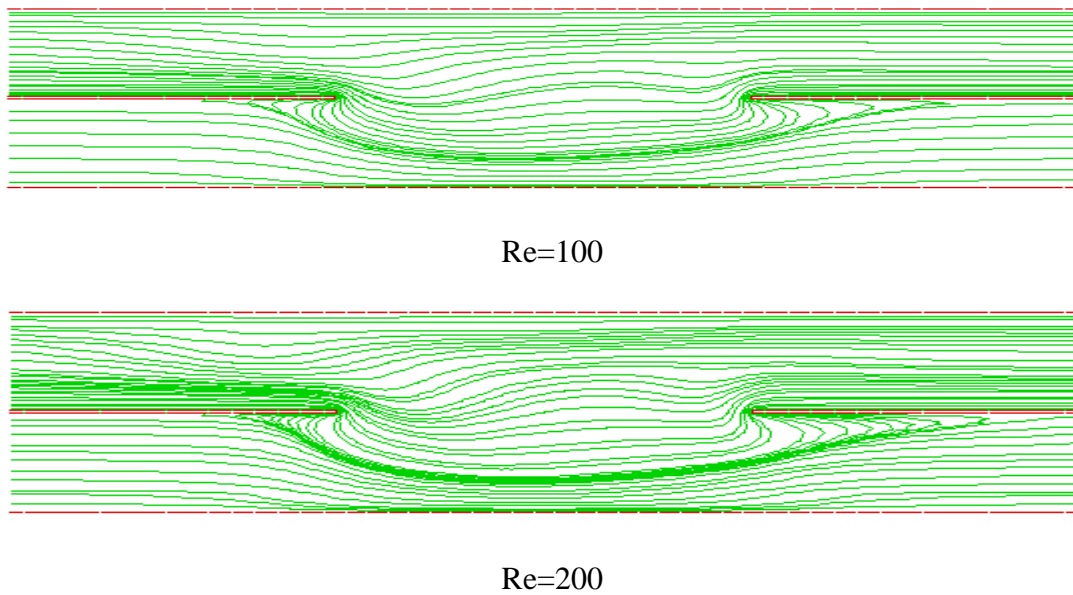


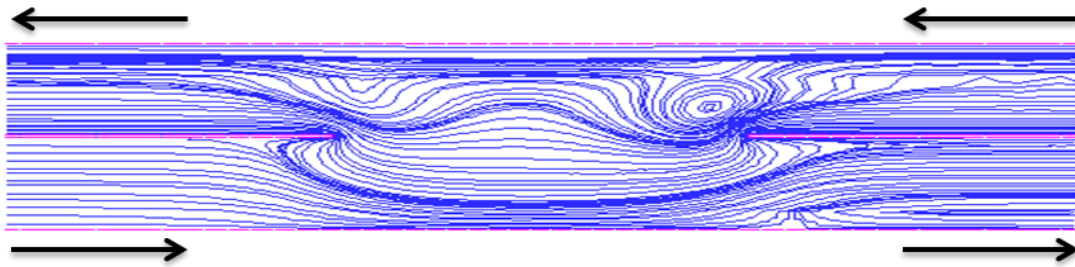
Figure 7.2 Streamlines for Newtonian mixing-separating flow of equal (1, 1) flow rate in a pipe filled with the non-porous medium, increasing Re from top to bottom.

### 7.5.2.2 Unequal (1, 2) flow rate

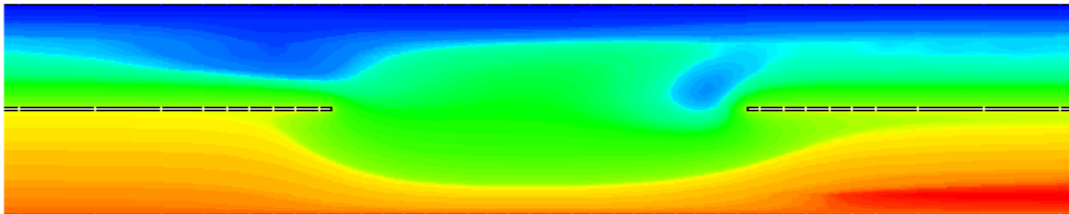
In order to understand the effects of inertia, the flow of a Newtonian fluid has been observed and numerical estimates are presented with increasing Reynolds number from  $Re=1$  to  $Re=200$  in Figure (7.3). To analyse the flow phenomena with changing flow rates from equal to unequal in both inner and outer pipes, it was deliberated to set up, double flow rate in outer pipe in opposite direction. A very interesting flow phenomena is observed, even at a low value of inertia at unity ( $Re = 1$ ). A strong recirculating region appears in the centre of the outer pipe at a nip/in the vicinity of separating region, the flow structure is shown in Figure (7.3).

As increased inertia was beyond  $Re = 1$ , this vortex activity increases and occupy centre of the domain. The vortices appeared in outer pipe in its upstream from right and left. With increasing Reynolds number at  $Re=50$  the above vertex discussed shifted down in the centre of a pipe.

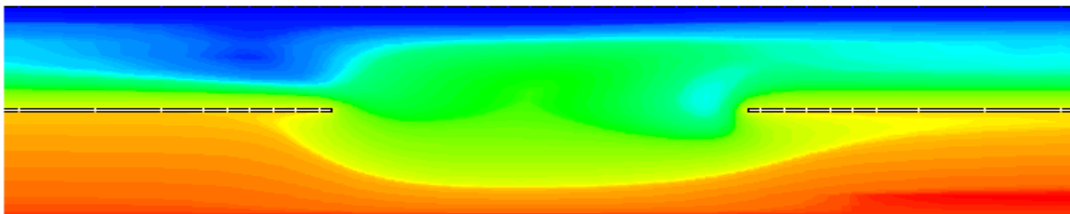
Also at  $Re=50$ , two other vortices occurred one strong vortex in the middle gap of the domain slightly above the central gap and the other vortex was developed in the downstream of the outer cylinder. With increase in the value of  $Re$  these all three vortices were strengthened and become stable with increasing Reynolds number up to 200. The presence of a vortex in the gap, caused fluid coming from inlet has been pushed an inner pipe. The double flow rate in the outer cylinder has pushed vortex near the plate into the inner pipe as well. Mixing of fluids was only observed in the inner pipe, due to pushing flows towards the line of symmetry.



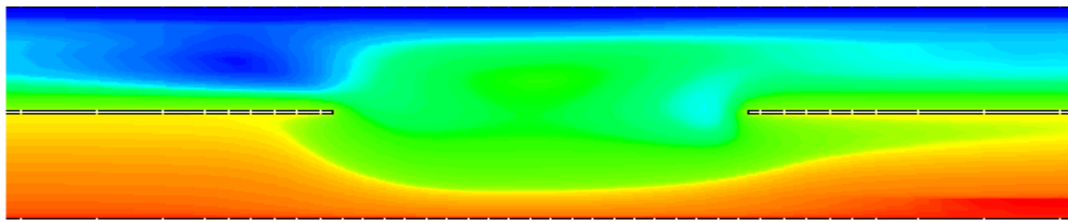
Re=1



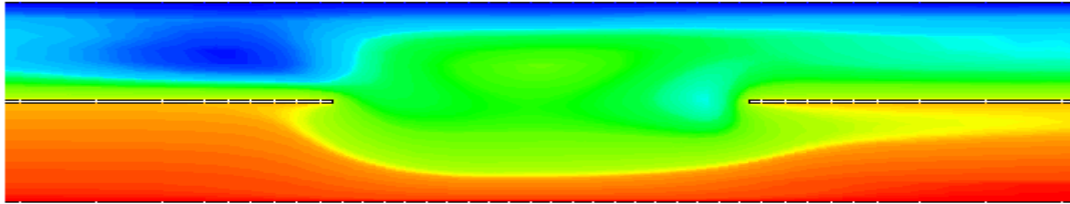
Re=25



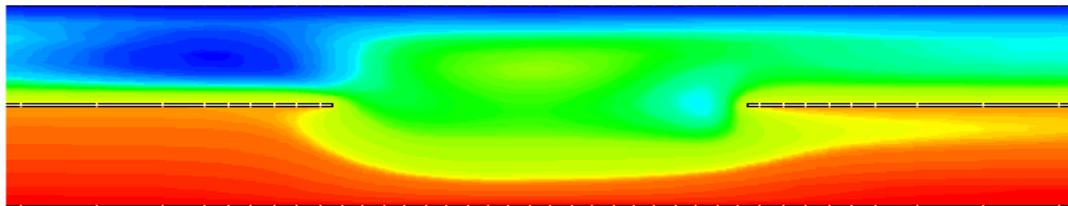
Re=50



Re=100



Re=150



Re=200

Figure 7.3 Streamlines for Newtonian mixing-separating flow of unequal (1, 2) flow rate in a pipe filled with the non-porous medium, increasing Re from top to bottom.

### 7.5.2.3 Influence of flow rate

The results from both equal (1, 1) and unequal (1, 2) flow rates of Newtonian fluids are shown in Figures [(7.2) to (7.3)]. Changing flow rate in outer cylinder has given much more rise in vortex intensity and vortex enhancement in the outer cylinder and also in the separation gap of the domain. In unequal flow rate fluid has been pushed in down in the separation gap of the inner pipe towards the line of symmetry. Double flow caused mixing only in inner pipe.

#### 7.5.2.4 Effects of flow rates and inertia on pressure

In Figure (7.4) Pressure in Newtonian mixing and separating flow of fluids in a pipe filled a non-porous medium is presented. Pressure has been scaled in the same way as discussed in Chapters five and six for Newtonian fluid flows in a channel filled with non-porous and porous media. For Newtonian fluid flows non-dimensional scaled pressure obtained in inner and outer pipes filled with non-porous media is  $1 \leq p_s \leq 1.132$  and  $1 \leq p_s \leq 1.6309$  under both equal (1, 1) and unequal (1, 2) respectively. Varying flow rate and increasing inertia have effects of increase in pressure. In a channel flow's frequency of vortex development was higher than pipe flows. For initial values of Re from (Re=1 to 50), increase in pressure is less than compared from (Re=100 to 200). As shown in Figure (7.4) under equal flow rate growth is linear but in double flow rate increase in scaled pressure is non-linear.

In channel flows increase in pressure for initial values was not significant but in pipe flows it is obvious. Results could be compared as shown in Figures [(5.5) and (5.13)] with Figure 5-7. In pipe flows influence of flow rate is also obvious when compared with the channels flows. For initial values of Re patterns of graph for each flow rate is almost had the same values but in pipe flows flow rate shows good difference. Even for higher values flow rate has obvious change as compared with channel flow discussed in chapter five. Figures [(5.5) and (5.13)] of channel flows give very good comparison against pipe flows shown in Figure (5.7).

### Effects of two Flow Rates and Inertia on Maximum Pressure

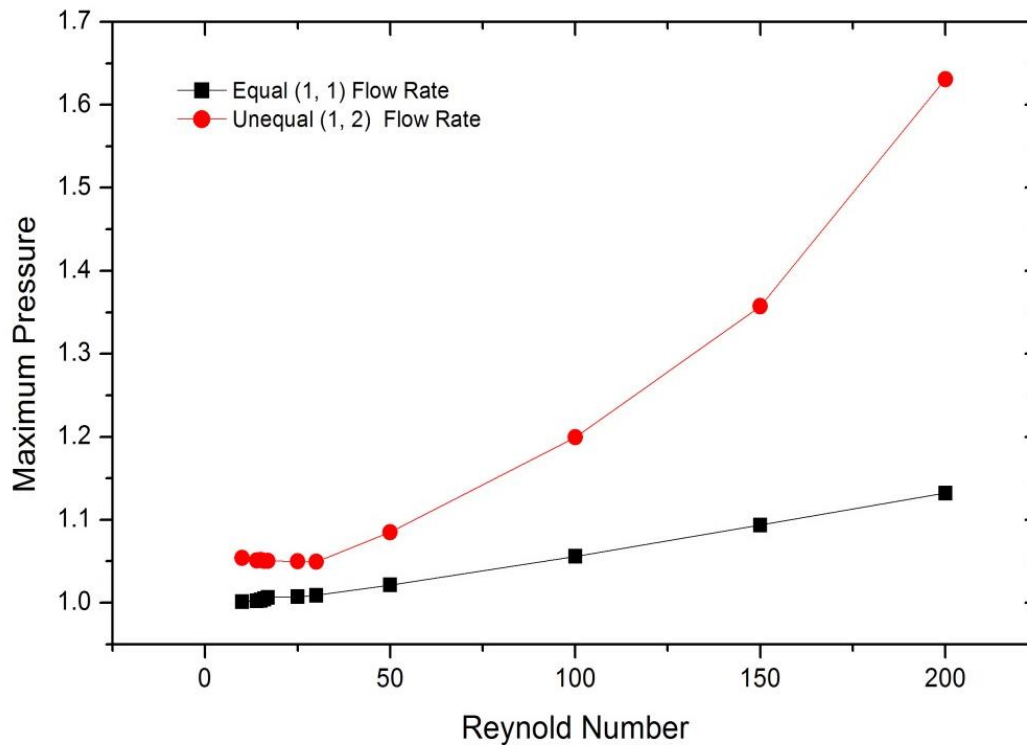


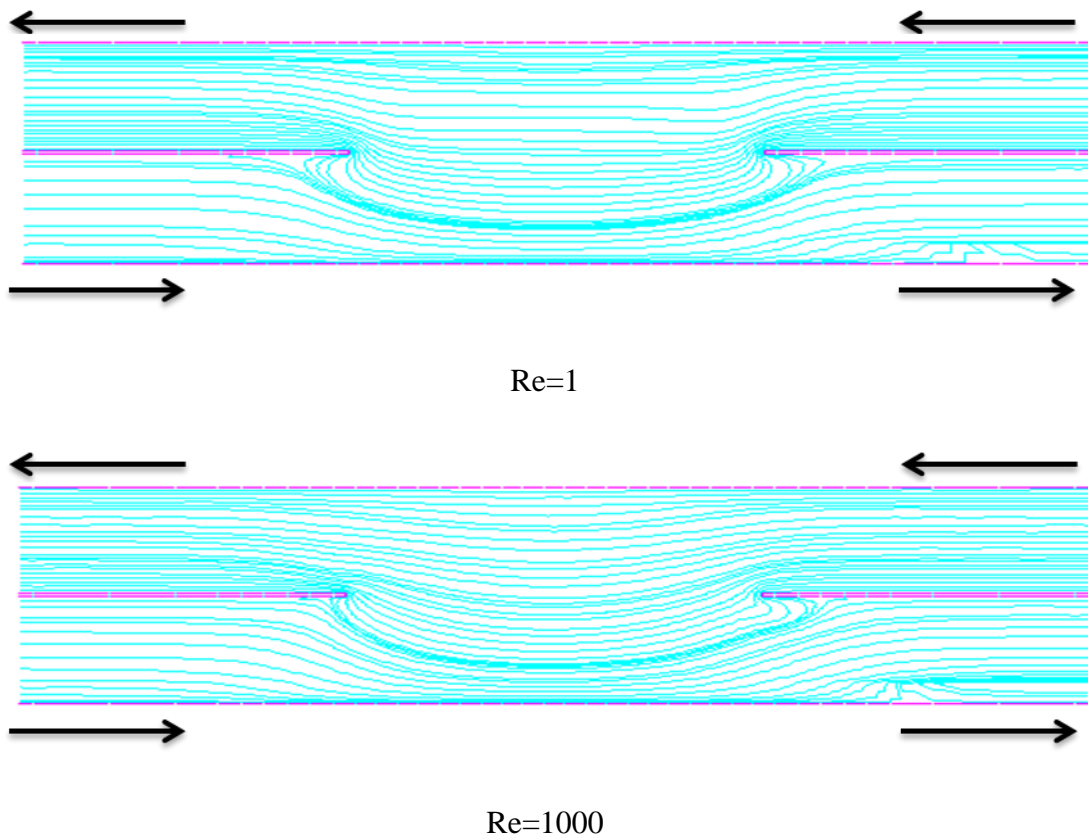
Figure 7.4 Comparison of maximum scaled pressure with inertia at different flow rates in Pipes filled with non-Porous Media.

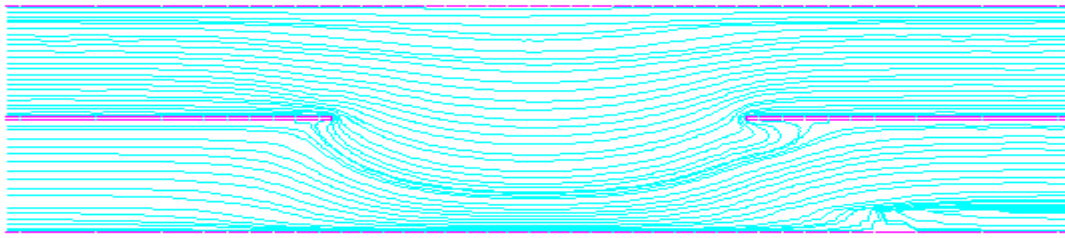
#### 7.5.3 Mixing and separating of Newtonian fluid flows in a pipe filled with porous media

The details of the particular combined mixing and separating flow problem are presented in Figure [7.1 (a)] with same specification discussed in section (7.5.2). In this section the domain is filled with porous media. Flows of Newtonian fluids filled with porous media have been displayed along with streamline projections from  $Re=1$  to  $Re=5000$  under both equal and unequal flow rates. Influence of increasing inertia, pressure difference and effects of porous media in the computational domain have been discussed.

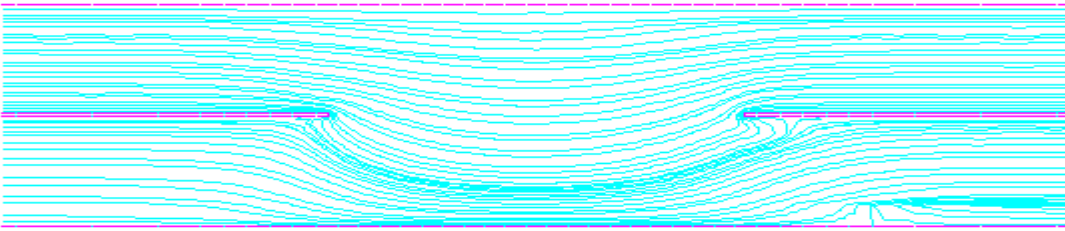
### 7.5.3.1 Equal (1, 1) flow rate

Numerical results of Newtonian fluids for increasing Reynolds number are presented in Figure (7.5) in a pipes filled with porous media. At the equal flow rate no noticeable activity of vortex development has been observed, however as fluid releases from the inlet cylinder and comes down to the central pipe and goes again back in the same cylinder in upper downstream. Subsequently no mixing has been observed as compared with flows without presence of the porous materials. For all increasing Reynolds number the same pattern of streamlines as have been seen that fluid flow has been pushed down in inner pipe towards the line of symmetry. As it appears in Figure (7.5), no significant inertial effect on the flow structure can be seen, therefore only few simulated results from  $Re=1$  to  $Re=5000$  are presented.





Re=3000

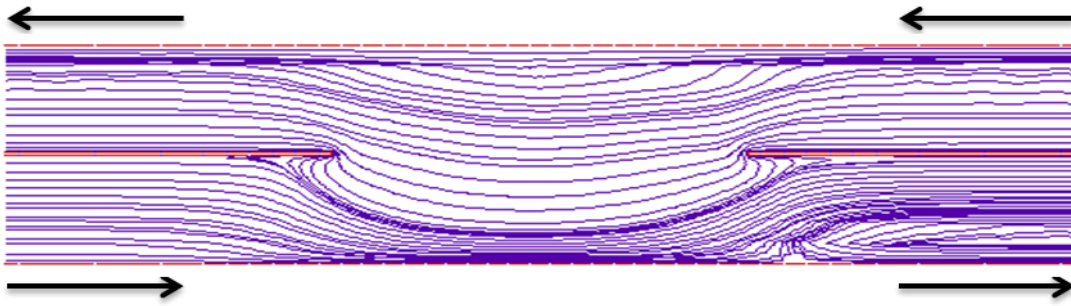


Re=5000

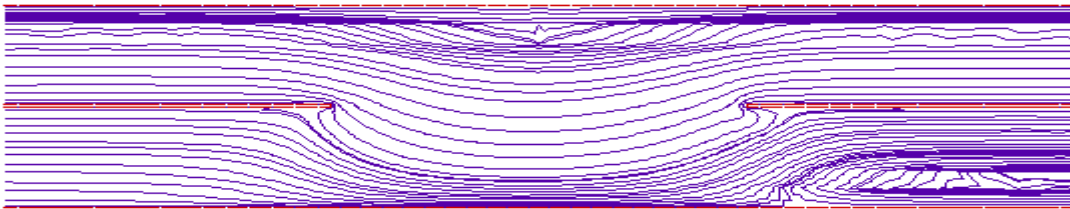
Figure 7.5 Streamline functions for Newtonian combined mixing and separating flow of equal flow rate (1, 1) in a pipe filled with a porous medium, increasing Re from top to bottom.

### 7.5.3.2 Unequal (1, 2) flow rate

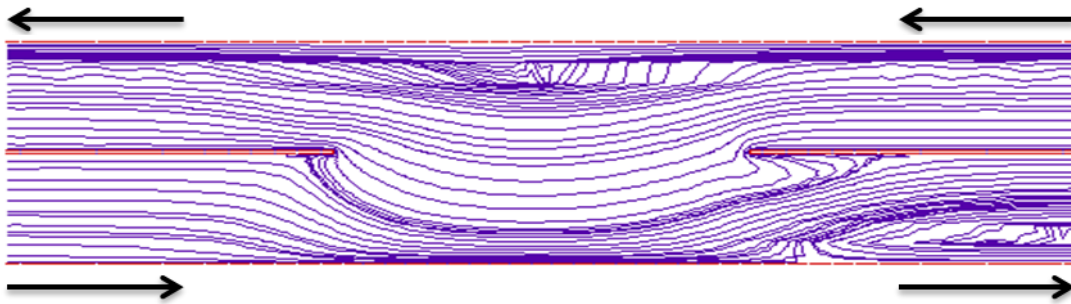
Figure (7.6) shows the simulated results from Newtonian fluids in the same domain filled with porous media from  $Re=1$  to  $Re=5000$ . It appears that with no noticeable activity of vortex development, subsequently no mixing has been observed compared with flows without presence of the porous materials. Due to double flow rate in the outer cylinder there appears a numerical artefact in the inner pipe which will be examined in later research. Similarly, fluid flows have been pushed down in the inner pipe as was the case in the equal flow rate shown in Figure (7.5).



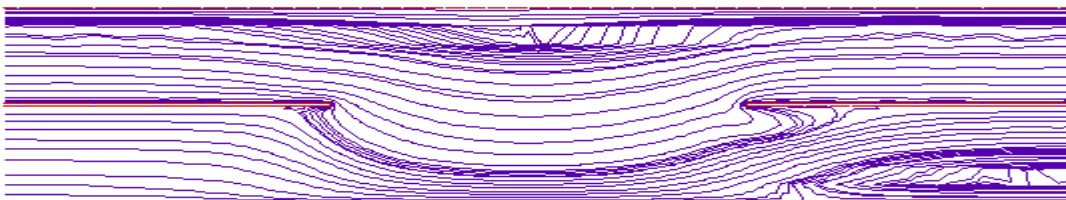
Re=1



Re=100



Re=3000



Re=5000

Figure 7.6 Streamline functions for Newtonian combined mixing and separating flow of unequal flow rate (1, 2) in a pipe filled with a porous medium, increasing  $Re$  from top to bottom.

### **7.5.3.3 Influence of flow rate**

Results for both equal (1, 1) and unequal (1, 2) flow rates in the computational domain are presented in Figures [(7.5) to (7.6)]. Numerically simulated results do not show any dramatic change with varying flow rate in outer the cylinder in the reversed direction. In an unequal flow rate fluids have been pushed down into a separation gap of the inner pipe towards the line of symmetry and again gone back to upstream of the outer cylinder. No mixing effects have been observed by changing flow rates in the outer cylinder. Some numerical artifact has been noticed in the inner pipe and will be examined future studies.

### **7.5.3.4 Effects of flow rates and permeability on pressure**

Numerically simulated results for pressure of Newtonian fluid flows in a pipe filled with porous media are presented in Figure (7.7). The graph shows trends under two different flow rates, increasing Reynolds number and varying values of permeability. Maximum and minimum scaled pressure for both equal and unequal flow rates are,  $1 \leq p_s \leq 991.8812$  and  $1 \leq p_s \leq 683.5631$  respectively. The results show a dramatic change in pressure with equal and unequal flow rates with changing values of permeability. In all conditions discussed in chapter five and in section (7.5.3) on Newtonian fluid flows either in channel or pipes filled with or

without porous media in the domain pressure increases with varying flow rates from equal (1, 1) to unequal (1,2) but in section it is opposite.

Pressure increases very fast with adding Darcy's effects in the computational domain compared with Newtonian fluid flows established in the domain without porous media in it. In this setting the value of  $\kappa$  varies for equal and unequal flow rates from  $0.001 \leq \kappa \leq 0.00001$  and  $0.01 \leq \kappa \leq 0.00001$  respectively. The value of Forchheimer number is fixed 0.001 for equal and 0.0001 for unequal flow rates. Influence of change in the values of permeability and Forchheimer number are obvious in pressure in the presence of varying flow rates and inertia. From  $Re=1$  to 4000 the value of permeability has been changed, it shows significant changes in the pressure as shown in Figure (7.7). From  $Re=4000$  to 10000 permeability is fixed and shows linear trend in the pressure as shown in Figure (7.7).

### Effects of two Flow Rates and Inertia on Maximum Pressure

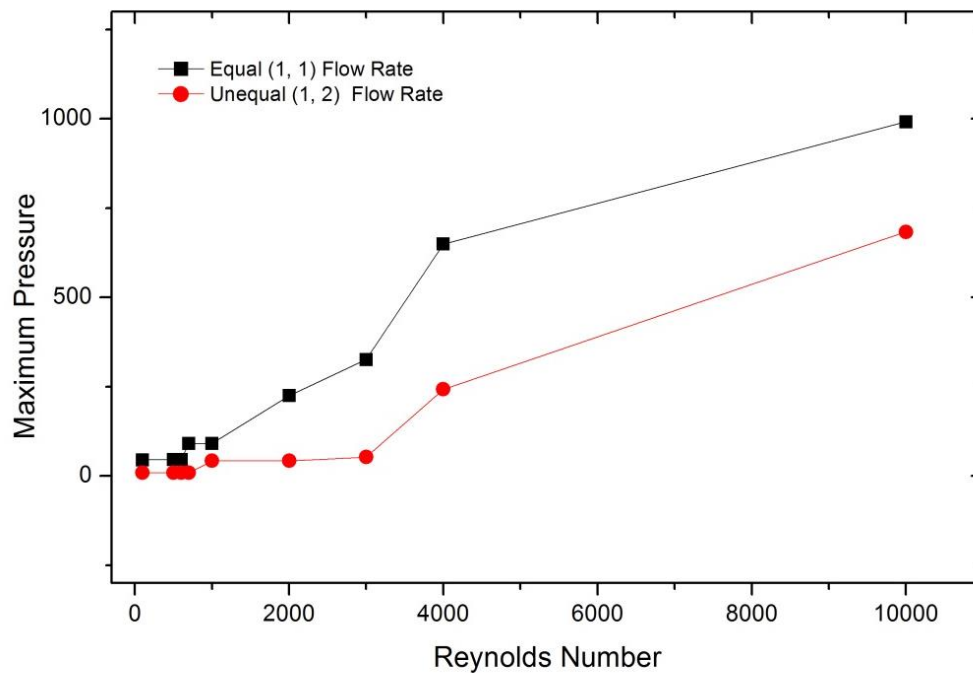


Figure 7.7 Comparison of maximum scaled pressure with inertia at different flow rates  
in Pipes filled with Porous Media

## 7.6 Summary

A numerical study has been conducted on Newtonian fluids filled with and without porous media in an inner pipe and outer cylinder under combing and separating flow configurations. Semi-implicit Taylor-Galerkin scheme found very useful in the study of pipes flow filled with or without porous media. Numerical solutions are presented through streamline patterns for stream functions and pressure difference with graphs to see the effects of changing flow rates from equal to unequal on a computational domain. The algorithm used has been found stable and accurate in its predictions. The numerical solutions obtained theoretically prove a very close agreement with results found in a channel filled with and without porous media as discussed from chapters five and six in this thesis.

The results presented in this work for Newtonian fluids in pipes initially filled with no porous media have demonstrated that there was no development of vortices in equal flow rate. In the same domain filled with non-porous media by changing flow rates in outer cylinder there has been a very effective development of vortices in the domain in the separation gap near the central plate in the outer cylinder even at low Reynolds number. In mixing and separating geometry for higher values of Reynolds number more vortices were observed in the downstream of outer cylinder and in the middle gap of the domain. By further increase of the value of  $Re$  these vortices grow in their size until being settled in the domain in the outer cylinder and in the separation gap.

Influence of changing flow rates, inertia and Darcy's number is obvious on pressure difference. Pressure increases with increasing inertia and flow rates in general. But an increase in pressure has been highly affected by equal to unequal flow rates along with varying values of

Forchheimer from 0.001 to 0.00001in pipes filled with porous media. The effects of permeability are seen on pressure. It can be seen in Figure (7.7) from  $Re=1$  to 4000 and again from  $Re=4000$  to 10000. The trend is non-linear for first half of the inertia values and then non-linear for the other half.

Lastly, Newtonian fluids have been passed in both pipes filled with porous materials. Results have shown no formation of vortices even if changing flow rate in outer cylinder or increasing the value of Reynolds number except flow has been pushed down in the inner channel toward symmetry. Again results are in good agreement with channel filled with porous media discussed in chapter 6.

Stream functions of computational domain for Newtonian fluids through circular pipes are presented with velocity profiles and velocity vectors as given in appendix-E. Stream functions are presented with contour number and its corresponding values of contours. Contour types are presented in lines, flood and in some case lines and flood both. Velocity Vectors are also presented for selected Reynolds number. These results are presented for equal (1, 1) and unequal (1,2) flow rates in both cases either domain is filled with non-porous or porous materials.

## **Chapter 8. Flows of Non–Newtonian Fluids through Tubes Occupied with and without a Porous Material**

### **8.1 Introduction**

For the numerical simulation of inelastic non–Newtonian fluids, this chapter presents a brief description of the mathematical models of flow in circular pipes filled with porous media. Details of the problem specification of combined mixing–separating domain are given. The modelling approaches used to capture the shear thinning behaviour of fluids are presented. Mathematically, the flow of inelastic non–Newtonian fluids can be modelled by means of continuity and time–dependent generalised momentum equations. For axisymmetric two–dimensional cylindrical polar frame of reference, these governing equations needs initial and boundary conditions and dimensionless forms are discussed.

Justification of applied numerical scheme is given which has been already used in chapters 5 to 7. The results and discussions of the numerical simulations are described for the used models. The effects of inertia on flow domain on the flow domain, under increasing  $Re$ , varying flow rates, power law index are presented with streamline functions. The influence of inertia, varying flow rates and permeability on pressure difference are debated. Finally, general discussions of the models, their effects on the flow domain due to changing power law index, increasing Reynolds number, permeability on pressure are summarized.

### **8.2 Problem specification**

Information related to the specific flow of combing and separating tube problems measured are given diagrammatically as shown in Figure [7.1(a)-(b)] of chapter 7 . Problem specification is

such that there are two pipes. One is with smaller diameter which is fitted within another cylinder of larger diameter. The inclusion of the inner pipe of small radius into the large tube domain produces dual inlets and outlets in both same as well as in opposite directions. Breaking of the inner pipe wall in the centre, creates separation (gap) between both pipes. For this investigation purpose, at entry and exit of computational domain, a fully developed flow is ensured. While, the length of an axi-symmetric two-dimensional computational domain is taken  $23 R$ . Where,  $R$  is taken as characteristic radius of inner tube, while, the non-dimensional thickness of inner pipe is taken as ( $\alpha = 0.0245$ ) in case of channel flow problem, discussed in earlier chapters.

Flow of non-Newtonian fluid passed pipes filled with porous material is simulated through circular rigid tubes having an axially symmetric gap and the size of a typical  $\beta = 3L$  discussed in previous chapters. All results presented here are computed with a mesh given in Figure [7.1 (b)]. The computational domain is discretised in small tessellation in reflected and symmetric fashion. In which, respectively, the total number of elements, nodes and degree-of-freedom are 5049, 19057 and 73953. Other details, diameters of the pipe and initial and boundary conditions of the domain may be referred to Figure (7.1) in chapter seven. Poiseuille flow was created in the two-dimensional domain as accessible in as discussed in previous chapters.

Couple of (Bird–Carreau and Power Law) models have been investigated to acquire the behaviour of inelastic non-Newtonian fluid. The effect of shear–rate dependent functional viscosity of fluid in a pipe can be investigated. The increasing levels of inertia were introduced by varying the Reynolds number and with varying flow rates in the outer cylinder. This allows an analysis of the effects of inertia on flow patterns and pressure difference.

### 8.3 The Power law model

The functional viscosity of inelastic non–Newtonian Power law model fluid is given in equation (8.1) as:

$$\mu(\dot{\gamma}) = \mu_0 (\dot{\gamma})^{n-1} \quad (8.1)$$

Where, zero shear viscosity ( $\mu_0$ ) also known as consistency index of the flow and the Power law index ‘ $n$ ’ taken as 0.9, 0.8 and 0.7. While, shear–rate is represented by ‘ $\dot{\gamma}$ ’ and defined as

$$\left| \frac{\partial v_z}{\partial r} \right| s^{-1}. \text{ The Power law index ‘} n \text{’ specifies the degree of the inelastic shear–thinning and –}$$

thickening behaviour of the fluid. When  $n < 1$ , then fluid behave shear–thinning, while,  $n > 1$  then fluid behave like shear–thickening [(Jung, et al., 2004) and (Solangi, et al., 2012b)].

In Figure (8.1), non–Newtonian Power law model depicts the variation of viscosity against shear–rate. With the increase of shear–rate viscosity decreases, graph in Figure (8.1), shows clearly the shear–thinning behaviour of the fluid captured by the Power law model.

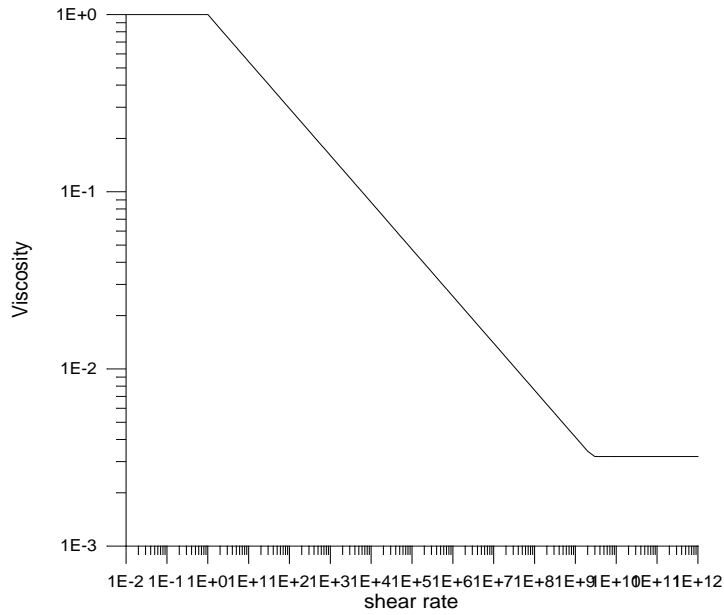


Figure 8.1 Graph of shear–rate dependent viscosity of Power law model.

For Power law model, the analytical solution is given below as (Neofytou, et al., 1994):

$$v_z = \frac{1}{4} \frac{6n+2}{(n+1)} \left( \frac{1}{R_i} \right)^2 \left( 1 - \left( \frac{r}{R_i} \right)^{\frac{n+1}{n}} \right), \quad 0 \leq r \leq R_i \quad (8.2)$$

Where,  $R_i$  is a constant taken as non-dimensional radius of an inner pipe. Pressure difference for Power law model is analytically computed from the z-component of a steady-state momentum equation. Employing Equation-(8.2) along with boundary conditions, at inlet, pressure difference become as used in (Solangi et al., 2012a):

$$p_{in} = \left[ 2k \left( \frac{3n+1}{2n} \right)^n z \right] \quad (8.3)$$

#### 8.4 The Bird-Carreau model

The governing non-Newtonian equation was indented to capture the variances in velocity profile due to the shear thinning behaviour of fluid by the given Carreau model as (Berthier et al., 2002) and published in (Solangi et al., 2012a):

$$\mu = \mu_{\infty} + (\mu_0 - \mu_{\infty}) \left[ 1 + (\lambda \dot{\gamma})^2 \right]^{\frac{n-1}{2}} \quad (8.4)$$

Where  $\mu_0$ ,  $\mu_{\infty}$ ,  $\lambda$  and  $n$  are the zero and infinite shear rate limit viscosities, relaxation time constant. Power law index taken  $n$  is as 1.0 kg/m-s, 0.9, 0.8 and 0.7 respectively. The relaxation time constant and the power law index control the respective transitions and slope in the Power law region.

The shear thinning behaviour of viscosity at low and high shear rates is displayed for Carreau model in Figure (8.2). Viscosity is dependent on shear rate; increase in shear rate decreases the viscosity. Therefore, shear rate and viscosity are inversely proportional. As shown in Figures [(8.1) and (8.2)], in Power law model viscosity decreases more than compared with Bird-Carreau model.

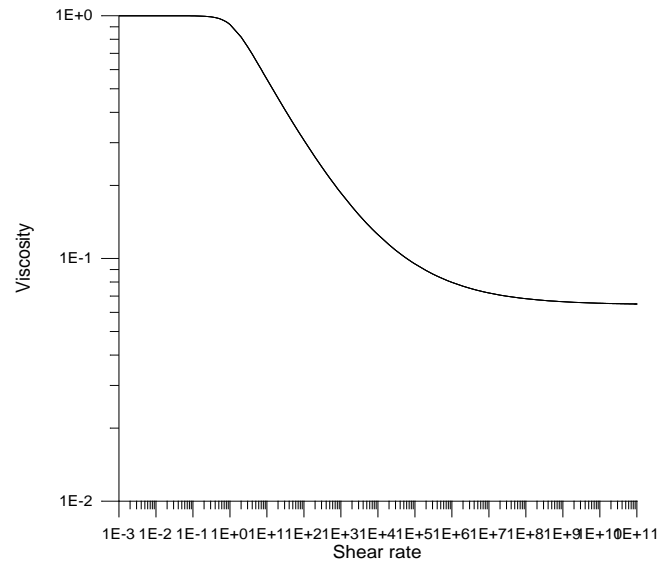


Figure 8.2 Variation of viscosity with shear rate according to Carreau model.

### 8.5 Governing system of equations

Flow of non-Newtonian fluid can be mathematically modelled by the continuity and generalised momentum balance equations. These governing equations, in the absence of body force, for two dimensional cylindrical polar coordinates are given as under [(Solangi, 2011) and (Solangi et al., 2012b)] :

Continuity equation:

$$\frac{1}{r} \frac{\partial}{\partial r} (r v_r) + \frac{\partial v_z}{\partial z} = 0 \quad (8.5)$$

Momentum balance equation: Momentum Balance Equation Component-wise:

r-component:

$$\rho \left( \frac{\partial v_r}{\partial t} + v_r \frac{\partial v_r}{\partial r} + v_z \frac{\partial v_r}{\partial z} \right) = \left( \frac{1}{r} \frac{\partial}{\partial r} (r \tau_{rr}) - \frac{\tau_{\theta\theta}}{r} + \frac{\partial}{\partial z} \tau_{rz} \right) - \frac{\partial p}{\partial r} - \frac{\mu}{\rho \kappa} v_r \quad (8.6a)$$

z-component: (Solangi et al., 2012b)

$$\rho \left( \frac{\partial v_z}{\partial t} + v_r \frac{\partial v_z}{\partial r} + v_z \frac{\partial v_z}{\partial z} \right) = \left( \frac{1}{r} \frac{\partial}{\partial r} (r \tau_{rz}) + \frac{\partial}{\partial z} \tau_{zz} \right) - \frac{\partial p}{\partial z} - \frac{\mu}{\rho \kappa} v_z \quad (8.6b)$$

Where,  $v_r$  and  $v_z$  are fluid velocity components in the radial and axial direction respectively,

$\rho$  is the fluid density,  $p$  is the isotropic fluid pressure and  $t$  is time. Then  $\tau_{rr}$ ,  $\tau_{rz}$ ,  $\tau_{zz}$  and  $\tau_{\theta\theta}$  denote the components of the extra stress tensor and defined as follows [(Solangi, 2011) and (Solangi et al., 2012b)]:

$$\tau_{rr} = 2\mu(\dot{\gamma}) \frac{\partial v_r}{\partial r} \quad (8.7)$$

$$\tau_{rz} = \mu(\dot{\gamma}) \left\{ \frac{\partial v_r}{\partial z} + \frac{\partial v_z}{\partial r} \right\} \quad (8.8)$$

$$\tau_{zz} = 2\mu(\dot{\gamma}) \frac{\partial v_z}{\partial z} \quad (8.9)$$

$$\tau_{\theta\theta} = 2\mu(\dot{\gamma}) \frac{v_r}{r} \quad (8.10)$$

Where,  $\mu(\dot{\gamma})$  is the functional viscosity of the fluid and  $\dot{\gamma}$  is a shear rate.

### 8.5.1 Initial and boundary conditions

The system of Equations [(8.5), (8.6a) and (8.6b)] with continuity equation are solved by imposing appropriate initial conditions on the region  $\Omega$  as detailed in the study of (Solangi, 2011).

$$v_r(r, z, t) = v_r^0(r, z, 0) \quad (8.11)$$

$$v_z(r, z, t) = v_z^0(r, z, 0) \quad (8.12)$$

$$p(r, z, t) = p^0(r, z, 0) \quad (8.13)$$

Where,

$$\nabla \cdot \mathbf{v}^0 = 0 \quad (8.14)$$

The appropriate boundary conditions on  $\Gamma$  as:

$$v = g_1(x, t) \quad \text{on } \Gamma_1 \quad (8.15)$$

$$(\sigma \cdot n) = g_2(x, t) \quad \text{on } \Gamma_2 \quad (8.16)$$

Where,

$$v \cong (v_r, v_z) \quad (8.17)$$

Here  $\Gamma(\Gamma_1 \cup \Gamma_2)$  enclosing the domain  $\Omega$ ,  $n$  is the unit outward normal to the boundary,  $g_1(x, t)$  represents the velocity vector prescribed on  $\Gamma_1$ ,  $g_2(x, t)$  designates the traction vector prescribed on  $\Gamma_2$ , and  $\sigma$  is the total Cauchy's stress tensor. Note that it is also possible to have mixed velocity–traction boundary conditions. Finally, if  $\Gamma_1 = \Gamma$  when vanishing tractions are imposed ( $\Gamma_2 = 0$ ), the prescribed velocity  $g_1(x, t)$  must satisfy consistency conditions.

$$\int_{\Gamma} n \cdot b d\Gamma = 0 \quad (8.18)$$

In this case, a consistent pressure datum must be supplied up to an arbitrary constant in order to avoid an indeterminacy or fluid dynamic inconsistency. No-slip condition is imposed on solid walls, while on axis of symmetry Dirichlet condition (vanishing cross component) and Neumann condition for axial component is imposed.

### 8.6 Numerical scheme and fully discrete system of weak formulation

The selection of algorithm for numerical simulation depends on accuracy, convergence rate, efficiency and stability. Literature review shows that semi-implicit techniques are preferred over the explicit schemes, which have a slow rate of convergence [(Hawken et al., 1990), (Carew et al., 1994), (Baloch et al., 1994), (Baloch, 1994), (Baloch et al., 1995a) and (Solangi et al., 2012a)]. For the enhancement of numerical stability, generally implicit methods are used; however, these methods are computationally no more expensive. A fully discrete system of the problem will be derived by defining appropriate finite dimensional subspaces  $V^h, V_0^h$  and  $P^h$  of  $V, V_0$  and  $P$  respectively. The equations are spatially discretised using Galerkin weighted residual technique and a mixed velocity-pressure formulation is used to solve the equations. The piecewise quadratic functions for velocities and piecewise linear functions for pressure

over triangular mesh subdivision are taken. Velocities  $(v_r, v_z)$  and pressure  $p$  are approximated over each element by the equations.

The fully discrete implicit and semi-implicit Taylor-Galerkin/pressure-correction scheme along with finite dimensional subspaces over a finite dimensional space of functions is presented in chapter 4.

### **8.7 Numerical results and discussions**

Numerical solutions are presented by streamline patterns and graphs for change in pressure difference due to changing flow rate. The effects of two different inelastic models, namely the Power law and Carreau model, have been compared. Increasing inertia Reynolds (density) numbers from (Re=1 to Re= 6000) and increasing inertia by changing the values of N (power law index) 0.9, 0.8 and 0.7, porosity 1, viscosity 1, values of permeability from 0.1 to 0.00001 and zero shear viscosity are taken. Power law index varies from 0.9 to 0.7 to monitor shear thinning behaviour on the flow domain of non-Newtonian fluids.

The numerical results are presented by stream line projections and graphs of pressure difference against increasing Reynolds number have been presented in for a pipe filled with porous materials. Comparisons of numerically simulated results have been made with the results presented in chapter six for channel flows through porous media.

#### **8.7.1 Mixing and separating of non-Newtonian fluid flows in a pipe filled with porous media (Power law model)**

Numerical results from inelastic Power law model have been displayed with increasing inertia. Flows of non-Newtonian fluid filled with porous media have been shown along with streamline projections in Figure- 8.4 with equal and unequal flow rate in an inner pipe and outer cylinder

with changing power law index from 0.9 to 0.7. Mixing and separating effects are discussed against changing flow rates and power law index. The value of permeability varies from 0.1 to 0.0001 along with a changing value of power law index to see its effects on pressure difference in both equal and unequal flow rates.

### **8.7.2 The influence of inertia on flow structure**

As shown in Figures [8.4(a) to 8.4(c)], the steady-state predicted streamline functions are presented with increasing  $Re$  from 1 to 6000 along with a change in power law index for both equal (1, 1) and unequal (1,2) flow rates in an inner pipe and outer cylinder respectively. As usual, a fluid has been pushed in the inner pipe as was the case in Newtonian fluids. Similarly, and reverse flow in the inner pipe along with the line of symmetry has been noted. Not any effect on inertia either with changing power law index or increasing the value of Reynolds has been observed.

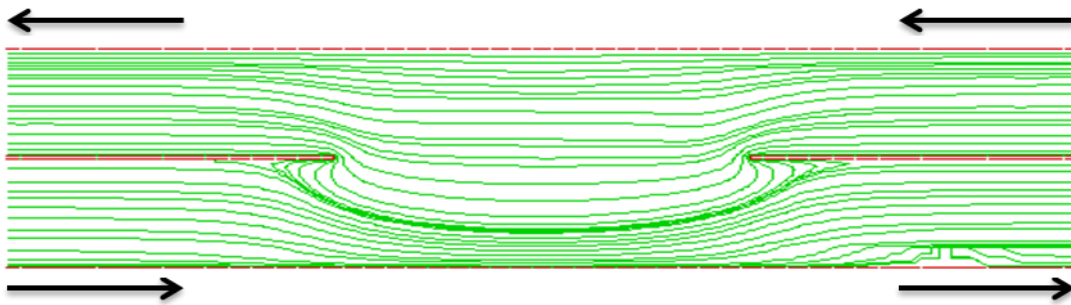
Changing flow rates in the outer cylinder has some effects on inertia at  $Re=1$  as shown in Figure 8.3 (a) when power law index is 0.9 but for other decreasing values that effects vanishes as in Figures [8.3 (b) and 8.3 (c)]. At  $Re=1$  vortex has been developed at the separation gap in the outer cylinder but with increasing value of  $Re$  it vanishes as shown in Figure 8.3 (a) [ $Re=1$  and 6000 when  $N=0.9$  and flow rate is (1, 2)]. No other obvious effects of inertia on flow structure have been noticed either by changing flow rates or power law index. Above observation are in agreement with the numerical results discussed in a channel filled with porous media in chapter 6.

Flows are unidirectional as was the case of Newtonian fluids in a pipe either filled with porous or porous media. Only some reverse flows due to some numerical error appeared in the inner pipe towards the exit section near the line of symmetry. Fluids are only mixed in an inner pipe in the separating gap. Mixing and separations appeared in all cases of changing flow rates and increasing inertia values. In this research no other evident influence of changing flow rate in outer cylinder has been seen.

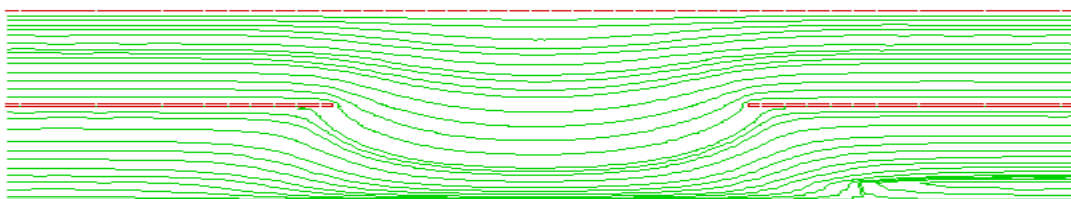
$N=0.9$

(a)

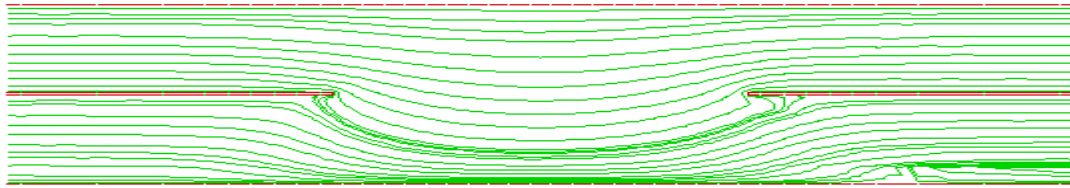
**Equal (1, 1) Flow Rate**



$Re=1$

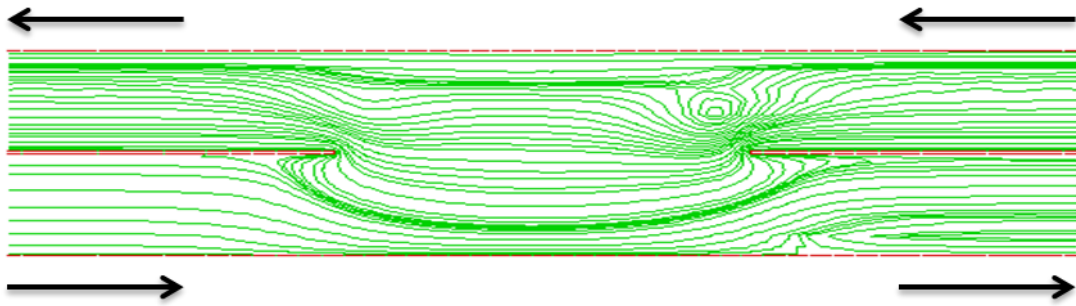


$Re=1000$

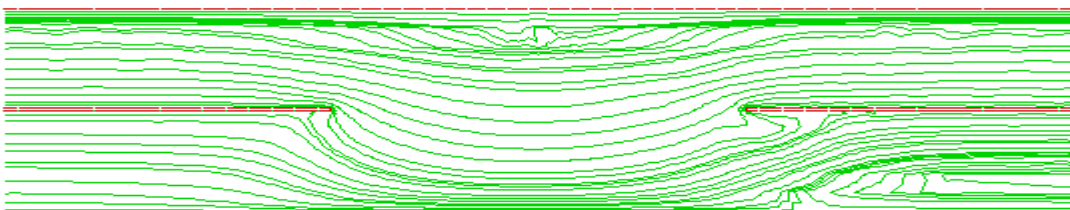


Re=6000

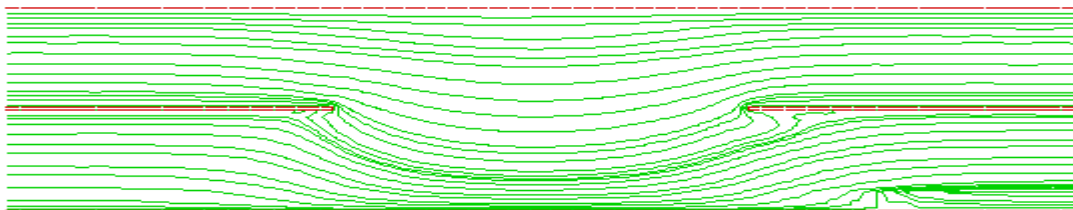
**Unequal (1, 2) Flow Rate**



Re=1



Re=5000

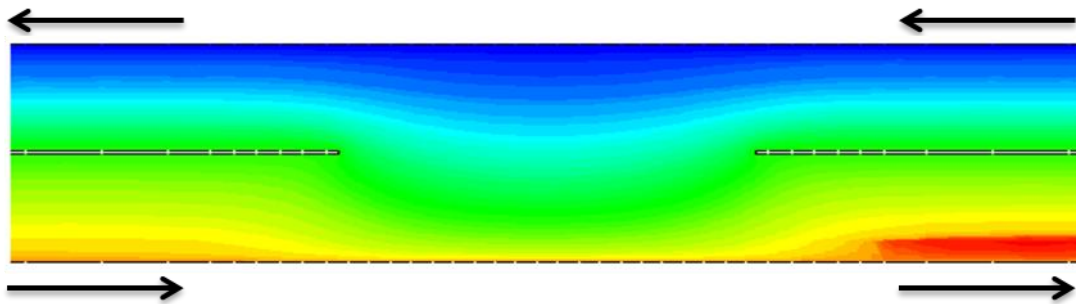


Re=6000

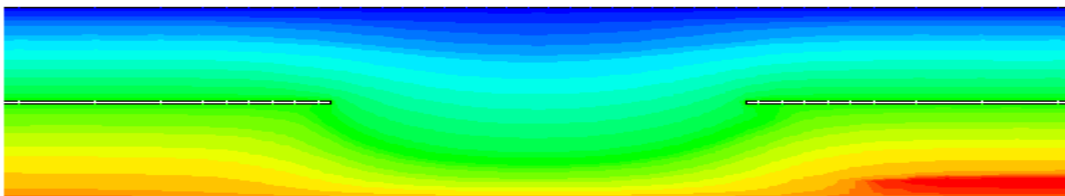
N=0.8

(b)

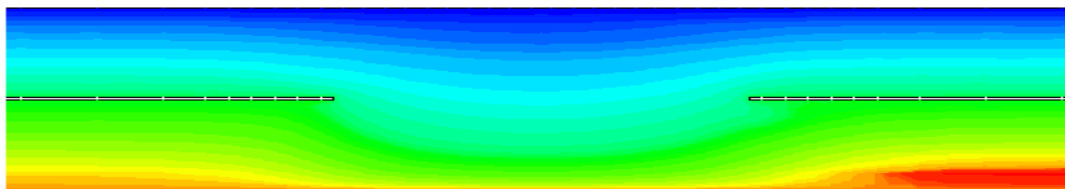
**Equal (1,1) Flow Rate**



Re=1

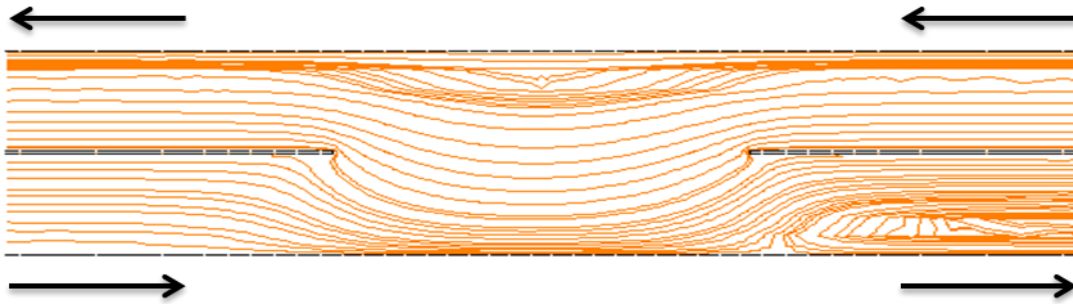


Re=3000

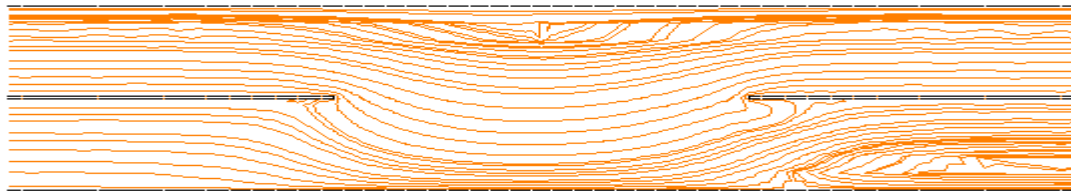


Re=6000

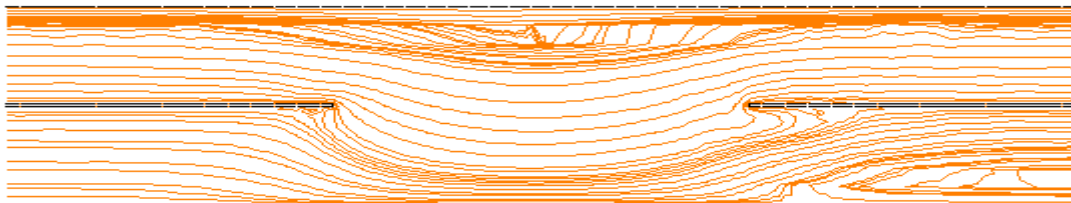
**Unequal (1,2)Flow Rate**



Re=1



Re=3000

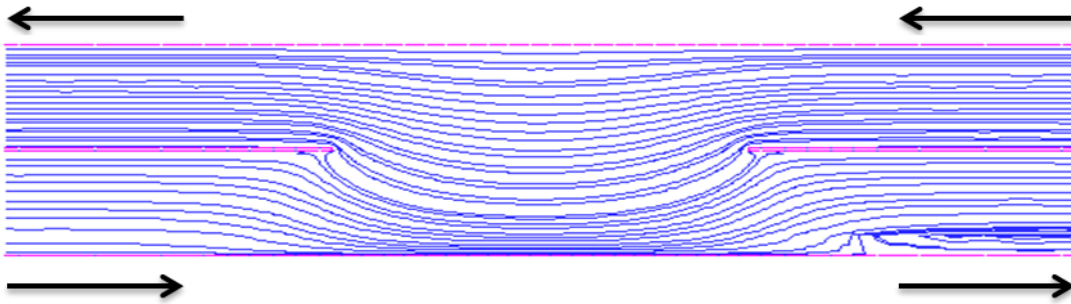


Re=5000

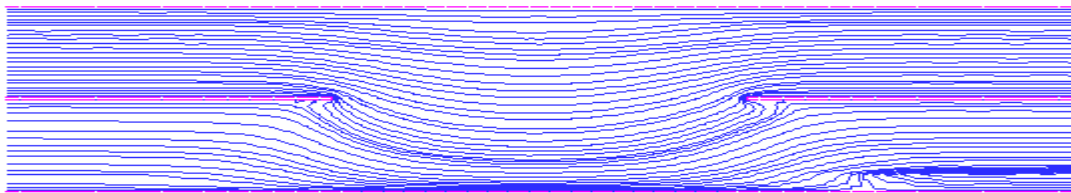
**N=0.7**

**(c)**

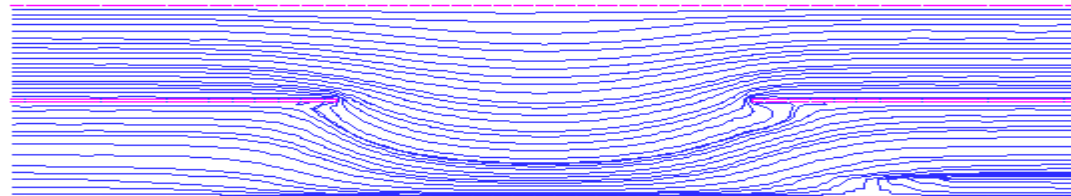
**Equal (1,1) Flow Rate**



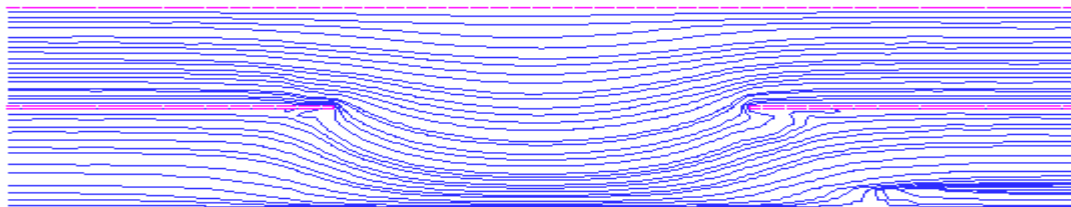
$Re=1$



$Re=3000$

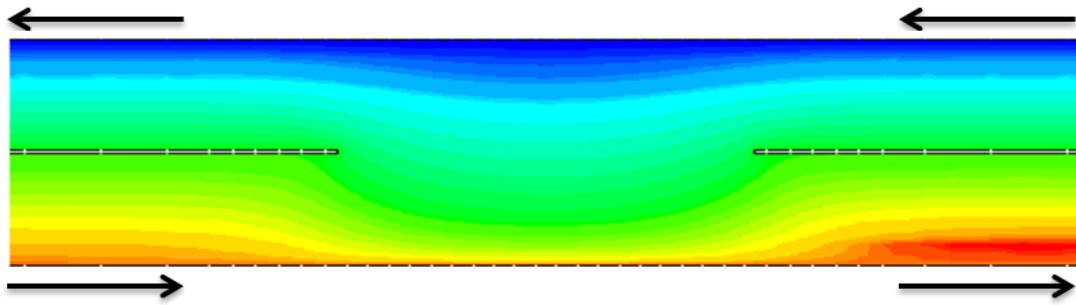


$Re=5000$

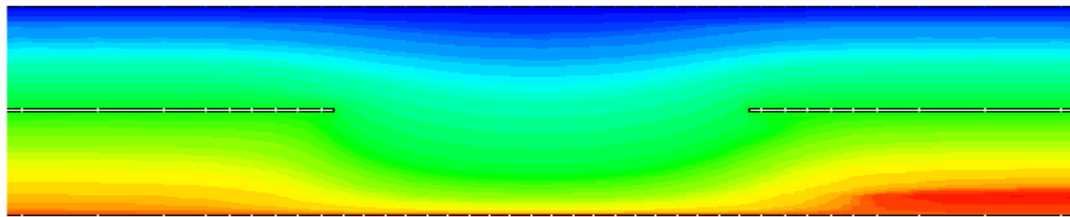


$Re=6000$

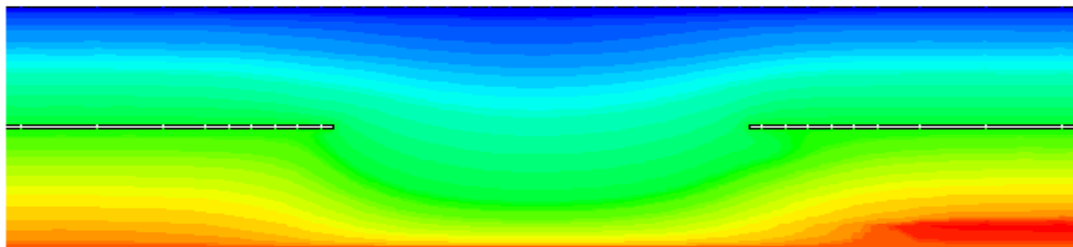
**Unequal (1, 2) Flow Rate**



Re=1



Re=3000



Re=6000

---

Figure 8.3 Streamline function of non-Newtonian fluid flows for Power law model under changing values of power law index from 0.9 to 0.7 with increasing Reynolds number from  $Re=1$  to 6000, from top to bottom. (a) Under an equal (1, 1) and unequal (1, 2) flow rates, (b) Under an equal (1, 1) and unequal (1, 2) flow rates, (c) under an equal (1, 1) and unequal (1, 2) flow rates.

### 8.7.3 Effects of changing flow rates and permeability on pressure

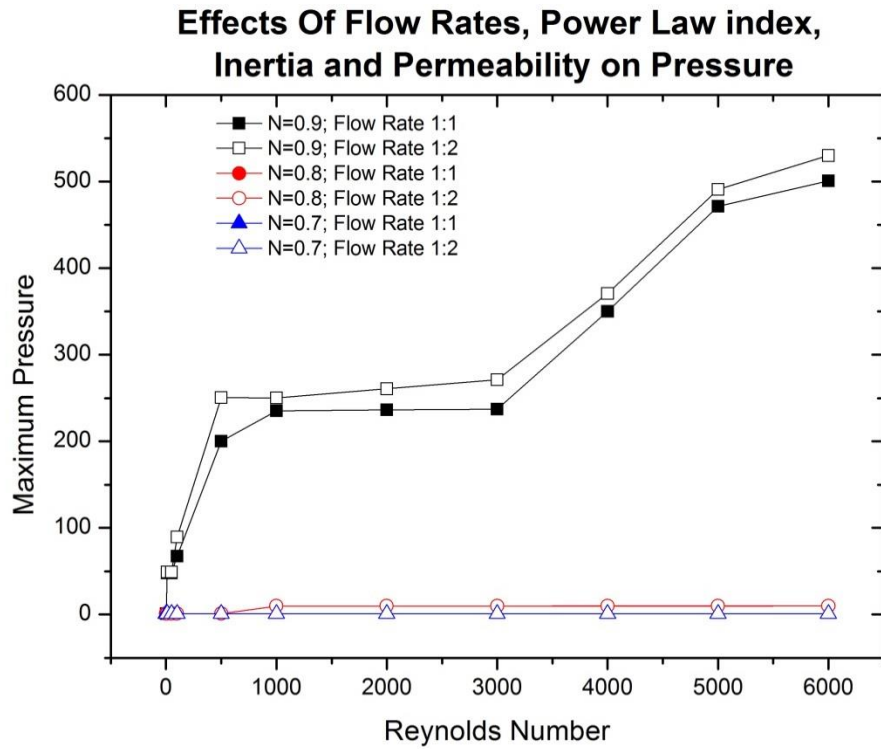
Non-Newtonian fluid flows in pipe filled with porous media with relative flow rates are presented in Figures [8.4(a) and 8.4(c)], to compare its effects on pressure. Maximum and minimum scaled pressures with both flow rates at  $N=0.9$  are  $1 \leq p_s \leq 500.9706$  and  $1 \leq p_s \leq 530.1138$  respectively with changing values of permeability from  $0.1 \leq \kappa \leq 0.0001$ . Maximum and minimum scaled pressures for both flow rates at  $N=0.8$  are  $1 \leq p_s \leq 9.9815$  and  $1 \leq p_s \leq 2.00$  respectively with changing values of permeability from  $0.001 \leq \kappa \leq 0.0001$ . Similarly, maximum and minimum scaled pressures with both flow rates at  $N=0.7$  are  $1 \leq p_s \leq 1.0094$  and  $1 \leq p_s \leq 1.012$  respectively with fixed value of permeability 0.0001 for all increasing values of inertia.

To monitor the effects of changing flow rates on pressure difference along with varying the value of power law index from 0.9 to 0.7 and value of permeability from 0.1 to 0.0001 together with varying value of Reynolds number from 1 to 6000. In this research pressure rises with changing flow rates. A decrease in the value of permeability also gives rise to pressure difference. In Figure 8.4(a) as shown in when power law index  $N=0.9$  and the value of permeability changes from 0.1 to 0.001, the pressure shoots up as shown in Figure 8.4 (at  $Re=1$

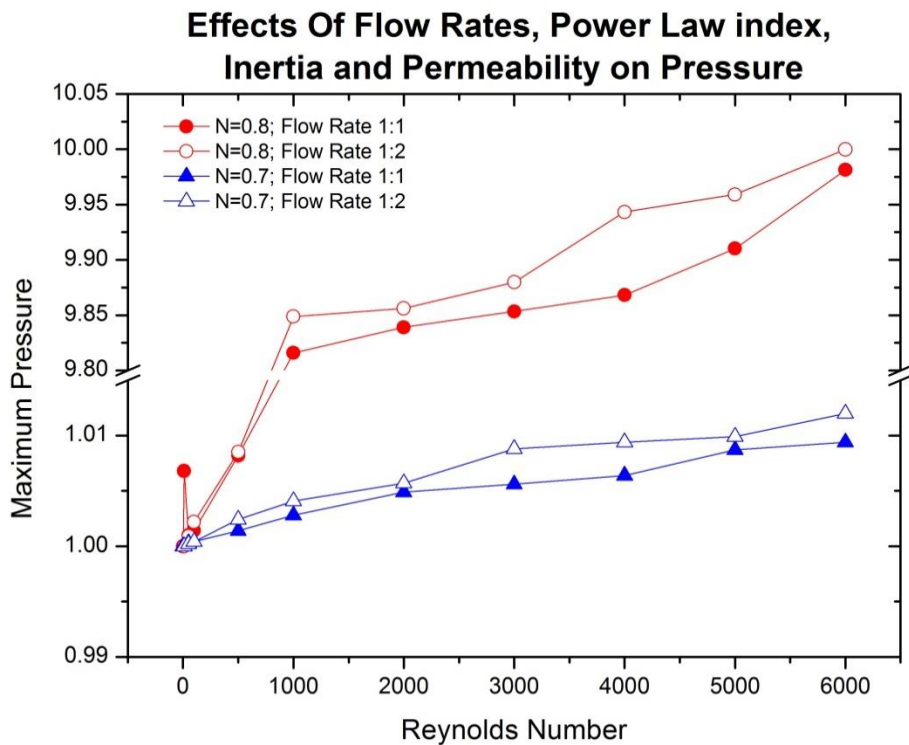
and 10) by keeping Darcy's number fixed to 1. At same power law index and changing value of permeability from 0.001 to 0.0001, the pressure increases as shown in Figure 8-5 (at  $Re=50$  and 100). Again at  $Re=500$  and 1000 the pressure rises when permeability decreases from 0.001 to 0.0001. In unequal flow rate pressure rises when permeability varies from 0.001 to 0.0002 as shown in Figure 8-5 (at  $Re=500$  to 1000).

At power law index  $N=0.8$  initially permeability was fixed, therefore, there is no dramatic change in pressure difference, when the value of permeability has been changed from 0.001 to 0.0001 which gives rise to pressure the same way as was the case when  $N=0.9$  as shown in Figure 8.4 ( $Re=500$  to 1000). As at  $N=0.8$  less permeable domain gives minimum change in pressure difference and trend tends to linear as compared with both flow rates at  $N=0.9$ .

The Figure 8.4(a) could not show us the clear picture of the effects on pressure with flow rates with changing power law index from 0.8 to 0.7 due to fixed value of permeability. Their effects have been shown in Figure [8.4(b)] by breaking the vertical axis to its smaller values of scaled pressure of flow rates at  $N=0.7$ . For the increase in the Reynolds number permeability is fixed in both the flow rates, where  $N=0.7$ , which means there is no significant effect of pressure, while inertia values increase smoothly. Changing flow rates and the value of permeability gives rise to pressure difference with increasing inertia.



(a)



(b)

Figure 8.4 [(a)-(b)] Pressure difference for an equal (1, 1) and unequal (1, 2) flow rates with changing power law index from 0.9 to 0.7 and with increasing Reynolds number from 1 to 6000. Re increasing from top to bottom.

#### **8.7.4 Mixing and separating of non-Newtonian fluid flows in a pipe filled with porous media (Bird-Carreau model)**

The results of numerical computation have been obtained using the inelastic model of Bird Carreau that displays the equal and unequal rate of flow within outer cylinder and inner pipe with porous materials filled in it. Flows of non-Newtonian fluid filled with porous media have been shown along with streamline projections in Figure (8.5) with increasing inertia and changing power law index from 0.9 to 0.7. Mixing and separating effects are discussed due to changing flow rate and power law index. Inertial effects have been discussed due to the presence of porous media and compared with those from the power law model.

#### **8.7.5 Influence of inertia on flow structure**

Non-Newtonian results are given in Figures [8.5(a) to 8.5(c)] to see an impact of inertia on flow structures with both equal and unequal flow rates in pipes filled with porous media. No impact on inertia in pipes filled with porous media either by changing flow rates or increasing the value of Reynolds number along with decreasing value of power law index has been observed. For both rates of flow as demonstrated there is an increase in the Reynolds number and decrease in the power law index, 1 to 6000 and 0.9 to 0.7, respectively. Similarly flows have been pushed in the inner pipe from both sides of the outer cylinder in the gap towards the

---

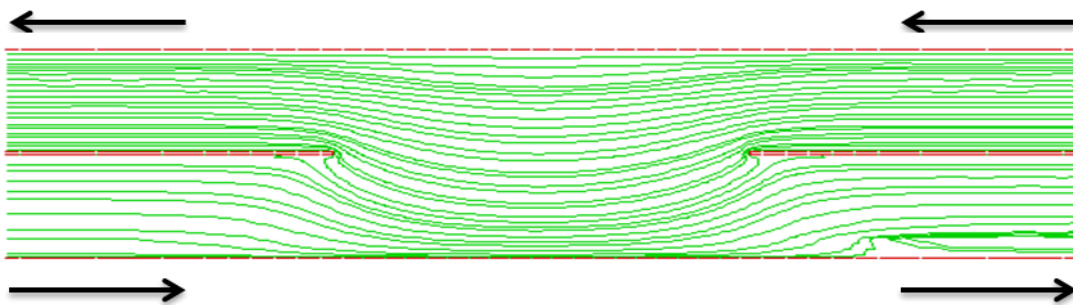
line of symmetry and some reverse flow has been observed in the inner pipe towards the downstream exit.

It is found that Bird Carreau has no effect on the inertia due to pressure, while there was only negligible inertia effect in the power law model. Flows are the same unidirectional as was the case in power law model. There is no influence of changing power law index. No impact of inertia has been noticed what so ever is the reason. Increasing inertia, varying flow rates, power law index along with variation in the values of permeability has not affected the flow. Cross flow in an inner pipe at the exit section has been noticed. That error could be dealt in future studies.

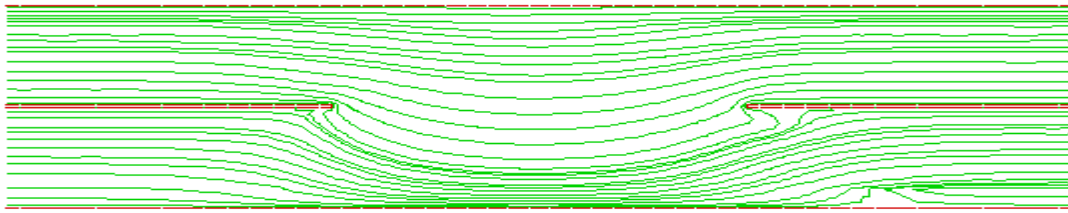
$$N=0.9$$

(a)

**Equal (1,1) flow rate**

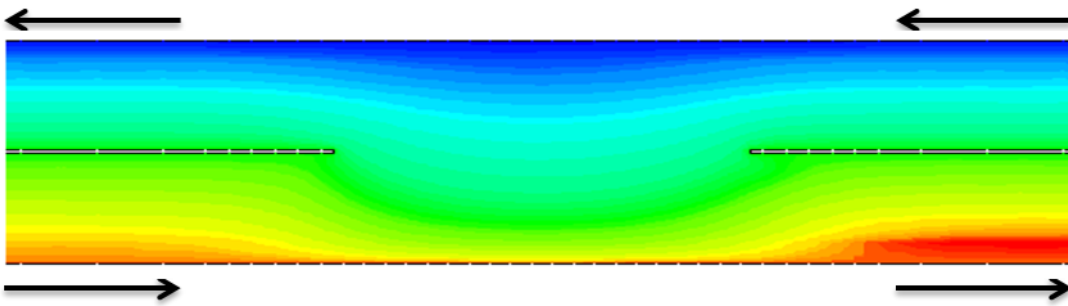


$$Re=1$$

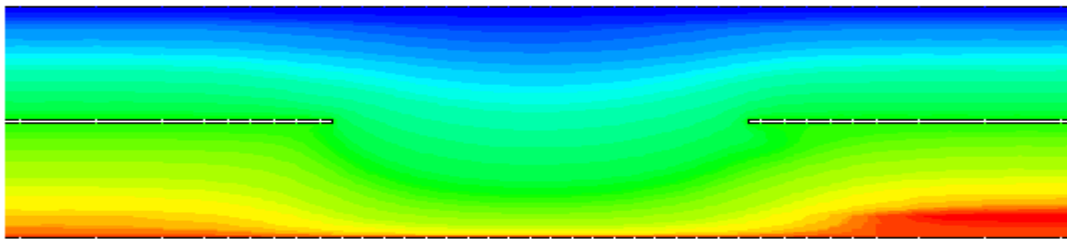


Re=6000

**Unequal (1,2) flow rate**



Re=3000

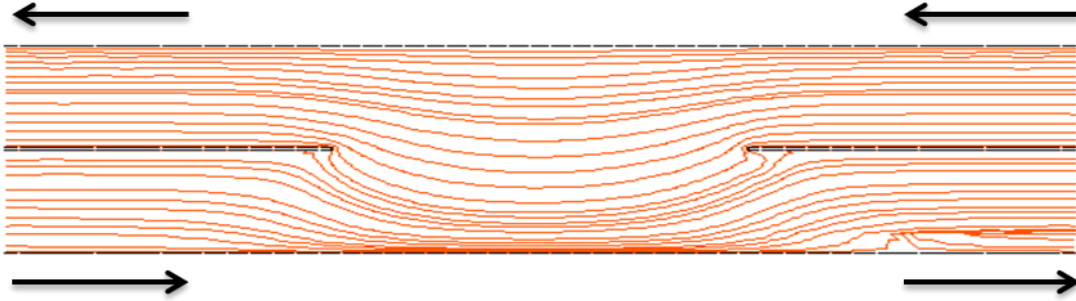


Re=6000

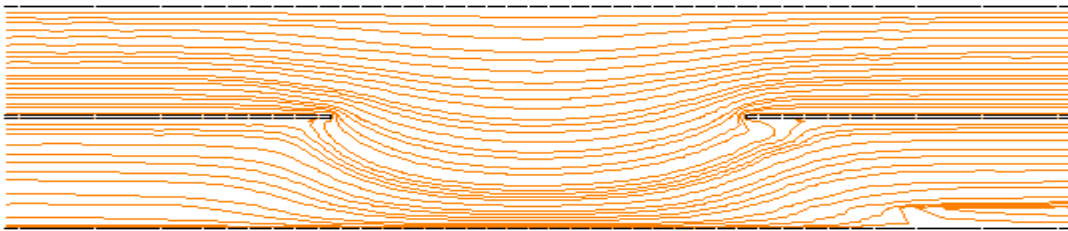
N=0.8

**(b)**

**Equal (1,1) flow rate**

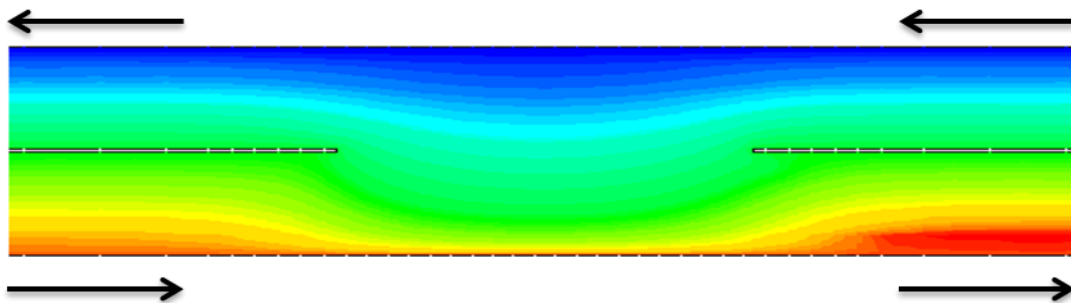


Re=3000

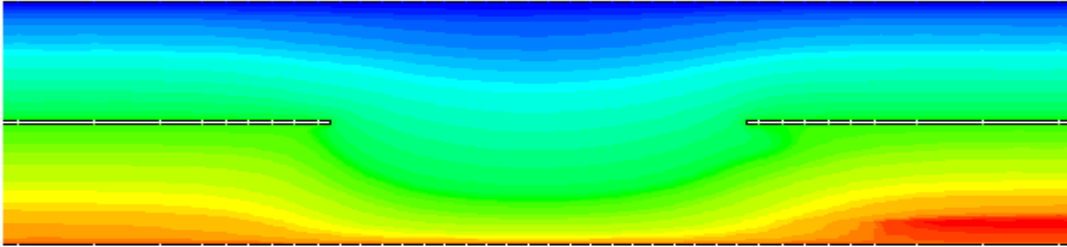


Re=6000

**Unequal (1, 2) flow rate**



Re=3000

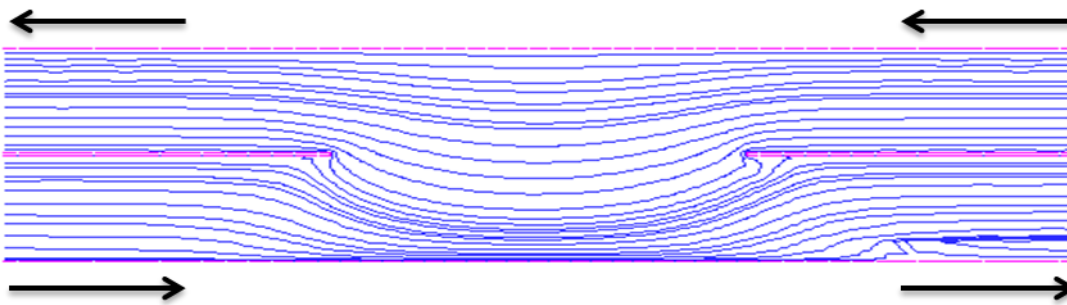


Re=6000

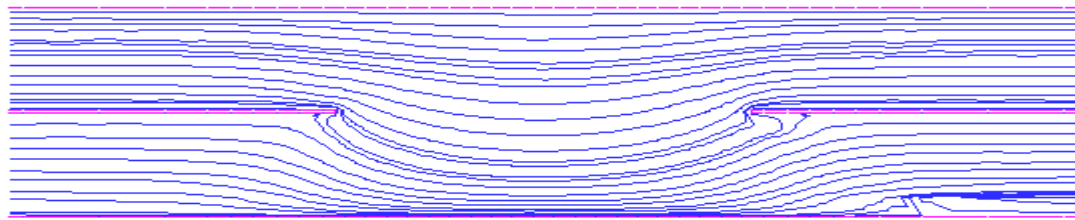
N=0.7

(c)

**Equal (1,1) flow rate**

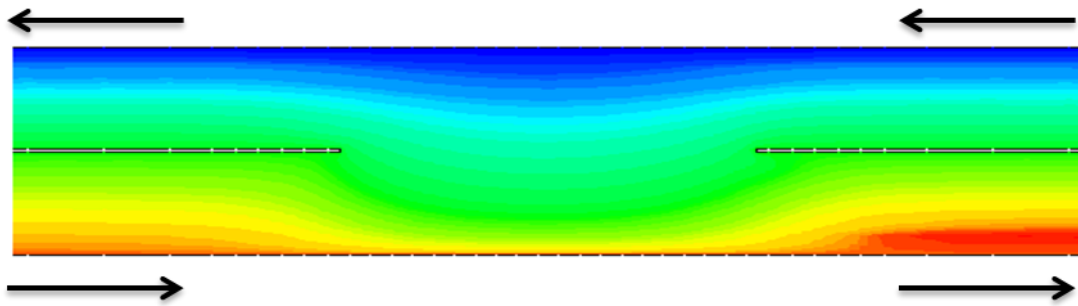


Re=3000

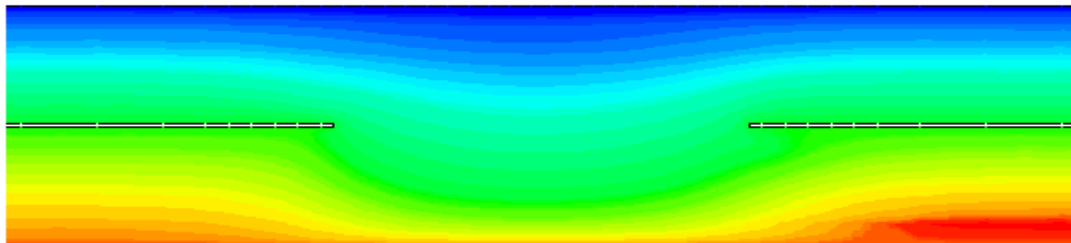


Re=6000

**Unequal (1, 2) flow rate**



Re=3000



Re=6000

Figure 8.5 Streamline function of non-Newtonian fluid flows for Bird Carreau model under changing values of power law index from 0.9 to 0.7 with increasing Reynolds number from Re=1 to 6000, from top to bottom. (a) Under an equal (1, 1) and unequal

(1, 2) flow rates, (b) Under an equal (1, 1) and unequal (1, 2) flow rates, (c) under an equal (1, 1) and unequal (1, 2) flow rates.

### **8.7.6 Effects of Power Law and Bird Carreau model on pressure when pipes are filled without porous media**

The Figure (8.6) displays the differences for the effect of Bird Carreau and power law due to pressure with an increase in the  $Re$  for flows of non-Newtonian fluid. Reynolds number has been taken from  $Re=1$  to 200 under equal (1, 1) flow rate when pipes are filled with non-porous media. With the increasing pressure there is no significant change observed for  $Re$  up to 50 th. The influence of Power law on pressure is higher than Bird Carreau model. Bird Carreau model shows linear trend in the increase of scaled pressure while Power law shows linear trend in an increase up to  $Re=150$  after that increase in pressure is non-linear. As discussed above in sections (8.7.2) and (8.7.5), Power laws have some inertia effects on flow behaviour whereas the Bird Carreau model shows no significant effects in inertia.

Like other situations discussed in chapters 6 to 7 in a channel and pipe flows, pressure increases with varying values of  $Re$  same trends has been observed in non-Newtonian flows when pipe is filled with non-porous media.

### Influence of Power law and Carreau Models on Pressure

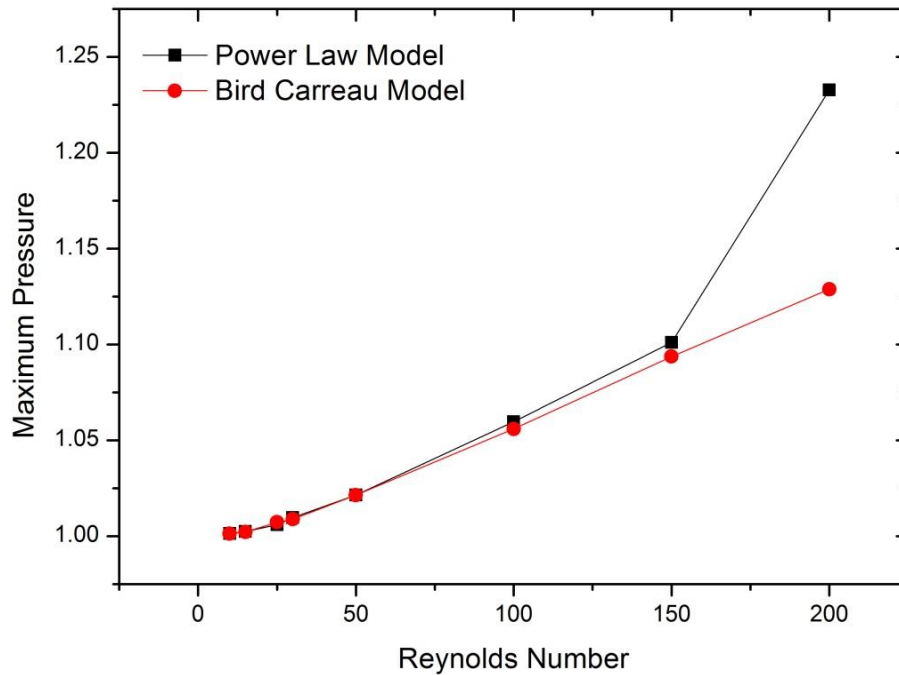


Figure 8.6 Comparison of Power Law and Bird Carreau model on pressure.

### 8.8 Summary

In this chapter, numerical simulations have been carried out with non-Newtonian rheological models, that is, the Bird-Carreau and Power law model under combing and separating flow configurations in an inner circular pipe and outer circular cylinder. With the increase in the Reynolds number the graphs and streamline patterns illustrates the numerical results, with varying power law index and changes in the flow rate in both pipes from dual- outlet/ inlet. Taylor-Galerkin/Pressure-Correction primitive variable finite element algorithm has been found accurate and stable in its performance and predictions. Numerical results obtained prove to be theoretically in close agreement with available numerical and results achieved in the channel filled with porous media.

For mixing separating flows in pipes filled with porous media, if non-Newtonian effects are added then Power law and Bird Carreau model found negligible inertial effects in the domain filled with porous media. In this work Power law model of has captured inertia effects on flow structure for low Reynolds number. With the higher values of power law index, these inertia effects vanished. With Bird Carreau model no impact on inertia has been noticed either varying values of power law index or flow rates. It has been noticed that there are some numerical errors in flows. This error appeared in the inner pipe in the exit section, which will be discussed later.

Considering the various mixing and separating flow conditions has obvious effect on the permeability, power law index, and flow rates in pipe. Increasing flow rate in outer cylinder gives rise in pressure during changing power law index. Decreasing values of permeability decreases pressure and increasing value of it increases pressure but fixed values of permeability shows a linear trend in the value of pressure. In comparison to Bird Carreau model, there are more effects noted for the inertia and flow on pressure than power law model. Pressure has not been affected too much in Bird Carreau model with changing flow rates, power law index and permeability in the entire computational domain. Figure (8.6) shows that for values from  $Re=1$  to 4000 where the values of permeability have been changed for different Reynolds numbers. After  $Re=400$  on fixed value of permeability and Forchheimer growth is linear.

Flows of non-Newtonian fluids through tubes are presented with Velocity profiles at  $Re=01$  for Power law model. In this an equal (1, 1) flow rate is shown when domain is filled with porous media as an example in the end of appendix-E. Stream functions with contour numbers its corresponding value are labelled and aligned vertically. Contour types are shown in flood, lines and lines and flood together as well. Velocity Vector is also presented for  $Re=01$ .

---

## Chapter 9. Discussion

### 9.1 Introduction

Overall general discussions on variety of the results achieved in this research are given below for four different categories of channel flows. In pipes mixing and separating flow involves the material changes, besides the application of the non-Newtonian models.

### 9.2 Channel flows through non-porous media

The chapter five of the thesis presented, computations, numerical modelling, and Newtonian fluids of the mixing and separating flows combined without porous media in the planar channel. For primitive variables numerical algorithm employed in the analysis is based on Taylor series expansion for temporal discretisation. Galerkin is a finite element for the approximation of the spatial discretisation. To achieve second order accuracy and deal with incompressibility constrain pressure–correction method is incorporated in the scheme. Details of this algorithm are debated in detail in chapter 4 and onwards in different sections of this thesis. Reversed and unidirectional flows with different flow bifurcations of computational domain and finite element mesh as shown in Figure (5.1) along with applied numerical scheme are discussed in chapter five in detail. Three flow rates in every condition are simulated and compared with each other to see the influence of changing flow rate on flow structure. In order to understand the effects of inertia on flow structure, flows are monitored with increasing value of Reynolds numbers, changing flow rates and flow directions. Comparison of pressure difference due to varying flow rates are presented into different sections of the chapter 5 for four different configurations (geometries  $G_1$  to  $G_4$ ). In the end results are compared with experimental and numerical results available literature.

---

Over all highlights of the general discussion in detail on the modelling and numerical results of Newtonian fluid for complex mixing–separating channel flows filled with non–porous media in first part of Figure [5.1(a)] with varying flow rates in the upper channel arm are given below. Reynolds numbers have been considered from 1 to 200. The aim of varying it from lower to higher values is a way to find the critical Reynolds number.

In equal (1, 1) flow rate the fluid mixes and separates in the middle gap and towards the exit sections of the domain under initial Reynolds numbers. When the Reynolds number increases, vortex forms and grows within the middle gap and move horizontally in the direction of separating plates, giving rise to a reverse flow. Other vortices formed will grow that resides on the central nip; these are stretched in horizontal direction and adjusts their positions of the plate. At the higher value of Reynolds number that is 200 eddies formed in the middle gap due to more recirculation twist their position clockwise. An increase in the value of  $Re$  has led to an increase the size, intensity of recirculation and stability in adjusting their positions of the vortices of the entire domain.

Due to unequal (1, 1.5) flow rate into the upper arm of fluid flows have been pushed to the lower channel arm in its gap. The vortex development taking place very early because of the flow rate changes is a predominant evidence of the effects of inertia on the flow structure and rates. Due to changing the flow rate in a top channel a vortex has been developed on only one plate its nip of in the exit sections of the domain for lower values of  $Re$ . In contrast with the equal flow–rate the vortex developed on side of the wall in upper channel arm in its middle. With increasing the value of  $Re$  the vortex developed on the wall grows in size and starts

---

moving in the middle gap of the domain in its gap along with the emerge of another vortex which was expected on the other side of the centrally located plate. In contrast to the equal flow rate in both arms of a mixing–separating domain, flows are both unidirectional as well as opposite direction until the exit of the channel. Fluid is mixed within the exit section and middle gap of the domain.

The more drastic effect in the flow is observed with the change (1, 1.5) to (1, 2) in flow rate. Again very early activity of vortex development has been observed in flow domain due to unequal (1, 2) flow rate contrast to equal (1, 1) and unequal (1, 1.5) flow rates. Vortices have been noticed in all three different locations of the domain but with more intensity and power of recirculation against increasing inertia. When the Re value increases vortices are split into small vortices in same eddies. For the mixing and separation of the domain in Reynolds numbers throughout the process there were both unidirectional and reversed flows. Changing flow rates as described in chapters five and six in computational domain from equal to unequal flow rates of Newtonian fluid flows in combining mixing separating geometry has a dramatic change on flow structure. Influence of unequal flow rate has been observed on inertia, positions of vortices and on fluid flow directions. In the study of Newtonian fluid flows in a channel a comparison of scaled pressure difference verses Reynolds numbers are presented with relative flow rates. The relative flow rates with increasing the value of inertia have the effects of increasing non-dimensional pressure difference.

In another unidirectional configuration discussed in chapter 5, as shown in Figure [5.1(b)], Newtonian flows in a channel have been simulated and detail discussions are given in chapter five. In such settings target is basically the results of, change in flow direction and its inertia

---

effect, changes in flow rate for equal and unequal, and effect of flow direction and rates on the pressure differences. Similarly, Reynolds number has been taken from 1 to 200 for this unidirectional situation.

In all three equal and unequal flow rates, vortices have been developed only in the silent zone of the upper channel arm. Fluids mix only in the lower arm towards the downstream of a channel. With increasing the value of  $Re$  along with varying flow rates in upper channel arm due to recirculation power vortices developed the splits and a merge. A weak vortex developed on the plate fitted towards right in the middle grows in size and becomes more visible with changing flow rates in the upper arm for higher values of  $Re$ . The pressure difference is same for the effects by the inertia and flow rate; however, there is a linear increase in pressure with the reverse flow.

The Figure [5.1 (c)] illustrates configurations for single outlet and dual inlet, considering the Reynolds number from 1 to 200 the study discussed the Newtonian fluid flows and numerical calculations. Flow rates have been changed in the top arm of a channel again to see the effects on flow structure and non-dimensional pressure difference. It is evident that Fluid flows have been pushed into the upper channel arm in the separation gap of the domain along with the appearance of vortices in the silent section of the same arm. With increasing  $Re$ , vortex developed in the left section of the upper arm grows in size and becomes an eddy and moves towards the middle gap horizontally. That eddy adjusts its position in the middle gap between the upper wall and due to a push of flow from the lower arm of channel. With increasing value of  $Re$ , two other vortices grow one from the upper wall and another on the plate fitted to the

---

left in the middle of the domain. To increase the Re values all eddies and vortices developed are adjusted in their position and increase in size.

The influence of unequal flow rates along with increasing inertia on flow behaviour has been mentioned and no other obvious dramatic change has been noticed except early development and intensity in the formation of vortices/eddies due to more recirculation. Flows are both unidirectional as well as reversed. Non-dimensional pressure difference shows same the pattern of increase as was the case of unidirectional flow case discussed earlier in above paragraphs.

Once again unidirectional flows of Newtonian fluid in a single inlet/outlet configuration as shown in Figure [5.1(d)] in chapter 5 are numerically simulated to see the effects of inertia and the effects on pressure difference. The value Re has been considered from 1 to 500 to observe its effects on the flow domain. Again similar development in vortices has been noticed in the silent section of the domain of the low pressure zones. With increasing Re vortices/eddies grow in size and horizontally parallel to the wall in the opposite directions towards the inlet and outlet of the domain. Both vortices/eddies near the plate and in the silent zones, narrows the path of fluid flows in the middle gap due to their movements. For the greater values of Re, in an upper arm more vortices have been noticed along with one on the central plate towards the exit section of the domain. Linear increase in the pressure difference has been observed due to increasing inertia which resembles with the unidirectional flow discussed above Figure [5.1(b)].

Numerically simulated results discussed in this section are in very good agreement with experimental and numerical results available in open literature [(Cochrane, et al., 1981), (Cochrane, et al., 1982), (Walter and Webster, 1982), (Baloch, et al., 1995b) and (Echendu, et

---

al., 2011)]. There are comparisons considering various flow rates and directions within Newtonian fluids. In Figure (9.1) flow visualizations taken by photographing images under experimental setup are presented from the study of (Cochrane, et al., 1981). Newtonian liquids used in the experiment are high maltose syrup-water mixtures, whose velocities are determined by using a Brookfield viscometer. The Weissenberg number ( $w$ ) is of course zero for Newtonian fluids. In the experimental study non-Newtonian fluids are also investigated to compare with the results with Newtonian fluids. In scope of current research channel flows are investigated under Newtonian fluids with varying flow rates and flow directions. The current study has not found the effects of Weissenberg on the domain's flow rate without porous media filled in the channel. Figure 9.1 also shows numerical results of this study and are compared against experimental results of (Cochrane, et al., 1981). The Figure 9.1 illustrates that there is equal rate of flow for each arm, thus, the current experimental results are consistent with this investigation.

In figure 9.2 experimental results also nearly agrees with the predictions of present analysis Figure 9.2, in which unequal (1, 2) flow rates are passed in both arms of a channel. In experimental results  $Re=0.75$  and  $W =0.17$  and in numerical results of this study at  $Re=1$  with  $w=0$ . The Figure 9.2 shows the unidirectional flow obtained in the current numerical results at  $Re=1$ , which are similar to  $Re= 1$  experimental results with  $w=0.23$ . If inertia effects of current study are compared with the experimental study of (Walter and Webster, 1982) at  $Re=1$ , then again result is almost same. The reversed flow of this study is also agrees with the experimental results of (Walter and Webster, 1982) but difference is, in this study double flow rate is in upper arm of a channel. Due to double flow rate in upper arm fluid has been pushed in the middle gap in the lower arm as shown in Figure (9.2), It is noted that (Walter and Webster,

1982) experiment found the lower channel arm with double rate of flow, which means that fluid is pushed towards the upper arm's middle gap.

- **Unidirectional and reversed flows with equal and unequal flow rates in both channel arm.**

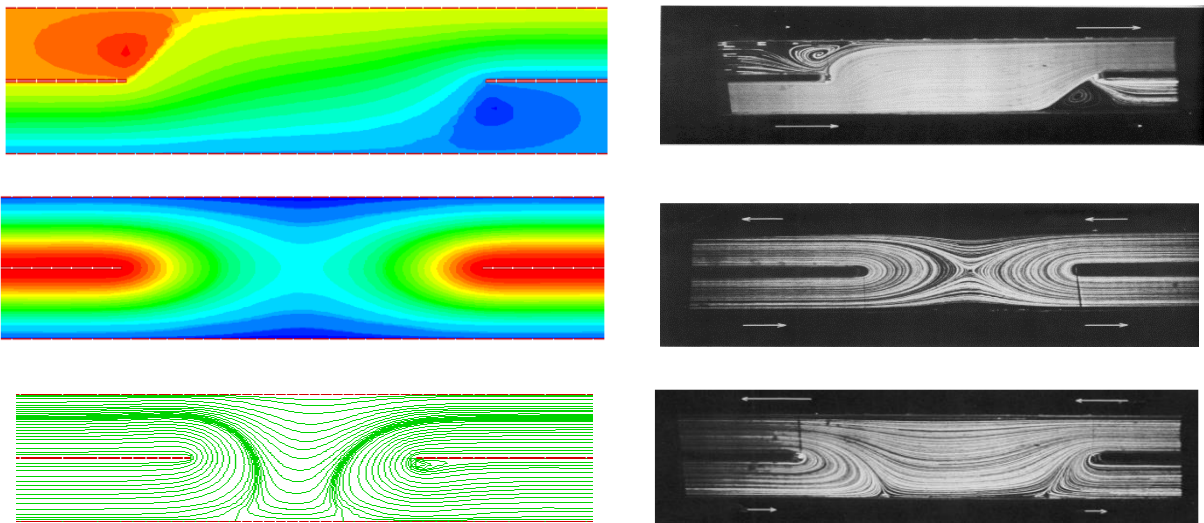
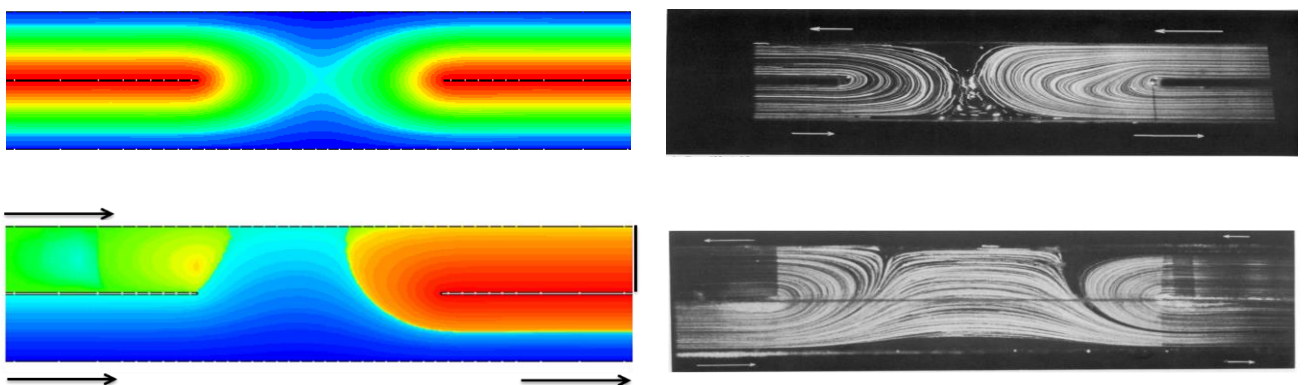


Figure 9.1 Numerical Results Compared with the experimental Results of (Cochrane et al., 1981).

- **Channel flows with changing flow directions and varying flow rate.**



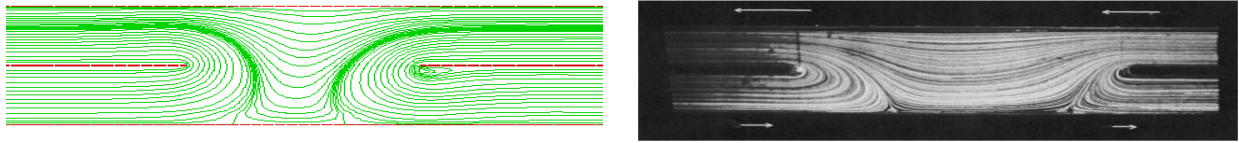


Figure 9.2 Numerical Results Compared with the experimental results of [(Cochrane et al., 1981) and (Walters and Webster, 1982)].

### 9.3 Channel flows through porous media

In this section detailed discussions are carried out for flows of Newtonian fluids through complex mixing–separating channel in the presence of porous material. In chapter five Figure (5.1), the study presented the different configuration with the same domain. For an incompressible flow through homogeneous porous material, continuity and a time–dependent Darcy–Brinkman momentum equation have been used. For primitive variable formulation a finite element based semi–implicit Taylor–Galerkin/Pressure–Correction algorithm is employed. Details of this scheme are discussed in detail in chapter four and onwards in different sections of this document. Detailed discussions on the effects of inertia, pressure and Darcy’s numbers on the flow domain have been given in chapter 6. The value of Darcy’s number ( $D_a$ ) is 1 and permeability ( $\kappa$ ) changes from 0.1 to 0.00001 with increasing Reynolds numbers  $Re$  from 01 to 10000.

Numerically simulated results for configuration presented in [Figure 5.1(a)] discussed in detail have been presented in chapters 6. In this section some useful findings are discussed. At  $Re=4000$ , the study found varying  $Re$  values with flow rate equal (1, 1) for the inertia effect on the structures of flow. The study found very weak appearance of vortex development at  $Re=5000$

---

for the central plate's lower head within the middle gap. For increasing values of  $Re$  vortex appeared, vanished and no other vortex has been found in the entire domain. For the end at  $Re$ , there are unidirectional and reversed flows.

For unequal (1, 1.5) flow rate flows have been pushed in the bottom channel arm due to higher flow rate in top arm as was the case for Newtonian flows in a channel filled with free of porous media. An early activity of vortex generation has been noticed with changing flow rate in the top channel arm which bears a resemblance with flows in the channel filled with non-porous media. But with increasing  $Re$  a vortex developed disappears is dissimilar to the flows in a channel filled without porosity. With the increase of flow rate with an increasing  $Re$  within the channel's upper arm results in generating early vortex. By increasing further, the value of  $Re$  the vortex developed on the nip of centrally located plate disappears as was the case in above equal (1, 1) and unequal (1, 1.5) flow rates. Thus, in the central gap fluid is mixed and streams down towards the channel exits.

The details given in section (6.5.2) of the chapter 6 presents the configuration of the Newtonian fluid flows for the unidirectional numerical simulations. Here discuss the important aspects of inertia on flow behaviour due to changing flow rates in upper channel arm are addressed. For the entire domain there were no activities involving the development of vortex in both unequal and even equal rates of flow. Fluids mix only in the lower channel arm in the downstream of the domain towards the exit.

As shown in the figure (5.1(c)), one-outlet/ two-inlet domain combination that are illustrated in section (6.5.3) of the chapter 6, where because of the middle gap flow is directed towards

---

the upper arm. There was not any early activity of vortex development for initial Reynolds number on the entire domain for equal flow rate conditions. At  $Re=2000$ , it was found that there were very weak vortices generated within the central plate nip and because of the increase in the  $Re$  value their size grows and positions stabilises. Flows are both unidirectional as well as reversed for the entire range of  $Re$ . It was found that there is vortex development in early activity for the unequal flow rates. Initially vortex appeared at the right side of the domain on the nip of central plate and later on left side. The effects of inertia and varying flow rates are obvious on pressure. Pressure increases with an increase in the value and changing the flow rate. That was also the case in channel flows of non-porous domains.

Under the last condition of unidirectional flows for separating domain as shown in the figure [5.1(d)], numerical calculations are presented in section (6.5.4) in detail. There were no inertial effects found based on the porous media filled within the domain to effect the flow behaviour. Increasing or decreasing the value of permeability affects the pressure difference. In the literature about fluid flow in a domains totally filled with porous media, it has been noticed that the local macroscopic inertial term is commonly small compared to the microscopic Darcy drag term and hence could be neglected (Nield, 1991). A quantitative plotting of the operating and geometrical parameters within which the local inertial term may be significant is not available in the literature yet. Therefore, it is not possible that numerically computed results of Newtonian fluid flows in a channel could be compared with the other experimental or numerical results.

---

#### 9.4 Pipe flows through non-porous media

Numerical study has conducted Newtonian fluid flows passing through two pipes filled with non-porous media. The problem specification is such that one pipe with small diameter placed within another pipe of the large diameter having sudden gap in the middle as shown in Figure (7.1) in chapter 7. Newtonian fluid flows are passing in reversed directions with varying flow rates in either circular pipe. The same method is adopted as in chapter four, five and six for numerical compilations. The scheme is fractional staged Taylor-Galerkin/pressure-correction finite element as discussed in chapter four in detail and applied in chapter seven along with imposed initial and boundary conditions discussed. The flow domain is meshed by employing a uniform conformal mappings, a technique which automatically aligns element sides with streamlines and preserves orthogonality of the elements. In the current research, the power and vortex length is calculated via stream function with the increase in Reynolds numbers. Thus, considering the stream functions' numerical predictions were established using the stream line patterns and pressure differences for the increasing inertia is monitored for outer and inner cylinder pipes with varying flow. Critical values of Reynolds number are identified during the vortex generation due to increasing the value of  $Re$  and with the changing flow rates in cylindrical pipes.

Reynolds number were used from 1 to 200 and the gaps within the mixes and unidirectional flow have been found using the Newtonian fluid. Newtonian fluid Flow merges in both upper and lower exits of the computational domain. For the flow rate at equal (1, 1) no relevant vortex development activity was found, even considering the higher value ( $Re= 200$ ). Flow structure stays the same except that fluid has been pushed to the inner pipe towards its line of symmetry.

---

In order to identify more effects of inertia on flow domain an unequal (1, 2) flow rate has been served from the inlets. The fluid passing from the outer cylinder is double as compared to the inner cylinder in volume, because of the increase in the flow rates. Even at  $Re=1$ , there is a significant flow phenomenon demonstrated within the flow rate changes. A strong recirculation region has been observed in the centre of outer pipe behind its centrally located plate in the vicinity of separating region. Increasing the value of  $Re$  increases the power of vortex development and the generated vortices grow in size and occupy the central gap of the domain. Most of the developed vortices remain in the outer cylinder on the central plate, in the middle gap and silent region. Similar push to flow in the inner pipe has been noticed towards the line of symmetry as was the case in equal flow rates. Increasing value of Reynolds number and varying flow rate have the collective effects on pressure difference. Influence of increase in scaled pressure difference has been shown in Figure 7-4 in seventh chapter of this thesis.

### **9.5 Pipe flows through porous media**

The porous media filled within the domain will pass with equal and unequal flow rates for both fluids (Newtonian and non-Newtonian). Details of the combined mixing-separating geometry are given in Figure (7.1) along with its associated initial conditions and boundary conditions. The Power law and Bird Carreau model have been used to capture the non-Newtonian behaviour of the fluid flows. When the value of Reynolds number are varied the level of inertia is increased. The semi-implicit time stepping Taylor-Galerkin/pressure-correction scheme has been used for the solution of the Navier-stokes equation and with the incompressible constraints. Numerical results are shown by stream line patterns with increasing inertia and plots of pressure difference due to changing flow rates in chapter eight.

---

For Newtonian fluid flows in pipes filled with porous media, flow phenomena are the same as was in equal flow rate in pipes filled without porous media. As shown in section (8.7) in chapter 8, no obvious activity of vortex generation has been noticed except the fluid has been pushed in the inner cylinder. Physically it is correct since the diameter of the outer pipe is large; thus the flow of fluid is also greater in the outer pipe as compared to the inner ones. During unequal flow rate a numerical artefact in inner pipe has been observed which will be examined in later. This research could not find any obvious change on flow behaviour due to changing flow rates. Flows in a pipe filled with porous media have a dramatic change on pressure difference due to an increase or decrease in the value of permeability. Due to the increasing or decreasing permeability value for the porous material filled in the pipe the pressure difference changes. Decreasing the value of permeability gives rise to pressure.

Non-Newtonian behaviour of fluid has been captured by using two inelastic models Power law and Bird Carreau in a domain filled with porous media. The effects of flow domain and pressure difference are analysed with increasing inertia, changing flow rates in inner and outer pipe, permeability and power law index. The power law index varies from 0.7 to 0.9 and permeability from 0.1 to 0.0001. Stream line functions are presented from  $Re=1$  to 6000. Fluid has been pushed the same way as was the case of Newtonian flows. No significant effects of inertia are observed to due changing flow rates or power law index. An error has been originated in an inner pipe towards the exit near the line of symmetry as it was in the case of Newtonian fluid flows through porous media. Results of pipe flows thorough are in agreement with results of channel flows through porous media.

The increase in inertia and change of flow rate effects the difference in pressure, but increase or decrease of permeability value have significant effect on the pressure. The power law and

---

Bird Carreau Model predict almost the same behaviour of flows in the domain filled with porous media but differ in forecasting pressure. Through the increase or decrease of permeability value when applying the Bird Carreau Model there was no effect on the pressure. As experimental and numerically simulated results are not available for the domain investigated during this study. Therefore, results are compared with channel flows. Simulated results are in good agreement.

---

## Chapter 10. Conclusions and Future Suggestions

### 10.1 Introduction

This chapter is based on providing the overview of the complete study. It specifies the main scientific ideas based on findings and future suggestions on further research work is presented. In the first chapter, the aims and objectives set out, are accomplished. The robustness of Taylor-Galerkin/pressure-correction algorithm and its viability is exhibited. The numerical predictions are validated by simulating several steady-state isothermal flows of incompressible fluids through complex mixing-separating channels and pipes filled with porous material or without considering porous media. Comparing against other experimental results and numerical solutions a well agreement is observed. The validation of the predicted results illustrate that the present technique is most promising and being robust incense of accuracy, rate of convergence and stability. In a channel flows through non-porous media comparisons are presented with the experimental results as shown in Figure [9.1 to 9.2]. The implemented algorithm can be utilised as an effective tool for performing numerical experiments and can be achieved insight appreciation of the flow phenomena, for the range of steady-state complex flows. The general conclusions of the research study have been given below; that are obtained through numerical results for pipe flows and mixing-separating channel with and without porous material.

### 10.2 Conclusion on channel flows

1. The research study found that changing the Newtonian fluids' material properties can be obvious with non-porous media filled in the channel. This was investigated by

---

without porous material and increasing the Reynolds number, thus inertia, which results to increase the size, recirculation power, and positional stability for adjustment.

2. Changing flow rates in a channel filled for Newtonian fluids without porous media has given rise to an early development of vortices. These vortices are formed under higher values of  $Re$  and eddies are noticed on only one side of the central plate for its initial Reynolds number in a channel filled with no porous media.
3. Flows of constant viscosity fluid in a planar channel in absence of porous material, with changing flow-rates, at both inlets, from an equal to unequal have still given unidirectional and reversed flows whereas this was not the case in equal flow rate for higher values of the Reynolds number.
4. In a channel flows, reversed flows show more inertia effects as compared with unidirectional flows.
5. There is a less chance of the development of vortex with porous material filled in the channel. The study found very weak vortices relative to very high number of Reynolds.
6. Pressure difference is effected by the variations within the flow rates
7. The performance and the capability of the numerical scheme are clearly demonstrated through its applicability for a wide range of inertia, flow rates on flow structure and porosity. In all cases the semi-implicit Taylor-Galerkin/pressure-correction scheme works well except simulating flows with very high Reynolds number.

### **10.3 Conclusions on pipe flows**

1. It was found that there is a varying flow rate due to inertia effect on the domain without porous media for the Newtonian fluid flows in combined separation and mixing. In the current study it was found that the vortex development within the unequal flow rates (1,

- 2) excites in the outer cylinder, while the flows are pushed closer to the symmetry line towards the inner pipe.
2. In a mixing-separating domain of pipes filled with Newtonian materials in which fluid passes through porous media; there is no significant change in the flow structure due to increasing inertia and varying flow rates. However, a dramatic change in pressure difference has been noticed due to increasing or decreasing value of permeability.
3. In non-Newtonian flows pressure is affected by varying flow rates and permeability in the domain filled with porous media. In comparison to Bird Carreau Model, the power law model captures some effects of inertia.
4. This study could find an influence of varying power law index on inertia but permeability has its more effects on pressure.
5. Numerical scheme is very good in capturing flow behaviour but some error has been noticed in an inner pipe filled with porous media under unequal flow rates in the outer cylinder.

#### **10.4 Novelties of the research project**

1. Darcy term has been added in momentum transport equation for monitoring the effects of porosity on the flow domain. The applied implicitness on the Darcy's term is to make mass matrix more stronger.
2. An analytical solution has been found during current study and has been imposed as an exact velocity profile on the inlets of a channel filled with porous media. Full details of its derivations are available in Appendix-B.
3. Numerical modelling for Pipe flows has been taken as test problem for the Newtonian and non-Newtonian fluid flows through porous and non-porous materials.

4. Initially problem was solved for equal flow rates. In current research flow directions and flow rates have been changed to monitor the inertia effects on the computational flow domain.
5. To improve the accuracy of the solution modified Euler method has been used instead of Euler method.
6. Numerical code has been enhanced by including all necessary parameters required for Newtonian and non-Newtonian flows in both porous media domains. Extended numerical code is attached in appendix-D.
7. Physical analysis was compared with experimental results for consistency and good agreement have been established.

### **10.5 Recommendations for future work**

The foremost recommendation for the implementation of numerical simulation is that it is not used as a substitute but only applicable for the experimental analyses. For the solution of realist physical problem using mathematical modelling approach, it is very important that the assumption must be based on realist physical conditions and should be very close as possible. The present study has raised many new issues and they need to be examined. Some of them are:

1. Total number of elements 1328, 5049 was used in a rectangular channel and circular pipes respectively. In presence of the computer capacity it is predicted that the accuracy can be achieved by increasing the number of nodes and elements.
2. Mesh refinement was used in current research, however many regions in a circular pipes were observed with numerical artefact and should be investigated.

3. In channel flows there are variety of ways to change directions and flow rates in either arms. In the current study using the varying flow rates, four combinations were analysed. Still there are more configurations possible and should be examined.
4. Pipe flows were taken as test problem during current study by applying same mesh used for channel flows. As these are three dimensional domains as well in many industrial applications, therefore three dimensional meshes should be used and simulated in the presence of cluster and parallel processing.
5. The pipe flow domain can be designed in a variety of ways. By keeping outer pipe fixed and rotating inner pipe clockwise or counter clockwise should be investigated. Even rotating one side of inner pipe clockwise and other counter clockwise will reveals many new phenomena.
6. During the implementation of Finite element analysis one the most critical decisions is the design of mesh. In many non-Newtonian flows, regions with steep stresses and gradients frequently occur or disappear or change their shape and location. It is therefore important to make sure that finite element mesh is sufficiently fine in these areas to accurately capture the solution.
7. During this study only two dimensional flows were studied, however, further investigation is need to extent the present research in three–dimension and may be for turbulent flow, due to its importance in the industrial context.
8. The problems related to time dependency may arise in the flows involving the moving objects, multi-layer injecting moulds, and free surface. Difficulty of handling moving meshes then may arise. In that case, consistent time dependent boundary conditions are needed because they add some freedom to the specification of the problem.

9. In the current study single relaxation time was considered; therefore, it is suggested that future studies use multiple-relaxation times for the pipe flows, as well as different models for viscoelastic and non-Newtonian in the pipe flow channels should be used.

---

## Appendix-A

### Publications

1. Khokhar, R. B., Chen, Y. K., Calay, R. K. and Xu, Y. (2013), Numerical scheme to simulate combined mixing and separating flow in a channel, *Applied Mechanics and Materials*, Vols. (303-306), pp. 2798-2805.
2. Khokhar, R. B., Chen, Y. K., Xu, Y. and Calay, R. K. (2013), Numerical simulation of combined mixing and separating flow in channel filled with porous media, *Advanced Materials Research* Vols. (694-697), pp. 639-647.
3. Solangi, M. A., Khokhar, R. B. and Baloch, A. (2013), A FEM Study for Non-Newtonian behaviour of blood in plaque deposited capillaries: analysis of blood flow structure, *Mehran University Research Journal of Engineering and Technology*, vol. 32 (2), pp. 277-282.
4. Solangi, M. A., Khokhar, R. B. and Blaoch, A. (2012), Computational modelling of pressure difference for non-Newtonian behaviour of blood in plaque deposited capillaries, *Sindh University Research Journal Science Series*, vol. 44(4), pp. 723-726.
5. Solangi, M. A., Shaikh, H., Khokhar, R. B. and Baloch, A. (2012), Numerical Study of Newtonian blood flow through a plaque deposited artery, *Sindh University Research Journal Science Series*, vol. 44 (04), pp.79-82.

## Appendix-B

### Analytical solution

#### Steady–state analytical solution of one–dimensional Darcy’s–Brinkman equation to impose boundary condition on the inlets of combined mixing–separating domain

Consider the steady–state incompressible isothermal flow of constant viscosity fluid through planar channel packed by porous media governed by one–dimensional Darcy–Brinkman equation, neglecting body force is written as:

$$\frac{\mu}{\varepsilon} \frac{\partial^2 u}{\partial y^2} - \frac{\mu}{\kappa} u = \frac{\partial p}{\partial x} \quad (1)$$

Where  $u$  is the axial velocity component,  $p$  is the isotropic pressure,  $x$  and  $y$  are axial and transversal coordinates respectively, while, respectively material parameters  $\mu$ ,  $\varepsilon$  and  $\kappa$  are fluid viscosity, porosity and permeability of porous material. After taking suitable scaling factors such as  $u = V_c u^*$ ,  $(x, y) = L_c (x^*, y^*)$  and  $p = \frac{\mu V_c}{\varepsilon L_c} p^*$ . Then dimensionless form of above

equation (1) with constant pressure gradient, takes the following form:

$$\frac{\partial^2 u}{\partial y^2} - \frac{1}{D_a} u = \frac{\partial p}{\partial x} \quad (2)$$

Here dimensionless Darcy's number  $D_a = \frac{\kappa}{\varepsilon L_c^2}$  and  $\frac{\partial p}{\partial x}$  are constants then partial differential equation reduces in an ordinary differential equation as:

$$\frac{d^2 u}{dy^2} - Au = -B \quad (3)$$

Where  $A = \frac{1}{D_a}$  and  $B = -\frac{dp}{dx}$

As we know boundary conditions are  $u(a) = 0$  and  $u(b) = 0$ .

Equation (3) is non-homogeneous linear partial differential equation with constant coefficient and conditions are homogeneous so that required general solution of Equation (3)  $u(y)$  is of the form:

$$u(y) = u_c + u_p \quad (4)$$

Where  $u_c$  and  $u_p$  stands for complementary function and particular integral.

For complementary function, the equation (3) becomes homogeneous as:

$$\frac{d^2 u}{dy^2} - Au = 0 \text{ or } u_{yy} - Au(y) = 0 \quad (5)$$

Or it can be written as:

$$\{D^2 - A\}u(y) = 0 \quad (6)$$

In Equation (6), replacing  $D$  by  $m$  :

$$m^2 - A = 0 \text{ or } m^2 = A \quad (7)$$

or

$$m = \pm\sqrt{A} \quad (8)$$

Here the roots are distinct so the particular solution will be exponential or hyperbolic; in hyperbolic form solution is as follows:

$$u_c = C_1 \cosh(\sqrt{A}y) + C_2 \sinh(\sqrt{A}y) \quad (9)$$

Now for particular integral ( $P.I$ ) equation (3) is  $\frac{d^2u}{dy^2} - Au = -B$  so that  $u_p$  is:

$$u_p = P.I = \frac{-B}{D^2 - A}$$

$$u_p = \frac{-B}{-A \left\{ 1 + \frac{D^2}{-A} \right\}}$$

$$\frac{B}{A} \left\{ 1 - \frac{D^2}{A} \right\}^{-1} \quad (10)$$

Apply Binomial Theorem, and then the result will be:

$$u_p = \frac{B}{A} \quad (11)$$

Now adding Equations (9) and (10), we will get the complete general solution as:

$$\therefore u(y) = C_1 \cosh(\sqrt{A}y) + C_2 \sinh(\sqrt{A}y) + \frac{B}{A} \quad (12)$$

Or

$$u(y) = C_1 \cosh\left(\frac{y}{\sqrt{D_a}}\right) + C_2 \sinh\left(\frac{y}{\sqrt{D_a}}\right) - D_a \frac{dp}{dx} \quad (13)$$

Now after applying boundary conditions  $u(a) = 0$ , it means  $u = 0$  at  $y = a$  and  $u(b) = 0$ ,

means  $u = 0$  at  $y = b$  then from Equation (13), we get as follows:

$$0 = C_1 \cosh\left(\frac{a}{\sqrt{D_a}}\right) + C_2 \sinh\left(\frac{a}{\sqrt{D_a}}\right) + \frac{B}{A} \quad (14)$$

$$0 = C_1 \cosh\left(\frac{b}{\sqrt{D_a}}\right) + C_2 \sinh\left(\frac{b}{\sqrt{D_a}}\right) + \frac{B}{A} \quad (15)$$

Solving simultaneous Equations (14) and (15) for constants  $C_1$  and  $C_2$ , by applying basic trigonometric identities and know formulae we get the values of  $C_1$  and  $C_2$ . By putting these values in Equation (13), we will get the steady-state analytical solution as below:

$$u(y) = U_{\max} \left[ 1 - \frac{\sinh \frac{y-a}{\sqrt{Da}} + \sinh \frac{b-y}{\sqrt{Da}}}{\sinh \frac{b-a}{\sqrt{Da}}} \right] \quad (16)$$

where  $U_{\max} = -\frac{\partial p}{\partial x}$ .

In figure below, the graphs for above solution equation (16) of axial velocity profile on both inlets, i.e., left bottom and right top of the mixing–separating channel flow.

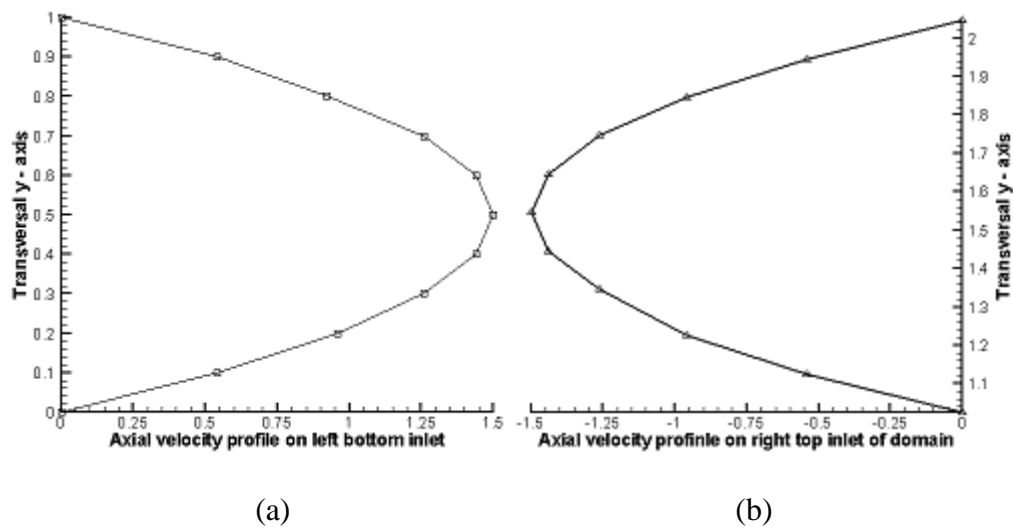
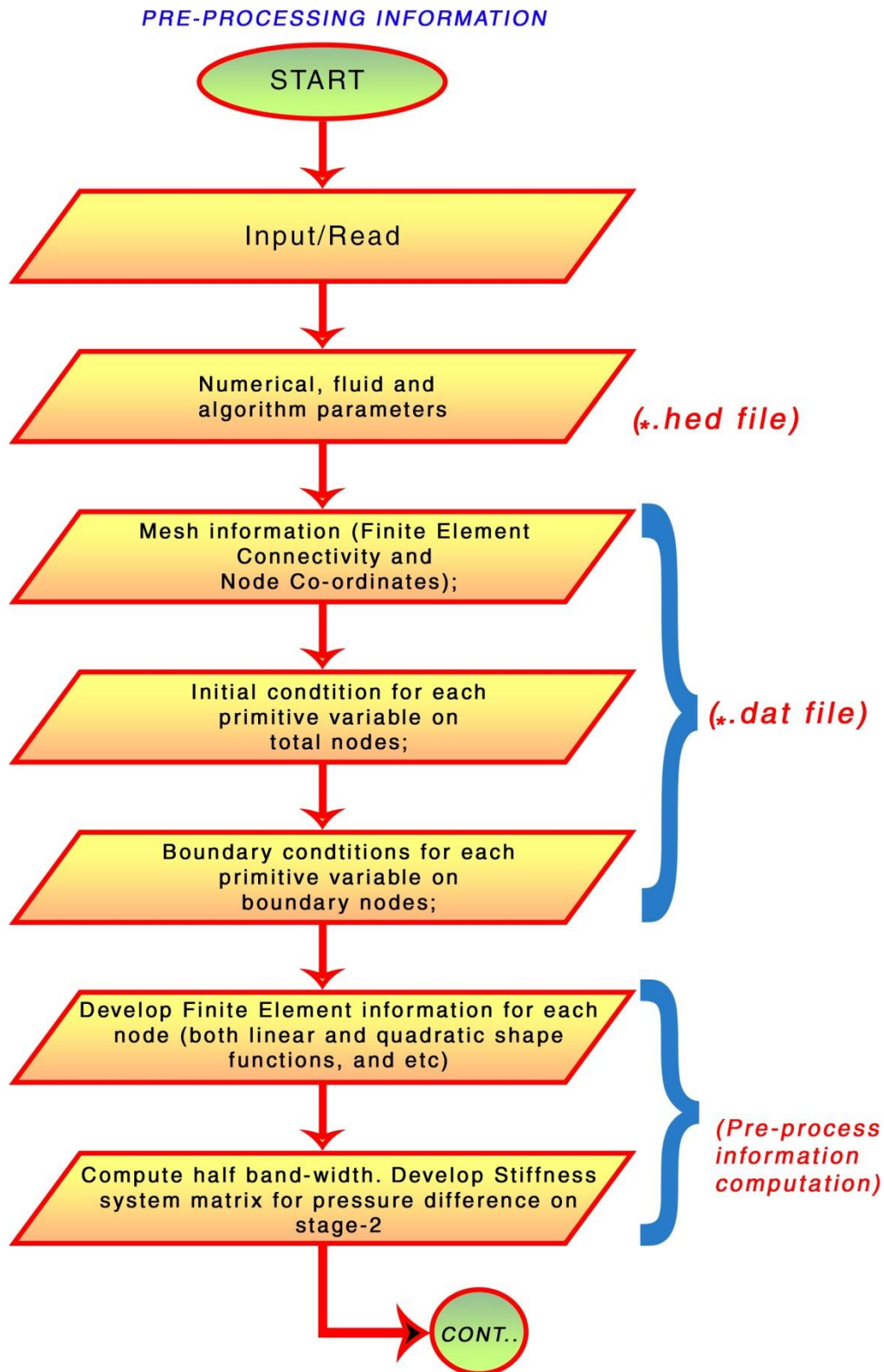
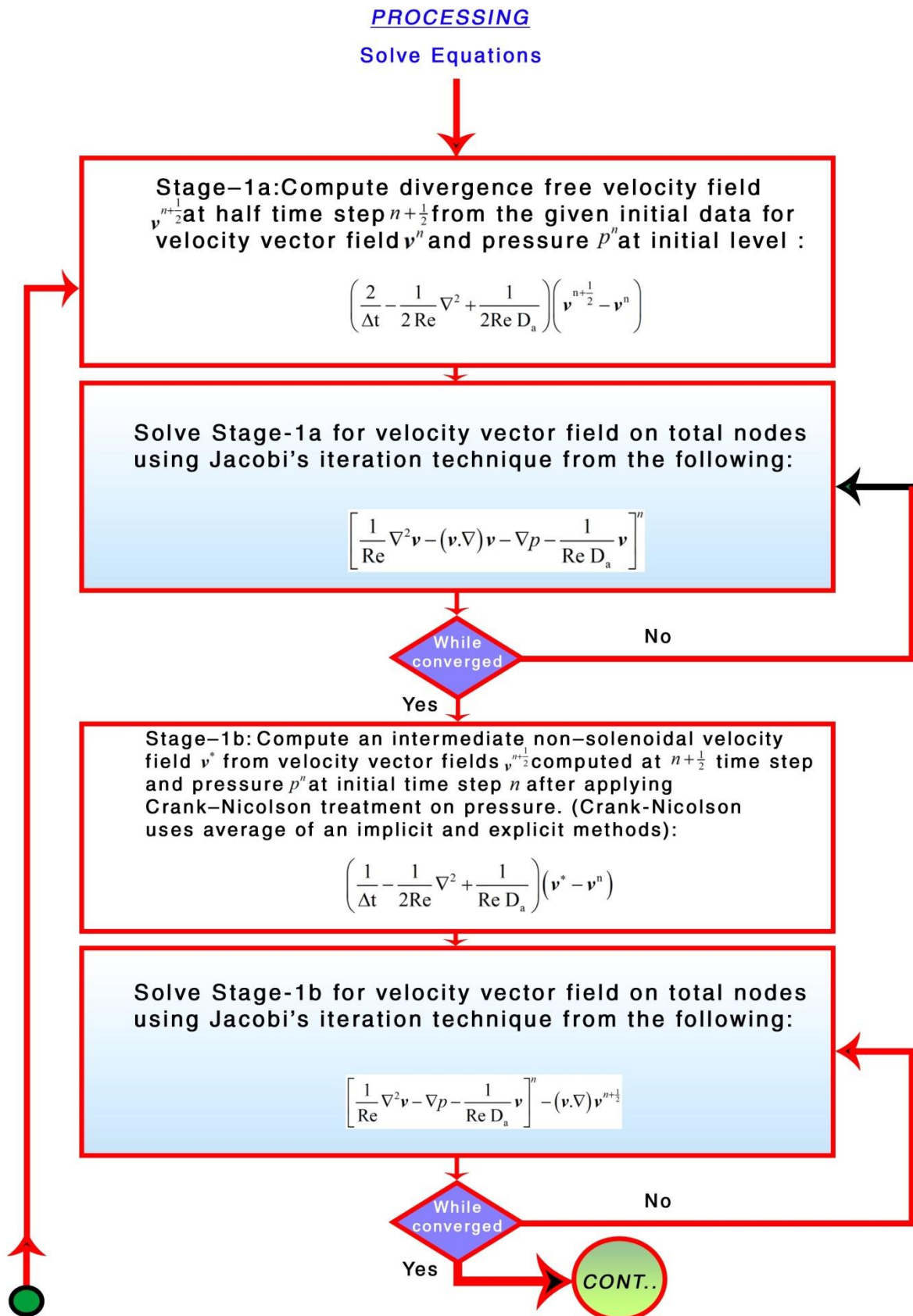


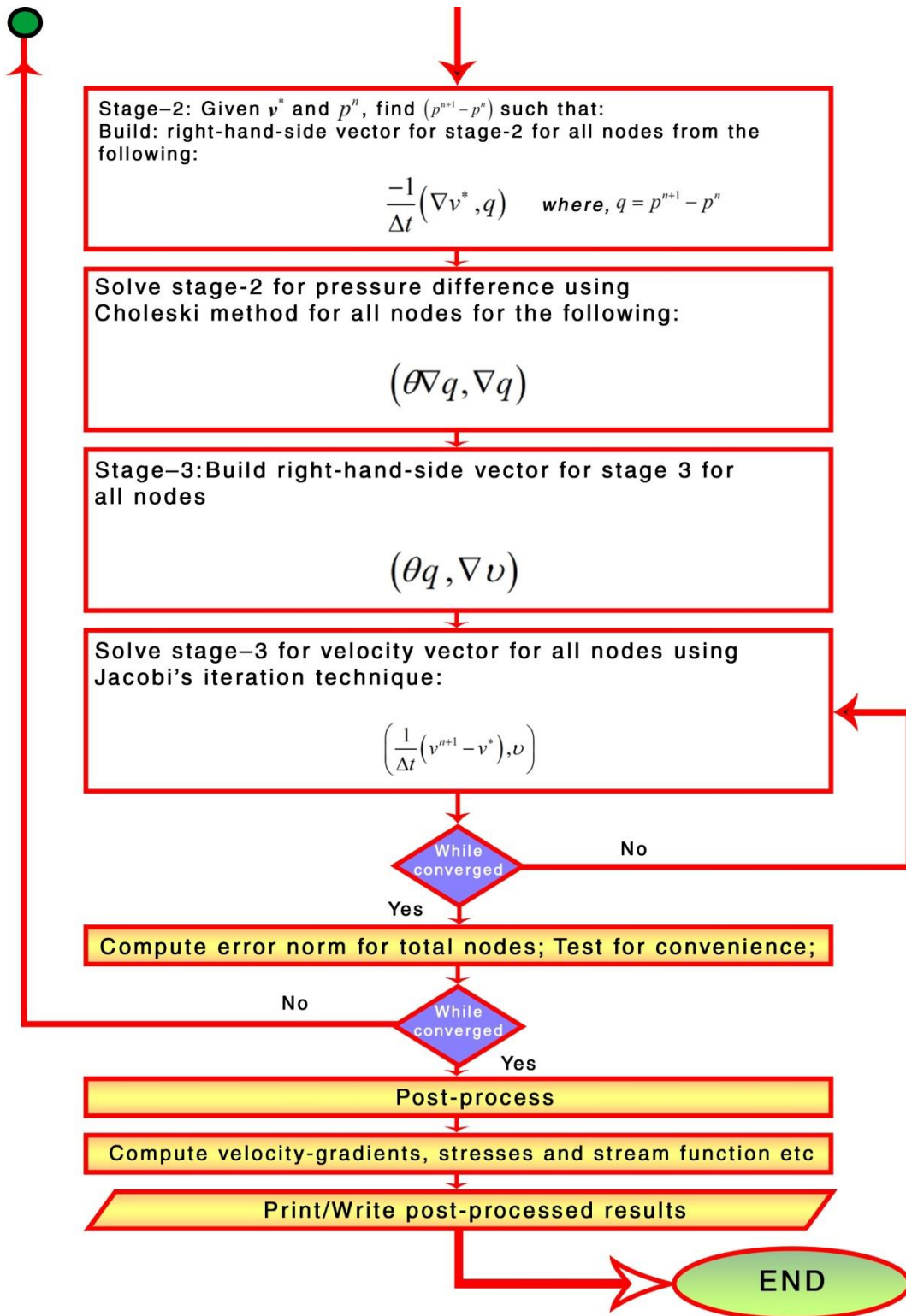
Figure 1 Velocity profiles imposed on the (a) left bottom inlet and (b) right top of the computational domain.

## Appendix-C

## Flow Chart of the of finite element scheme







## Appendix-D

### Two dimensional code

```

!*****
!*****
!*****
!*****
!***** SEMI-IMPLICIT *****
!***** TAYOR-GALERKIN + PROJECTION METHOD *****
!*****
!***** PLANE TWO-DIEMSIONAL *****
!*****
!***** NEWTONIAN *****
!*****
!*****
!*****
!
! Started : 14th Sept. 2014
! Last Modified :
!
! Authors : A. Baloch
!
! Location : Mehran University of Engineering and Technology,
! Jamshoro, Sindh, Pakistan
!
!-----
!
! #if cflag1 || cflag2 && !cflag3
! #elif cflag4
! #elif
! #endif
! means if cflag1 or cflag2 and not cflag3
! else if cflag4
! else
!
!=====
!
Include 'local_def.f90'
Include 'Common_h.f90'
Include 'Pvm_cb.f90'
!
Include 'Assemble.f90'
Include 'BuildDiag.f90'
Include 'BuildRhsMom.f90'
Include 'Cholesky.f90'
Include 'CompErr.f90'
Include 'Dmpfmt.f90'
Include 'ExacElmMat.f90'
Include 'FixBry.f90'
Include 'GaussQuan.f90'
Include 'Get_Area_steer.f90'
Include 'GetRhsStage1.f90'
Include 'GetRhsStage2.f90'
Include 'GetRhsStage3.f90'
! Include 'GNVisCos.f90'
Include 'LhsDiagStage1.f90'
Include 'MasItn1FV.f90'
Include 'Meshuty.f90'
Include 'Naguty.f90'
Include 'Postprocess.f90'
Include 'PorousM.f90'

```

```

Include 'Prepare1.f90'
Include 'Preprocess.f90'
Include 'Profit.f90'
Include 'Psetup.f90'
Include 'QuadElmMat.f90'
Include 'ReadCont.f90'
Include 'ReadStrt.f90'
Include 'SetGauss.f90'
Include 'Setup.f90'
Include 'SetupMat.f90'
Include 'SetupSteer.f90'
Include 'SetupShape.f90'
Include 'ShearExten.f90'
Include 'SolveEqu.f90'
Include 'SolveStage1.f90'
Include 'SolveStage2.f90'
Include 'SolveStage3.f90'
Include 'VisCosGenN.f90'
! Include 'Gradrec2d.f90'
!
!-----
!
PROGRAM MAIN
!
USE local_def, ONLY : ZNumNodes, ZTNODP, ZNumElements
USE common_h, ONLY : ZBAND, ZBTNOD, ZDIM, ZDOF, ZMFAC, &
ZNOD2, ZNODLP, ZNODLV, ZNVAR, ZNQP, &
ZNUMT, BTNOD, CONTUE, DOFNOD, DSCALE, &
DSMALL, ICOORD, IELTOP, INF, ING, &
INH, IPSTR, ISOL, ISOLP, ISYSK, &
ISYSM, ITEST, IVSTR, IWORK1, IWORK2, &
IWORK3, JCOORD, JELTOP, JNF, JSOL, &
JSYSK, JWORK3, MFAC, NQP, NSTEP, &
NTER, NUMT, NVAR, NVET, PNODEL, &
PICON, PNODS, VNODEL, NStepPr
!
USE pvm_cb
!
IMPLICIT NONE
!
!-----
!
! Data (parameters) initialisation
!
ICOORD=ZNumNodes; IELTOP=ZNOD2; ISOL=ZNumNodes; NQP= ZNQP;
ISOLP=ZTNODP; ISYSK=ZTNODP; ISYSM=ZNumNodes; IWORK2=ZTNODP;
IWORK3=ZNumNodes; INF=ZNumNodes; ING=ZNumNodes; INH=ZNumNodes;
JCOORD=ZDIM; JELTOP=ZNumElements; JSOL=ZNVAR; JSYSK=ZBAND;
JWORK3=ZDIM; JNF=ZDOF; DOFNOD=ZDOF; PNODEL=ZNODLP;
VNODEL=ZNODLV; NVAR=ZNVAR; PNODS=ZDIM; MFAC=ZMFAC;
BTNOD=ZBTNOD; NUMT=ZNUMT; DSCALE = 1.D+20; DSMALL = 1.D-10
NSTEP=0; ITEST=0; PICON=.TRUE.; CONTUE=.TRUE.
!
!-----
!=====
! Pre-processing part:
! Setup requirement for the time-stepping loop
!
Call Preprocess_setup
!
!-----
! MAIN TIME LOOP processor for various fractional stages
!

```

```

Call SolveEquations
!
!-----
! Post processor:
! FINAL SOLUTION PRINTOUT
!
Call Postprocess_results
!
!-----
!
STOP
END PROGRAM MAIN
!
!=====
!-----
!
SUBROUTINE GetMassMom( Nele, QuotM, RhsB, IRhsB )
!
! Called in GetRhsStage1 for Mass like term MP,
! For Darcy's term (Porous media) in RHS RBK
! Planar case at STAGE 1 only
! With "exact integration" (1 = true) or a quadrature rule
! (1 = false).
!
USE common_h
!
IMPLICIT NONE
!
! Parameter list
INTEGER :: Nele, IRhsB
DOUBLE PRECISION :: QuotM
DOUBLE PRECISION :: RhsB( IRhsB, * )
!
INTEGER :: I, J, JST, IVAR
DOUBLE PRECISION :: SOLIJ, VSC
!
!-----
! evaluate MMATE(VNODEL,VNODEL ) by exact integr.
! Make use of zero elements in matrix for the calculation of
! the rhs contributions
!-----
!
DO IVAR = 1, 2 ! loop over variables
DO J = 1, VNODEL
JST = VSTEER( J, Nele )
VSC = GNVisc( JST )
SOLIJ = QuotM * Sol( JST, IVAR ) * VSC
DO I = 1, VNODEL
RhsB( I, IVAR ) = RhsB( I, IVAR ) + MMATE(I, J) * SOLIJ
ENDDO
ENDDO
ENDDO ! end loop over variables
!
!-----
!
RETURN
END SUBROUTINE GetMassMom
!
!=====
!-----
!
SUBROUTINE GetForchhMom( NEle, QuotM, RhsB, IRhsB )

```

```

!
! Called in GetRhsStage1 for Forchheimer term (Porous Media)
! Calculate of solution arrays Fa * v^2 at the Gauss points
! Planar case at STAGE 1 only
! With quadrature rule setup interpolated values of velocity
! array terms at the Gauss points for Darcys law
!
USE common_h
!
IMPLICIT NONE
!
! Parameter list
INTEGER :: NEle, IRhsB
DOUBLE PRECISION :: QuotM
DOUBLE PRECISION :: RhsB( IRhsB, * )
!
INTEGER :: I, IQ, IVar, J, JST
DOUBLE PRECISION :: SolIJ1, SolIJ2
DOUBLE PRECISION :: SOLVN1, SOLVN2
DOUBLE PRECISION :: VelN( ZNqp, NVel )
!
!-----
! Make use of zero elements in matrix for
! the calculation of the rhs contributions
!-----
!
! Initialize
VelN = 0.0d0
!
!-----
!
Do J = 1, VNODEL
JST = VSTEER(J, NEle)
! The most recent velocity
SolVN1 = SolN(JST, 1)
SolVN2 = SolN(JST, 2)
Do Iq = 1, ZNqp
VelN(Iq, 1) = VelN(Iq, 1) + SOLVN1 * FUNV(Iq, J)
VelN(Iq, 2) = VelN(Iq, 2) + SOLVN2 * FUNV(Iq, J)
End Do
End Do ! End of loop J over VNODEL
!
Do Iq = 1, ZNqp
SolIJ1 = QuotM * VelN(Iq, 1) * VelN(Iq, 1)
SolIJ2 = QuotM * VelN(Iq, 2) * VelN(Iq, 2)
Do I = 1, VNodeL
RhsB( I, 1 ) = RhsB( I, 1 ) + FUNV(IQ, I) * SolIJ1
RhsB( I, 2 ) = RhsB( I, 2 ) + FUNV(IQ, I) * SolIJ2
End Do
End Do
!
!-----
!
RETURN
END SUBROUTINE GetForchhMom
!
!-----
!-----
!-----
!
SUBROUTINE GetMasPM(NEle, Del, IDel, JDel, QuotPM, RhsB, IRhsB)
!
! Called in GetRhsItMom for step 1, for porous media
!

```

```

! evaluate symmetric element mass matrix MMATE(VNODEL,VNODEL)
! contribution to the rhs using exact integration.
! Elements with straight sides only!!!
!-----
!
! USE common_h
!
! IMPLICIT NONE
!
! INTEGER :: NEle, IDel, JDel, IRhsB
! DOUBLE PRECISION :: QuotPM
! DOUBLE PRECISION :: Del(IDel, JDel), RhsB(IRhsB, JDel)
!
! INTEGER :: I, J, JST, IVar
! DOUBLE PRECISION :: DelJ1, VSC
!
!-----
! 2D planar coordinates
!-----
!
! Do J = 1, VNodeL
! JST = VSTEER(J, NEle)
! VSC = GNVisc( JST )
! Do IVar = 1, NVel
! DelJ1 = Del(JST, IVar) * QuotPM * VSC
! Do I = 1, VNodeL
! RhsB(I, IVar) = RhsB(I, IVar) + MMate(I, J) * DELJ1
! End Do
! End Do
! End Do
!
!-----
!
! RETURN
! END SUBROUTINE GetMasPM
!
!-----
!=====
!-----
!
! SUBROUTINE GetMasDiagPM( NEle, Quot, RhsB, IRhsB )
!
! Called in GETMAT
! Calculation of diagonalised mass matrix (transient) terms
! either the max row sum or just the diagonal of MMATE is
! evaluated, depending on what is stored in MMATD
! Elements with straight sides only!!!
!
! USE common_h
!
! IMPLICIT NONE
!
! INTEGER :: NEle, IRhsB
! DOUBLE PRECISION :: Quot, RhsB(IRhsB,*)
!
! INTEGER :: I, LST1, LST2, LST3
! DOUBLE PRECISION :: MMATH, RadL1, RadL2, RadL3, QuotPM
!
!-----
! 2D planar coordinates
!-----
!
! DO I = 1, VNODEL
! RhsB(I, 1) = Quot * MMATD(I)

```

```

ENDDO
!
!-----
!
RETURN
END SUBROUTINE GetMasDiagPM
!
!-----
!=====
!=====
!-----
!
SUBROUTINE GetRhsStage1( elpha )
!
! Called in SolveStages - the main iteration loop
! PSETUP - initialise pressure
! Get the rhs for the stage 1 equations
! Returns the rhs for stage 1 in matrix work.
!
! ZNumNodes = total number of nodes
! nstres = znvar = zdof - 1 = (vel dof + stress dof)
! per node, in 2D viscoelastic = 5
!-----
!
USE common_h
!
USE pvm_cb
!
IMPLICIT NONE
!
! parameter list
INTEGER :: elpha
!
! local variables
INTEGER :: i, j, k, imode
!
!-----
!
! Computes Gen. Newt. Viscosity per node in global array
! Call GenNVisCos
!
!-----
!
! First initialise the work array
! index is ( total_no_nodes, velocity_and_stress_index )
!
Work = 0.0d0
!
!-----
!
! Build RHS for momentum equation,
! only for non-fixed velocity field
!
CALL GetRhsStage1Vel( elpha )
!
!-----
!
! print*, 'Work vector-Stage-1'
! do j = 1, TOTNOD
! write( *, * ) j, ( Work( j, k ), k = 1, nvar )
! end do
10 format( i5, 8e16.6 )
9000 FORMAT(I4,5D15.8)
!

```

```

!-----
!
RETURN
END SUBROUTINE GetRhsStage1
!
!-----
!=====
!-----
!
SUBROUTINE GetRhsStage1Vel( elpha )
! Called in GetRhsStage1.
!
! Get the rhs for the stage 1 momentum equations
! Returns the rhs for the momentum equations (stage 1)
! in multiple (matrix) work vector.
!
! ZNumNodes = total number of nodes
! NVEL = number of velocity dof per node, in our case = 2
! elpha = pressure parameter to include the pressure term in
! the momentum equations (=1) or not (=0). The latter
! is used to initialize the pressure field, or for a
! first order pressure-correction implimentation
!
! momentum rhs vector and constitutive rhs vector:
! fractional step one of projection method
!-----
!
USE common_h, ONLY : NVEL, SOL, SOLN, REYNLD2, VISC1, &
VISC2, VISCTY, NDTYPE, TOTELS, &
RELAX, REYNLD1, VNODEL, VSTEER, &
WORK, ELDET, ISOL, ZNODLV, ZNQP, &
ZNumNodes, TOTNOD
USE pvm_cb
!
IMPLICIT NONE
!
INTEGER :: Elpha
! local variables
INTEGER :: BNEle, NEle, i, j, k, jst
DOUBLE PRECISION :: Det, CrjacC, CrjacF, CrjacM, CrjacS, &
QuotC, QuotD, QuotF, QuotM, QuotS
DOUBLE PRECISION :: RadGss( ZNQP )
DOUBLE PRECISION :: rhsb( ZNODLV, NVEL ), &
VelGssN( ZNQP, NVEL )
!
!-----
!
CrjacC = REYNLD2; CrjacS = 1.0d0 / REYNLD1;
CrjacM = CrjacS / permibility;
CrjacF = Forchheimer
! print*, porous, permibility
!
!-----
! Loop over finite elements (momentum eqn)
!-----
!
Do NEle = 1, TotEls
!
Det = ElDet(NEle) * Relax
!
!-----
! Nullify rhs b vector
rhsb = 0.0d0
!-----

```

---

```

! Get quantities in Gauss points for quadrature
Call SetGaussMom( NEle, VelGssN, RadGss, ZNqp, &
SolN, ISol, NVel )
!
!-----
! update rhs vector with diffusion terms, 2 eta_s d
! For the semi-implicit method this term has to be applied
! on sol and not on soln
!-----
QuotS = -Det * CrjacS ! scaling factor for matrix SS
Call GetDiffMom( NEle, Sol, ISol, NVel, QuotS, &
RhsB, ZNodIV, RadGss )
!
!-----
! (partially integrated) grad.tau term (tau = elastic stress)
!-----
! alpha == elpha = 1: take into account the L^T p term
! in the momentum equation
If( Elpha == 1 ) Then
Call GetGradPMom( NEle, Det, RhsB, ZNodIV, RadGss )
End If
!
!-----
! convection term (for non-zero reynolds number only)
QuotC = -Det*CrjacC ! scaling factor for matrix CMATE
Call GetConMom( NEle, QuotC, RhsB, ZNodIV, SolN, ISol, &
VelGssN, ZNqp, RadGss )
!
!-----
! Mass like term (for non-zero Darcy's number only)
If( porous == 1 ) Then
QuotM = -Det * CrjacM !Scaling factor for matrix MMATE
Call GetMassMom( NEle, QuotM, RhsB, ZNodIV )
End If
!
!-----
! Mass like term (for non-zero Darcy's number only)
If( porous == 2 ) Then
!
! Mass like term (for non-zero Darcy's number only)
! - v / ( Da * Re )
QuotM = -Det * CrjacM !Scaling factor for matrix MMATE
Call GetMassMom( NEle, QuotM, RhsB, ZNodIV )
!
! - Fa * ( v * V (u^2 + v^2) )
! Mass like term due to Forchheimer
QuotF = -Det * CrjacF !Scaling factor for matrix MMATE
Call GetForchhMom( NEle, QuotF, RhsB, ZNodIV )
End If
!
!-----
! information generated is in spatially local matrix "rhsb"
! now transfer it to spatially global matrix "work".
! NVEL = 2 (u,v)
! vnode = 6 (6 nodes on the element)
! Nele = do loop counter over all elements
!-----
Do j = 1, vnode ! j = 1..6 (nodes_per_element)
jst = vsteer(j,Nele) ! jst = steering --> global node index
Do k = 1, NVEL ! k = 1..2 (u,v)
Work(jst,k) = Work(jst,k) + RhsB(j,k)
End Do
End Do
! end of Nele counting though all Finite Element elements

```

```

End Do
!
!-----
!
! print*, 'Work vector at Stage-1 vel.'
! Do j = 1, TOTNOD
! write(nout,10) j, ( Work( j, k ), k = 1, nvel )
! write( 16, 10 ) j, ( Work( j, k ), k = 1, nvel )
! write( 17, 10 ) j, ( Work( j, k ), k = 1, nvel )
! End Do
!
! Stop
!
!-----
!
10 Format( i5, 3e16.6 )
!
RETURN
END SUBROUTINE GetRhsStage1Vel
!
!-----
!=====
!=====
!
SUBROUTINE SolveStage1( dteff )
!
! Called ONLY from SolveStages.F and call various stage1
! solve routines
!
USE common_h
!
IMPLICIT NONE
!
! parameter list
DOUBLE PRECISION :: dteff ! the effective time-step
!
! local variables
Integer :: i, j
!-----
! Solve the momentum equations if velocity field is not fixed.
!??? Has to be solved after the stress, to use velocity at correct
!??? time level in SUPG upwind function (iterative part) for stress
!-----
!
CALL SolveStage1Vel( dteff )
!
!-----
! print*, 'End of SolveStage1'
!-----
! print*, 'Work vector as solution difference'
! do i = 1, TOTNOD
! write(*,10) i, (Work(i,j), j=1,nvar)
! end do
! print*, 'Old solution vector Sol'
! do i = 1, TOTNOD
! write(*,10) i, (Sol(i,j), j=1,nvar)
! end do
! print*, 'New solution vector SolN'
! do i = 1, TOTNOD
! write(*,10) i, (Soln(i,j), j=1,nvar)
! end do
10 format(i4,3f12.6)
!
!-----

```

```

!
RETURN
END SUBROUTINE SolveStage1
!
!-----
!=====
!-----
!
SUBROUTINE SolveStage1Vel( dteff )
!
! fix boundary AND calculate solution for fractional step 1
! momentum balance equation
!
USE common_h, ONLY : NVEL, TOTNOD, SOL, SOLN, WORK, ZNumNodes
!
IMPLICIT NONE
!
! parameter list
DOUBLE PRECISION :: dteff ! the effective time-step
!
! local variables
INTEGER :: i,j
!
!-----
!
! mass matrix iteration for increment of solution component
! (Delta u, Delta v)
CALL MasItn1FV( dteff ) ! updates velocity in work.
! Also calls FixBry1Vel.
!
!-----
!
! Update the velocity solutions with (Delta u, Delta v)
DO j = 1, NVel ! loop through just u and v
DO i = 1, TotNod
SolN( i, j ) = Sol( i, j ) + Work( i, j )
ENDDO
ENDDO
!
!-----
! print*, 'Work vector as solution difference'
! print*, 'Solution vector'
! do i = 1, TOTNOD
! write(*,10) i, (Work(i,j), j=1,nvel)
! write(*,10) i, (Soln(i,j), j=1,nvel)
! end do
10 format(i4,3e18.8)
!
!-----
!
RETURN
END SUBROUTINE SolveStage1Vel
!
!-----
!=====

```

---

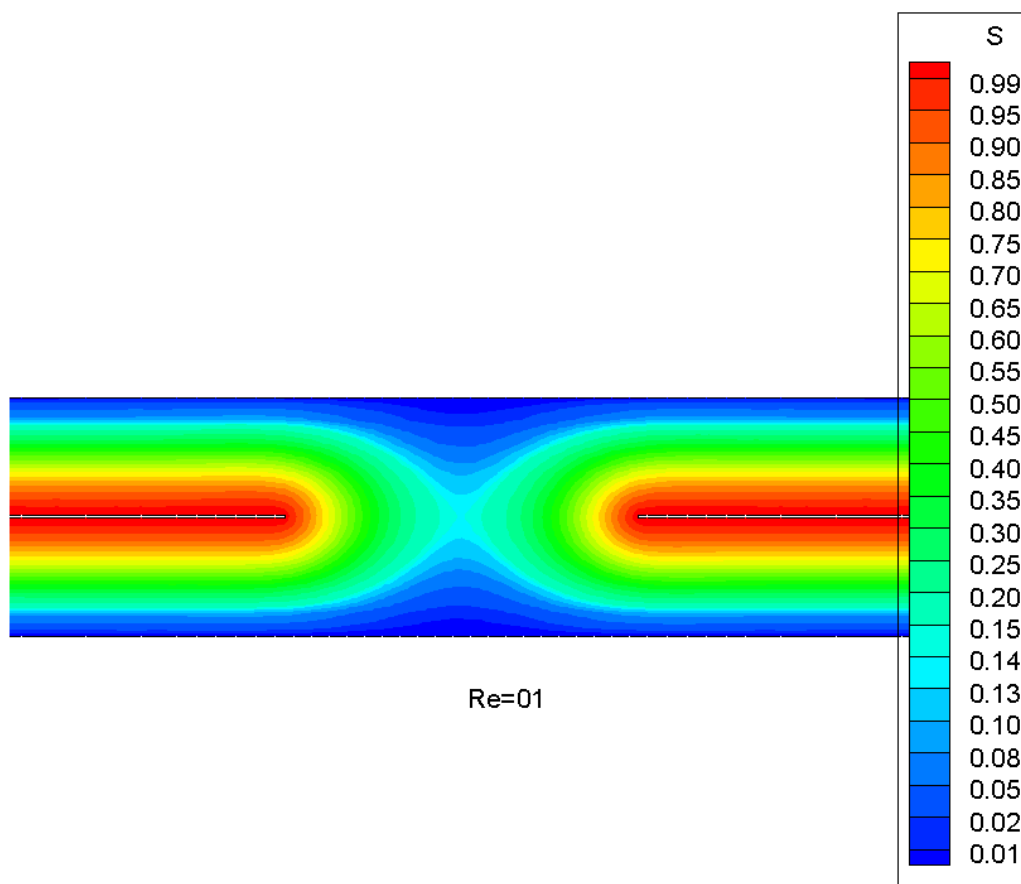
## Appendix-E

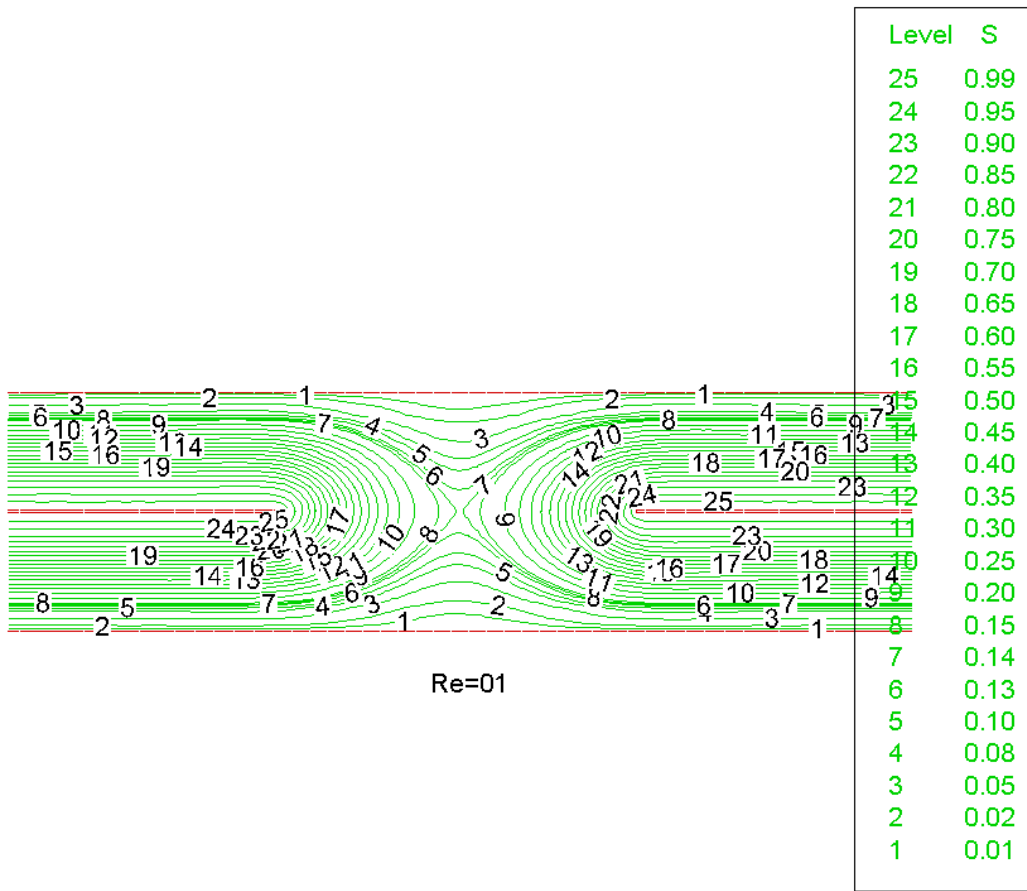
Numerically simulated results with velocity profiles, colour bars and velocity vectors

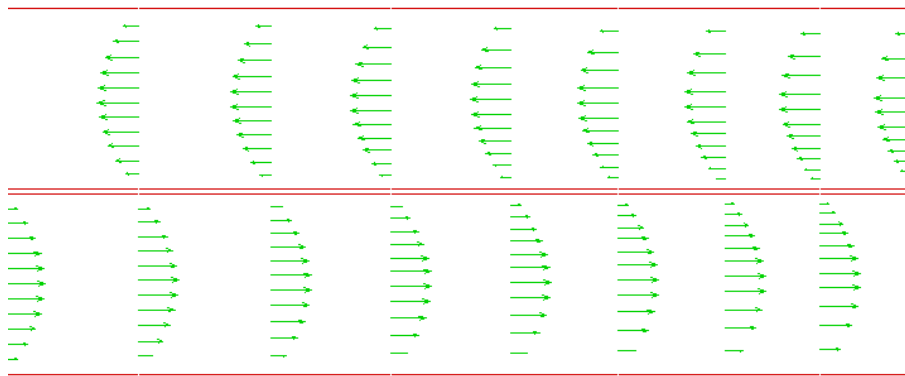
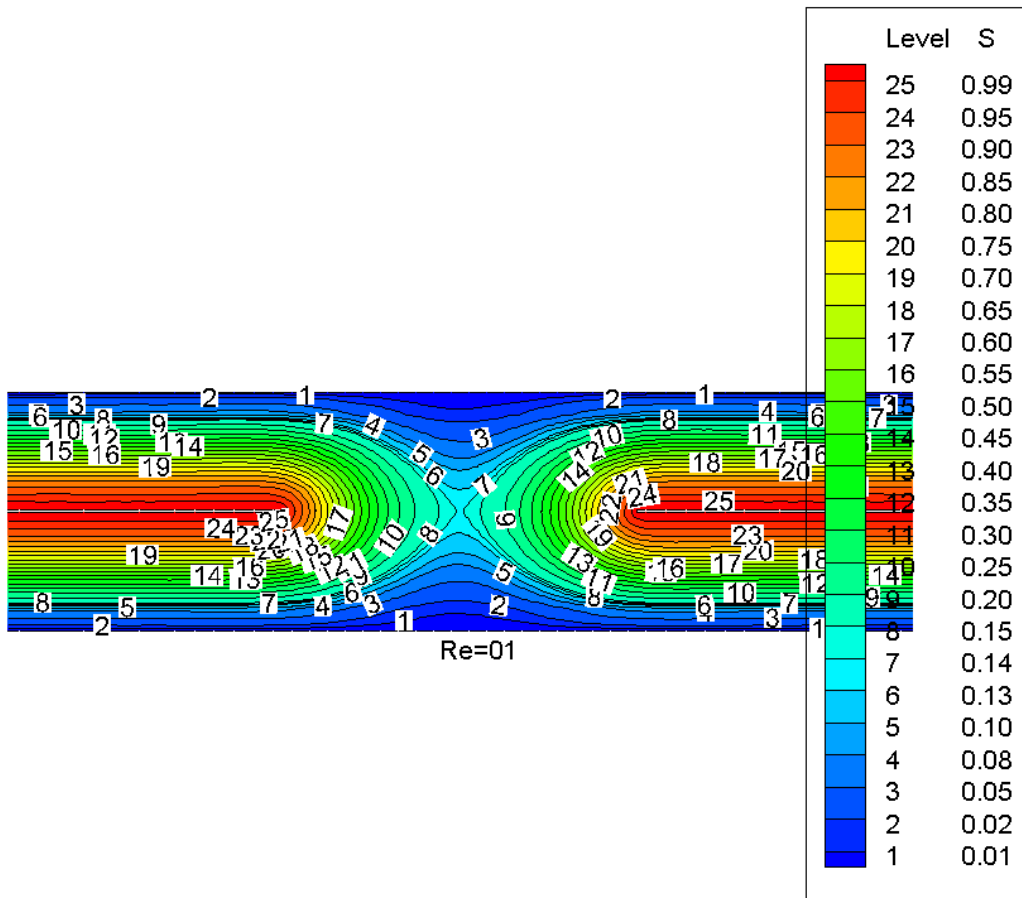
### 1. Chapter-5

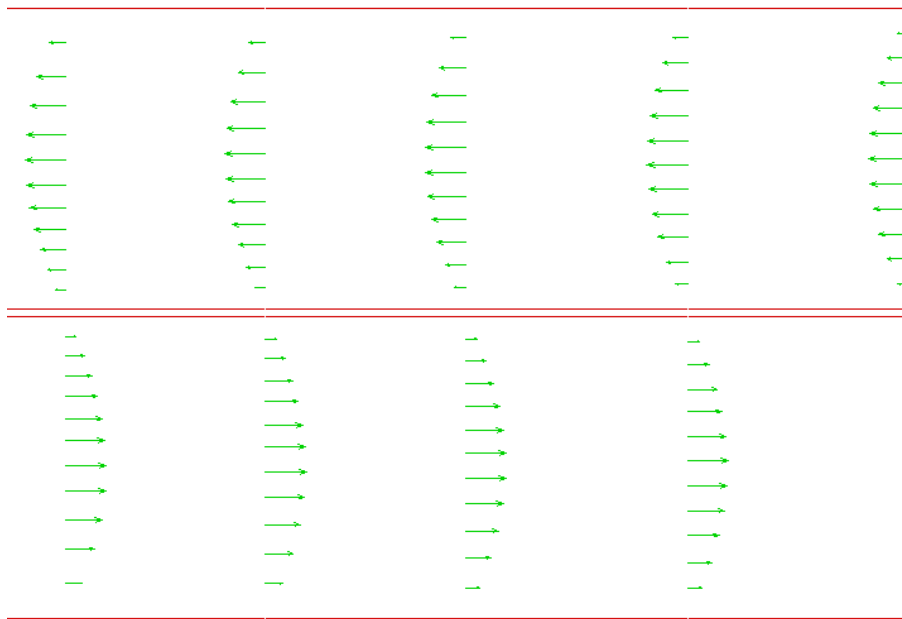
1.1 Mixing and separating of Newtonian fluid flows in a channel filled with non-porous media (Geometry  $G_1$ )

Equal (1, 1) flow rate

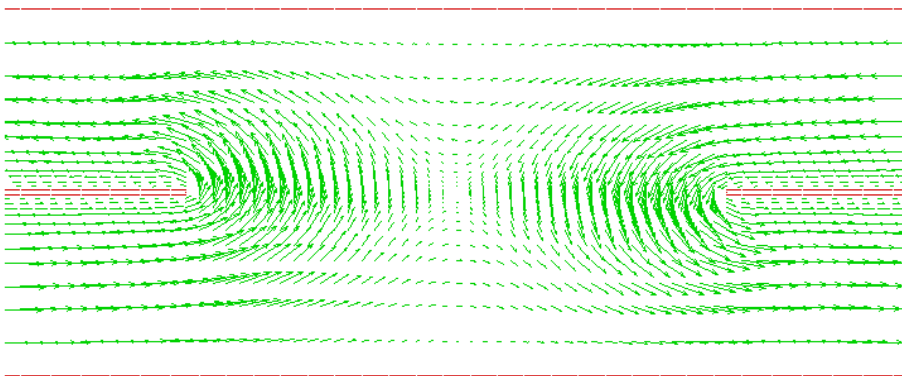




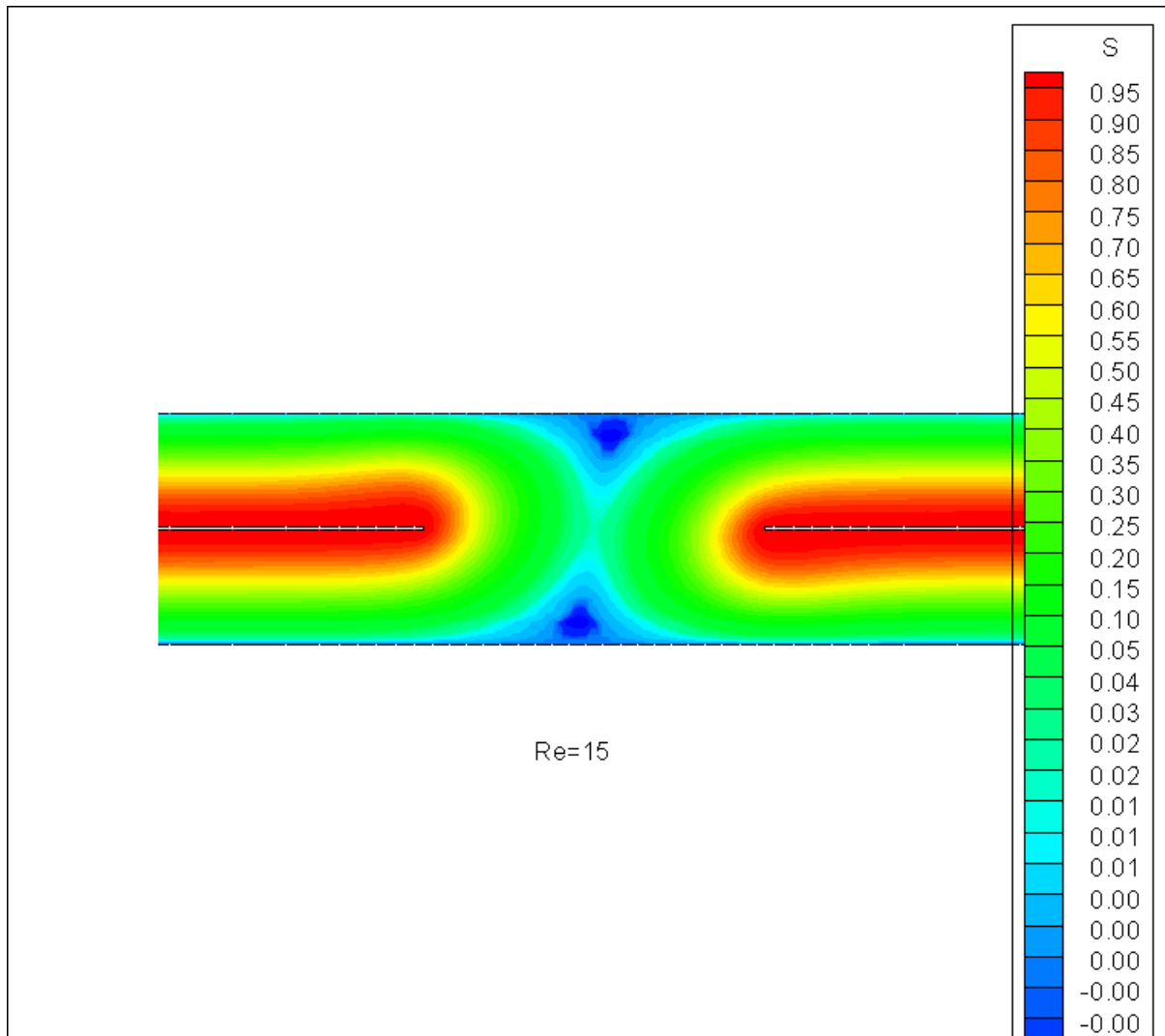


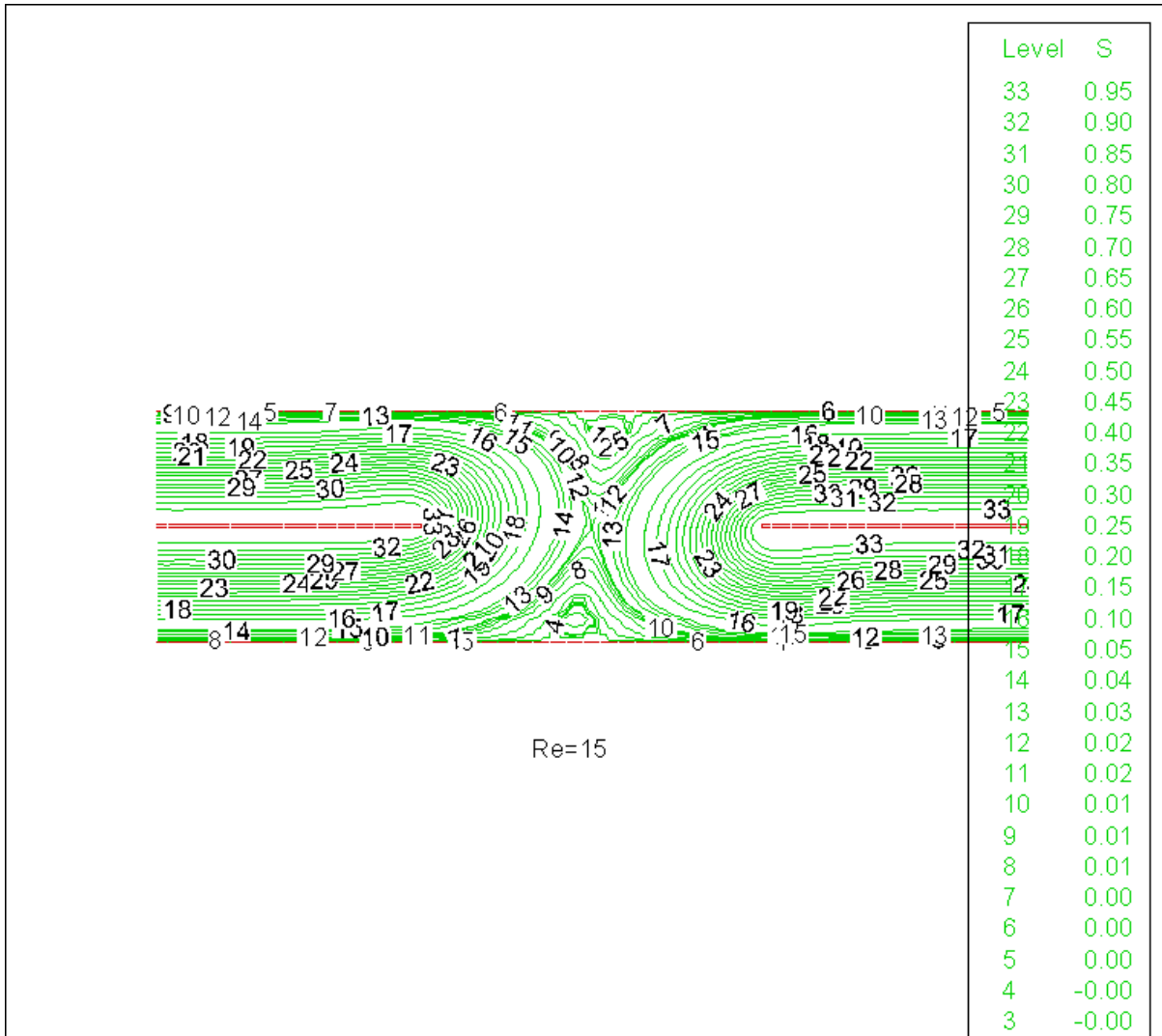


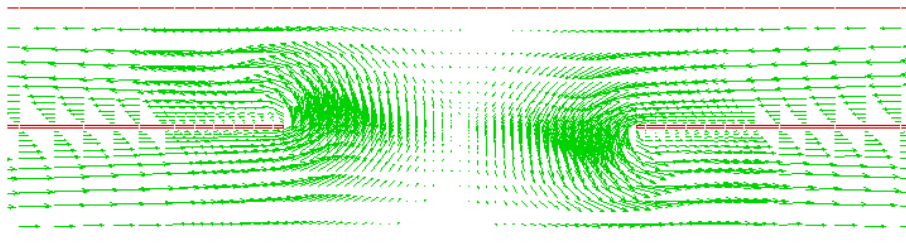
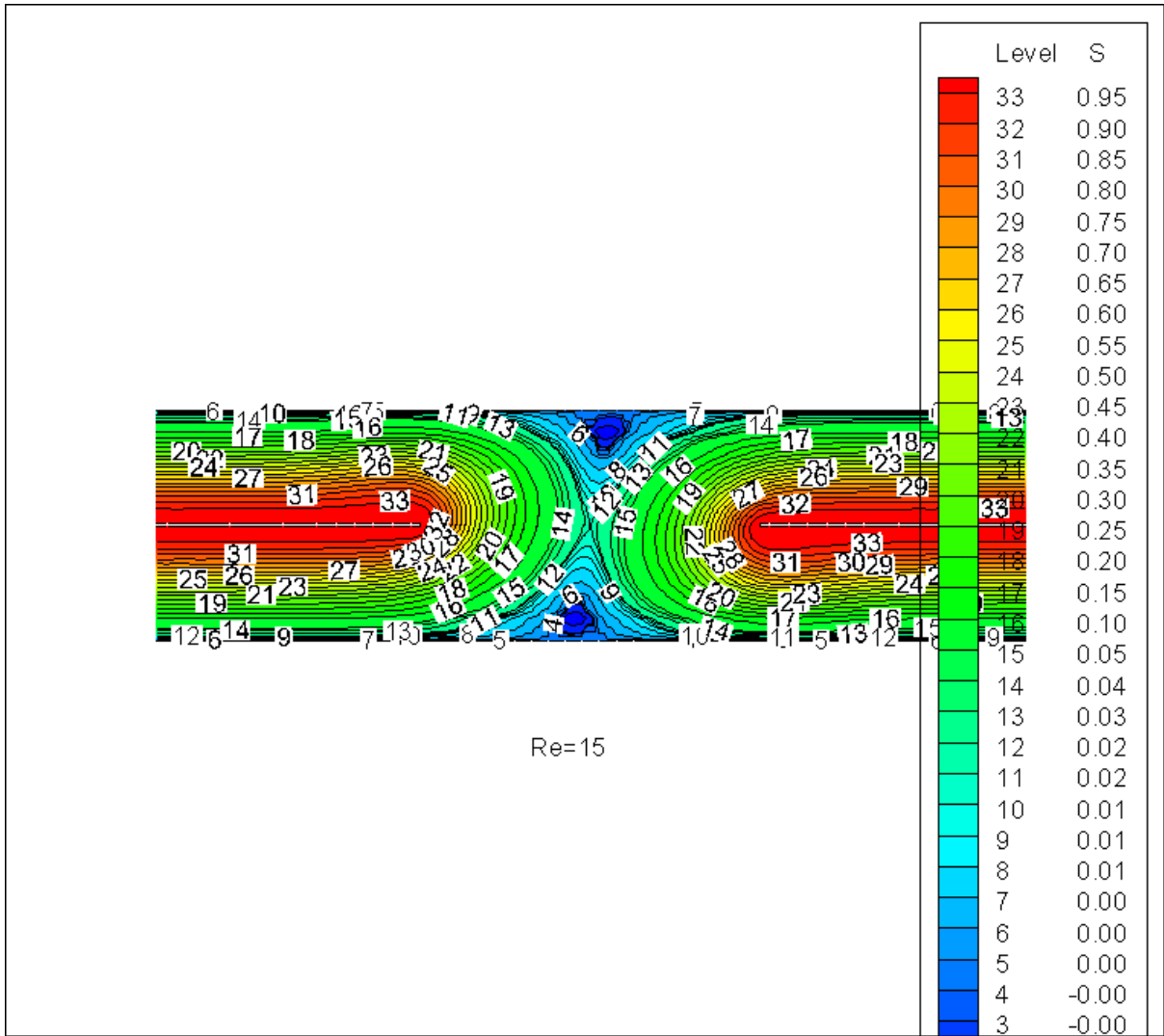
Re=01(R)



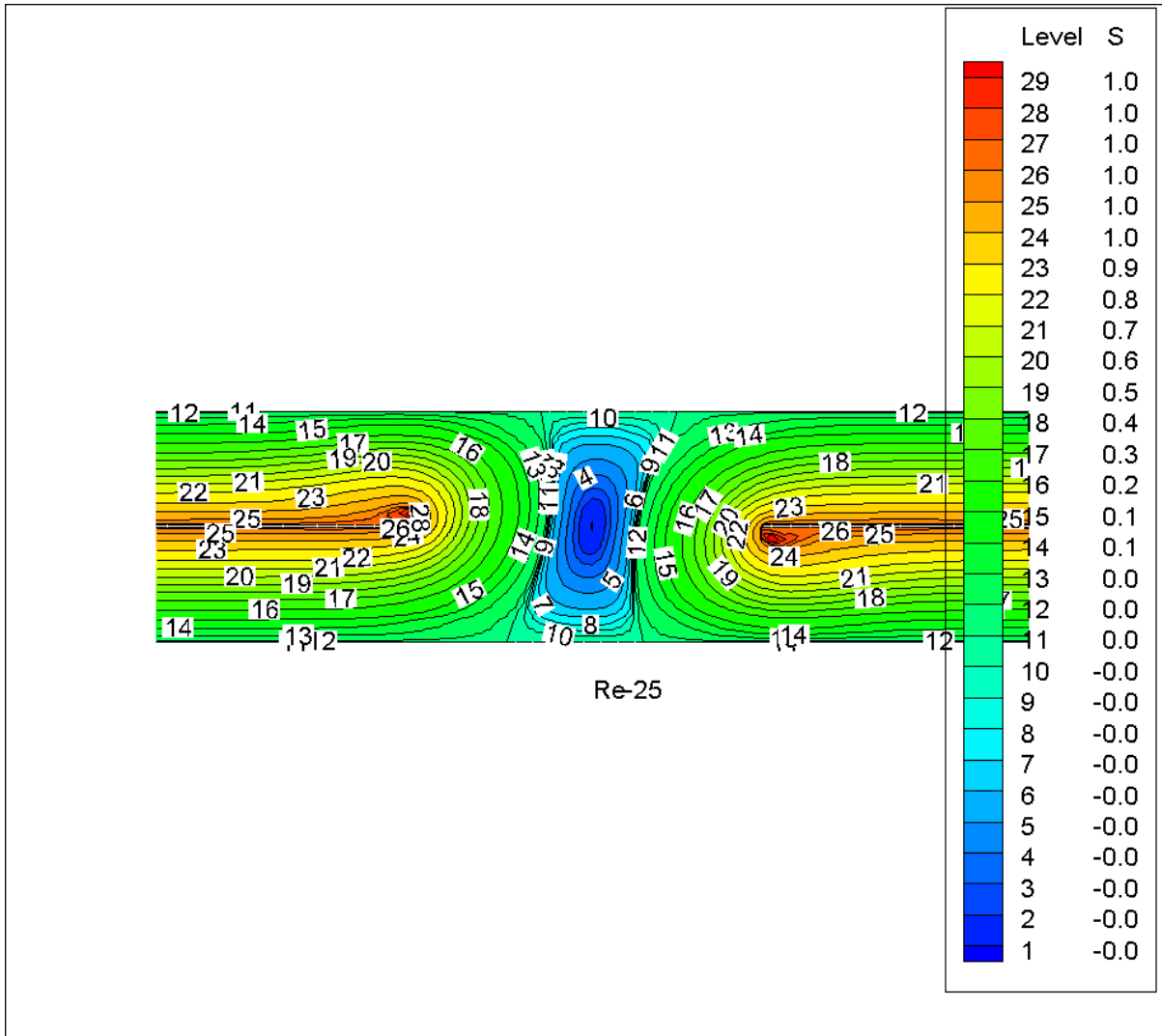
Re=01

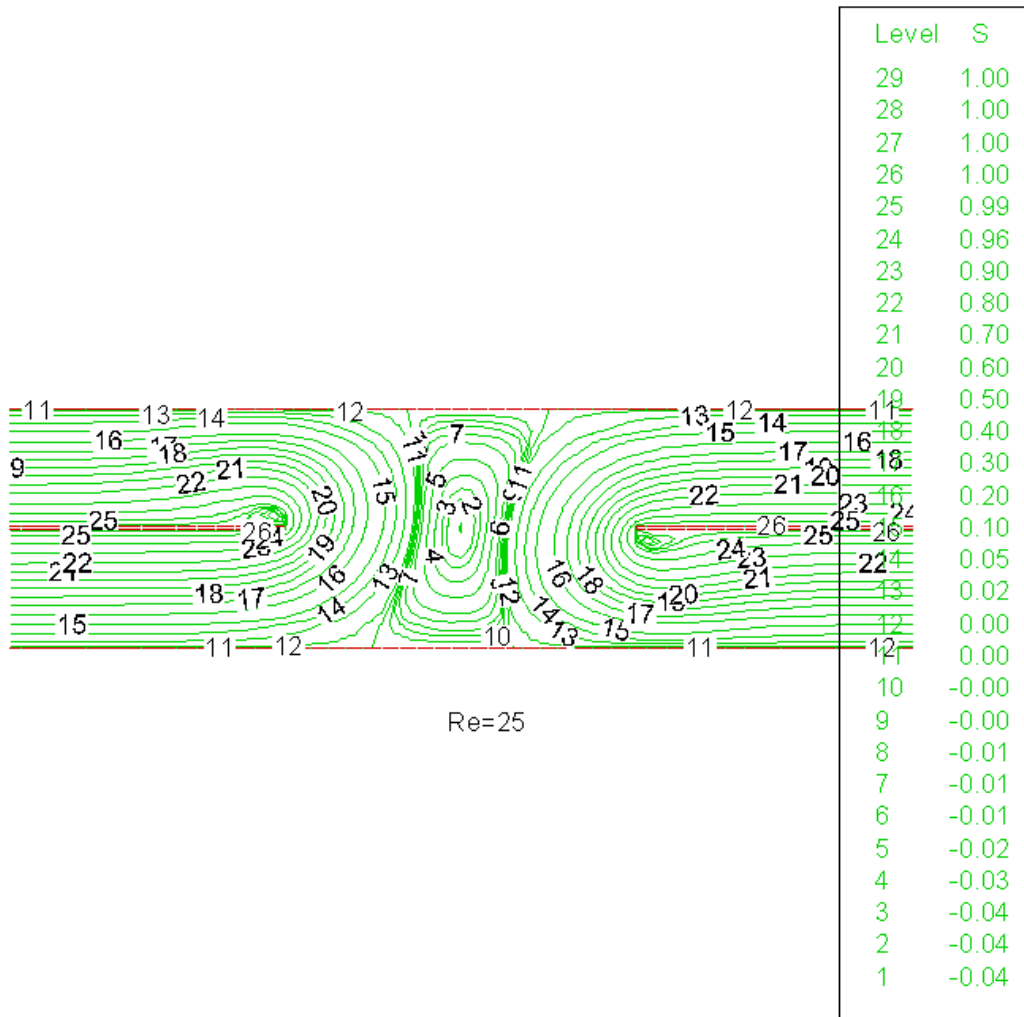


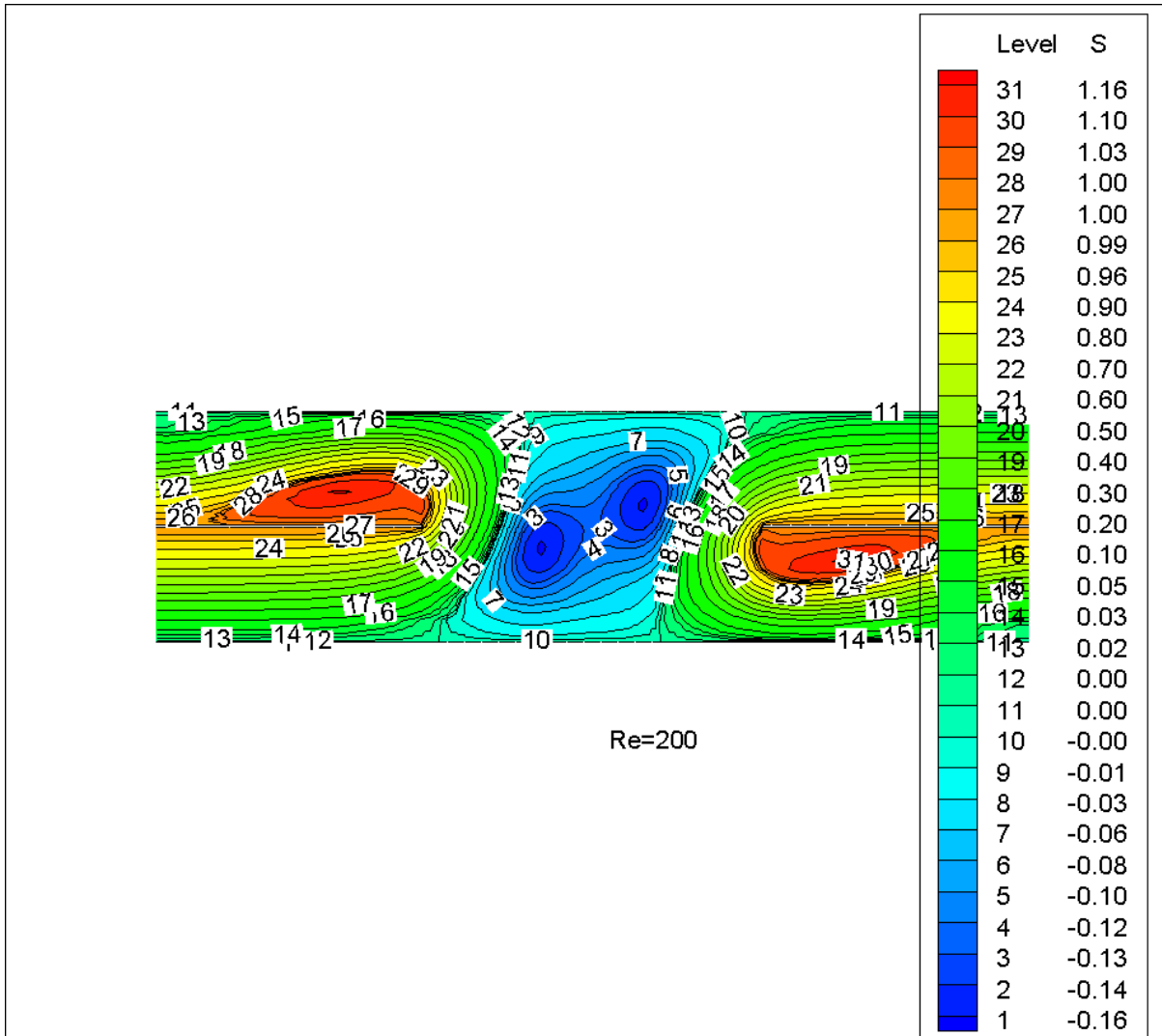


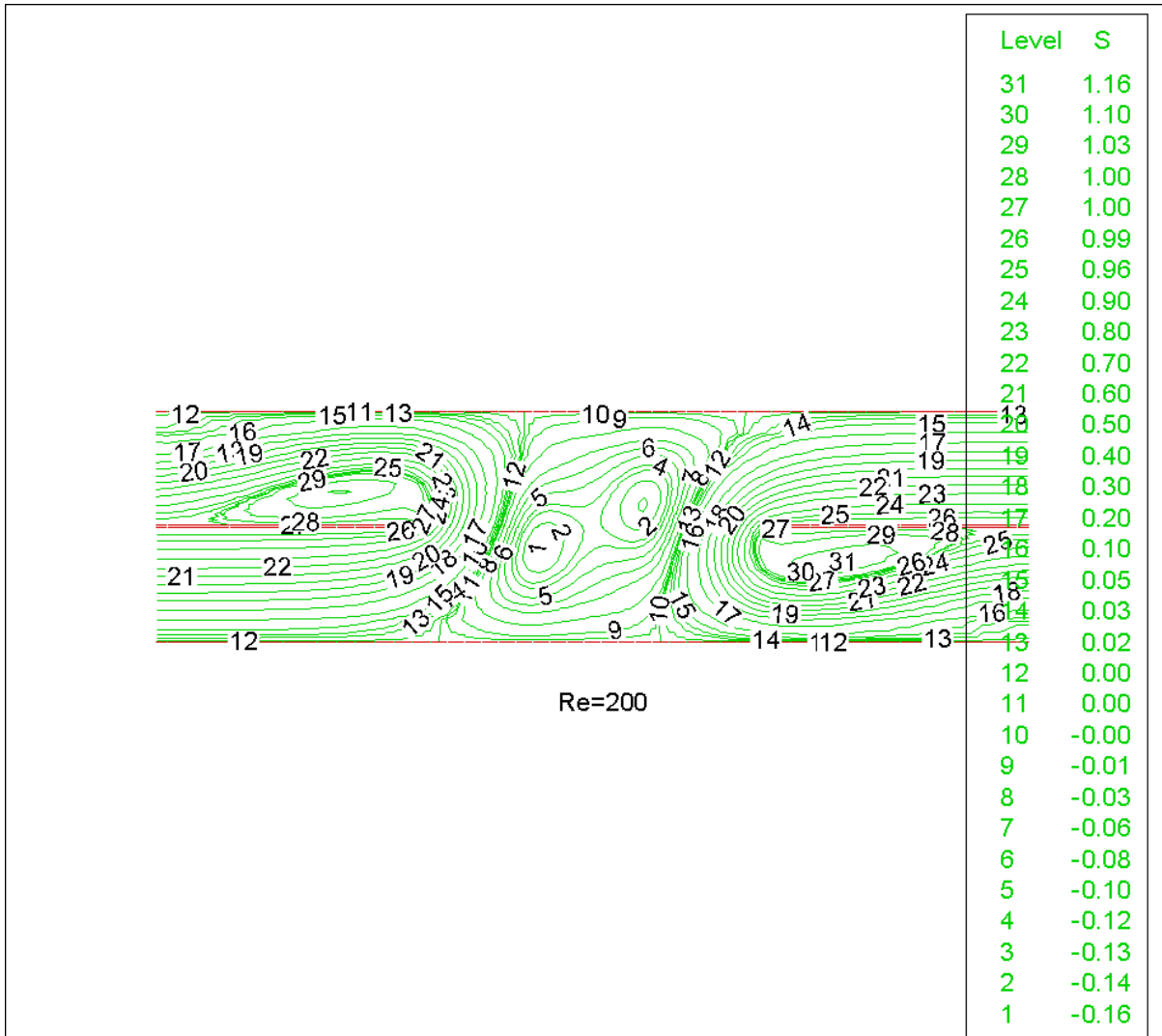


Re=15  
257

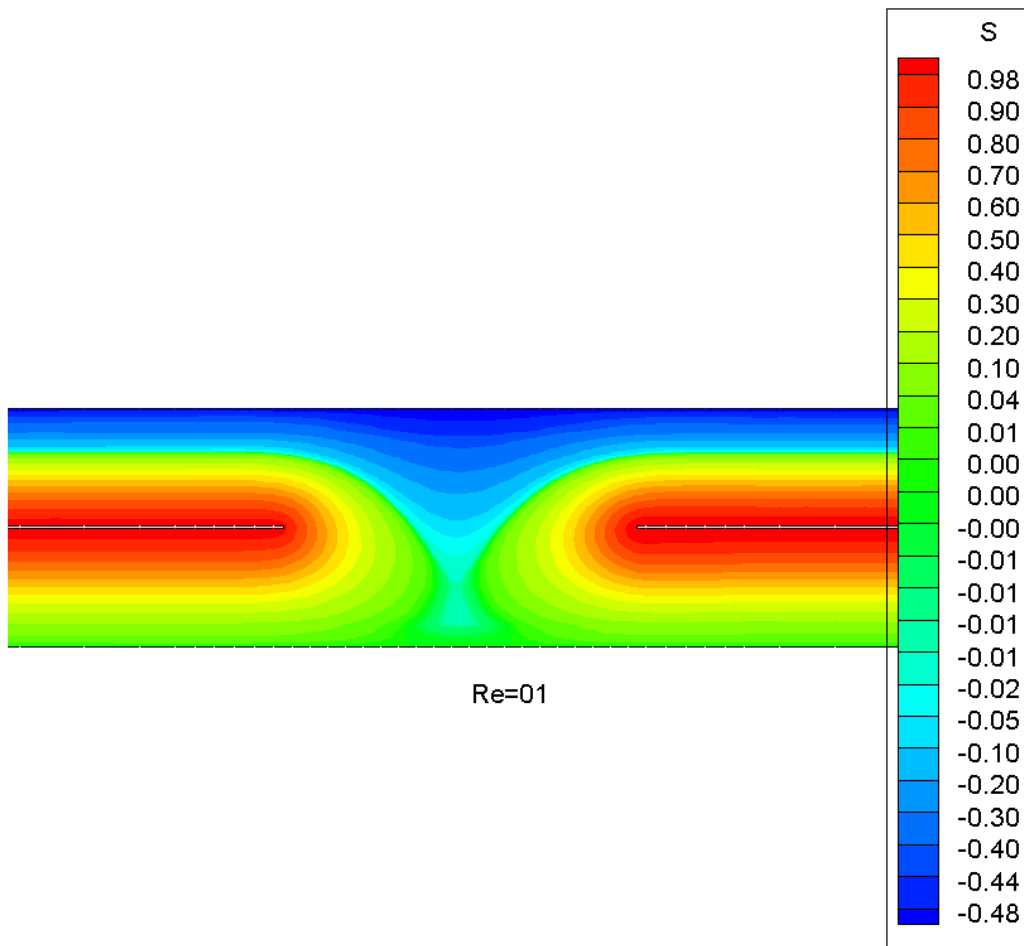


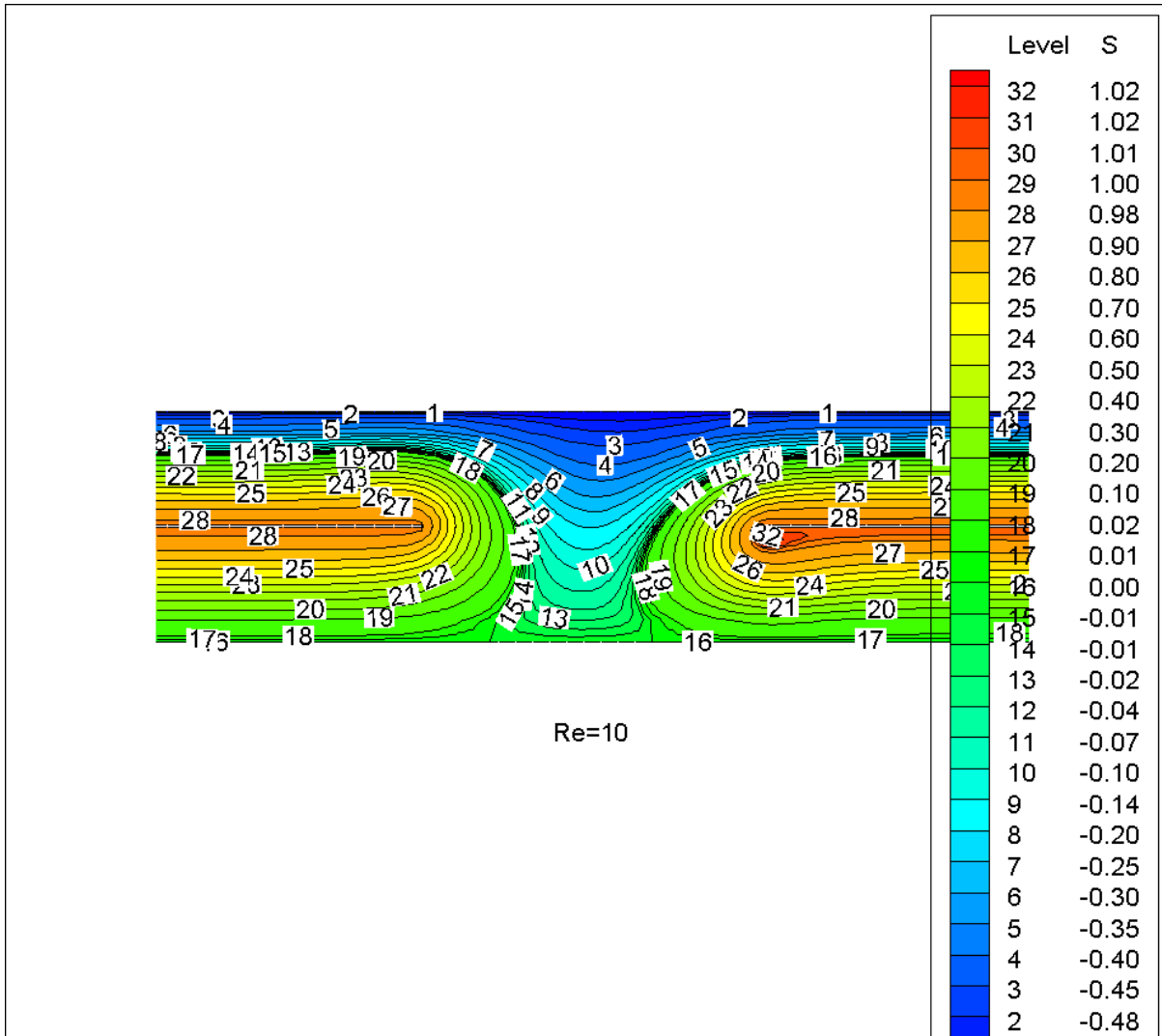


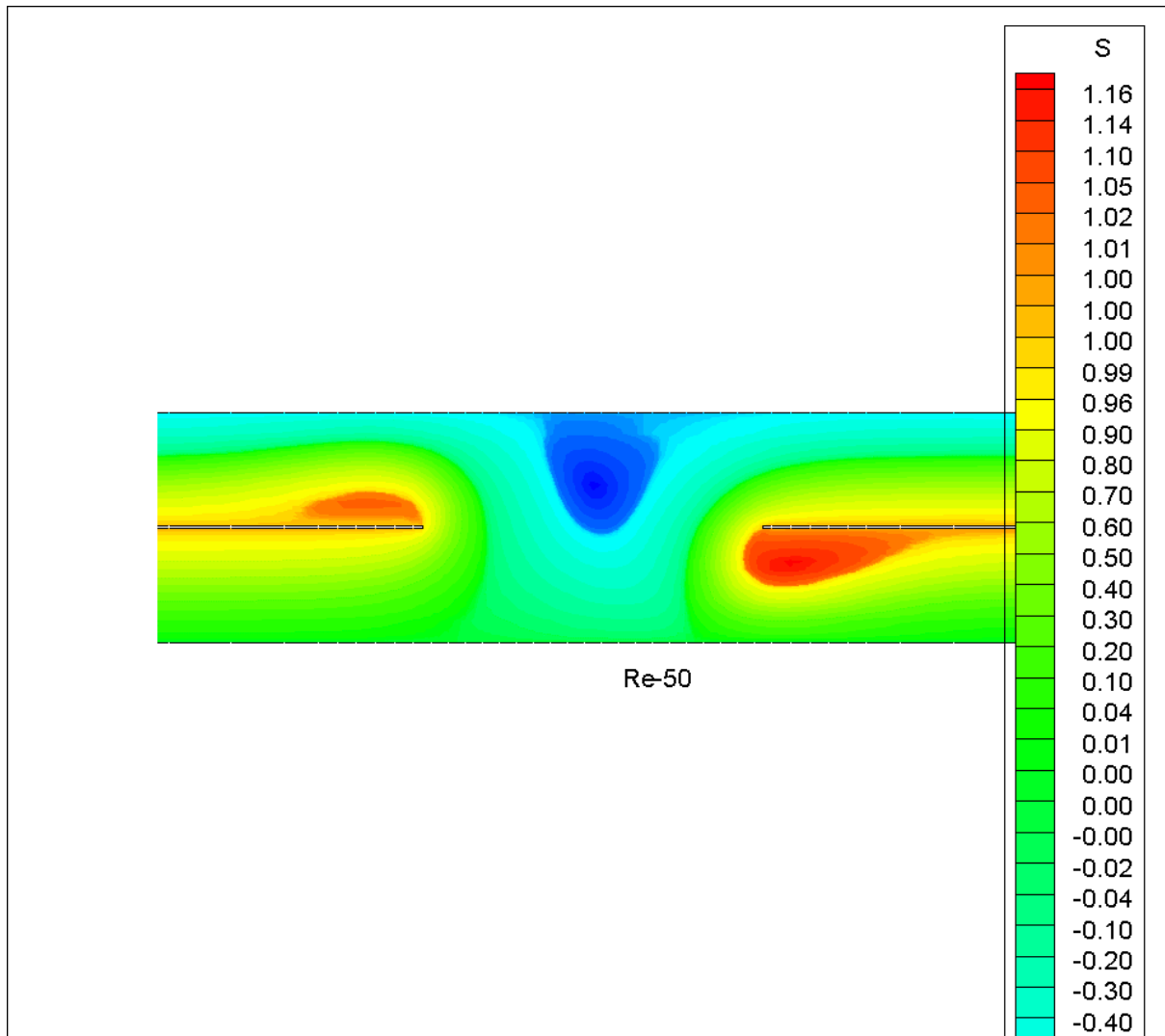


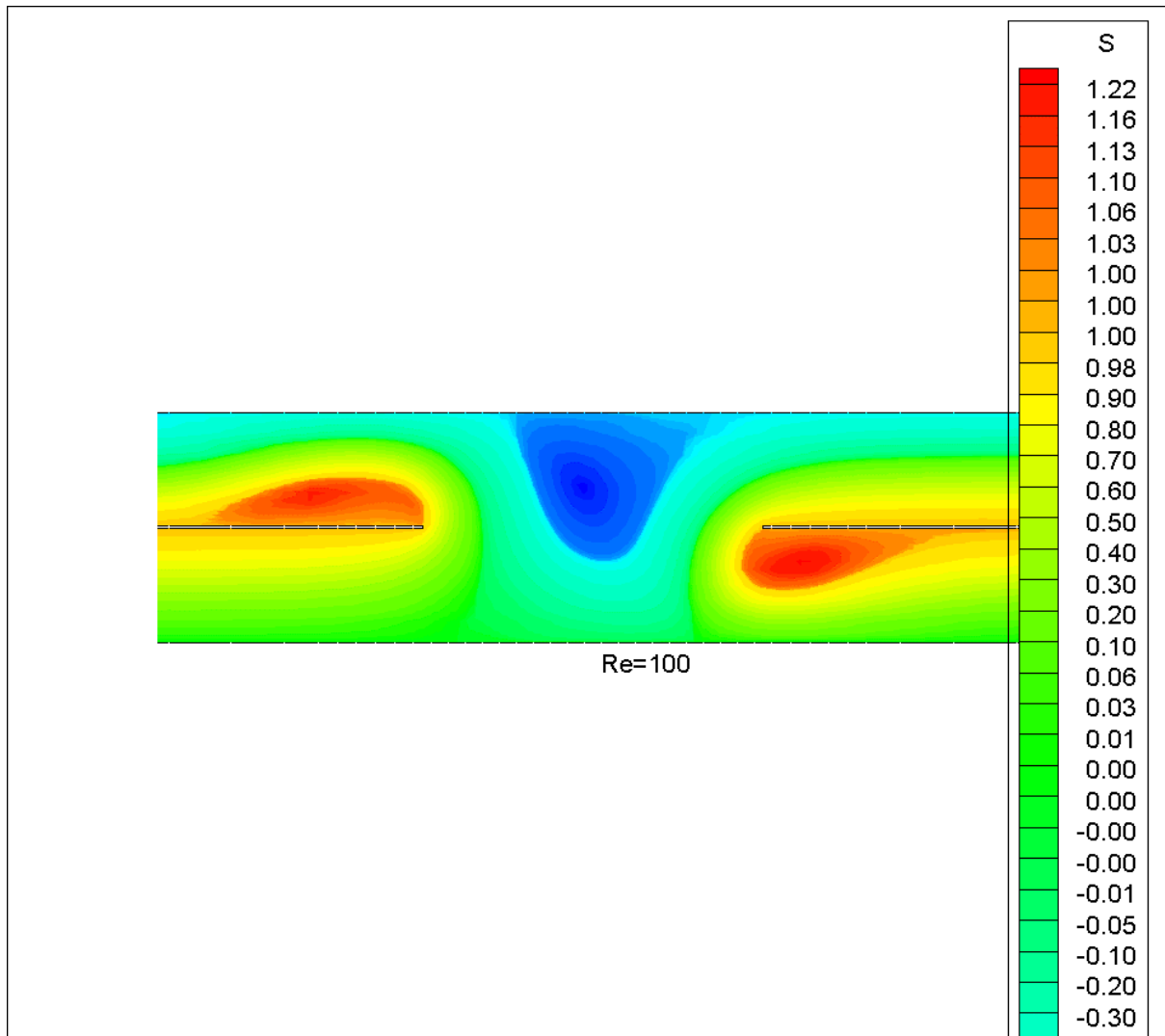


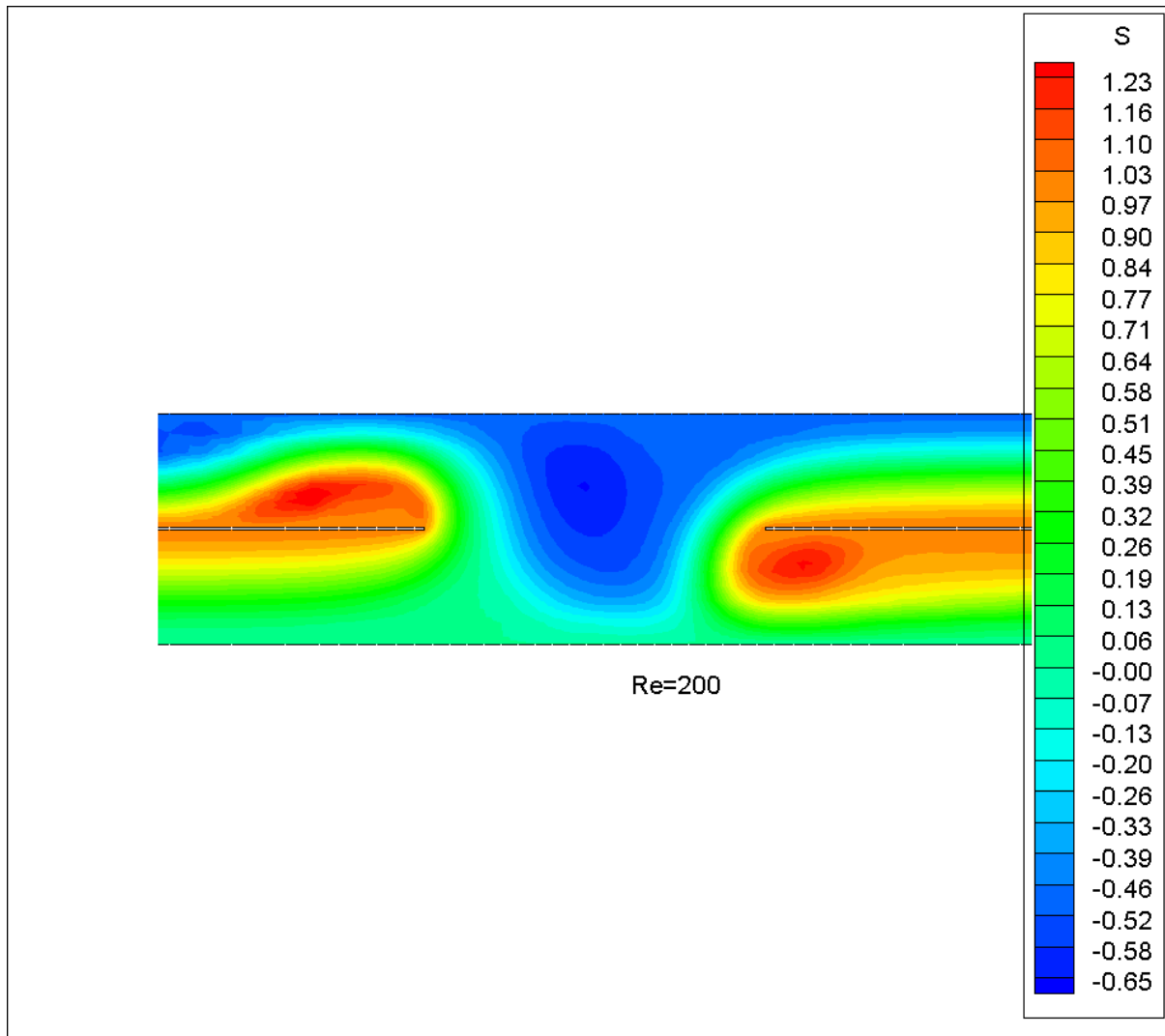
---

**Unequal (1, 1.5) flow rate**

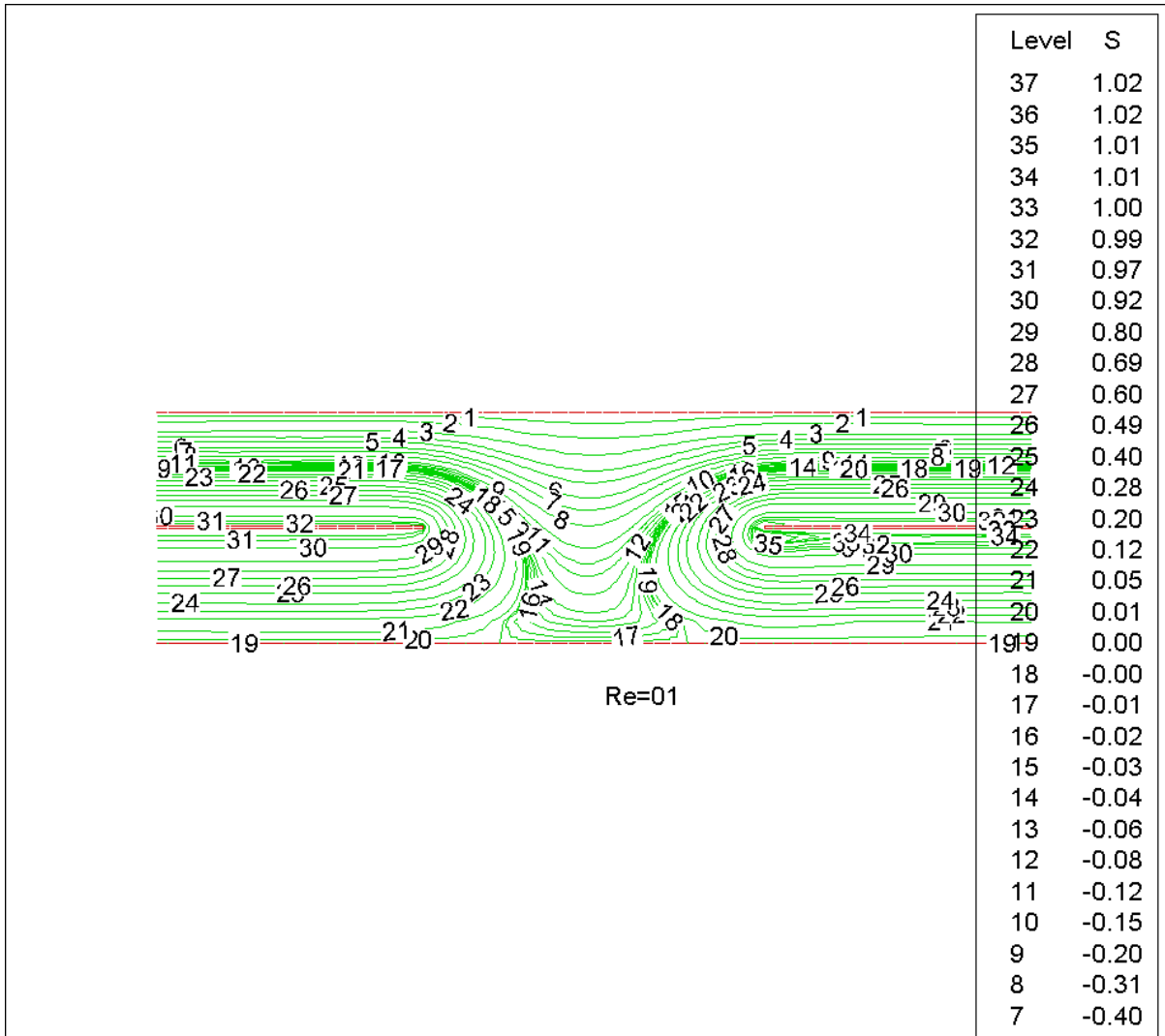


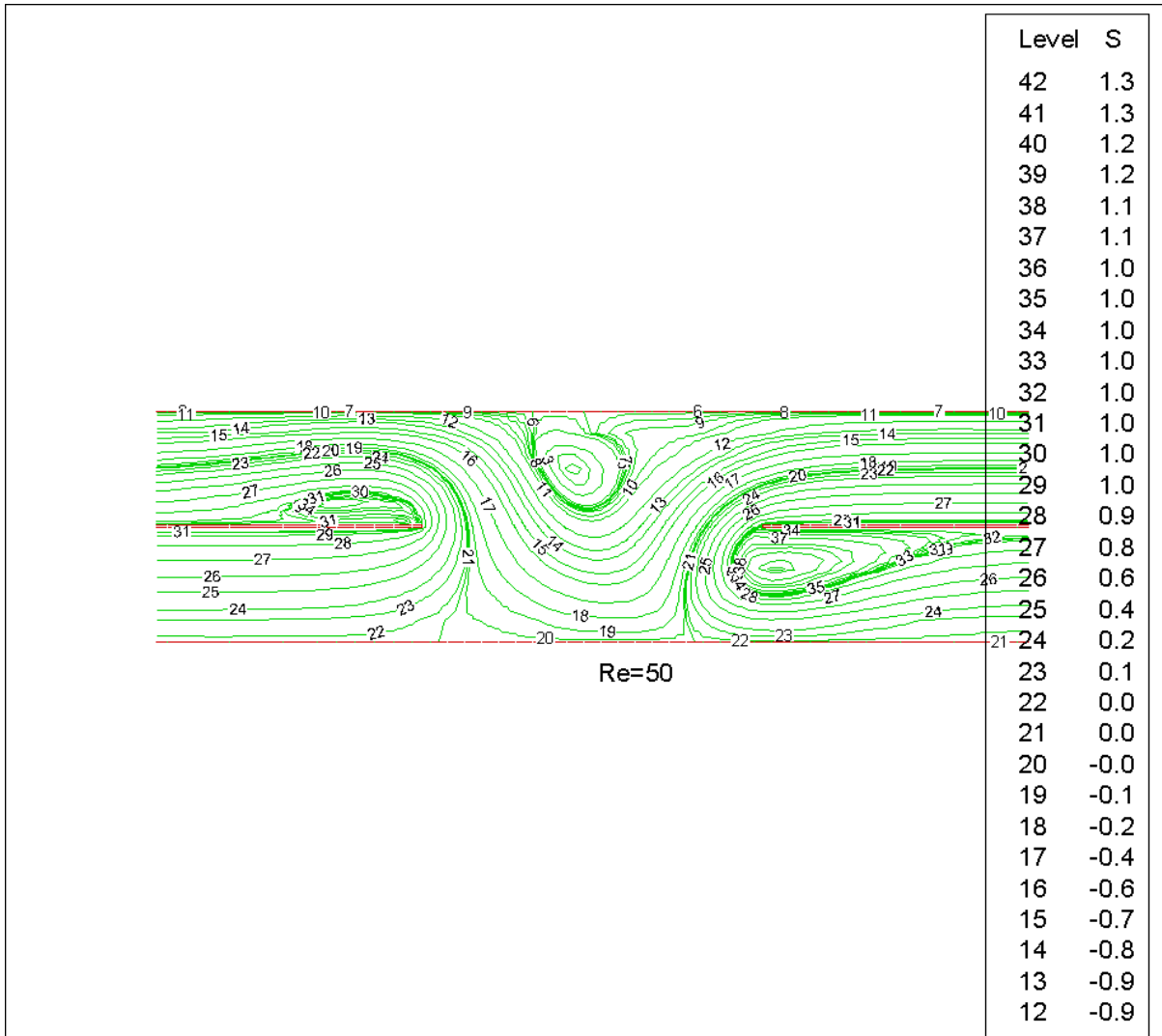


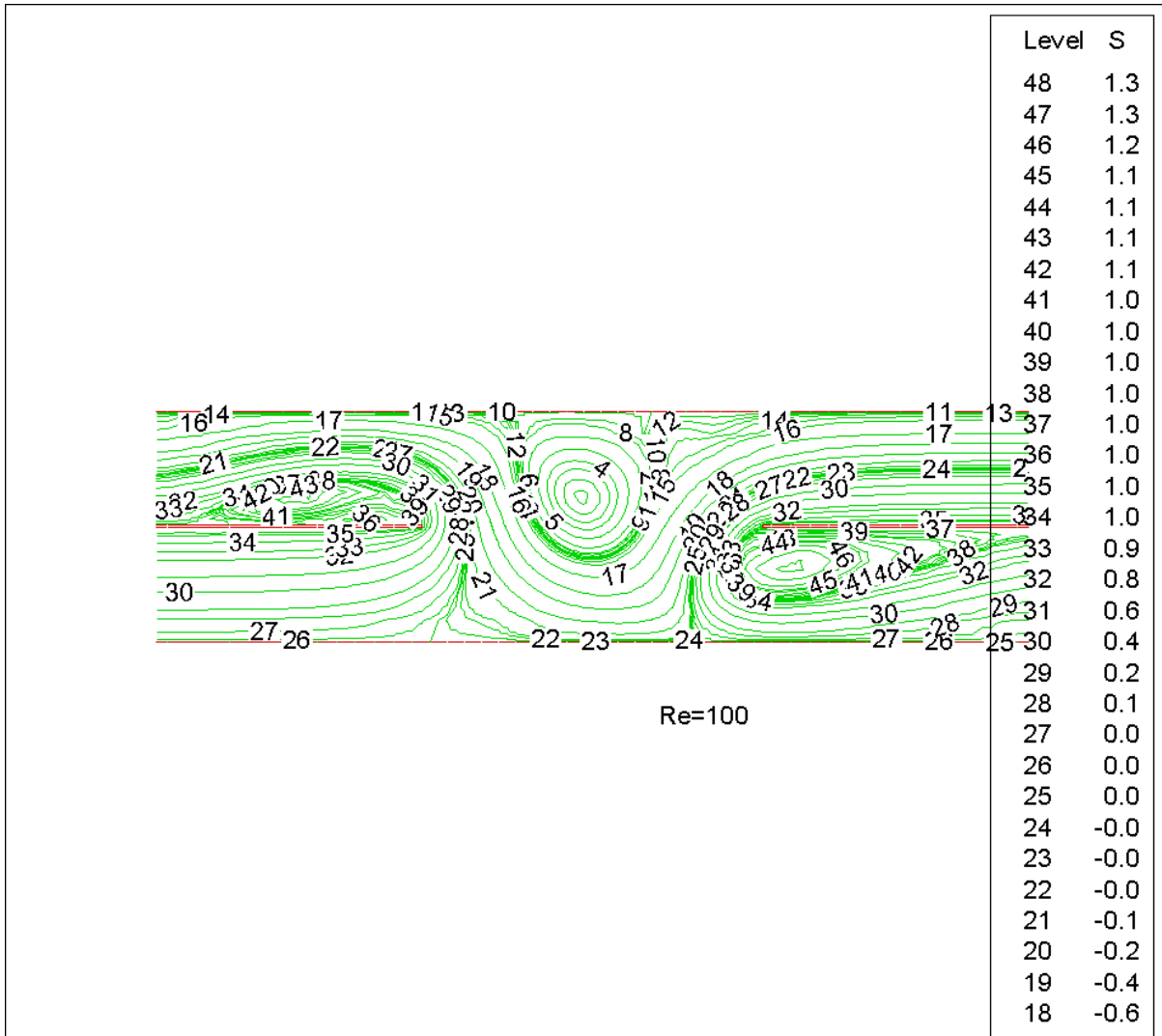


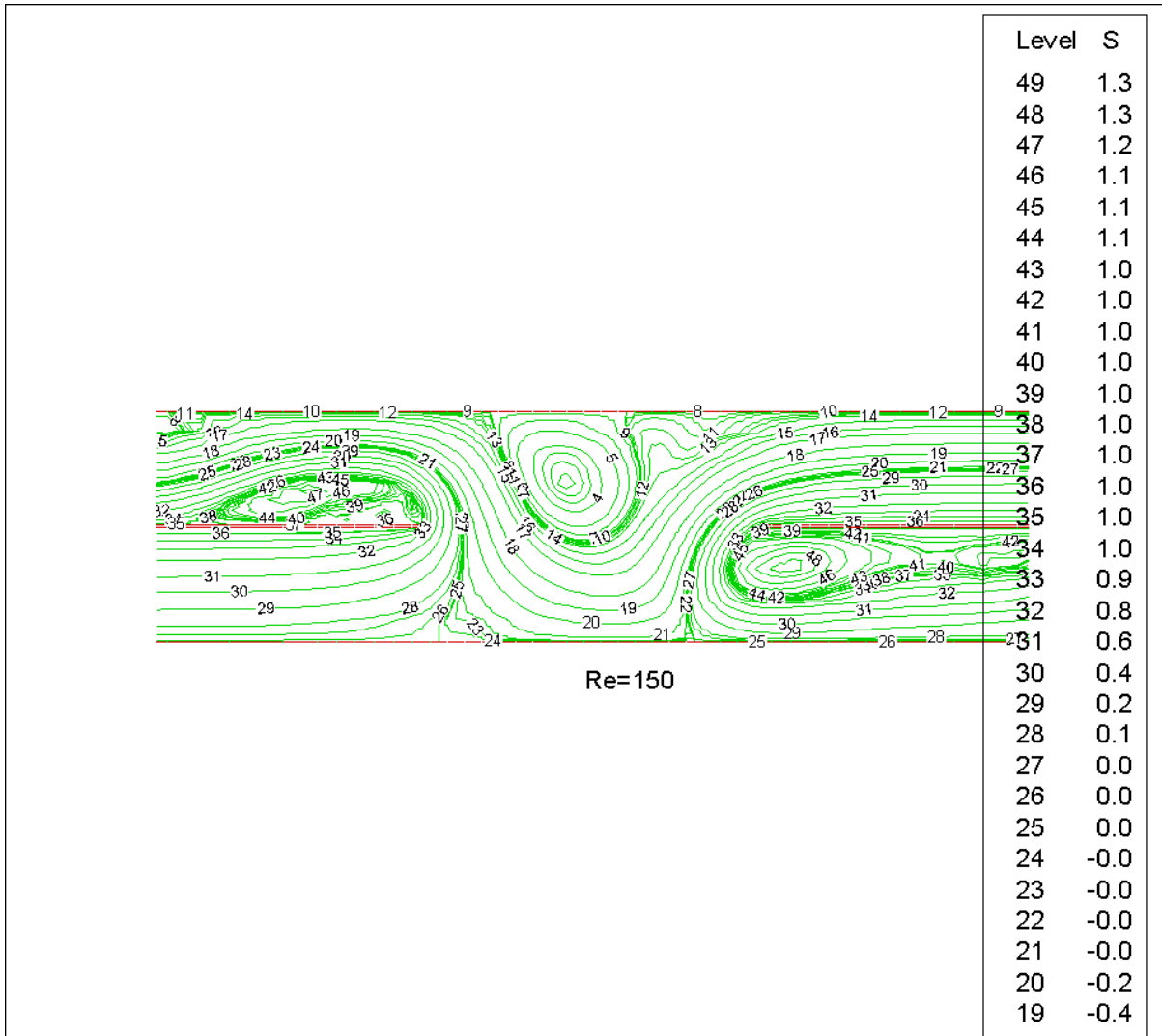


Equal (1, 2) flow rate

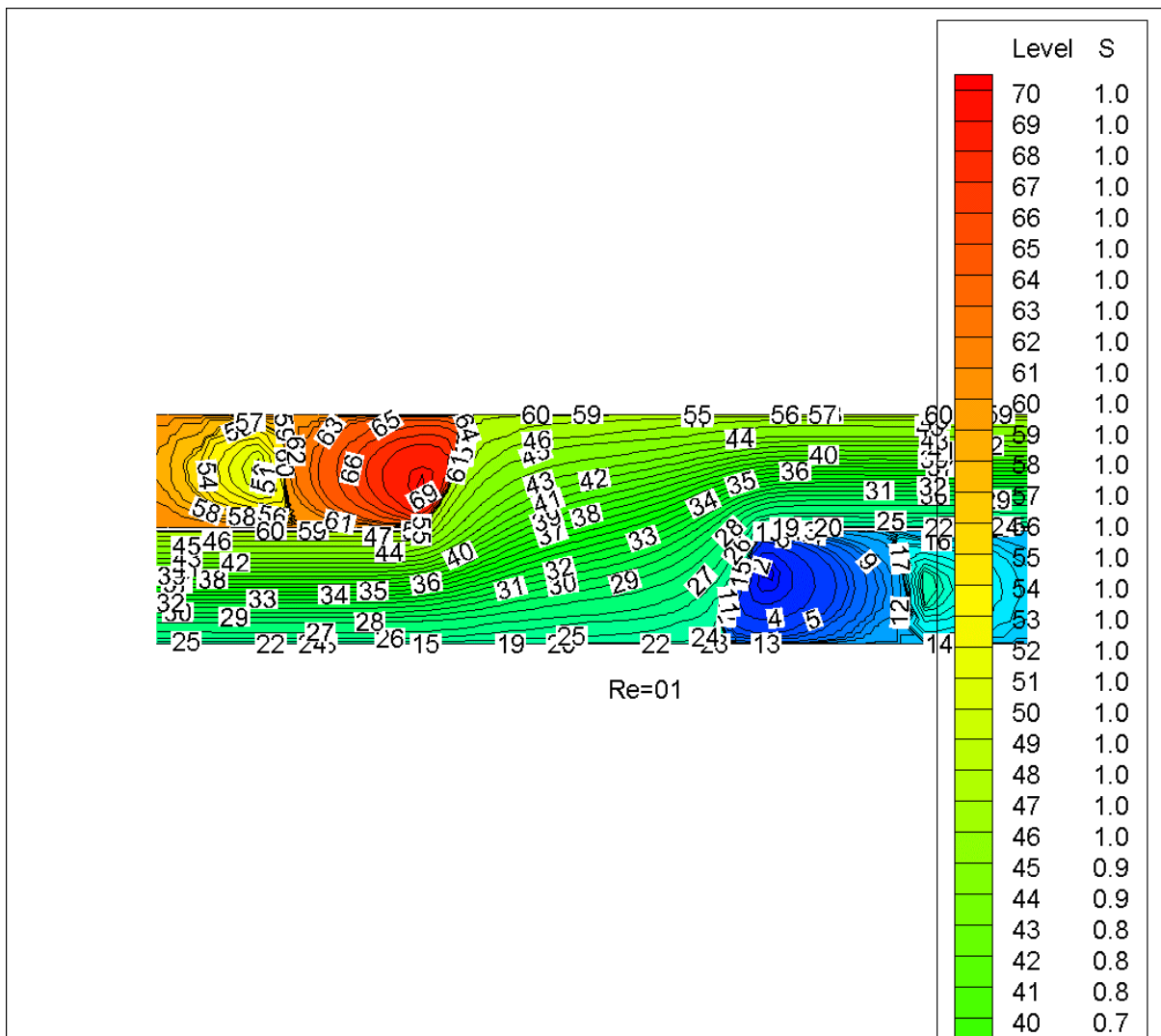


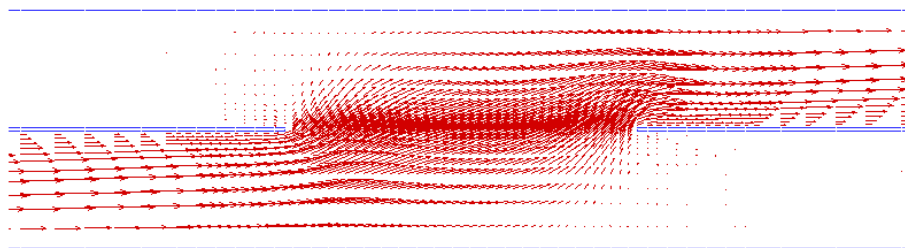
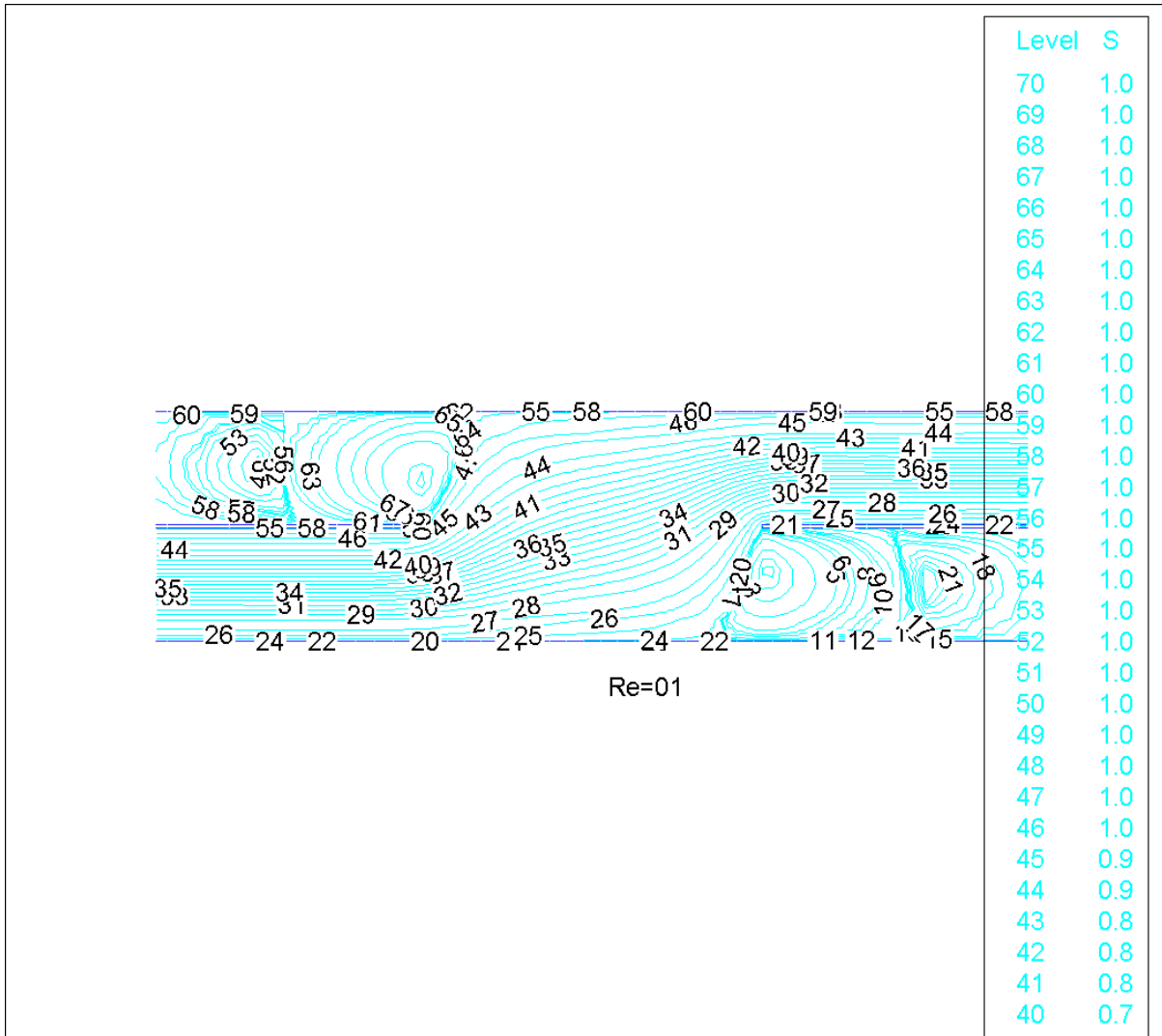






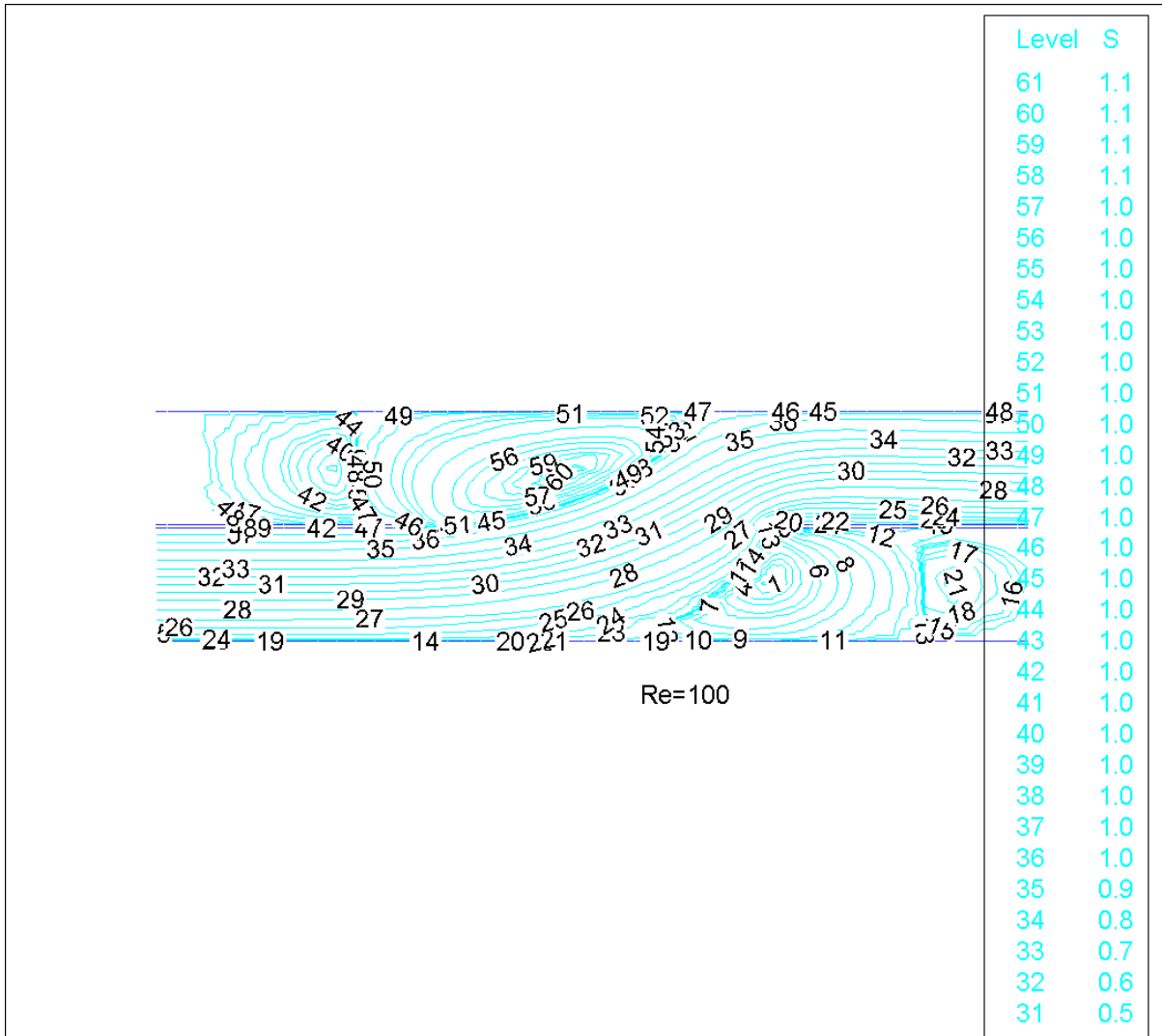
## 1.2 Mixing and separating of Newtonian fluid flows in a channel filled with non-porous media ( $G_4$ )

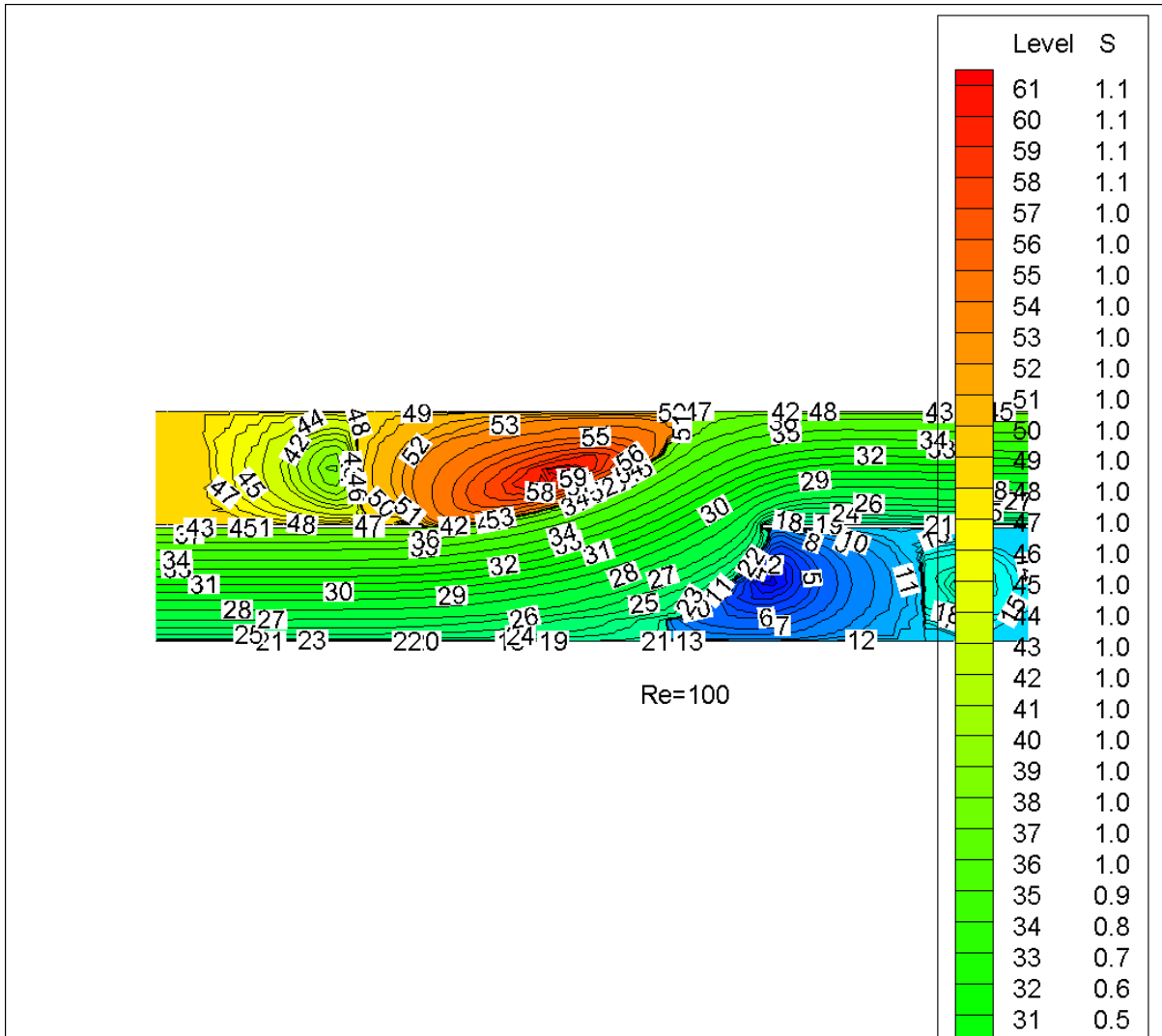


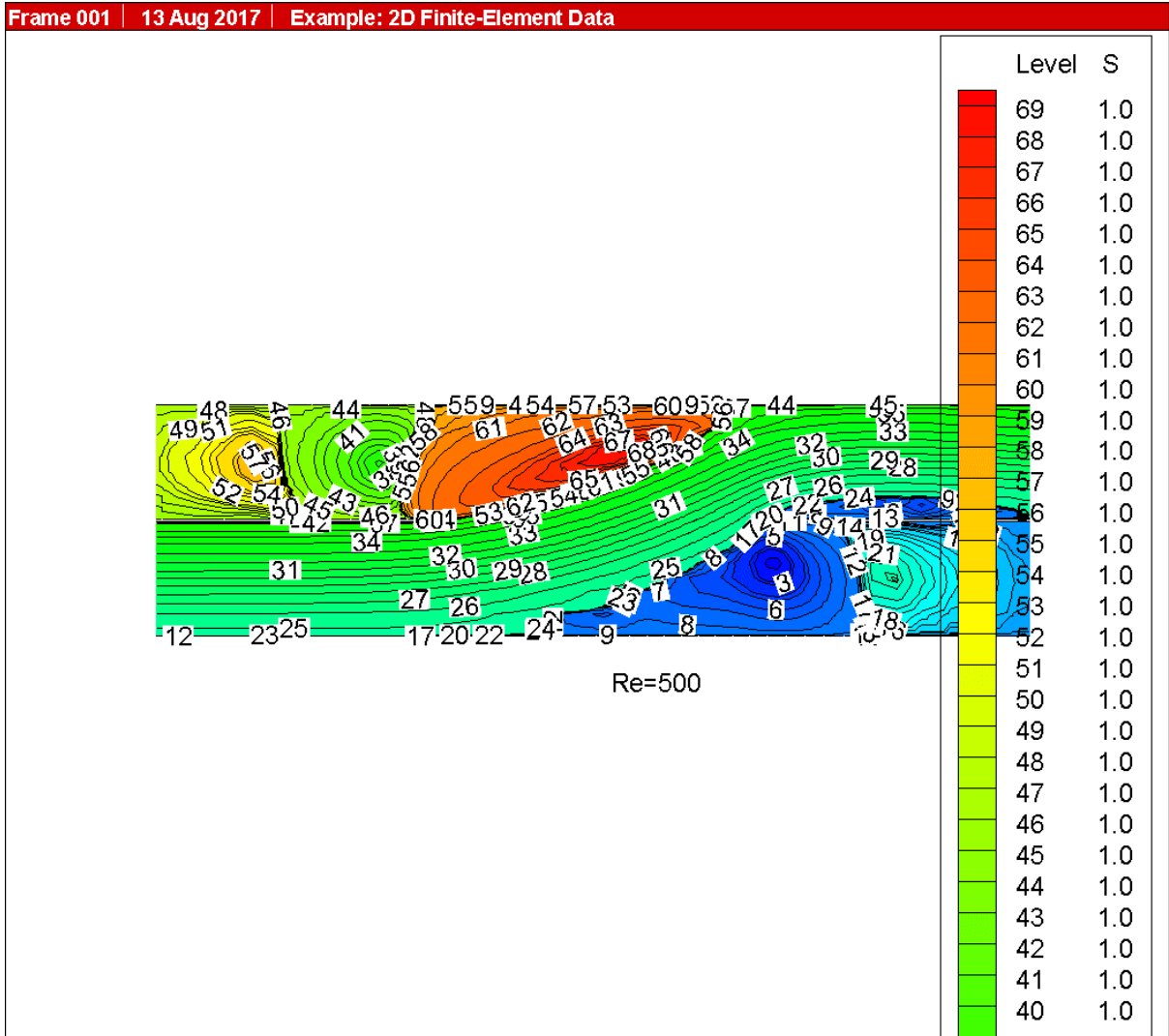


Re=01

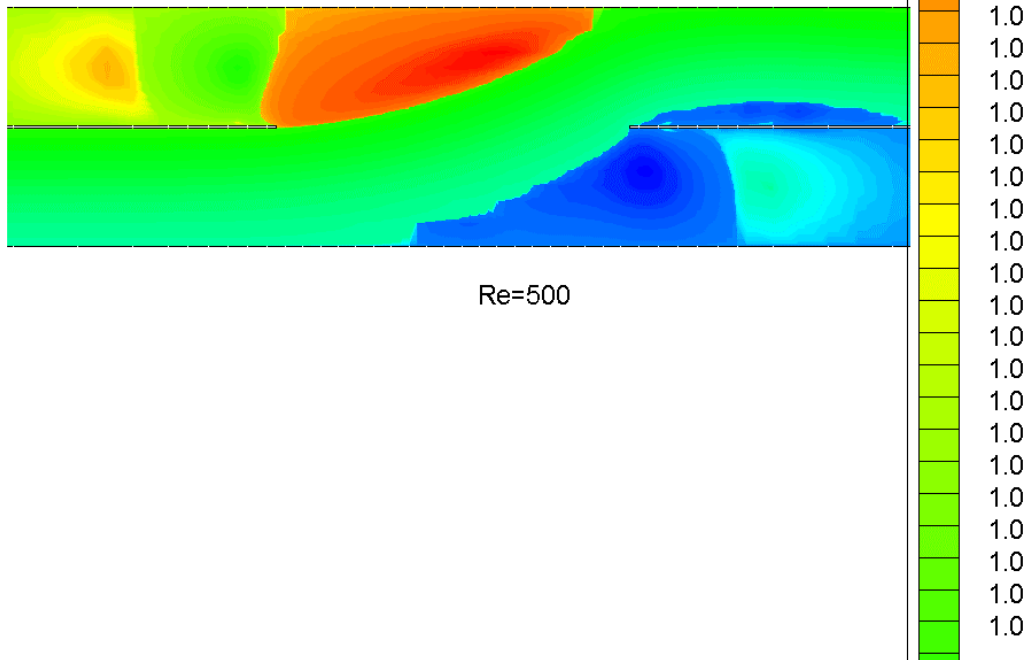


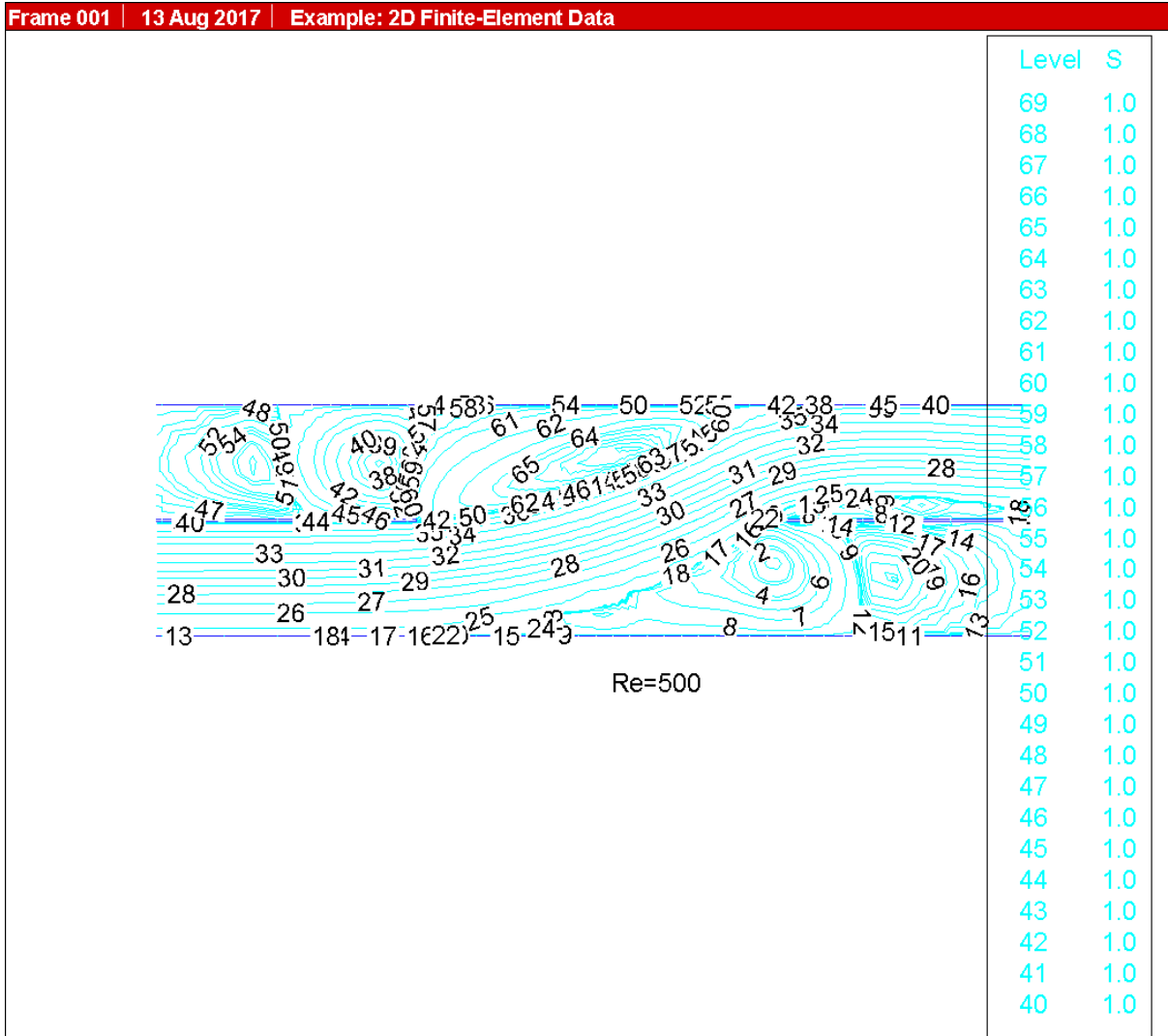




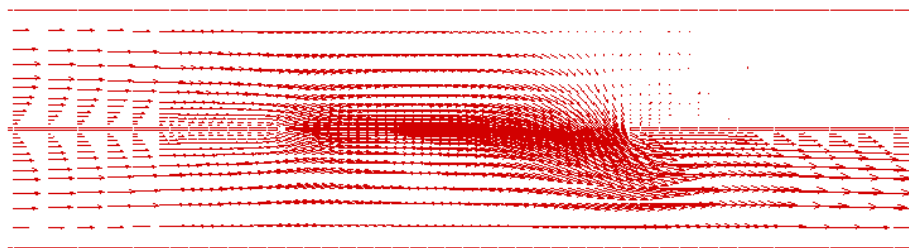
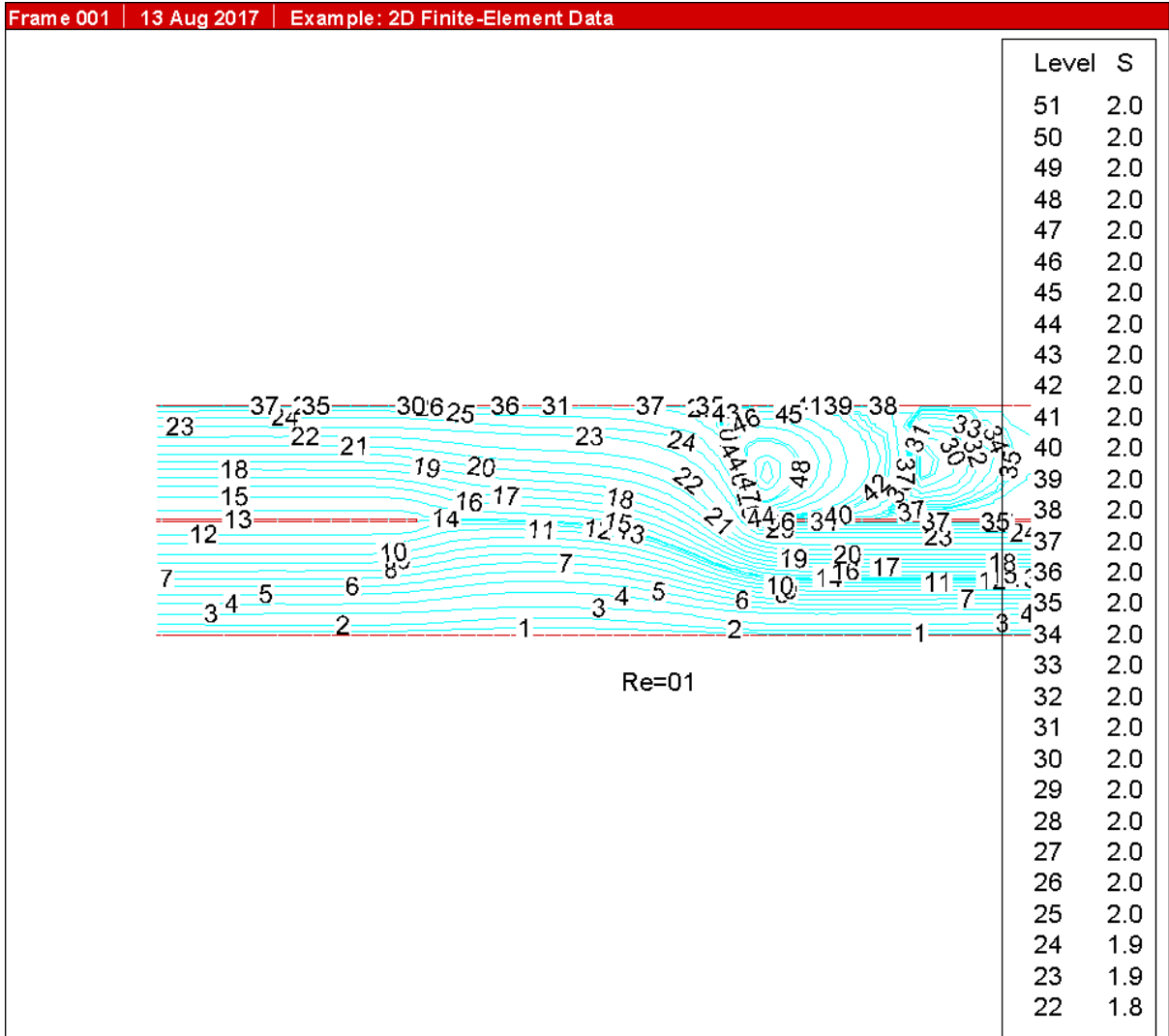


Frame 001 | 13 Aug 2017 | Example: 2D Finite-Element Data

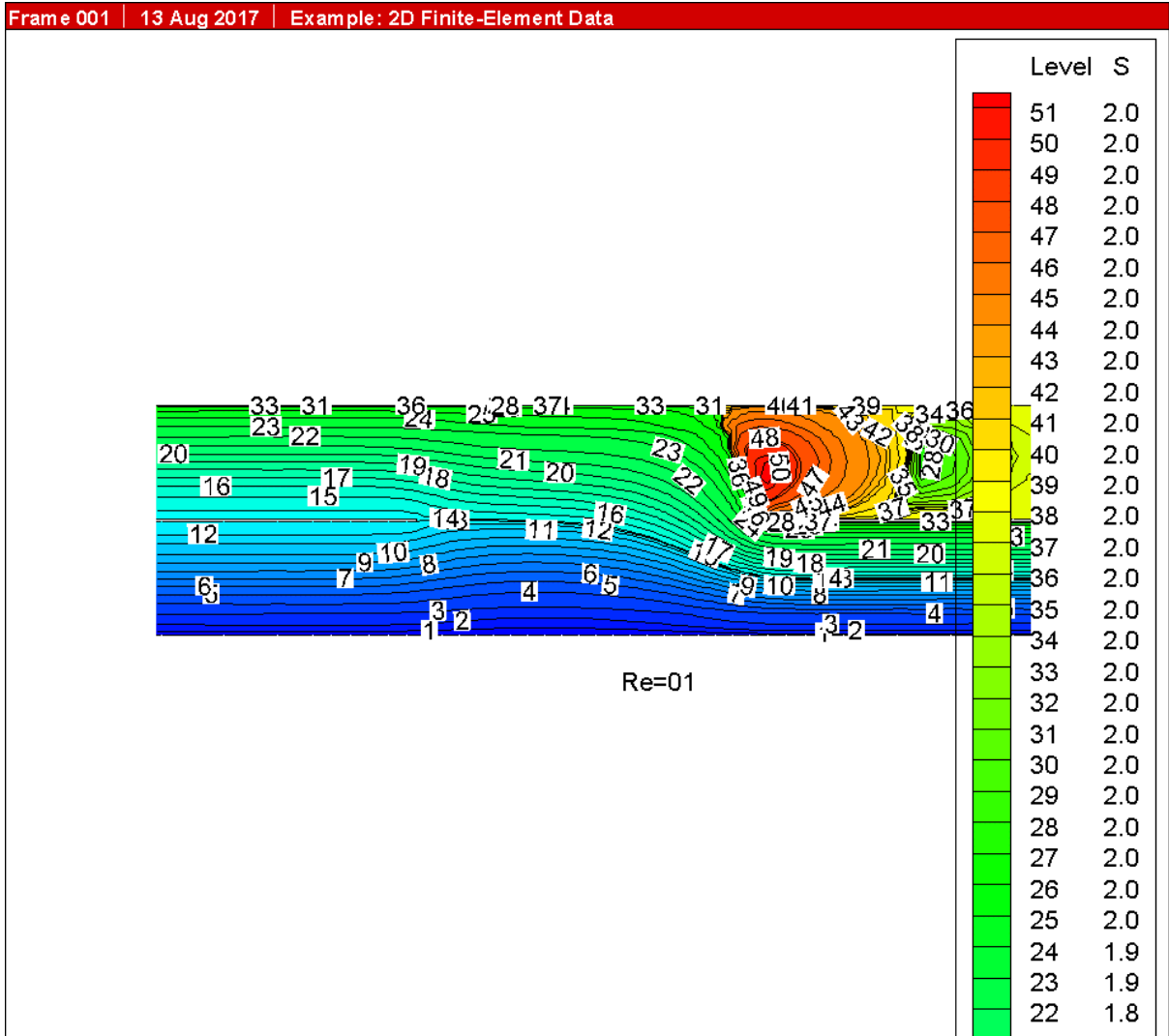




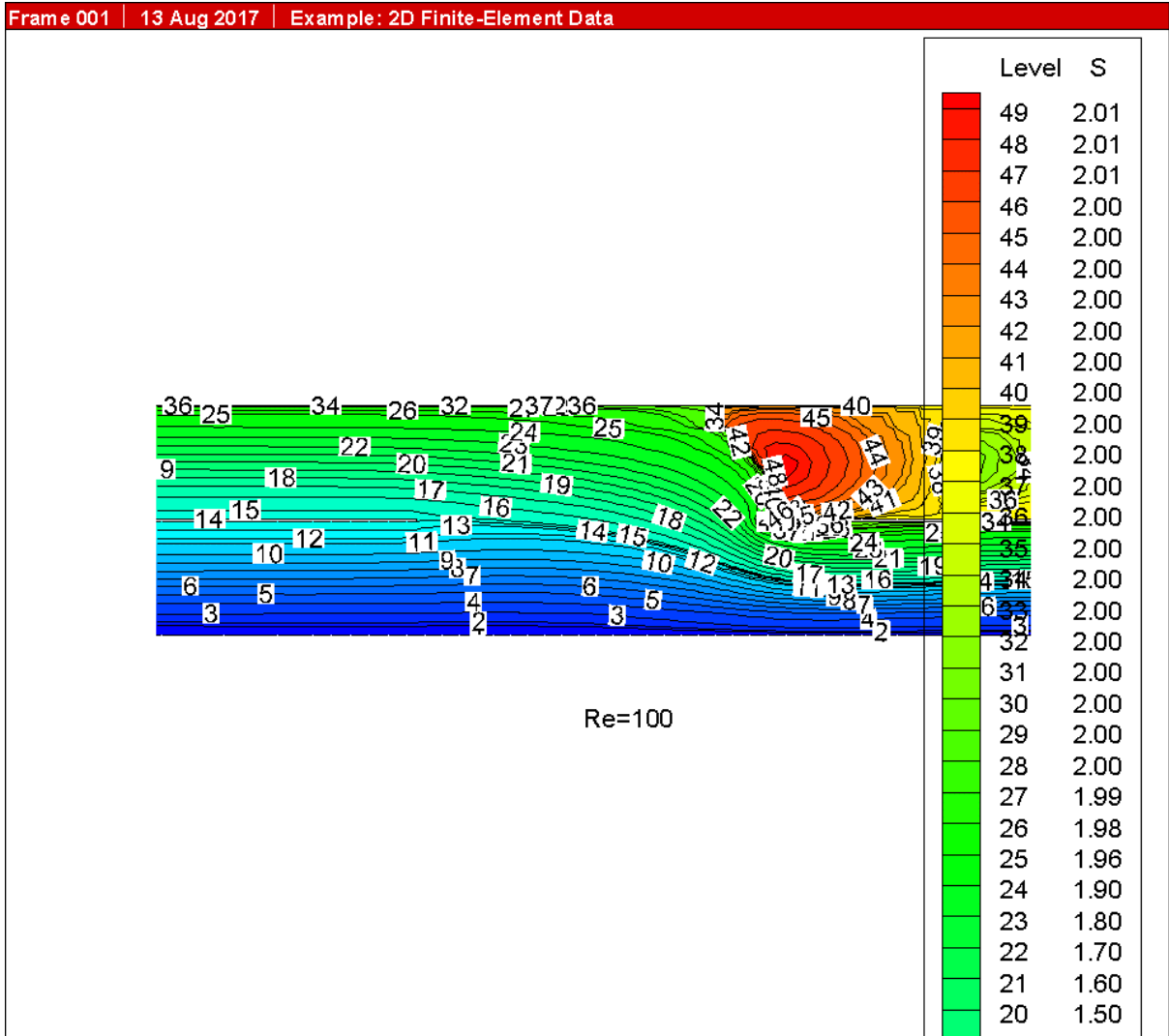


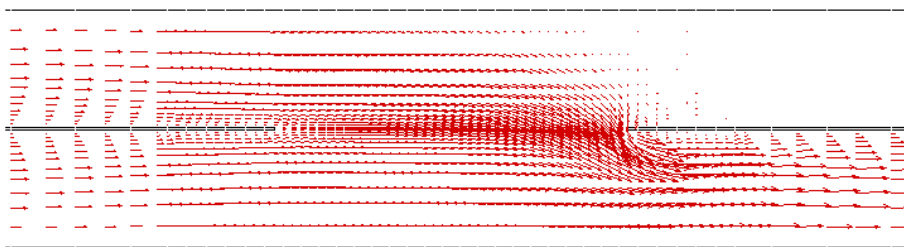
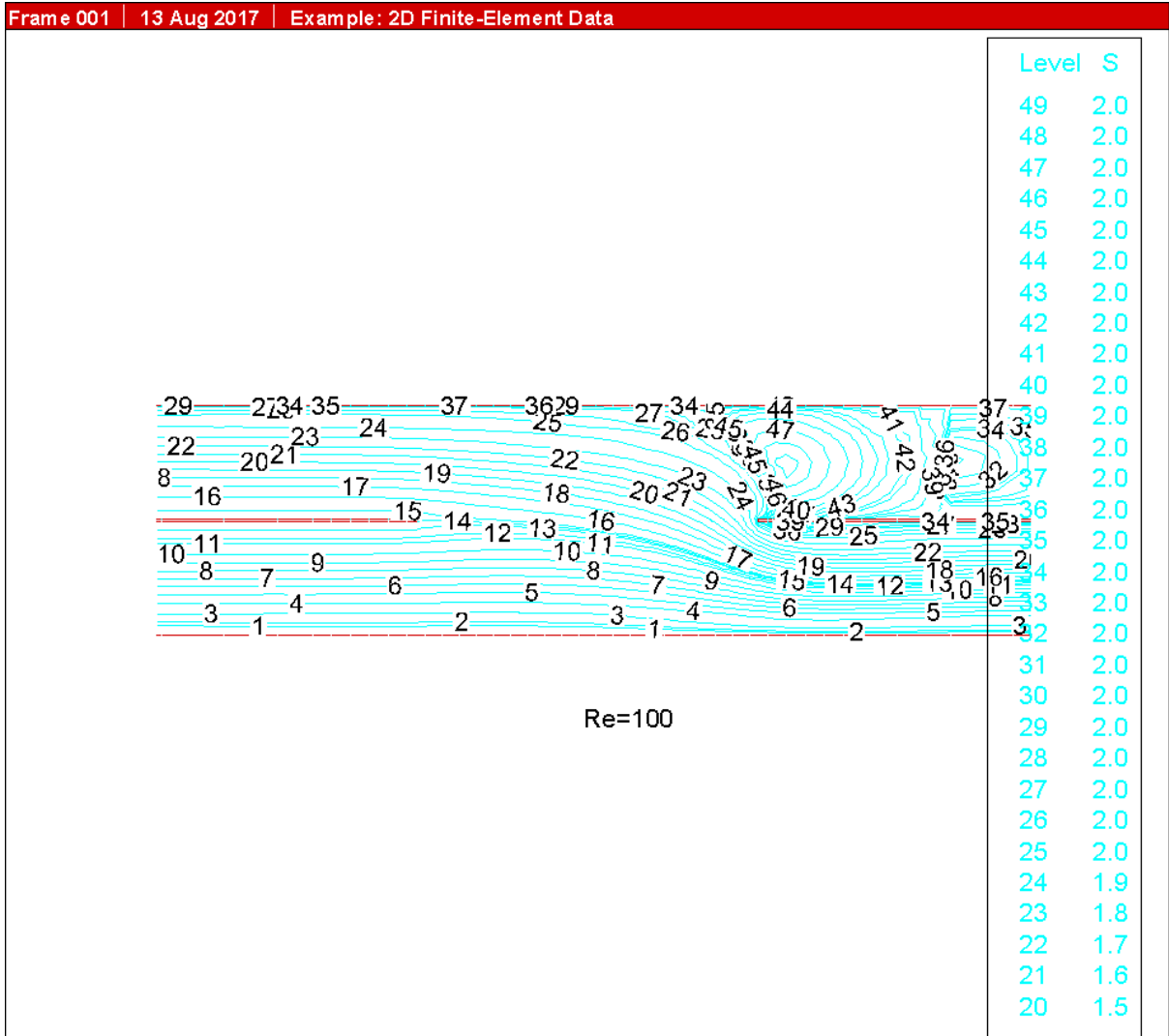


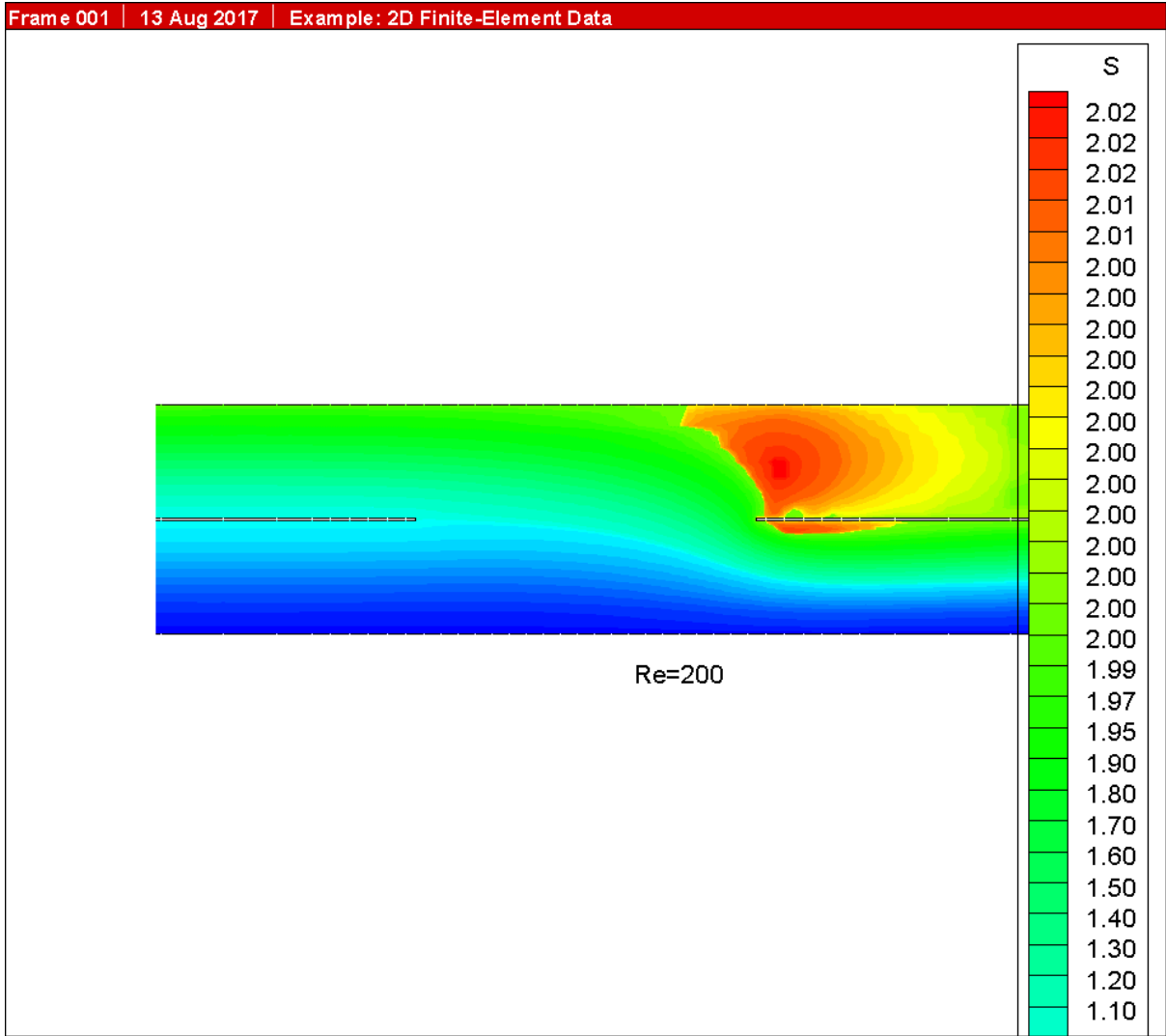
Re=01

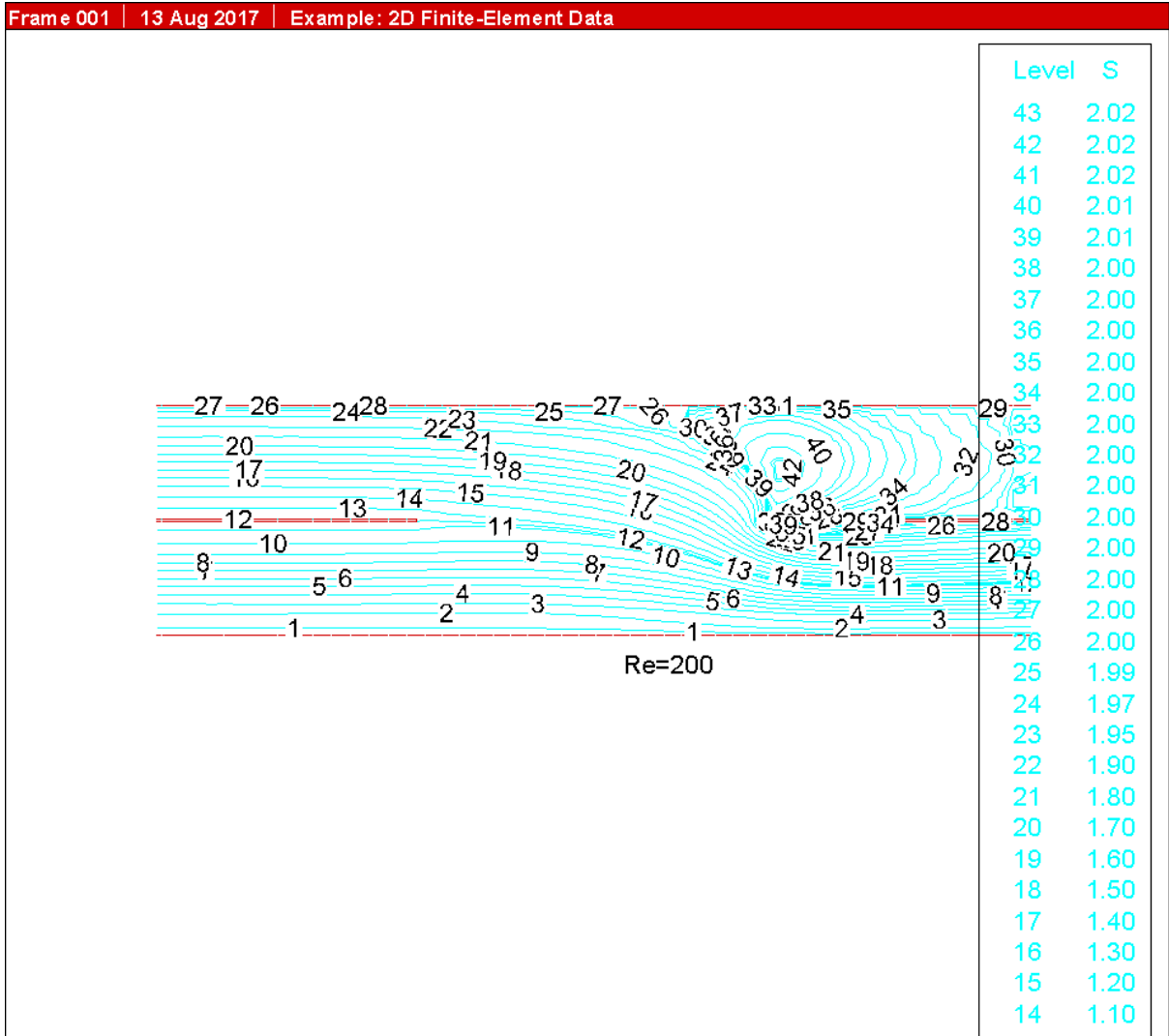


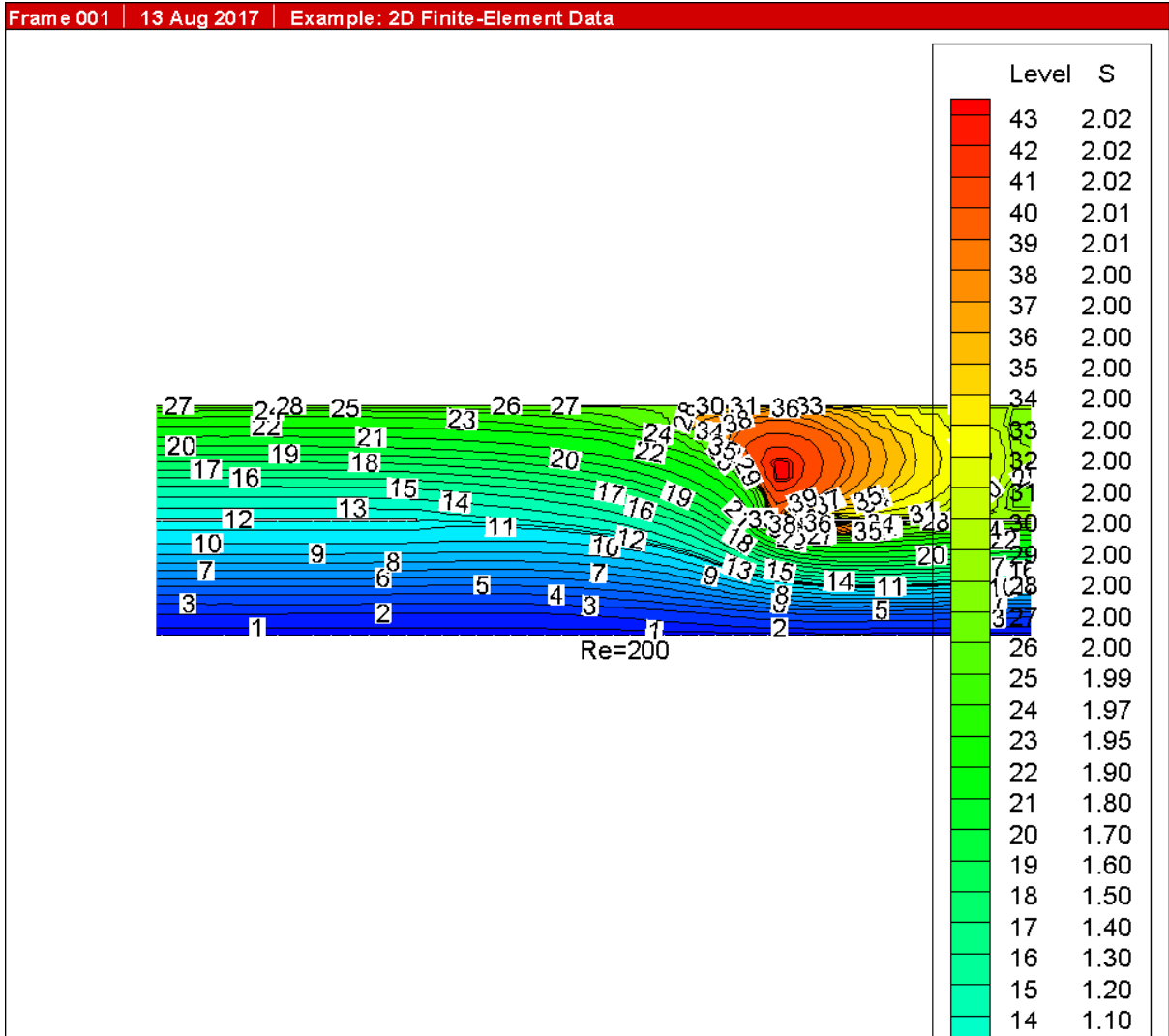


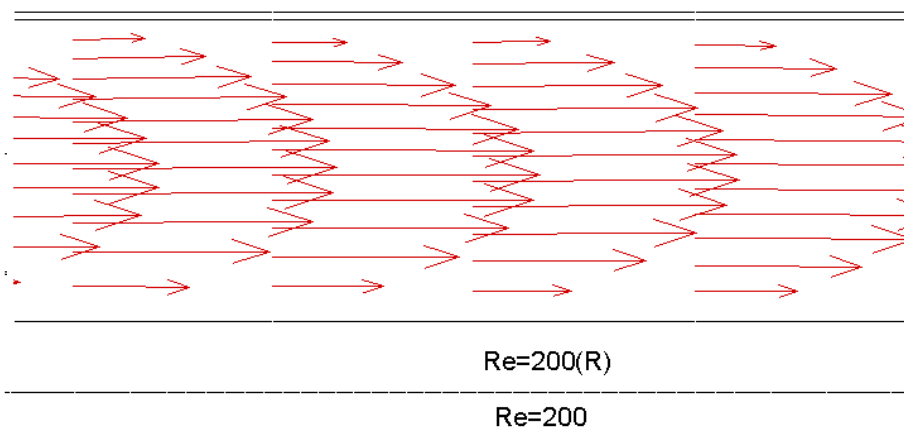




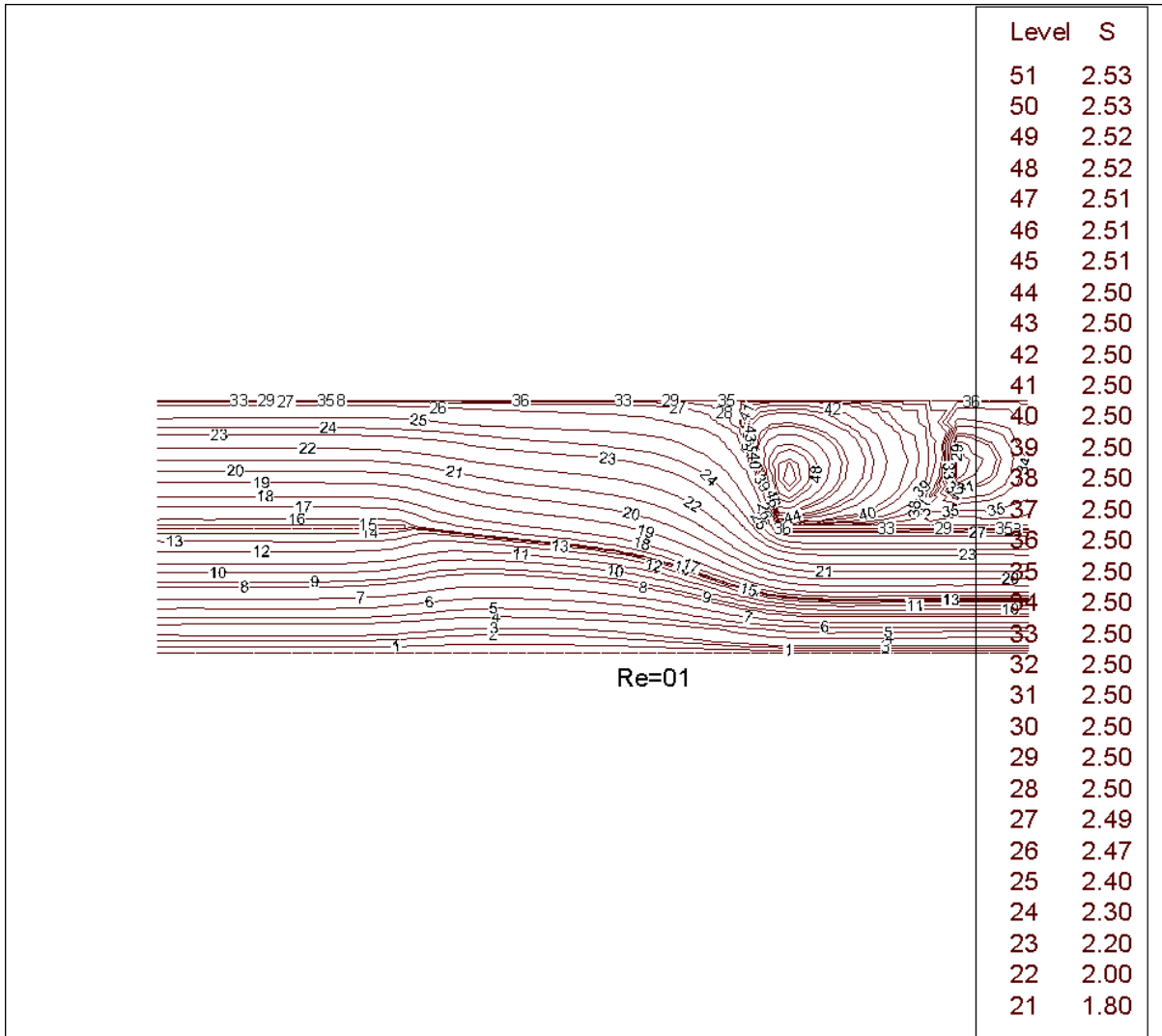


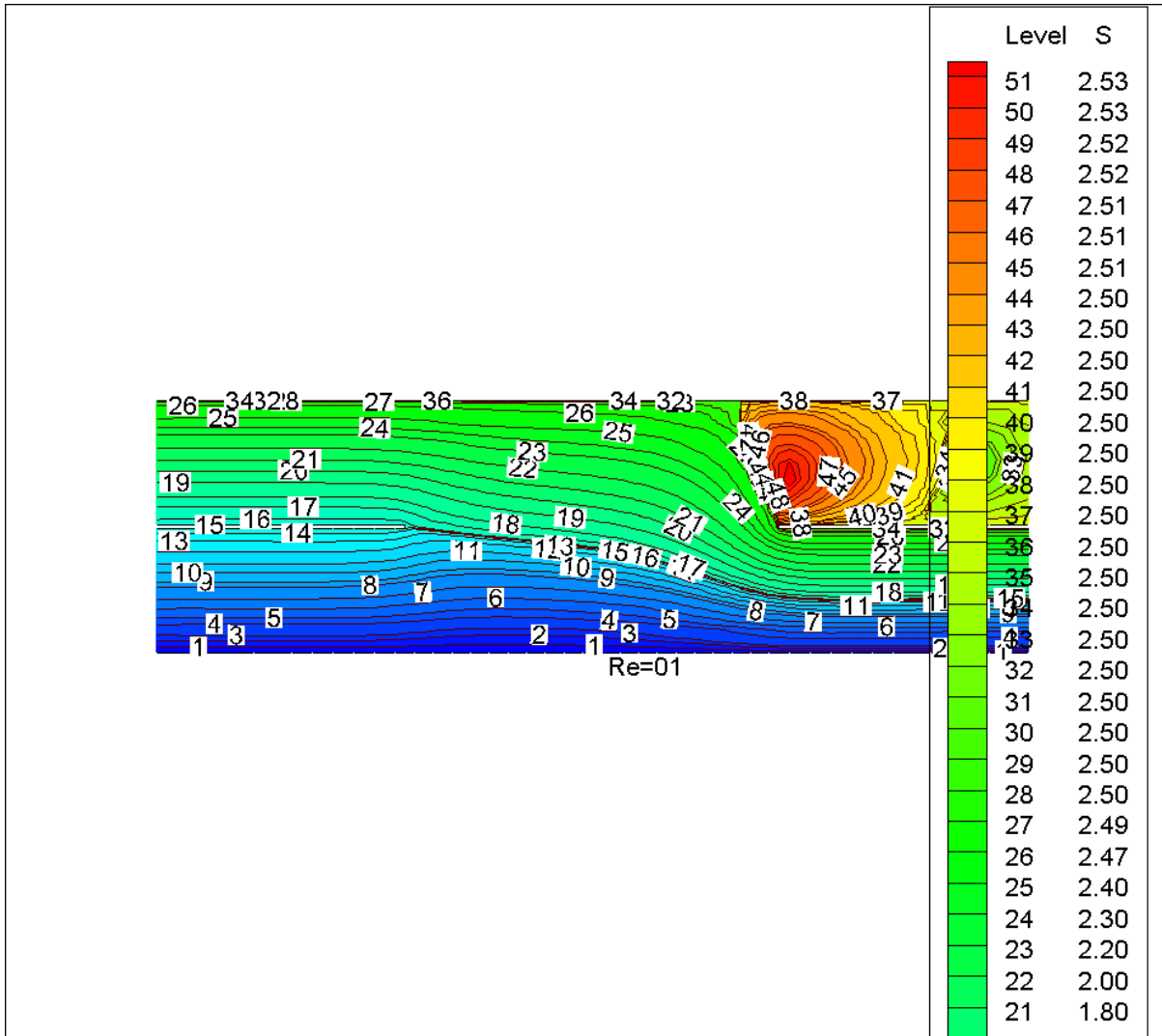




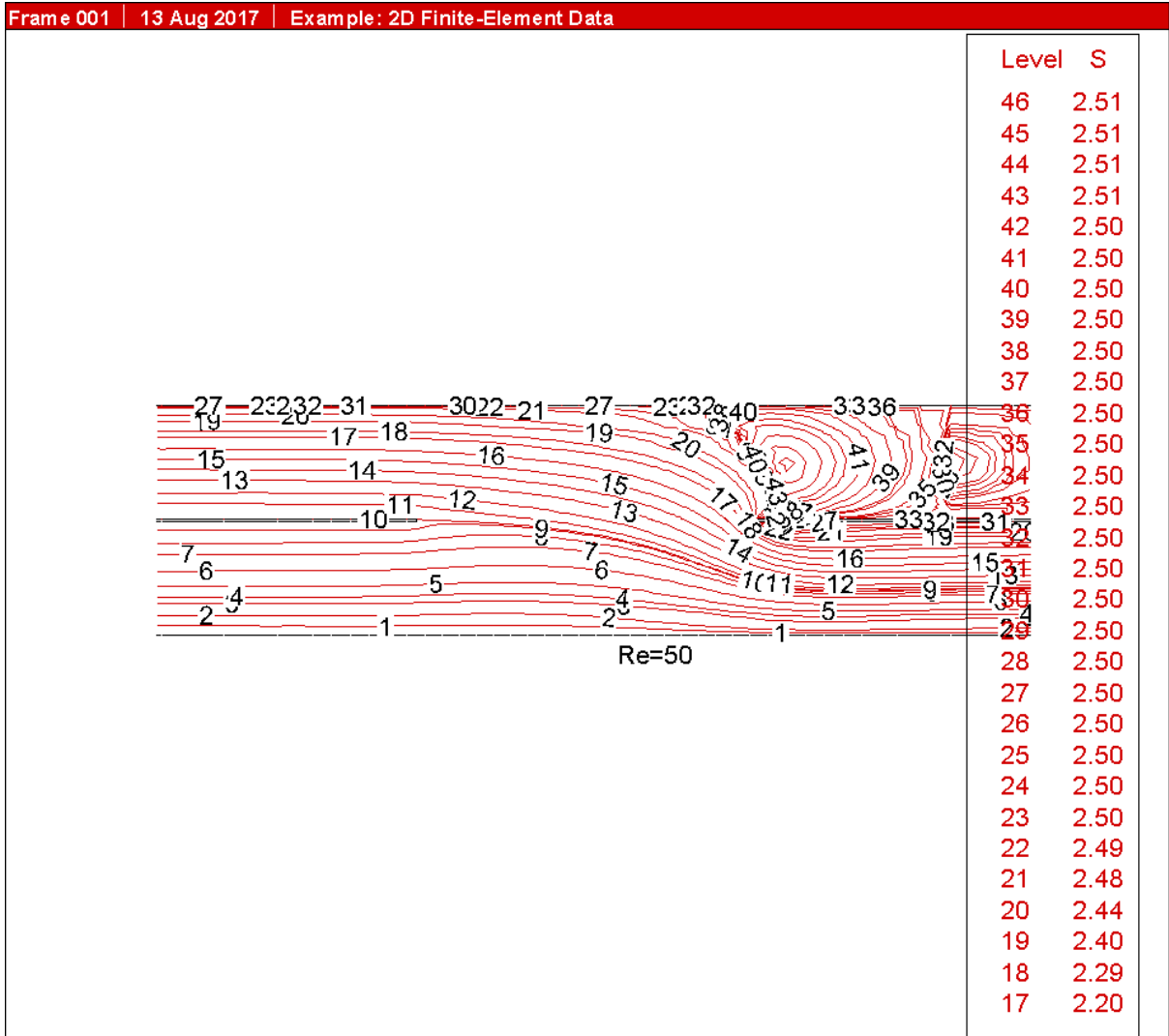


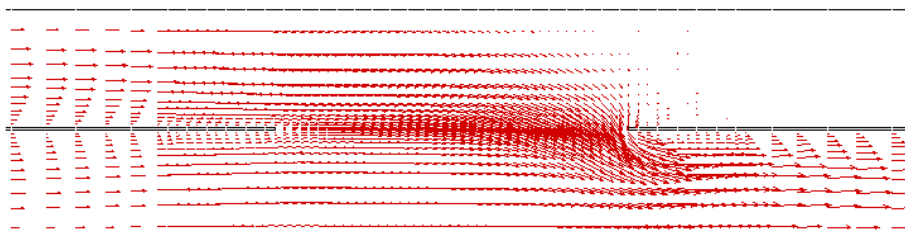
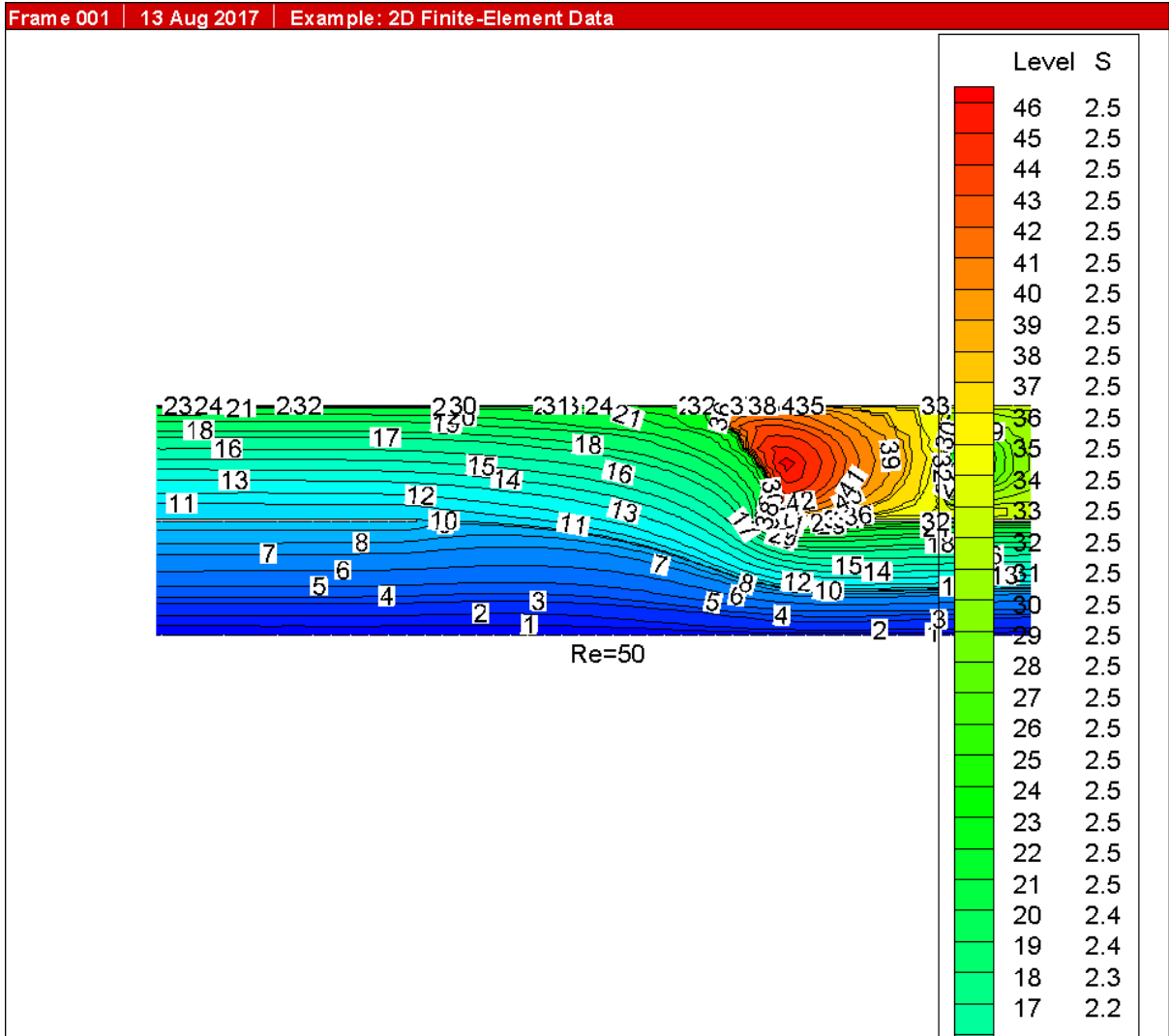




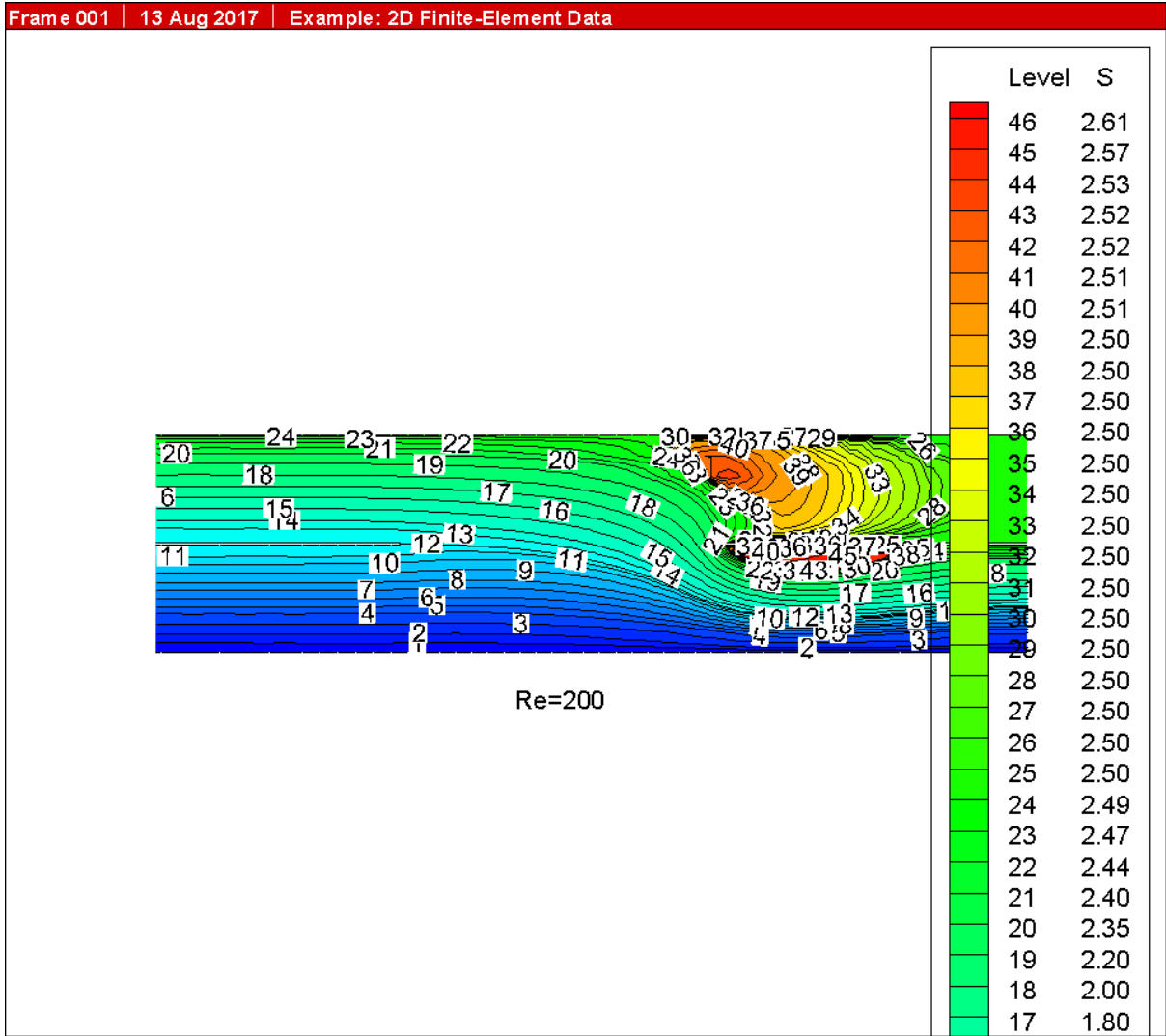


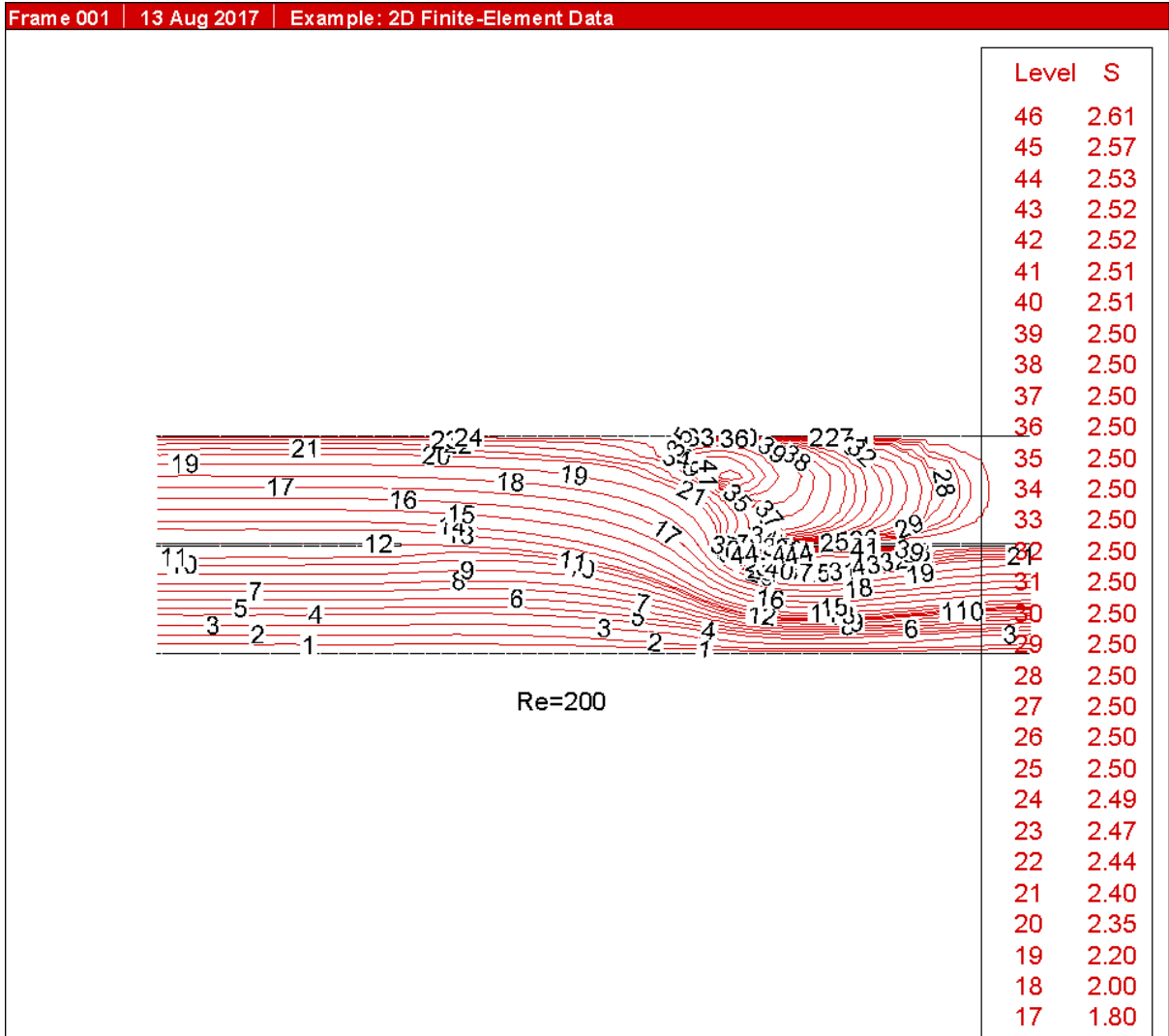






Re=50  
294

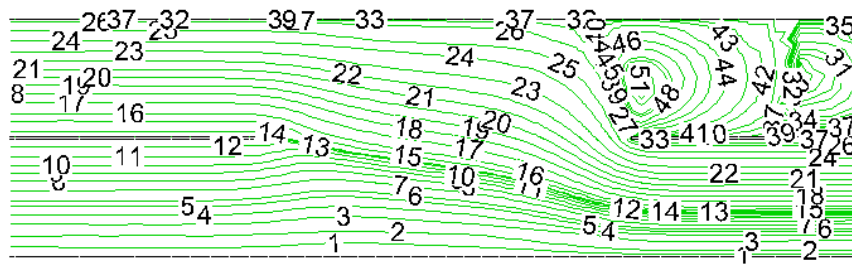






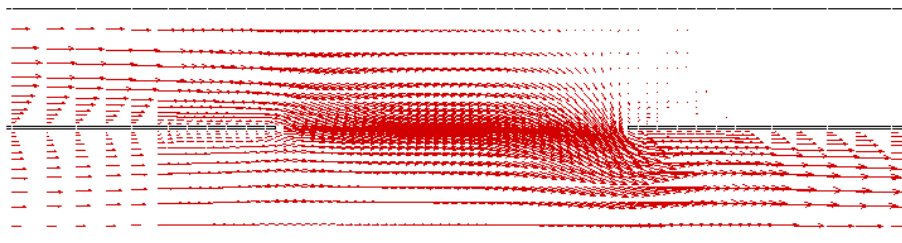
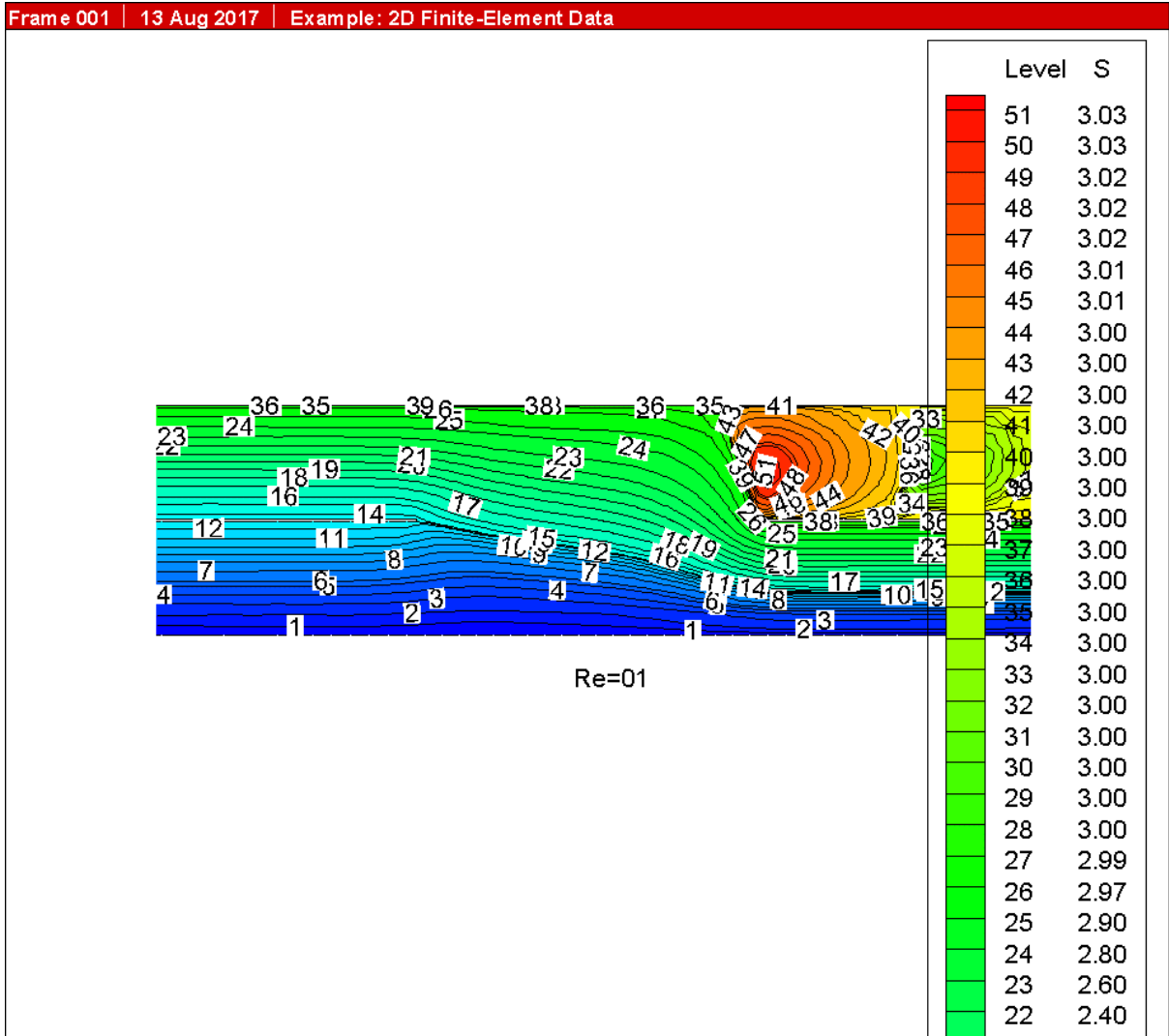


Frame 001 | 13 Aug 2017 | Example: 2D Finite-Element Data

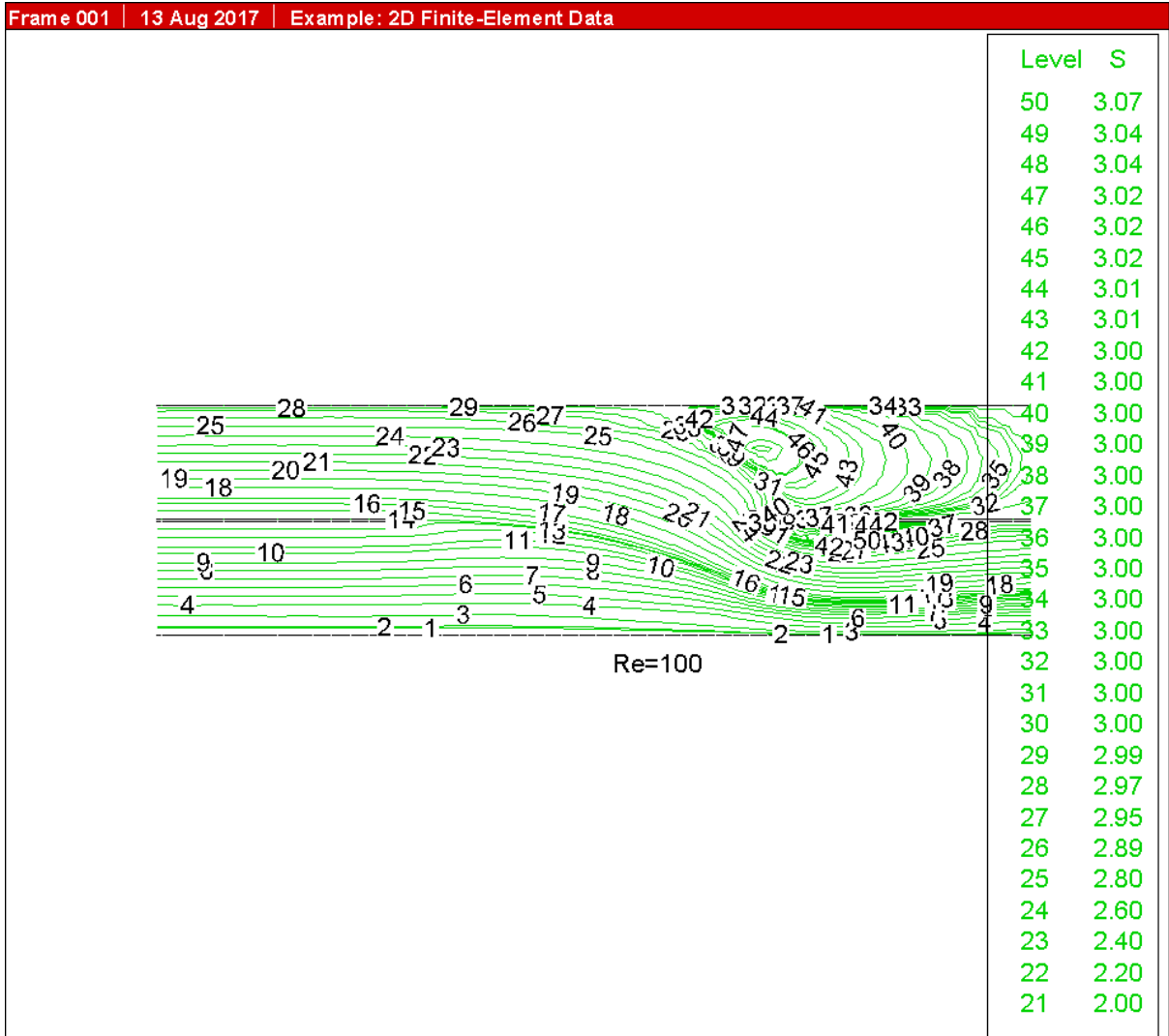


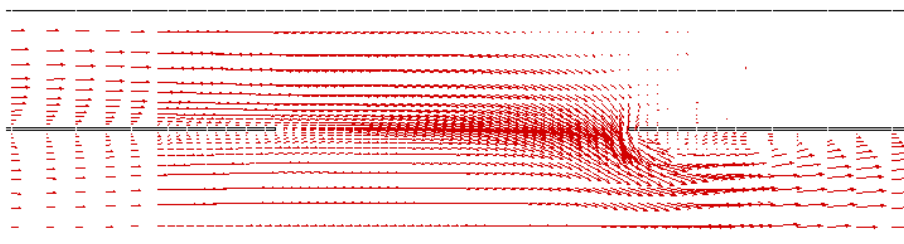
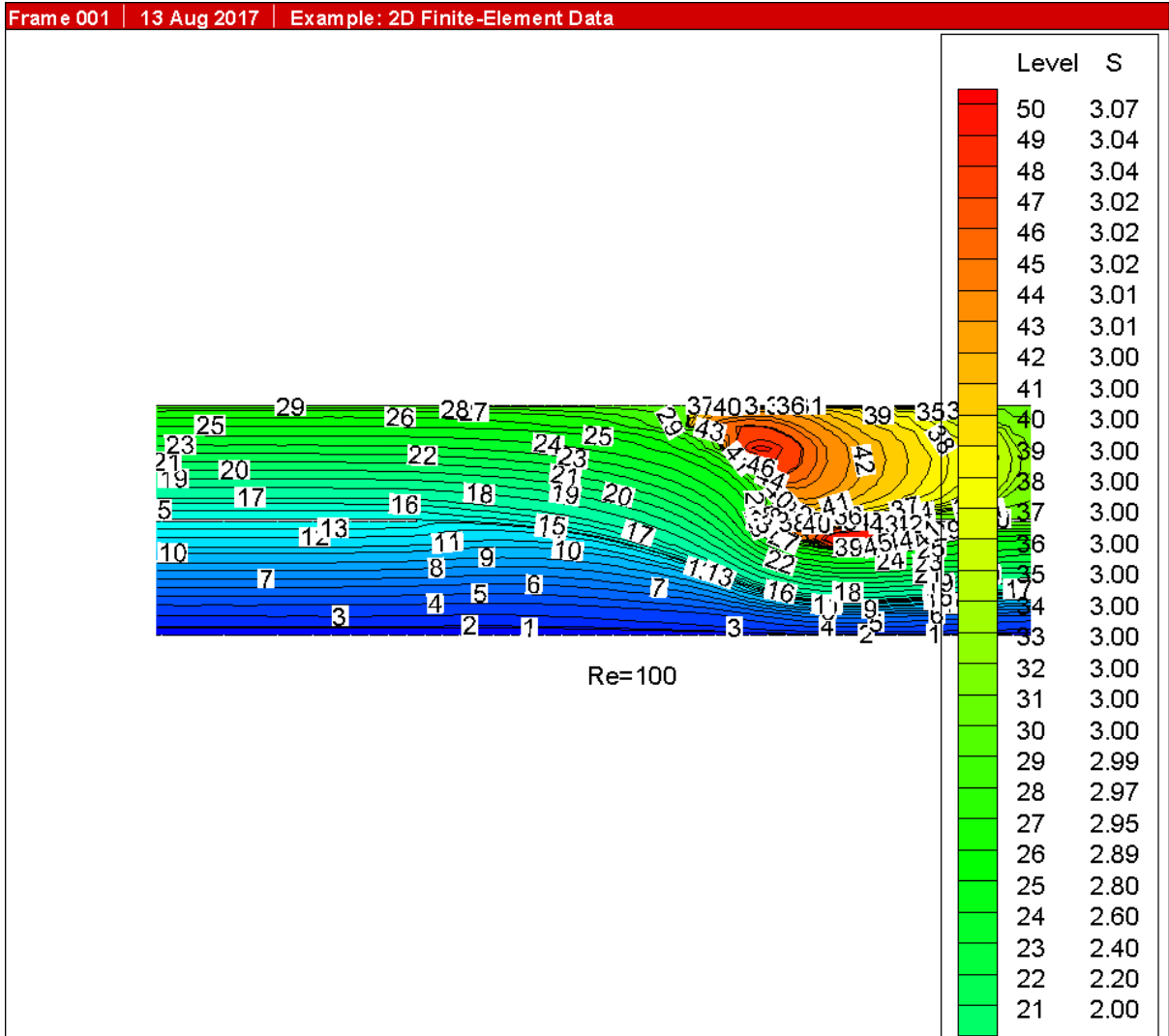
Re=01

Level	S
51	3.03
50	3.03
49	3.02
48	3.02
47	3.02
46	3.01
45	3.01
44	3.00
43	3.00
42	3.00
41	3.00
40	3.00
39	3.00
38	3.00
37	3.00
36	3.00
35	3.00
34	3.00
33	3.00
32	3.00
31	3.00
30	3.00
29	3.00
28	3.00
27	2.99
26	2.97
25	2.90
24	2.80
23	2.60
22	2.40



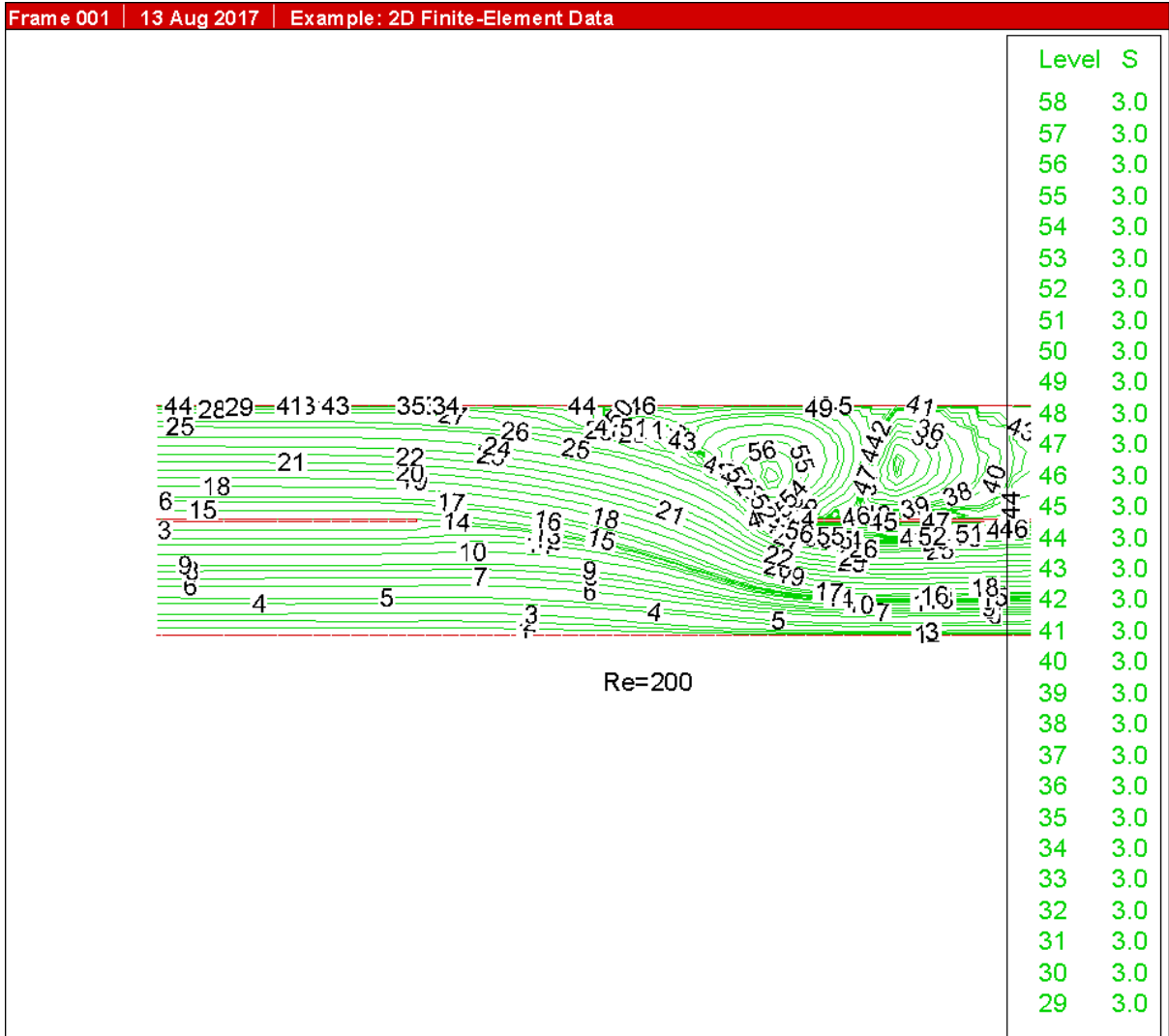


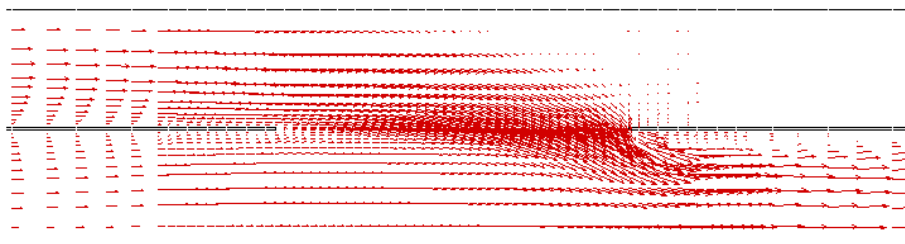
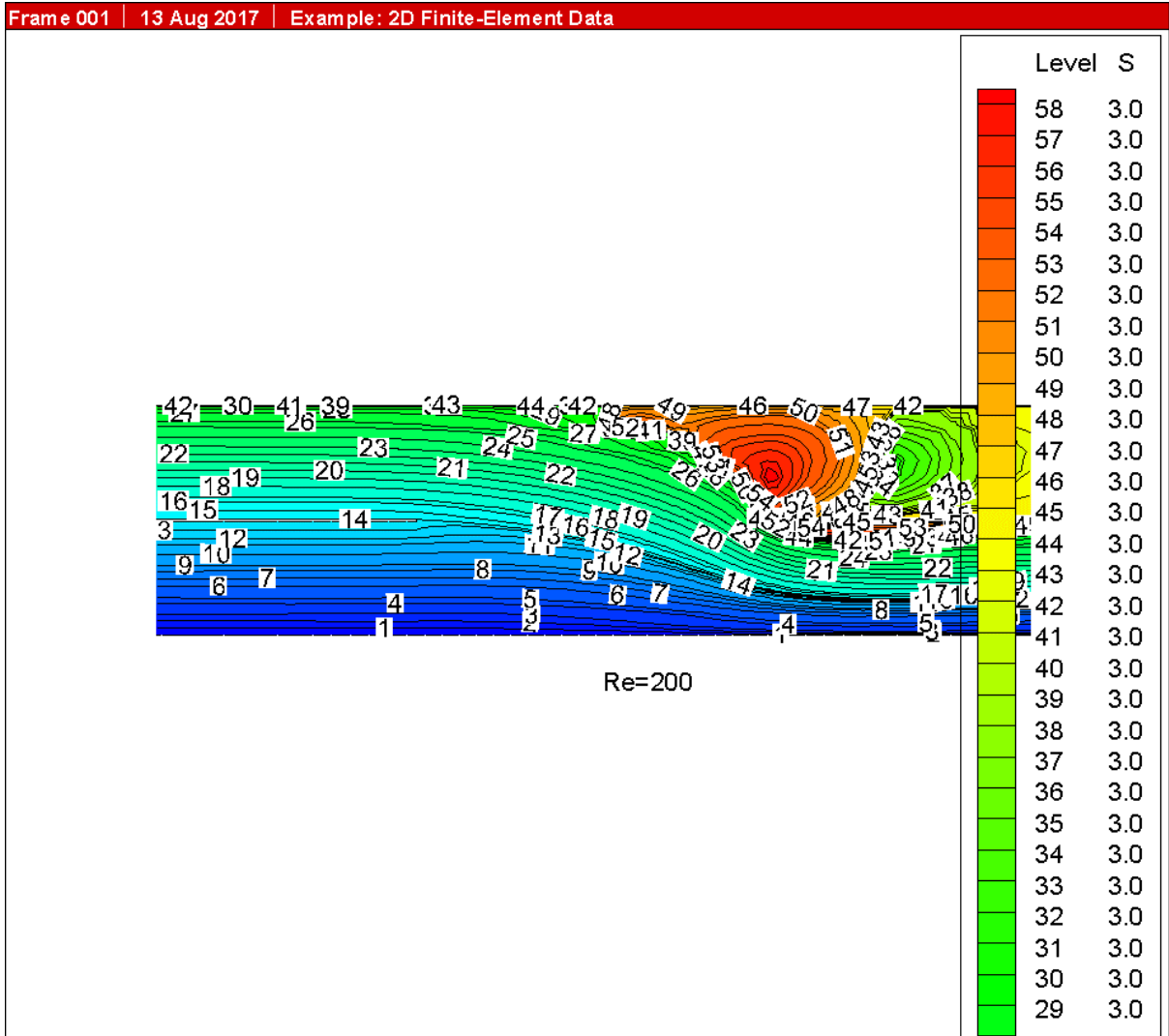




Re=100  
303

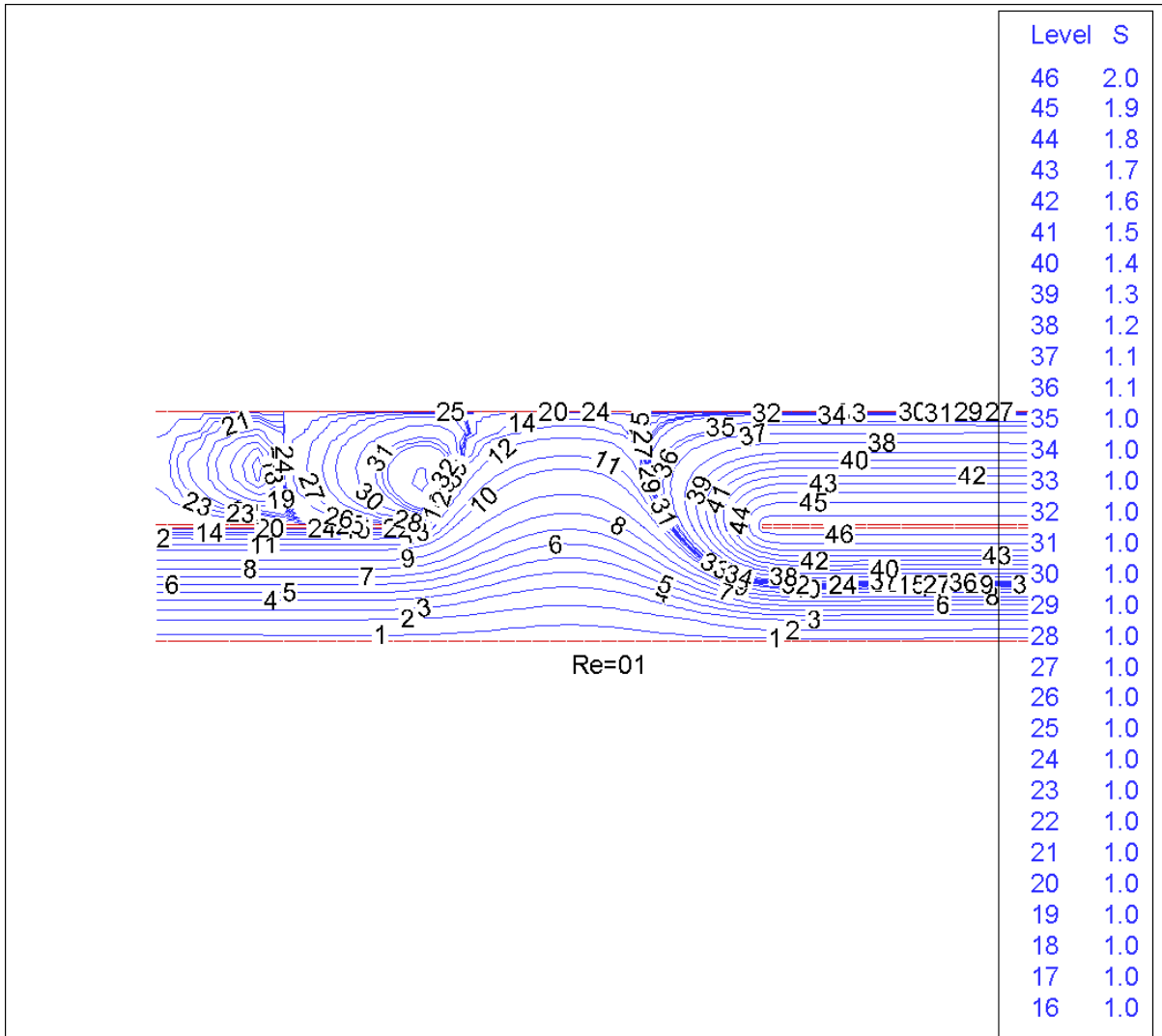


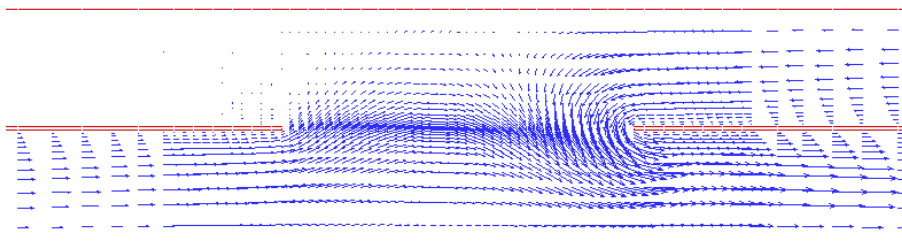
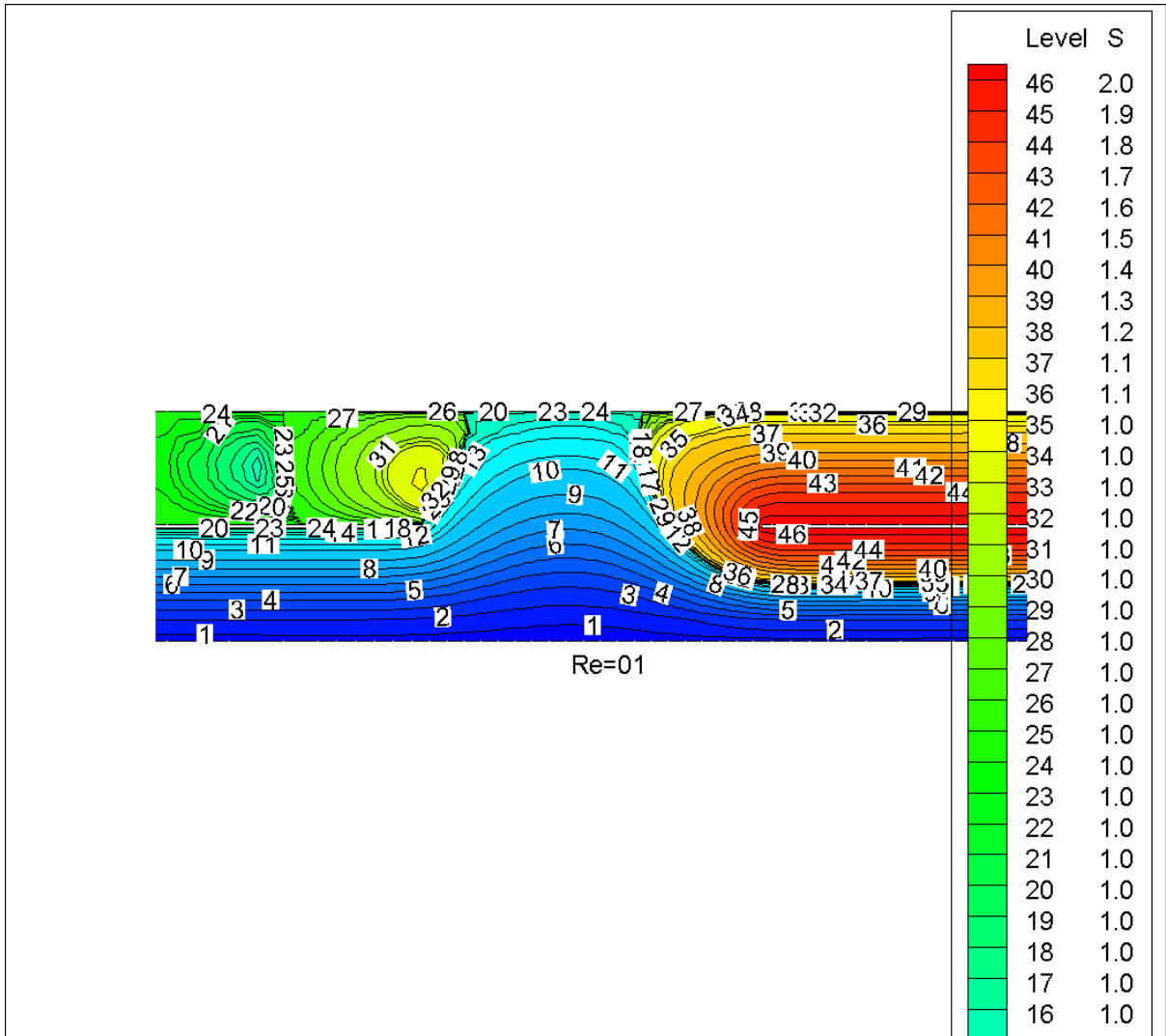




Re=200  
306

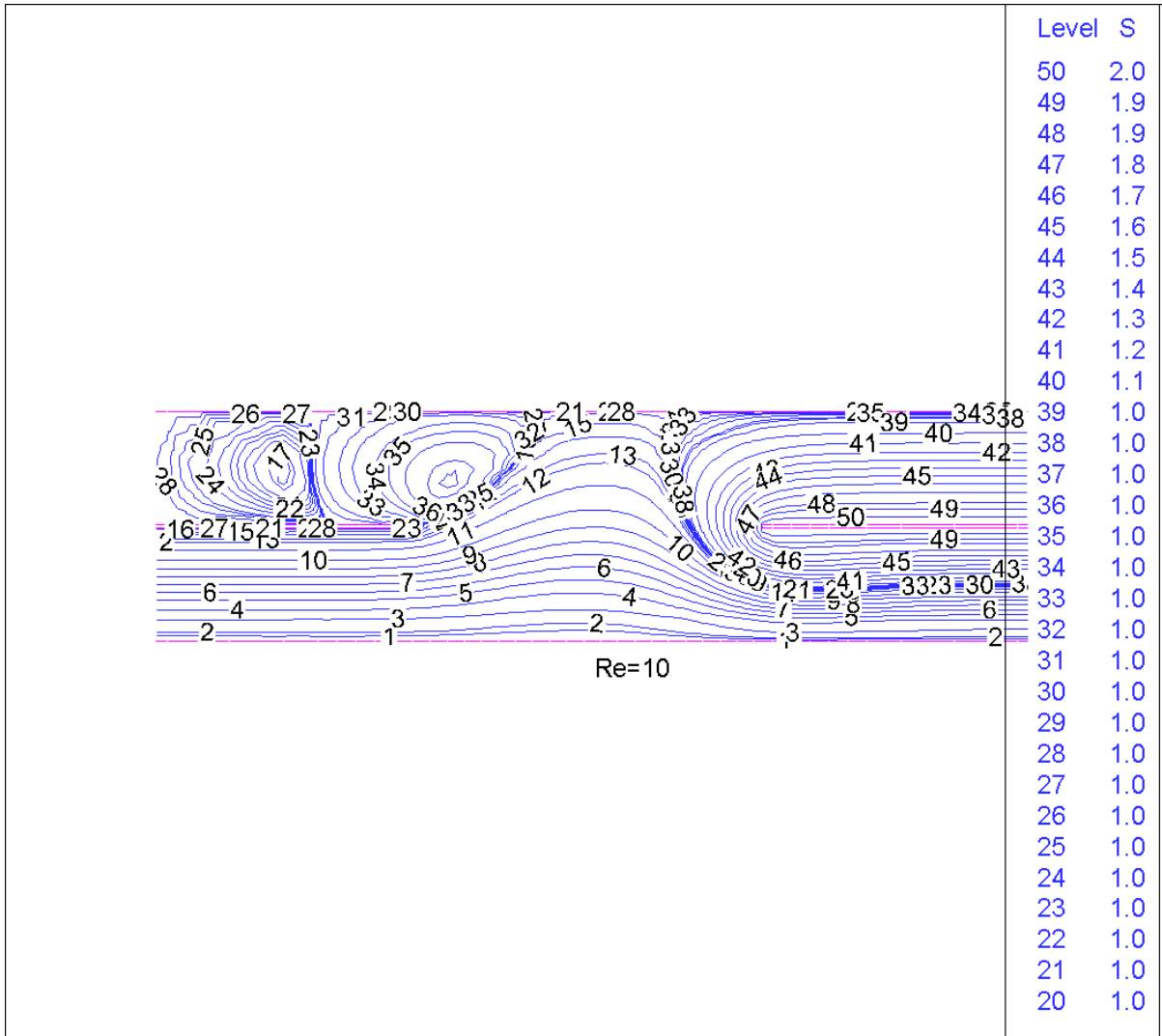


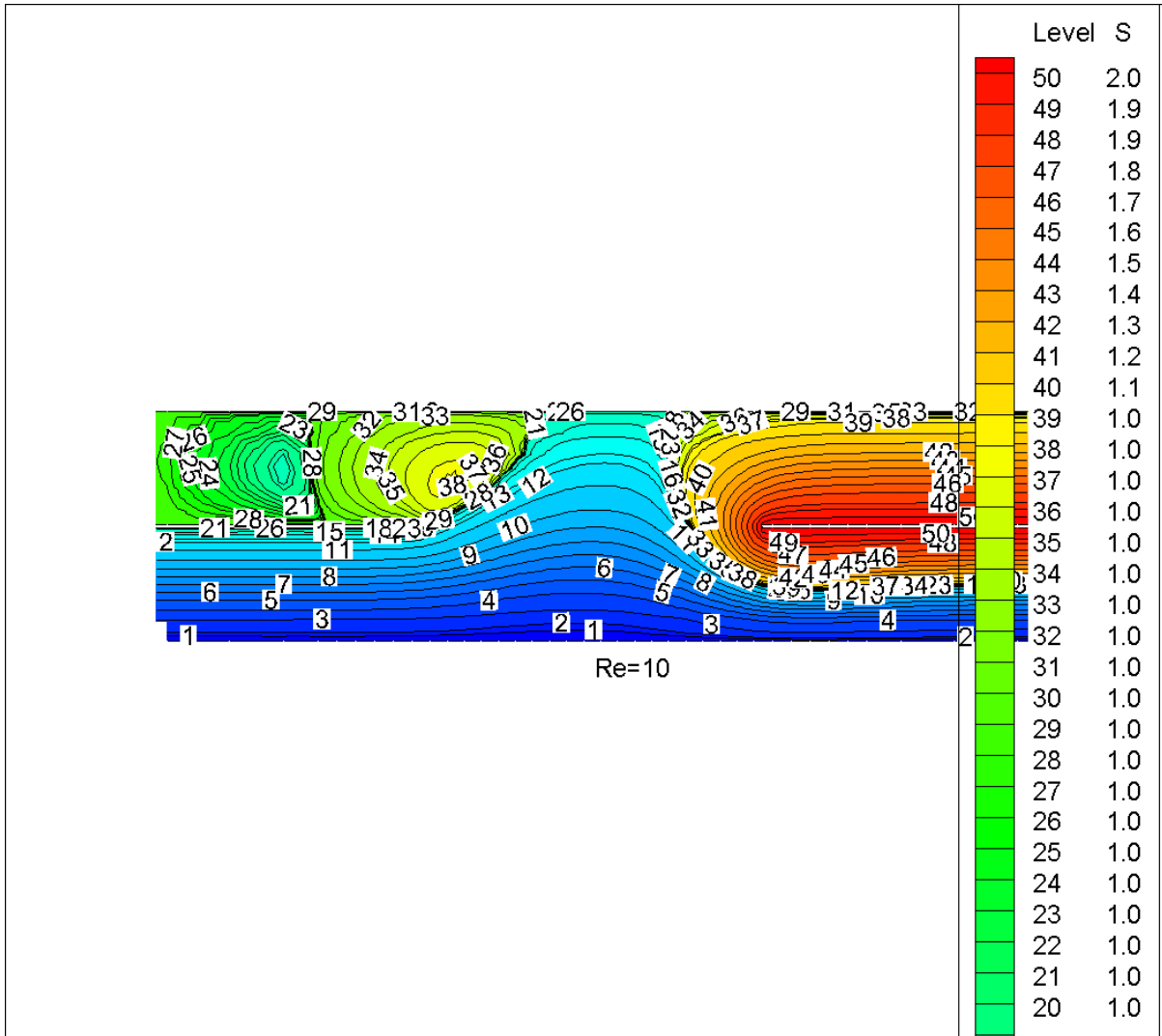




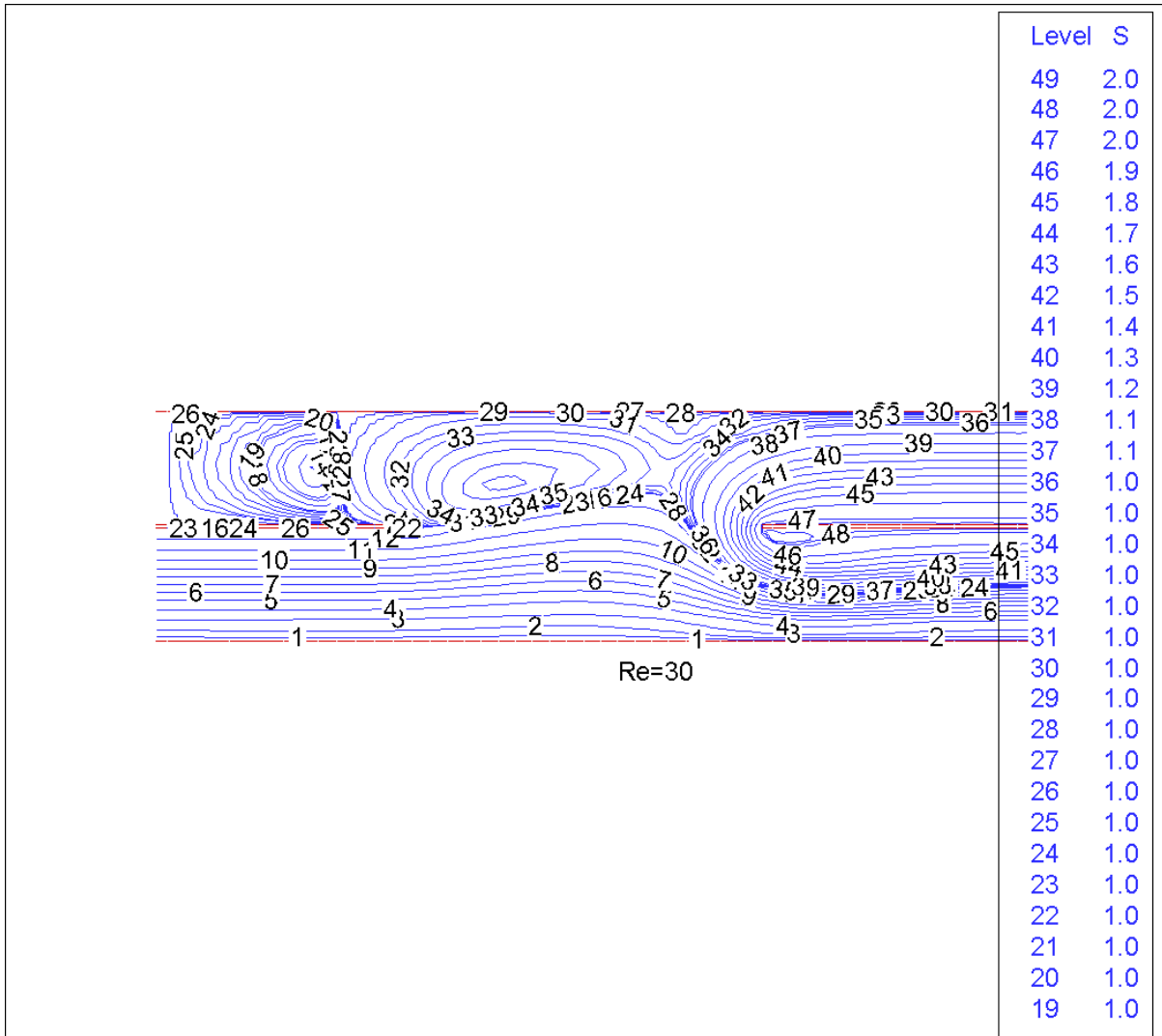
Re=01  
309

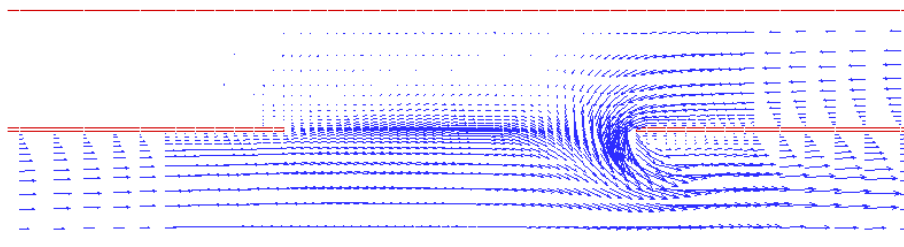
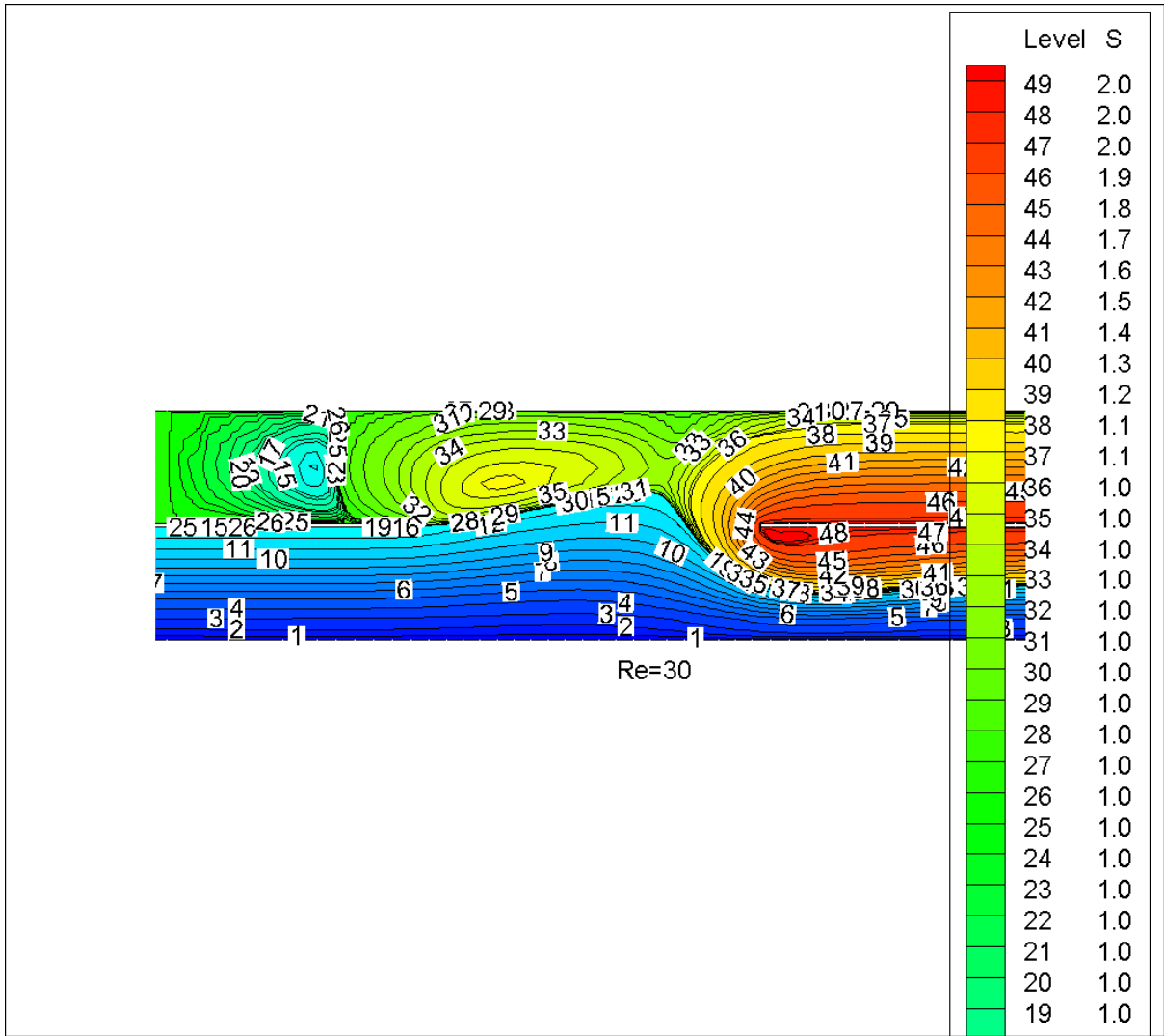






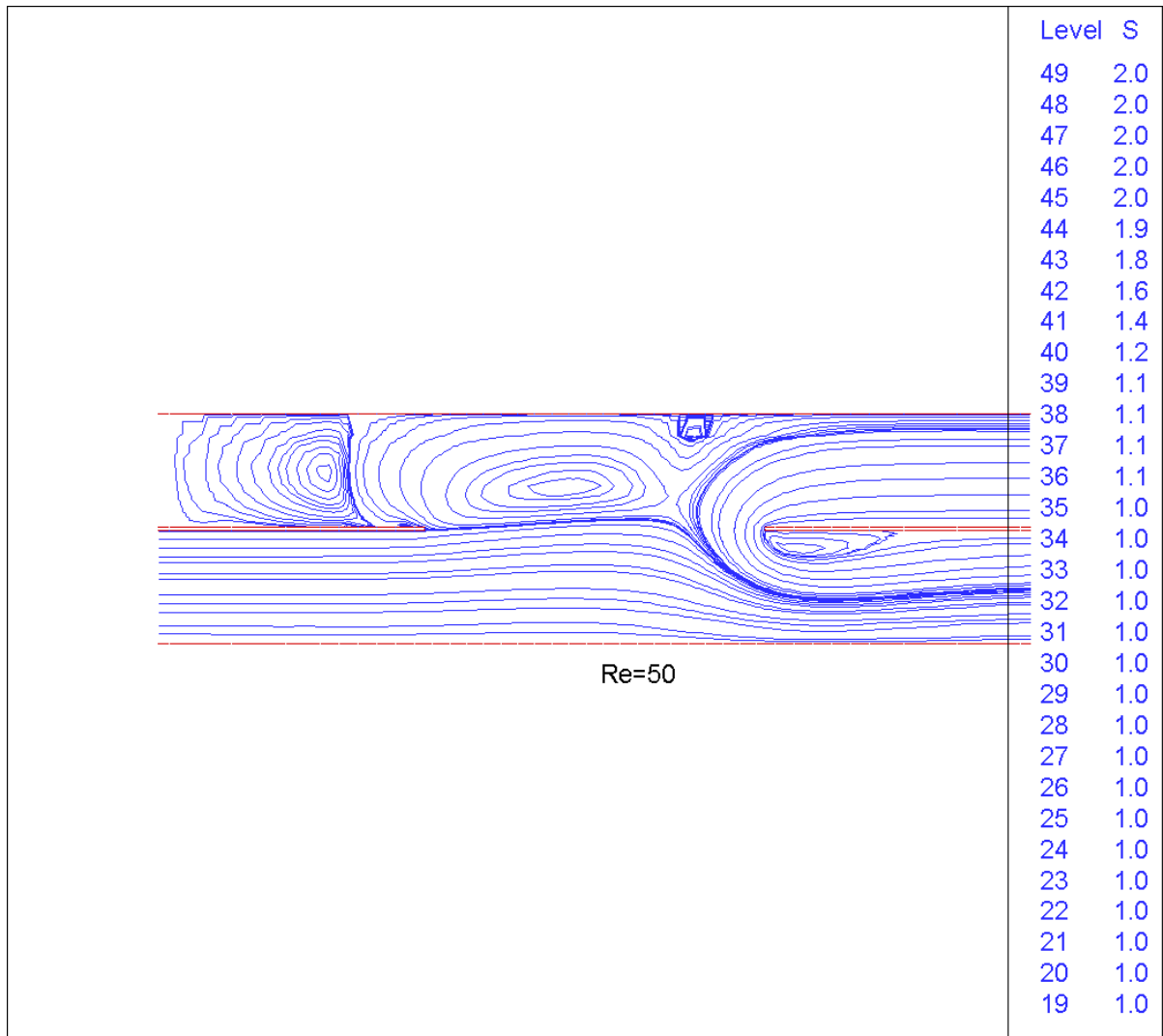


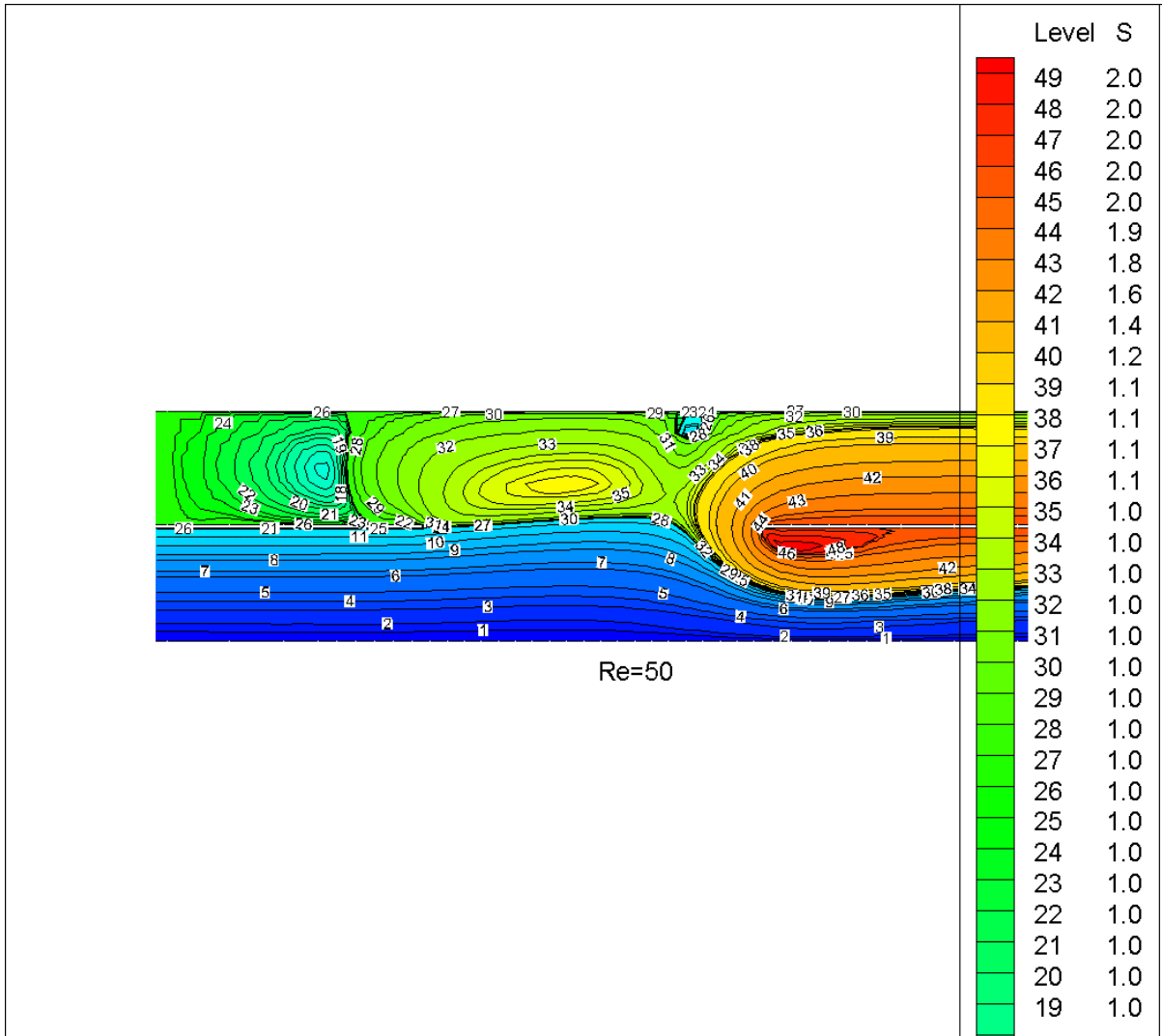


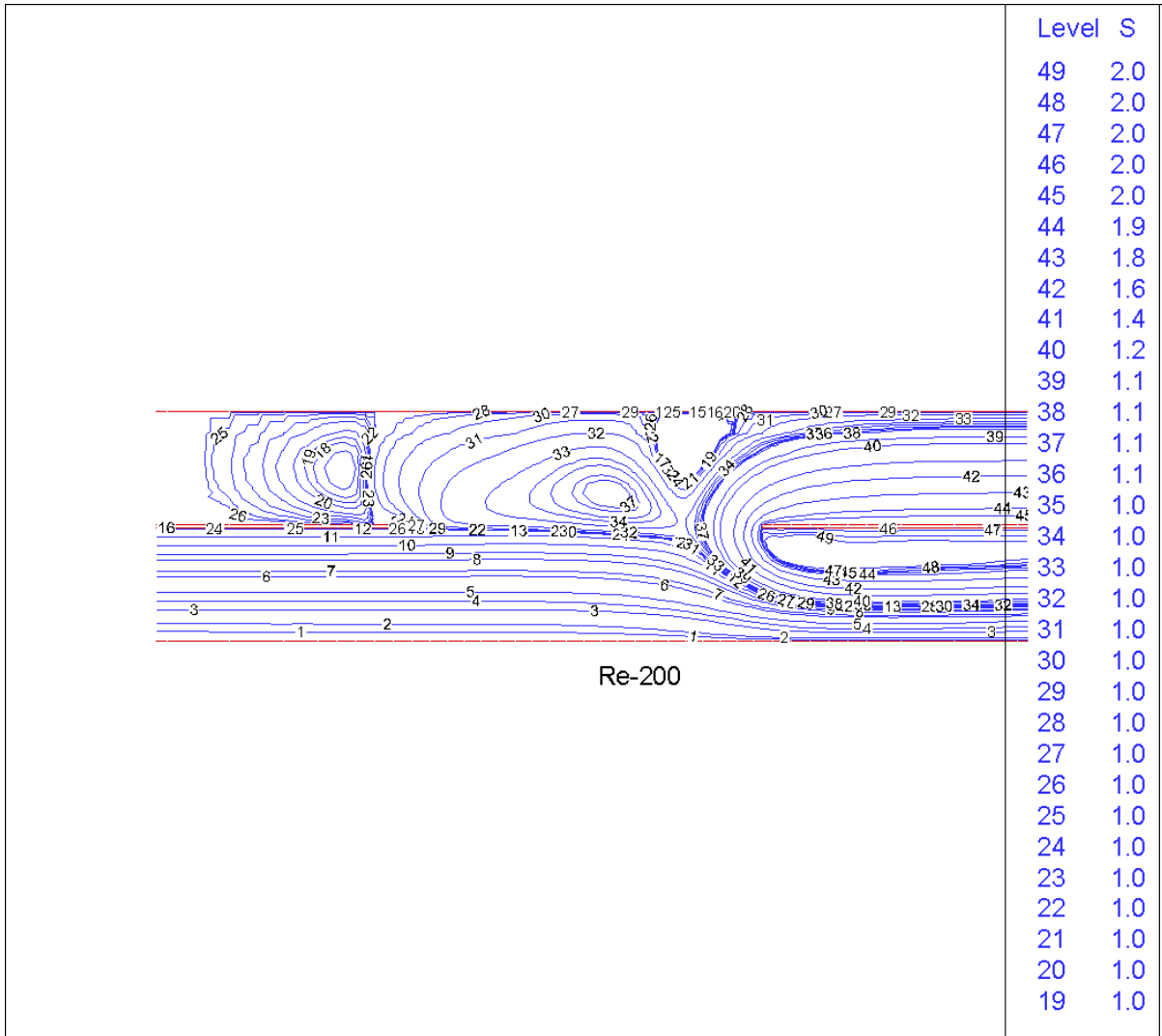


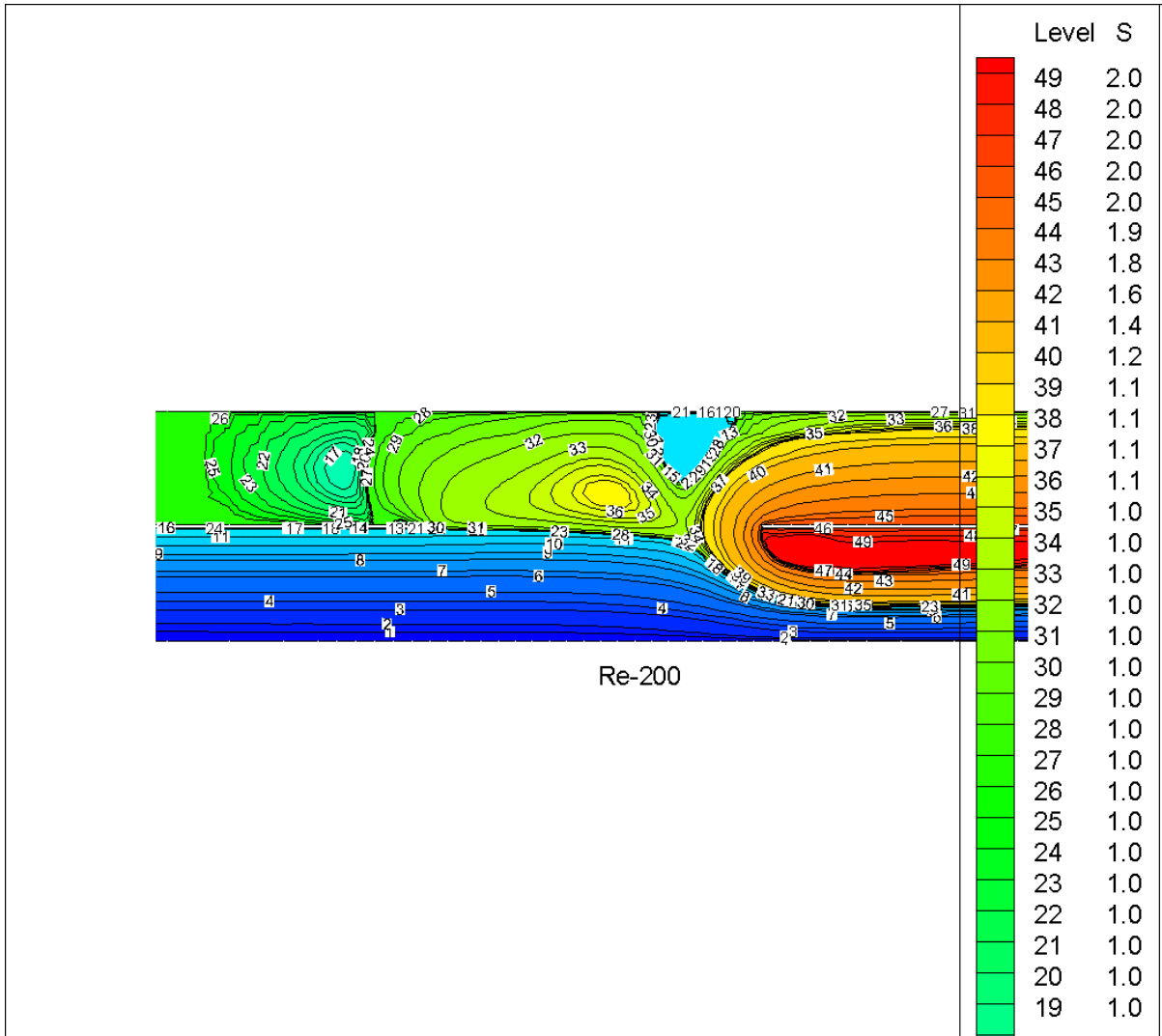
Re=30  
315

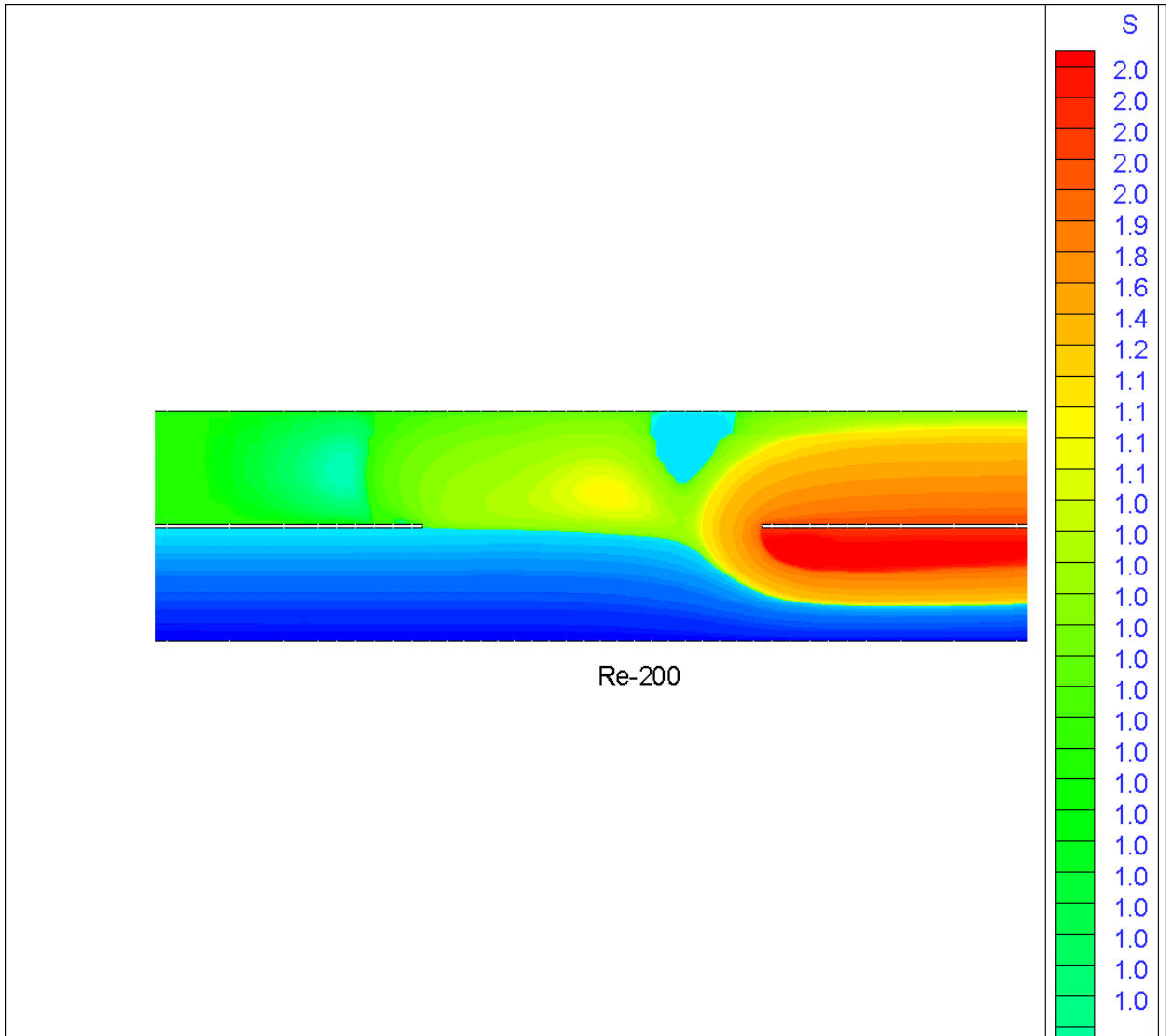




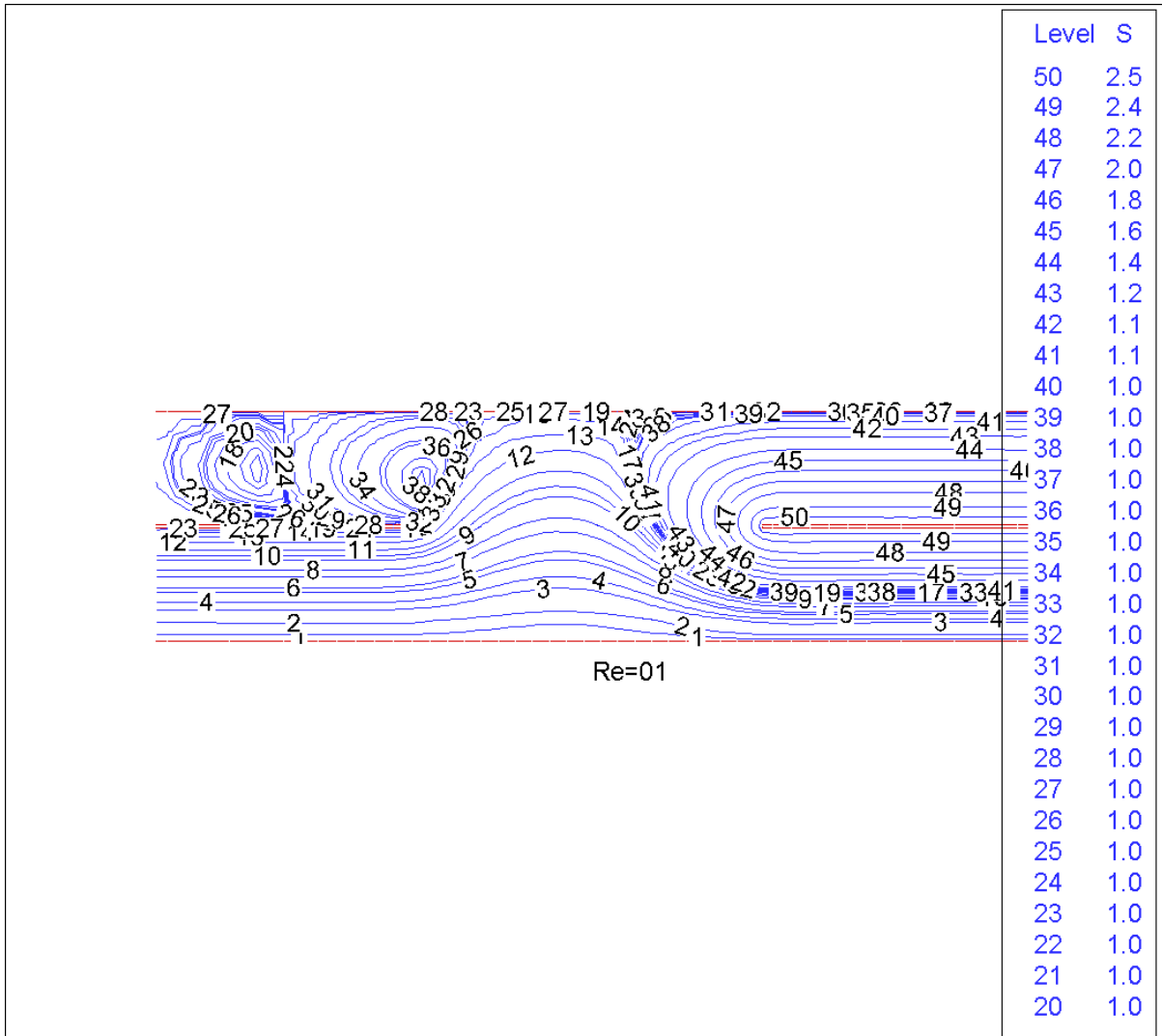


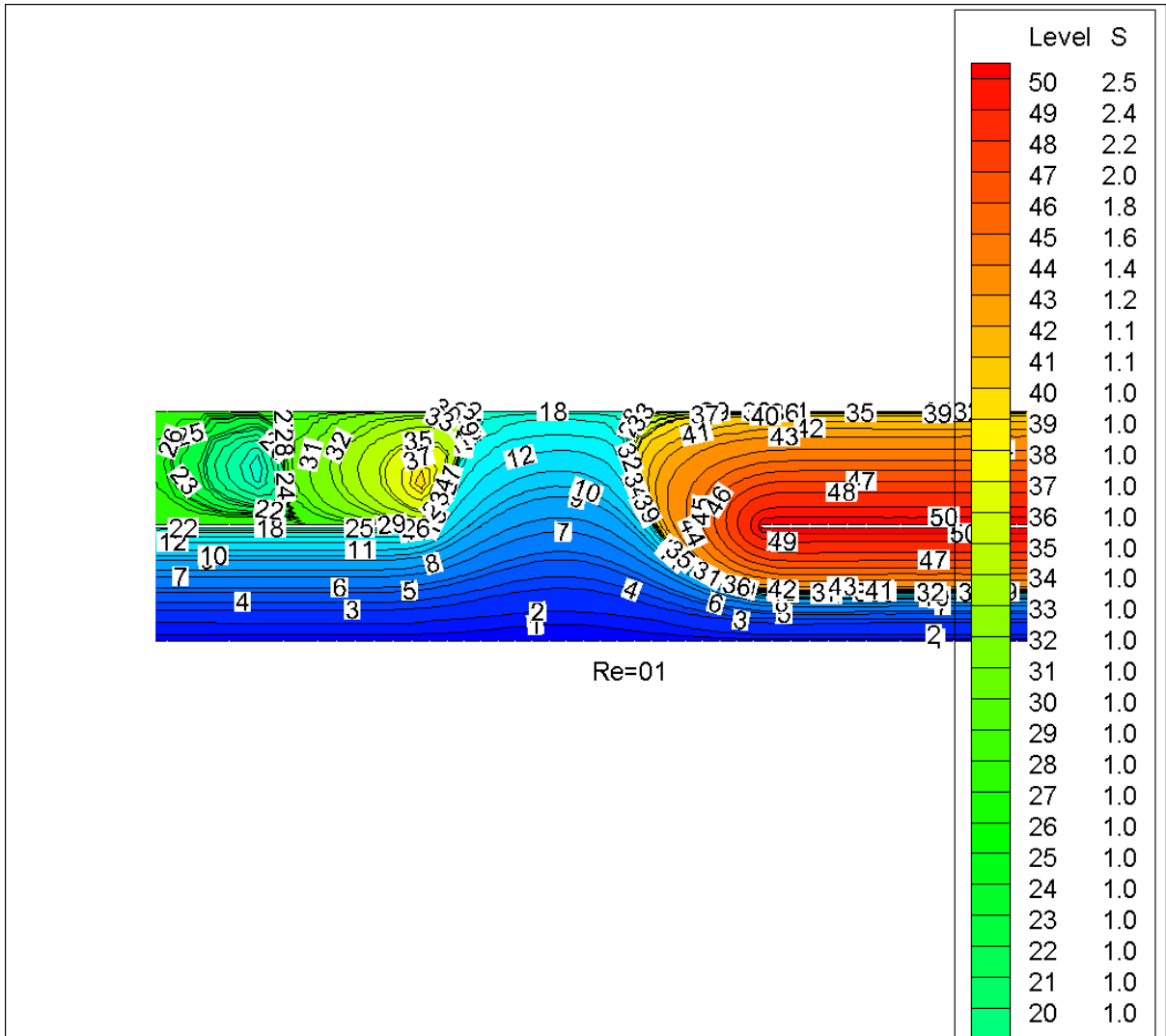




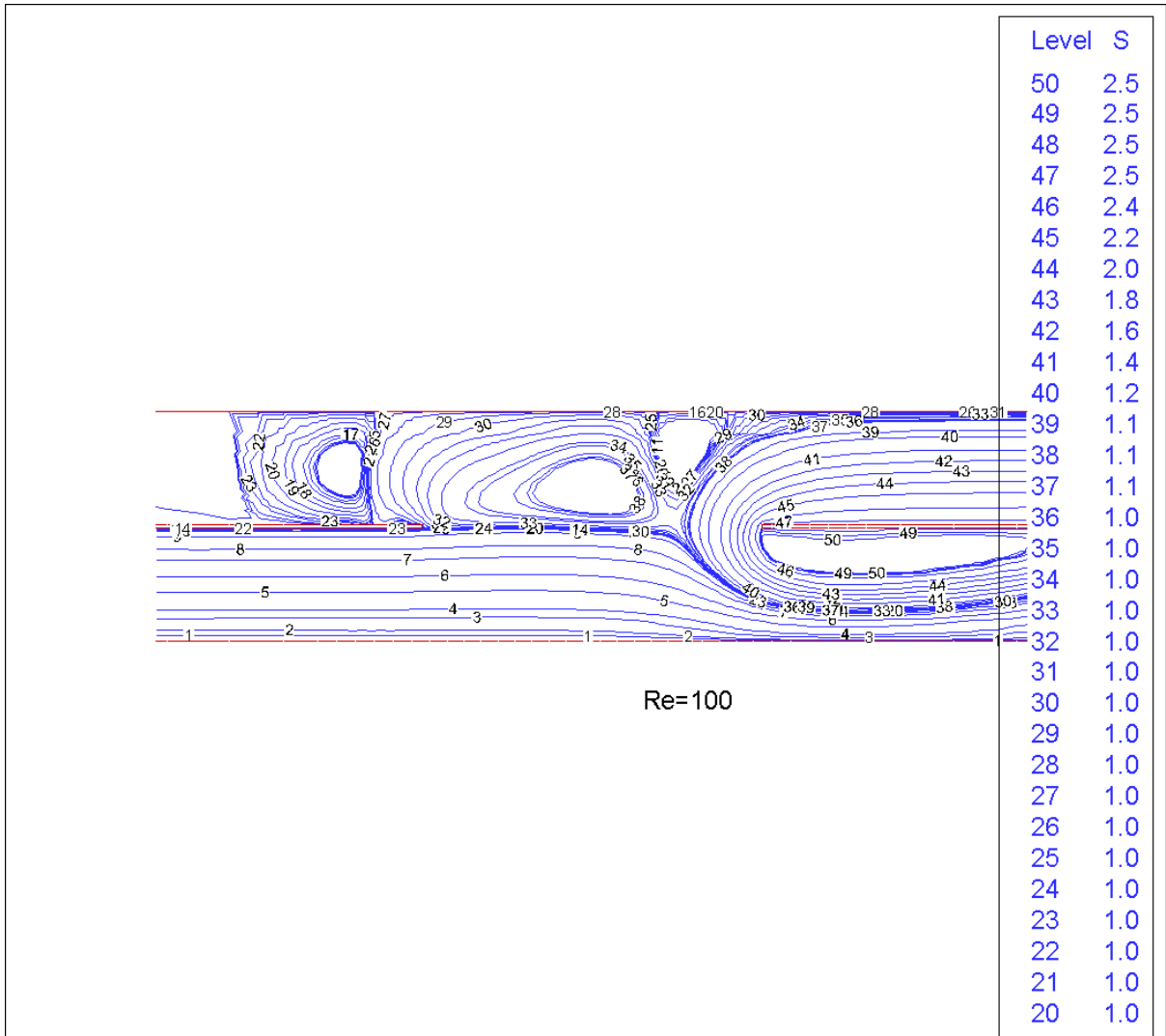


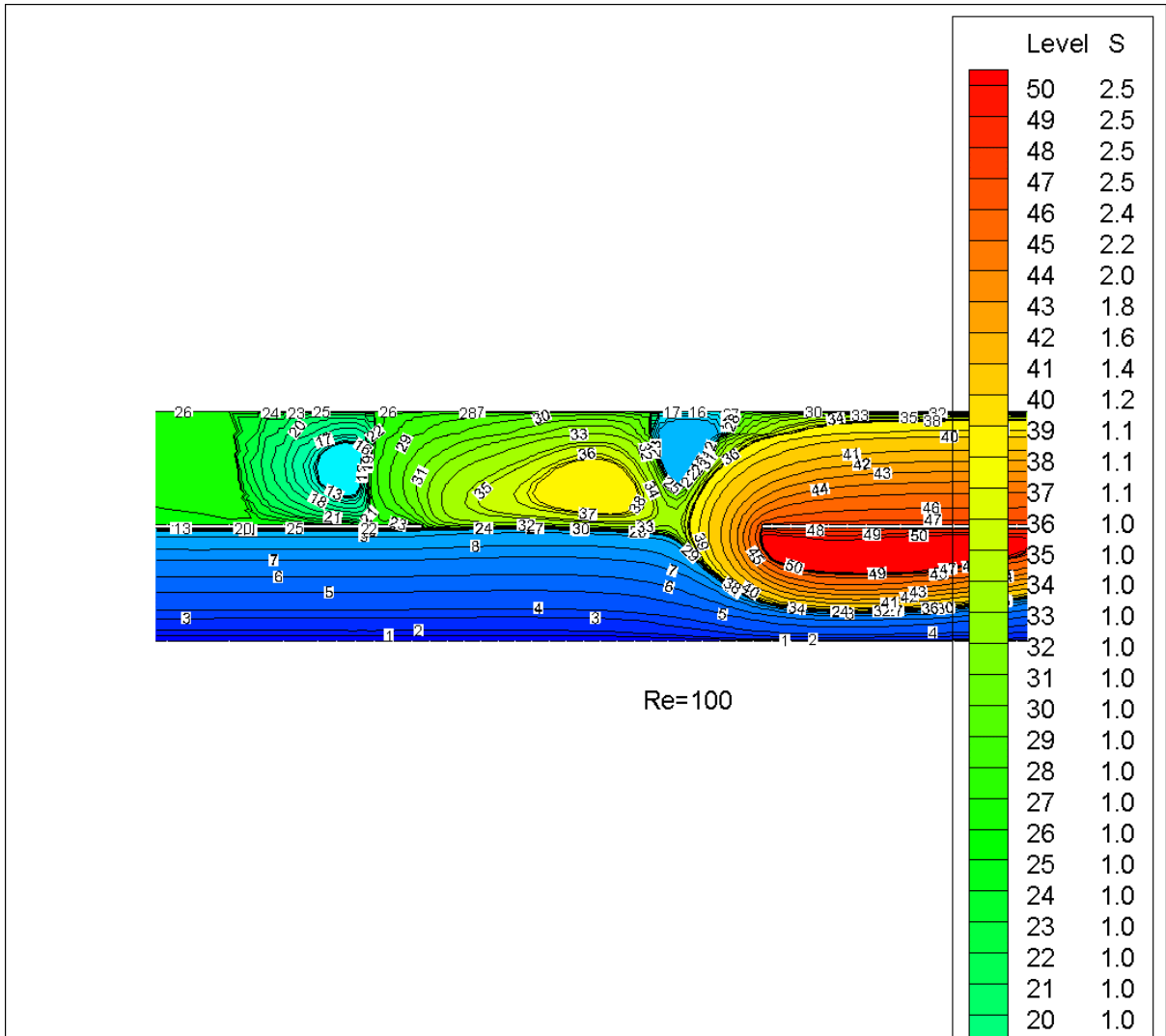


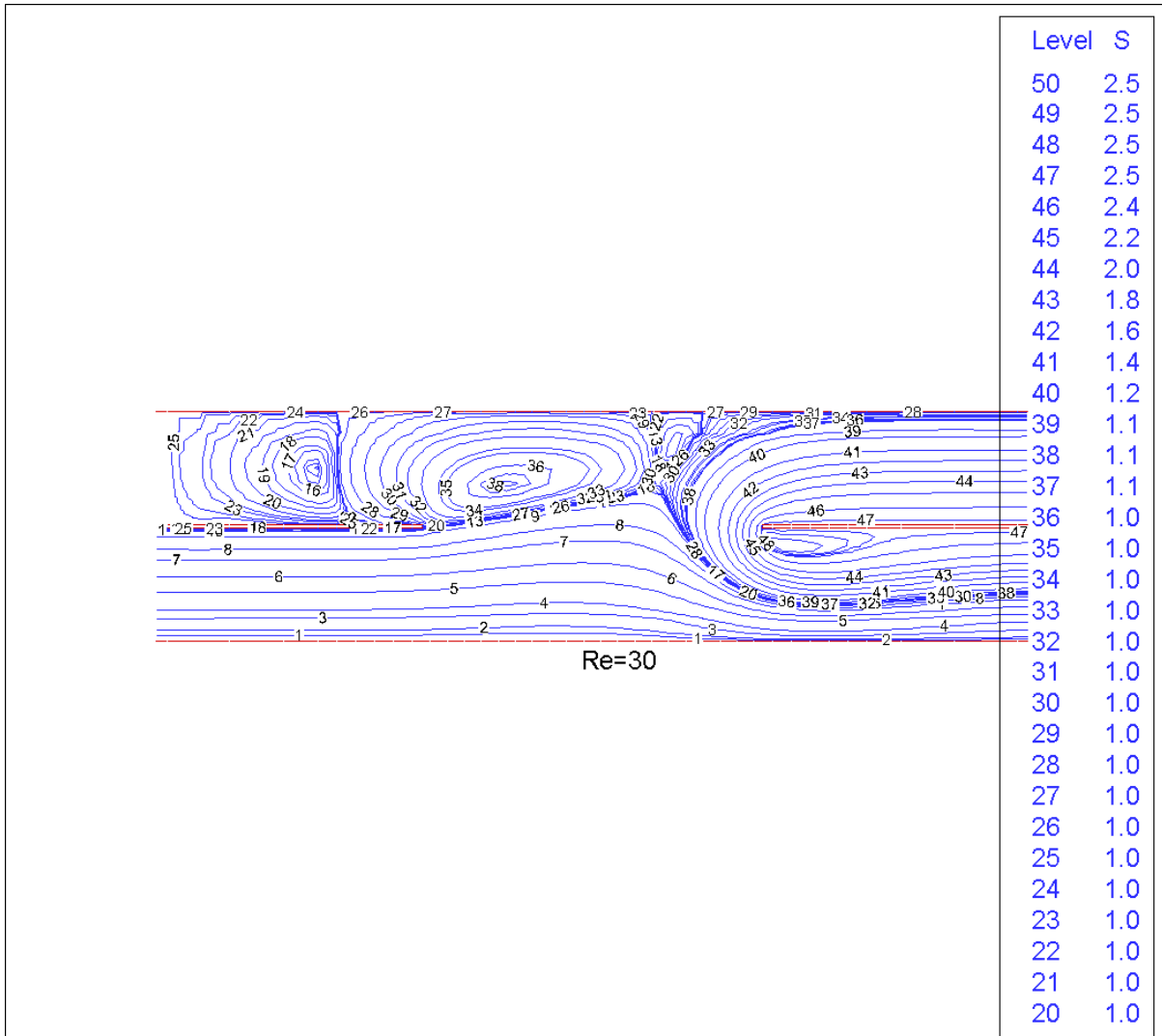


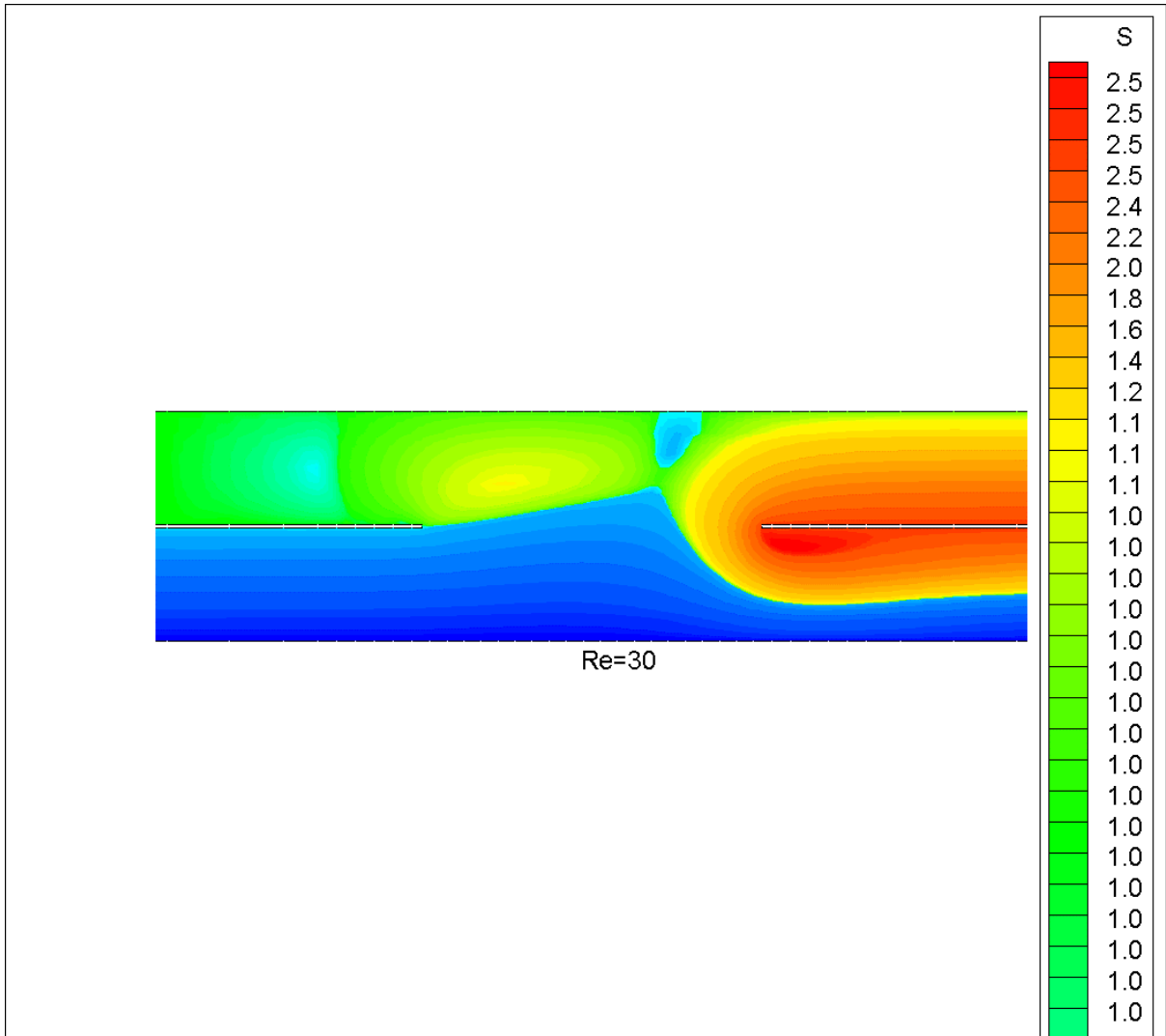


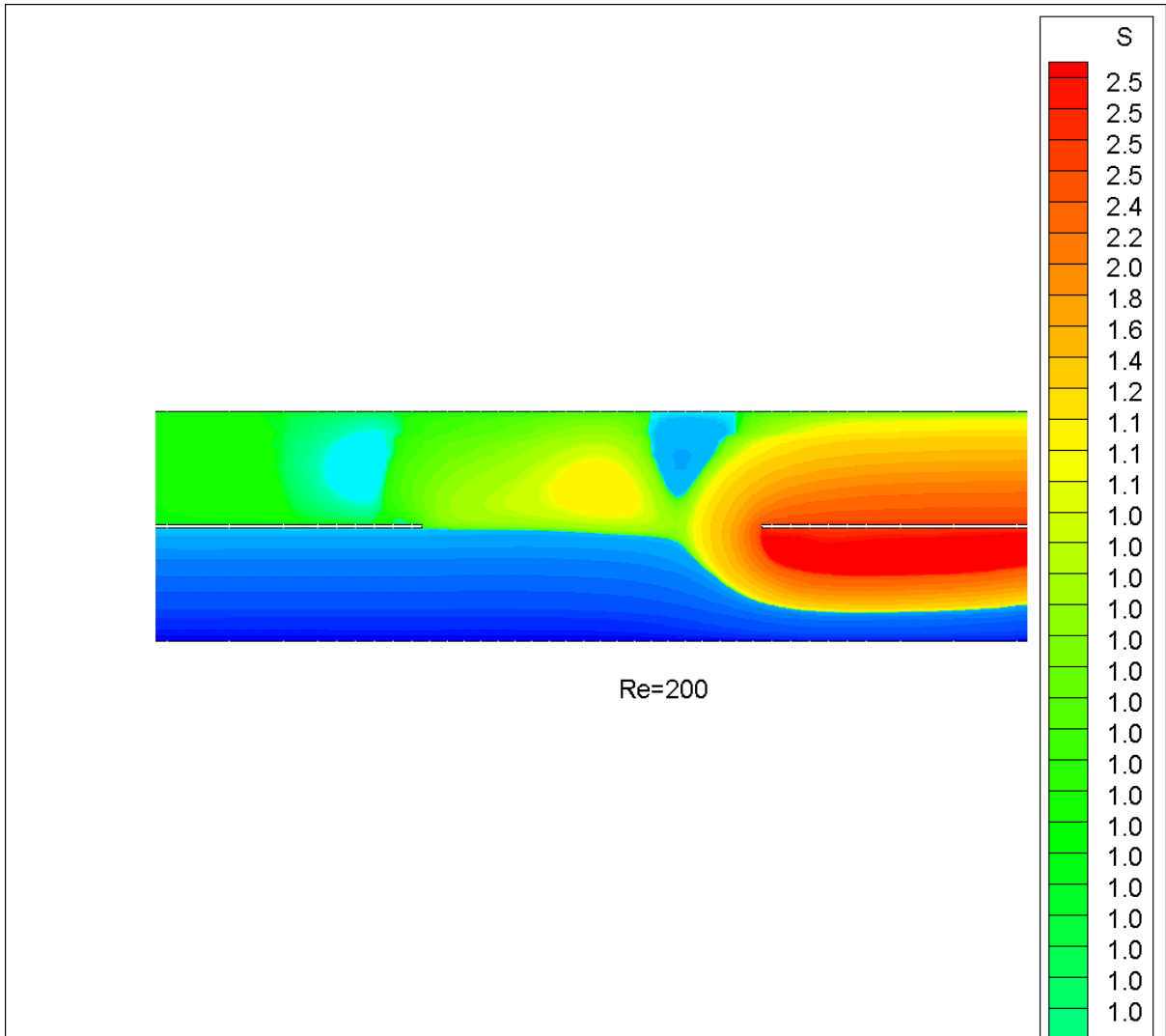


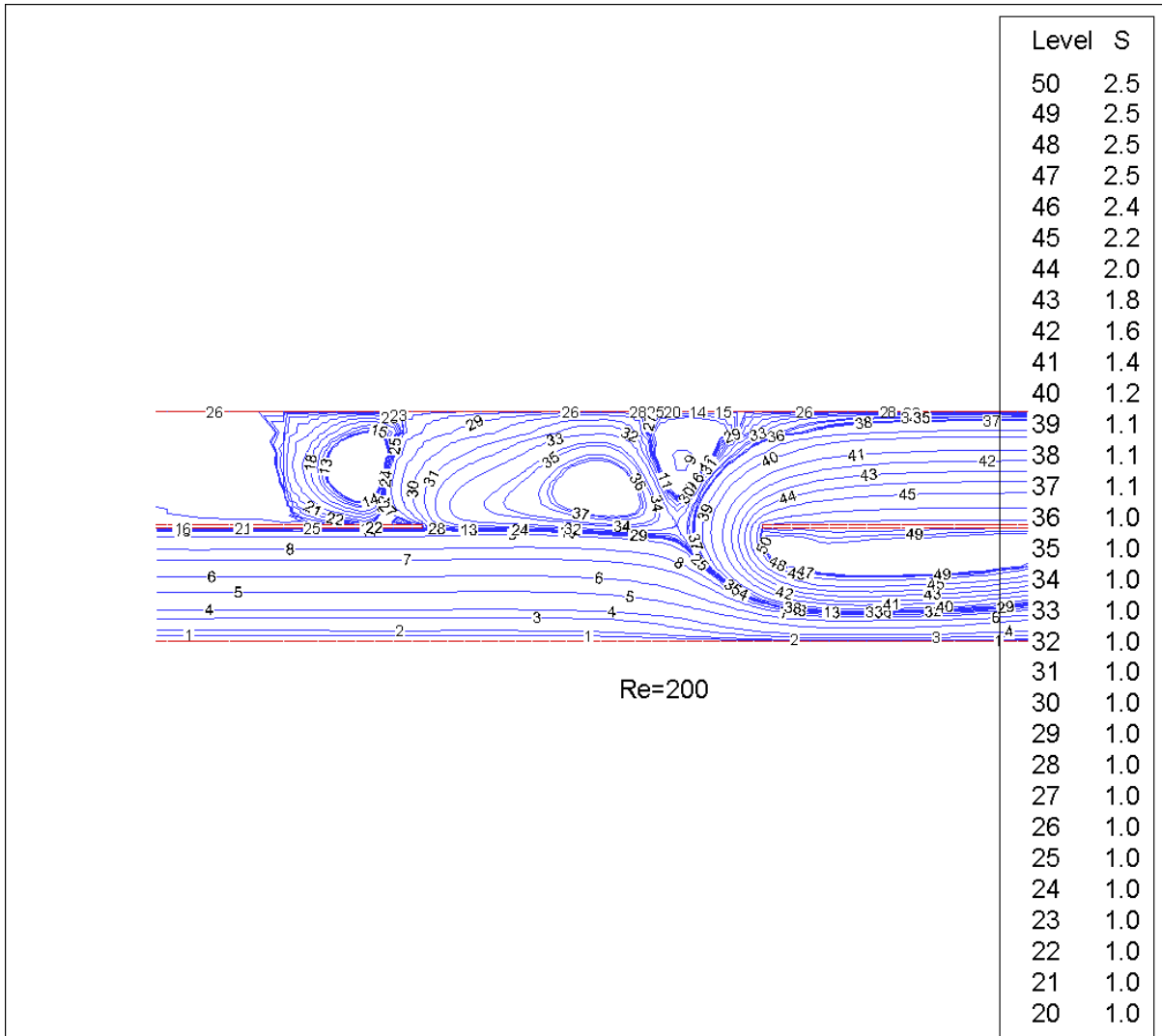


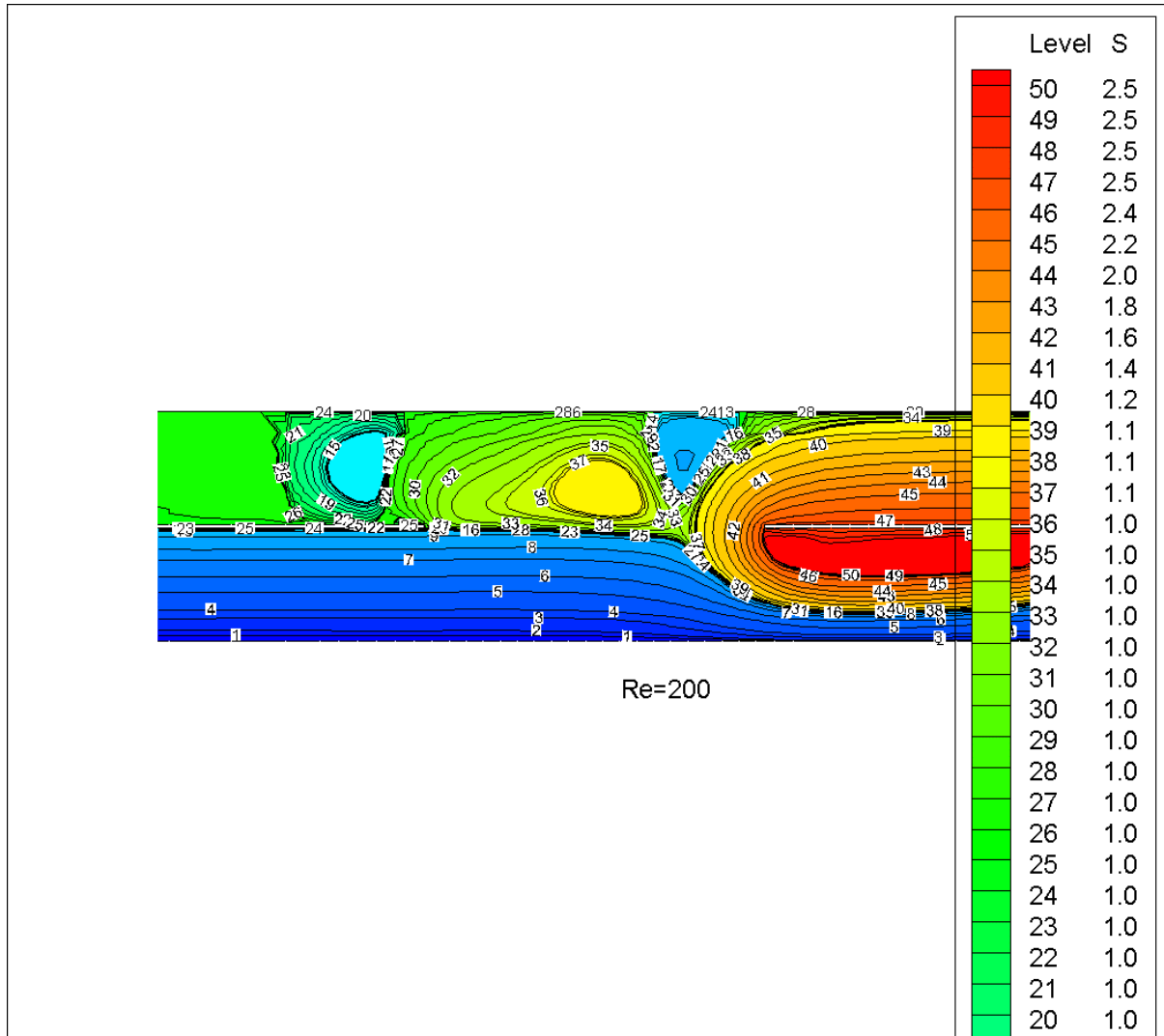




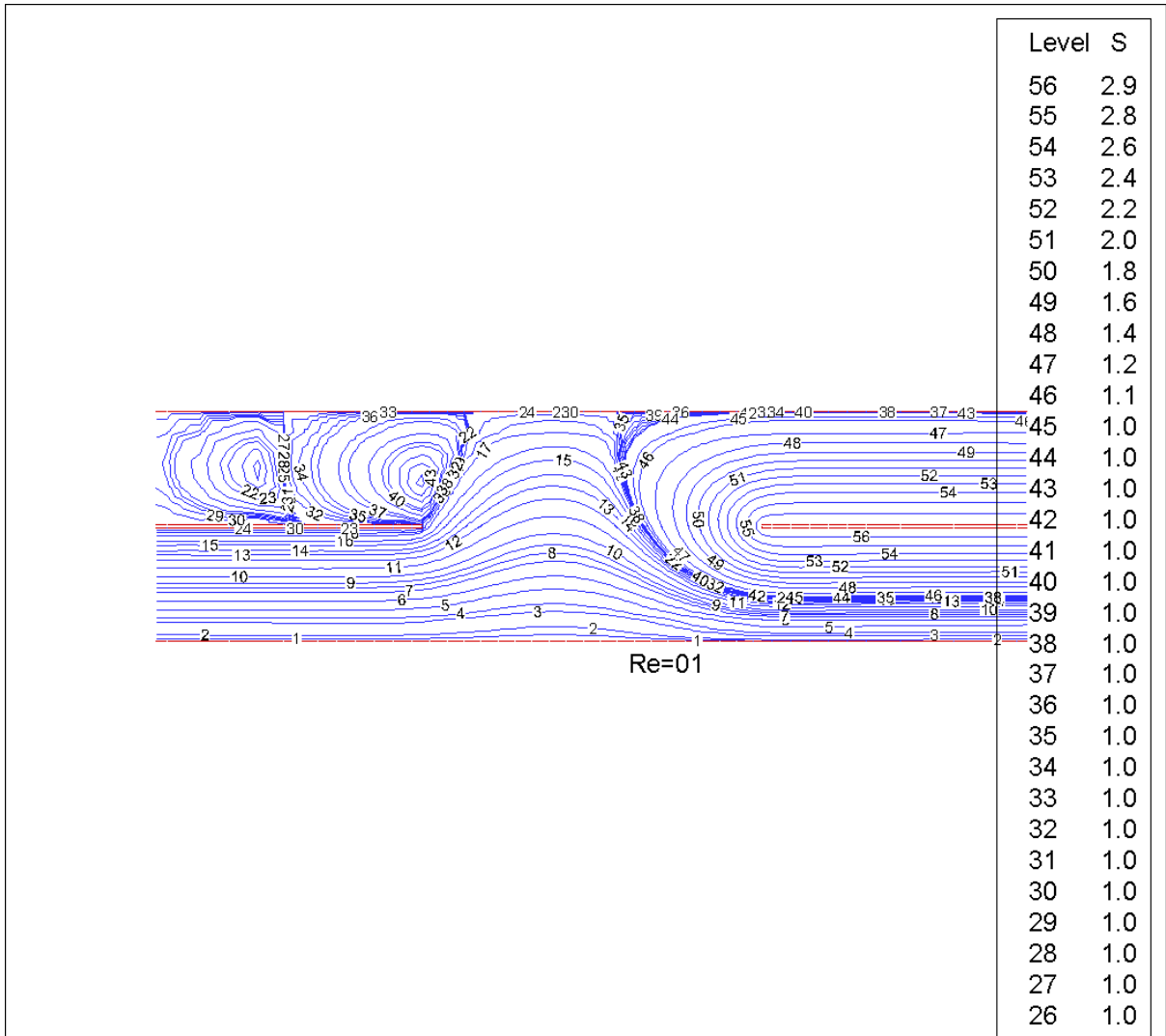


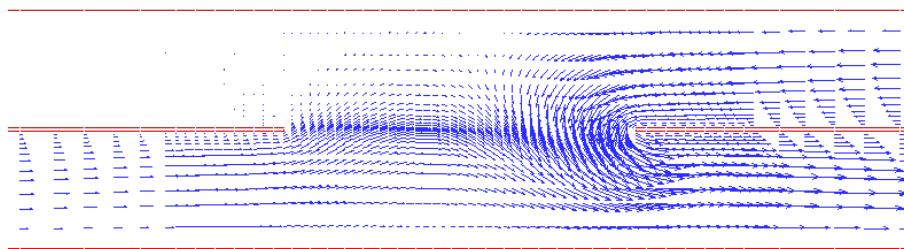
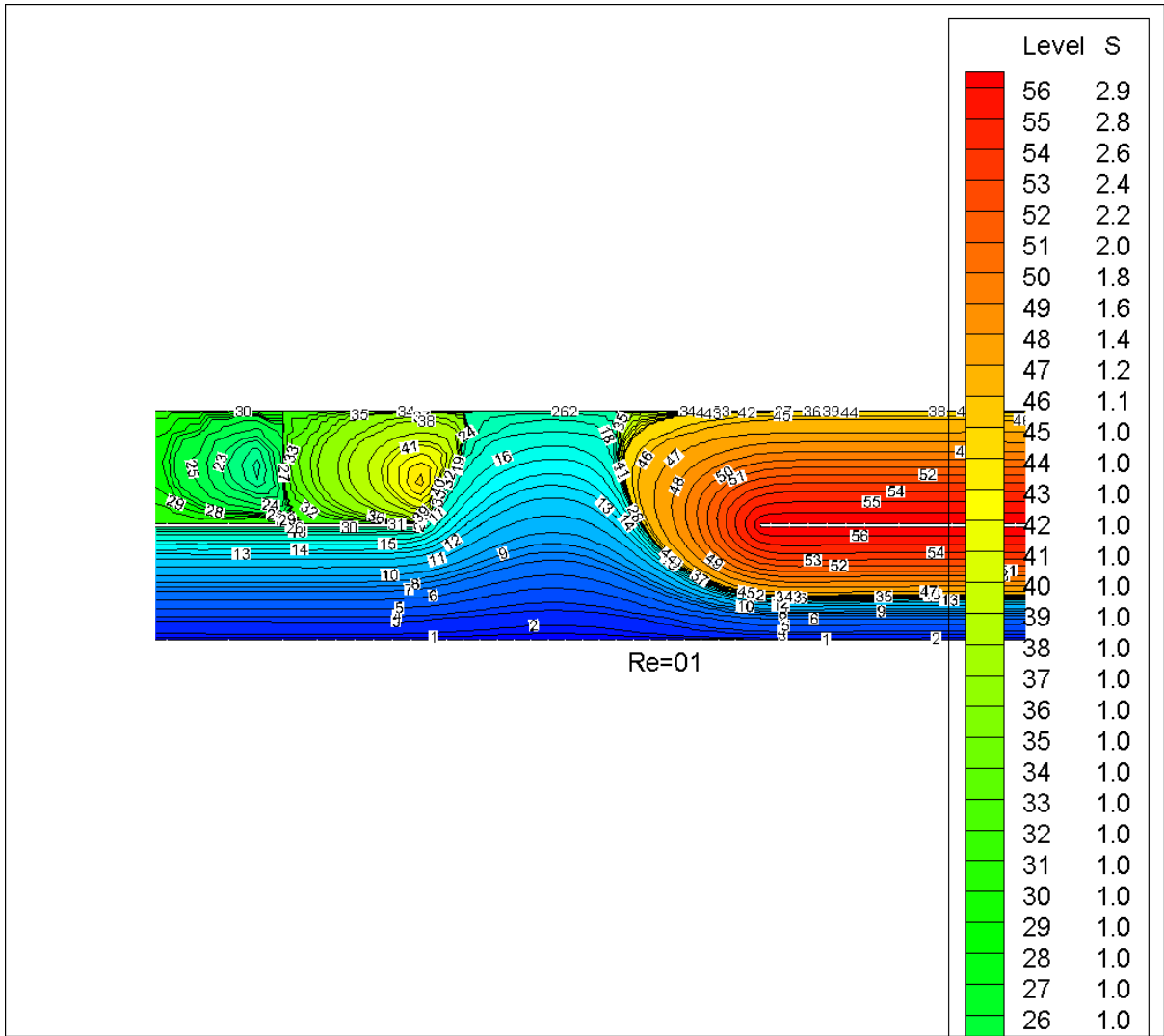




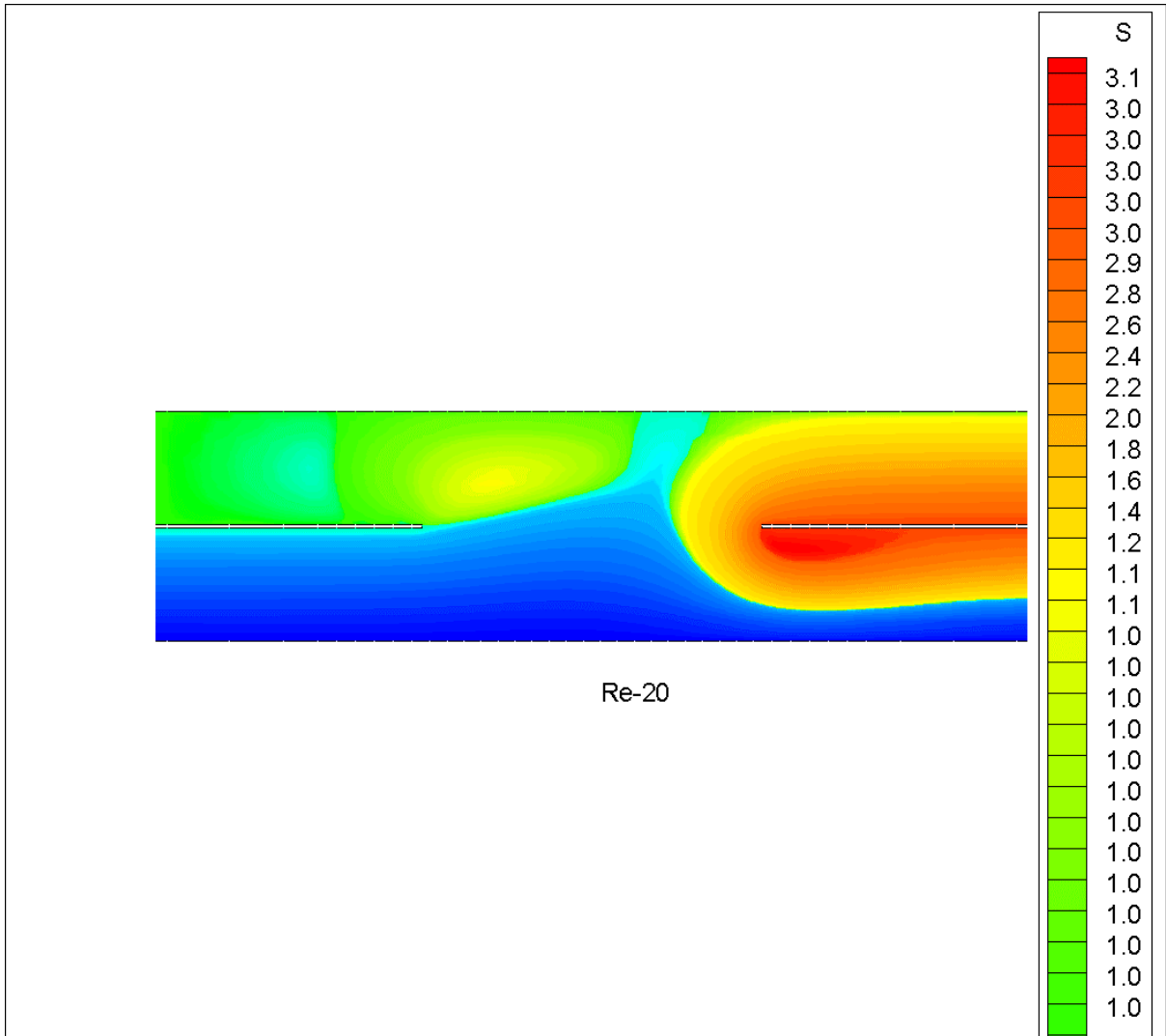


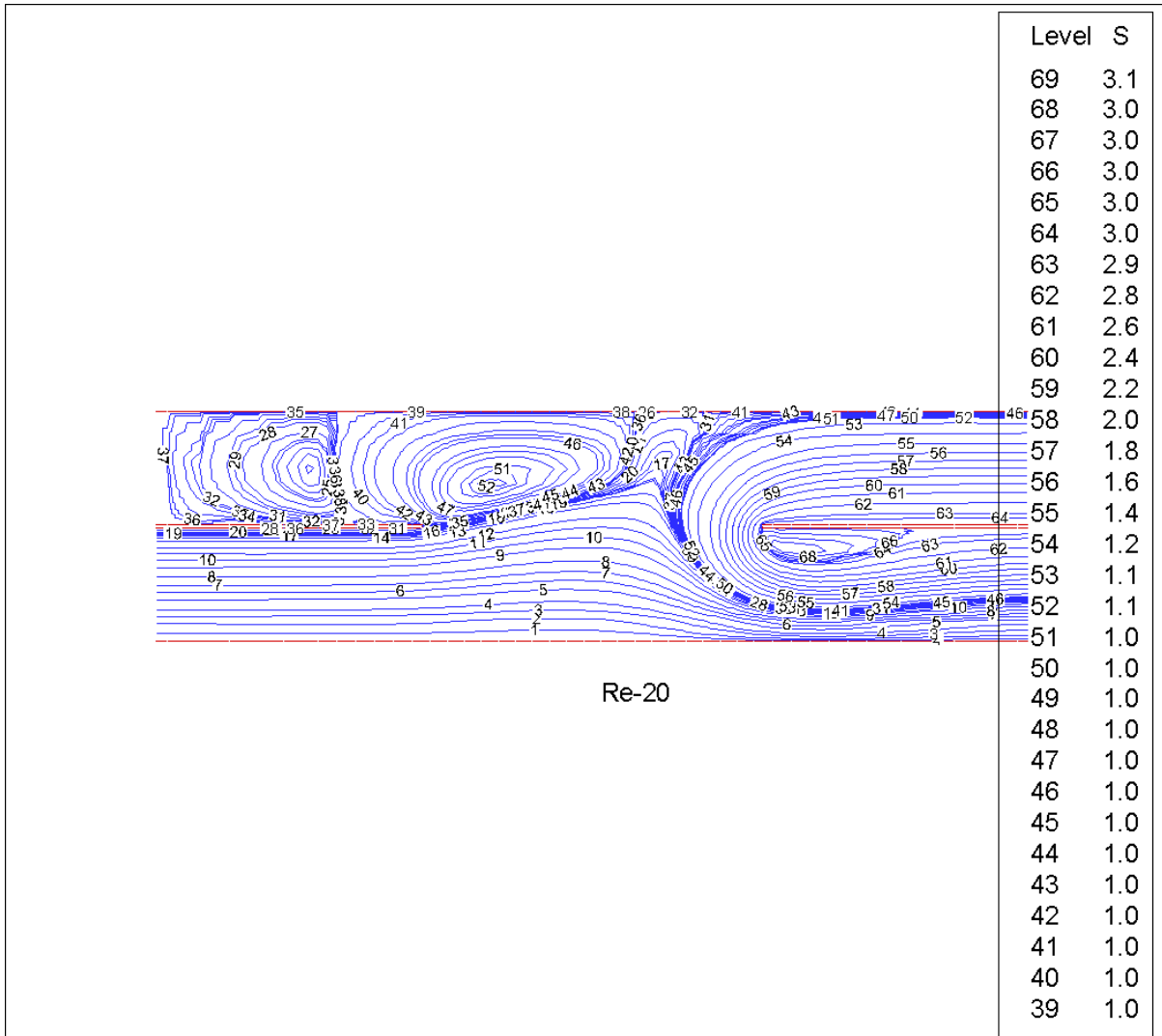


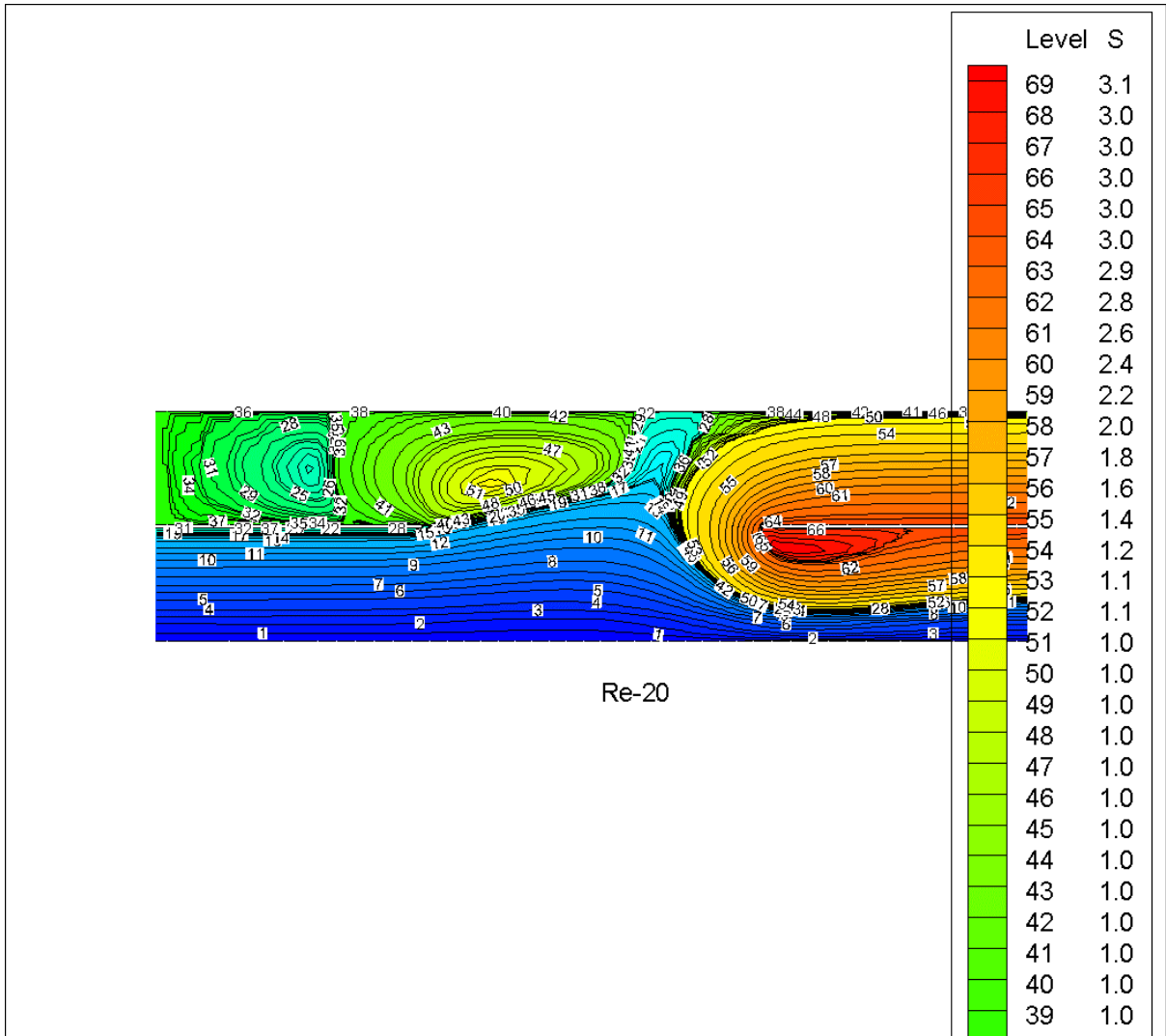




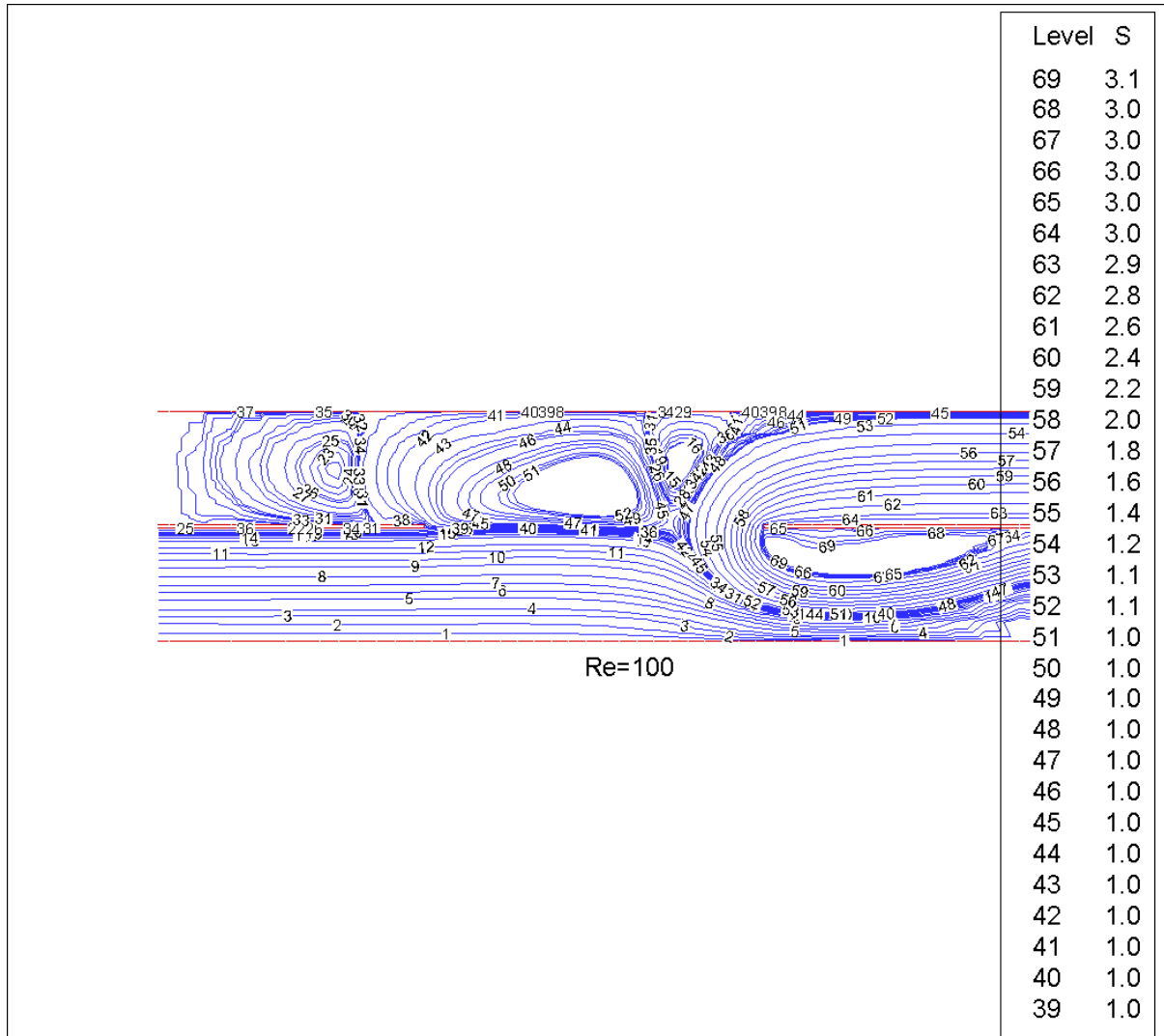
Re=01

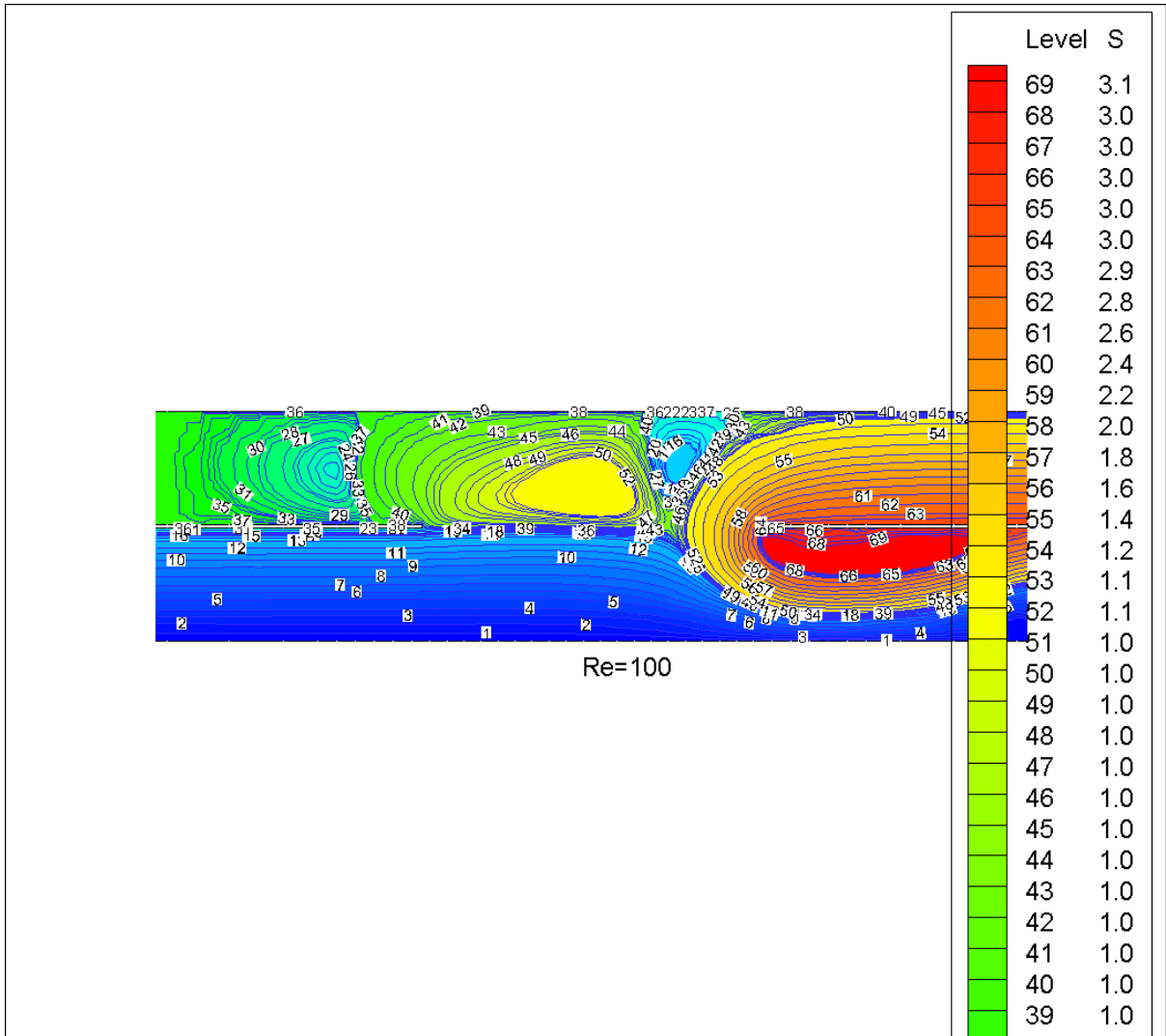








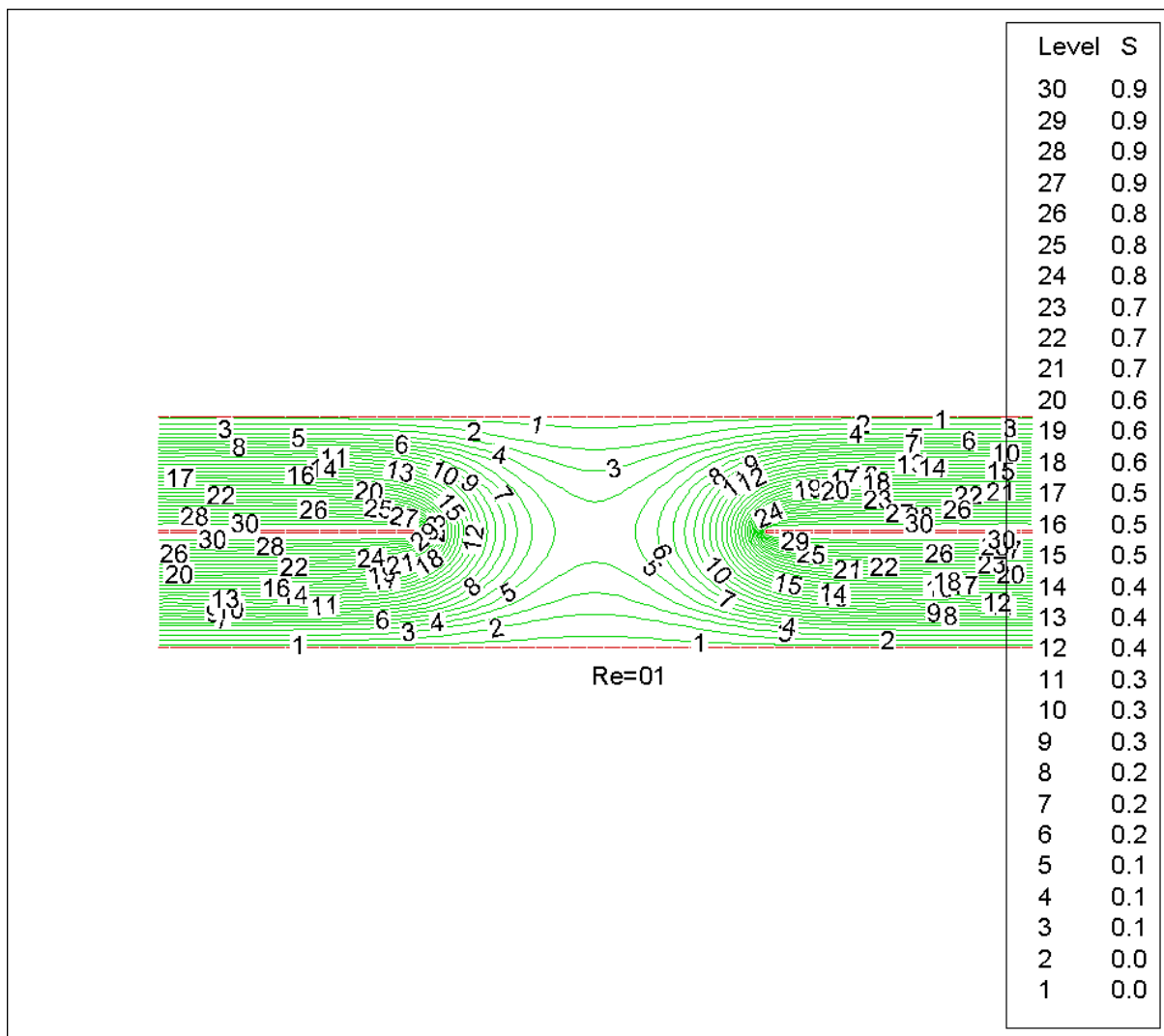


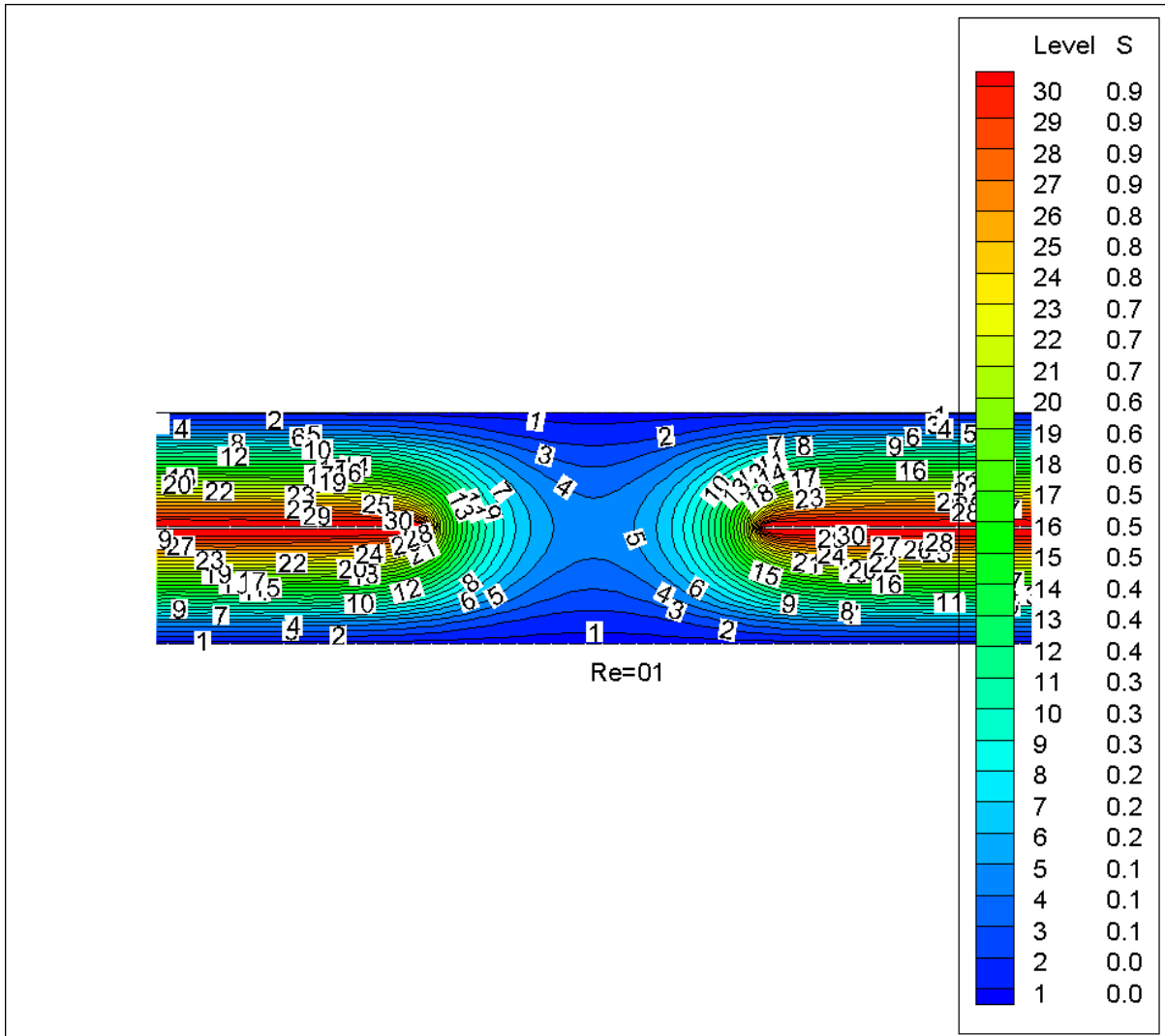


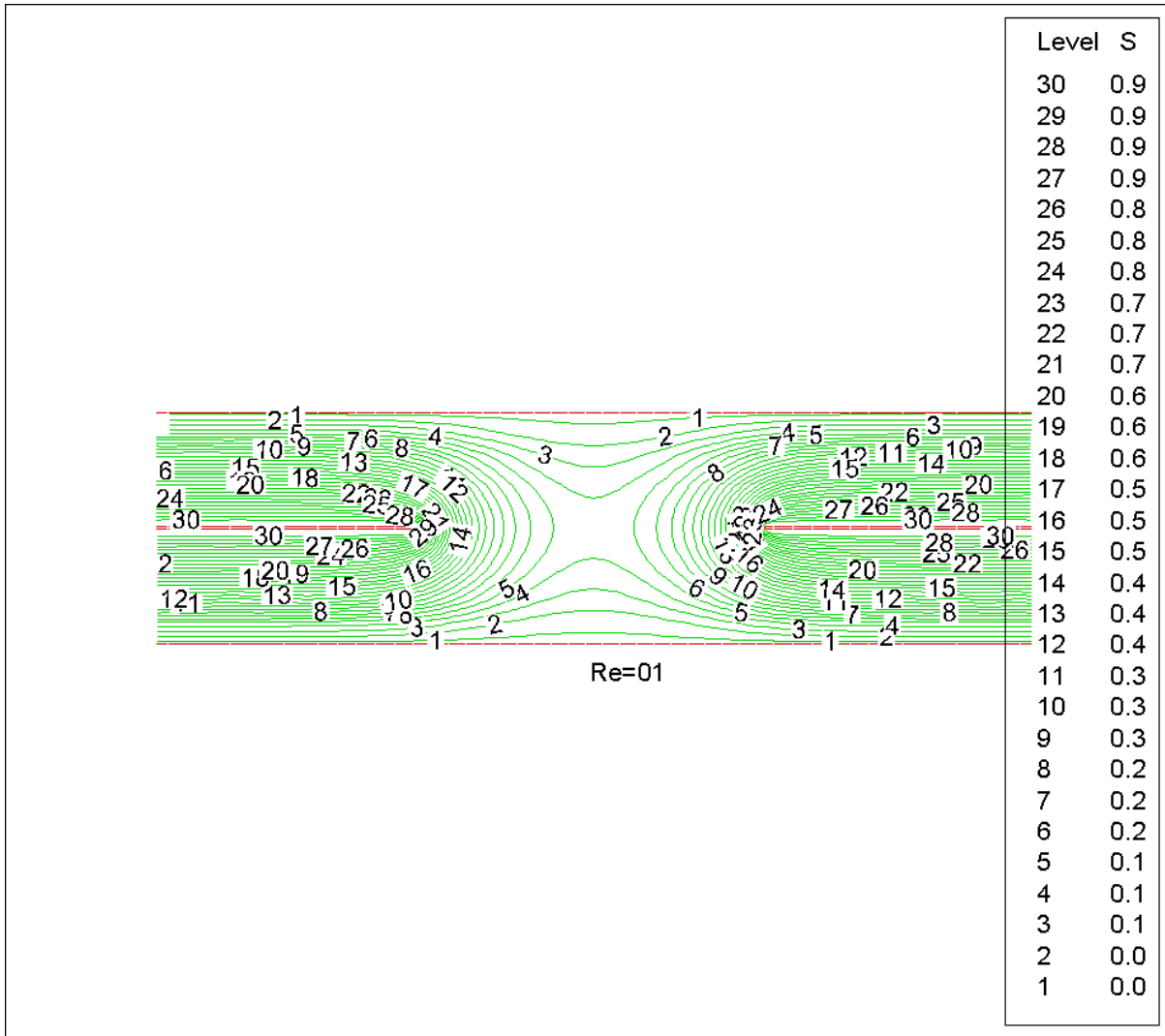
## 2. Chapter-6

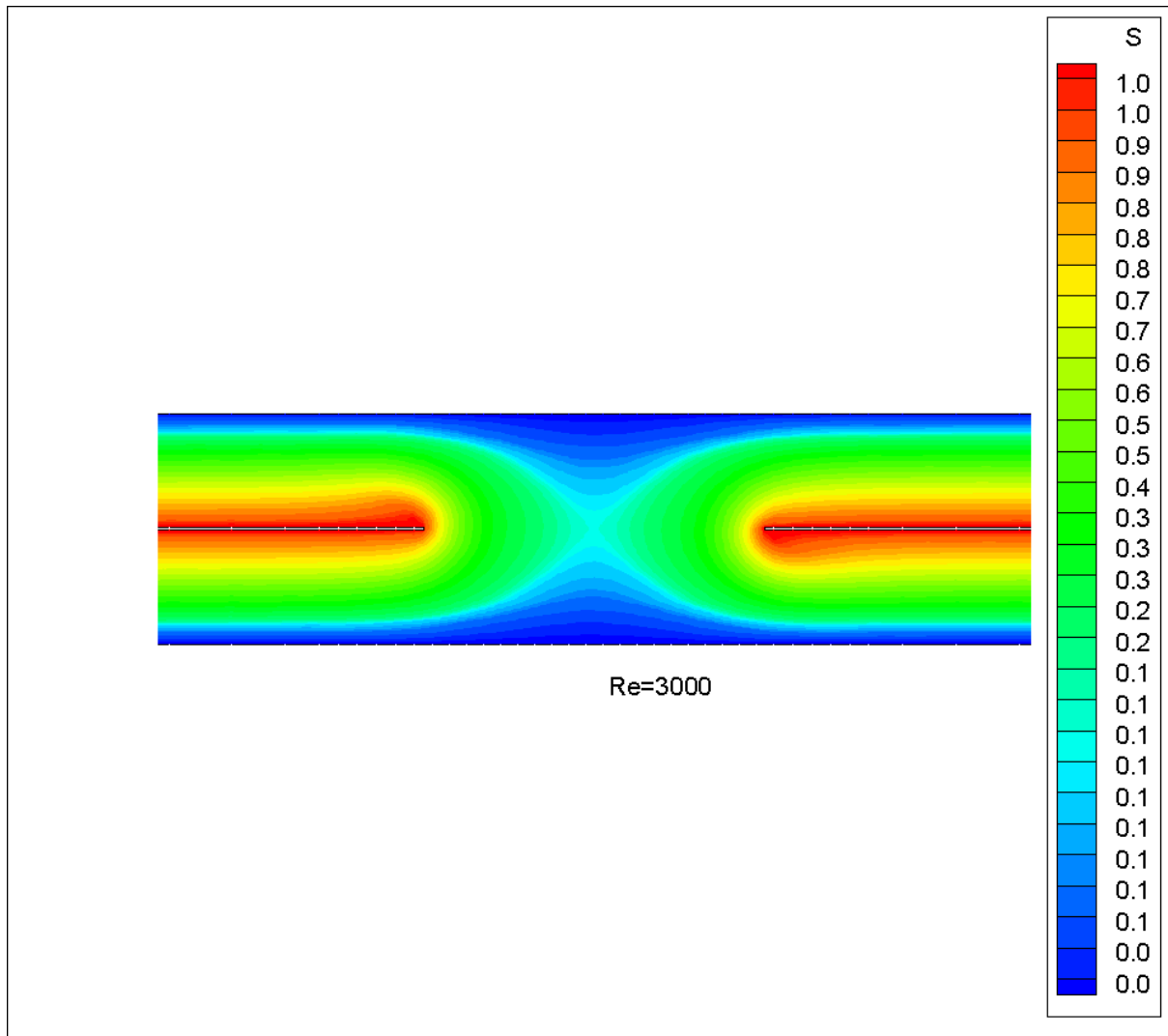
### 2.1 Mixing and separating of Newtonian fluid flows in a channel filled with porous media ( $G_1$ )

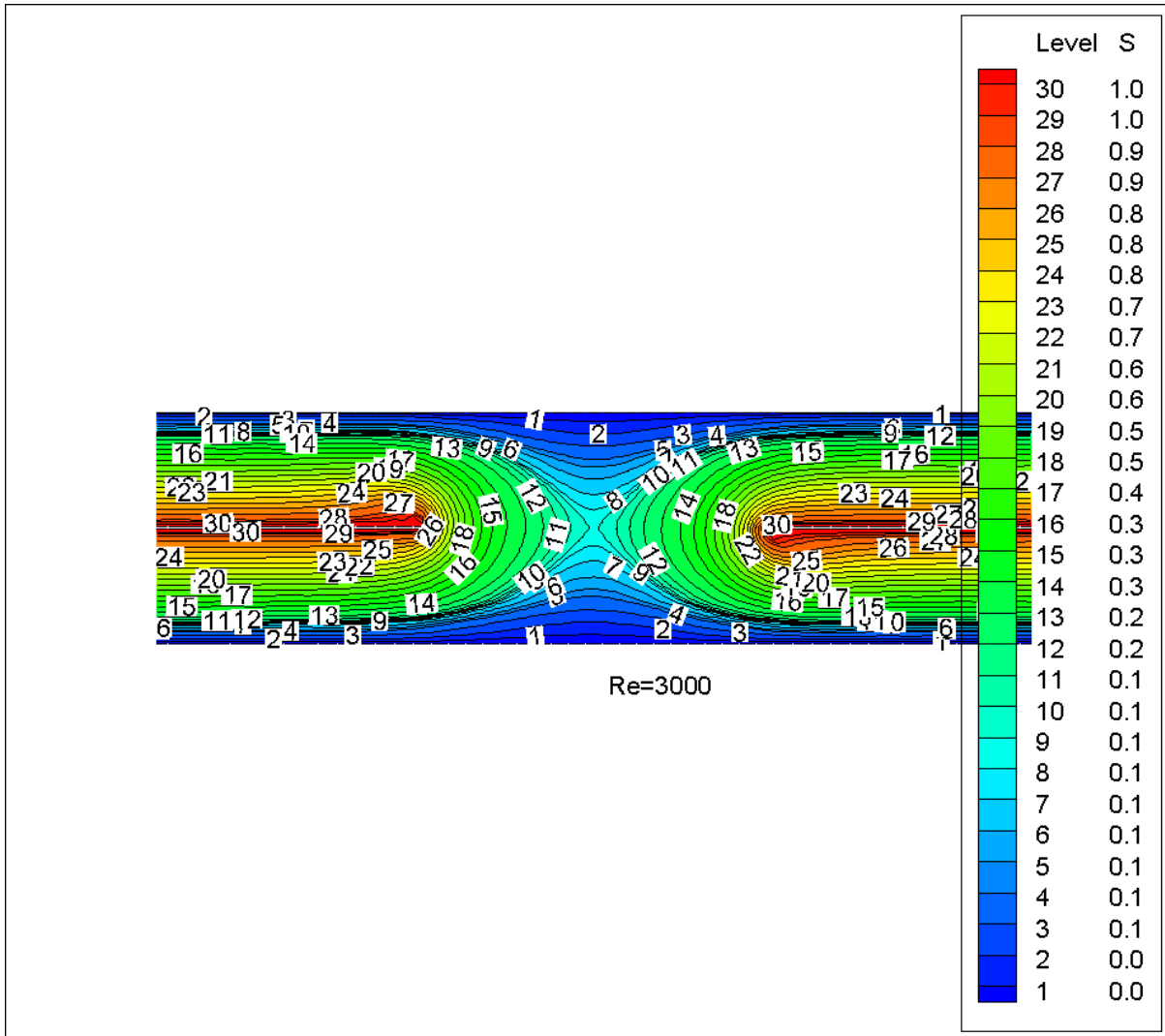
Equal (1, 1) flow rate

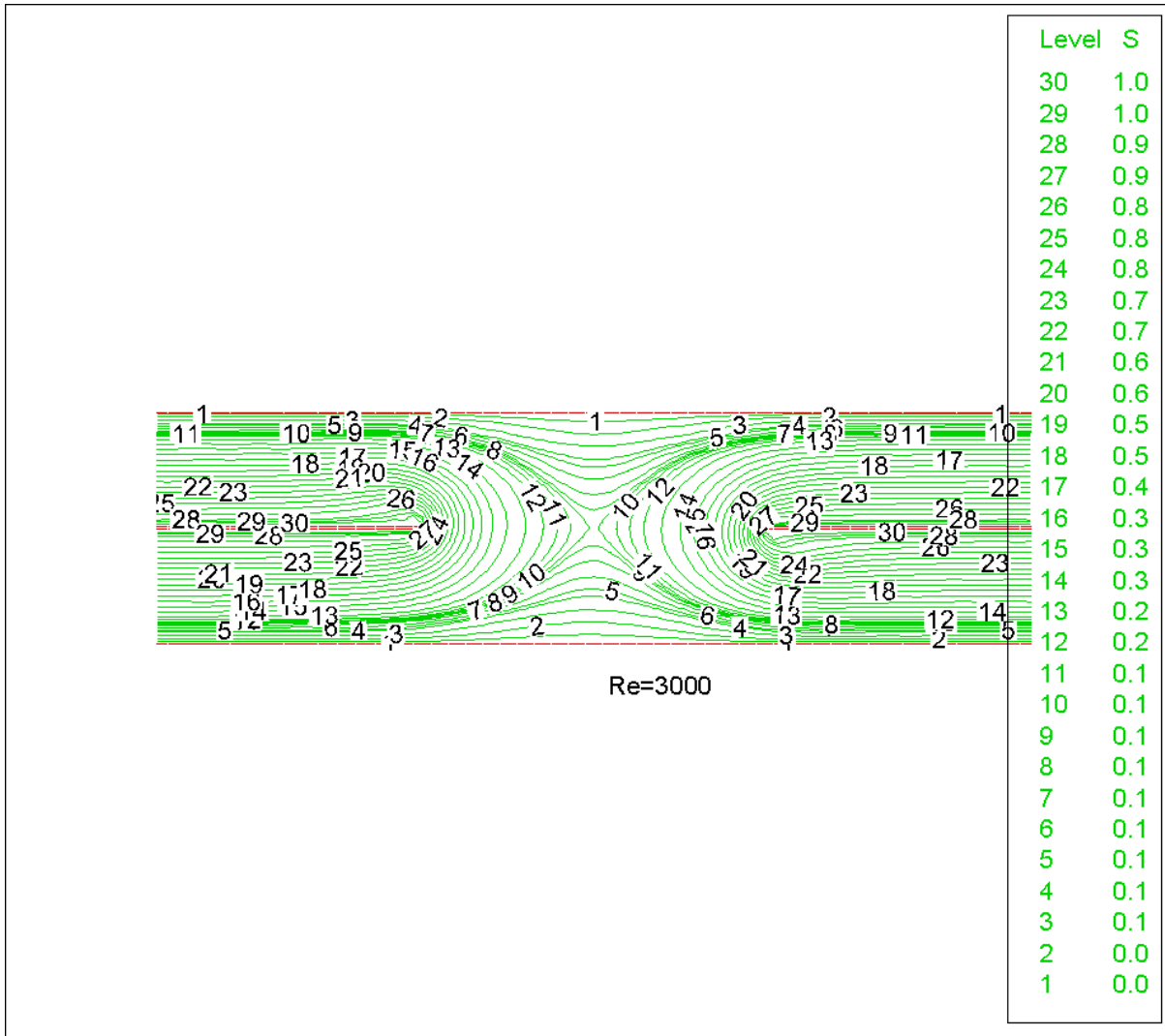


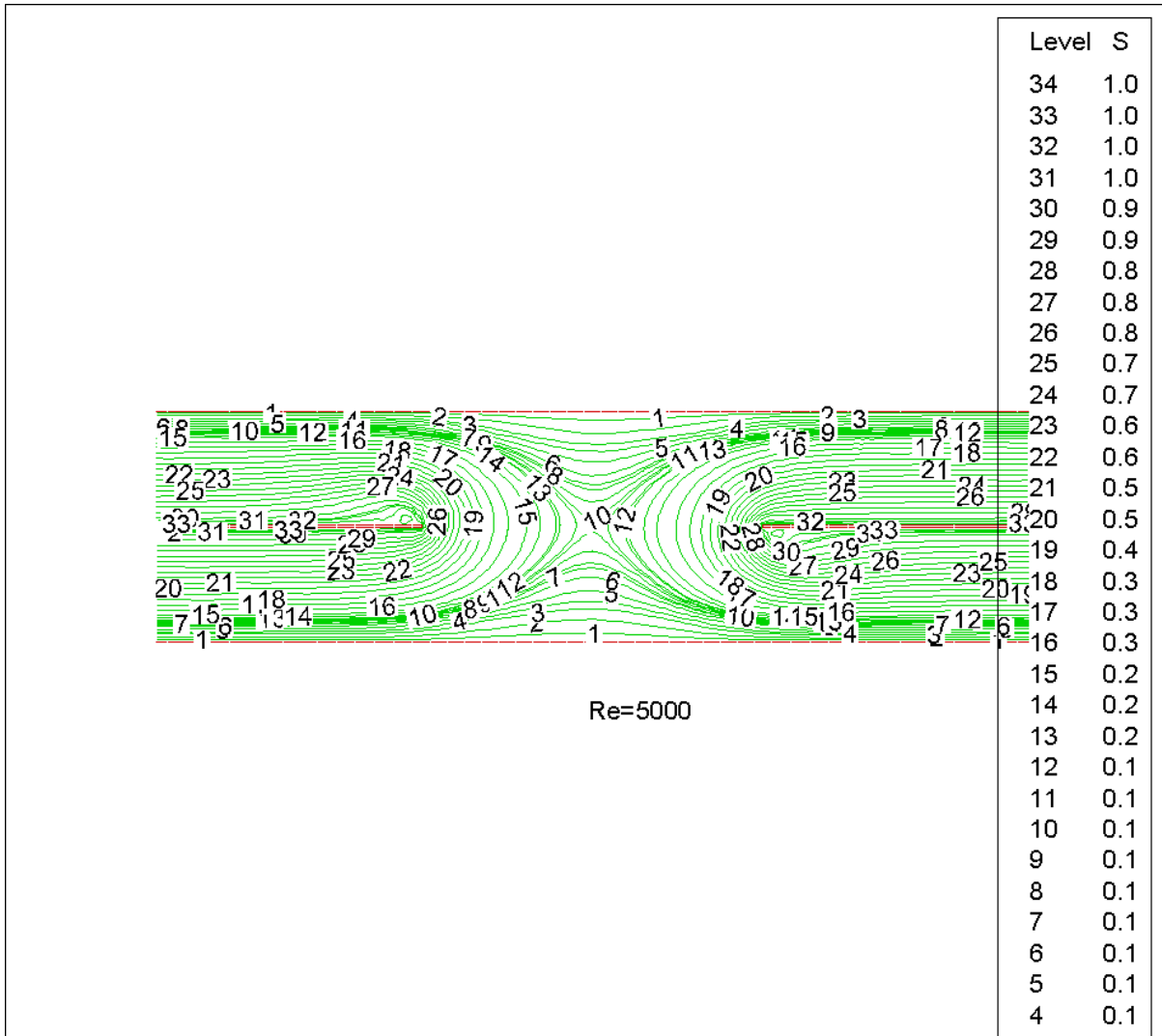


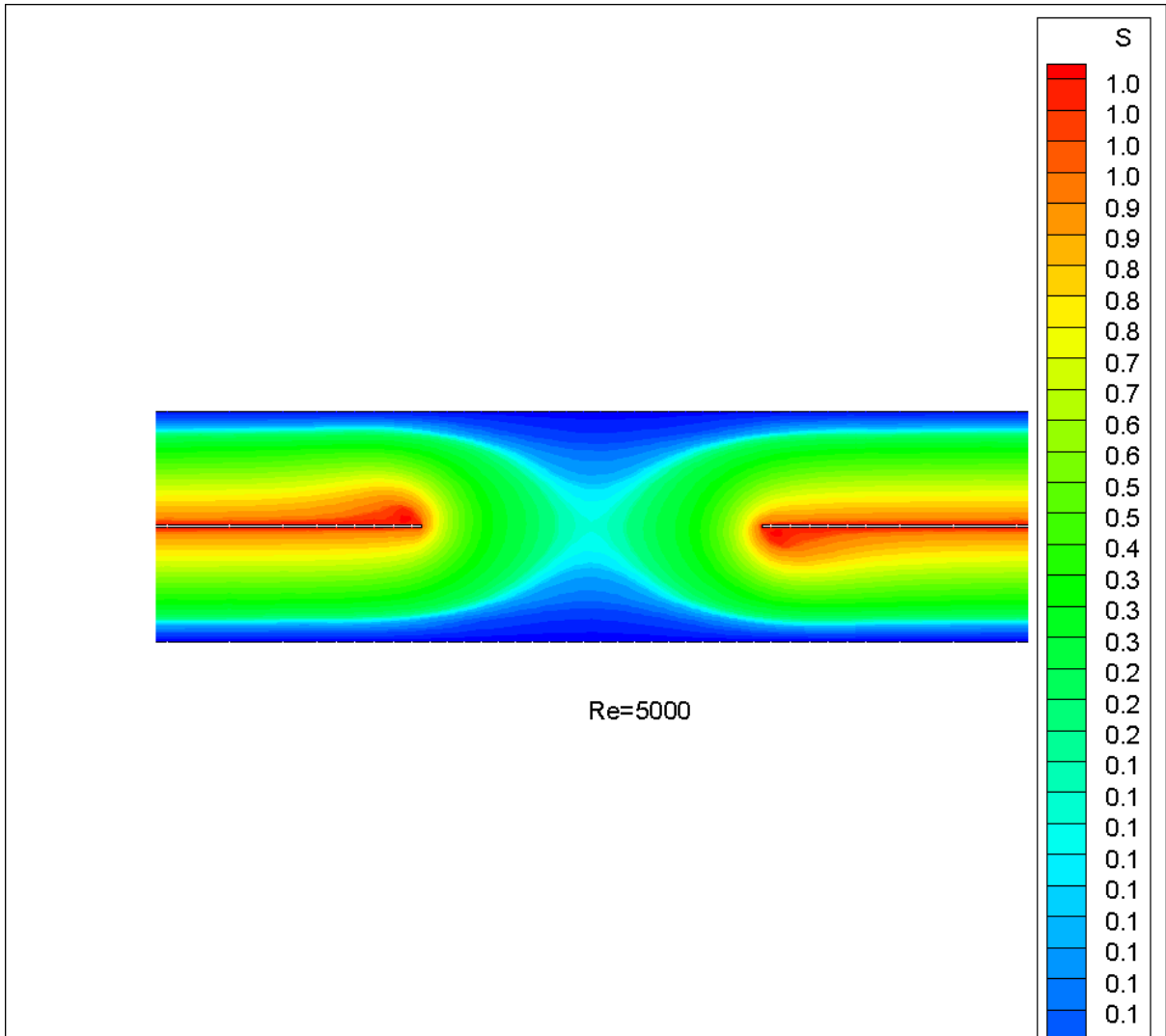


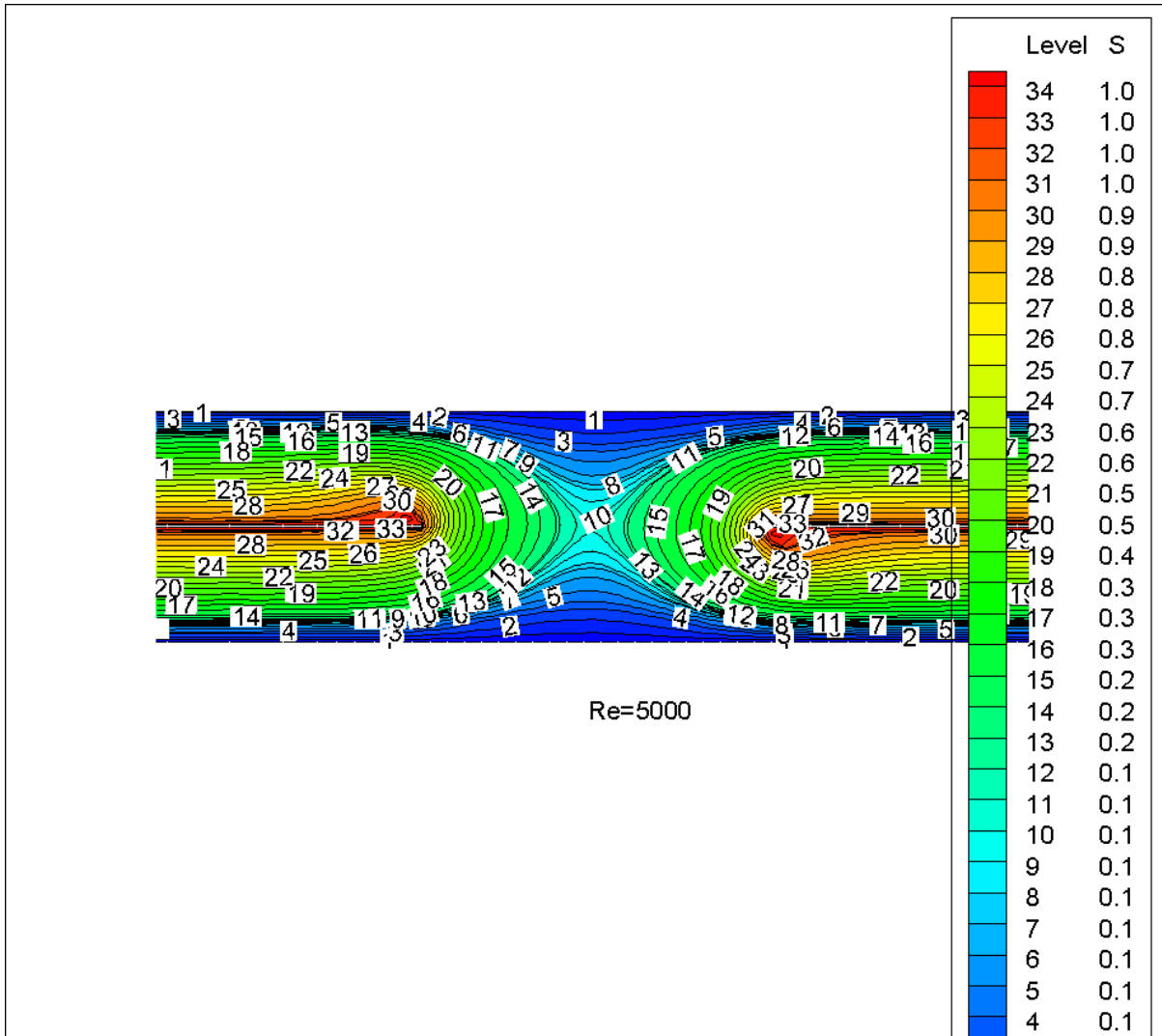




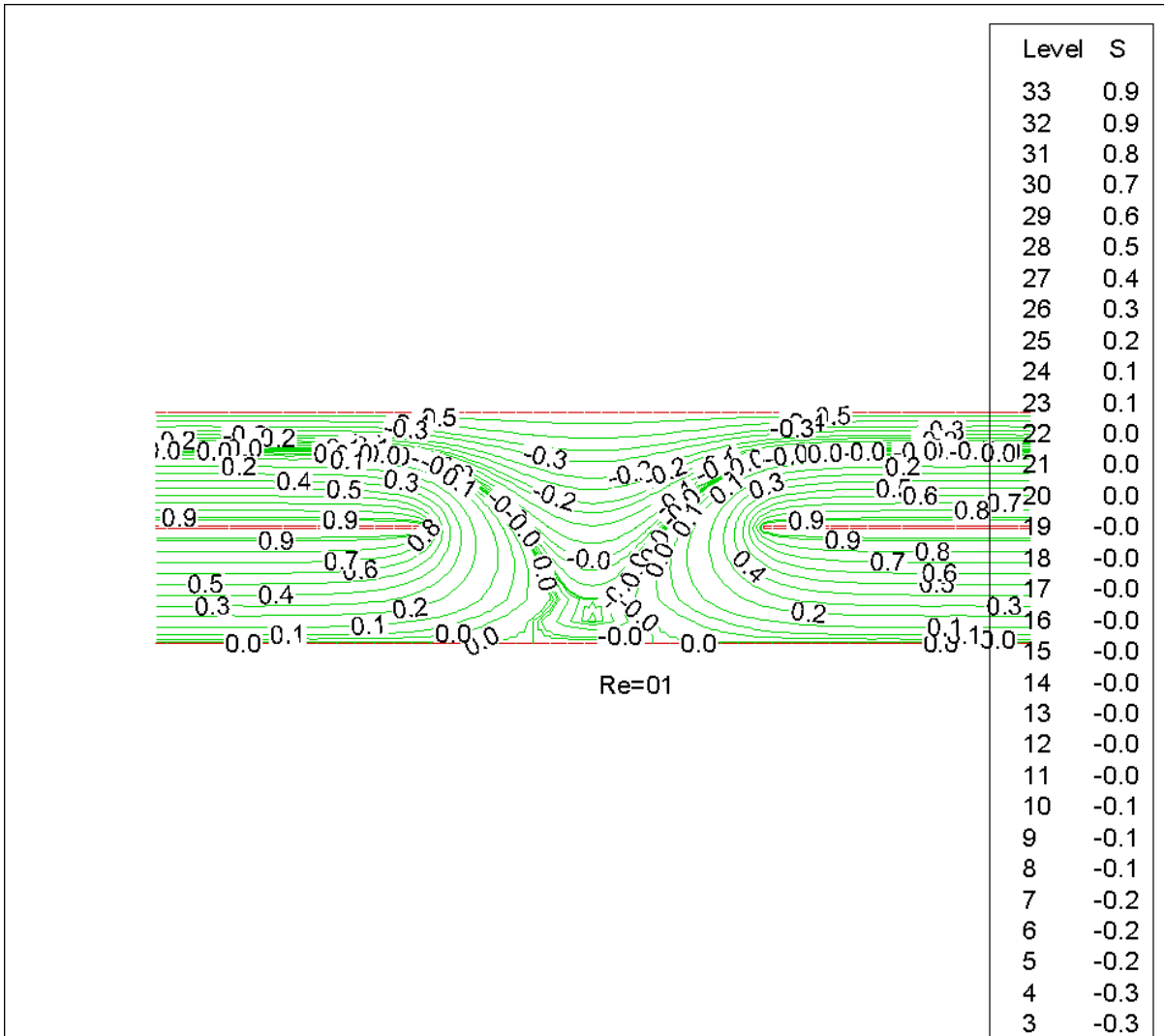


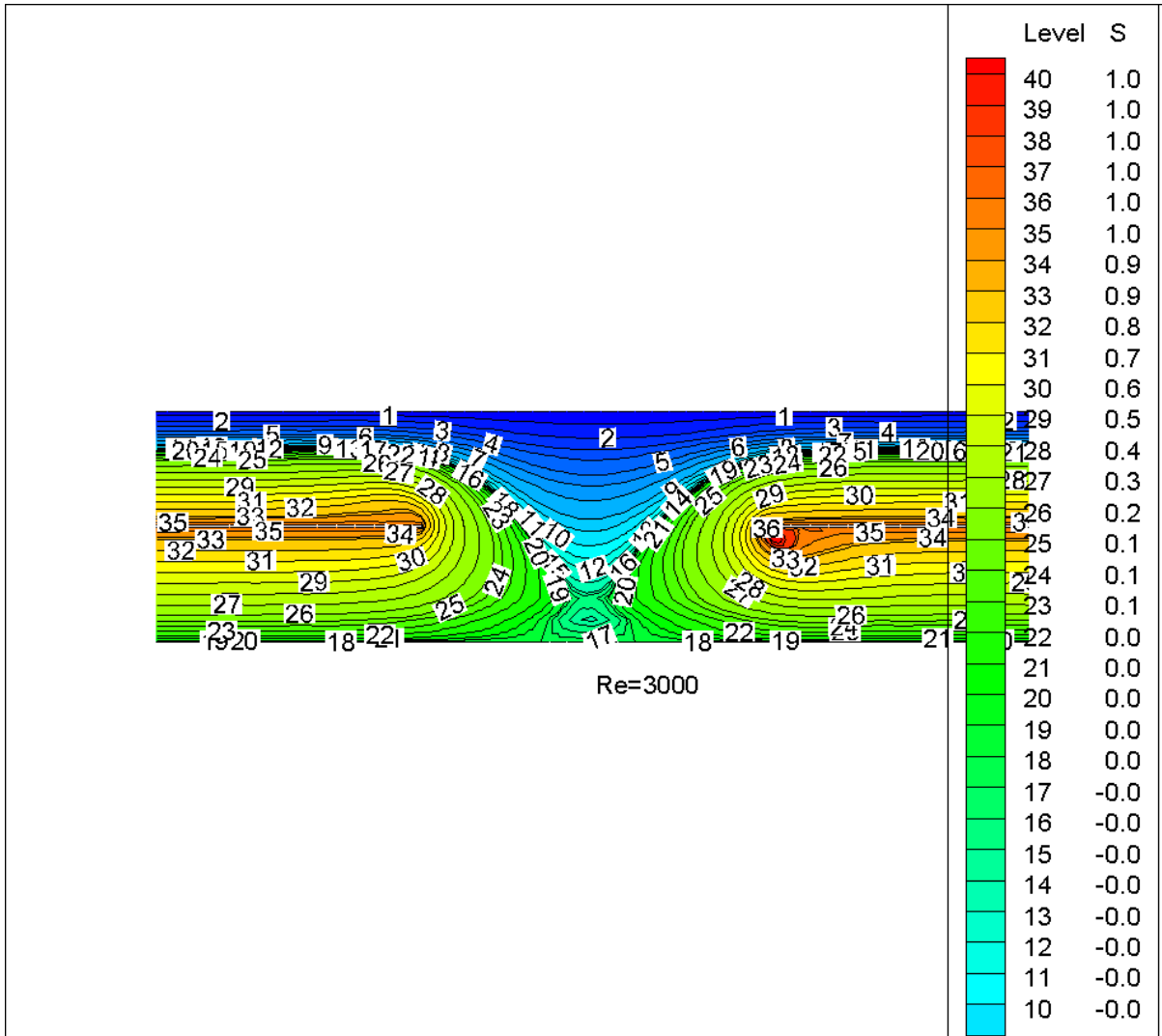






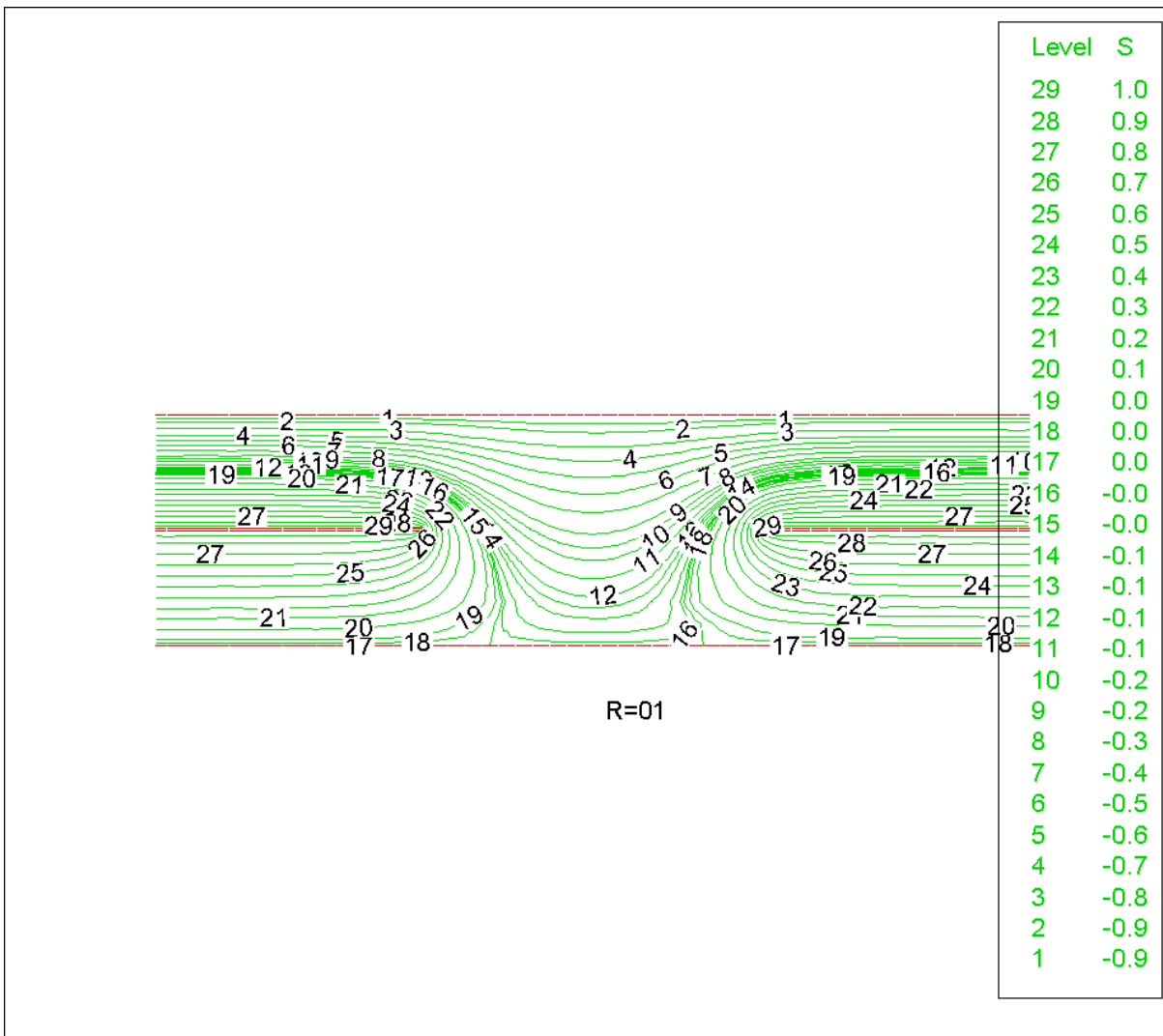
Unequal (1, 1.5) flow rate

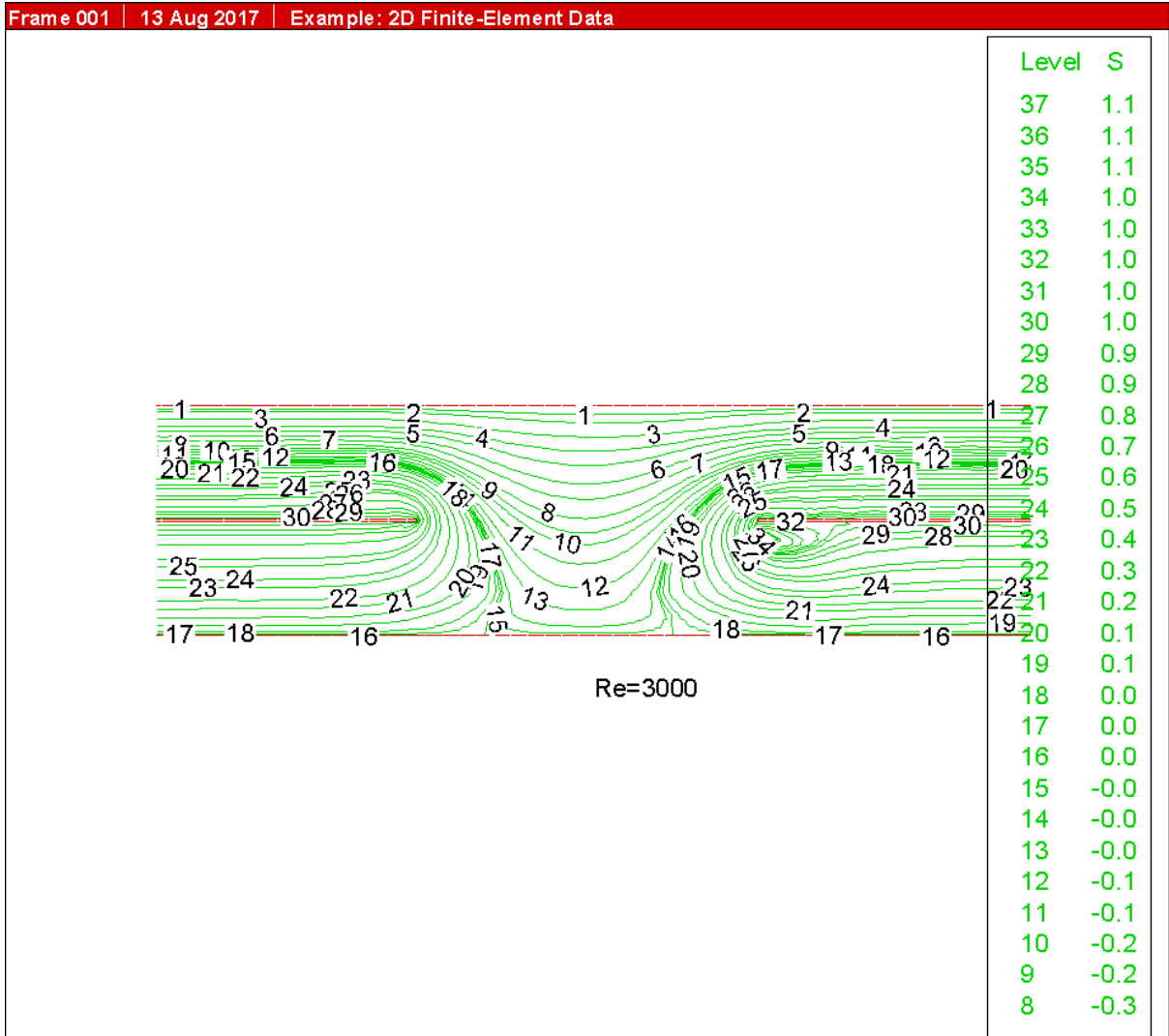




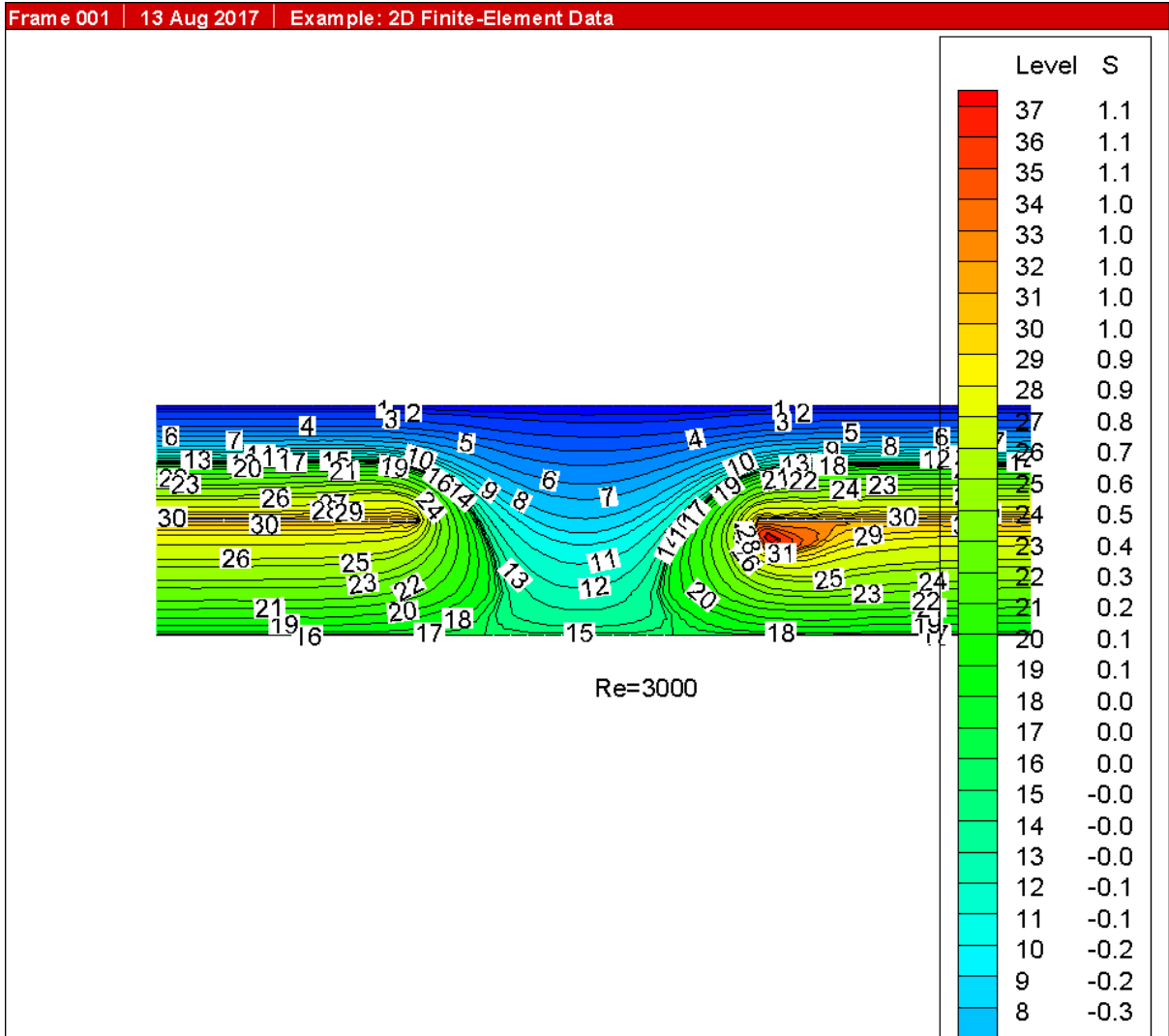


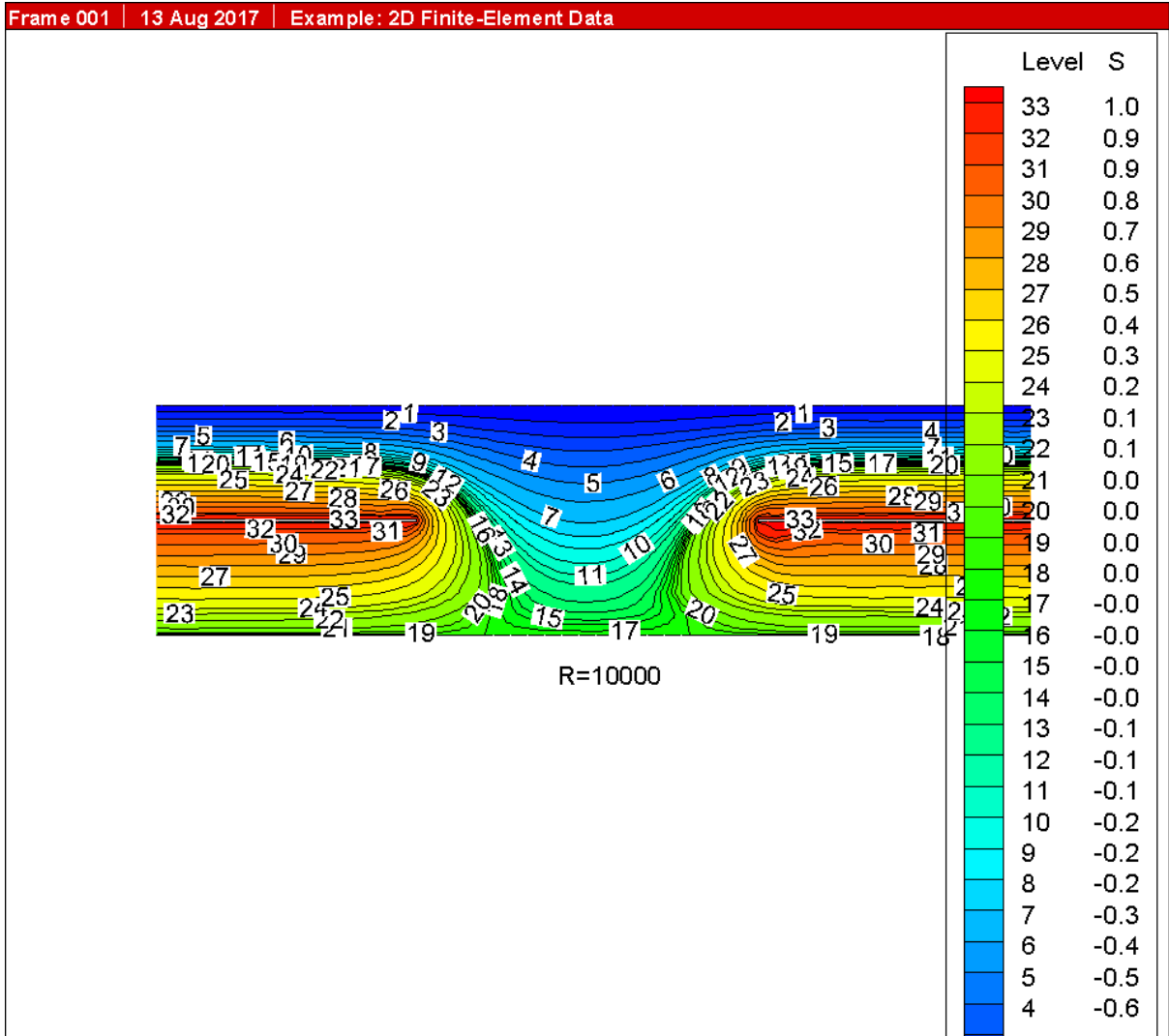
Unequal (1, 2) flow rate

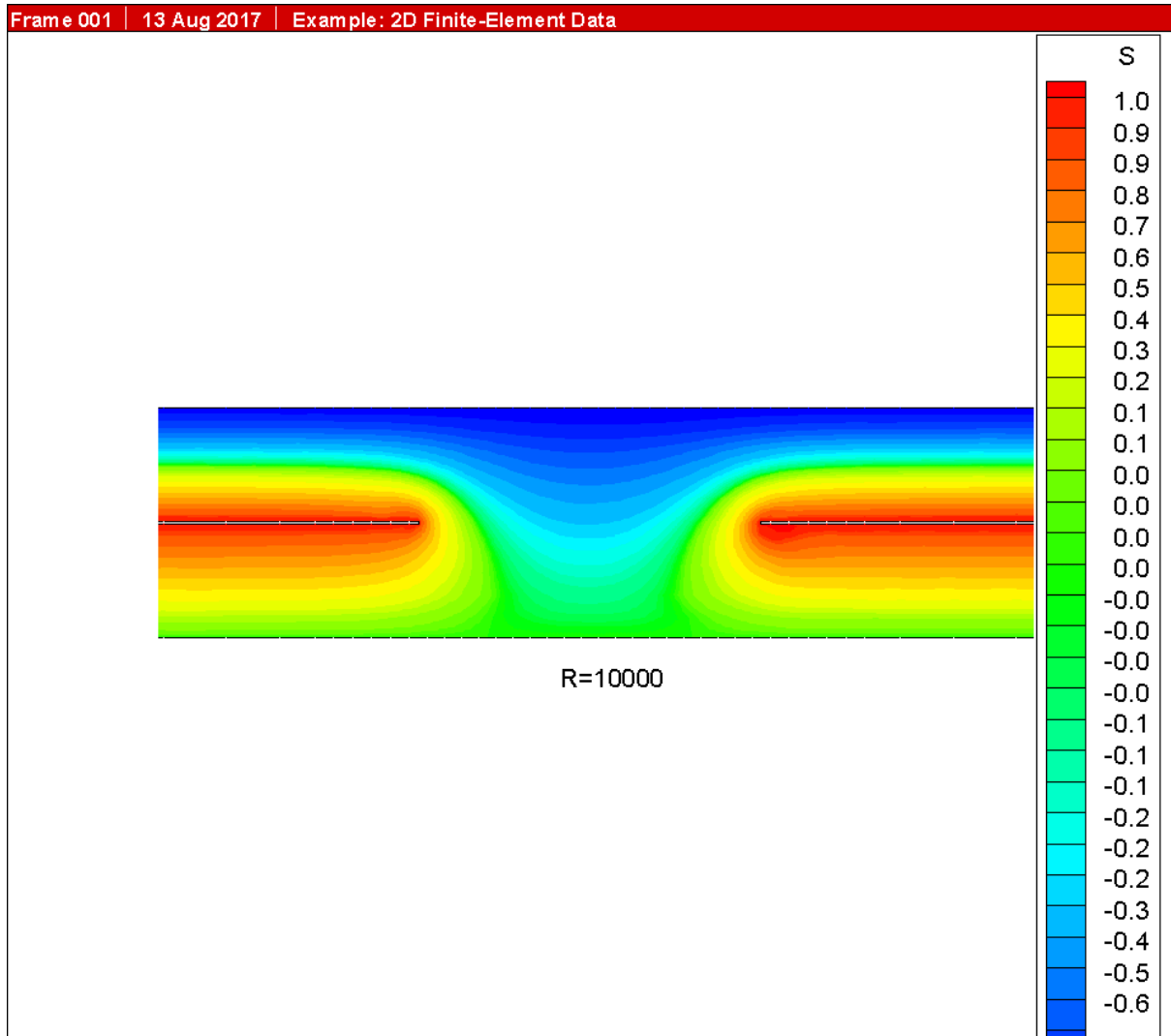


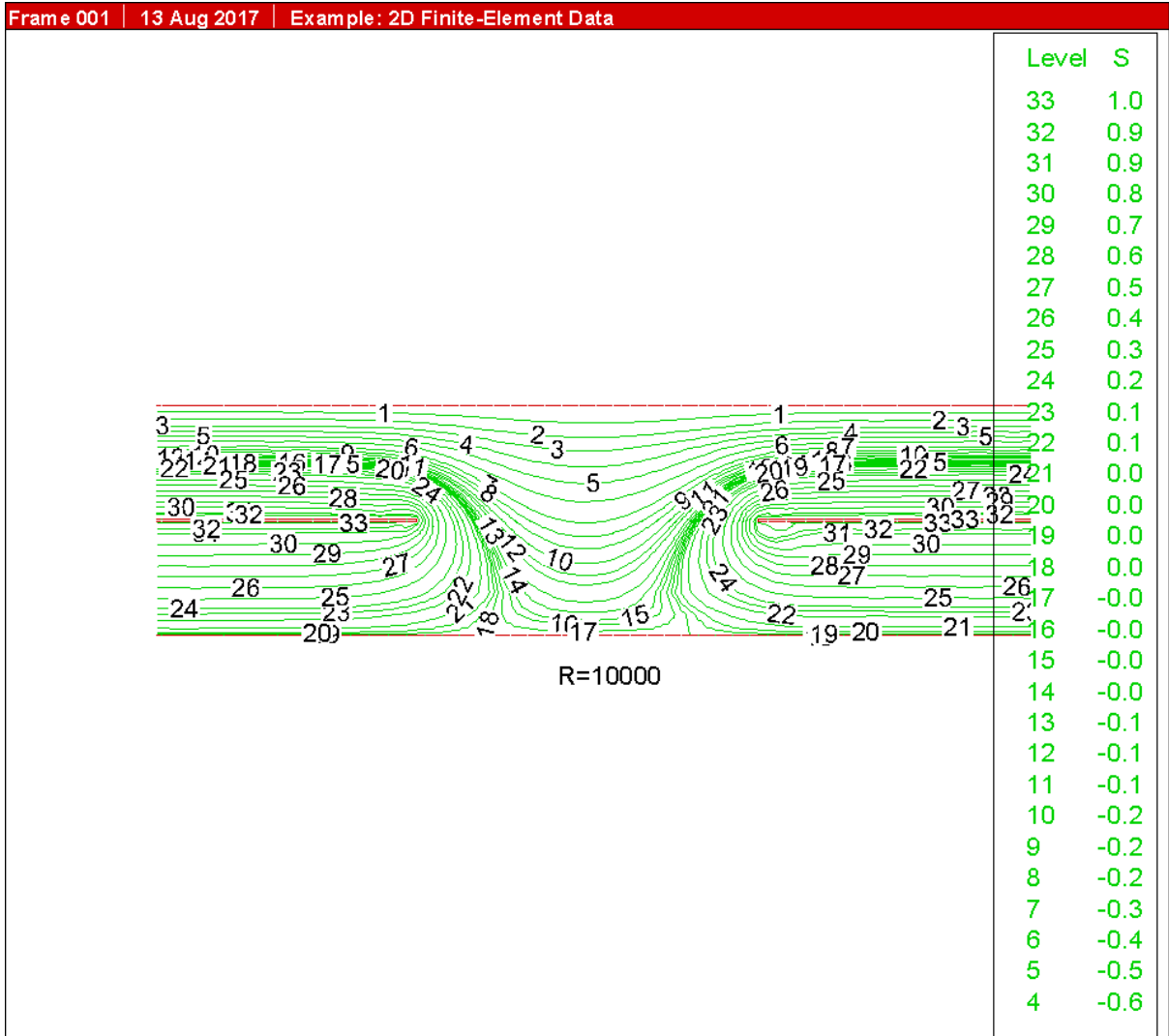










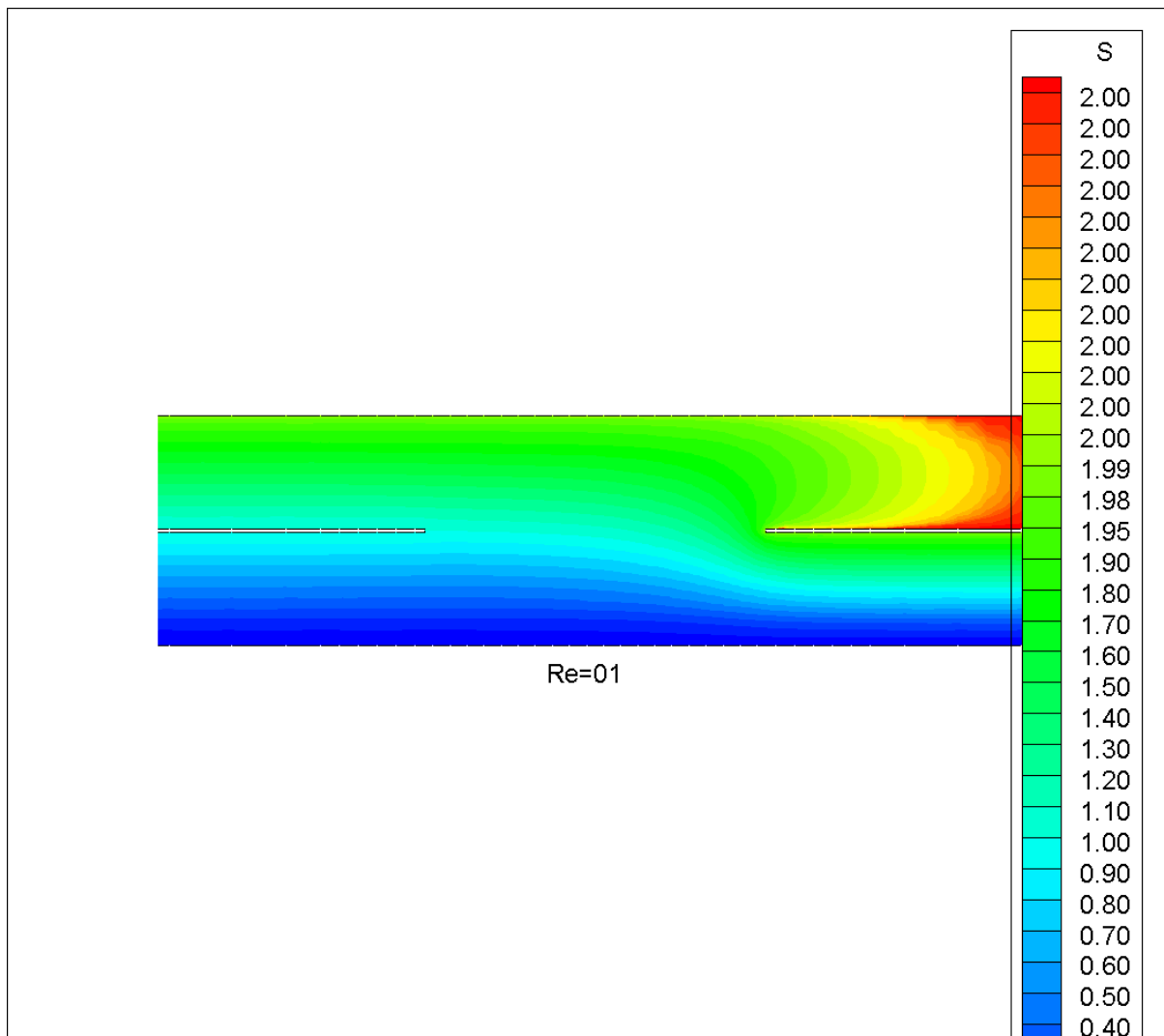


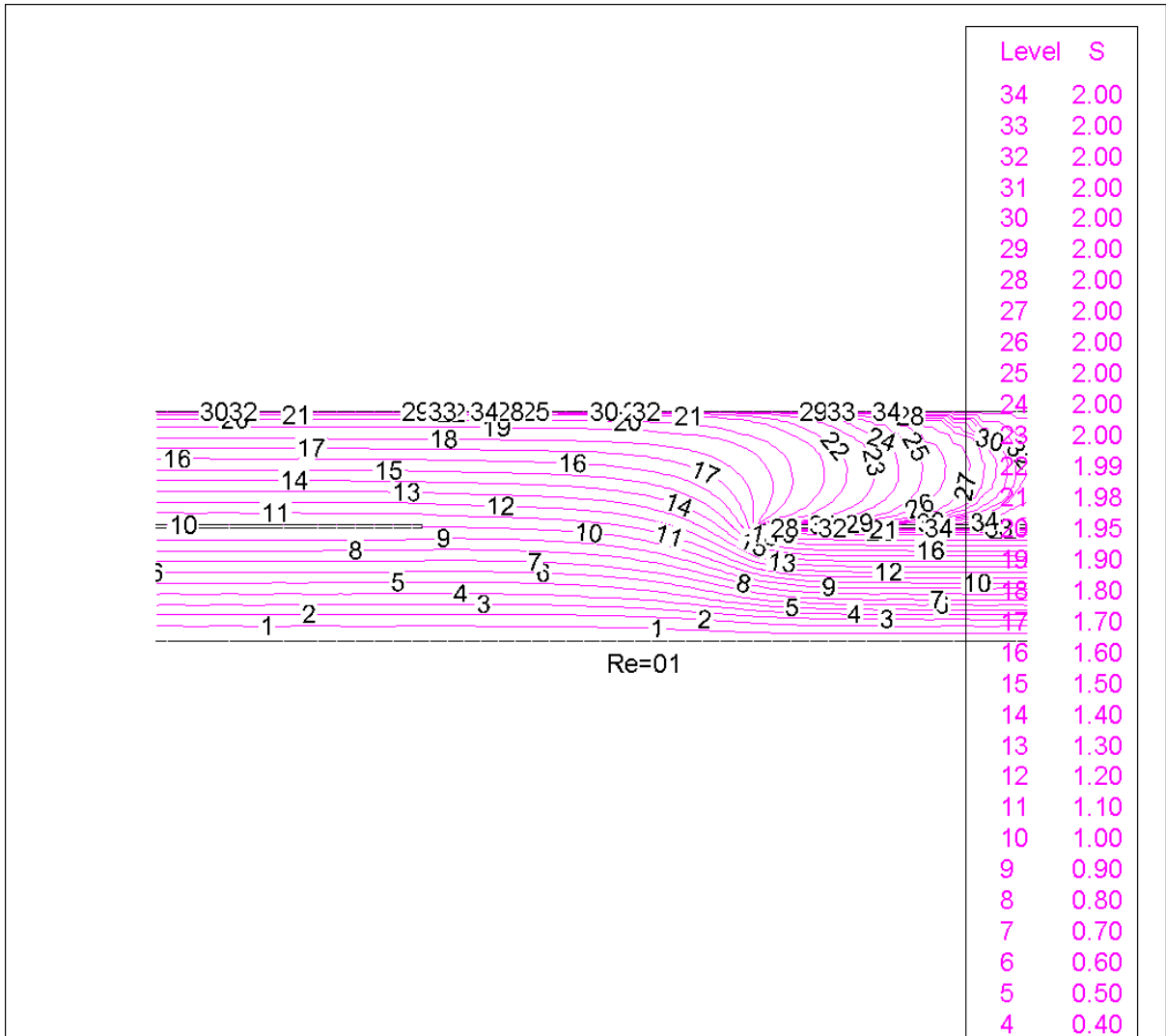
---

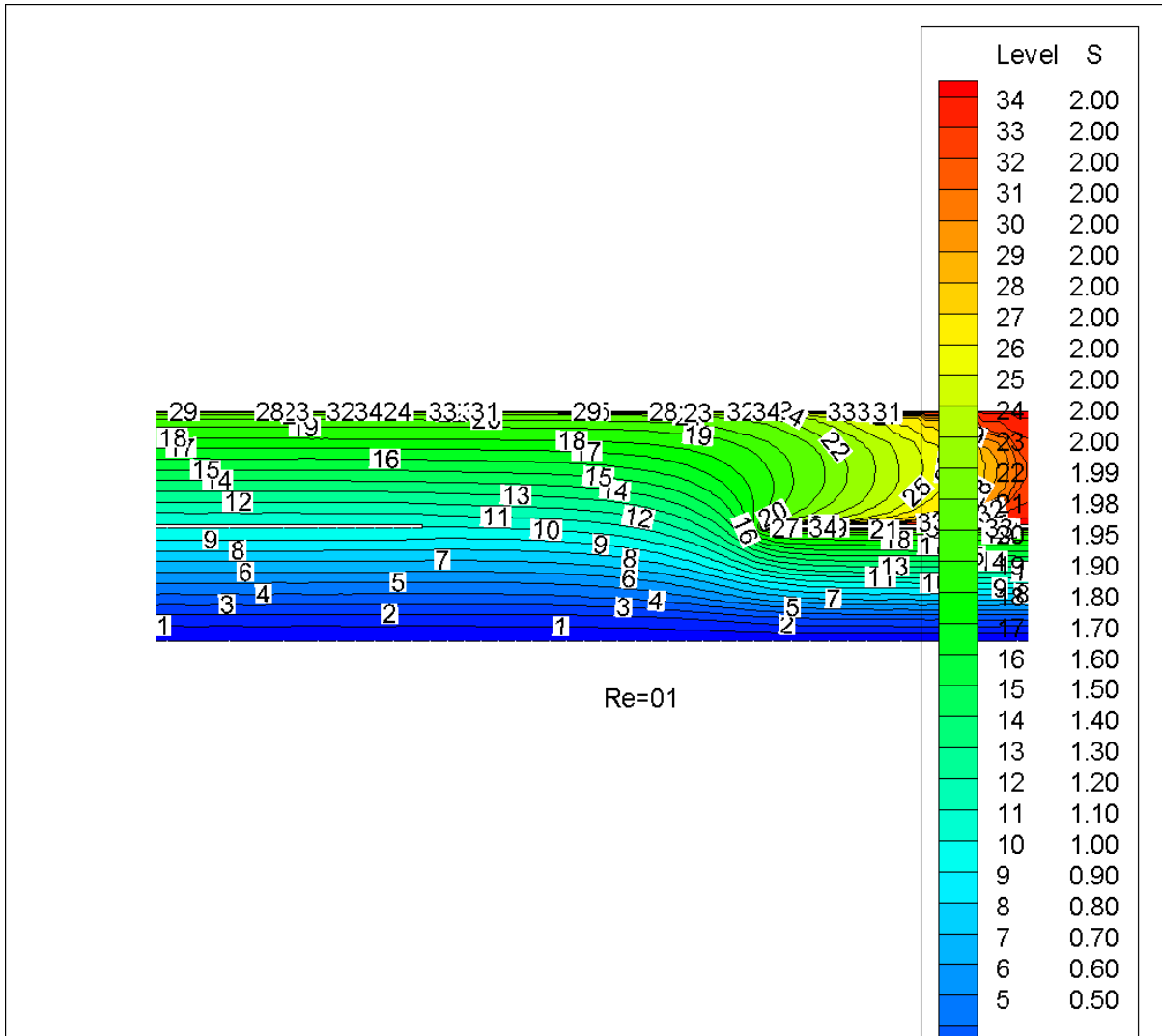
## 2.2 Mixing and separating of Newtonian fluid flows in a channel through porous media

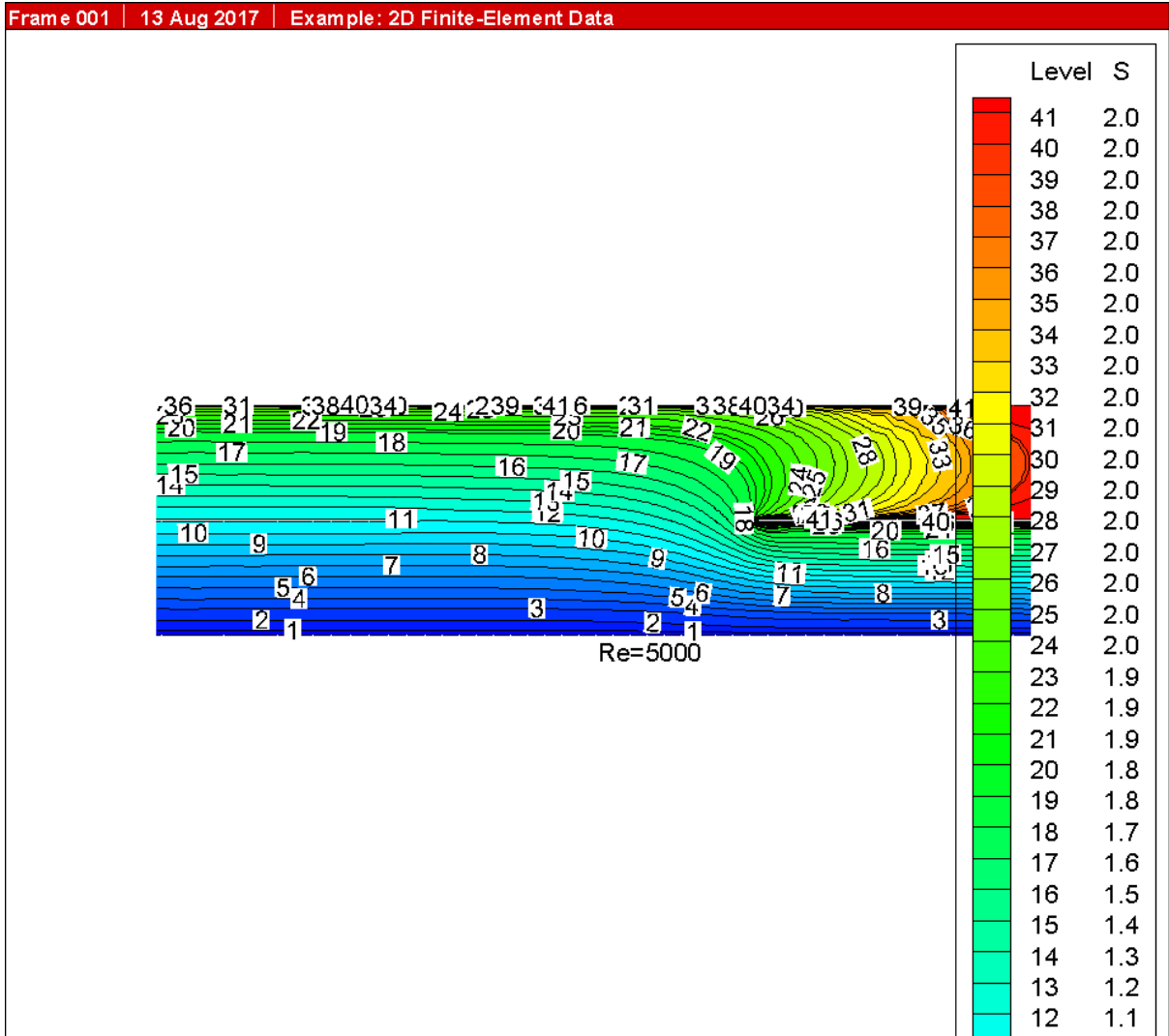
( $G_2$ )

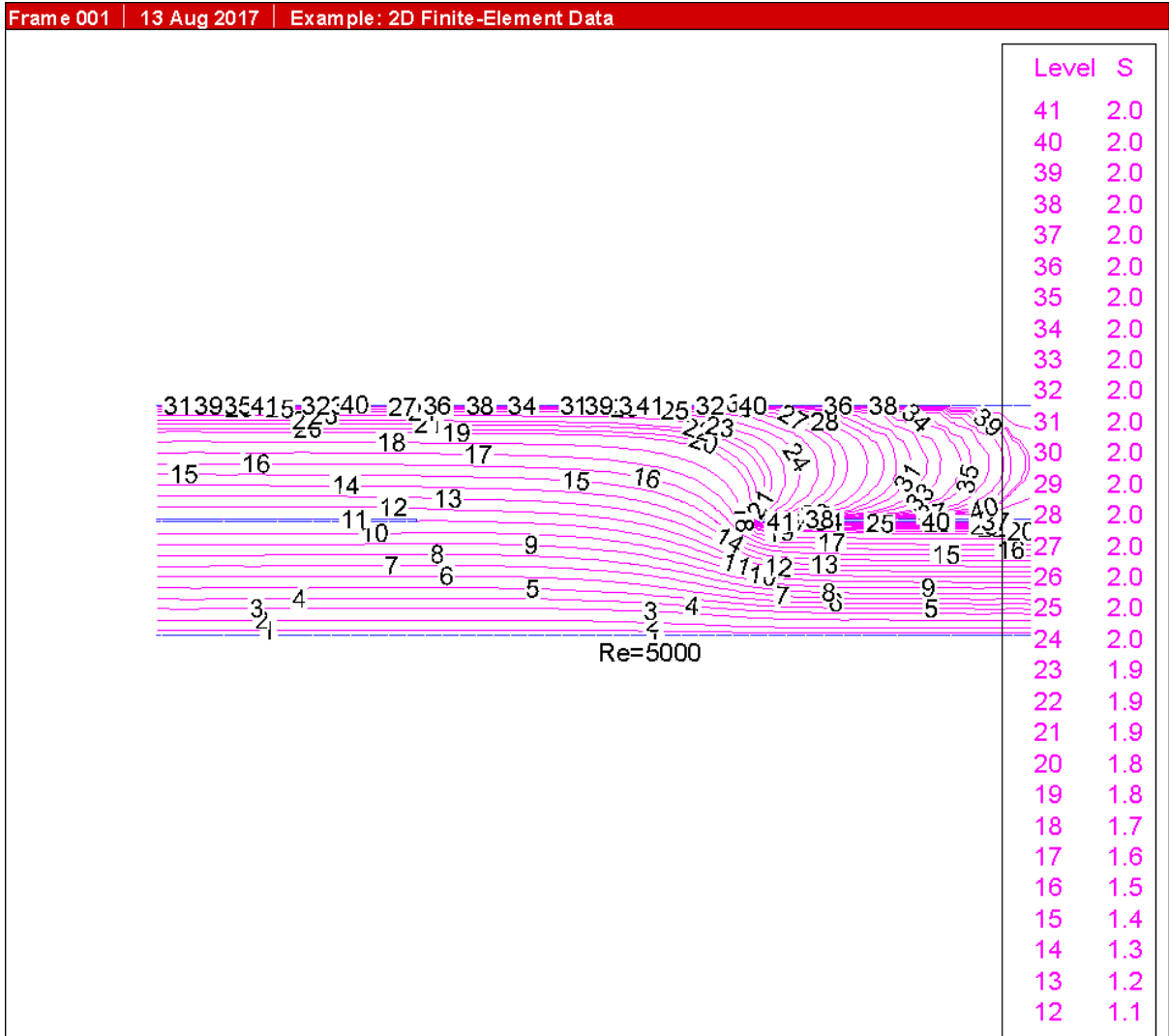
Equal (1, 1) flow rate

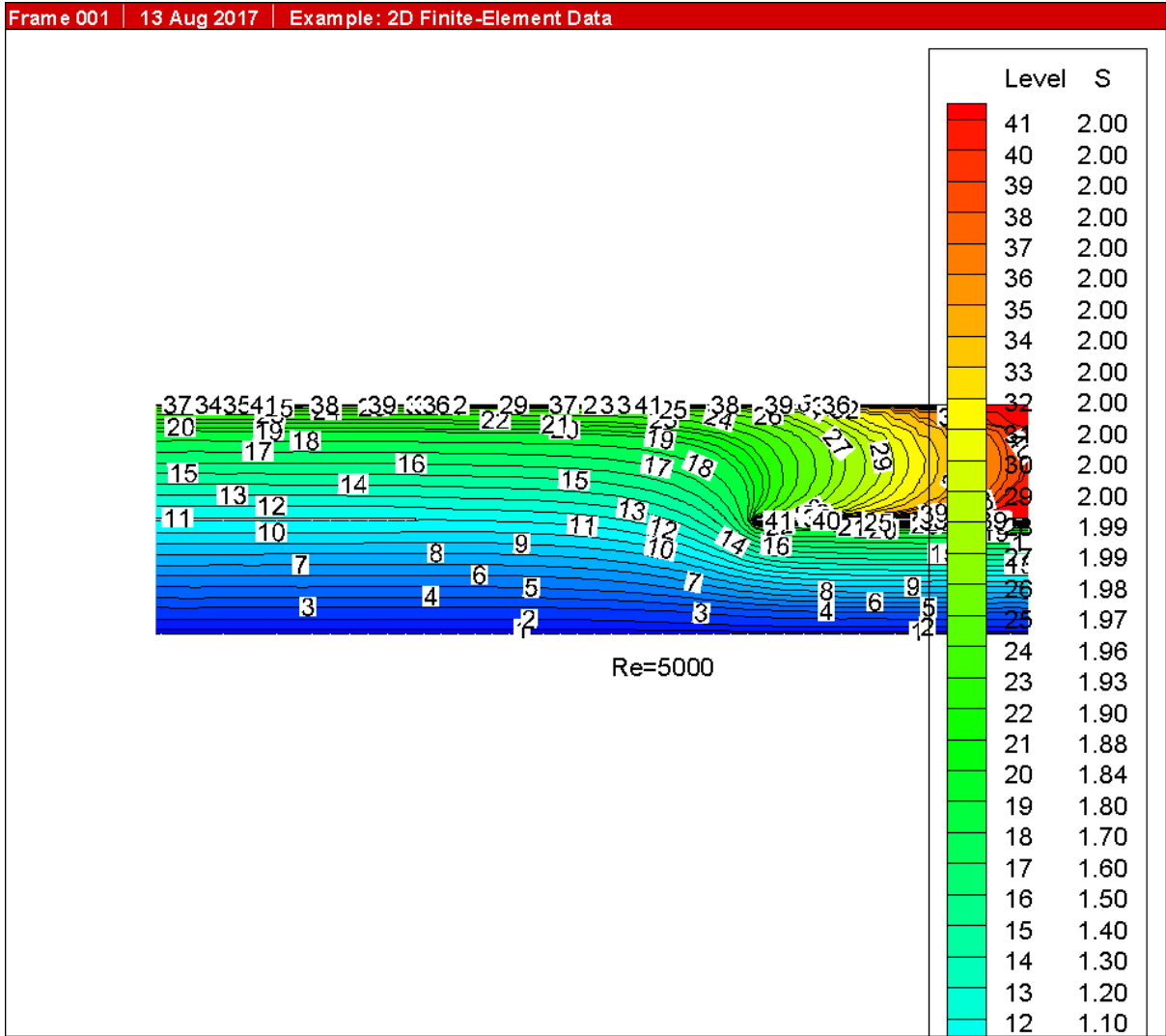


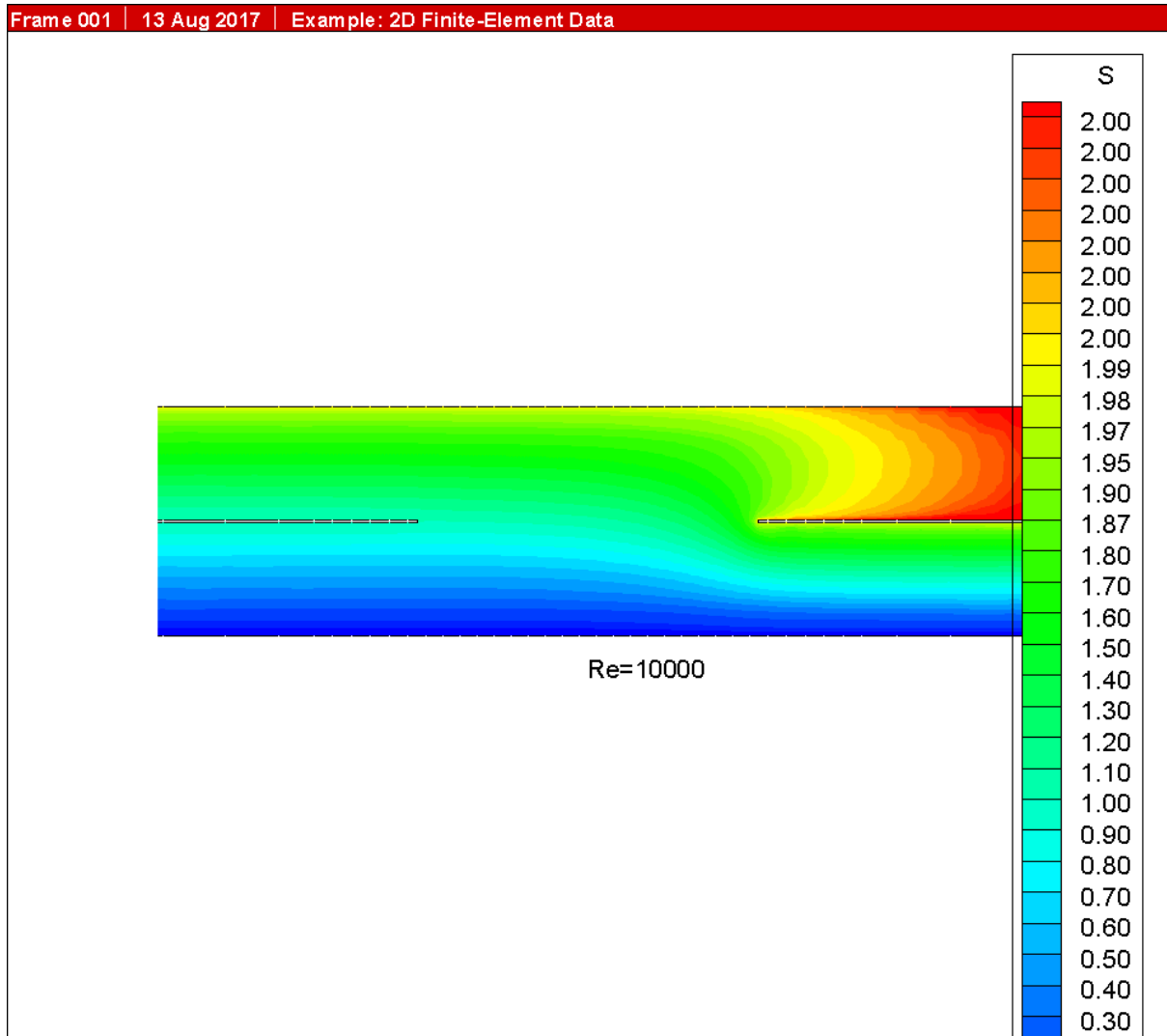


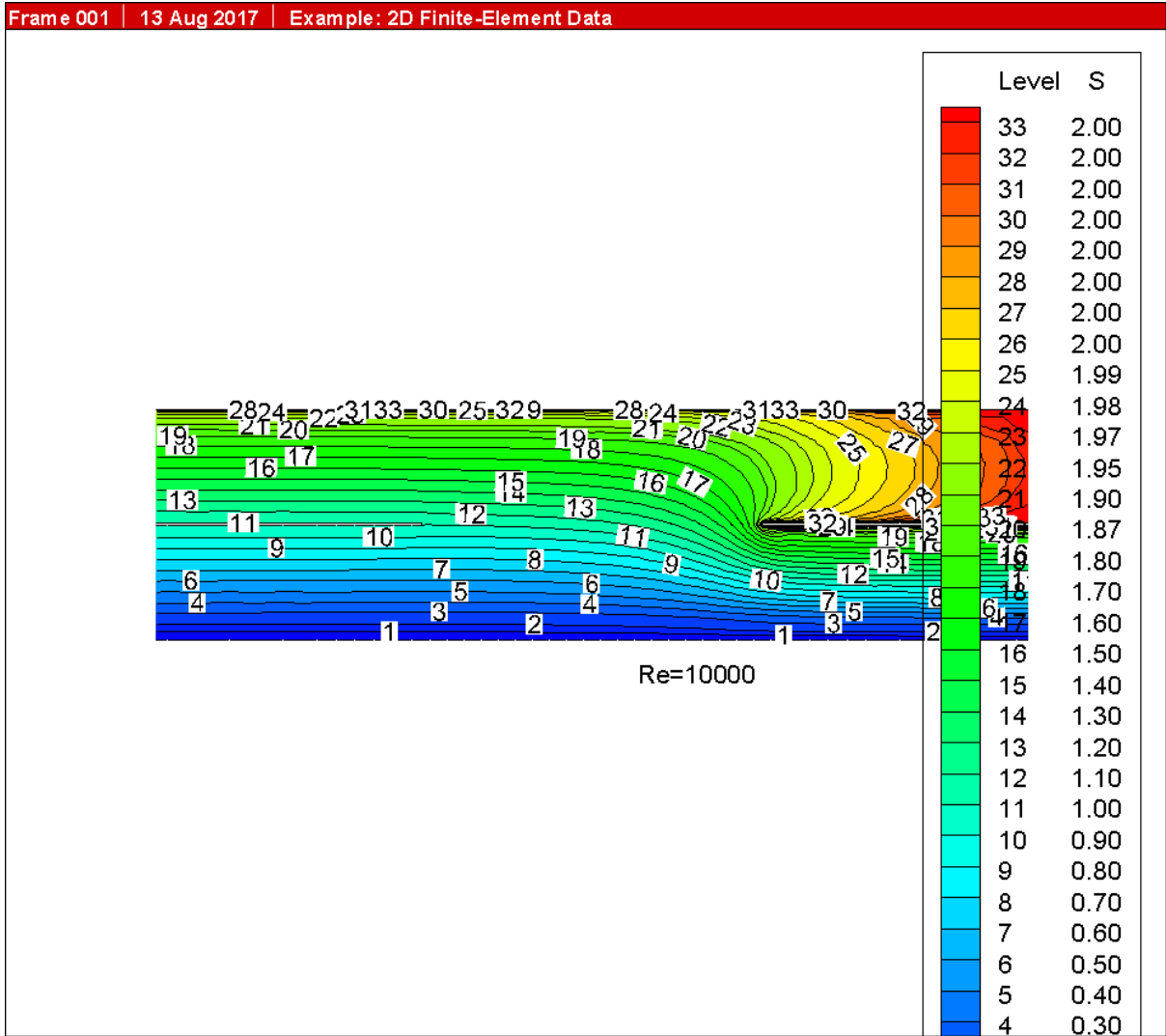


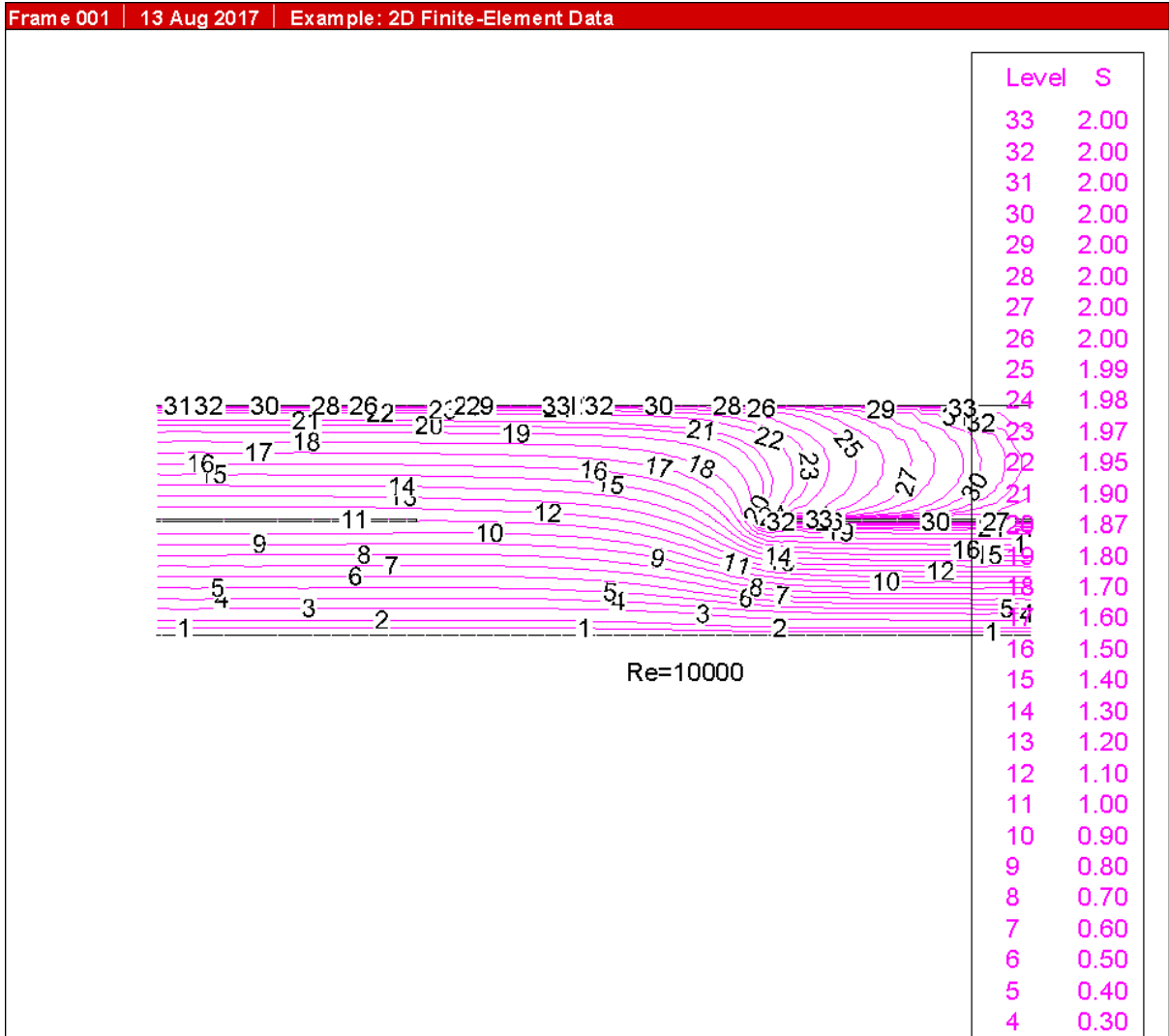




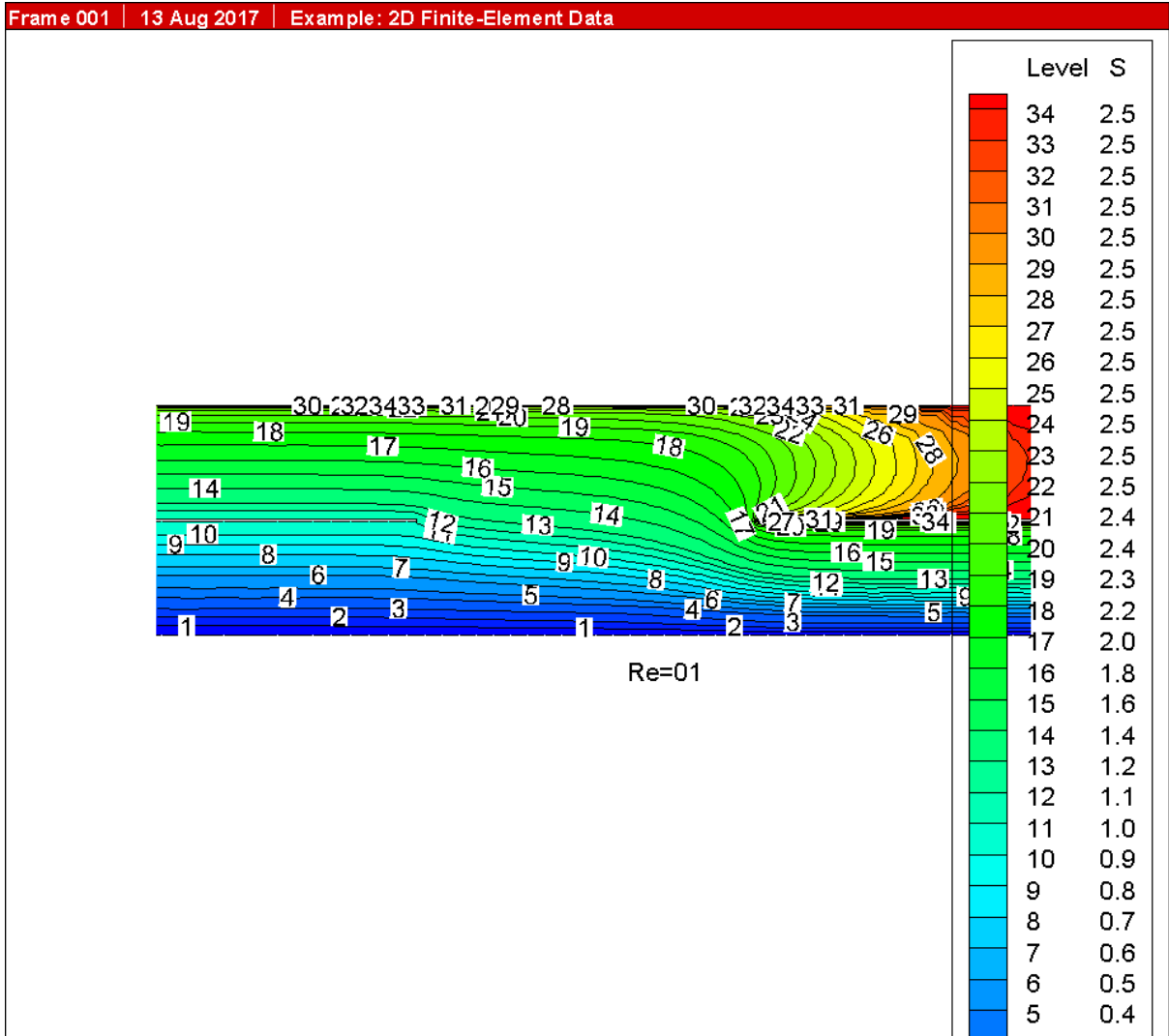


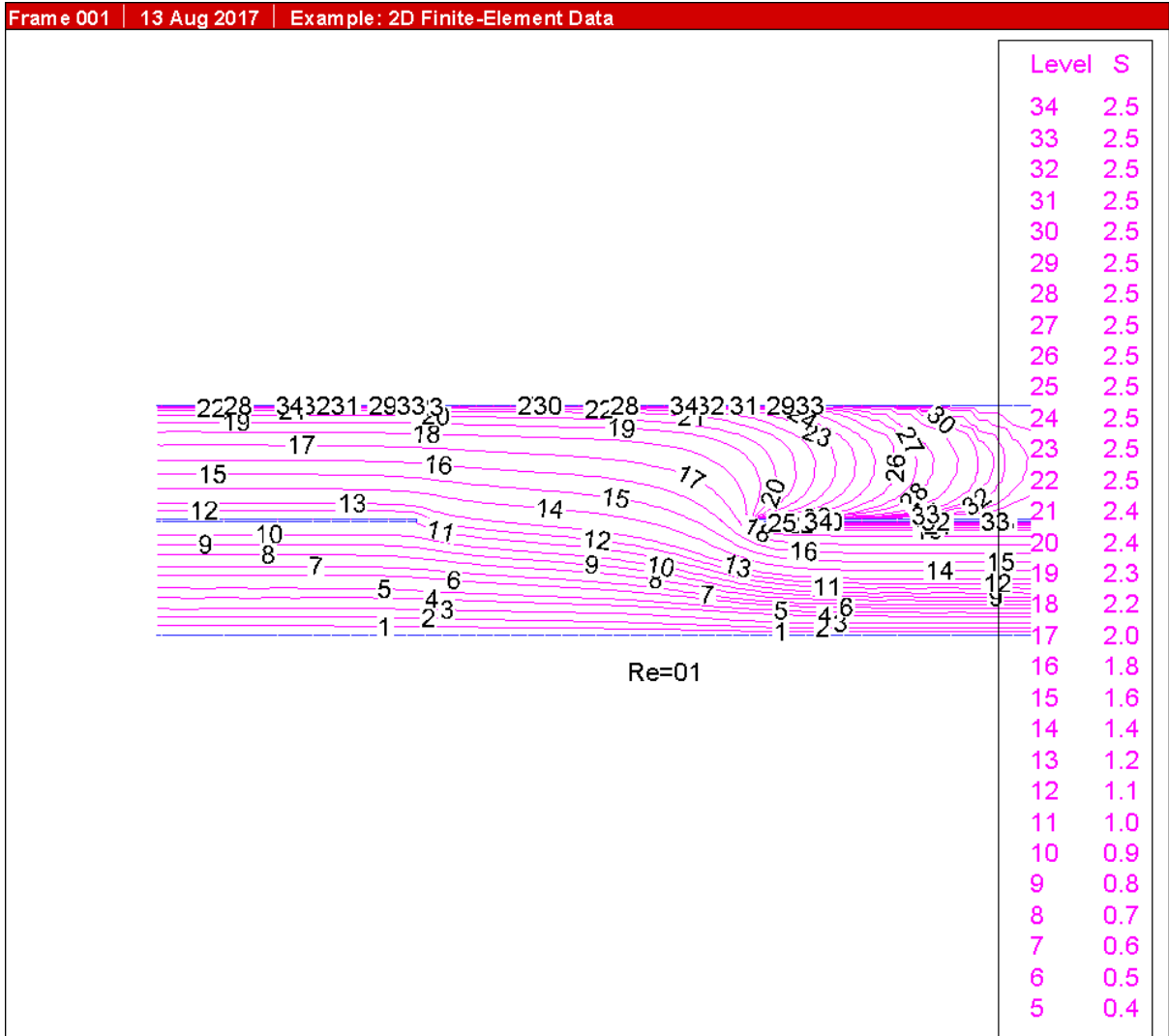




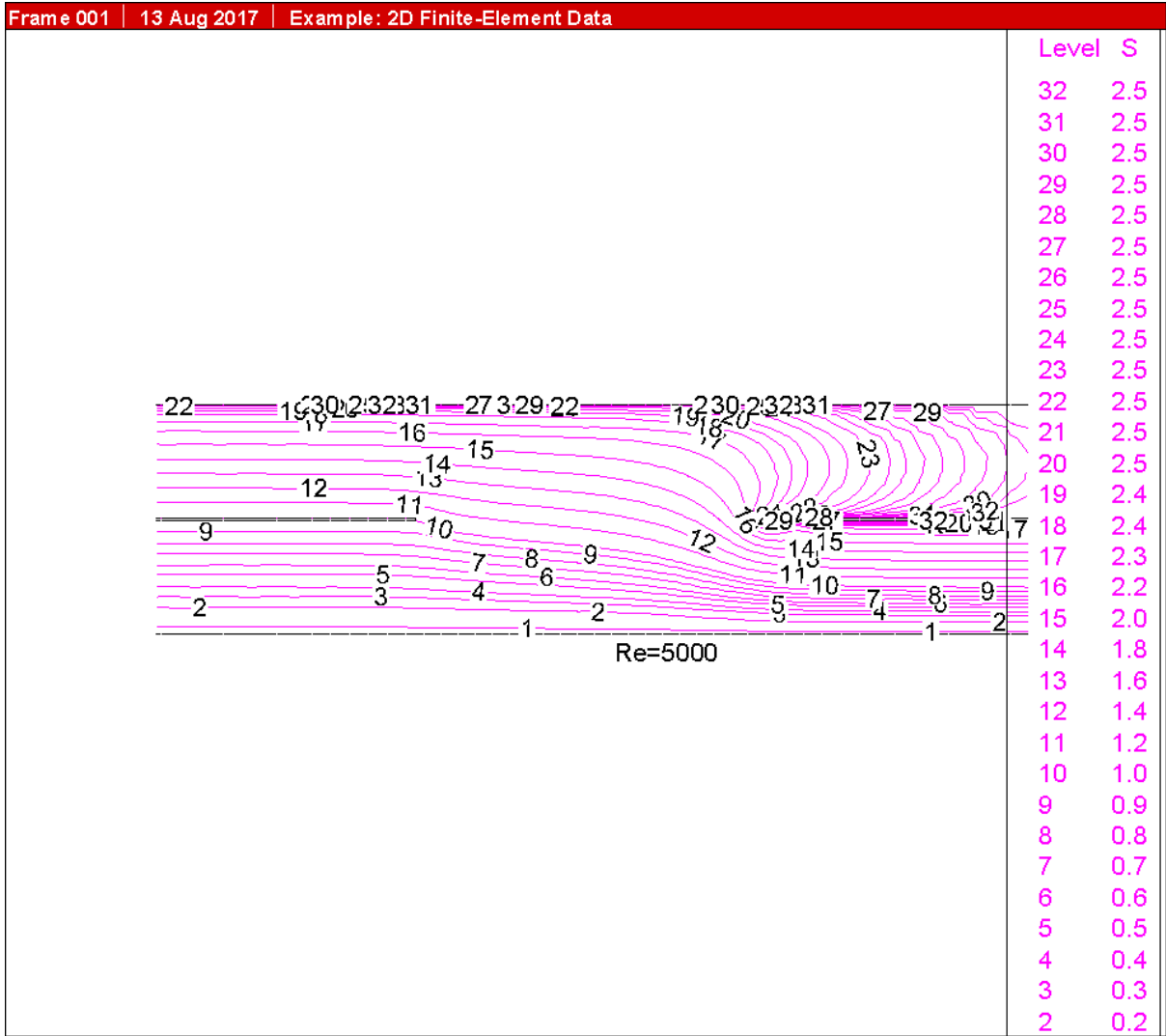


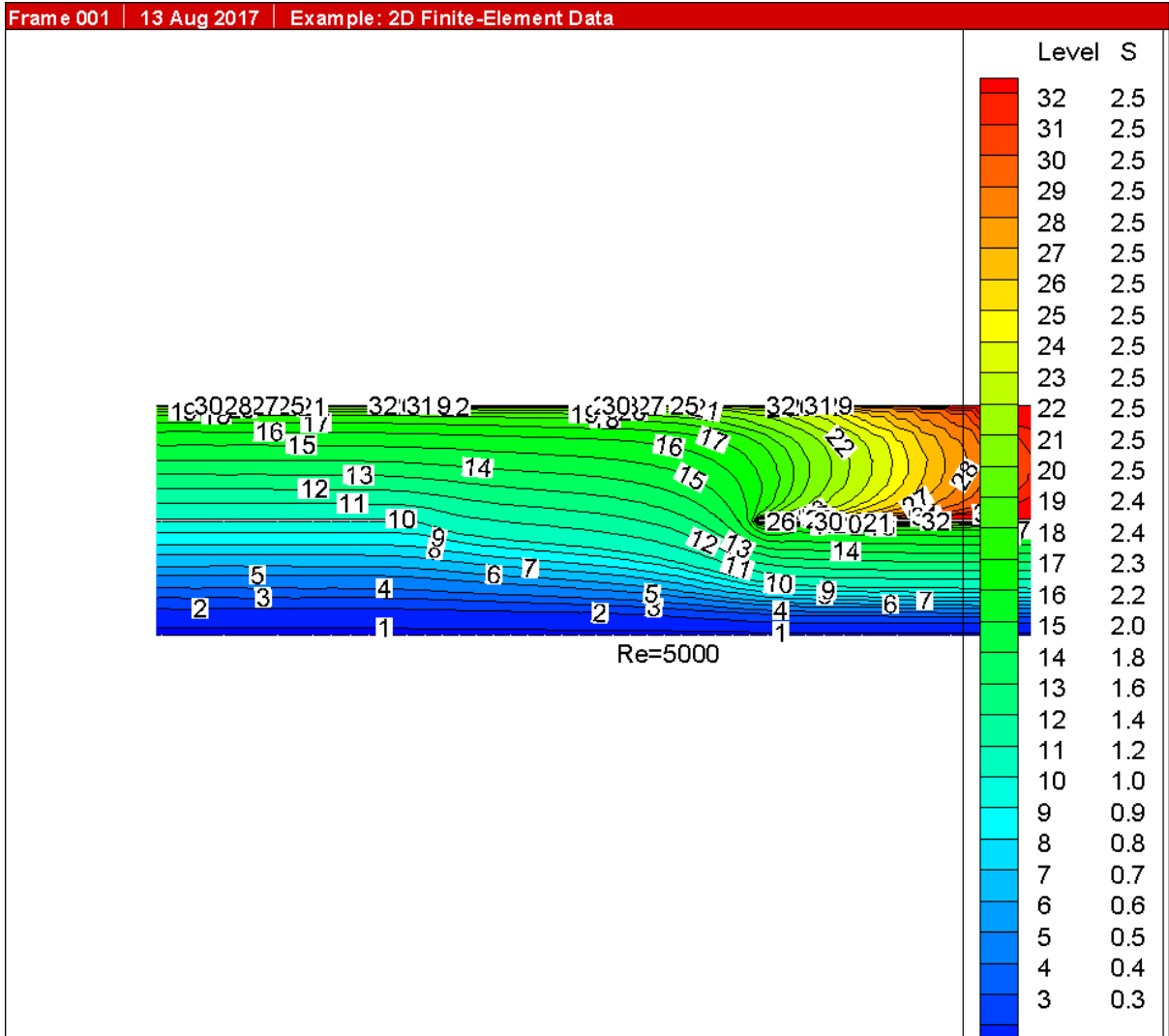




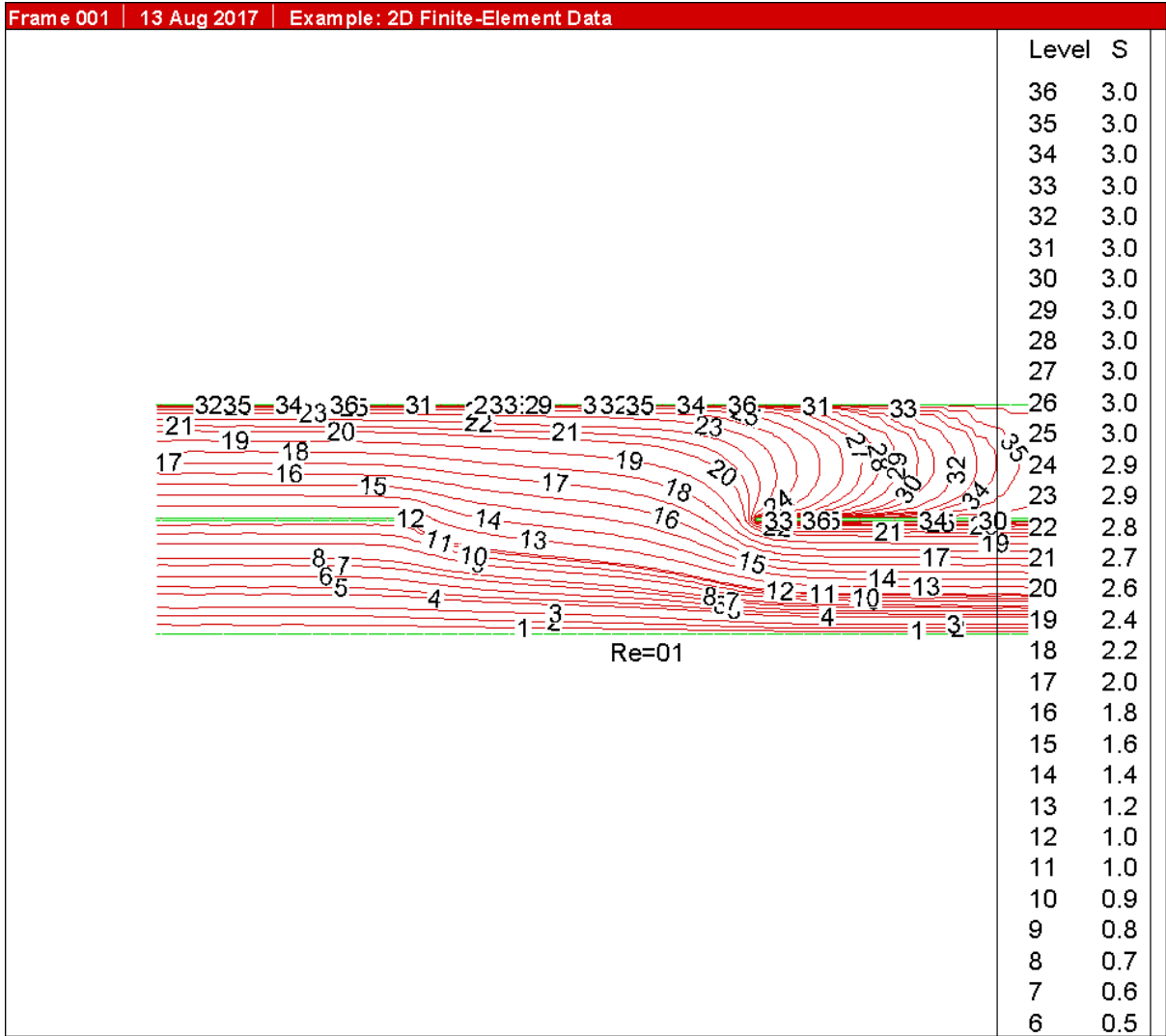


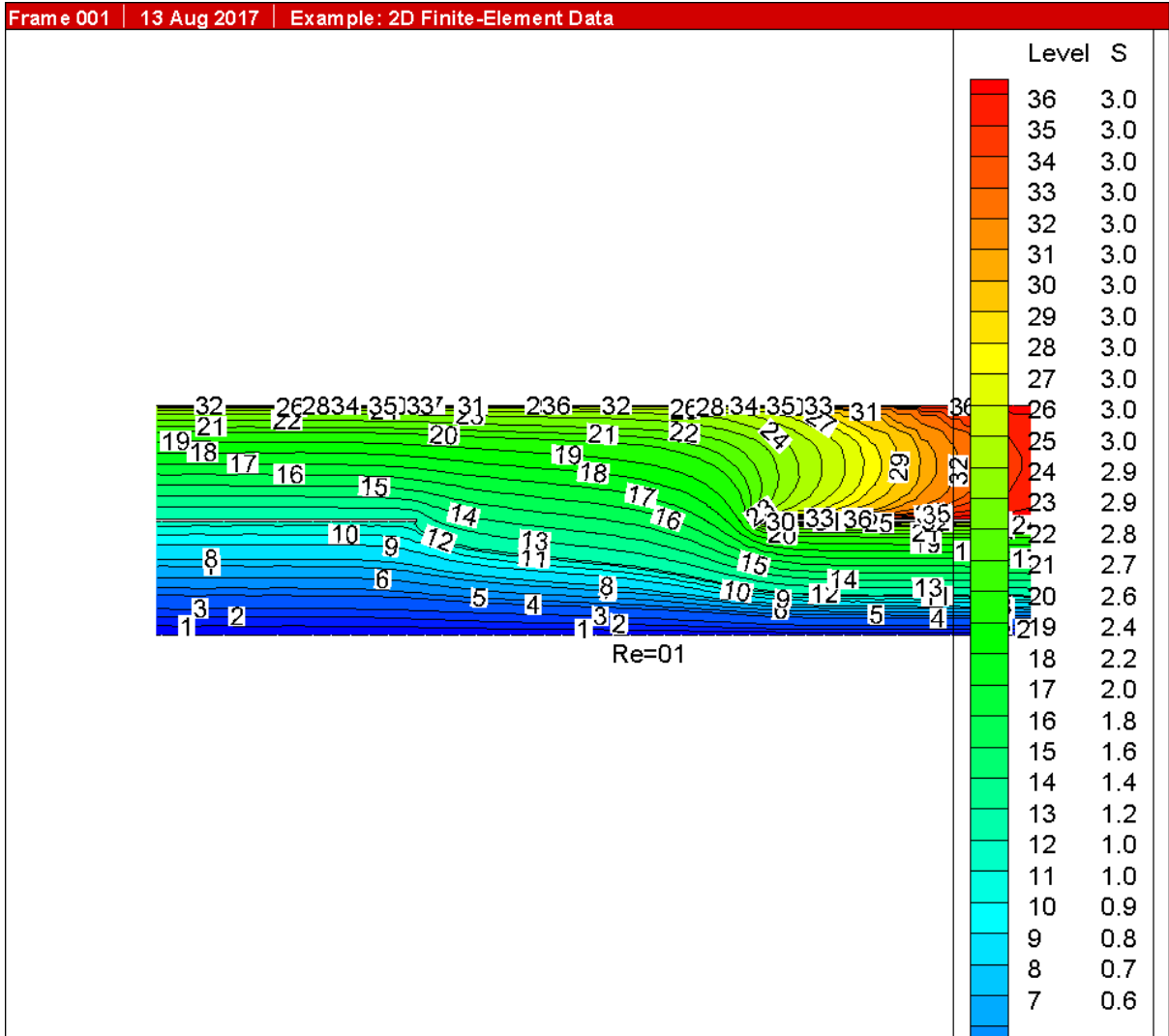




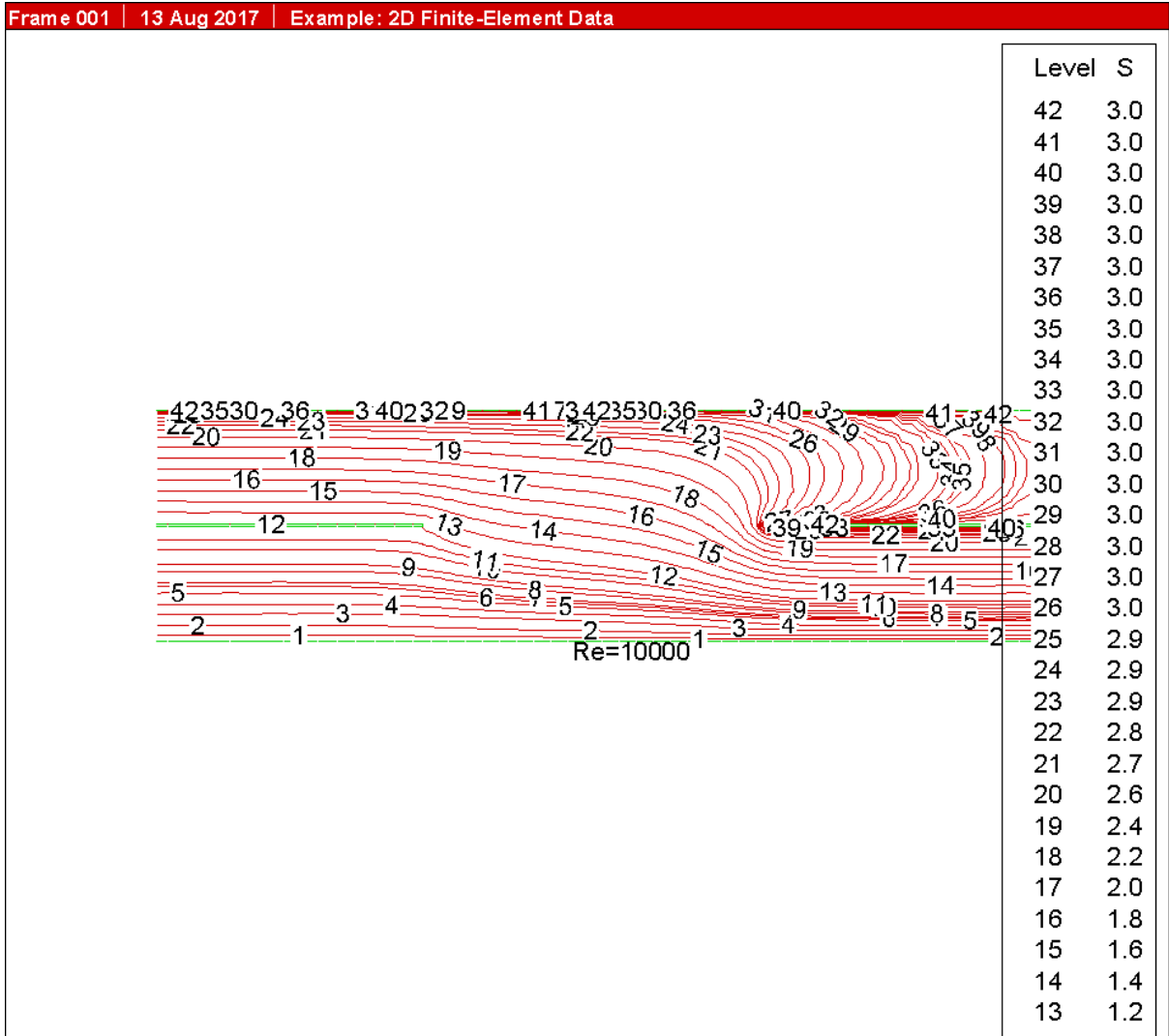


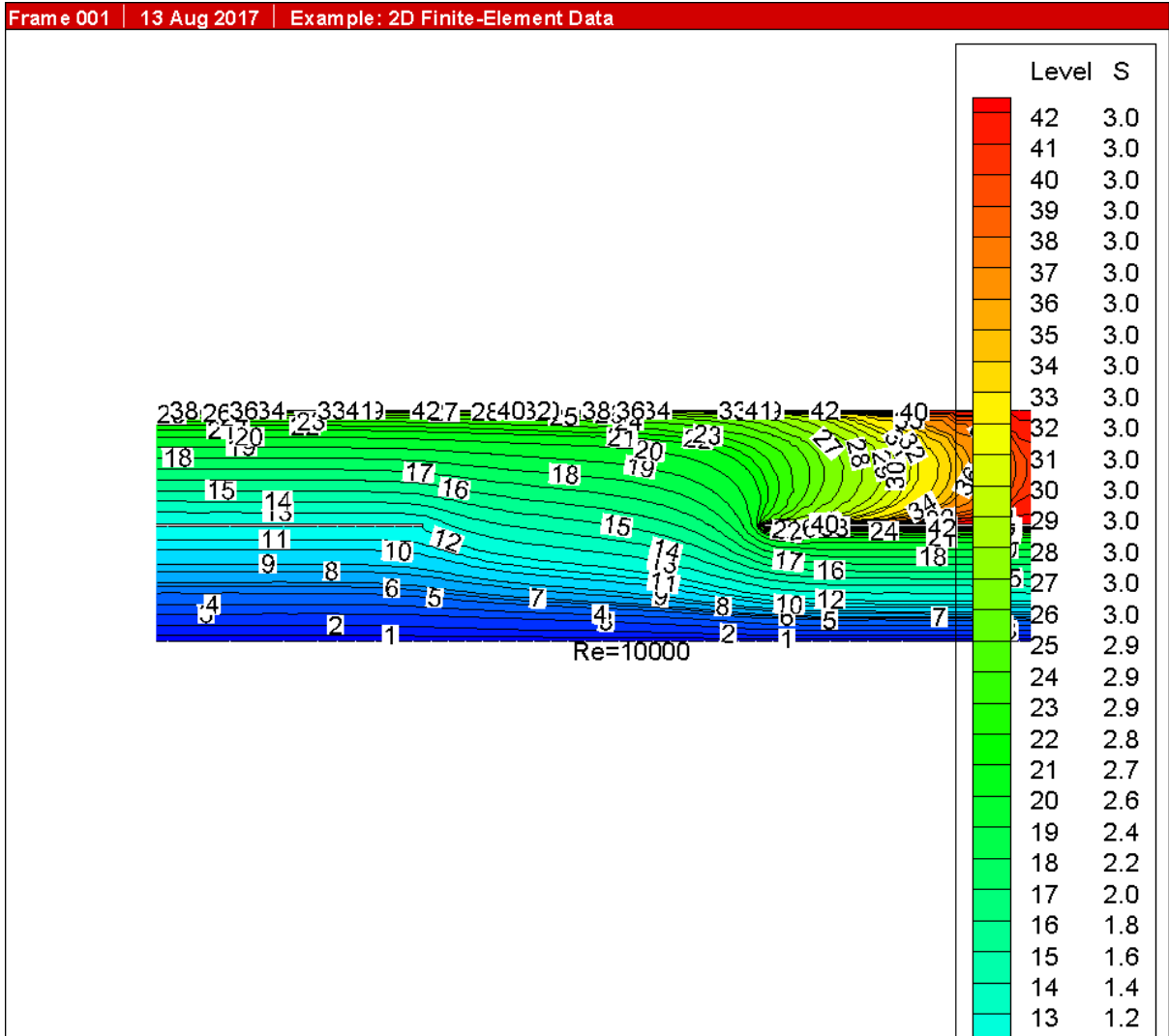




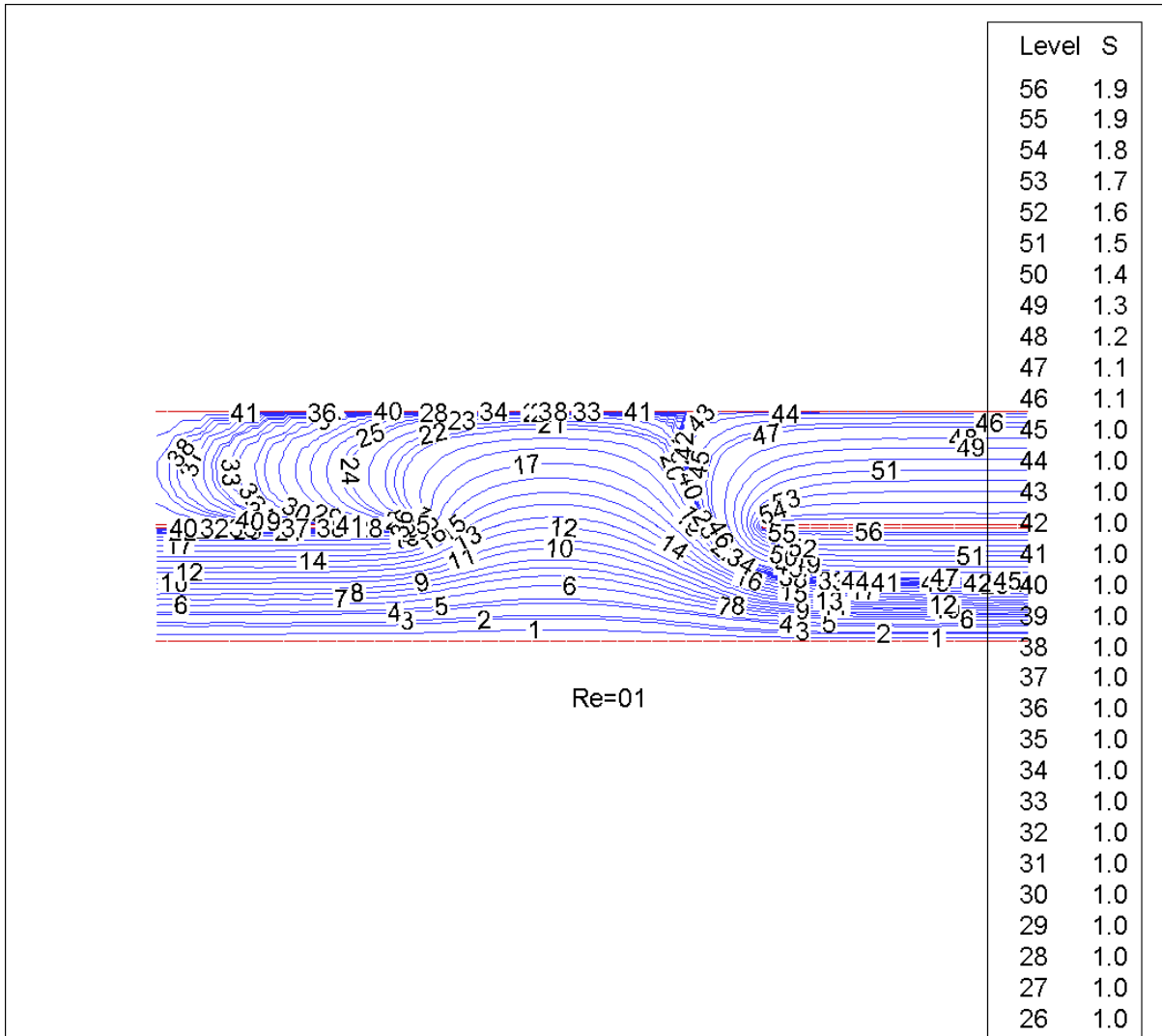


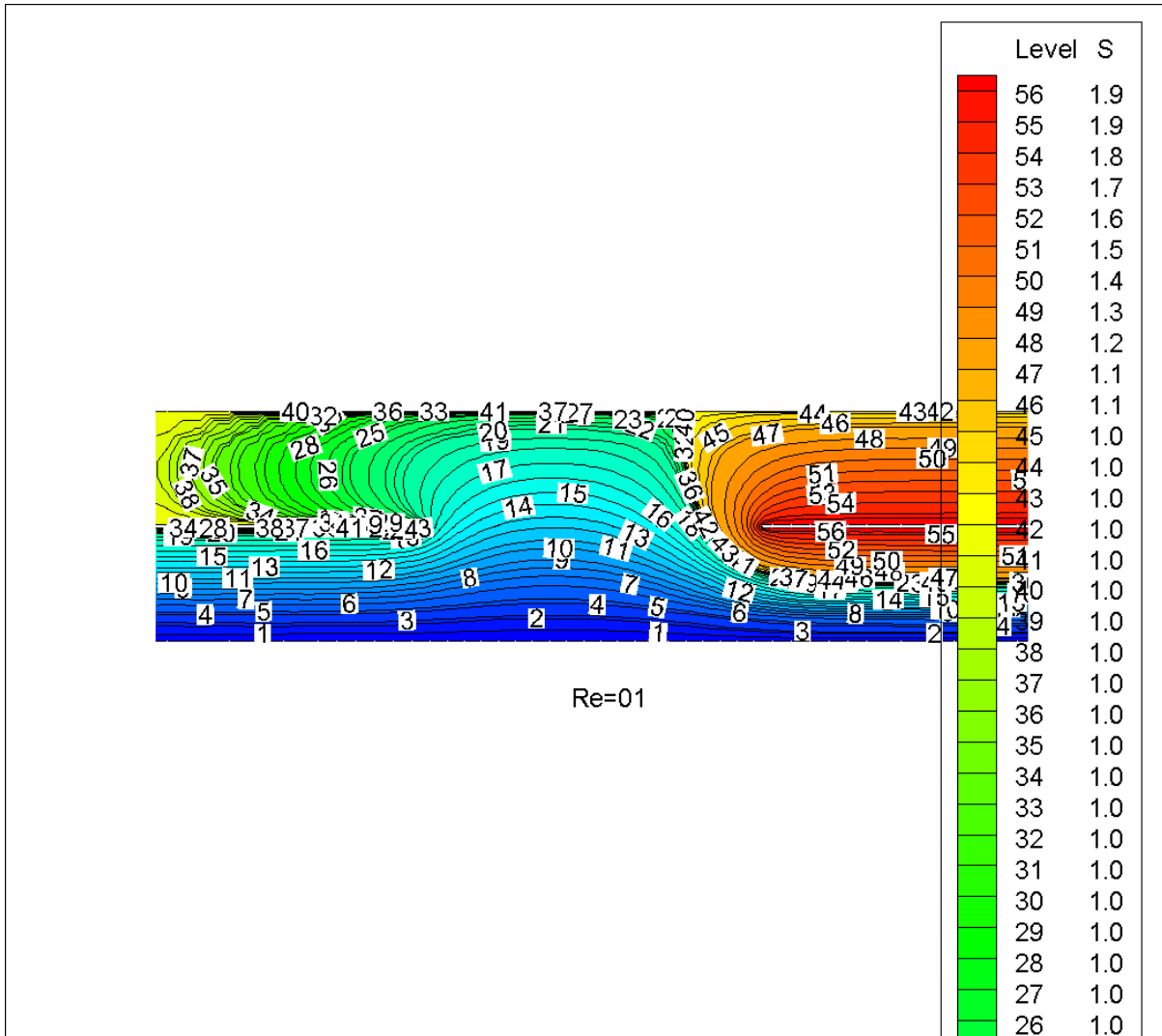


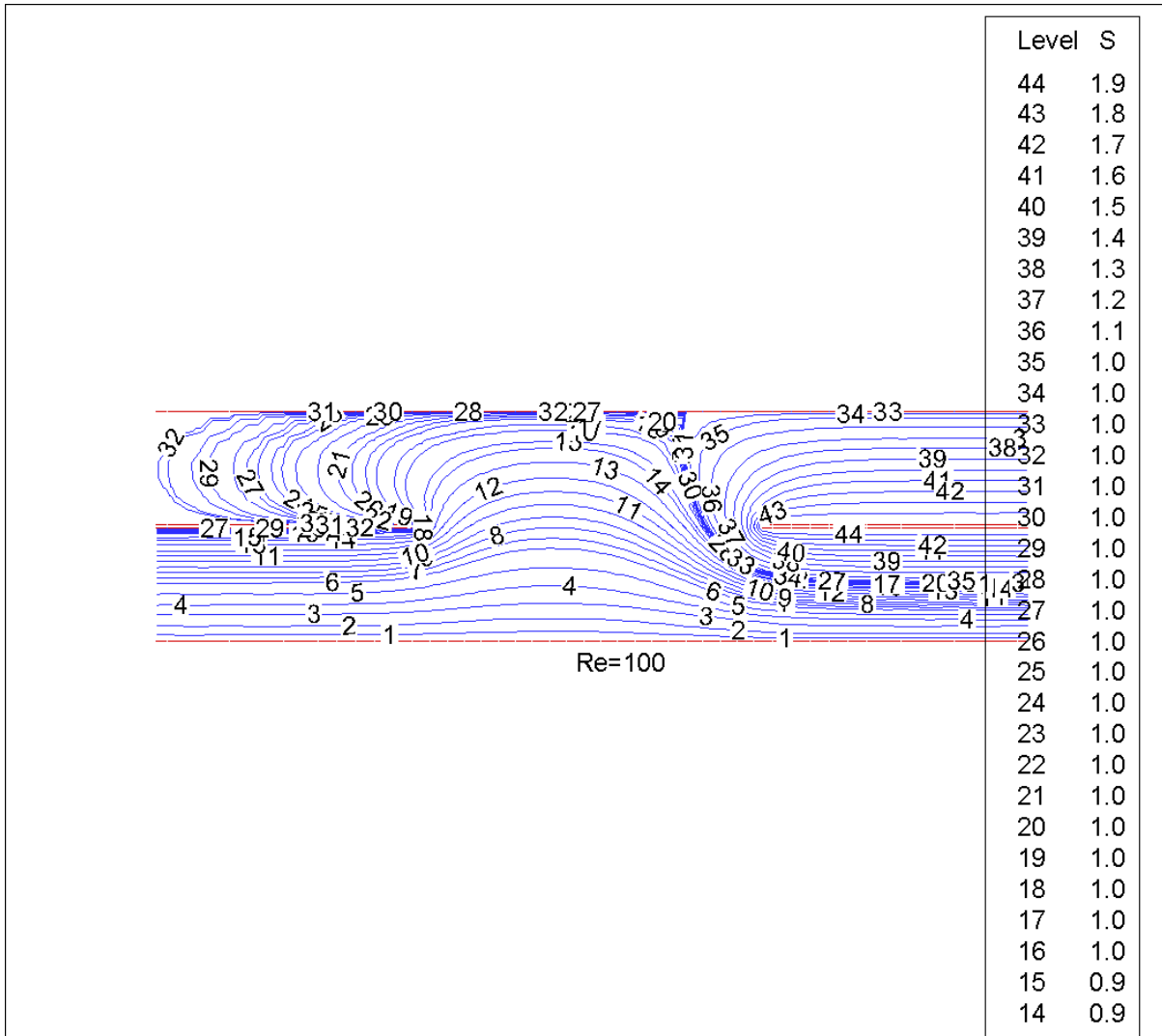


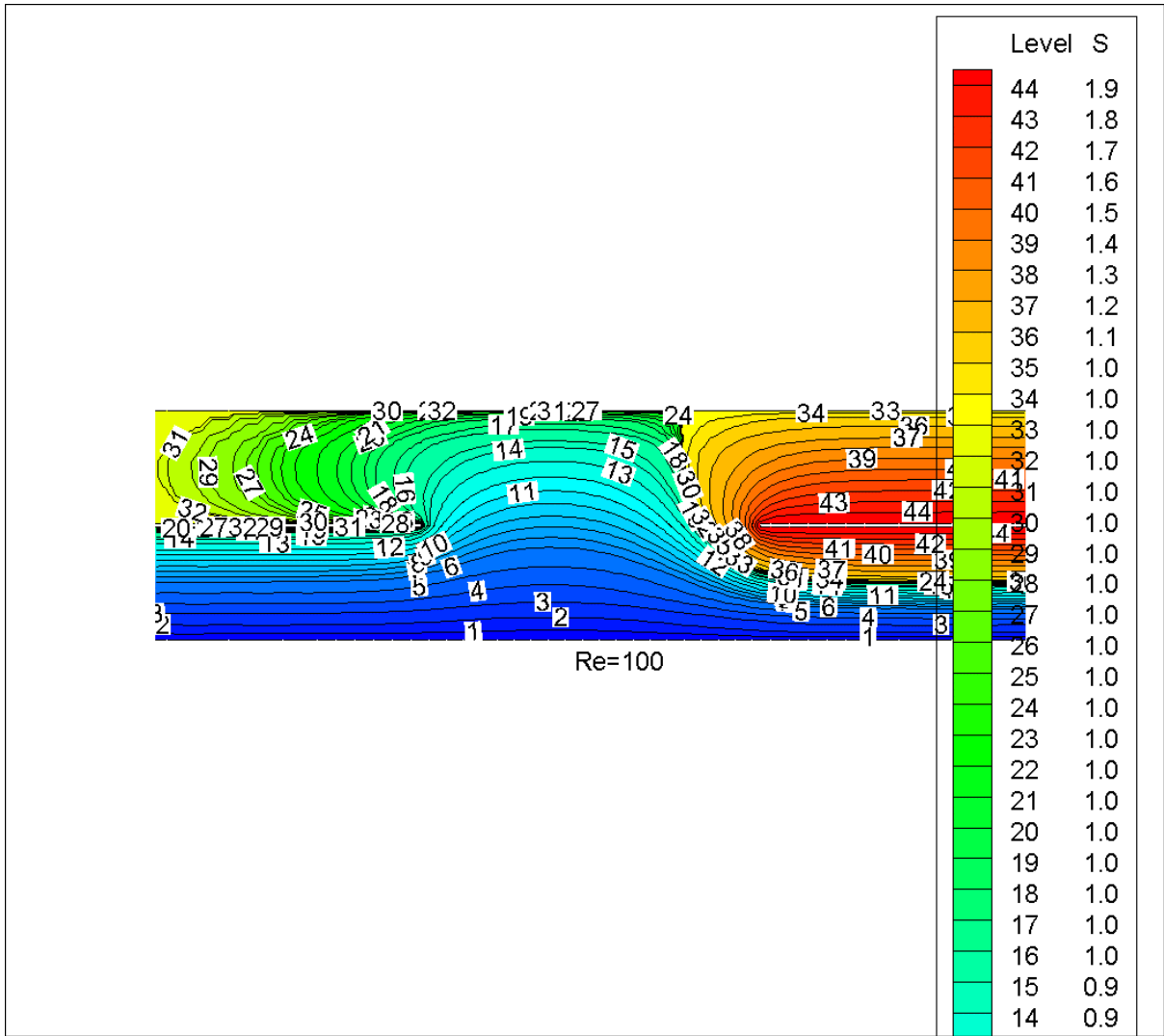






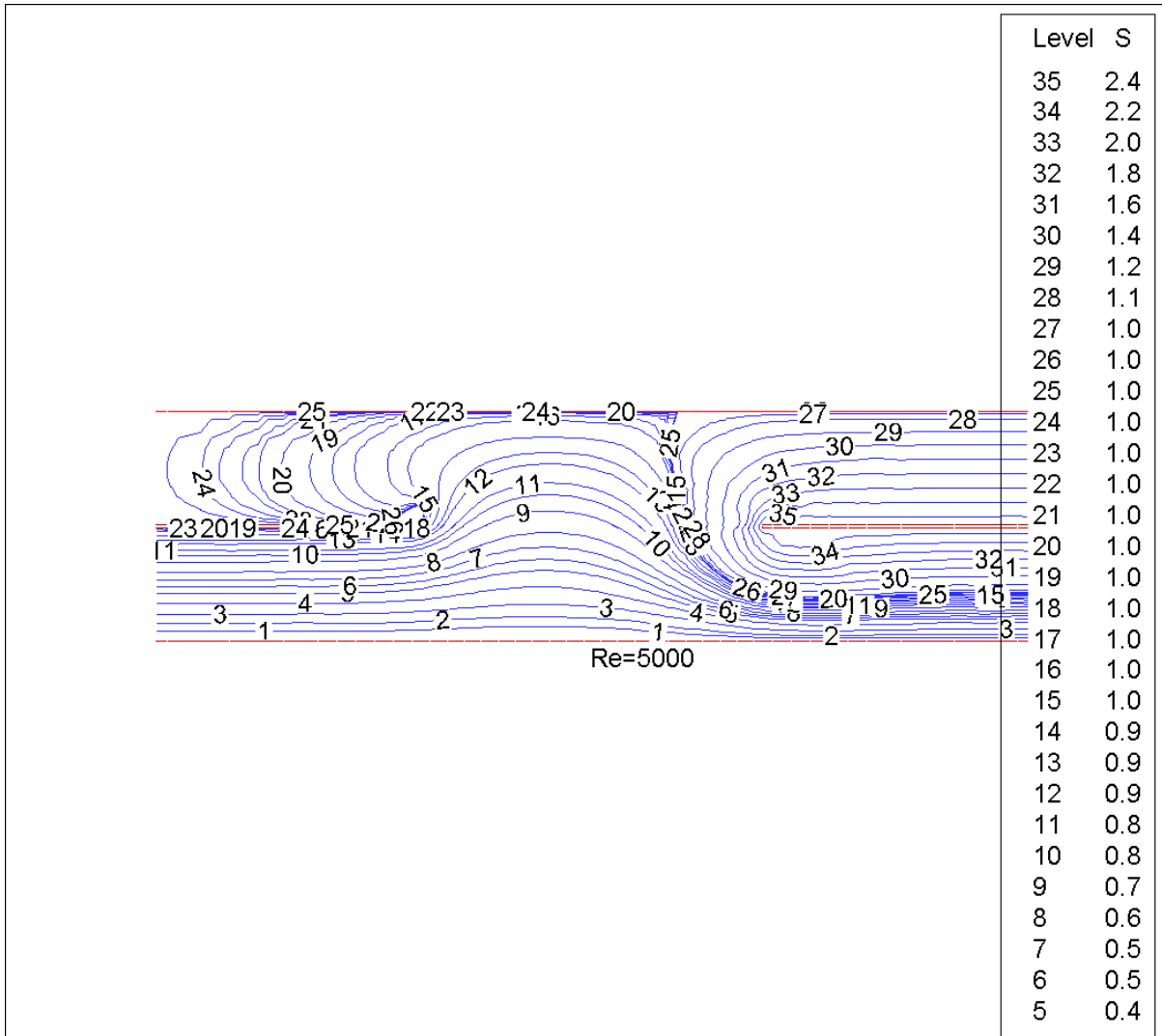


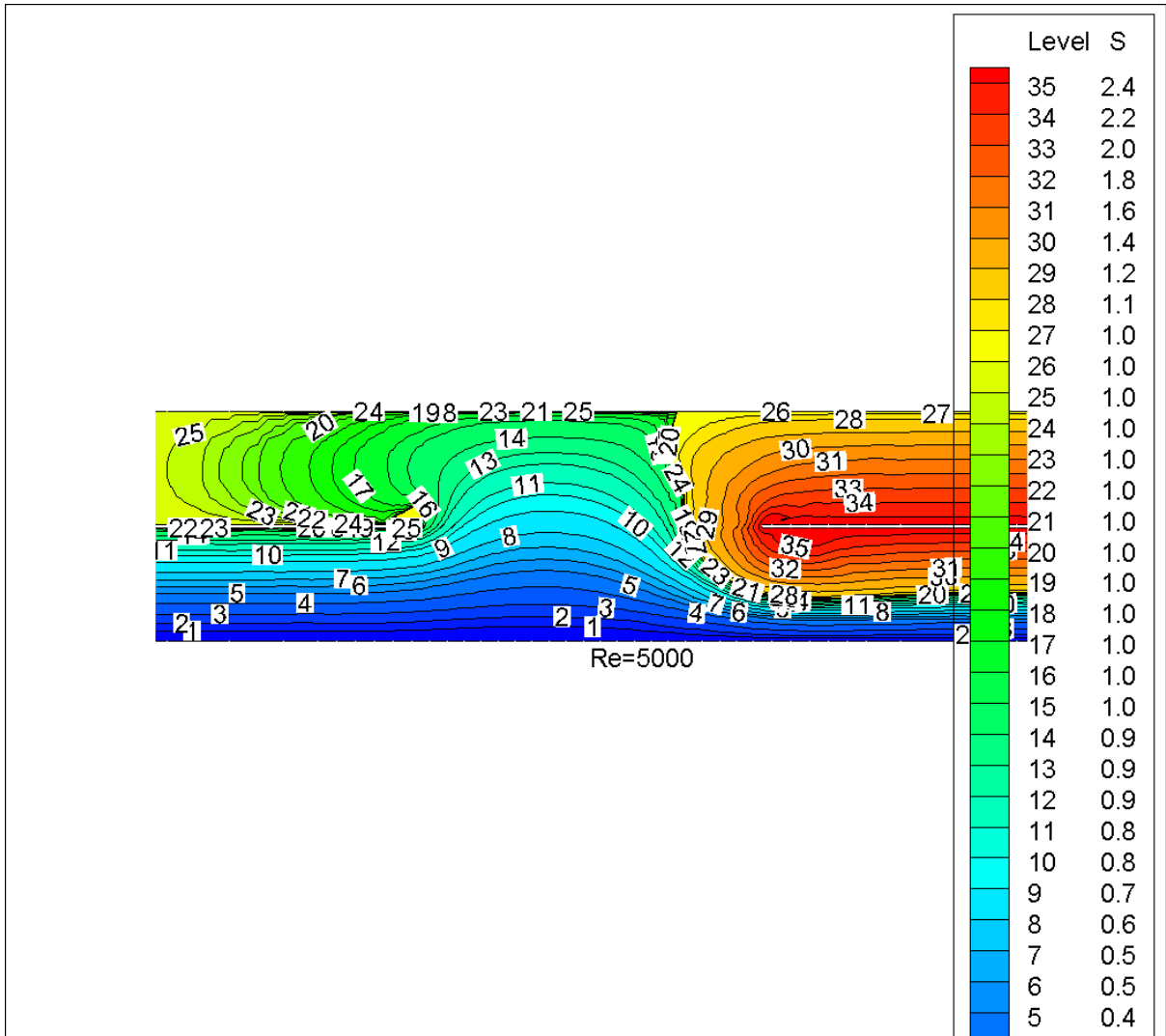






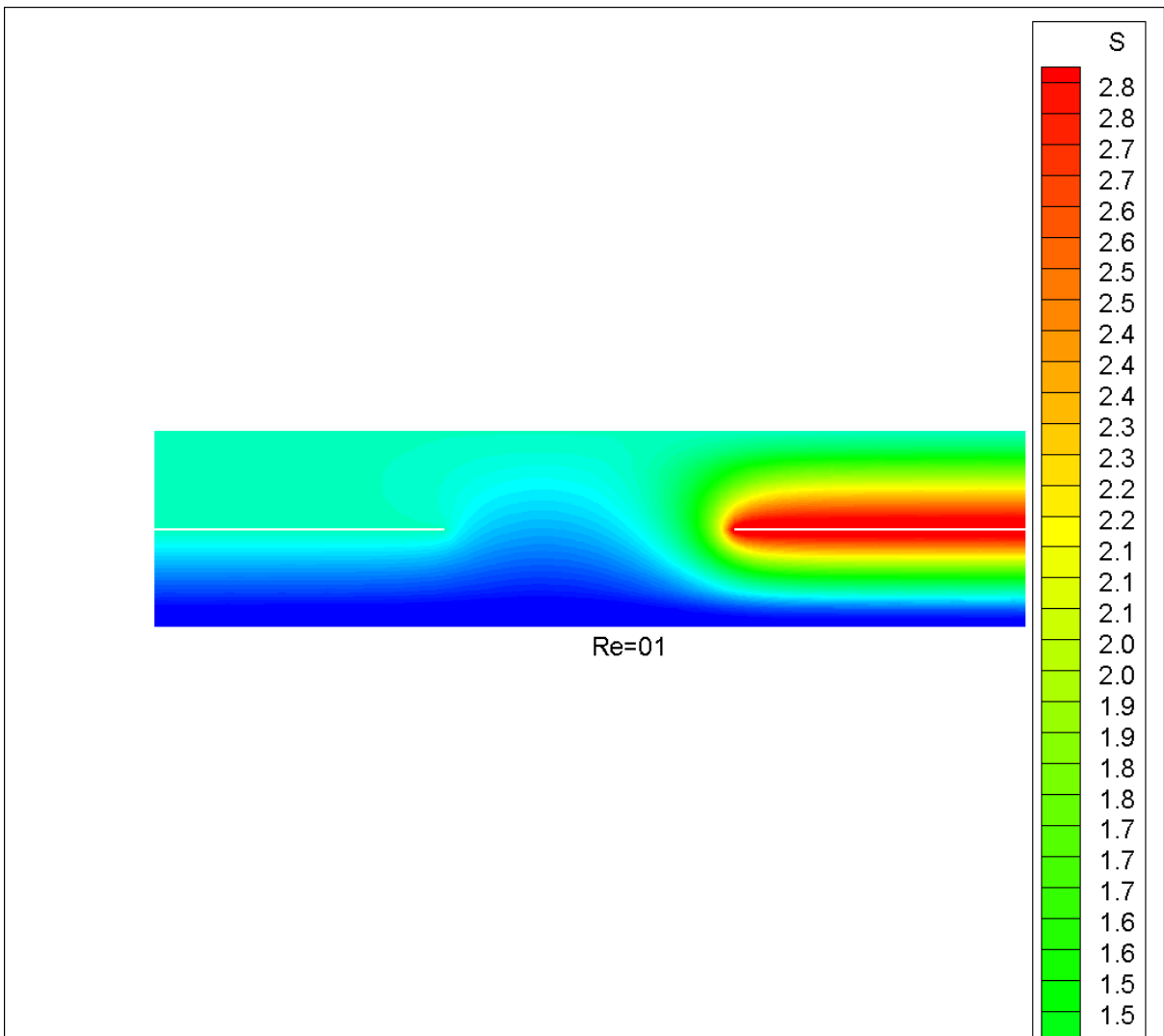


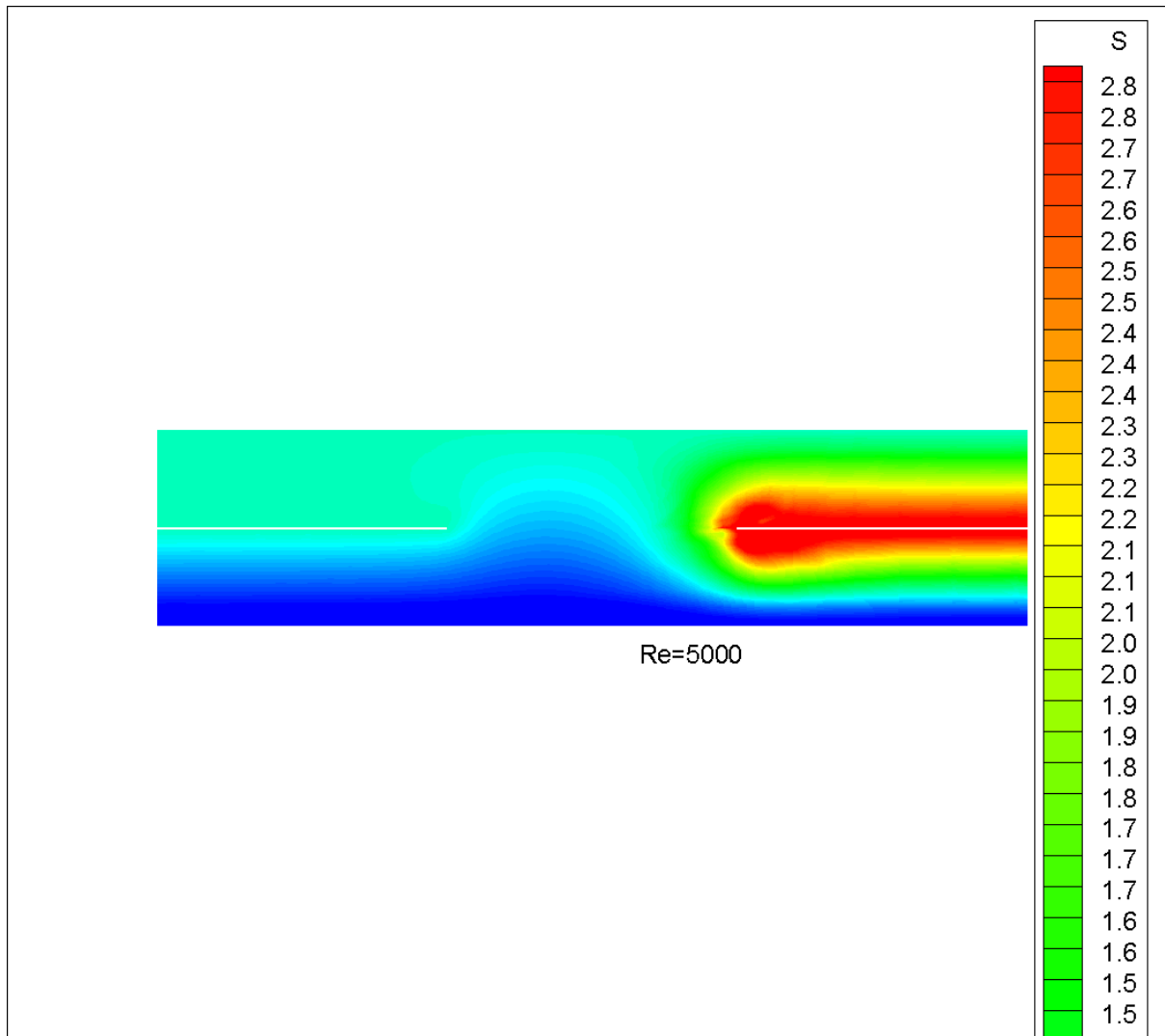




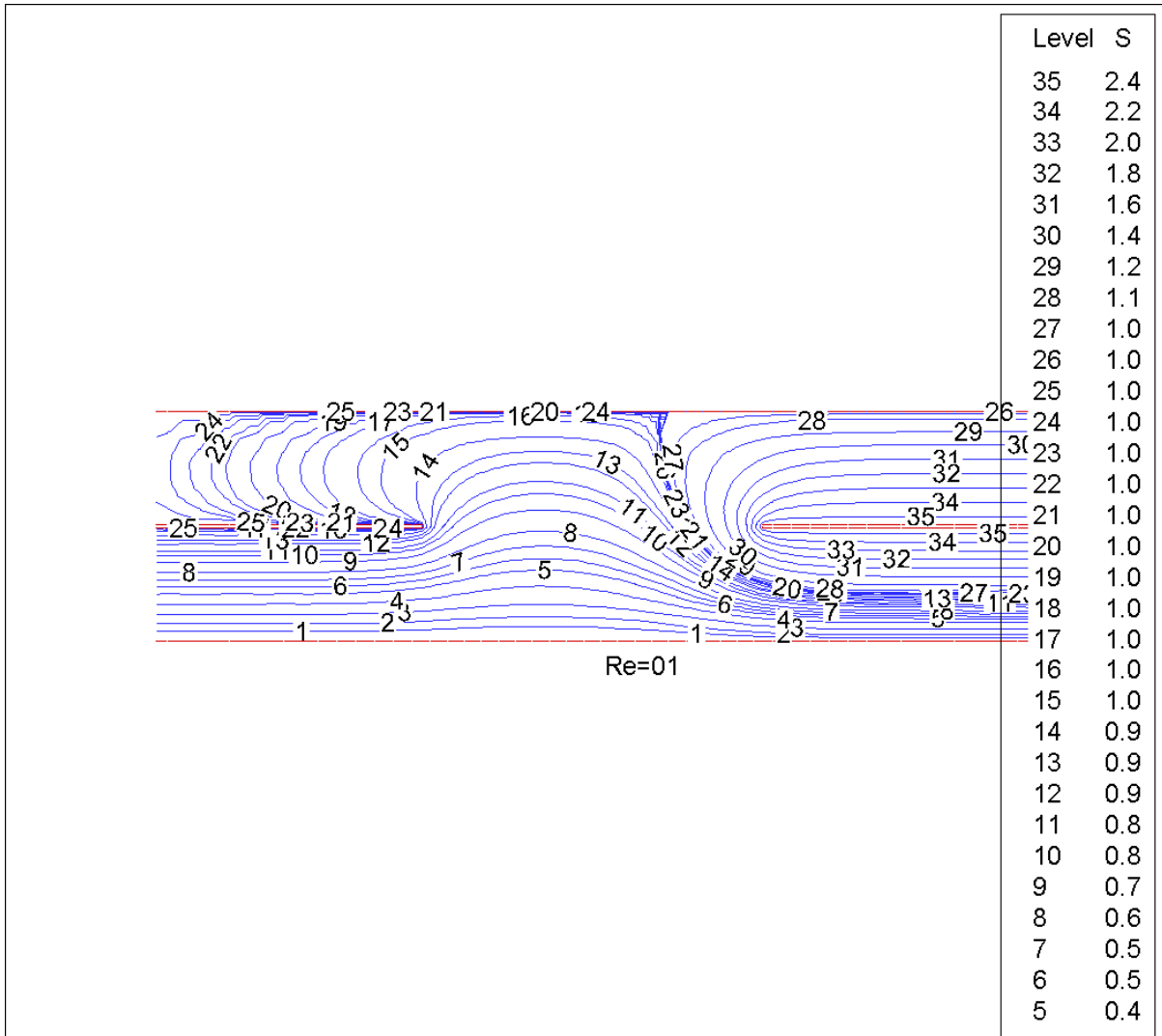
---

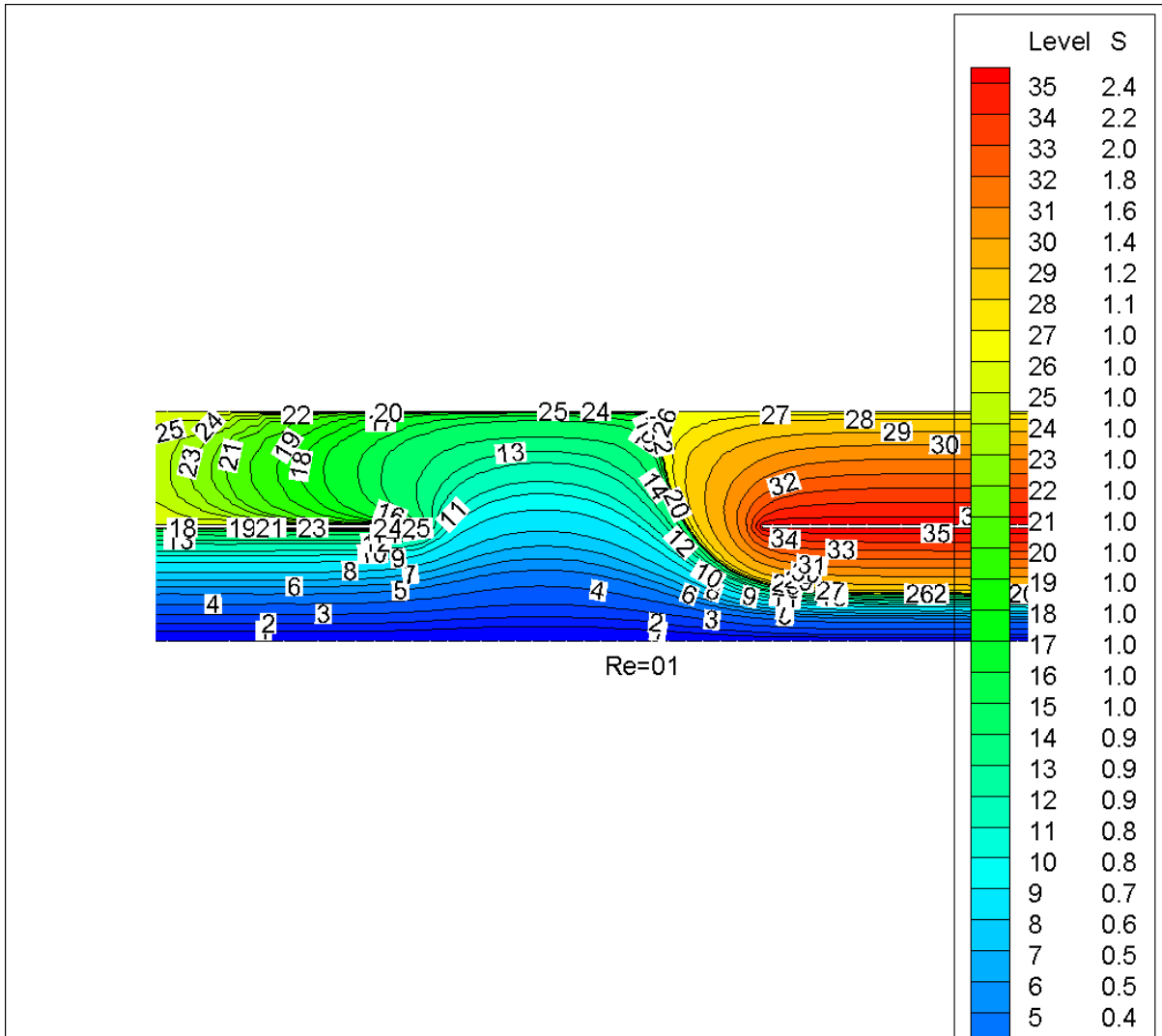
Unequal (1, 2) flow rate





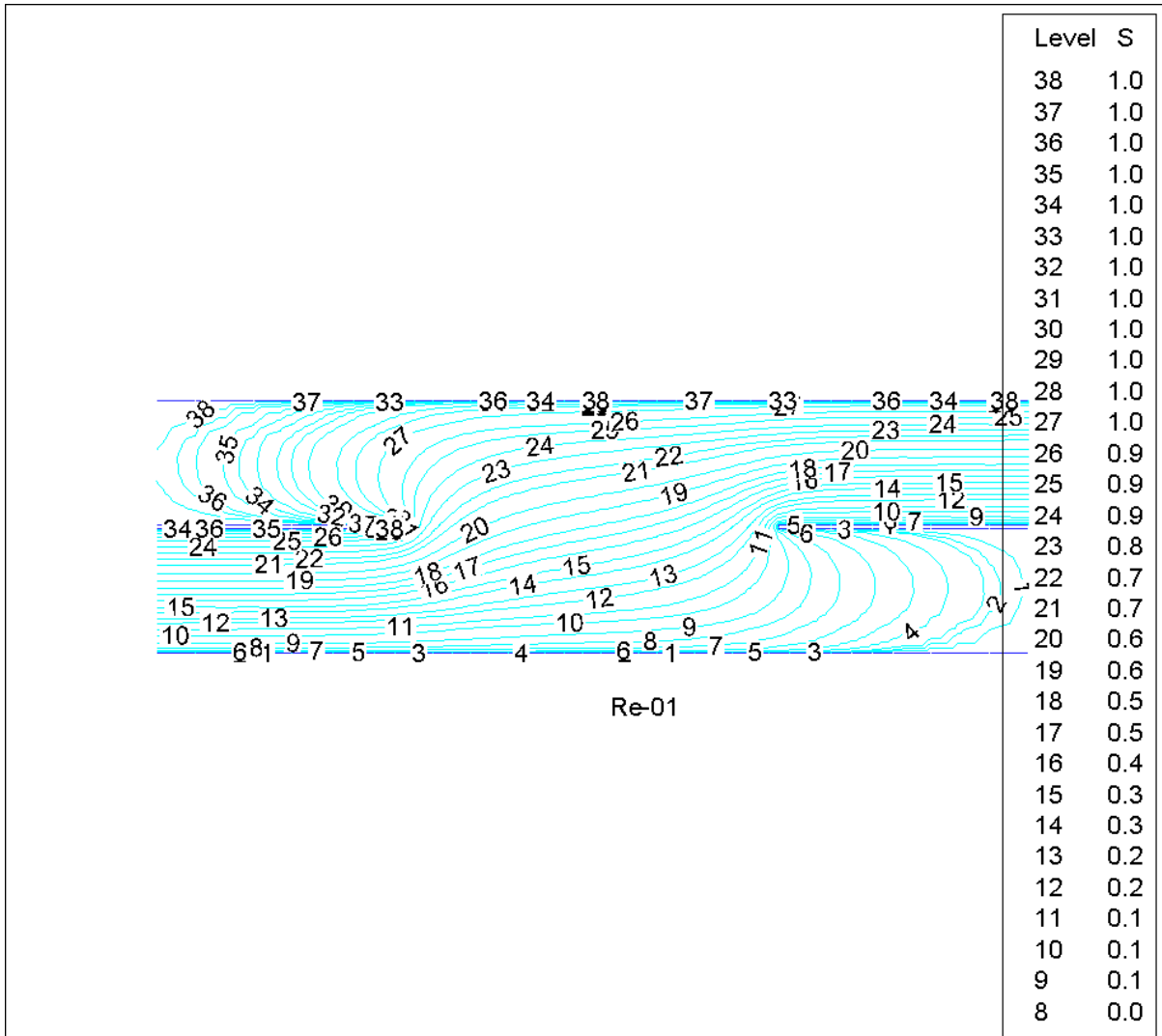


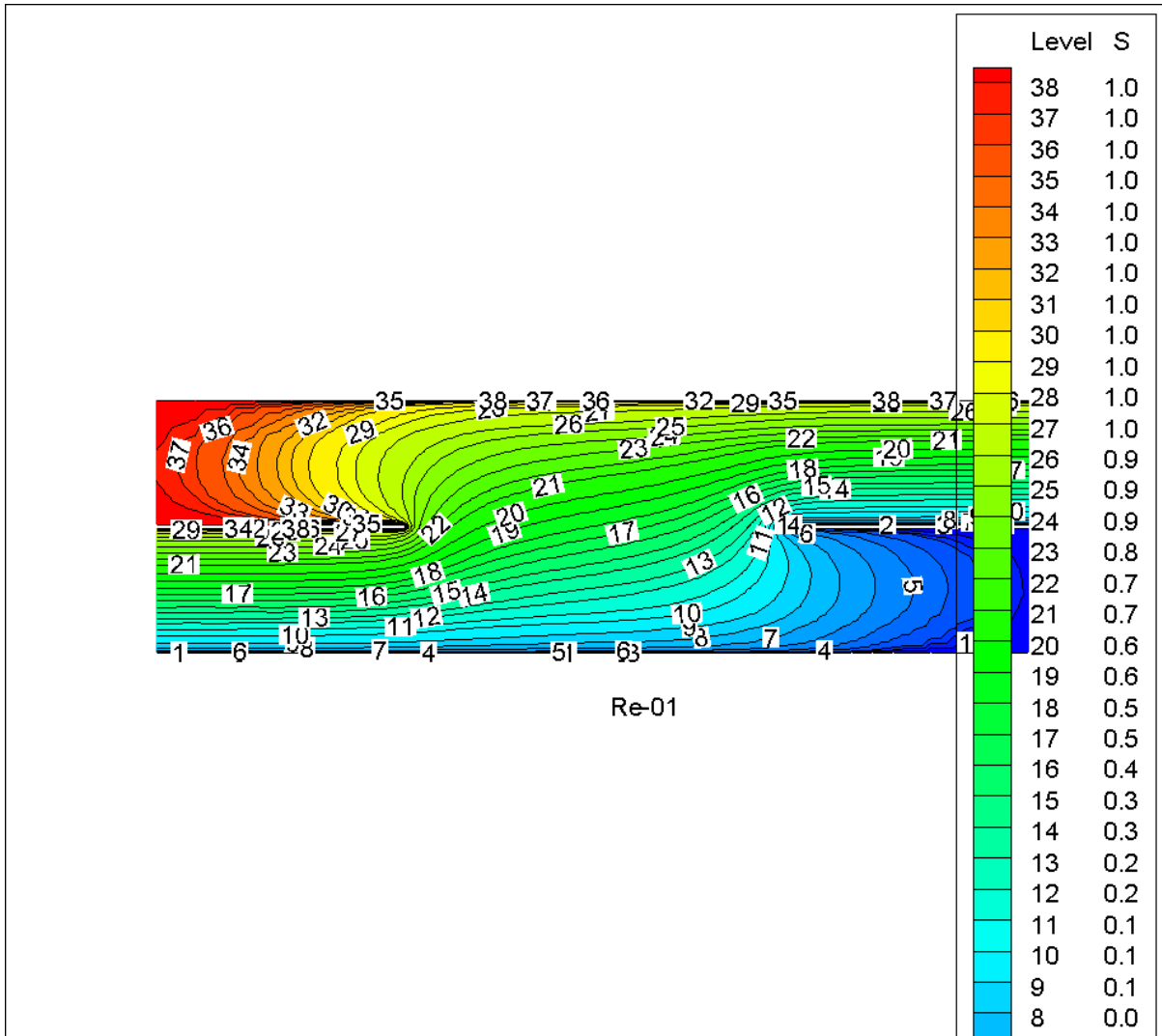


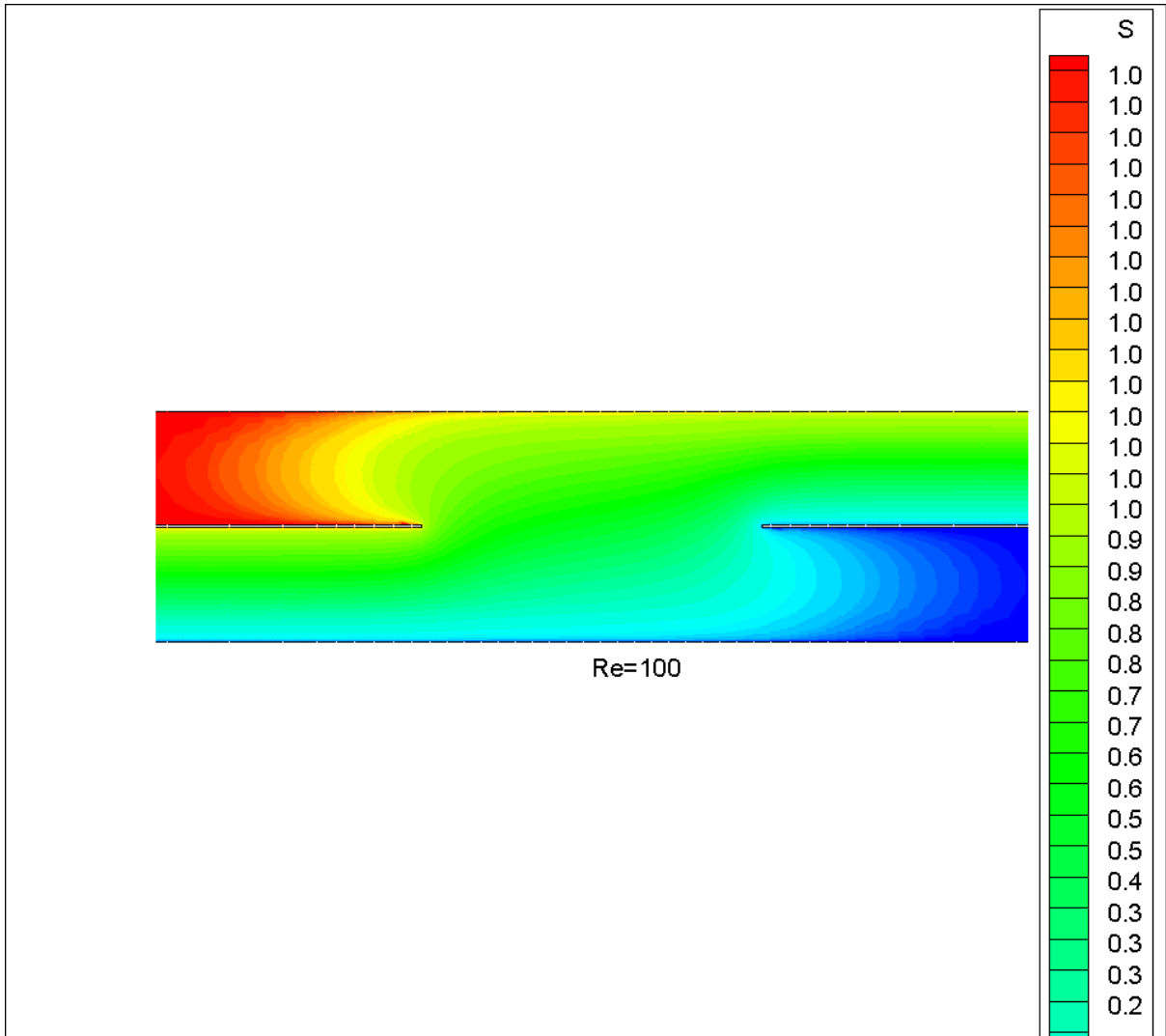


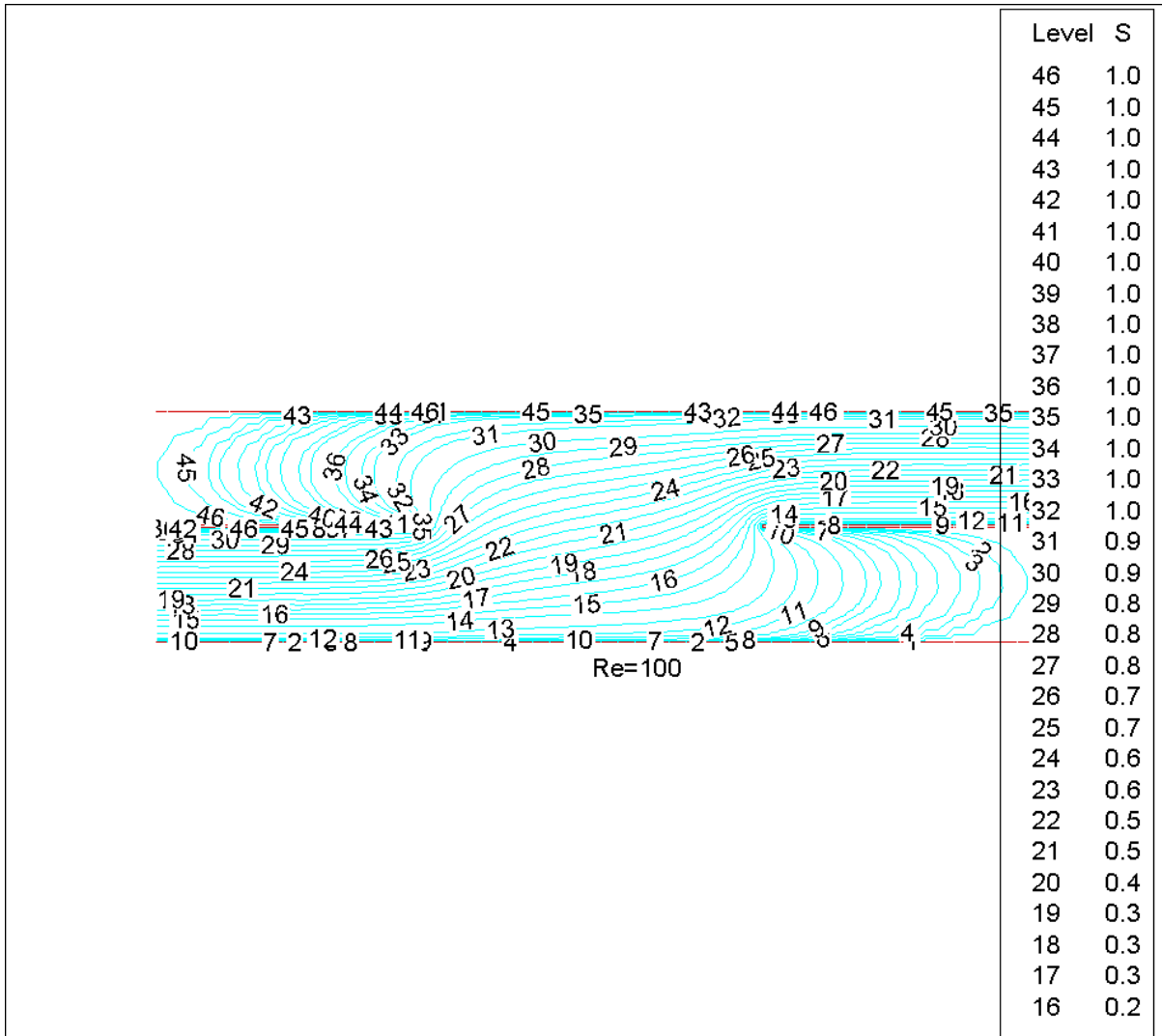
4.

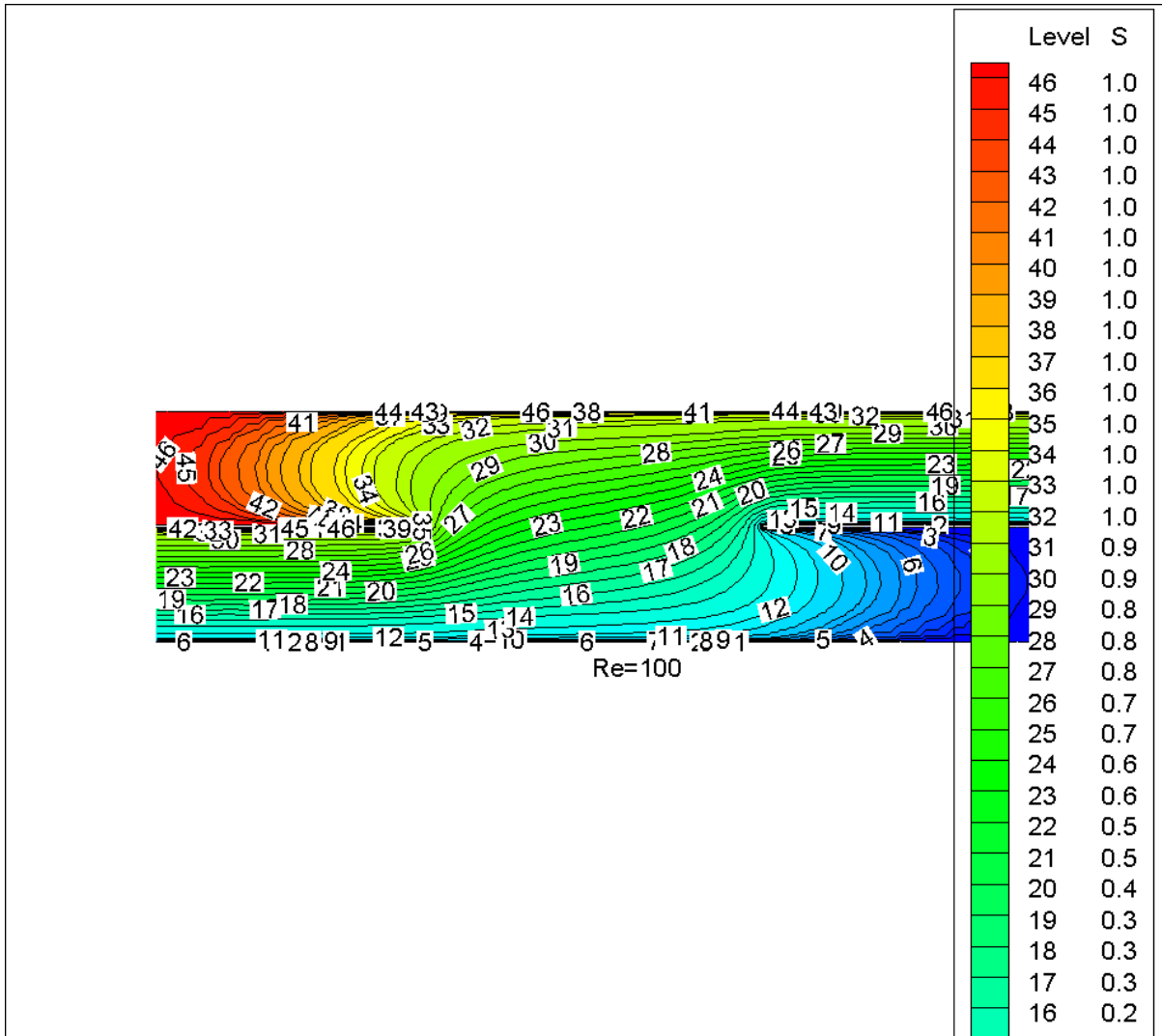


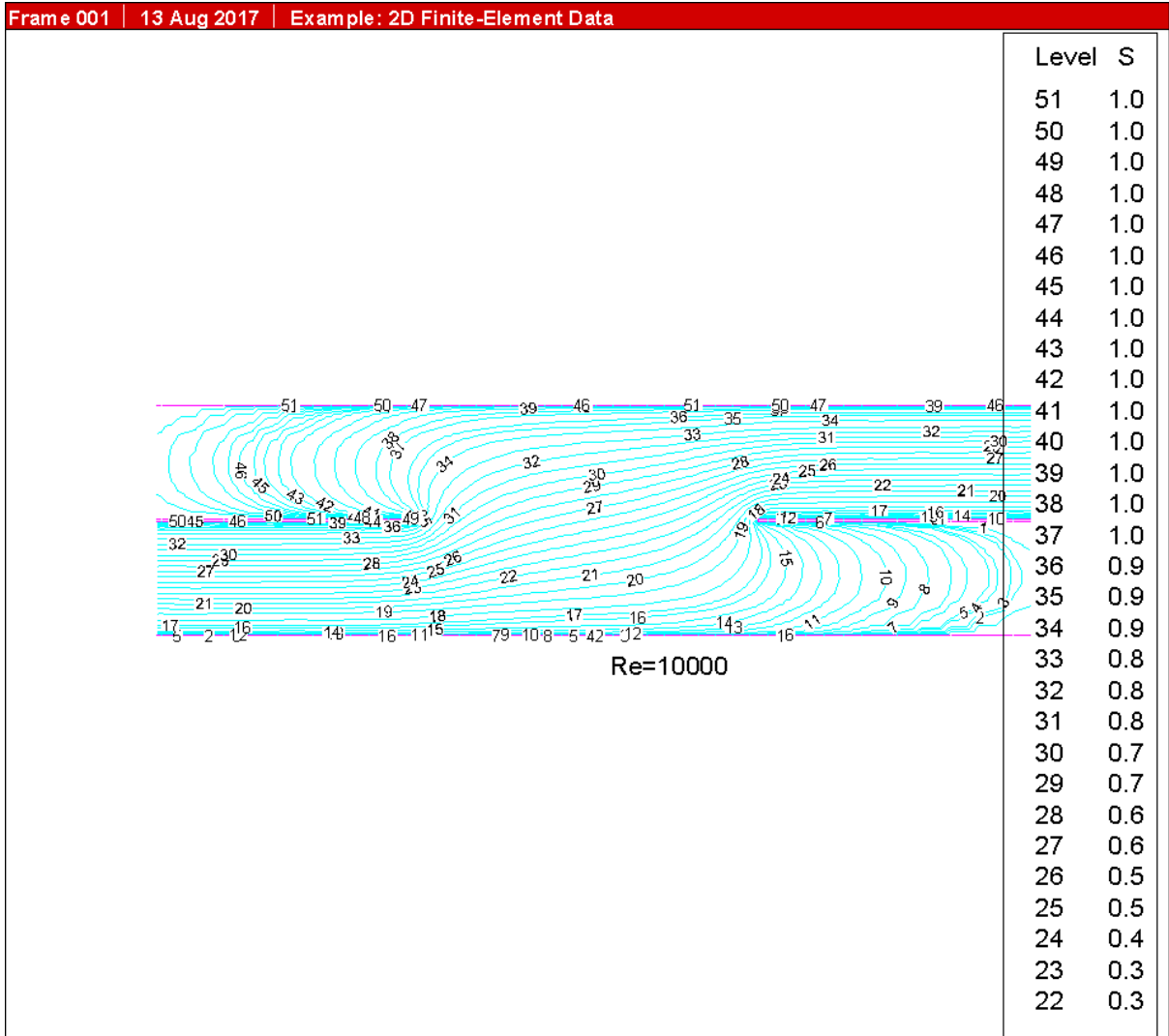


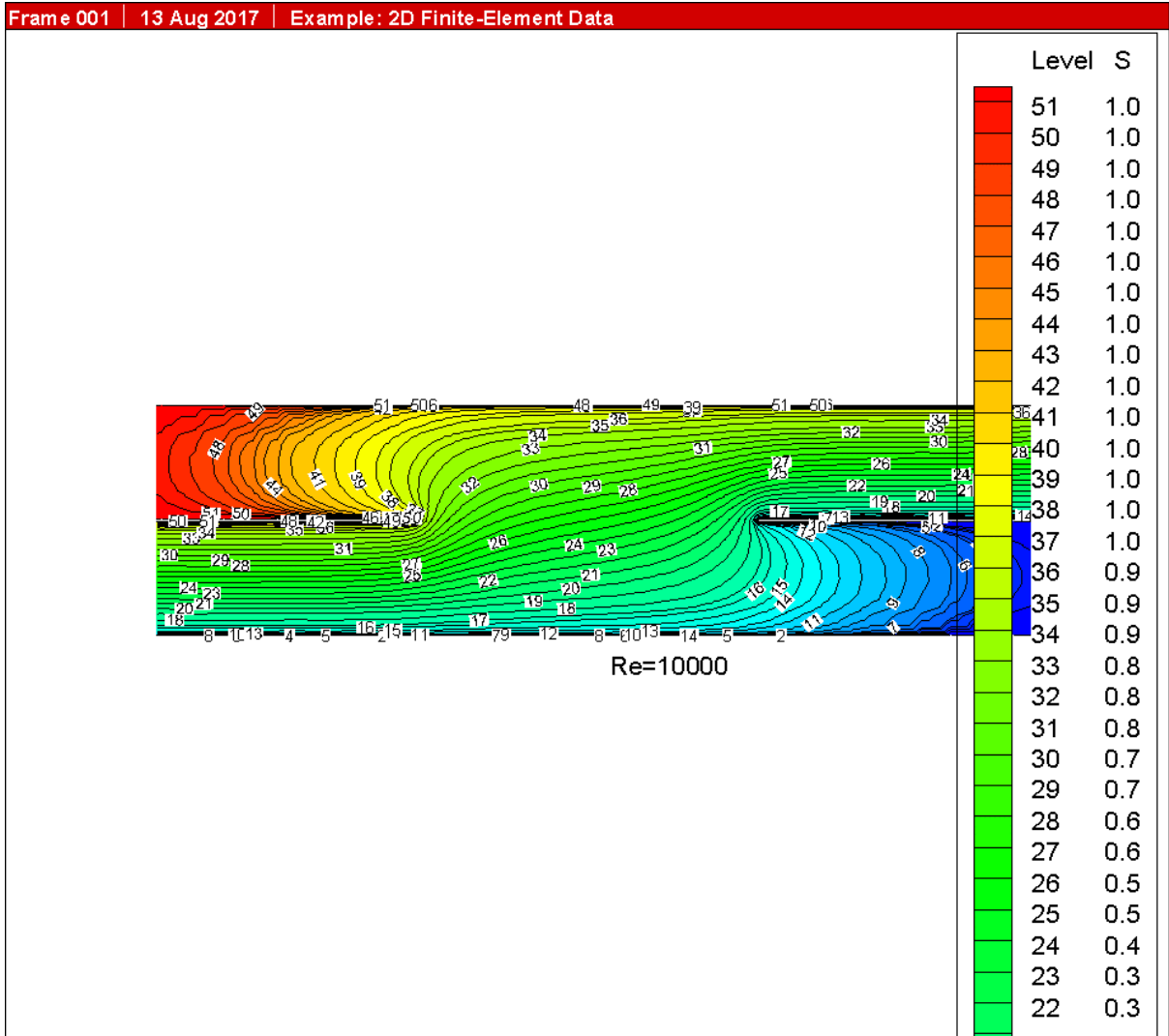










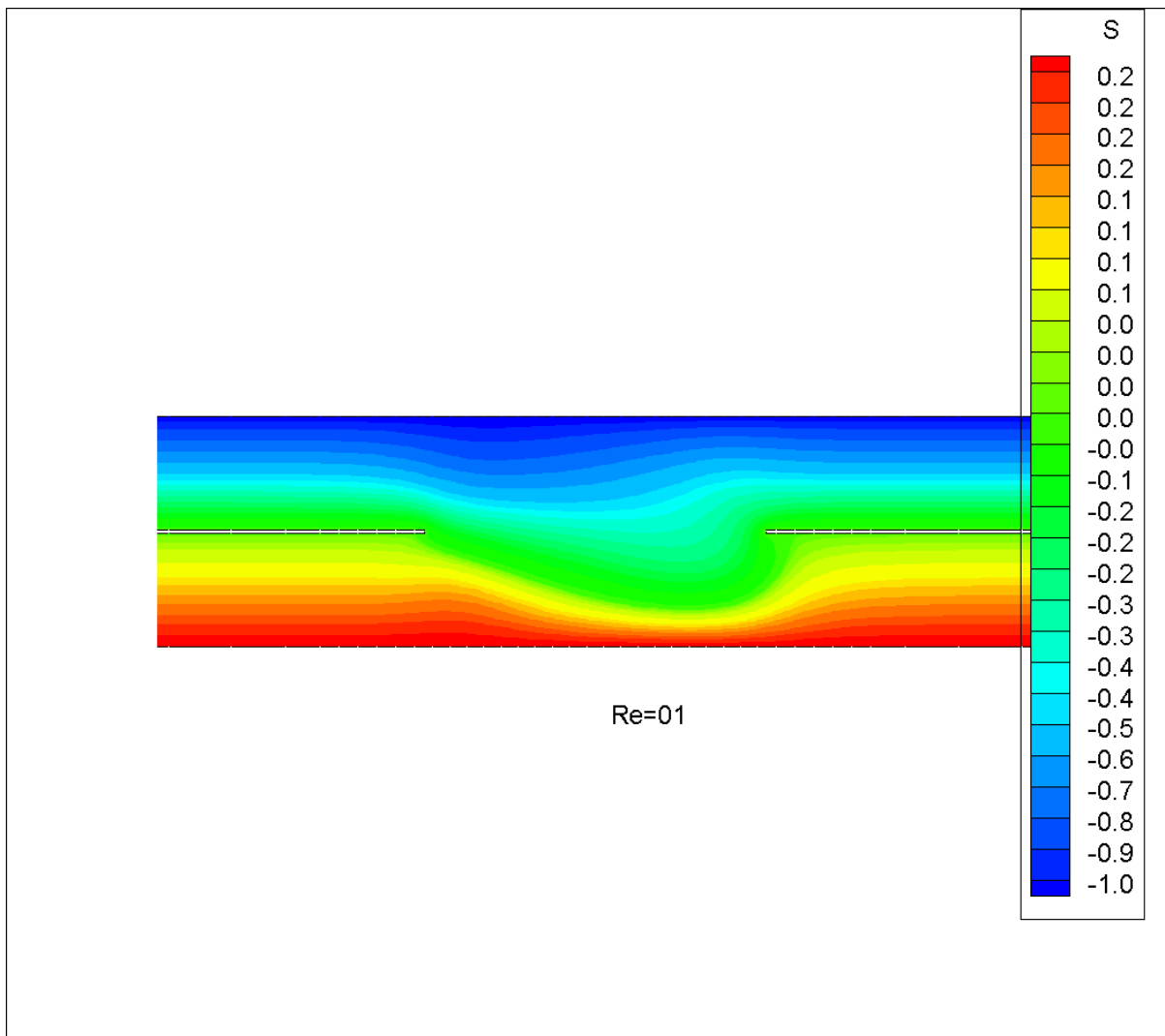


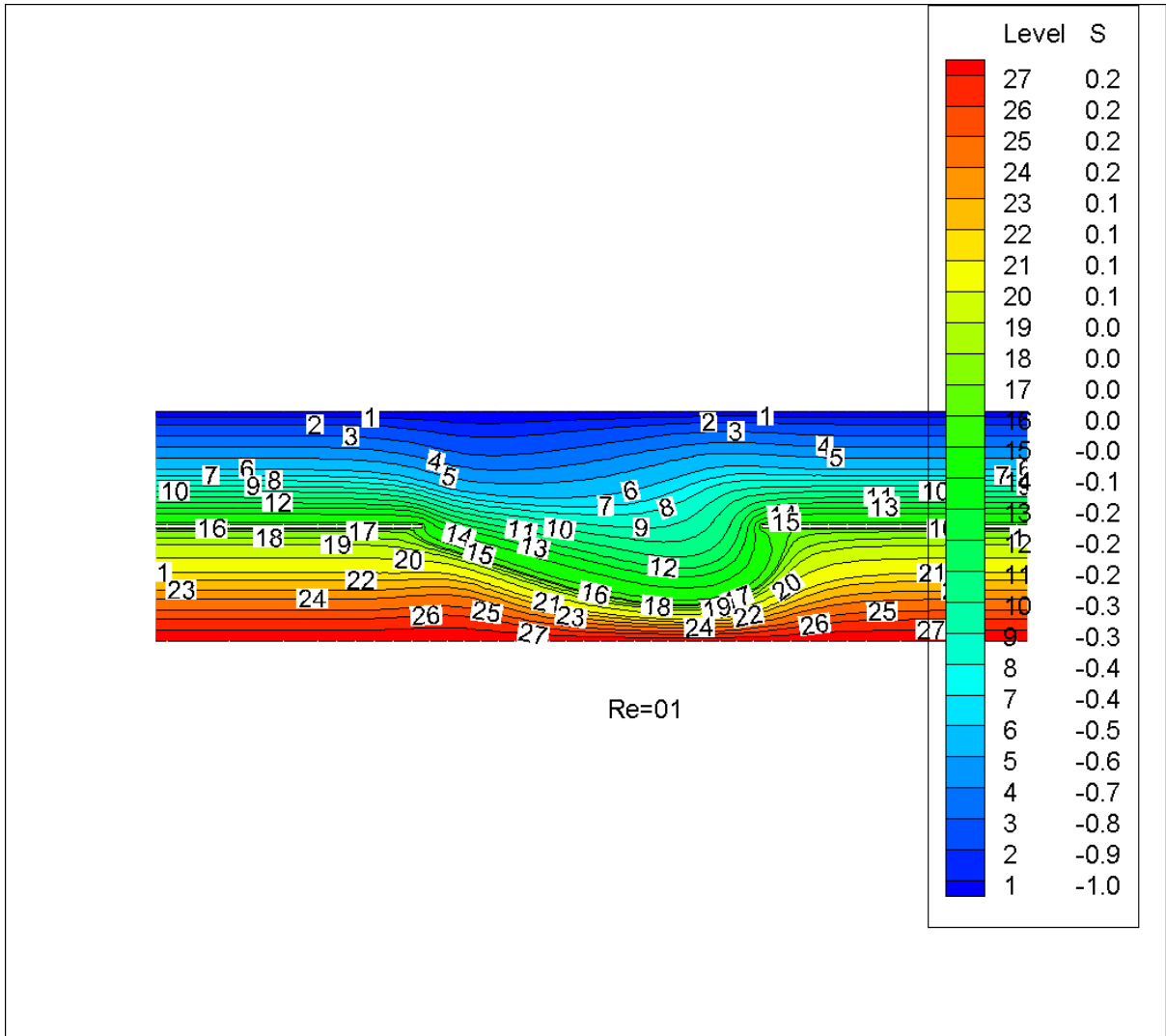


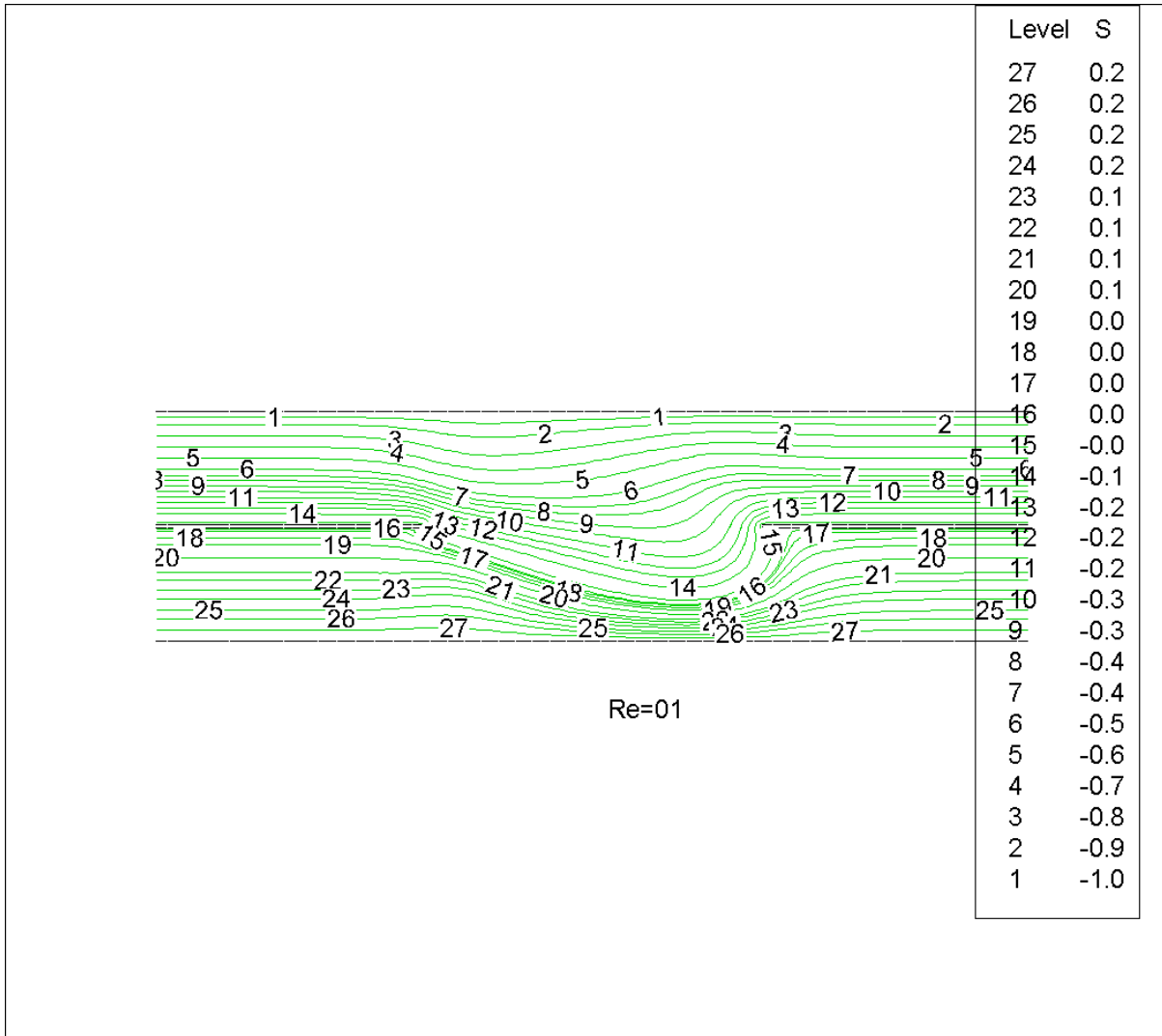
### 3. Chapter-7

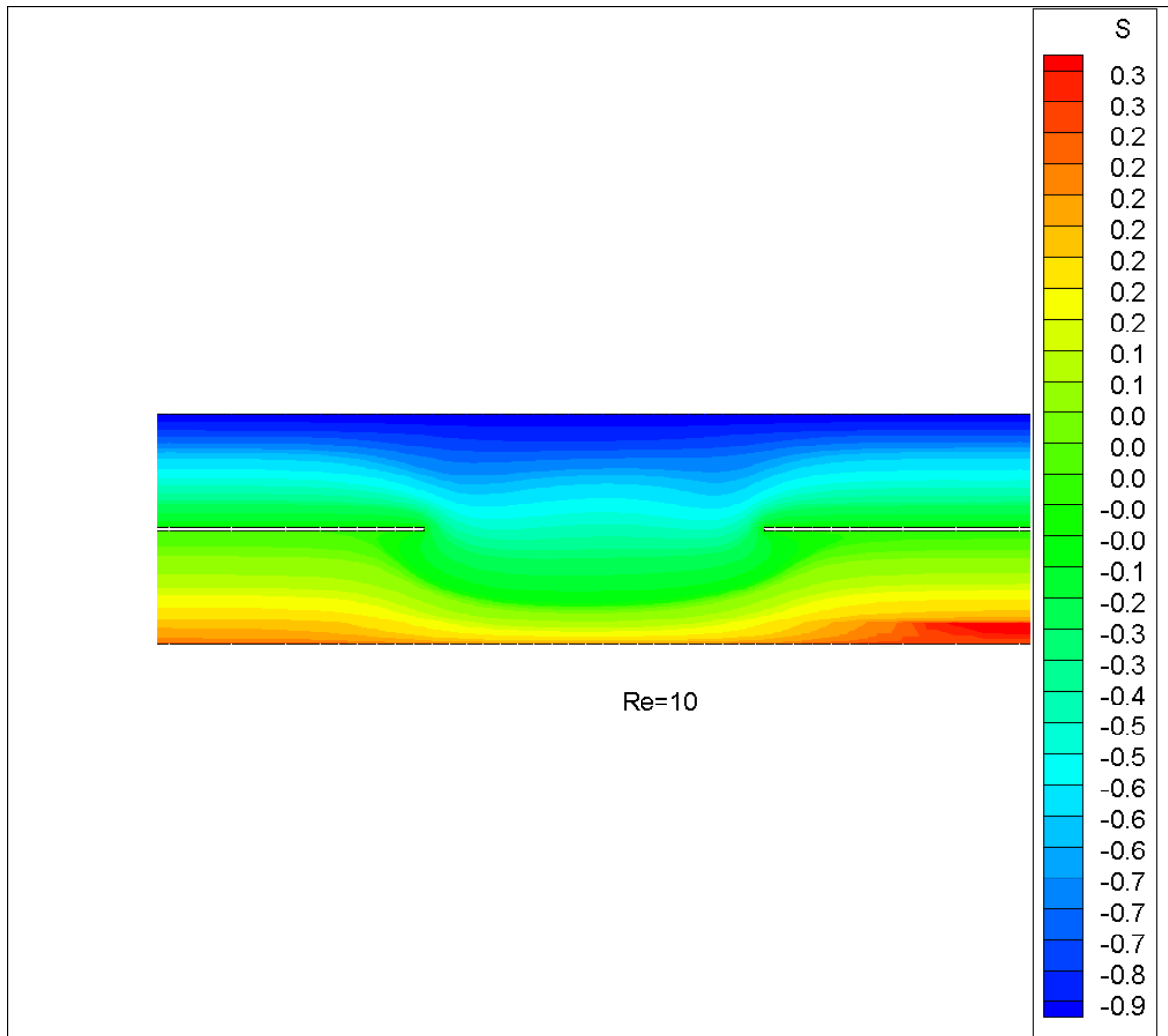
#### 3.1 Newtonian flows in a circular pipes filled with non-porous media

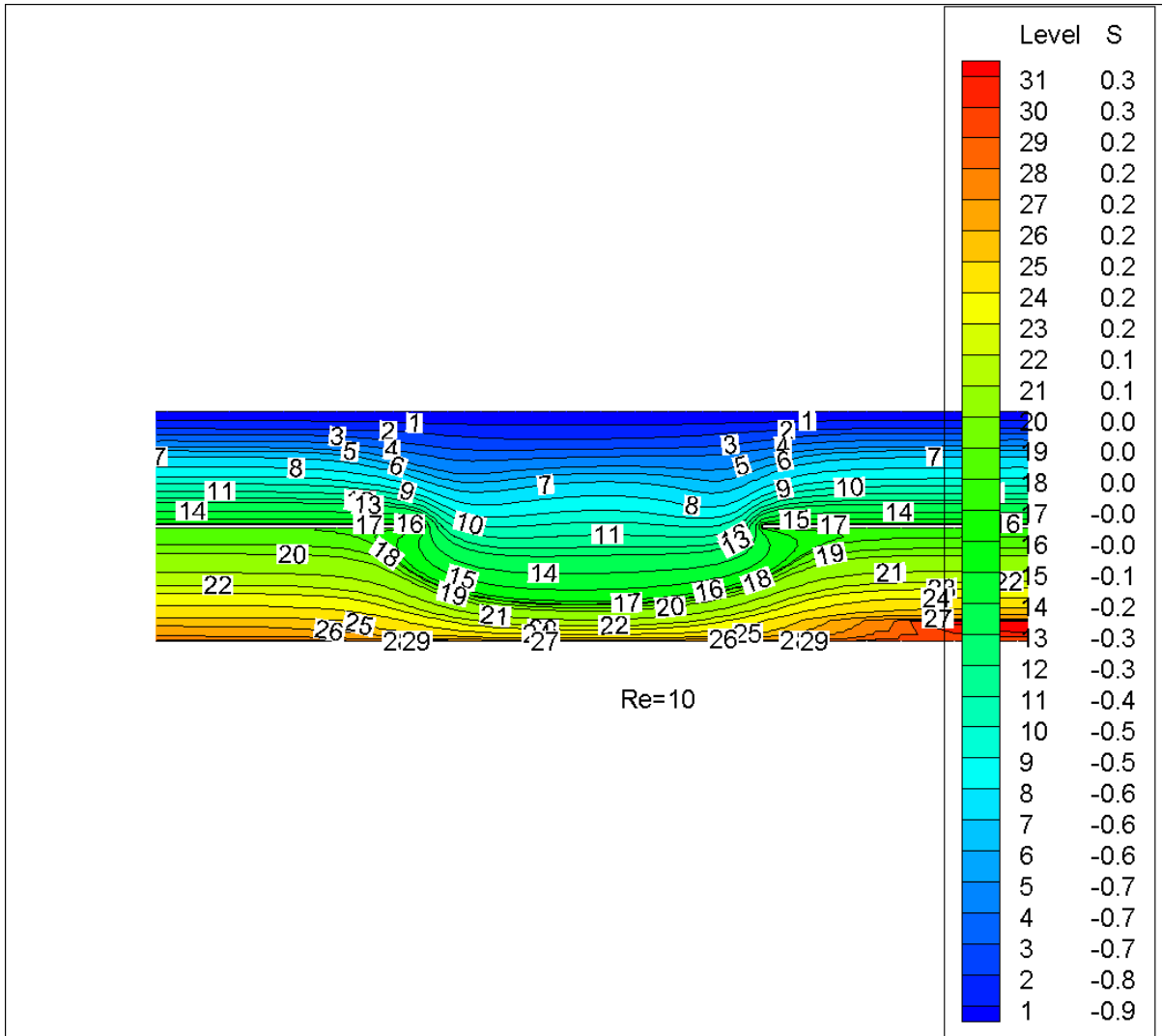
Equal (1, 1) flow rate

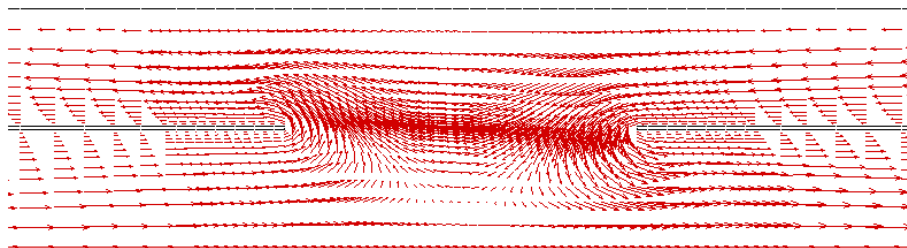
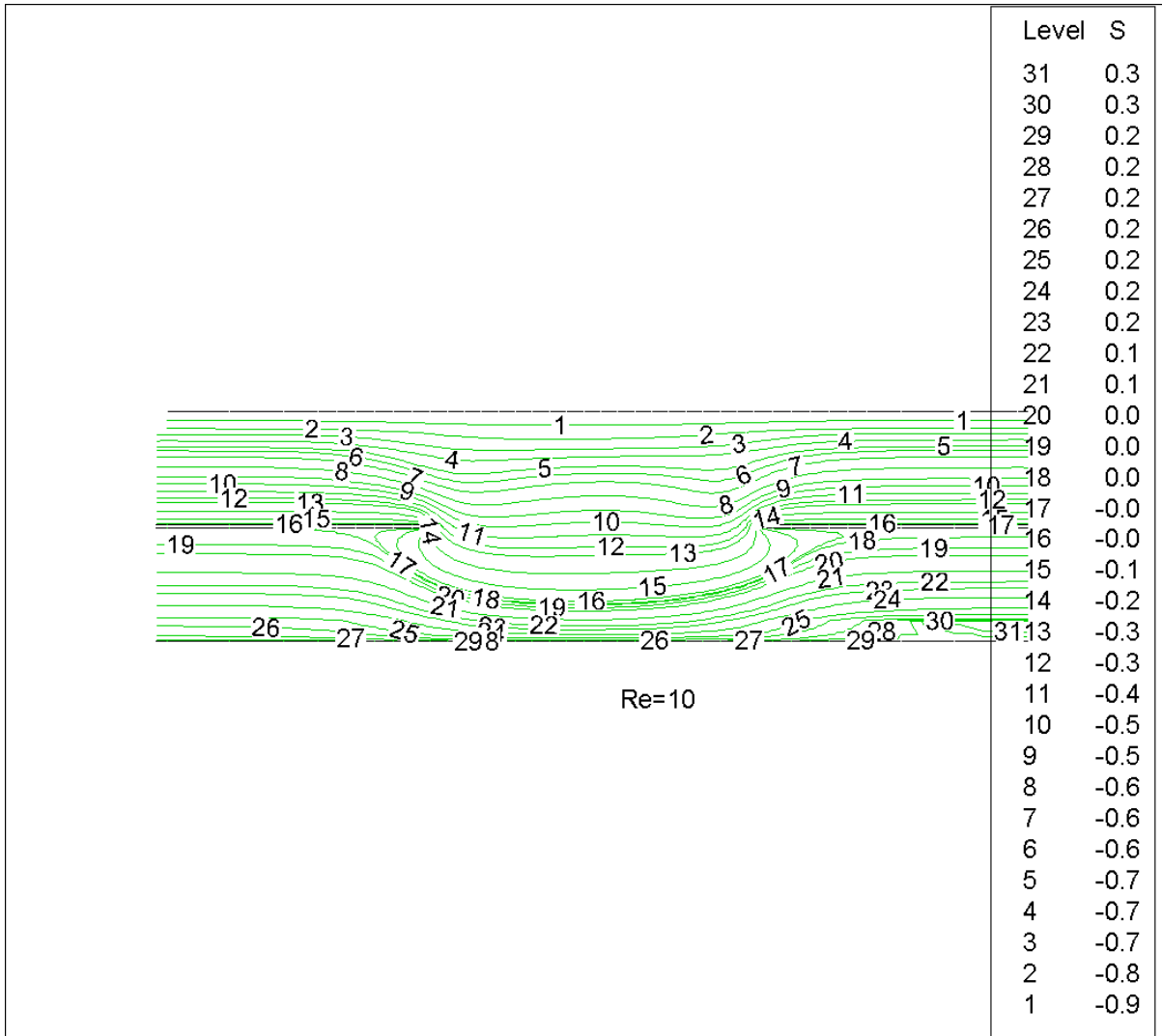




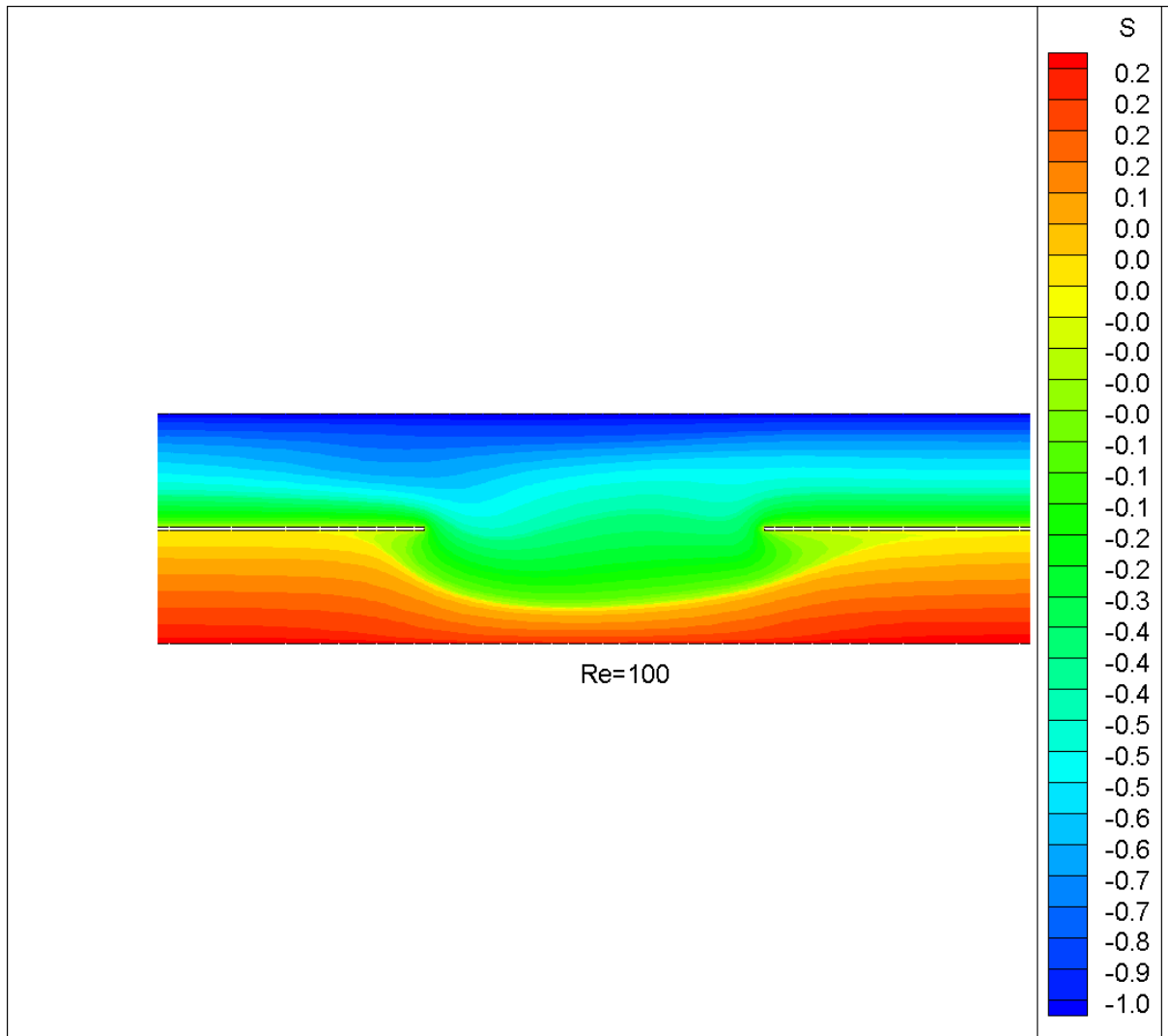


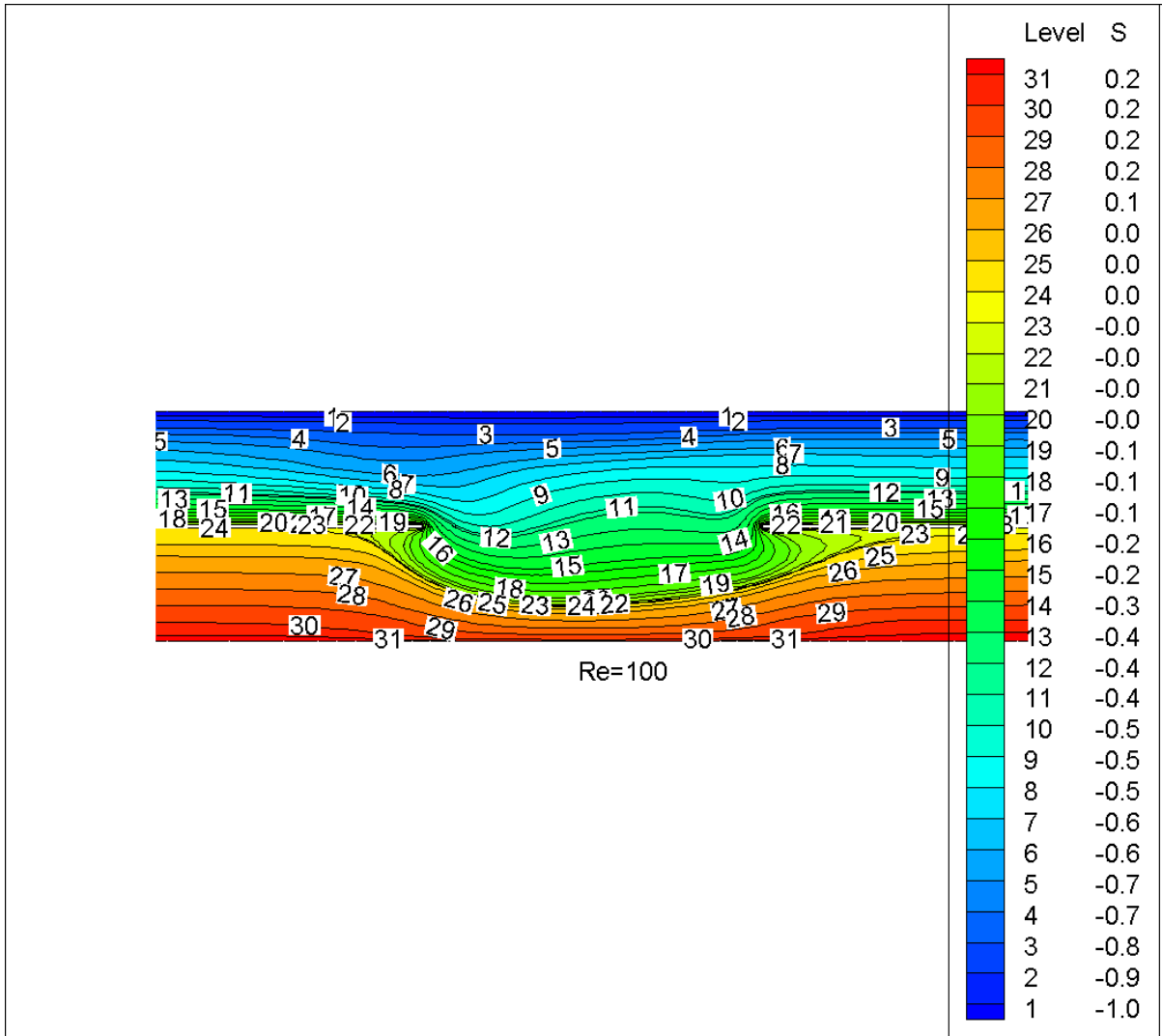


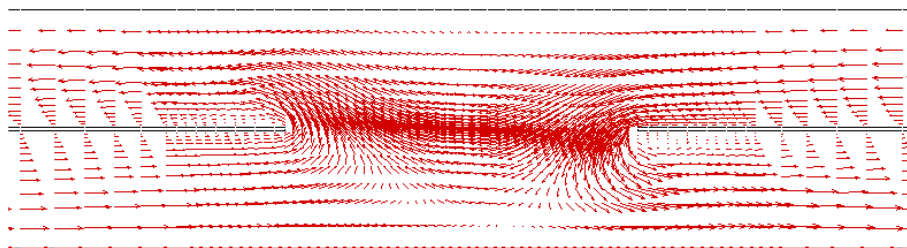
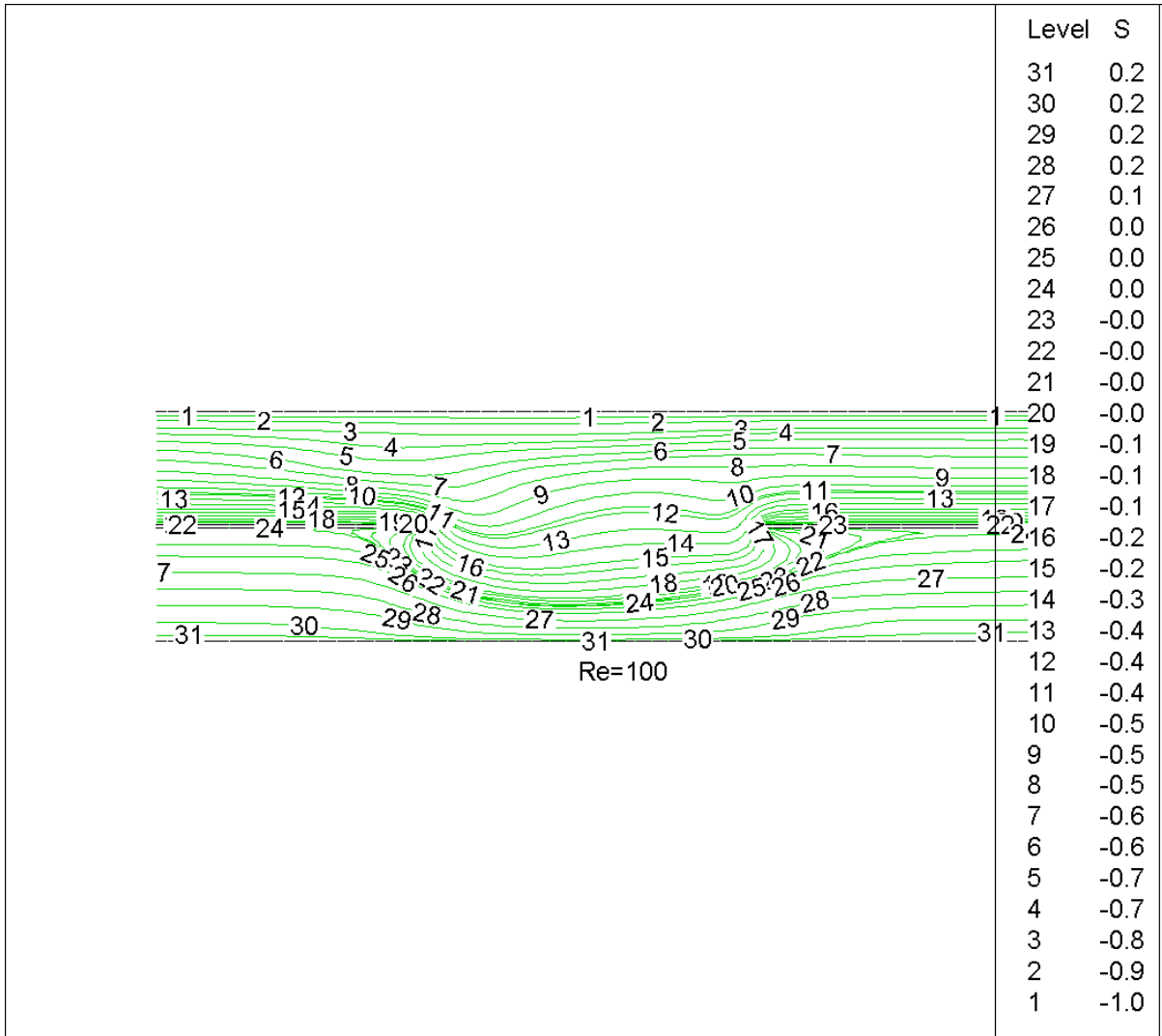




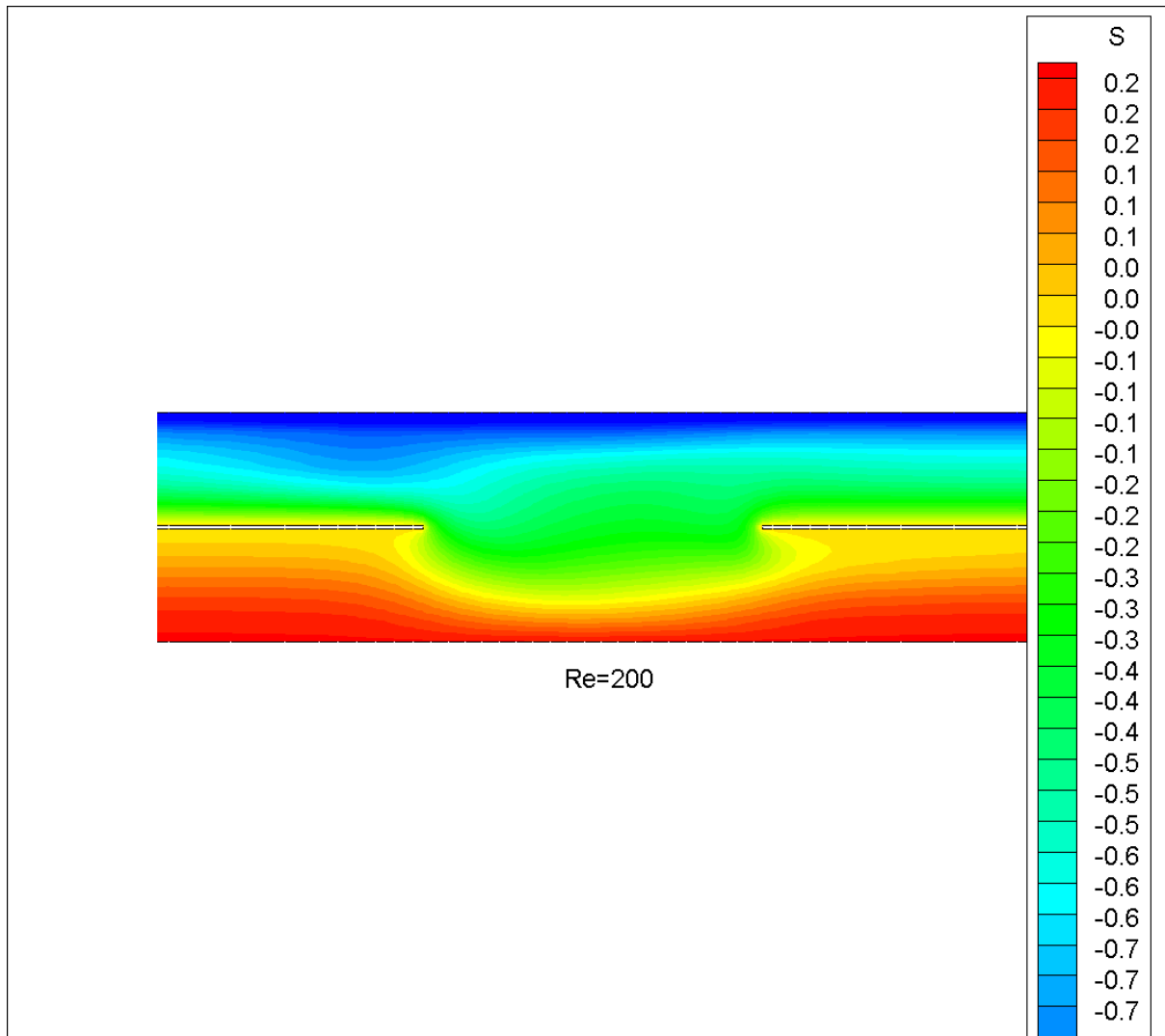
Re=10

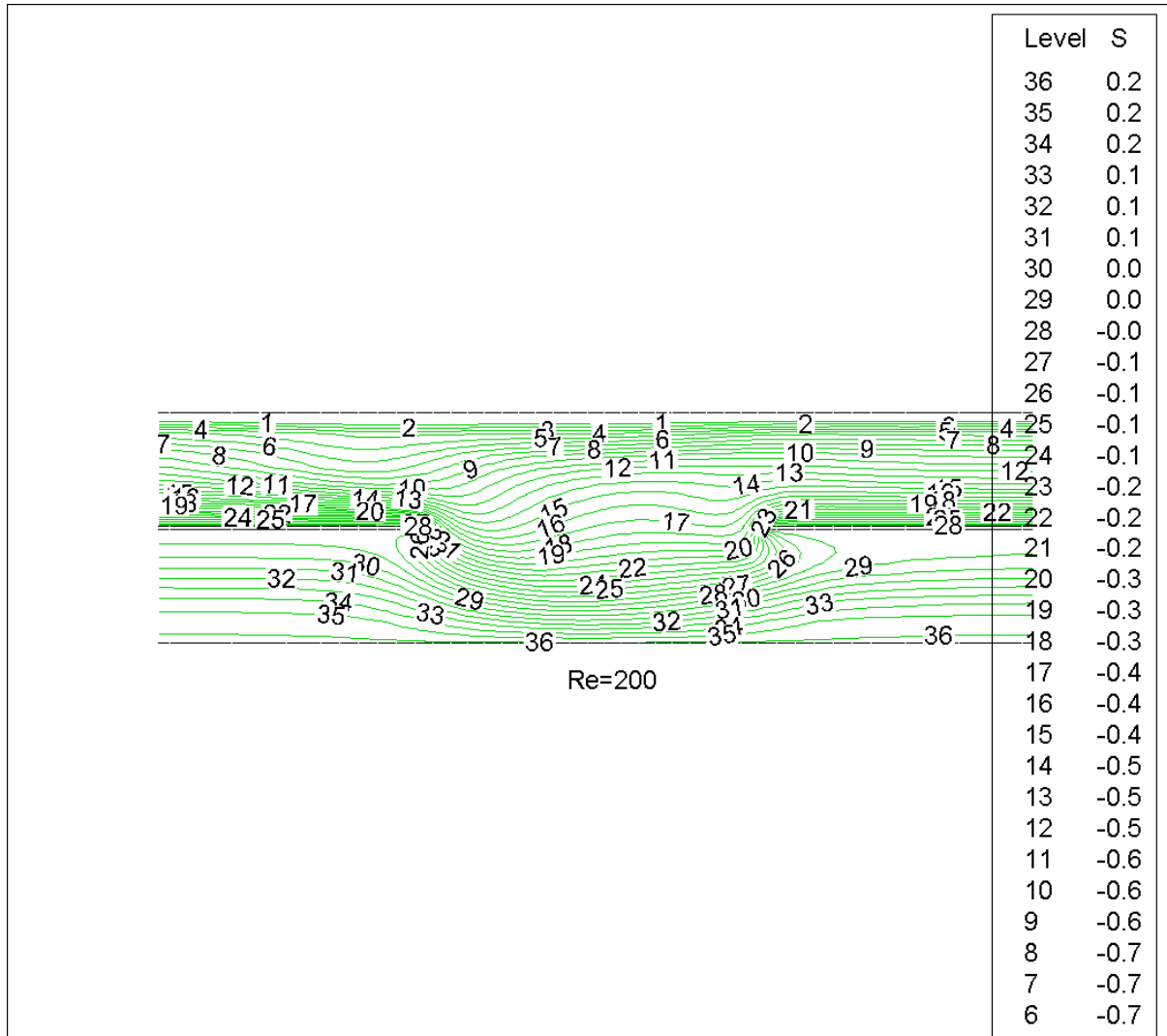


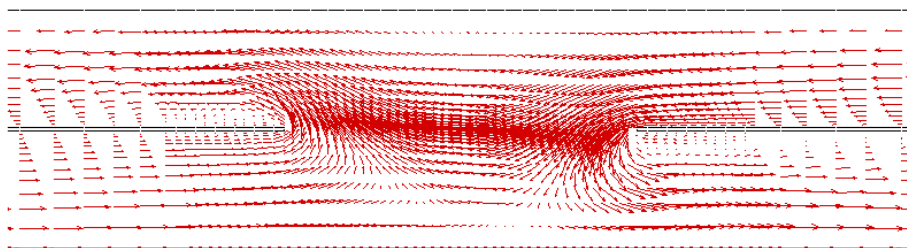
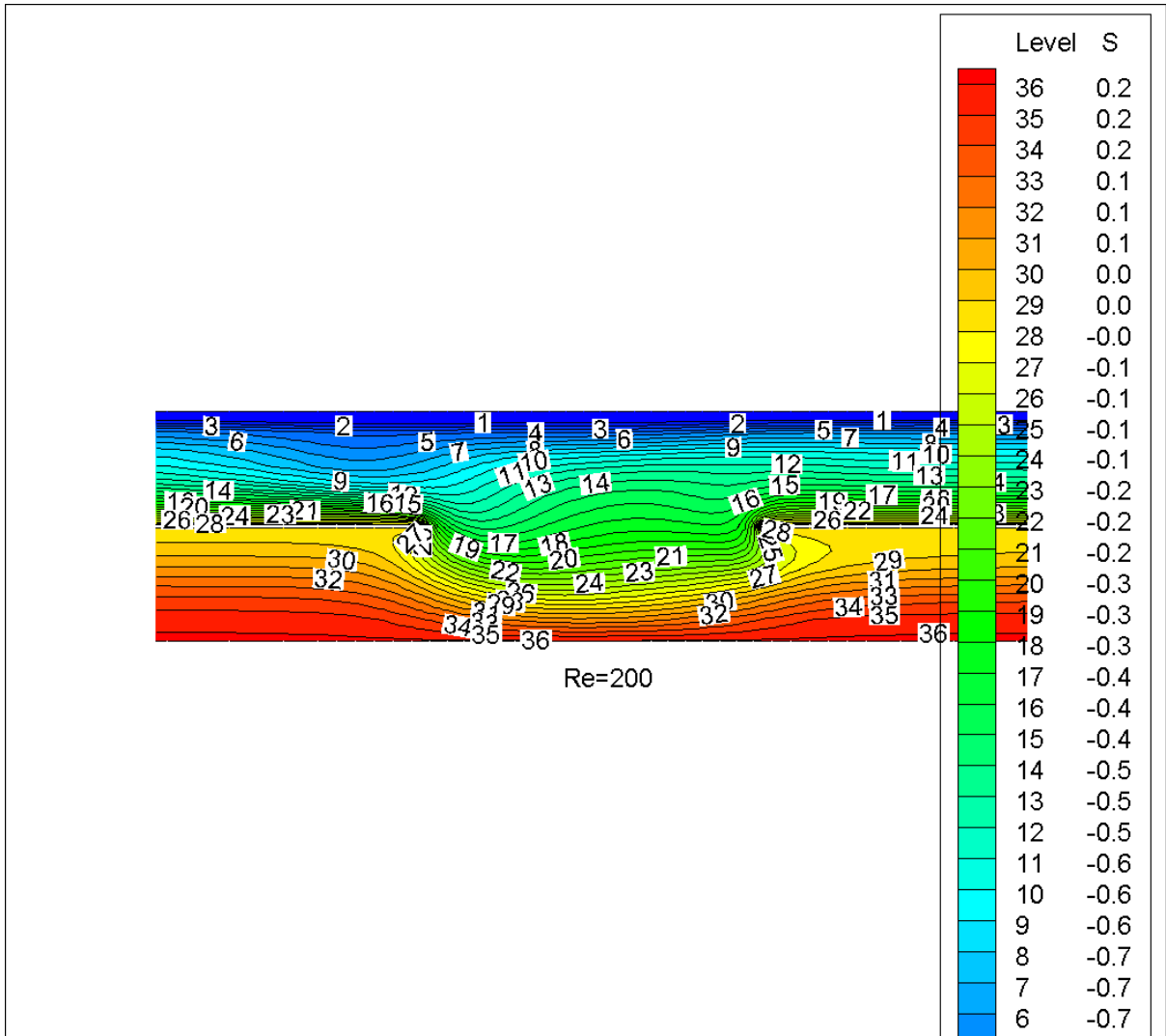




Re=100  
413



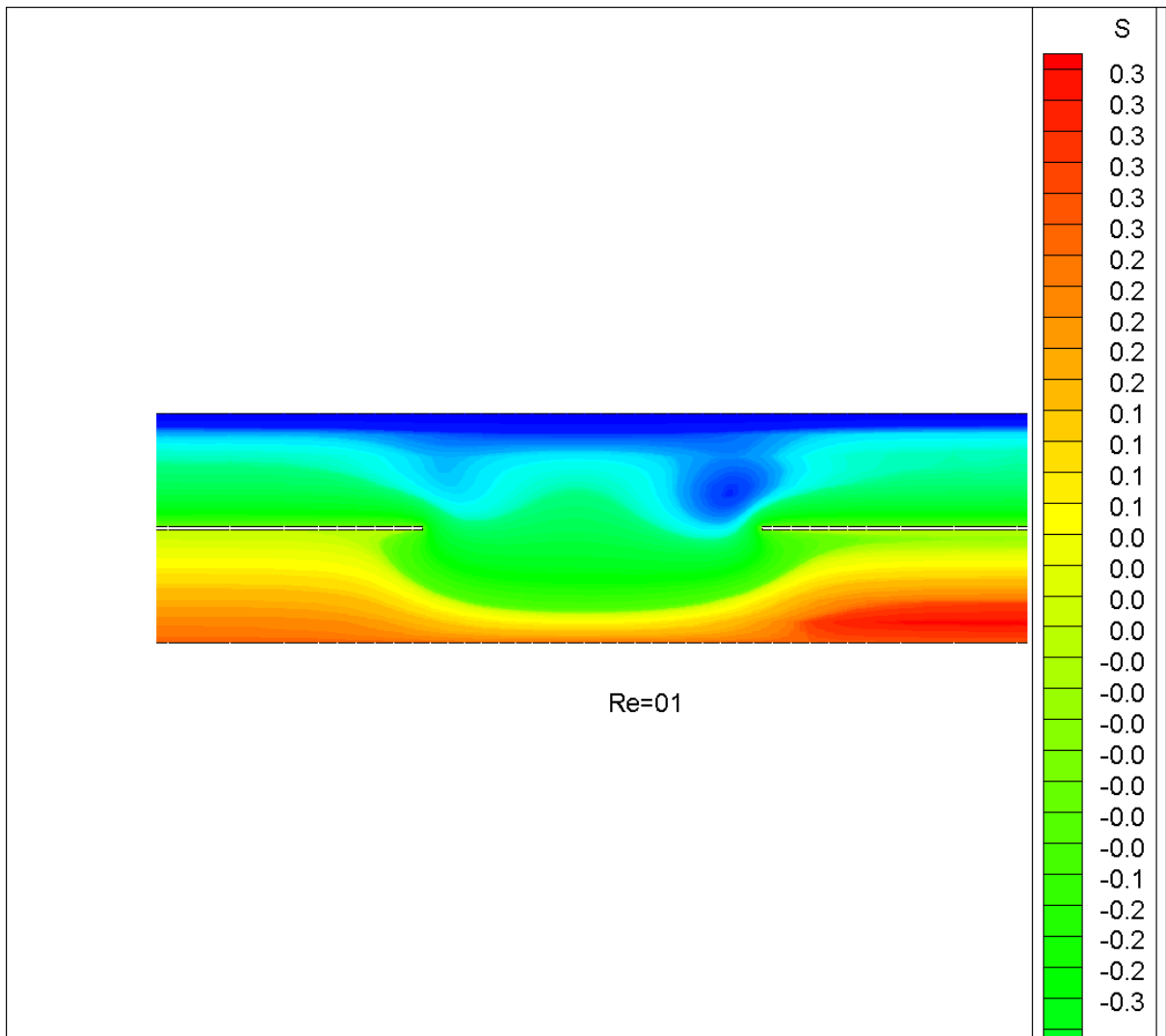


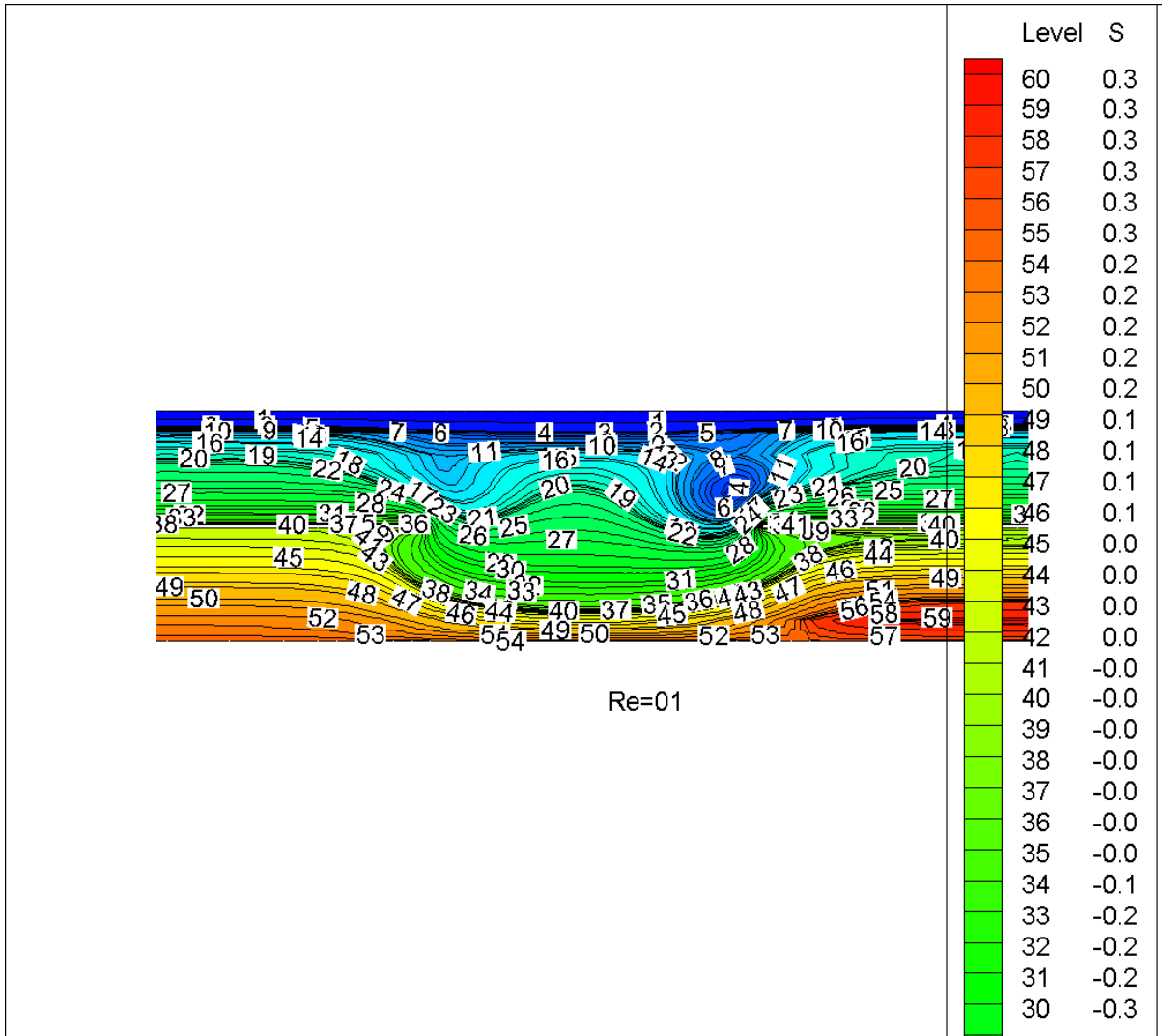


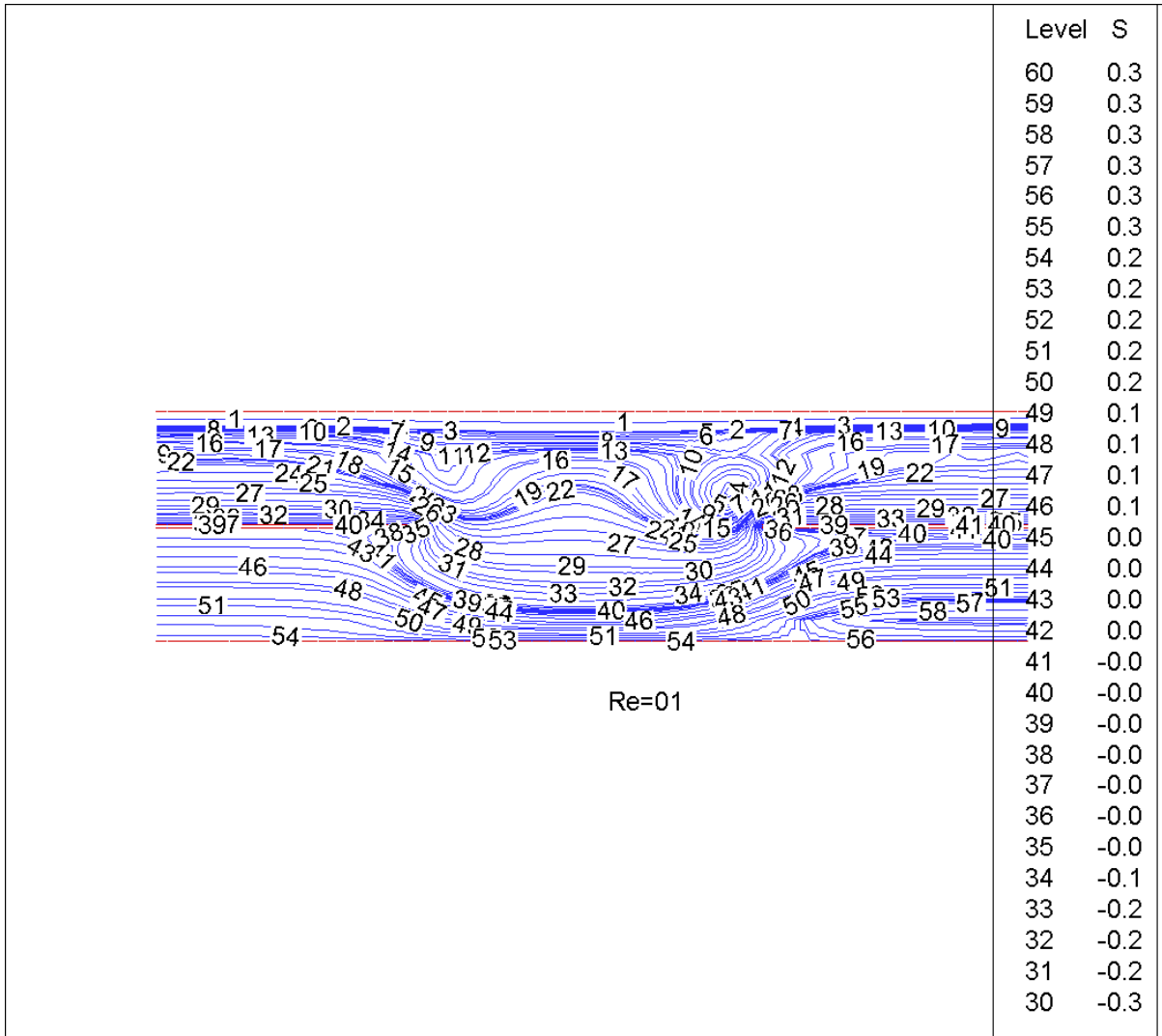
Re=200  
416

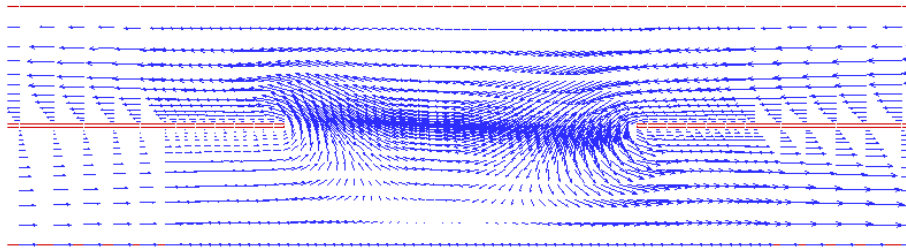
---

**Unequal (1, 2) flow rate**

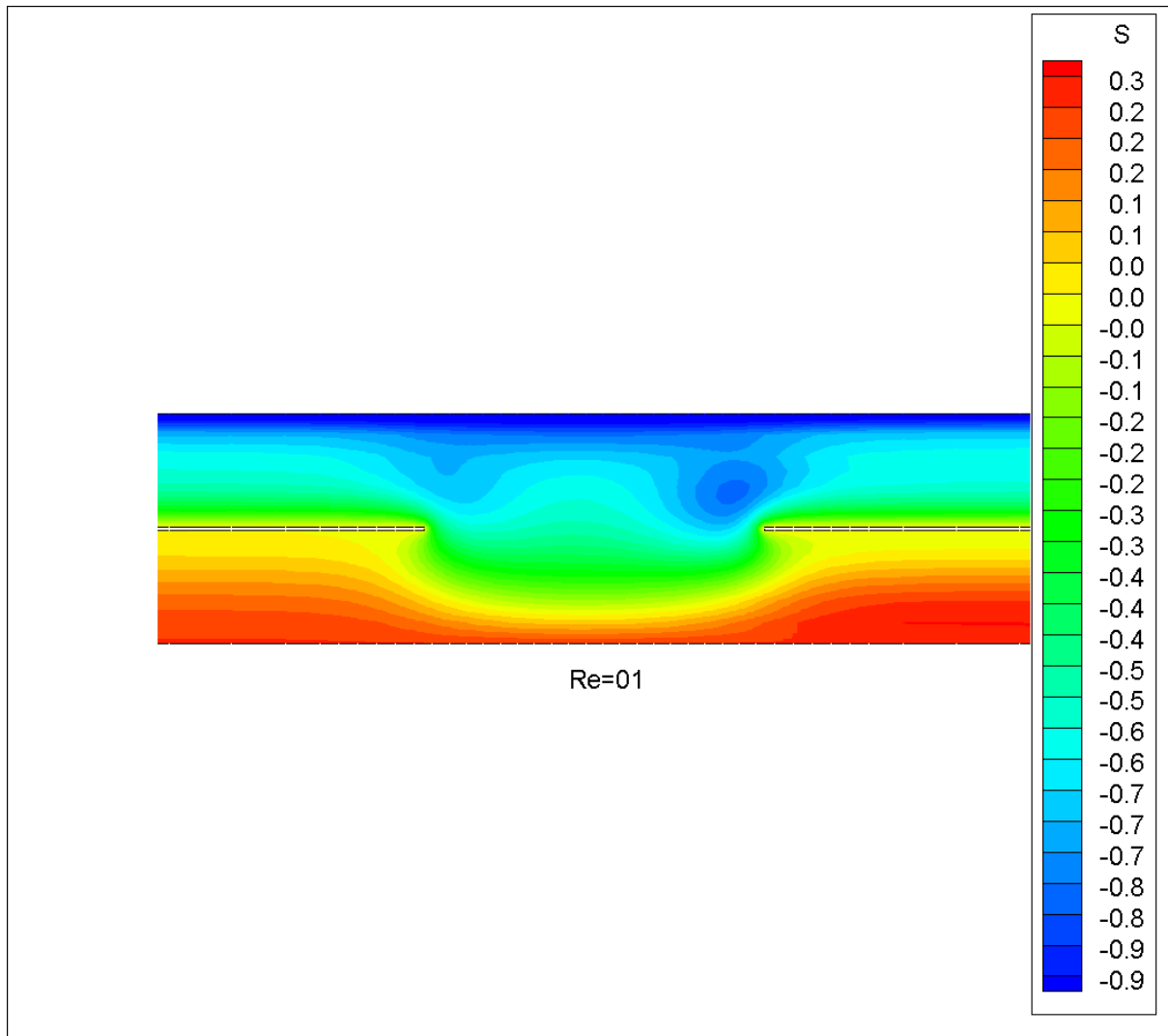


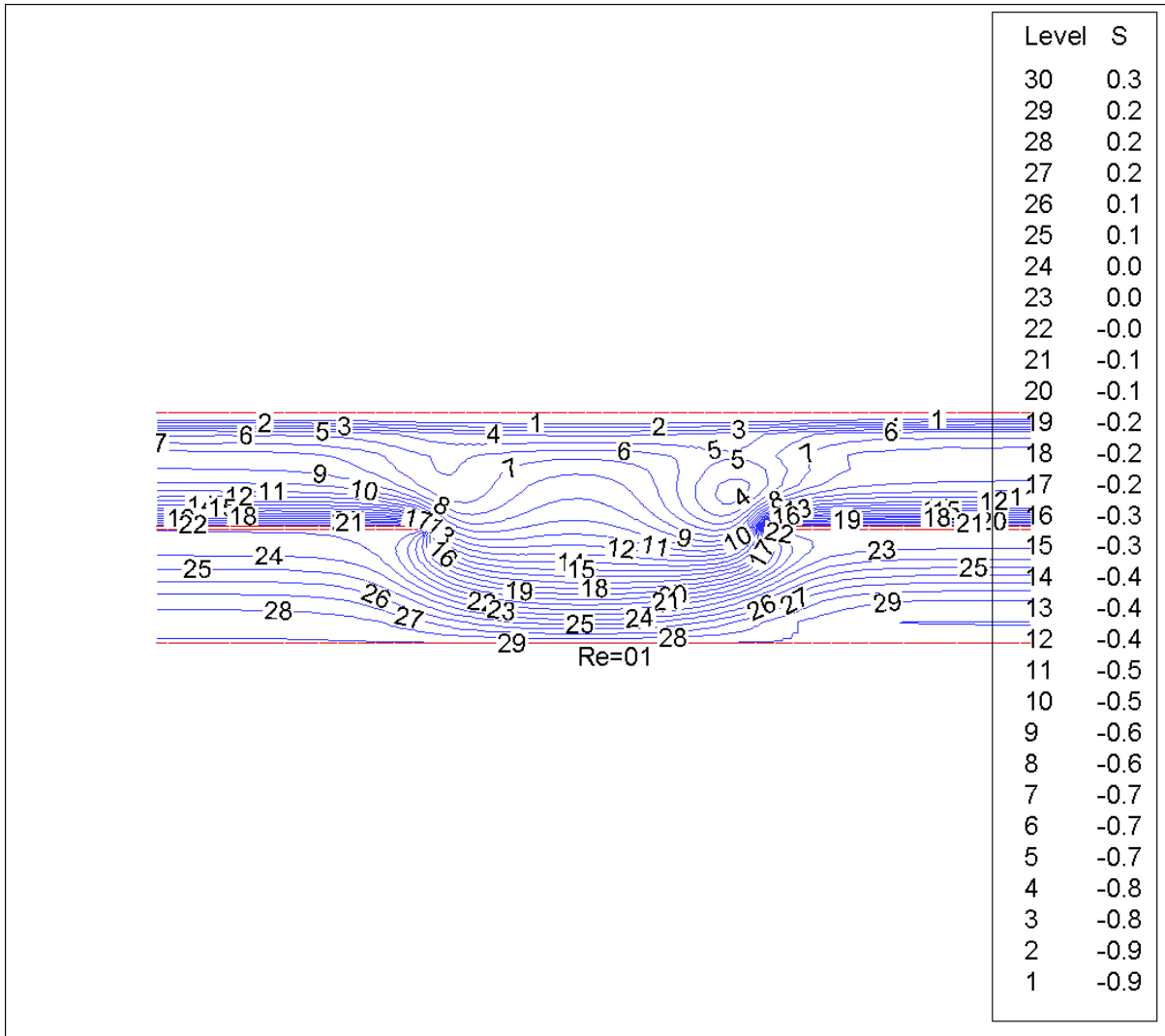


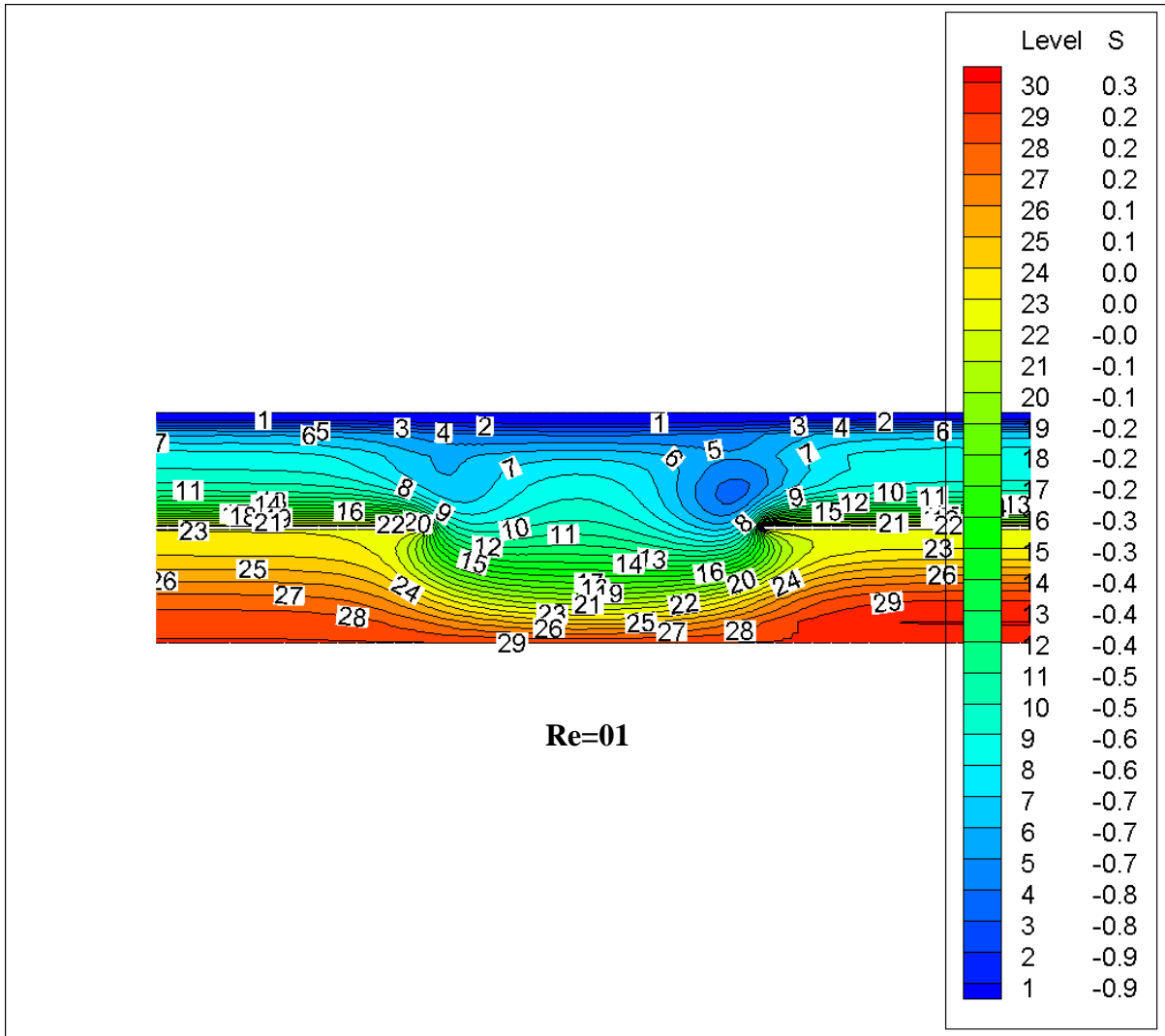




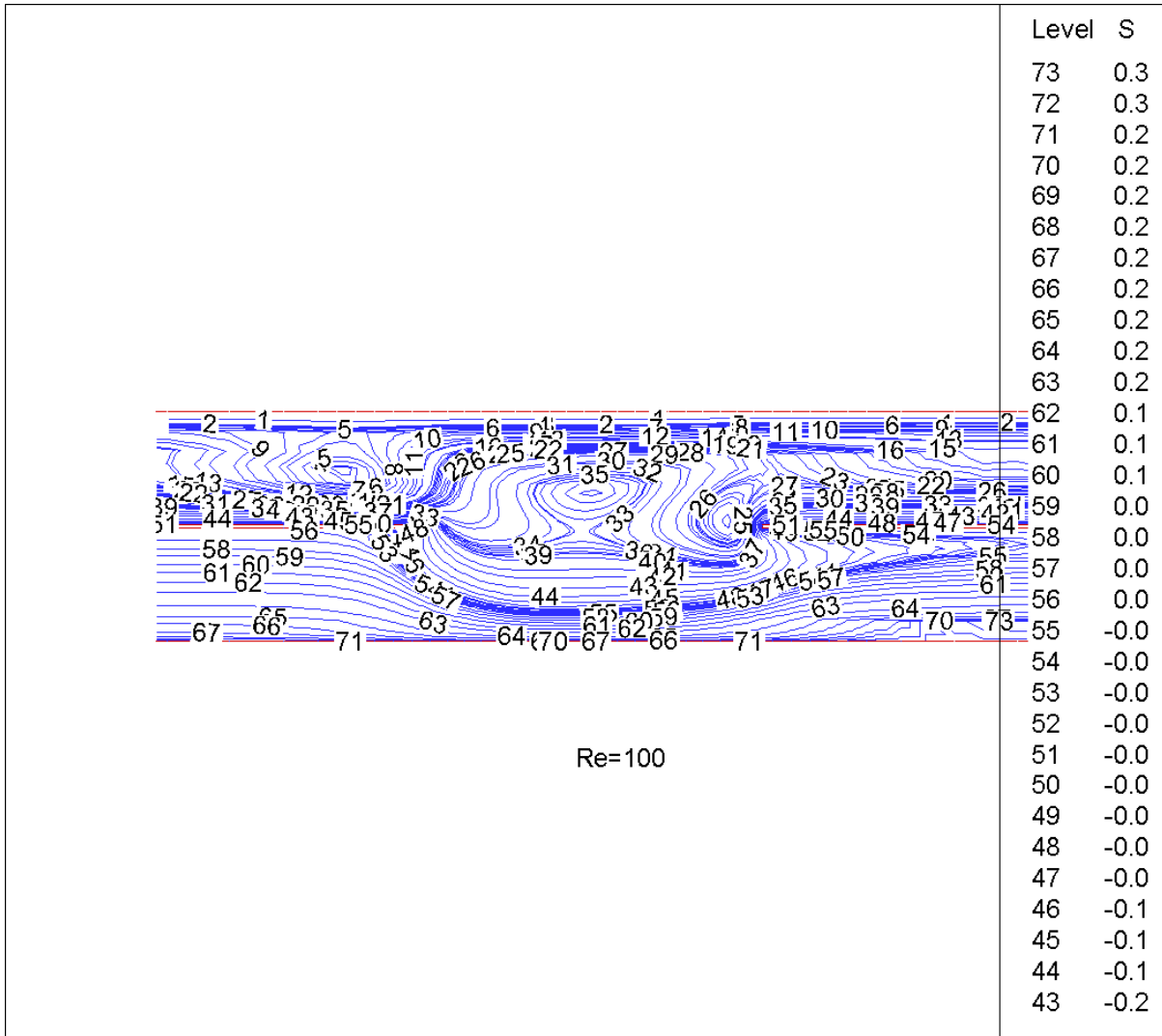
Re=01

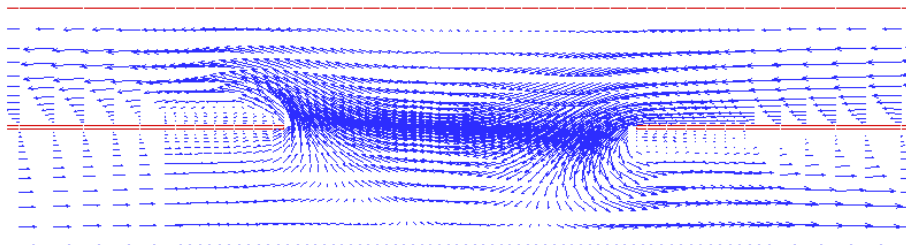
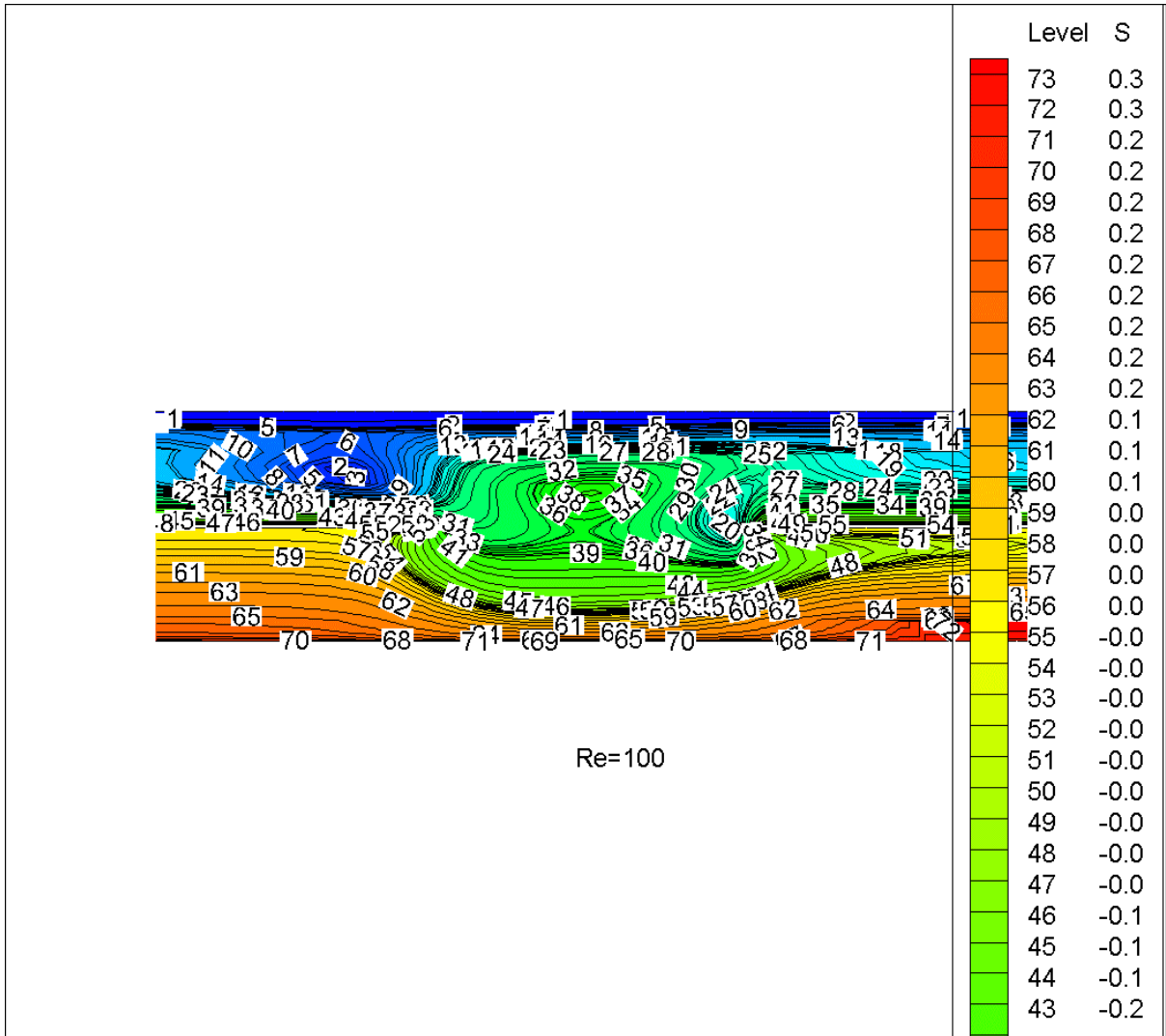




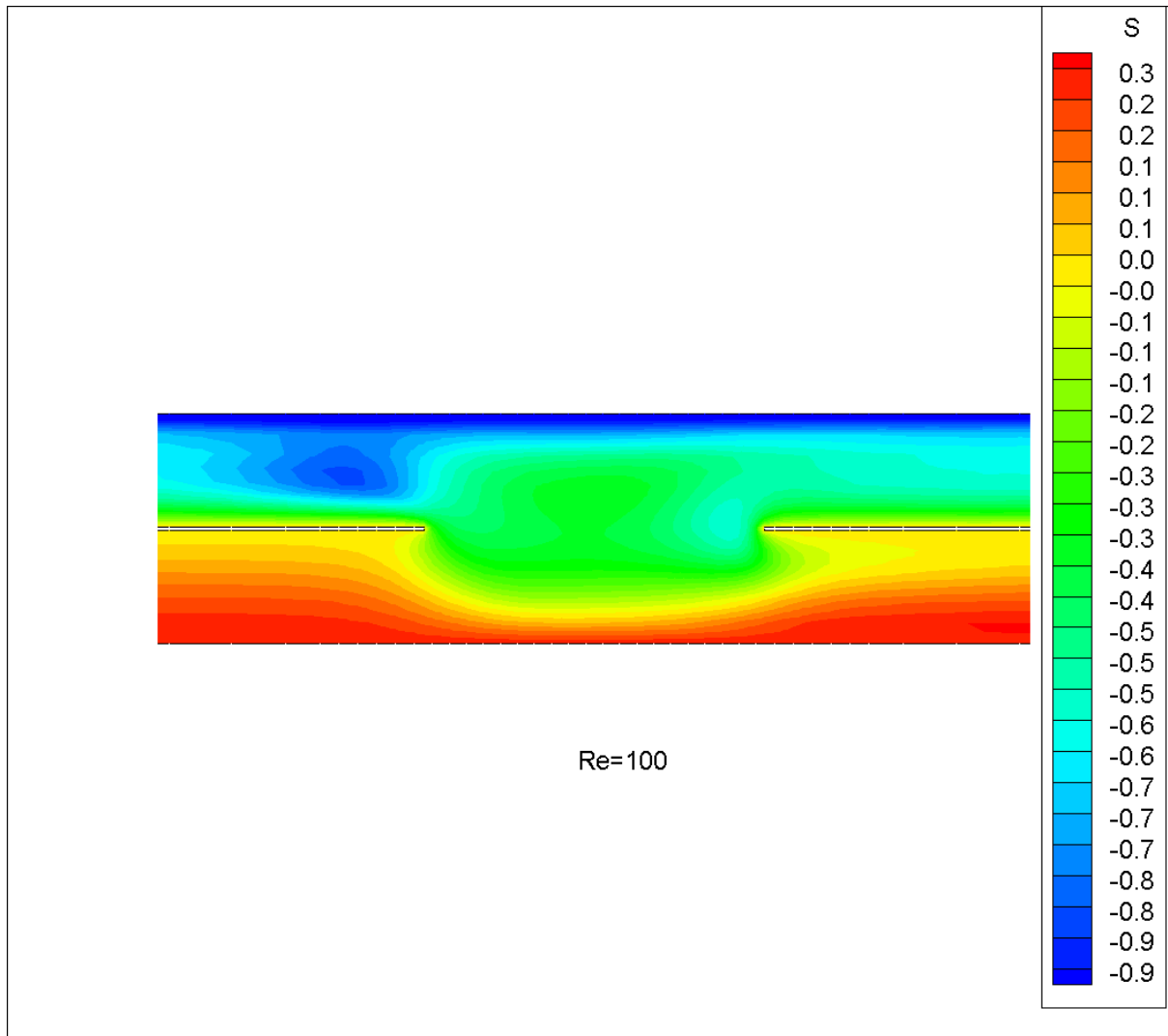


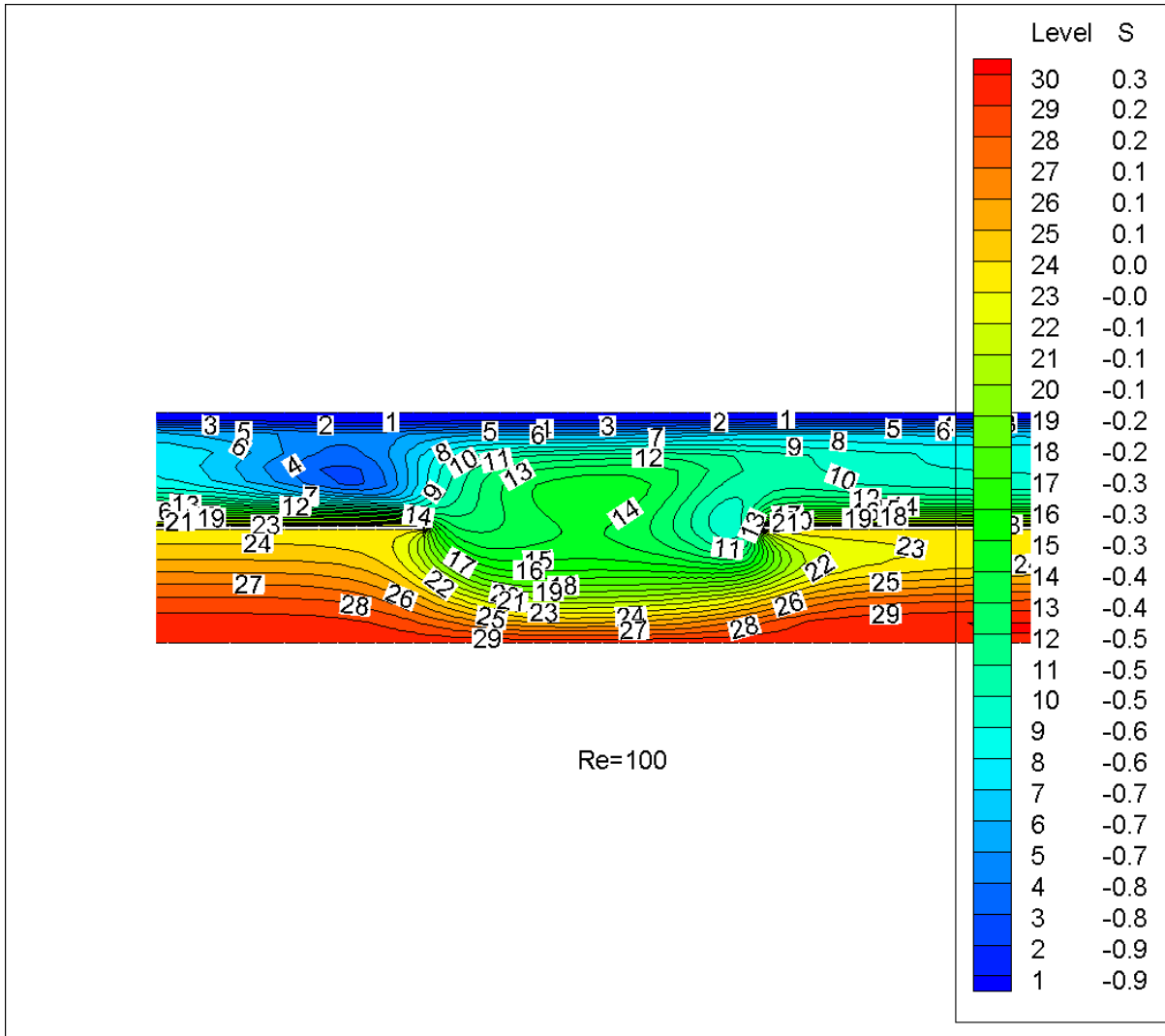


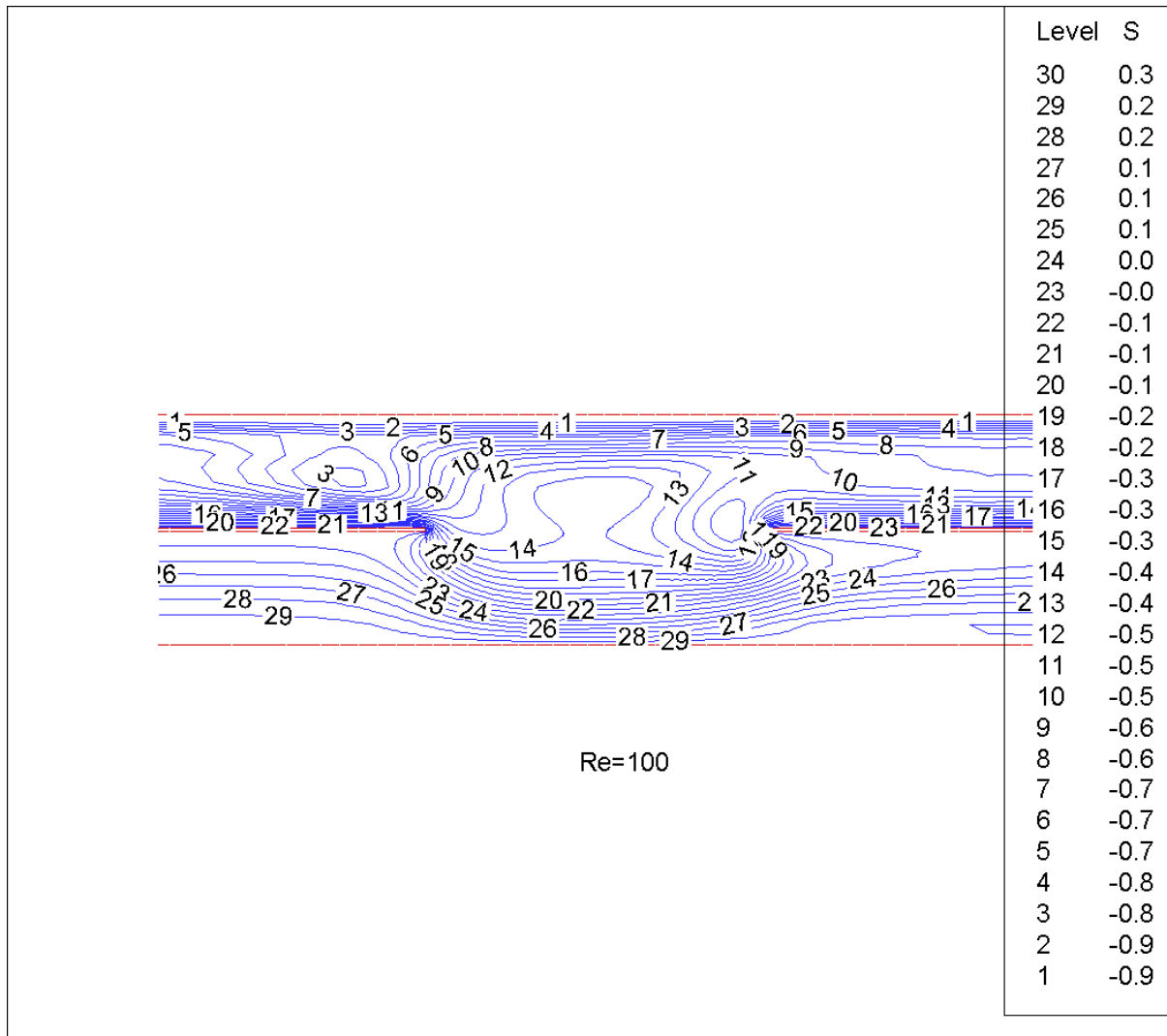


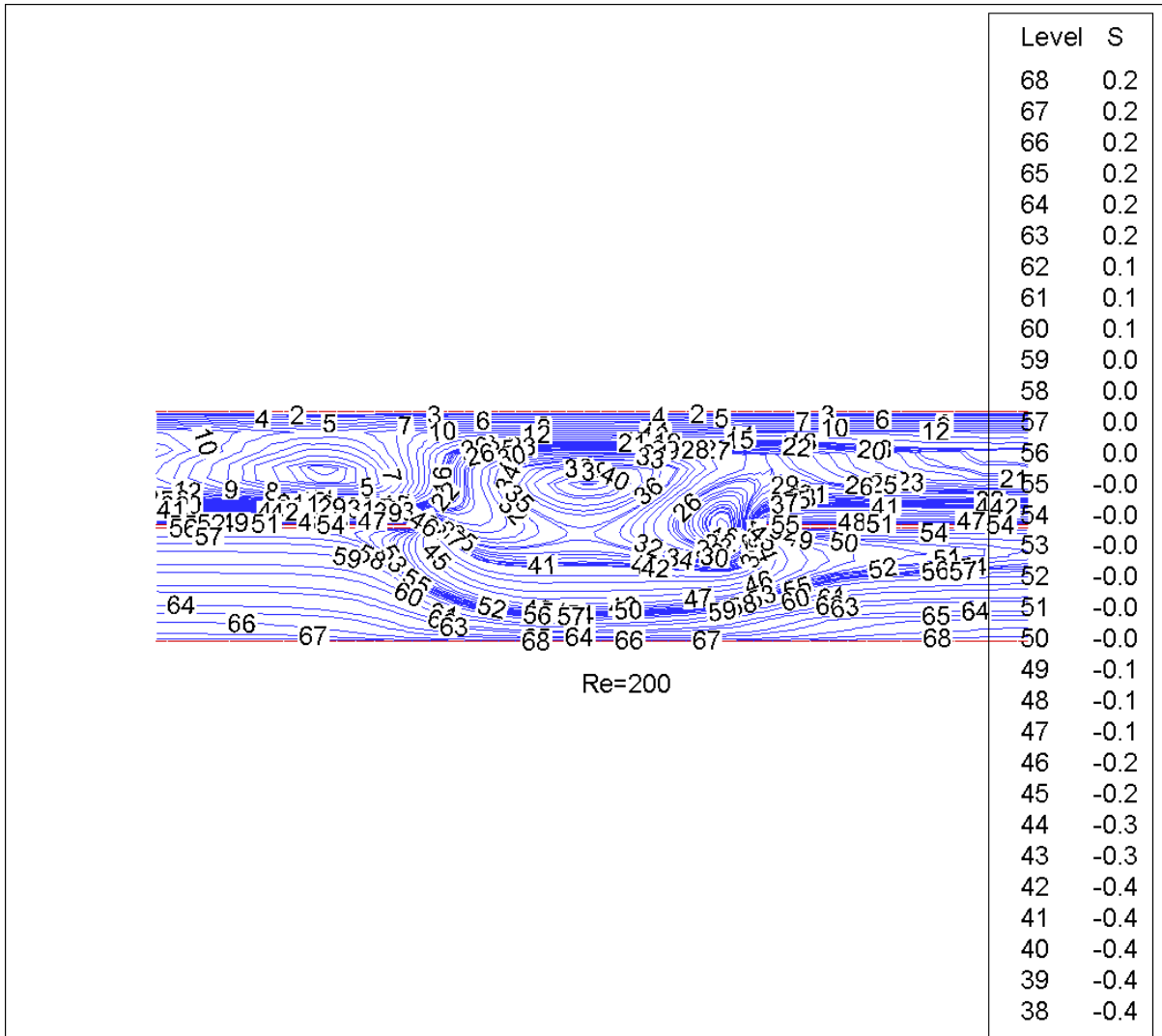


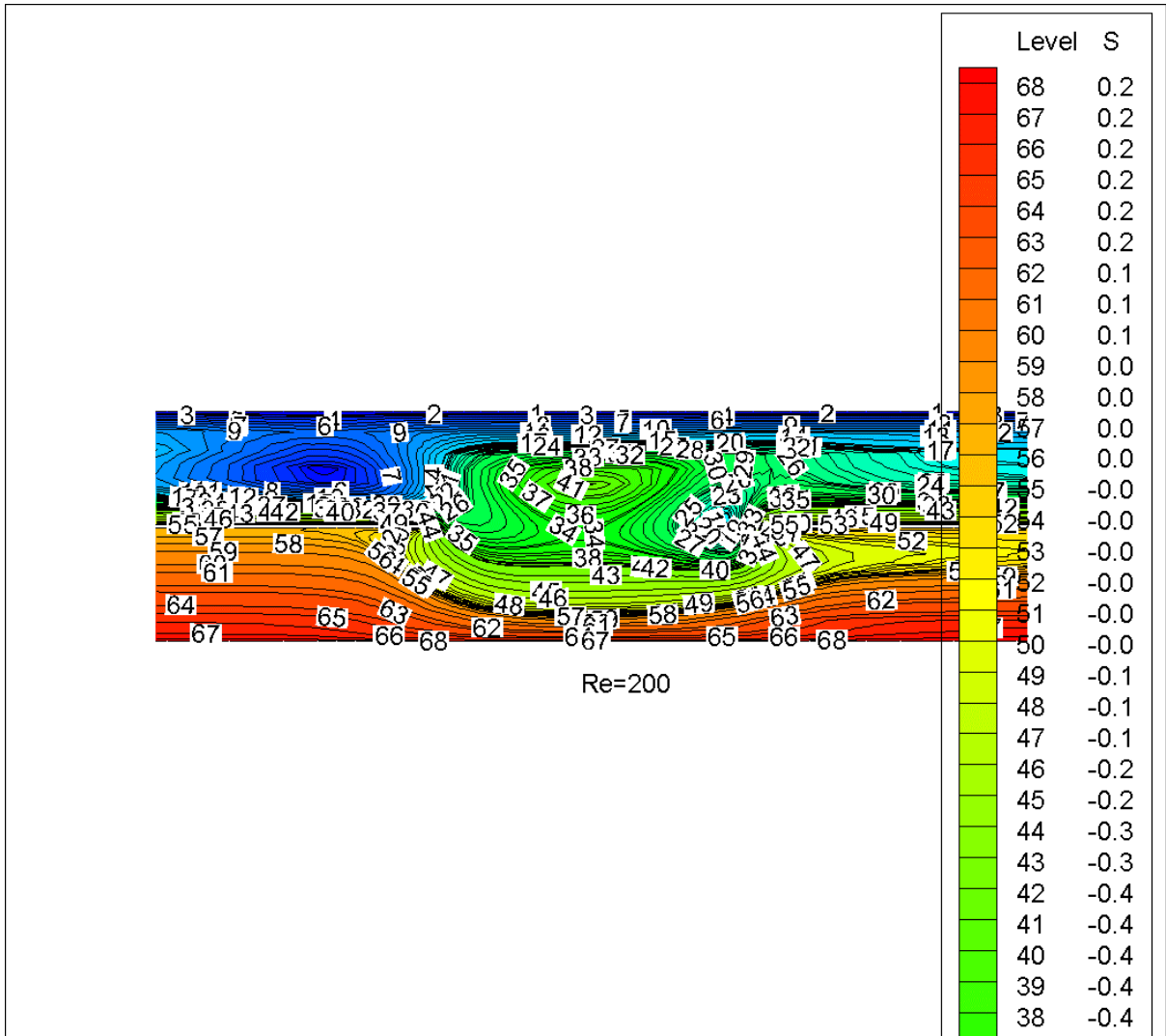
Re=100  
426

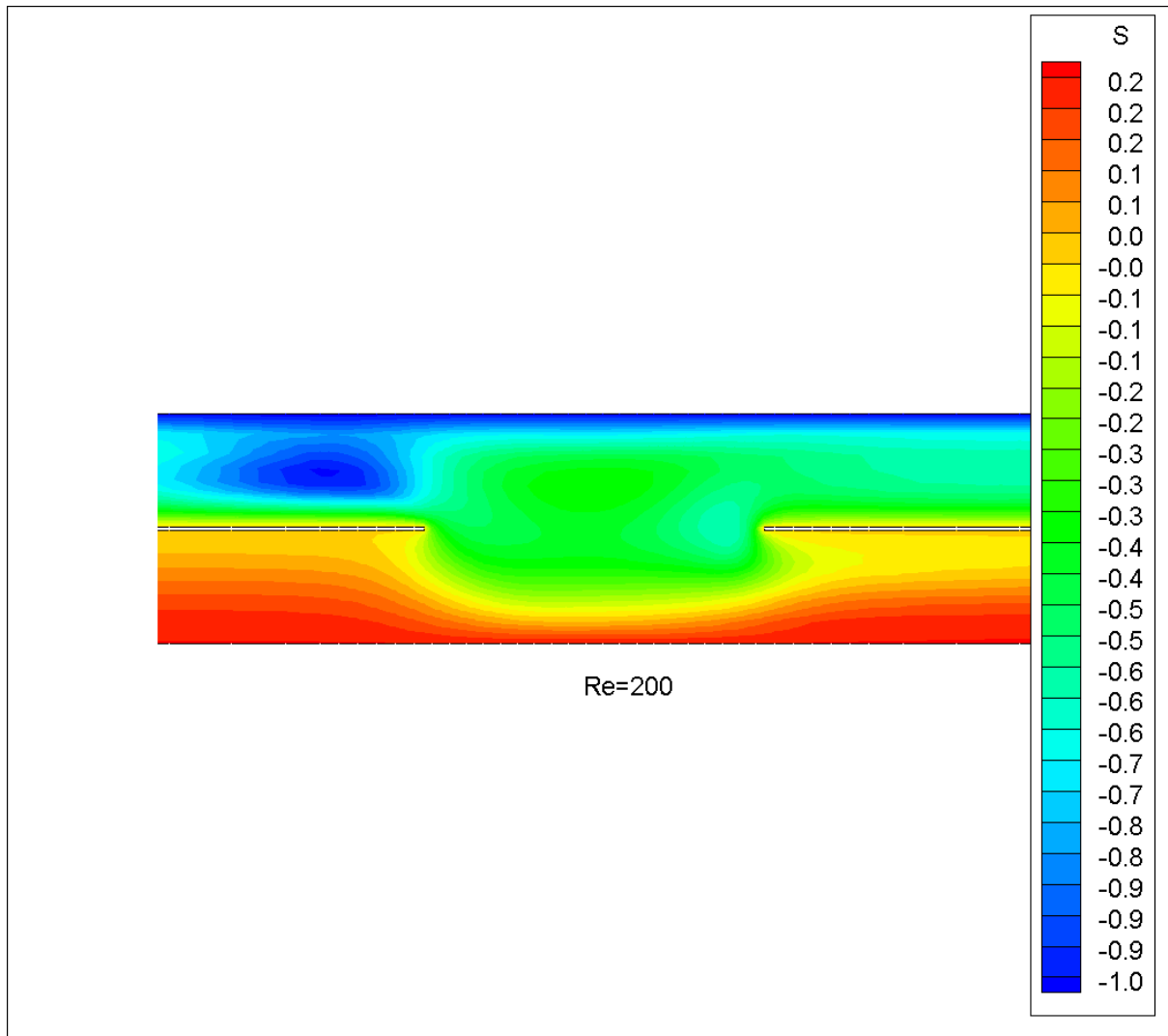






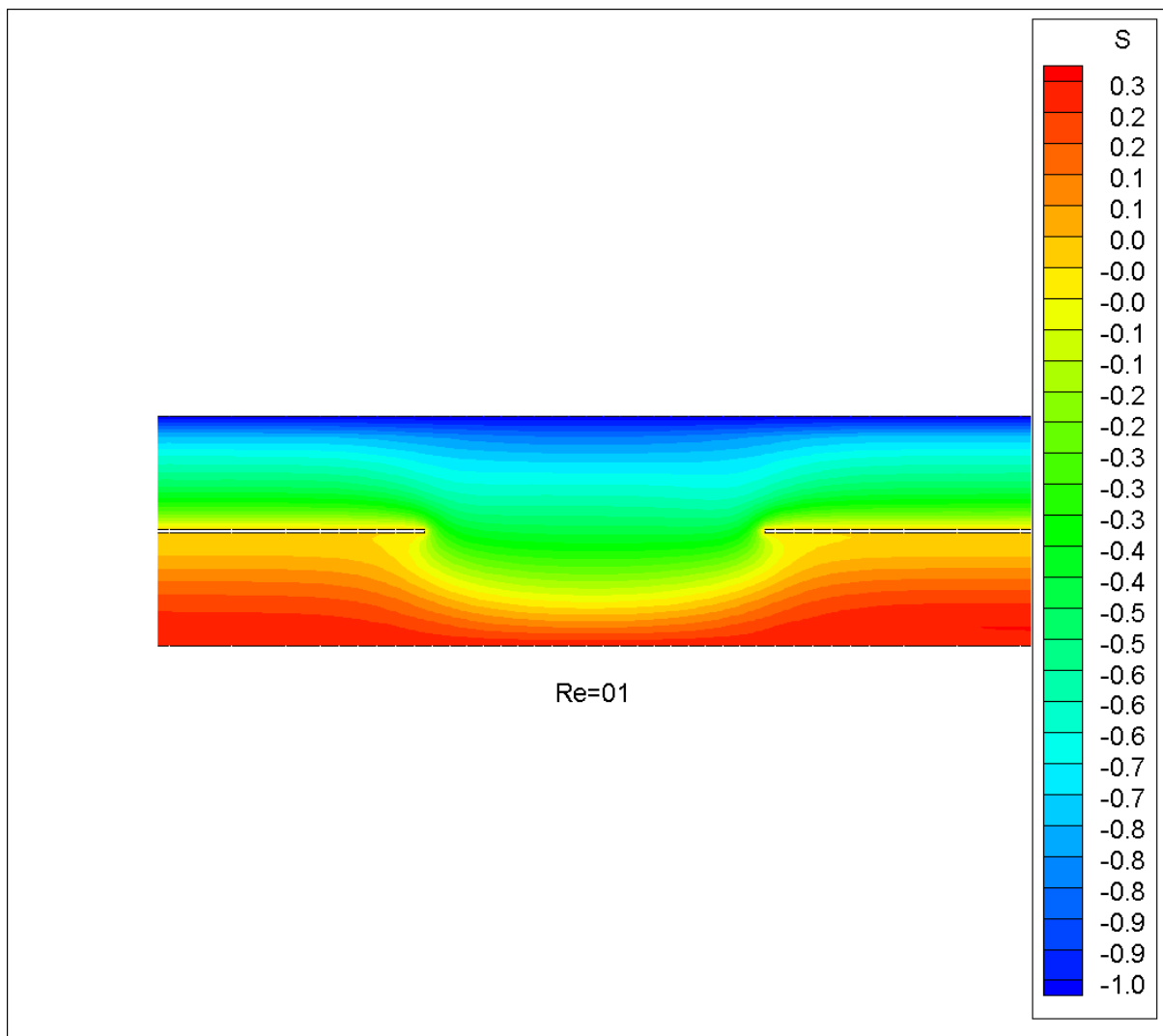


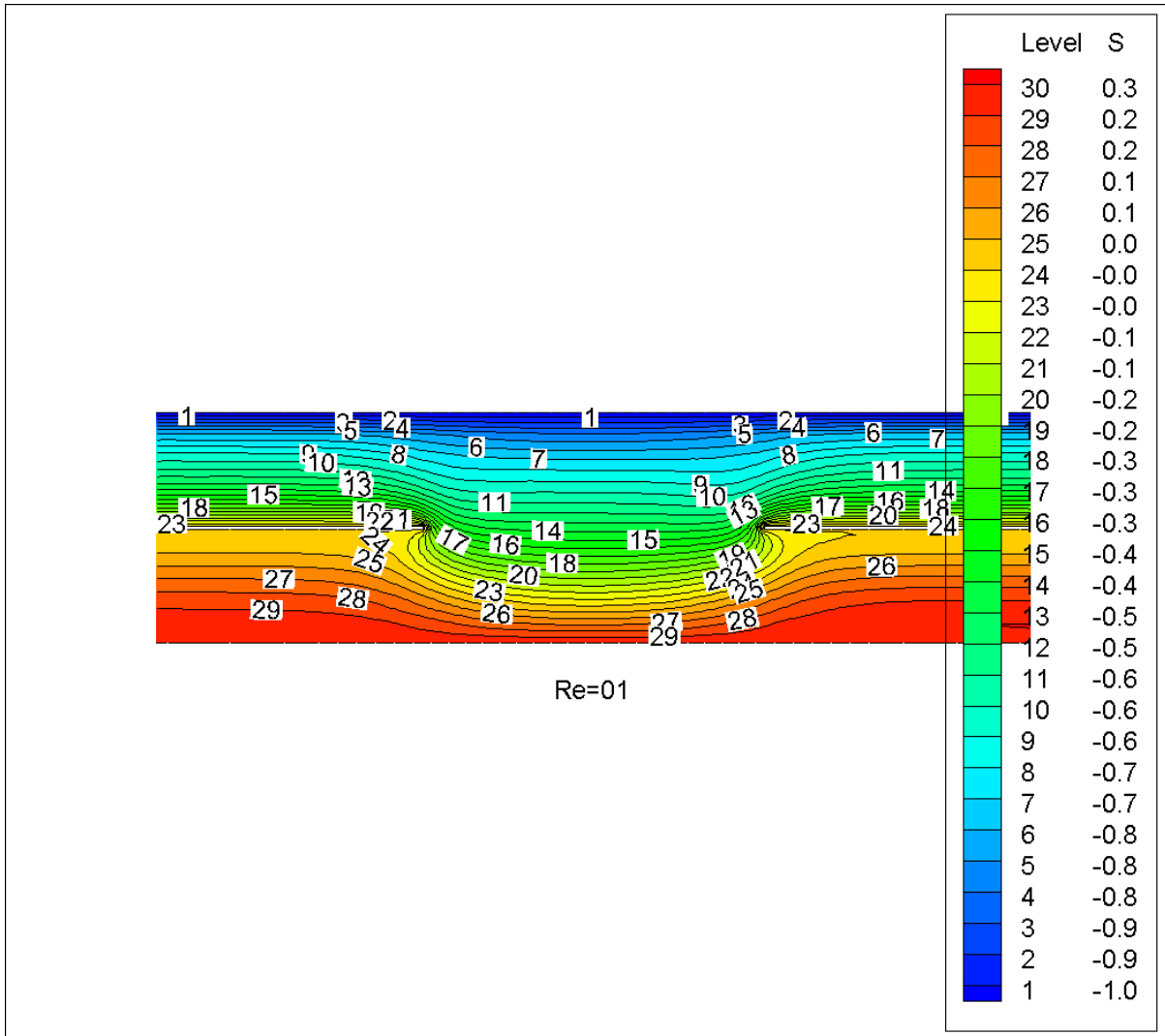


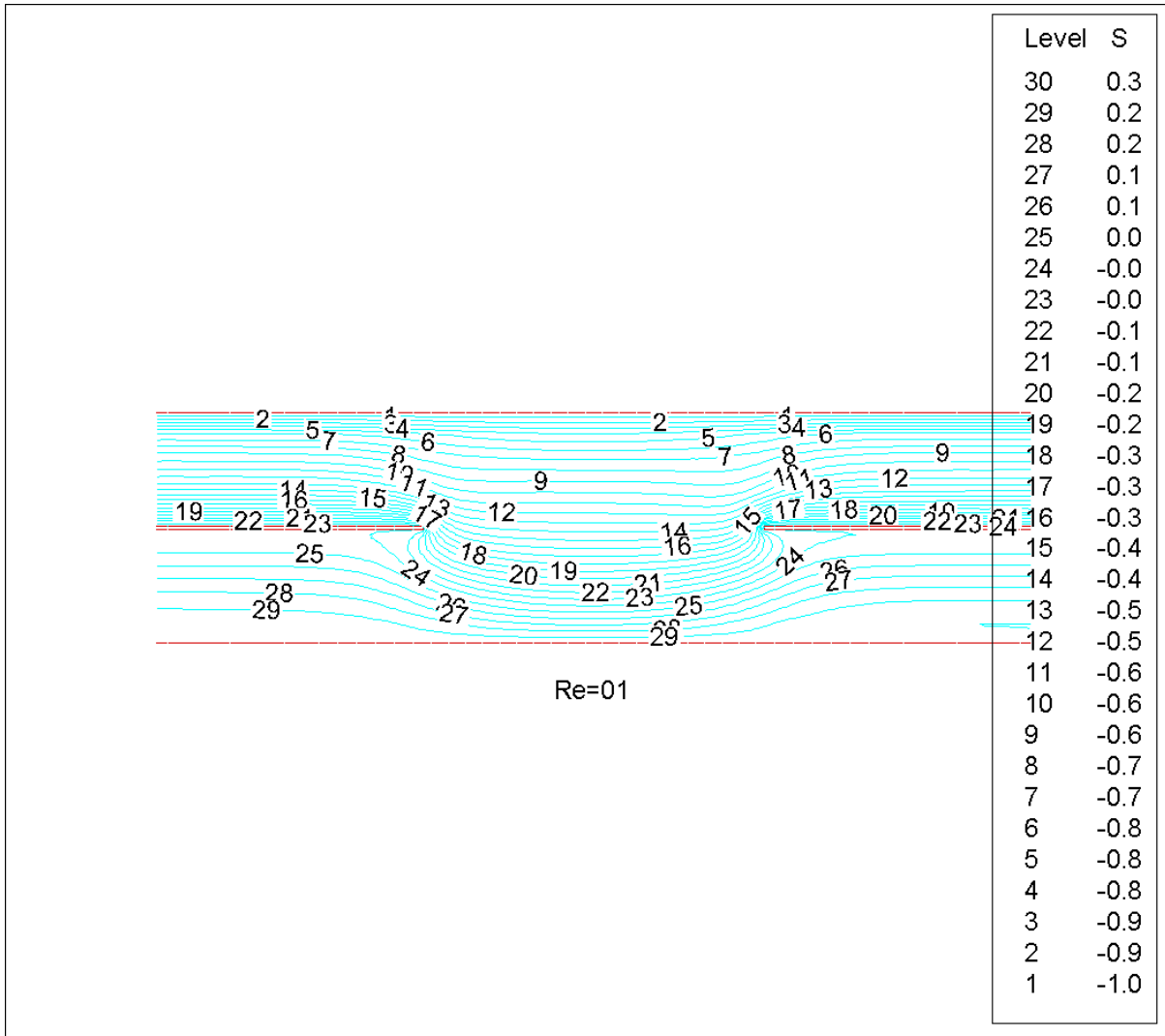


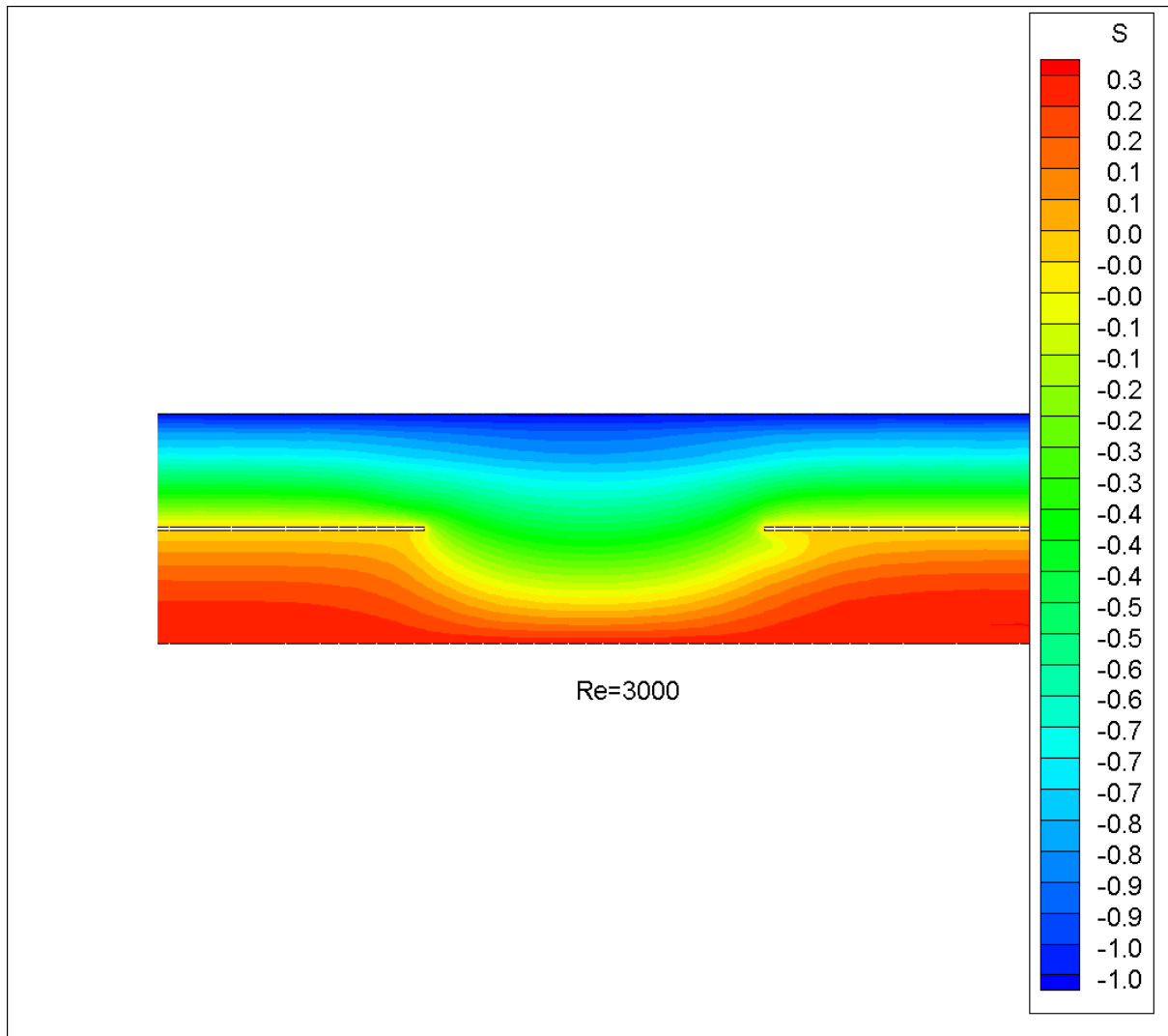
### 3.2 Mixing and separating of Newtonian fluid flows in a circular pipes filled with porous media

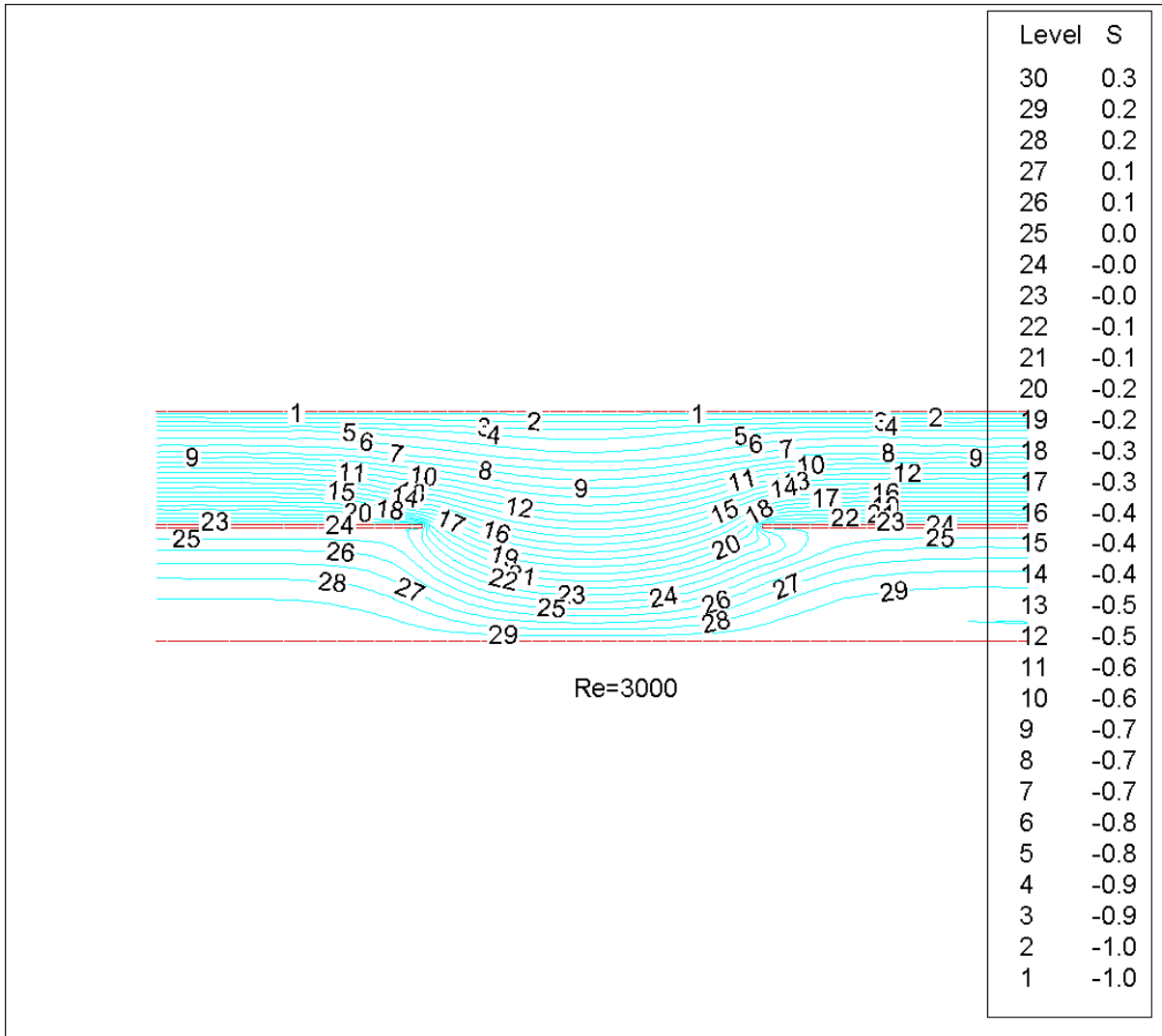
Equal (1, 1) flow rate

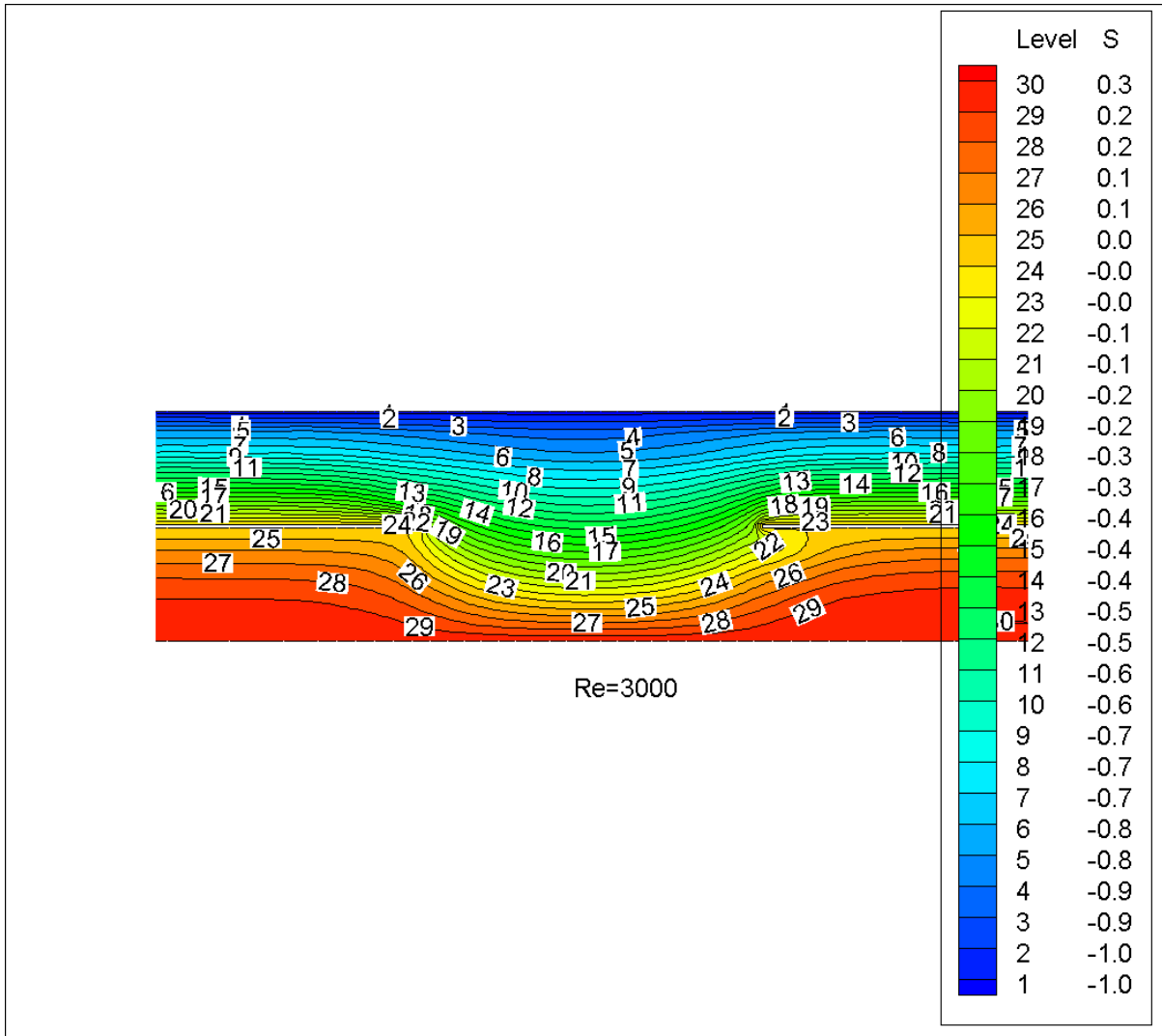


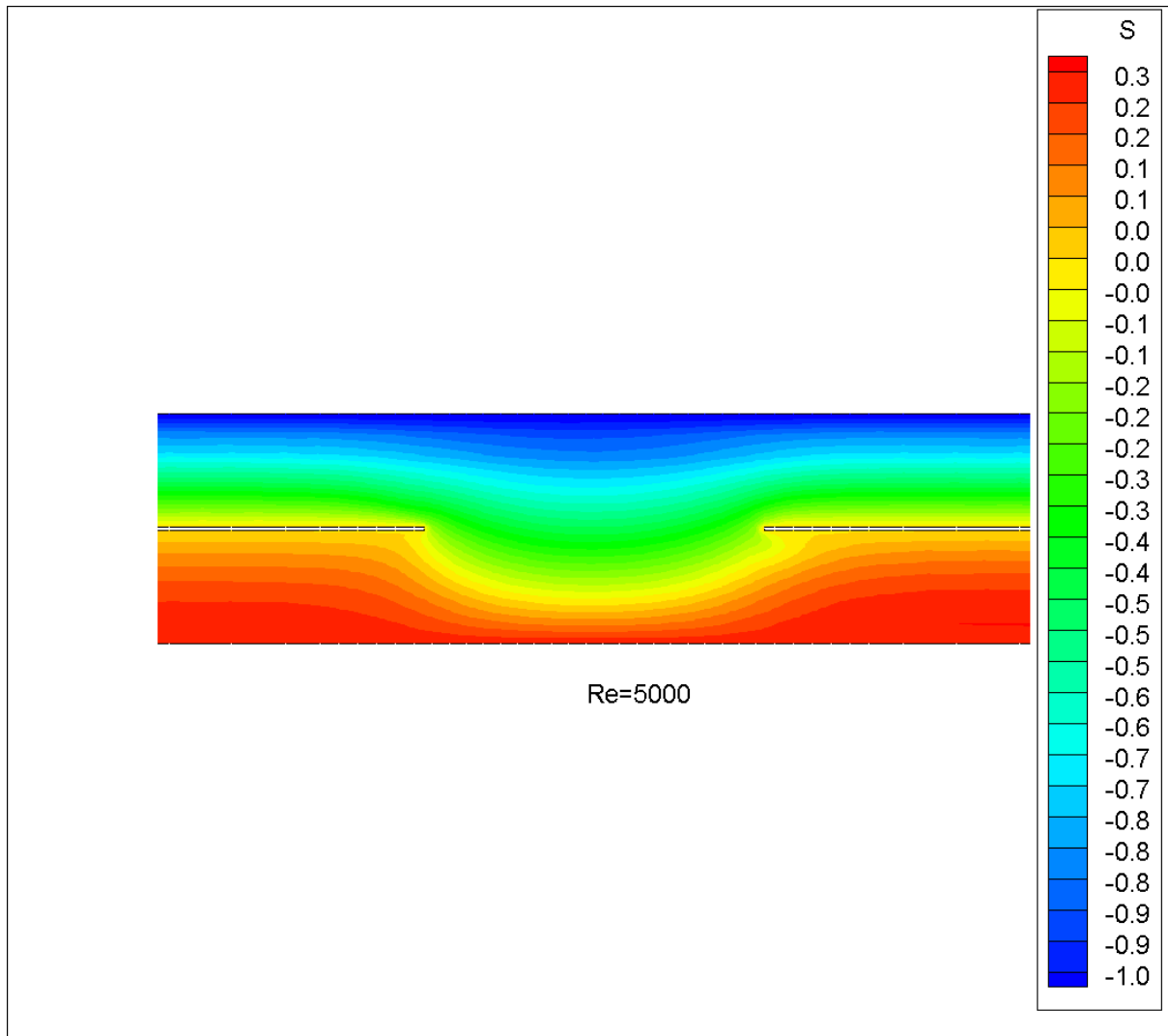


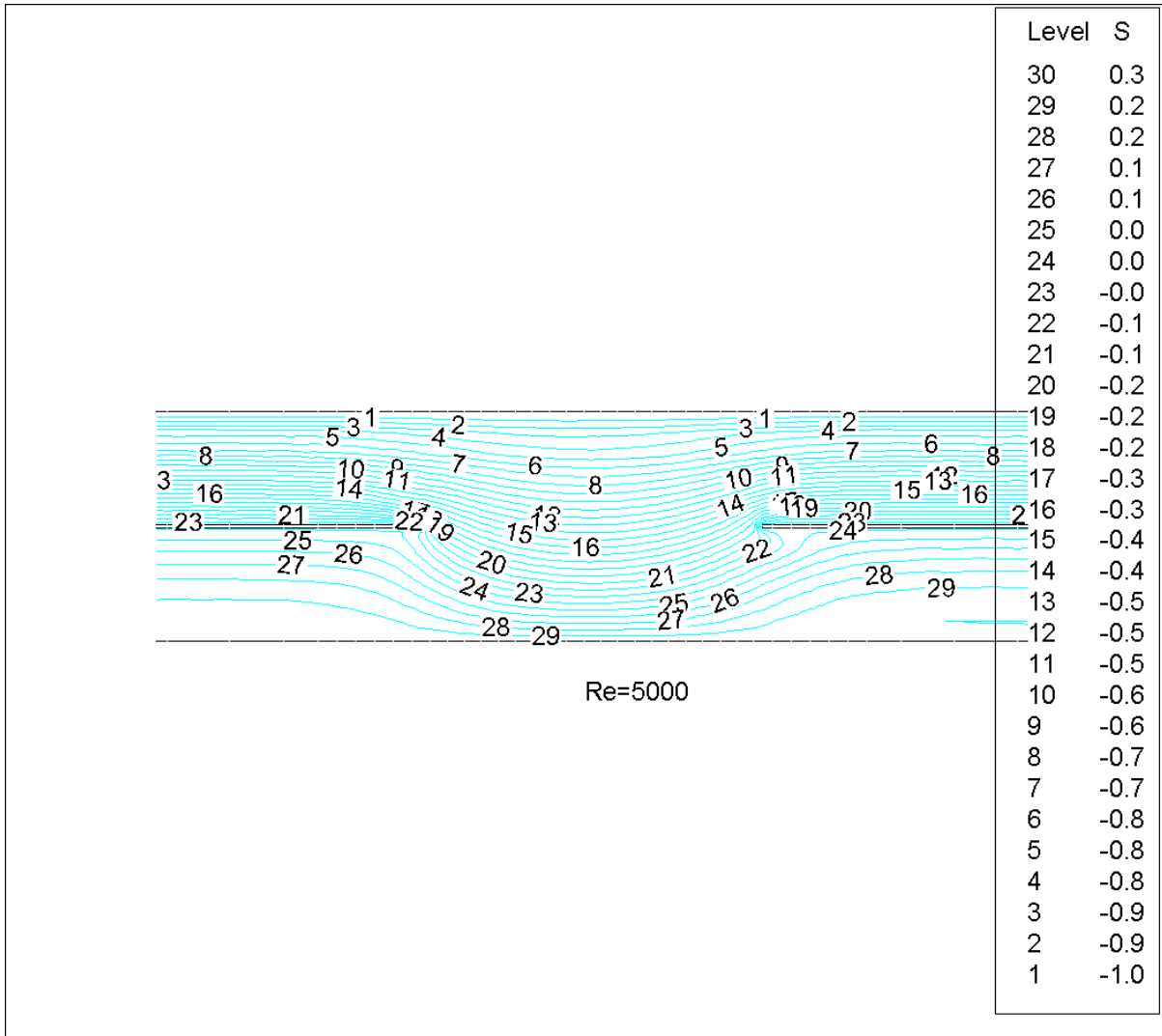


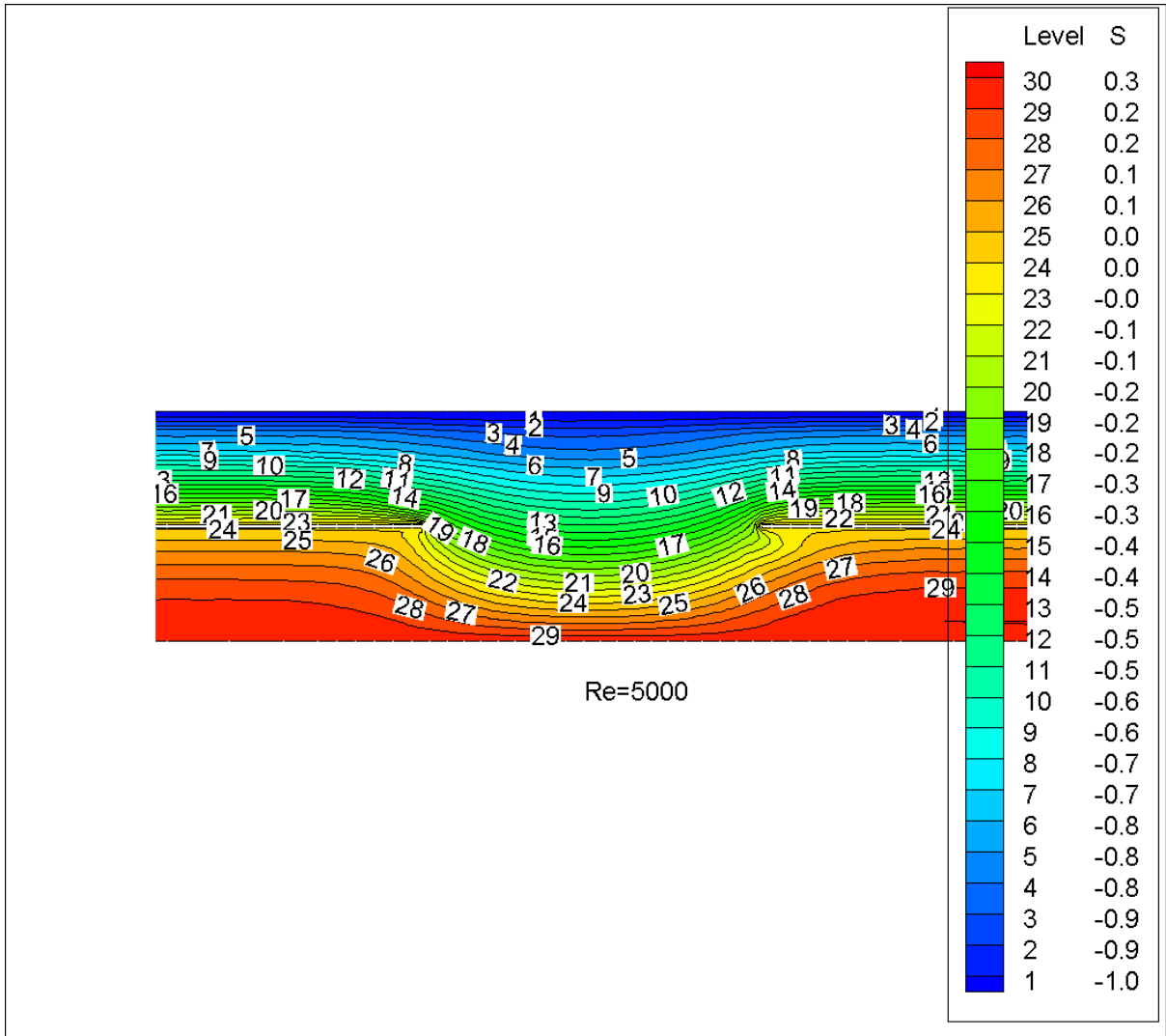




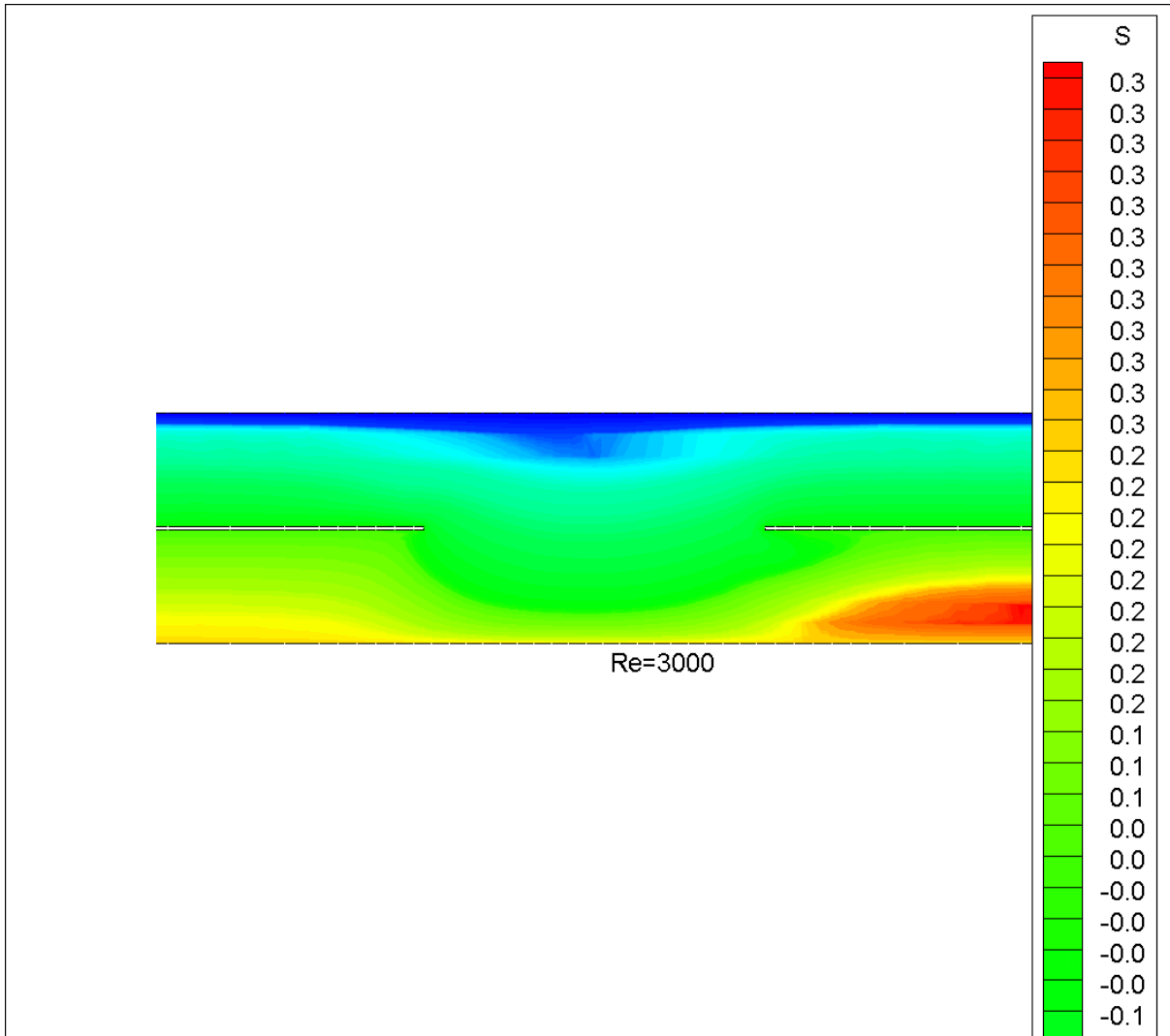


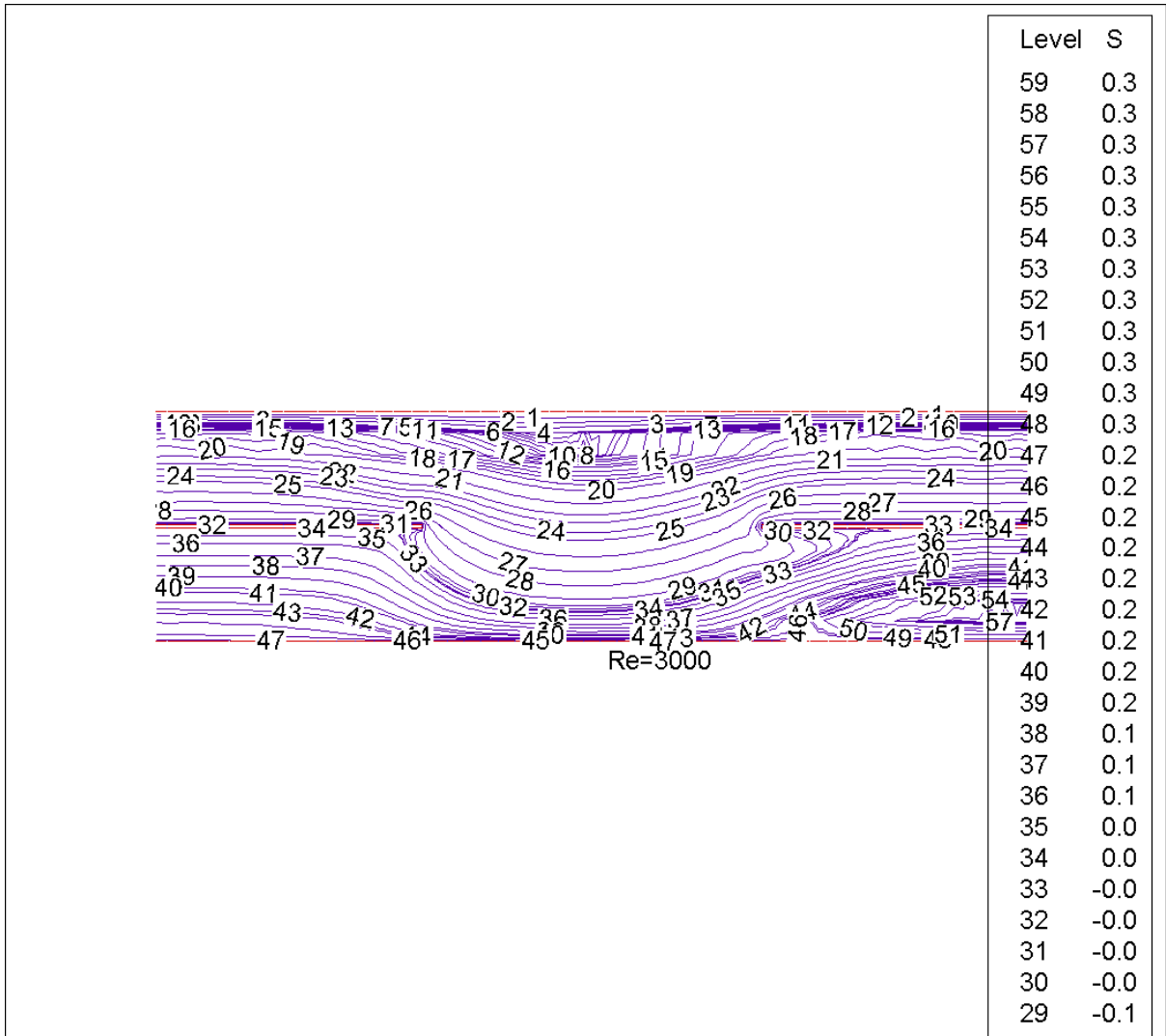


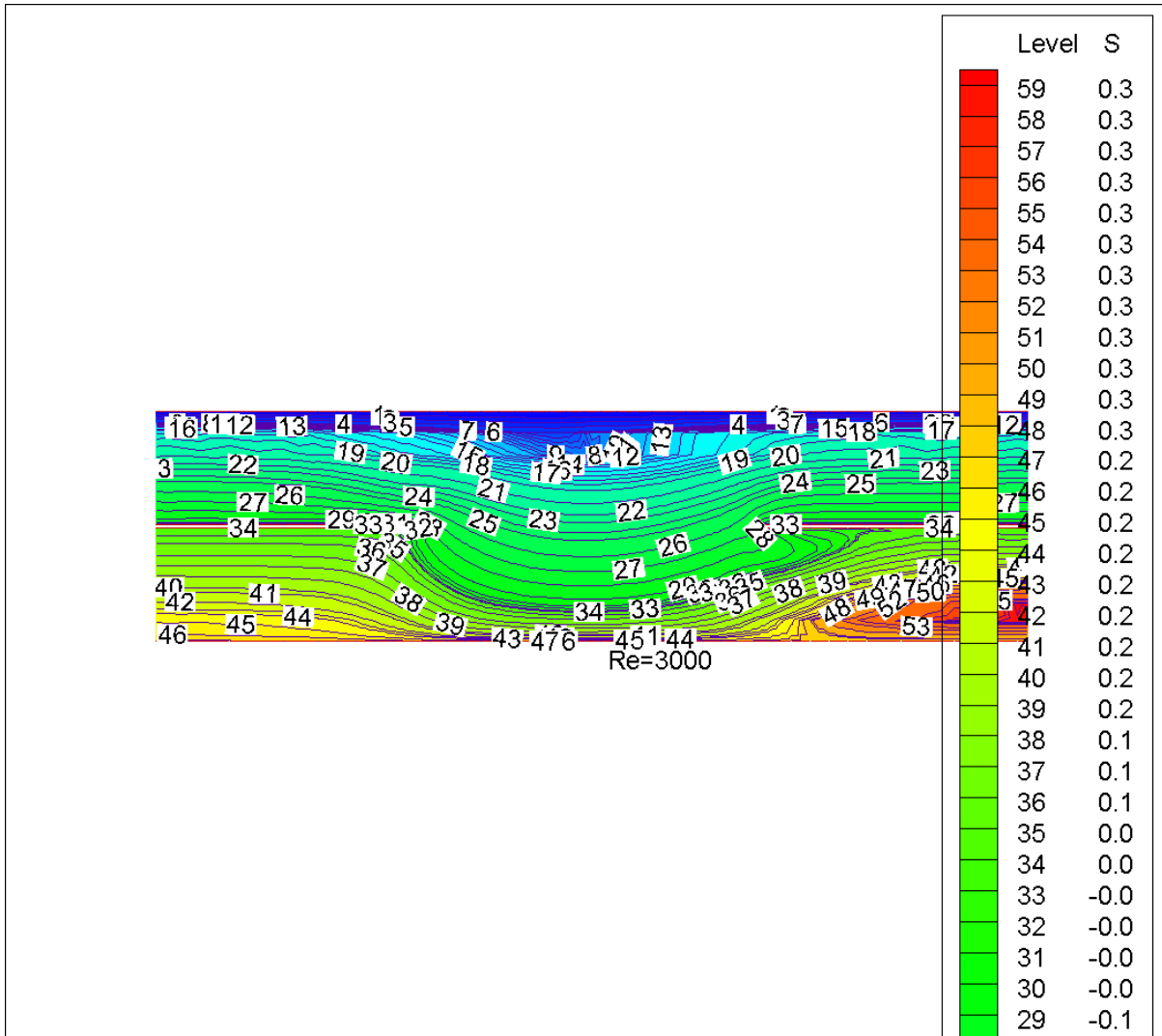




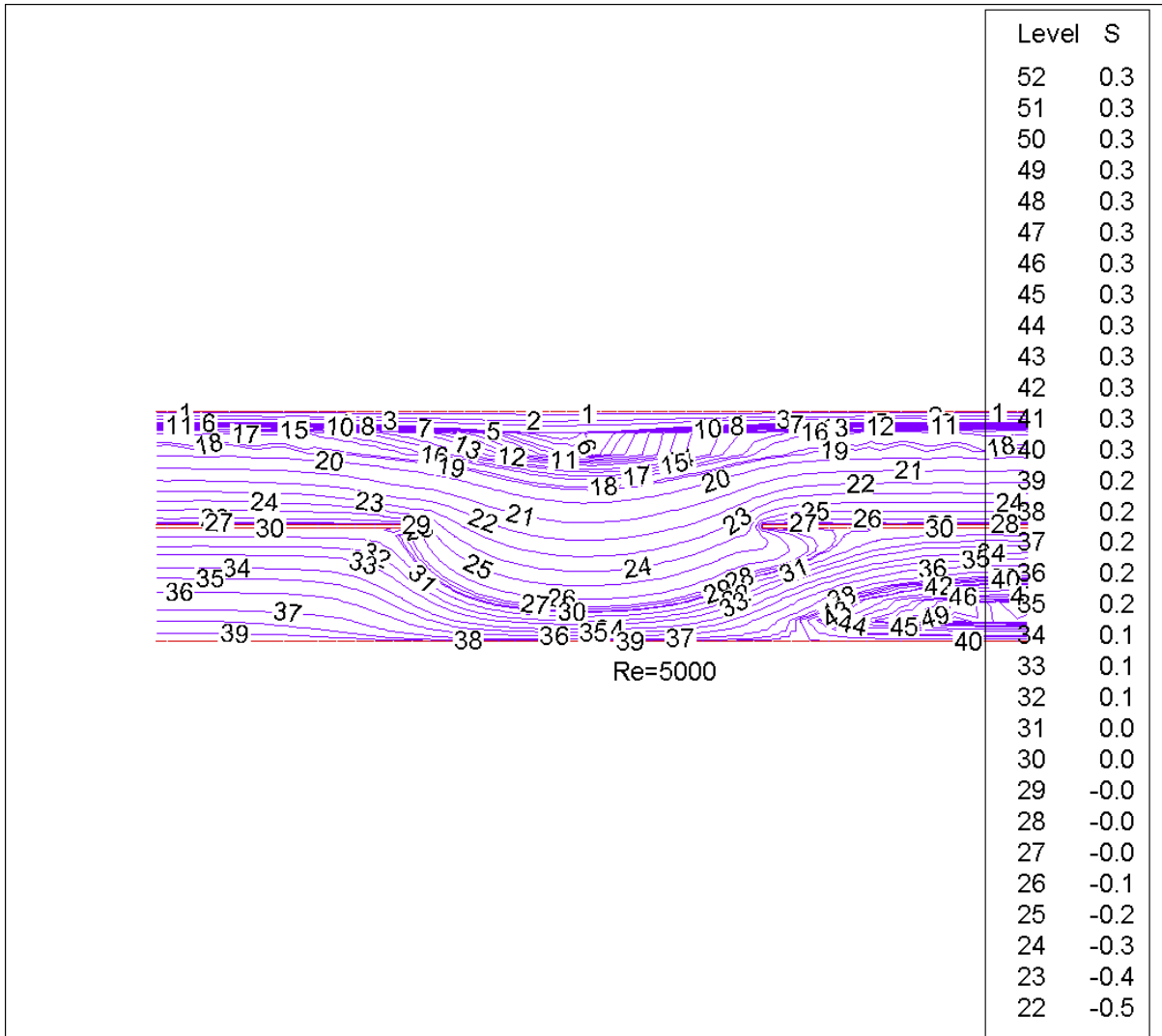
---

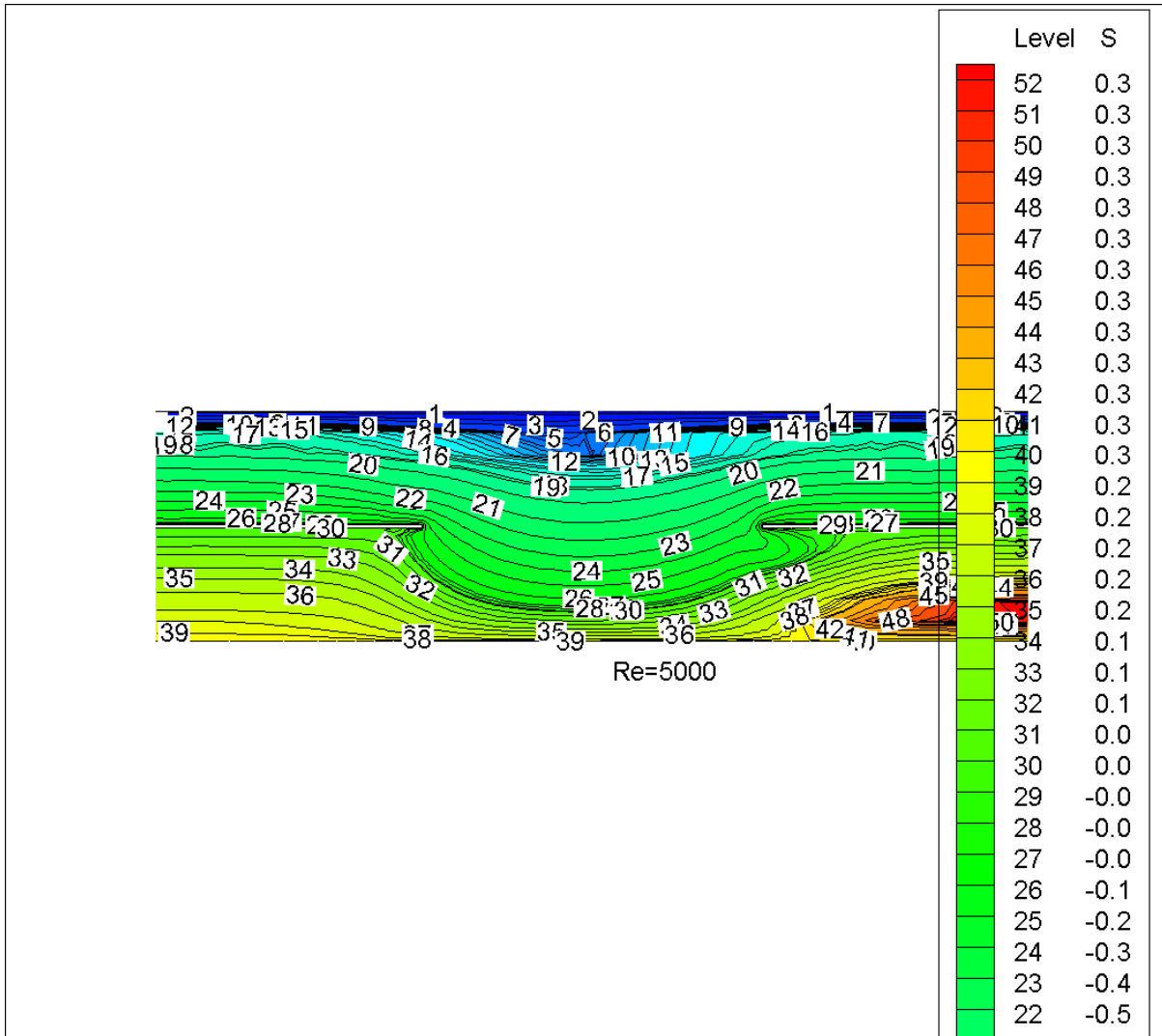
**Unequal (1, 2) flow rate**







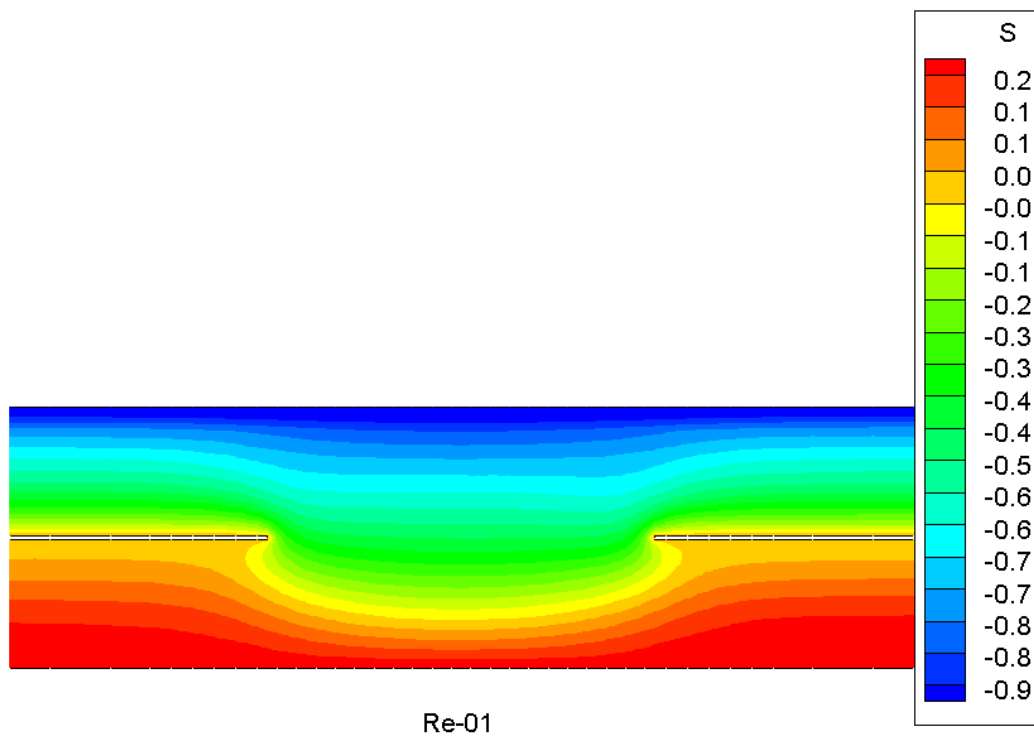


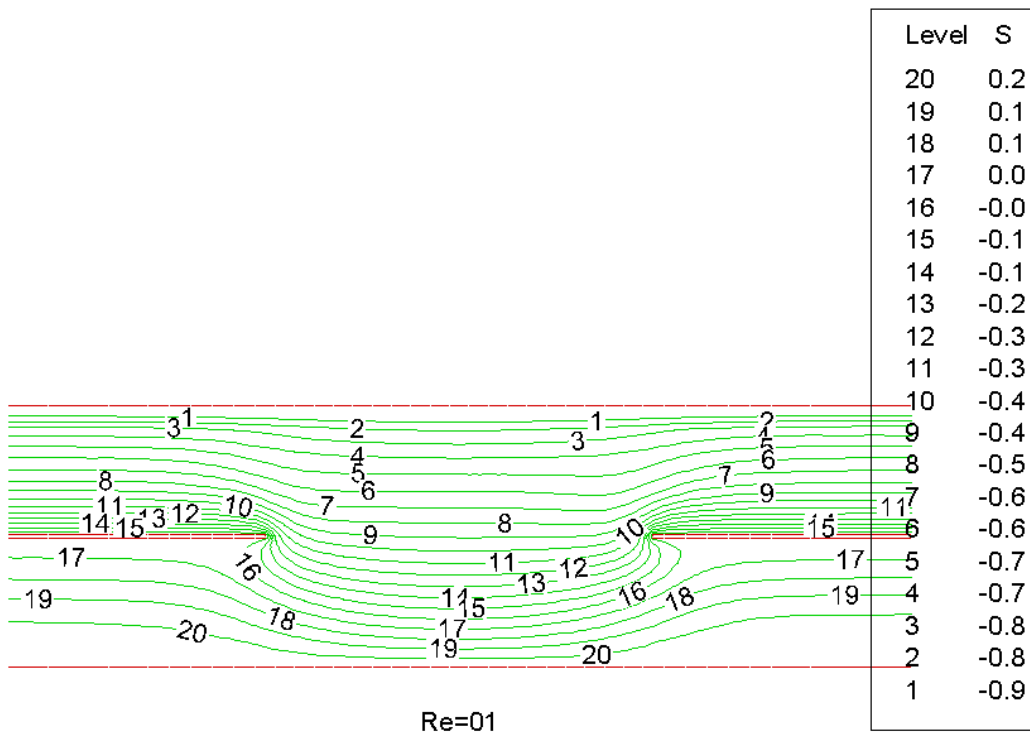
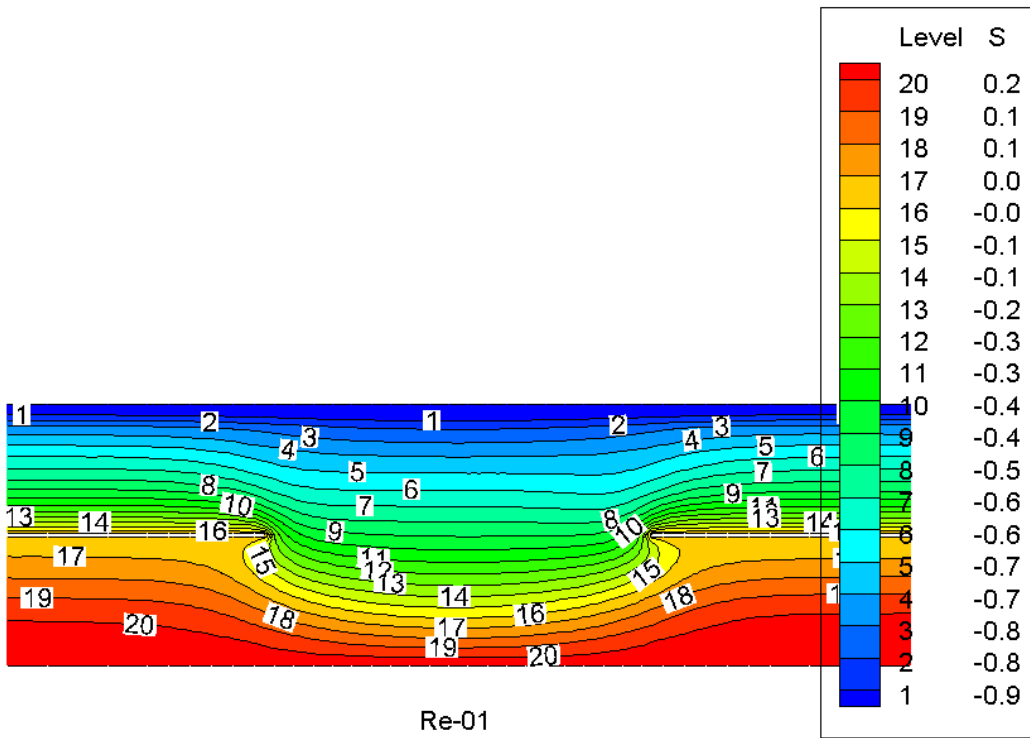


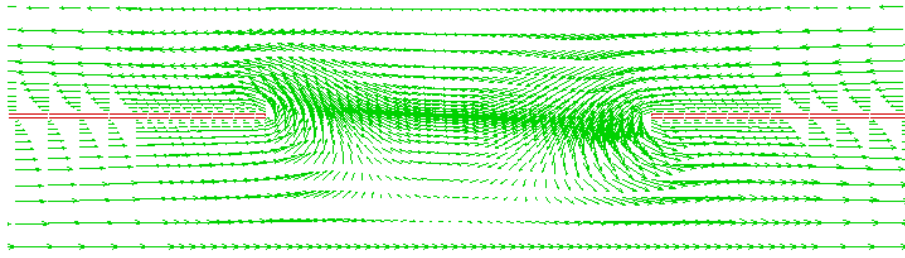
#### 4. Chapter-8

Mixing and separating of non-Newtonian fluid flows in a circular pipes filled with porous media (Power law model) at the value of Power law index ( $N=0.9$ )

Equal (1, 1) flow rate







Re=01

---

## Bibliography

- Aboubacar, M., Phillips, T. N., Tamaddon-Jahromi, H. R., Snigerev, B. A. & Webster, M. F. (2004), High-order finite volume methods for viscoelastic flow problems, *Journal of Computational Physics*, vol.199, no.1, pp.16-40.
- Abu-Hijleh, B. A. & Al-Nimr, M. A. (2001), The effect of the local inertial term on the fluid flow in channels partially filled with porous material, *International Journal of Heat and Mass Transfer*, vol.44, no.8, pp.1565-1572.
- Adler, P. M. (1992). *Porous media: Geometry and transports*, Butterworth-Heinemann Limited.
- Afonso, A., Alvis, M. A., Poole, R. J., Oliveira, P. J. & Pinho, F. T. (2008) Published. *Viscoelastic low- reynolds- number flows in mixing- separating cells*. Civil- Comp Press, Stirlingshire, Scotland. 1-12.
- Afonso, A. M., Alves, M. A. & Pinho, F. T. (2010), Purely elastic instabilities in three-dimensional cross-slot geometries, *Journal of Non-Newtonian Fluid Mechanics*, vol.165, no.13, pp.743-751.
- Afonso, A. M., Alves, M. A., Poole, R. J., Oliveira, P. J. & Pinho, F. T. (2011), Viscoelastic flows in mixing-separating cells, *Journal of Engineering Mathematics*, vol.71, no.1, pp.3-13.
- Al-Nimr, M. & Aldoss, T. (2004), The effect of the macroscopic local inertial term on the non-newtonian fluid flow in channels filled with porous medium, *International journal of heat and mass transfer*, vol.47, no.1, pp.125-133.
- Alazmi, B. & Vafai, K. (2001), Analysis of fluid flow and heat transfer interfacial conditions between a porous medium and a fluid layer, *International Journal of Heat and Mass Transfer*, vol.44, no.9, pp.1735-1749.

- 
- Alkam, M. K., Al-Nimr, M. A. & Hamdan, M. O. (2001), Enhancing heat transfer in parallel-plate channels by using porous inserts, *International Journal of Heat and Mass Transfer*, vol.44, no.5, pp.931-938.
- Anderson, J. D. (1995). *Computational fluid dynamics: The basics with applications*, MacGraw Hill.
- Baijens, F. P. T. (1998), Mixed finite element methods for viscoelastic flow analysis: A review, *J. Non-Newtonian Fluid Mechanics*, vol.79pp.361-385.
- Baloch, A. (1994), *Numerical simulation of complex flows of non-newtonian fluids*, PhD, University of wales.
- Baloch, A., Townsend, P. & Webster, M. (1995a), On the simulation of highly elastic complex flows, *Journal of non-newtonian fluid mechanics*, vol.59, no.2, pp.111-128.
- Baloch, A., Townsend, P. & Webster, M. F. (1994), Extensional effects through circular contraction with abrupt and rounded re-entrant corners, *J. non-Newtonian Fluid Mech.*
- Baloch, A., Townsend, P. & Webster, M. F. (1995b), On the simulation of highly elastic complex flows, *Journal of Non-Newtonian Fluid Mechanics*, vol.59, no.2-3, pp.111-128.
- Barnes, H. A., Hutton, J. F. & Walters, K. (1989). *An introduction to rheology*, Elsevier.
- Bear, J. (1988). *Dynamics of fluids in porous media*, New york, Dover Publications, INC.
- Benque, J., Labadie, G. & Ronat, J. (1982) Published. A new finite element method for navier-stokes equations coupled with a temperature equation. *Finite element flow analysis*. 295-302.
- Berthier, B., Bouzerar, R. & Legallais, C. (2002), Blood flow patterns in an anatomically realistic coronary vessel: Influence of three different reconstruction methods, *Journal of biomechanics*, vol.35, no.10, pp.1347-1356.

- 
- Brooks, A. N. & Hughes, T. J. R. (1982), Streamline upwind/petrov-galerkin formulations for convection dominated flows with particular emphasis on the incompressible navier-stokes equations, *Computer Methods in Applied Mechanics and Engineering*, vol.32, no.1-3, pp.199-259.
- Carew, E., Townsend, P. & Webster, M. (1993), A taylor-petrov-galerkin algorithm for viscoelastic flow, *Journal of non-newtonian fluid mechanics*, vol.50, no.2, pp.253-287.
- Carew, E. O., Townsend, P. & Webster, M. F. (1994), Taylor-galerkin algorithms for viscoelastic flow: Application to a model problem, *Numerical Methods for Partial Differential Equations*, vol.10, no.2, pp.171-190.
- Carey, G. F. & Jiang, B. (1988), Least-squares finite elements for first-order hyperbolic systems, *International journal for numerical methods in engineering*, vol.26, no.1, pp.81-93.
- Carey, G. F. & Shen, Y. (1989), Convergence studies of least-squares finite elements for first-order systems, *Communications in Applied Numerical Methods*, vol.5, no.7, pp.427-434.
- Chorin, A. J. (1968), Numerical solution of the navier-stokes equations, *Math. Comp.*, vol.22, pp.745-762.
- Cochrane, T., Walters, K. & Webster, M. F. (1981), On newtonian and non-newtonian flow in complex geometries, *Philosophical Transactions of the Royal Society of London. Series A, Mathematical and Physical Sciences*, vol.301, no.1460, pp.163-181.
- Cochrane, T., Walters, K. & Webster, M. F. (1982), Newtonian and non-newtonian flow near a re-entrant corner, *Journal of Non-Newtonian Fluid Mechanics*, vol.10, no.1-2, pp.95-114.

- 
- Costa, V. a. F., Oliveira, M. S. A. & Sousa, A. C. M. (2004), Numerical simulation of non-darcian flows through spaces partially filled with a porous medium, *Computers & Structures*, vol.82, no.17.19, pp.1535-1541.
- Coussot, P. (2005). *Rheometry of pastes, suspensions, and granular materials: Applications in industry and environment*, New Jersey, John Wiley and Sons Inc.
- Crank, J. & Nicolson, P. (1996), A practical method for numerical evaluation of solutions of partial differential equations of the heat-conduction type, *Advances in Computational Mathematics*, vol.6, no.1, pp.207-226.
- Crochet, M. J., Davies, A. R. & Walters, K. (eds.) 1984. *Numerical simulation of non-newton flow*.
- Crochet, M. J. & Walters, K. (1993), *Computational rheology: A new science*, *Endeavour*, vol.17, no.2, pp.64-77.
- Cuvelier, C., Segal, A. & Sttenuhoven., A. A. (1986). *Finite element methods and navier-stokes equations*, Holland, D. Reidel Publishing and Company.
- Cuvelier, C., Segal, A. & Van Steenhoven, A. A. (1986). *Finite element methods and navier-stokes equations*, Springer.
- David Gottlieb & Orszag, S. A. (1993). *Numerical analysis of spectral methods: Theory and applications*, SIAM
- Ding, D., Townsend, P. & And Webster, M. F. (1992), The iterative solution of taylor-galerkin augmented mass matrix equations, *International Journal for Numerical Methods in Engineering*, vol.34pp.241-253.
- Donald A. Nield & Bejan, A. (2006). *Convection in porous media*, New York, Springer.
- Donea, J. (1984a), Recent advances in computational methods for steady and transient transport problems, *Nuclear Engineering and Design*, vol.80, no.2, pp.141-162.

- 
- Donea, J. (1984b), A Taylor–Galerkin method for convective transport problems, *International Journal for Numerical Methods in Engineering*, vol.20, no.1, pp.101-119.
- Donea, J., Giuliani, S. & Halleux, J. (1982a), An arbitrary Lagrangian–Eulerian finite element method for transient dynamic fluid–structure interactions, *Computer Methods in Applied Mechanics and Engineering*, vol.33, no.1, pp.689-723.
- Donea, J., Giuliani, S., Laval, H. & Quartapelle, L. (1982b), Finite element solution of the unsteady Navier–Stokes equations by a fractional step method, *Computer Methods in Applied Mechanics and Engineering*, vol.30, no.1, pp.53-73.
- Donea, J., Quartapelle, L. & Selmin, V. (1987), An analysis of time discretization in the finite element solution of hyperbolic problems, *Journal of Computational Physics*, vol.70, no.2, pp.463-499.
- Douglas, J., Jim & Russell, T. F. (1982), Numerical methods for convection-dominated diffusion problems based on combining the method of characteristics with finite element or finite difference procedures, *SIAM Journal on Numerical Analysis*, vol.19, no.5, pp.871-885.
- Echendu, S. O. S., Belblidia, F., Tamaddon-Jahromi, H. R. & Webster, M. F. (2011), Modelling with viscous and viscoplastic materials under combining and separating flow configurations, *Mechanics of Time-Dependent Materials*, vol.15, no.4, pp.407-428.
- Escudier, M., Poole, R., Presti, F., Dales, C., Nouar, C., Desaubry, C., Graham, L. & Pullum, L. (2005), Observations of asymmetrical flow behaviour in transitional pipe flow of yield-stress and other shear-thinning liquids, *Journal of Non-Newtonian Fluid Mechanics*, vol.127, no.2, pp.143-155.
- Fortin, M., Peyret, R. & Temam, R. (1971), *Lecture Notes in Physics*, Springer vol.8 pp.337-382.

- 
- Fox, E. A. & Gex, V. E. (1956), Single-phase blending of liquids, *AIChE Journal*, vol.2, no.4, pp.539-544.
- Fu, C. C. (1972), On the stability of explicit methods for the numerical integration of the equations of motion in finite element methods, *International Journal for Numerical Methods in Engineering*, vol.4, no.1, pp.95-107.
- Fujii, H. (1973), Some remarks on finite element analysis of time-dependent field problems, *Theory and practice in finite element structural analysis*, pp.91-106.
- Glowinski, R. & Pironneau, O. (1992), Finite element methods for navier-stokes equations, *Annual Review of Fluid Mechanics*, vol.24, no.1, pp.167-204.
- Graham, F. C. & Jiannig, B. N. (1988), Least-squares finite elements for first-order hyperbolic systems, *International Journal for Numerical Methods in Engineering*, vol.26, no.1, pp.81-93.
- Gresho, P. M., Lee, R. L. & Sani, R. L. (1976). Advection-dominated flows, with emphasis on the consequences of mass lumping. [galerkin finite-element method].
- Guo & Kuo, P.Y. ( 1998 ), *Spectral methods and their applications*, Singapore, World Scientific publishing company pte. ltd.
- Hawken, D. M., Tamaddon-Jahromi, H. R., Townsend, P. & And Webster, M. F. (1990), A taylor-galerkin-based algorithm for viscous incompressible flow, *International Journal for Numerical Methods in Fluids*, vol.10, no.3, pp.327-351.
- Heldman, D. R. (2003). *Encyclopedia of agricultural, food, and biological engineering*, New York, Marcel Dekker, Inc.
- Hinton, E. & And Owen, D. R. J. (1977). *Finite element programming*, London, Academic Press INC.

- 
- Hirsh, C. (2007). Numerical computation of internal & external flows: The fundamentals of computational fluid dynamics, Burlington, John Wiley & Sons, ltd.
- Hossain, M., Acar, M. & Malalasekera, W. (2009), Modelling of the through-air bonding process.
- Hossain, M., Islam, S. Z., Colley-Davies, A. & Adom, E. (2013), Water dynamics inside a cathode channel of a polymer electrolyte membrane fuel cell, *Renewable Energy*, vol.50, no.0, pp.763-779.
- Hubbert, M. K. (1957), Darcy's law and the field equations of the flow of underground fluids, *Hydrological Sciences Journal*, vol.2, no.1, pp.23-59.
- Huebner, K. H., Dewhurst, D. L., Smith, D. E. & G., A. B. T. ( 2001 ). The finite element method for engineers, New York, John Wiley & Sons Inc.
- Hughes, T. J. R., Franca, L. P. & Balestra, M. (1986), A new finite element formulation for computational fluid dynamics: V. Circumventing the babuska-brezzi condition: A stable petrov-galerkin formulation of the stokes problem accommodating equal-order interpolations, *Computer Methods in Applied Mechanics and Engineering*, vol.59, no.1, pp.85-99.
- Hughes, T. J. R., Franca, L. P. & Hulbert, G. M. (1989), A new finite element formulation for computational fluid dynamics: Viii. The galerkin/least-squares method for advective-diffusive equations, *Computer Methods in Applied Mechanics and Engineering*, vol.73, no.2, pp.173-189.
- Hughes, T. J. R., Franca, L. P. & Mallet, M. (1987), A new finite element formulation for computational fluid dynamics: Vi. Convergence analysis of the generalized supg formulation for linear time-dependent multidimensional advective-diffusive systems, *Computer Methods in Applied Mechanics and Engineering*, vol.63, no.1, pp.97-112.

- 
- Ingham, D. (1998). *Transport phenomena in porous media*, Elsevier.
- Jayanti, S. (2001), Hydrodynamics of jet mixing in vessels, *Chemical engineering science*, vol.56, no.1, pp.193-210.
- Jen, T.-C. & Yan, T. Z. (2005), Developing fluid flow and heat transfer in a channel partially filled with porous medium, *International Journal of Heat and Mass Transfer*, vol.48, no.19–20, pp.3995-4009.
- Jiyuan Tu, Guan Heng Yeoh & Liu, C. (2008). *Computational fluid dynamics: A practical approach*, Burlington, Elsevier Inc.
- Johnson, C., Nävert, U. & Pitkäranta, J. (1984), Finite element methods for linear hyperbolic problems, *Computer Methods in Applied Mechanics and Engineering*, vol.45, no.1-3, pp.285-312.
- Johnson, C., Szepessy, A. & Hansbo, P. (1990), On the convergence of shock-capturing streamline diffusion finite element methods for hyperbolic conservation laws, *Mathematics of computation*, vol.54, no.189, pp.107-129.
- Jung, H., Choi, J. W. & Park, C. G. (2004), Asymmetric flows of non-newtonian fluids in symmetric stenosed artery, *Korea-Australia Rheology Journal*, vol.16, no.2, pp.101-108.
- Kan, J. V. (1986), A second-order accurate pressure-correction scheme for viscous incompressible flow, *SIAM Journal on Scientific and Statistical Computing*, vol.7, no.3, pp.870-891.
- Kawahara, M. & Takeuchi, N. (1977), Mixed finite element method for analysis of viscoelastic fluid flow, *Computers & Fluids*, vol.5, no.1, pp.33-45.

- 
- Khokhar, R., Chen, Y., Xu, Y. & Calay, R. K. (2013), Numerical simulation of combined mixing and separating flow in channel filled with porous media, *Advanced Materials Research*, vol.694pp.639-647.
- Khokhar, R. B., Chen, Y. K., Calay, R. K. & Xu, Y. 26-27, December (2012) Published. Numerical scheme to simulate combined mixing and separating newtonian fluid flow in a channel. In: Yarlagadda, Y.-H. K. a. P., ed. *Sensors, Measurement and Intelligent Materials*, Guilin, China. Switzerland  
Trans Tech Publications, Switzerland, 2798-2805.
- King, R. C., Apelian, M. R., Armstrong, R. C. & Brown, R. A. (1988), Numerically stable finite element techniques for viscoelastic calculations in smooth and singular geometries, *Journal of Non-Newtonian Fluid Mechanics*, vol.29pp.147-216.
- Kozo Ishizaki, Sridhar Komarneni & Nanko, M. (1998). *Porous materials: Process technology and applications*, Dordrecht, Kulwar Academic Publishers.
- Lax, P. & Wendroff, B. (2005). *Systems of conservation laws. Selected papers volume i*.
- Leong, K. C. & Jin, L. W. (2004), Heat transfer of oscillating and steady flows in a channel filled with porous media, *International Communications in Heat and Mass Transfer*, vol.31, no.1, pp.63-72.
- Ley, H. & Lessman, F. (1992). *Finite difference equations*, Mineola, Dover Publications.
- Liu, S. & Masliyah, J. H. (1999), Non-linear flows in porous media, *Journal of Non-Newtonian Fluid Mechanics*, vol.86, no.1-2, pp.229-252.
- Lohner, R. (2001). *Applied computational fluid dynamics techniques: An introduction based on finite element methods*, West sussex, John Wiley & Sons Ltd.
- Löhner, R. (1987), Finite elements in cfd: What lies ahead, *International Journal for Numerical Methods in Engineering*, vol.24, no.9, pp.1741-1756.

- 
- Malin, M. R. (1997a), The turbulent flow of bingham plastic fluids in smooth circular tubes, *International Communications in Heat and Mass Transfer*, vol.24, no.6, pp.793-804.
- Malin, M. R. (1997b), Turbulent pipe flow of power-law fluids, *International Communications in Heat and Mass Transfer*, vol.24, no.7, pp.977-988.
- Mohamad, A. A. (2003), Heat transfer enhancements in heat exchangers fitted with porous media part i: Constant wall temperature, *International Journal of Thermal Sciences*, vol.42, no.4, pp.385-395.
- Mutsuto, K., Nobutoshi, Y., Katsuya, N. & Hajime, O. (1976), Steady and unsteady finite element analysis of incompressible viscous fluid, *International Journal for Numerical Methods in Engineering*, vol.10, no.2, pp.437-456.
- Neale, G. & Nader, W. (1974), Practical significance of brinkman's extension of darcy's law: Coupled parallel flows within a channel and a bounding porous medium, *The Canadian Journal of Chemical Engineering*, vol.52, no.4, pp.475-478.
- Neofytou, P., Tsangaris, S. & Kyriakidis, M. Numerical study of the flow induced effects by different blood constitutive equations in a stenosed artery model.
- Nguyen, H. & Reynen, J. (1984), A space-time least-square finite element scheme for advection-diffusion equations, *Computer Methods in Applied Mechanics and Engineering*, vol.42, no.3, pp.331-342.
- Nicosia, M. A. (2007), A planar finite element model of bolus containment in the oral cavity, *Computers in biology and medicine*, vol.37, no.10, pp.1472-1478.
- Nicosia, M. A. & Robbins, J. (2001), The fluid mechanics of bolus ejection from the oral cavity, *Journal of Biomechanics*, vol.34, no.12, pp.1537-1544.

- 
- Nield, D. (1991), The limitations of the brinkman-forchheimer equation in modeling flow in a saturated porous medium and at an interface, *International Journal of Heat and Fluid Flow*, vol.12, no.3, pp.269-272.
- Nield, D. A. & Bejan, A. (2006). *Convection in porous media*, springer.
- Nield, D. A. & Kuznetsov, A. V. (2007), Forced convection with laminar pulsating flow in a channel or tube, *International Journal of Thermal Sciences*, vol.46, no.6, pp.551-560.
- Nield, D. A. B., A. (1999). *Convection in porous media*, New York, Springer-Verlag New York, Inc.
- Noll, W. (1958), A mathematical theory of the mechanical behavior of continuous media, *Archive for Rational Mechanics and Analysis*, vol.2, no.1, pp.197-226.
- Oden, J. T. (1970), Finite-element analogue of navier-stokes equation, *Journal of the Engineering Mechanics Division*, vol.96, no.4, pp.529-534.
- Oldroyd, J. G. (1950), On the formulation of rheological equations of state, *Proceedings of the Royal Society of London. Series A. Mathematical and Physical Sciences*, vol.200, no.1063, pp.523-541.
- Patera, A. T. (1984), A spectral element method for fluid dynamics: Laminar flow in a channel expansion, *Journal of Computational Physics*, vol.54, no.3, pp.468-488.
- Peixinho, J., Nouar, C., Desaubry, C. & Théron, B. (2005), Laminar transitional and turbulent flow of yield stress fluid in a pipe, *Journal of Non-Newtonian Fluid Mechanics*, vol.128, no.2-3, pp.172-184.
- Peyret, R. & T. D. Taylor (1985), *Computational methods for fluid flow*, The SAO/NASA Astrophysics Data System (ADS)
- Qureshi, A. L., Mahessar, A. A. & Baloch, A. Finite element model for unsteady open channel flows with sudden contraction/expansion.

- 
- Roger Peyret & Taylor., T. D. (1983). Computational methods for fluid flow, New York, Springer-Verlag
- Kakac, S., B. Arinç, K., F. and Faruk Arinç (1991), Convective heat and mass transfer in porous media, *Meccanica*, vol.27, no. November, pp.143-144.
- Savins, J. G. (1969), Non-newtonian flow through porous media, *Industrial & Engineering Chemistry*, vol.61, no.10, pp.18-47.
- Sendilkumar, K., Kalaichelvi, P., Perumalsamy, M., Arunagiri, A. & Raja, T. (2007) Published. Computational fluid dynamic analysis of mixing characteristics inside a jet mixer for newtonian and non newtonian fluids. World Congress on Engineering and Computer Science. Citeseer, 120-128.
- Sod, G. A. (1978), A survey of several finite difference methods for systems of nonlinear hyperbolic conservation laws, *Journal of Computational Physics*, vol.27, no.1, pp.1-31.
- Solangi, M. A. (2011), Finite element modeling of blood flow: Relevance to atherosclerosis, PhD, Mehran University of Engineering and Technology, Jamshoro.
- Solangi, M. A., Khokhar, R. B., Sheikh, W. & A., B. (2012a), Computational modeling of pressure difference for non-newtonian behavior of blood in plaque deposited capillaries, *Sindh University Research Journal (Science Series)*, vol.44, no.04, pp.723-726.
- Solangi, M. A., Khokhar, R. B., Sheikh, W. & Baloch, A. (2012b), A fem study for non-newtonian behaviour of blood in plaque deposited capillaries: Analysis of blood flow structure, *Mehran University Research Journal of Engineering & Technology*, vol.32, no.02, pp.277-282.
- Solangi, M. A., Khokhar, R. B. & Baloch, A. (2013), A fem study for non-newtonian behaviour of blood in plaque deposited capillaries: Analysis of blood flow structure.

- 
- Solangi, M. A., H. Sheikh, R. B. Khokar & Baloch., A. (2013), Numerical study of newtonian blood flow through a plaque deposited artery, *Sindh University Research Journal (Science Series)*, vol.45(01)pp.79-82.
- Strang, G. & Fix, G. J. (1973). *An analysis of the finite element method*, Prentice-Hall Englewood Cliffs, NJ.
- Strikwerda, J. C. (2004). *Finite difference schemes and partial differential equations*, SIAM.
- Tamaddon-Jahromi, H. R., Townsend, P. & Webster, M. F. (1992), Numerical solution of unsteady viscous flows, *Computer Methods in Applied Mechanics and Engineering*, vol.95, no.3, pp.301-315.
- Tanner, R. I. (2000). *Engineering rheology*, Oxford University Press.
- Tanner, R. I. & Walters, K. (1998). *Rheology: An historical perspective: An historical perspective*, Elsevier.
- Taylor, C. & Hood, P. (1973), A numerical solution of the navier-stokes equations using the finite element technique, *Computers & Fluids*, vol.1, no.1, pp.73-100.
- Temam, R. (1995). *Navier-stokes equations and nonlinear functional analysis*, Philadelphia, PA, Society for Industrial and Applied Mathematics, .
- Thien, N. P. & Tanner, R. I. (1977), A new constitutive equation derived from network theory, *Journal of Non-Newtonian Fluid Mechanics*, vol.2, no.4, pp.353-365.
- Thomas, J. R. H. (1987), Recent progress in the development and understanding of supg methods with special reference to the compressible euler and navier-stokes equations, *International Journal for Numerical Methods in Fluids*, vol.7, no.11, pp.1261-1275.
- Tian, Y. & Zhao, C. Y. (2011), Natural convection investigations in porous phase change materials, *Nanoscience and Nanotechnology Letters*, vol.3, no.6, pp.769-772.

- 
- Tian, Y. & Zhao, C. Y. (2013), A review of solar collectors and thermal energy storage in solar thermal applications, *Applied Energy*, vol.104pp.538-553.
- Townsend, P. & Webster, M. F. (1987), An algorithm for the three-dimensional transient simulation of non-newtonian fluid flows, *Proc. Int. Conf. Num. Meth. Eng: Theory and Applications*, pp.T12/1-11.
- Usmani, A. S., Cross, J. T. & Lewis, R. W. (1993), The analysis of mould filling in castings using the finite element method, *Journal of Materials Processing Technology*, vol.38, no.1-2, pp.291-302.
- Vafai, K. (2010). *Handbook of porous media*, Crc Press.
- Van Kan, J. (1986), A second-order accurate pressure-correction scheme for viscous incompressible flow, *SIAM Journal on Scientific and Statistical Computing*, vol.7, no.3, pp.870-891.
- Versteeg, H. K. & Malalasekera, W. (2007). *An introduction to computational fluid dynamics: The finite volume method*, Pearson Education.
- Walters, K. & Hafez, M. M. (1982), On dominating elastico-viscous response in some complex flows, *Philosophical Transactions of the Royal Society of London. Series A, Mathematical and Physical Sciences*, vol.308, no.1502, pp.199-218.
- Walters, K. & Webster, M. F. (2003), The distinctive cfd challenges of computational rheology, *International Journal for Numerical Methods in Fluids*, vol.43, no.5, pp.577-596.
- Webster, K. W. a. M. F. (1982), On dominating elasto- viscous responds in some complex flows, *Philos. Trans. R. Soc. London*, vol.A 308pp.199-218.
- Whitaker, S. (1986), Flow in porous media: A theoretic derivation of dary's law, *Transport in Porous Media*, vol.Volume 1pp.3-25.

- 
- Wolfgang Ehlers & Bluhm, J. (2002). Porous media: Theory, experiments and numerical applications  
Newyork, Springer-Verlag Berlin Heidelberg.
- Wood, W. (1990). Practical time-stepping schemes, Clarendon Press Oxford.
- Xia, B. & Sun, D. W. (2002), Applications of computational fluid dynamics in the food industry: A review, Computers and Electronics in Agriculture, vol.34, no.1-3, pp.5-24.
- Zhou, D., Zhao, C.Y. & Tian, Y. (2012), Review on thermal energy storage with phase change materials (pcms) in building applications, Applied energy, vol.92pp.593-605.
- Zienkiewicz, O. C., Richard Lawrence Taylor & Taylor, R. L. (2005a). The finite element method for solid and structural mechanics, Oxford, Elsiver Butterworth-Heinemann.
- Zienkiewicz, O. C., Richard Lawrence Taylor & Taylor, R. L. ( 2005). The finite element method for solid and structural mechanics, Oxford, Elsiver Butterworth-Heinemann.
- Zienkiewicz, O. C., Robert Leroy Taylor, Taylor, R. L. & Nithiarasu., A. P. (2005b). The finite element method for fluid dynamics,, Oxford, Elevier Butterworth-Heinemann.
- Zienkiewicz, O. C. & Taylor, R. L. (2000). The finite element method: Solid mechanics, Butterworth-heinemann.
- Zienkiewicz, O. C. & Zhu, J. Z. (1991), Adaptivity and mesh generation, International Journal for Numerical Methods in Engineering, vol.32, no.4, pp.783-810.
- Zienkiewicz, O. C. & Codina, A. R. (1995), A general algorithm for compressible and incompressible flow - part i. The split, characteristic-based scheme, International Journal for Numerical Methods in Fluids, vol.20, no.8-9, pp.869-885.